UNCLASSIFIED

AD NUMBER

AD844315

NEW LIMITATION CHANGE

TO

Approved for public release, distribution unlimited

FROM

Distribution authorized to U.S. Gov't. agencies and their contractors; Administrative/Operational use; Oct 1968. Other requests shall be referred to AFML [Maya], Wright-Patterson Air Force Base, Oh 45433 [________].

AUTHORITY

AFML, Ltr, 11 Sep 1969.

THIS PAGE IS UNCLASSIFIED

AD-844315

AFML-TR-68-189

ELECTRON SPECTROSCOPY FOR CHEMICAL ANALYSIS

KAI SIEGBAHN, CARL NORDLING, ANDERS FAHLMAN, et al.

Institute of Physics
Uppsala, Sweden

TECHNICAL REPORT AFML-TR-68-189

OCTOBER 1968

AIR FORCE MATERIALS LABORATORY
AIR FORCE SYSTEMS COMMAND
WRIGHT-PATTERSON AIR FORCE BASE, OHIO

NOTICES

300 - November 1968 - CO455 - 56-1280

REPRODUCTION QUALITY NOTICE

ELECTRON SPECTROSCOPY FOR CHEMICAL ANALYSIS

KAI SIEGBAHN, CARL NORDLING, ANDERS FAHLMAN, et al.

This document is subject to special export controls and each transmittal to foreign governments or foreign nationals may be made only with prior approval of the Air Force Materials Laboratory (MAYA), Wright-Patterson Air Force Base, Ohio 45433.

FOREWORD

This report was prepared by Uppsala University, Institute of Physics, under Contract AF 61(952)-795, Project Nos. 7360 and 7367, Task Nos. 736005 and 736702; and covers work performed during the period 1 May 1964 - 30 April 1968.

This work was administered under the direction of the Air Force Materials Laboratory, Materials Physics Division, Analytical Branch, with Mr. William L. Baun acting as Project Engineer.

The results are published under the title: ESCA, Atomic, Molecular and Solid State Structure Studied by Means of Electron Spectroscopy by Kai Siegbahn, Carl Nordling, Anders Fahlman, Ragnar Nordberg, Kjell Hamrin, Jan Hedman, Gunilla Johansson, Torsten Bergmark, Sven-Erik Karlsson, Ingvar Lindgren, Bernt Lindberg, Nova Acta Regiae Societatis Scientiarum Upsaliensis Ser. IV, Vol. 20 (1967).

This technical report has been reviewed and approved.

Freeman F. Bentley
FREEMAN F. BENTLEY
Chief, Analytical Branch
Materials Physics Division
AirForce Materials Laboratory

UNCLASSIFIED ABSTRACT

In this monograph, a report is given of our work leading to the development of high resolution electron spectroscopy. The work started in the early part of the fifties and has now been brought to a stage where we believe that this kind of spectroscopy is ready for a more general use. The energies that can be measured by our present equipment range from 1 MeV down to 0.01 eV, i.e. 26 octaves. It will be shown that new information about atoms and molecules can be obtained by electron spectroscopy. Samples may be prepared in the solid, liquid or gaseous phase. The material to be presented is comparatively extensive and we therefore start in Chapter I with a general survey in order to acquaint the reader with the main features of this type of spectroscopy before presenting a more detailed account in the chapters that follow. Some results of theoretical work and design studies are collected in appendices together with some tables required for ESCA.

CONTENTS

Appendices

ILLUSTRATIONS

ILLUSTRATIONS

ILLUSTRATIONS

ILLUSTRATIONS

ILLUSTRATIONS

ILLUSTRATIONS

ILLUSTRATIONS

ILLUSTRATIONS

ILLUSTRATIONS

ILLUSTRATIONS

ILLUSTRATIONS

ILLUSTRATIONS

ILLUSTRATIONS

ILLUSTRATIONS

ILLUSTRATIONS

ILLUSTRATIONS

(contd)

ILLUSTRATIONS

TABLES

TABLES

TABLES

PREFACE

In this monograph, a report is given of our work leading to the development of a high resolution electron spectroscopy. The work started in the early part of the fifties and has now been brought to a stage where we believe that this kind of spectroscopy is ready for a more general use. The energies that can be measured by our present equipment range from 1 MeV down to 0.01 eV, i.e. 26 octaves. It will be shown that new information about atoms and molecules can be obtained by electron spectroscopy. Samples may be prepared in the solid, liquid or gaseous phase. The material to be presented is comparatively extensive and we therefore start in Chapter I with a general survey in order to acquaint the reader with the main features of this type of spectroscopy before presenting a more detailed account in the chapters that follow. Some results of theoretical work and design studies are collected in appendices together with some tables required for ESCA. Our ambition has not been to include a complete account of related fields of research for which review articles can be found in the literature. Thus we have not dealt in detail with X-ray emission and absorption spectroscopy, electron energy loss studies etc. We have, however, given a list of papers to which reference has been made in the text and which we believe to be of direct relevance. These publications may in their turn help the reader to find his way to other papers bearing on the subject.

Uppsala in June 1967

Kai Siegbahn *Carl Nordling* *Anders Fahlman*
Ragnar Nordberg *Kjell Hamrin* *Jan Hedman*
Gunilla Johansson *Torsten Bergmark* *Sven-Erik Karlsson*

Institute of Physics, University of Uppsala

Ingvar Lindgren
Department of Physics,
Chalmers University
of Technology, Gothenburg

Bernt Lindberg
Institute of Chemistry,
University of Uppsala and
Research Division,
Pharmacia AB, Uppsala

1. INTRODUCTORY SURVEY OF ESCA

Most of the phenomena that are studied in a physics laboratory and utilized in technology take place in the electronic structure of atoms, molecules and solid material. Different kinds of spectroscopy have been developed for investigating these structures, the most well-known being optical, infrared (IR), Raman, and ultraviolet (UV) spectroscopy, optical rotational dispersion (ORD), X-ray emission and absorption spectroscopy, nuclear magnetic resonance (NMR), nuclear quadrupole resonance (NQR), electron spin resonance (ESR), Mössbauer spectroscopy, microwave spectroscopy, and mass spectroscopy. In the following sections we describe a recently developed high resolution spectroscopy, named ESCA (*E*lectron *S*pectroscopy for *C*hemical *A*nalysis). It is based on a magnetic or electrical analysis at high resolution of the electrons which are emitted from a substance on irradiation with X-rays. ESCA reproduces directly the electronic level structure, from the innermost shells to the atomic surface. All elements from lithium to the heaviest ones can be studied even if the element occurs together with several other elements and represents only a small part of the chemical compound. This spectroscopy is characterized by sharp electron lines and by a high sensitivity. The precision has been brought to the limit set by the inherent widths of the atomic levels themselves. ESCA is applicable in a variety of fields of research in physics and chemistry. Applications are, for example, found in organic chemistry, since the important light elements carbon, nitrogen, oxygen etc. are easy to study. Shifts of inner levels due to chemical structure effects are characteristic features, and ESCA provides information on the chemical bonding in molecules.

From the middle of the nineteen tens to the middle of the nineteen thirties some research workers in England (H. Robinson)[101, 102, 103] and in France (M. de Broglie)[104] investigated the energy distribution of electrons in various elements irradiated with X-rays. (For further references see Refs. 105 and 106). The distributions were recorded photographically with the help of a homogeneous magnetic field for the energy analysis. A given anode material in the X-ray tube, for example silver or molybdenum, emits a continuous spectrum plus characteristic X-ray lines, of which the $K\alpha_1\alpha_2$ doublet is the strongest. If this unfiltered and unmonochromatized radiation impinges on a foil of an element, photoelectrons are emitted which can be recorded in the magnetic spectrograph on a photographic plate. In this way, electron distributions were obtained which were characterized by long tails with edges at the high energy end. By measuring the positions of the edges it was possible to determine the energy of the photoelectrons ejected from the different atomic shells of the element under investigation. From the known energy of the X-ray lines in the primary X-ray beam, the binding energies of electrons in the different shells could be calculated.

Another approach is to let the X-ray beam pass through a thin foil and to study the absorption spectrum with an X-ray spectrometer. In this case edges are also obtained, and their positions correspond to the energy required to excite an electron from one of the inner shells to the nearest empty level in the atom, which is very near its surface. Clearly, the data obtained by the two methods are closely related, although not identical. Nowadays X-ray absorption spectroscopy is a well established technique.

X-ray emission gives a line spectrum (superimposed on a continuous bremsstrahlung spectrum) instead of the edges obtained in X-ray absorption. The X-ray emission spectrum constitutes one of our most accurate sources of information on atomic level structure. It must be remembered, however, that X-ray emission spectra are excited in an X-ray tube by an intense electron bombardment of the anode, a condition which normally leads to decomposition of chemical compounds. Hence, in order to study the X-ray emission spectra of chemical compounds it is usually necessary to resort to a fluorescence technique, in which a primary X-ray beam excites secondary X-ray emission spectra from the compound under investigation. By

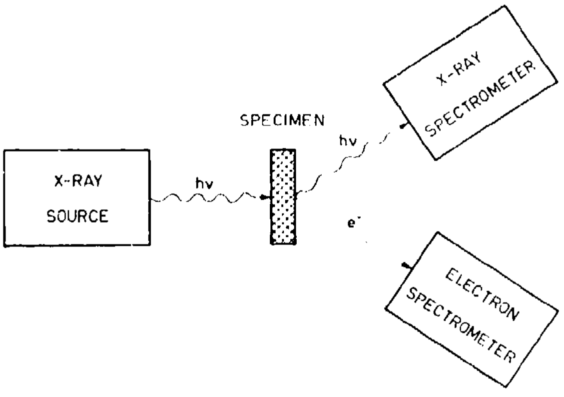

Fig. 1:1. Two different methods for the spectroscopy of atoms and molecules. The upper branch to the right represents X-ray fluorescence and X-ray absorption spectroscopy. The lower branch represents the electron spectroscopic method ESCA.

emission spectroscopy the energy differences within the atom are obtained, but it does not yield the electron binding energies.

After the above-mentioned early investigations, the electron spectroscopic approach almost completely disappeared. The reason for this recession is that the results could not compete in accuracy with those obtained by the X-ray absorption technique, and even less with those obtained by the X-ray emission technique. The edge positions of the electron distributions were not well defined, because of the energy absorption of the electrons emerging from the foil. A comparison of the observed binding energies showed considerably greater spread and greater uncertainty throughout.[105,106] Only few further attempts[107-111] have been made to extend the early works by H. Robinson and M. de Broglie, but these experiments met with limited success in comparison to contempory X-ray spectroscopy work.

The different ways of using X-rays for gaining information on atomic and molecular structure are illustrated in Fig. 1:1. A specimen is irradiated with X-rays. The upper branch to the right of the figure represents the well-known X-ray fluorescence and X-ray absorption spectroscopy. The lower branch represents electron spectroscopy as the alternative source of information. Since every process in the upper branch is accompanied by emission of electrons (by means of photo- and Auger effect) leading to the lower branch, one can in principle expect that each of these branches is of comparable value. The outcome of this approach and the conclusions which can be drawn from it depend entirely on how the experimental difficulties can be mastered. The first condition for favorable competition between the lower branch and the upper one is that an electron spectroscopy based on well defined criteria for the precise evaluation of significant energies can be developed. At first sight and with the early attempts in mind, the possibility of fulfilling this condition seems rather faint.

The absorption of photons in the material will not affect the energy of those photons which are transmitted but the intensity will be decreased. The intensity of fluorescence radiation produced in the specimen will be attenuated on its path out but the lines will retain their energies, as defined by the peak positions. Whether the position of an X-ray absorption edge is independent of the finite thickness of the absorption layer is less clear, but in the case of electrons it is very probable that the absorption process will destroy any precise information originally contained in the spectrum. This is because the energy and the intensity of electrons produced inside the material by the X-radiation would be expected to diminish considerably on their way out. The early studies in fact confirmed this general behaviour and the difficulty of getting precise energy criteria greatly limited electron spectroscopy as a competitor to X-ray spectroscopy.

The problem of this energy absorption of electrons

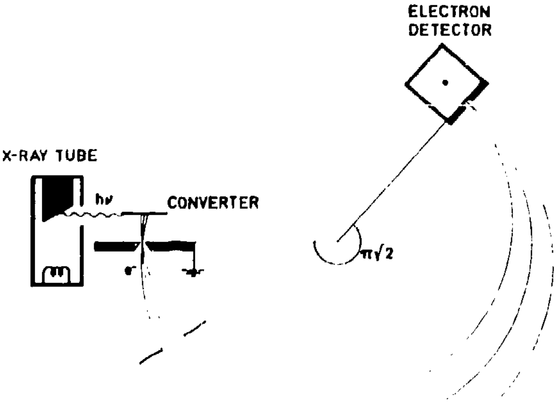

Fig. 1:2. Schematic view of an ESCA arrangement for the study of electrons expelled by X-rays.

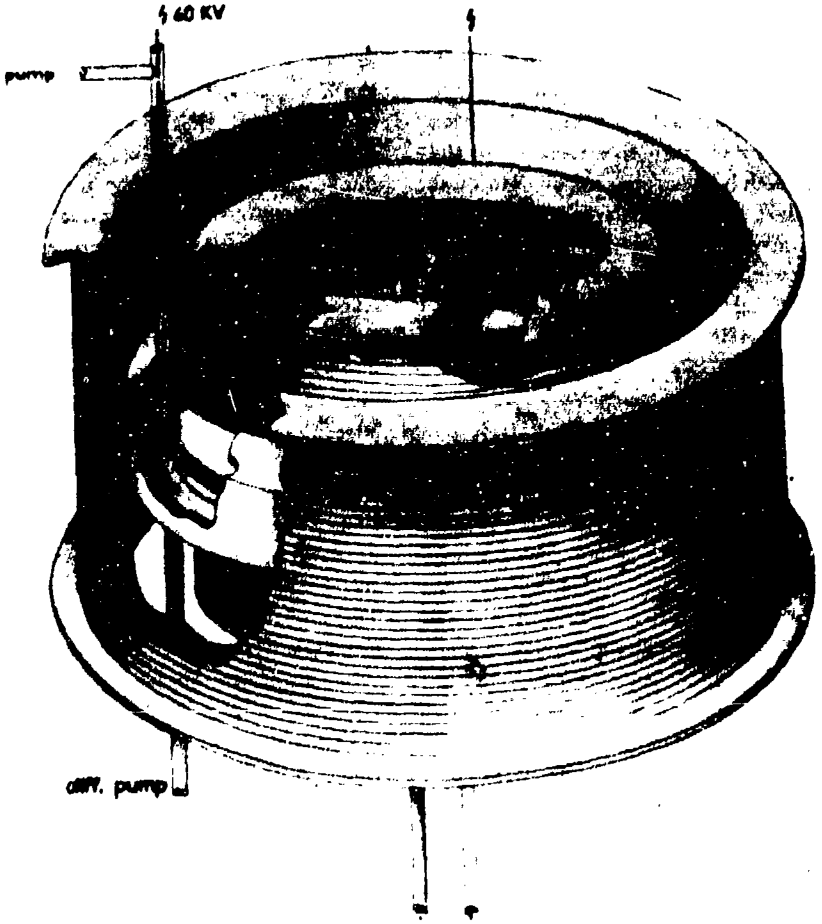

Fig. 1:3. First iron-free double focussing spectrometer adapted for ESCA. The magnetic field is obtained from two co-axial coils with radii 24 cm and 36 cm, and height 48 cm.[5]

is well known in high resolution beta spectroscopy. A radioactive source which has a finite thickness is known to emit electron lines which are broadened and shifted towards lower energies. For extreme precision in the measurements the radioactive atoms have to be collected completely carrier free on the surface of the backing material. High resolution instruments can easily detect line broadenings and shifts if the radioactive atoms are allowed to penetrate the material to some depth. A special technique which retards the radioactive ions produced in a mass separator before they are collected on the backing has been used to minimize β line distortion.[146] The energy of a β line is usually of the order of at least 25 keV, and in order to observe an absorption effect of, say, 5 eV on such a line, the resolution has to have the extreme value $\Delta B\varrho / B\varrho \approx 1 : 10^4$. Since line broadenings are also observed at more moderate resolutions, and even when great precautions have been taken to produce thin surface layers of the electron emitting radioactive layer, one has good reason to doubt whether the elimination of line distorsions of less than 1 eV for electrons produced in a thick target by X-radiation can be achieved.

In 1951, one of the authors (K. S.) initiated a research program aimed at the very high resolution study of the energy spectrum of electrons expelled by X-rays. A sketch of the experimental arrangement is shown in Fig. 1:2. An X-ray tube of compact construction (situated close to the specimen) is built into a high resolution, large dispersion magnetic spectrometer ($\varrho_0 = 30$

cm) of the double focussing type, see Fig. 1:3. The principle of two-directional or double focussing was conceived in 1946 by one of the authors (K. S.) in collaboration with N. Svartholm[112] and it was primarily developed for nuclear spectroscopy using radioactive sources. For low energy electron spectroscopy, in the range 0—10 keV, which is the energy region of interest for the ESCA method, it is difficult to use iron pole plates to shape the magnetic field according to the $1/\sqrt{\varrho}$ form, required for double focussing. Fortunately, it was found that the same field could be obtained over a limited region avoiding iron by using a coil arrangement, consisting of two co-axial coils of special dimensions[5]; see Fig. 1:3. This kind of electron spectrometer was subsequently constructed in increasingly elaborate forms and with radii of curvature of the central orbit up to 100 cm[46,52,279]. These instruments have large dispersion and the precision obtained with them exceeds that previously typical for semicircular magnetic instruments, used in radioactive work with radii 5–10 cm, by one or even two powers of ten while at the same time the intensity, due to the high luminosity, is appreciably increased. If a copper anode is used in the X-ray tube, a relative momentum resolution of, say $3 \cdot 10^{-4}$ of the electron spectrometer would correspond to an absolute energy resolution of 3 or 4 eV for loosely bound electrons and correspondingly better for the more tightly bound electrons in the inner shells. An absolute energy resolution of 1 eV corresponds to a relative momentum resolution of $5 \cdot 10^{-4}$ for 1000 eV electrons. This would be typical for electrons expelled by means of X-radiation from anode material like aluminum or magnesium. Furthermore, a precision of 0.1 eV in the measurement of a line peak position requires in the 5 keV region a relative precision of $\approx 1 \cdot 10^{-5}$ in the measurement of momentum. These requirements were substantially more severe than those met with previously. In addition to the resolution problem discussed above one also had to face the problems of intensity at high resolution. An efficient geometry for the X-ray tube and high transmission and large dispersion of the electron spectrometer were greatly needed. The investigation of low energy electrons calls for a completely iron-free instrument with highly reproducible field settings and a special electron detecting technique. All external magnetic fields, in particular the earth's magnetic field, have to be compensated for. An instrument of this kind had not been designed before and it took three years to build the first iron-free double focussing magnetic spectrometer and to test it so that the radioactive sources could be replaced by the X-ray unit. This first part of the work was described in a paper[5] entitled "Beta ray spectroscopy in the precision range of 1: 10^5" and also in some previous publications[1,2] and in the book "Beta- and Gamma-Ray Spectroscopy"[4] (new edition, Ref. 52).

In 1954 the first instrument was ready and attempts were made to record at high resolution photoelectron spectra produced by X-rays. A new observation then changed the course of the future development of the method. This was the appearance, under high resolution, of a very sharp line which could be resolved from the edge of each electron veil. This line has the important property that it does not undergo any energy absorption, and its sharp peak thus corresponds to the binding energy of the relevant inner shell. In principle, and also in practice, the line width can be made so small that it corresponds to the width of the atomic energy levels. This is of the order of a few electron volts for the lighter elements. The situation is illustrated in Fig. 1:4 which shows an electron spectrum obtained from MgO with an X-ray beam from a copper anode. The double focussing instrument was in this case set for a momentum resolution of $\approx 3 \cdot 10^{-4}$. The sharpness of the electron lines is so great that the energy scale must be multiplied by a factor of 100 in order to bring out the finite width as shown in the inset for one of the lines. The peak can be determined with considerable precision, to a few tenths of an electron volt. In a special investigation of the reproducibility in the determination of the position of this line, under identical conditions and for a thin source, the spread of the values for eleven recordings was within $1 \cdot 10^{-5}$.

A more detailed study of a photoelectron line obtained with the ESCA method shows that it consists of the principal line together with a more or less continuous energy distribution immediately to the left of the line; and with the resolution now attainable this can be distinguished from the principal line by an intensity minimum. This minimum occurs because electrons passing through the specimen can only lose energy in certain discrete amounts, a phenomenon which had been observed earlier in other connections,[113] but had not previously been observed here. The discrete energy losses are due to so called plasmon excitations of the electron plasma in the specimen, i.e.

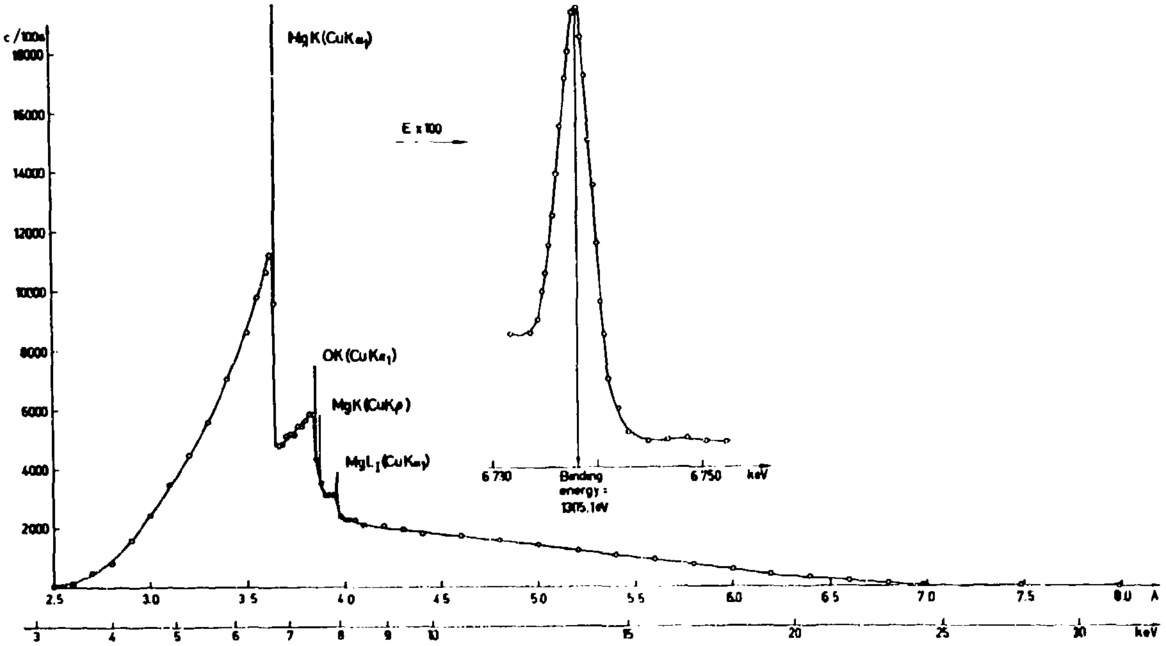

Fig. 1:4. Electron spectrum obtained from magnesium oxide with copper X-radiation. Edges are found at energies corresponding to atomic levels of magnesium and oxygen. A very sharp electron line can be resolved from each edge. Such an electron line is shown in the insert figure with the energy scale expanded by a factor of one hundred to bring out the finite width of the line.

collective electron vibrations in the plasma (of surface and volume type), plus ionisation, and excitation in interband transitions[147].

The discrete character of the electron energy losses and the high resolution are of fundamental importance for ESCA. Thus, since an electron line obtained in the way described above is not disturbed by the energy absorption processes, only the following factors contribute to the line width: (a) the natural width of the incident X-ray line, (b) the width of the atomic level from which electrons are ejected, (c) the aberration of the spectrometer and (d) the widths of the source and the detector slits.

The choice of anode material is dependent on the binding energy of the particular atomic shell studied. As a rule, one should use anode material from the light elements except in those cases where inner levels of higher Z elements are being studied. The advantages of using soft X-radiation are several: (a) the inherent widths of the levels of light elements are smaller, thus contributing less to the line width of the resulting electron line, (b) the energy of the expelled electrons is smaller, which means a high energy resolution on an absolute scale (since $\Delta B\varrho/B\varrho$ is a constant for the instrument),[52] (c) the photoelectric cross section is higher at low photon energies and although the range of the photoelectrons is smaller the net result is generally a gain in intensity of the electron lines, (d) the electron lines expelled by softer X-rays dominate completely over the low energy veils. In fact, the resulting electron spectra look very similar to the line spectra obtained in, for example, X-ray emission spectroscopy. As an example, Fig. 1:5 shows the electron spectra of the spin doublet L_{II}, L_{III} ($2p_{1/2}$ and $2p_{3/2}$, respectively) in copper excited by the Mg$K\alpha$ radiation. For comparison, a corresponding X-ray line spectrum of the same doublet as obtained by Sandström[114] is shown in the upper part of the figure. It is interesting to note that the ESCA lines from the $L_{II,III}$ shells of copper are even sharper than the $K\alpha_1$ and $K\alpha_2$ X-ray lines, although the latter were recorded under almost ideal conditions (fourth order reflection in a high dispersion instrument) and reproduced the X-ray transitions with essentially their inherent widths. The fact that the

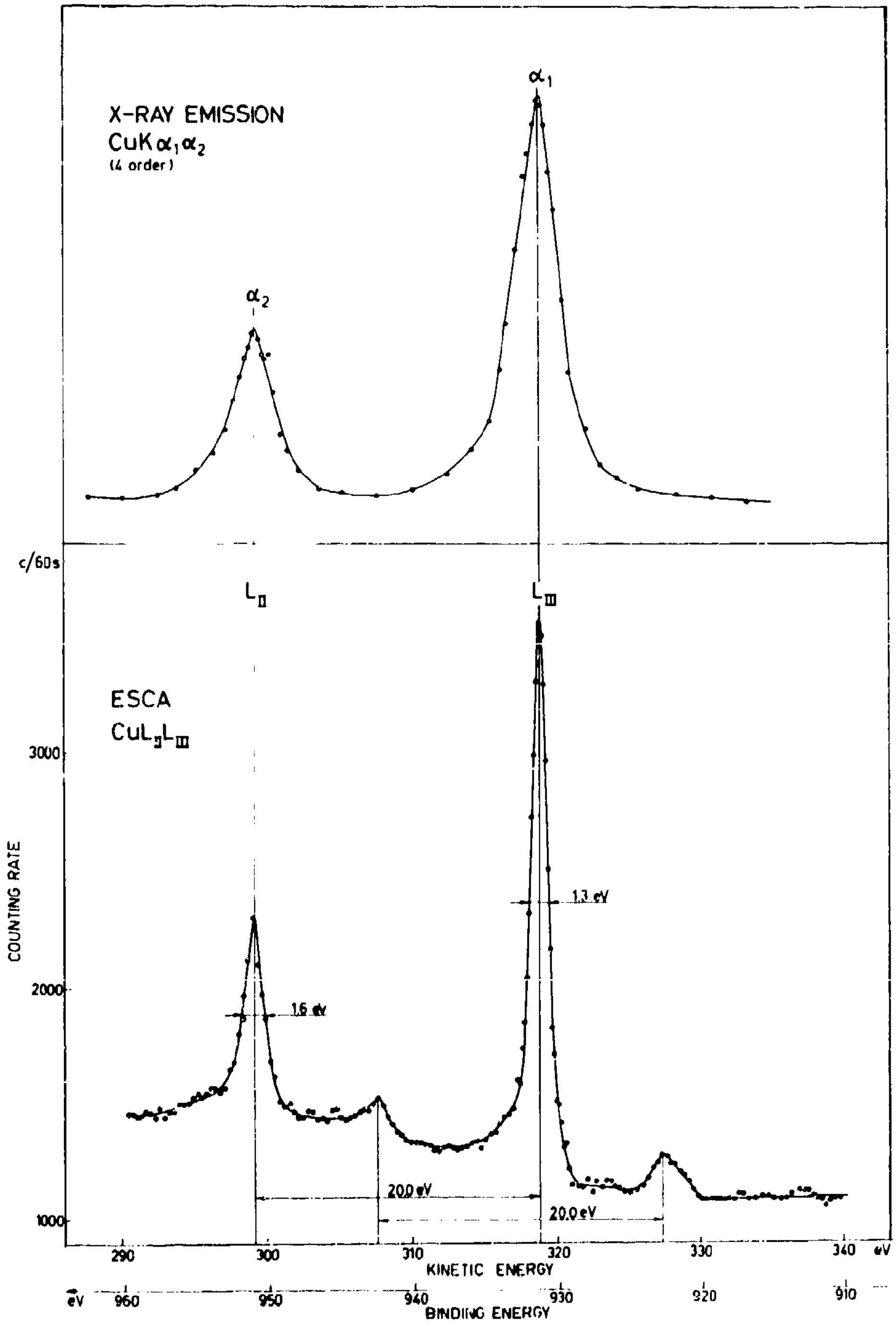

1:5. Electron spectrum of the L_{II}, L_{III} subshells of copper obtained with Mg*K*α radiation. For comparison, the Cu*K*$\alpha_1\alpha_2$ X-ray emission spectrum of the same doublet, recorded by Sandström[114], is shown in the upper part.

ESCA lines can be made even sharper than the inherent widths of the corresponding X-ray lines is readily explained by the small inherent width of the Mg$K\alpha$ radiation involved in the photoelectric process compared to the large width of the copper K level that is involved in the X-ray transition. The situation cannot be improved in the case of the X-ray line spectrum by studying the $L\alpha_2$ and $L\beta_1$ lines. These lines have a considerable width, since they result from transitions from M_{IV} to L_{II} and L_{III}, and the M_{IV} level in copper lies in the band structure with a width of several eV. One can notice a small difference in level width between L_{II} and L_{III}. In the electron spectrum the $K\alpha_3\alpha_4$ satellite in the Mg X-radiation gives rise to two lines of low intensity.[287] Although of lower intensity, these satellite lines show the L_{II} and L_{III} levels of copper in much the same way as do the main lines. The distance between the L_{II} and L_{III} levels as obtained from the electron spectrum is in good agreement with the X-ray difference between $K\alpha_1$ and $K\alpha_2$, namely 20.0 eV.[115] This agreement is of particular interest for the theoretical comparison of ESCA and X-ray spectroscopy data (when binding energies are concerned). The photoelectric release of an electron from the atom takes place in the ground state of the atom whereas the X-ray transition occurs between two excited states (i.e. starting with a hole in the K shell and ending with one hole in the L shell). One, consequently, could imagine a difference between the results of ESCA and X-ray spectroscopy. According to Fig. I:5 there is, however, good agreement between the energy difference $L_{II}-L_{III}$ as obtained from ESCA and the corresponding $K\alpha_1-K\alpha_2$ difference. A closer theoretical analysis of the experimental evidence, presented in Section III:9, suggests that an accurate approach would in this case be obtained by treating the electronic system of the atom as a whole after the removal of a photoelectron or the emission of an X-ray quantum.

As pointed out earlier the electron line spectrum maps out each individual atomic level, whereas the characteristic X-ray spectrum reveals differences between the levels involved in the transitions. According to the result presented above (Fig. I:5), the energy difference between two electron lines yields similar information to that obtained from X-ray emission spectroscopy.

The advantage with X-ray absorption spectroscopy as with electron spectroscopy is that it gives the binding energies of the individual levels. In this case ESCA spectra offer advantages mainly because they appear as sharp line spectra. Let us illustrate this (Fig. I:6) from a comparison between an absorption spectrum and an ESCA spectrum of the M_I and $M_{II,III}$ levels in the same element as in the preceding figure, namely copper. The absorption spectra is due to Johnston and Skinner[116] (also reproduced in Tomboulian's review article in Encyclopedia of Physics[117]), and although it might be claimed that the absorption spectrum could be further improved it is still obvious that the information gained from the electron spectrum is far more detailed.

During the ten years of development following the resolution and recording of the first ESCA spectra by our group, a large body of data on the electron binding energies of most elements from lithium to plutonium in the Periodic System has been accumulated and systematized (see first section of reference list). The accuracy of the binding energies is consistently higher than that offered by the X-ray absorption method. As one particular example, it was found that the previously accepted L_I binding energies for a sequence of light elements had to be revised by as much as 50 %,[51] owing to earlier difficulties in the interpretations of X-ray absorption spectra in this region. Even in cases where one has to deal with closely spaced levels, the ESCA method is satisfactory.

In order to obtain electron spectra from the inner levels of heavier elements, one must use anode materials of correspondingly higher Z, like molybdenum and tungsten. If one restricts oneself to the lighter elements or to the outer levels, anode materials like sodium, magnesium or aluminum are more advantageous. With such anode materials we have found that ESCA permits a study of the band structure in metals and alloys. The photoelectrons then have nearly the full X-ray photon energy, which is 1253.6 eV for magnesium radiation.[115] Fig. I:7 shows an ESCA spectrum for the outer part of the gold level system. Although the N_{VI} and N_{VII} levels differ by only 3.7 eV, they are completely resolved in the spectrum and recorded with high intensity. The satellite line Mg$K\alpha_{3,4}$ also produces this doublet. An O line of low intensity is recorded and finally, in the region close to binding energy zero, the conduction band is reproduced. This part of the spectrum is displayed separately in the figure and shows

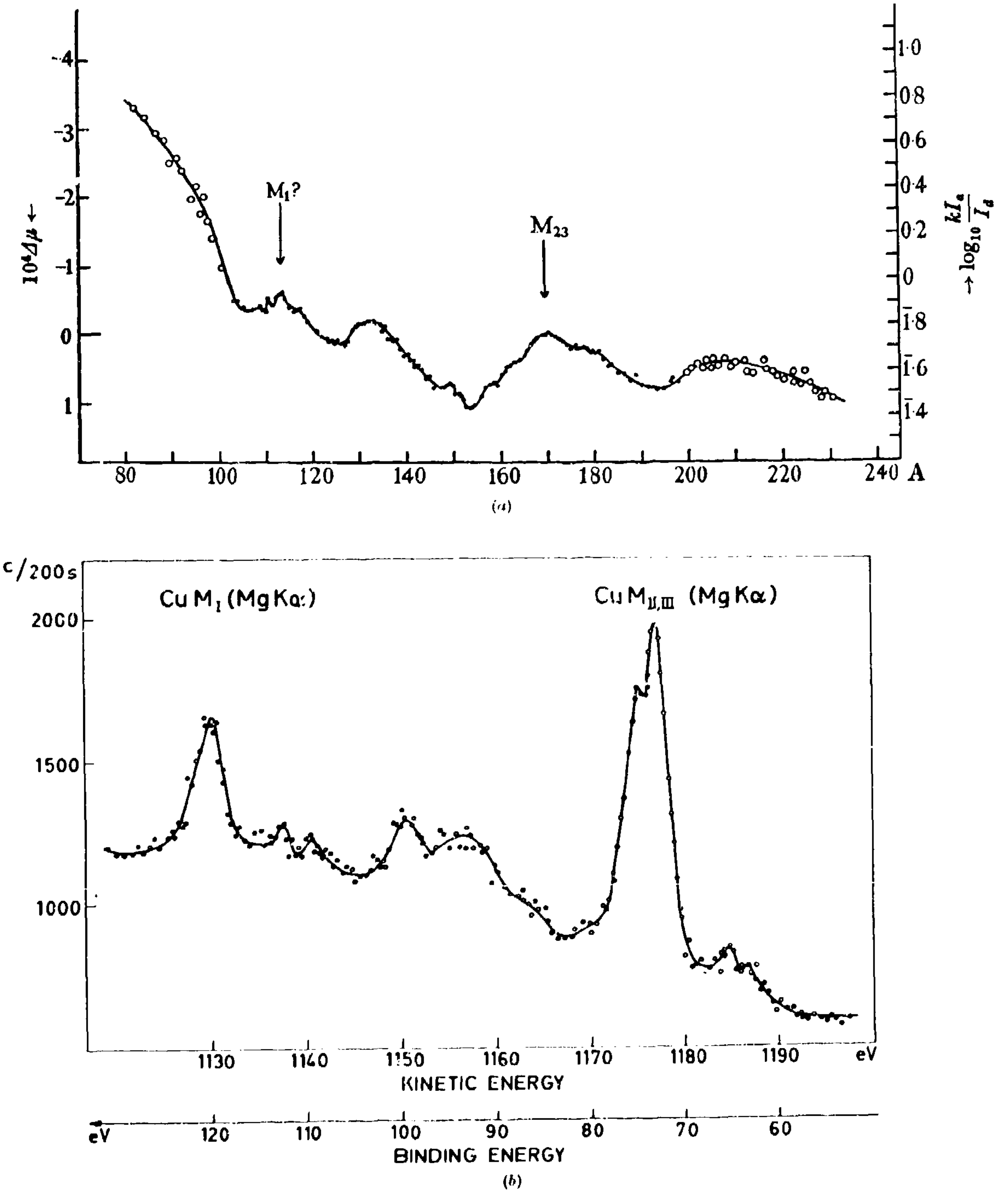

Fig. 1:6. A comparison between an X-ray absorption spectrum recorded by Skinner and Johnston[116] (a) and an ESCA spectrum (b) of the M_I and $M_{II,III}$ levels in copper. The $M_{II,III}$ levels are partly resolved in the ESCA spectrum. Two discrete energy losses can be seen in this spectrum on the low-energy side of the $M_{II,III}$ line.

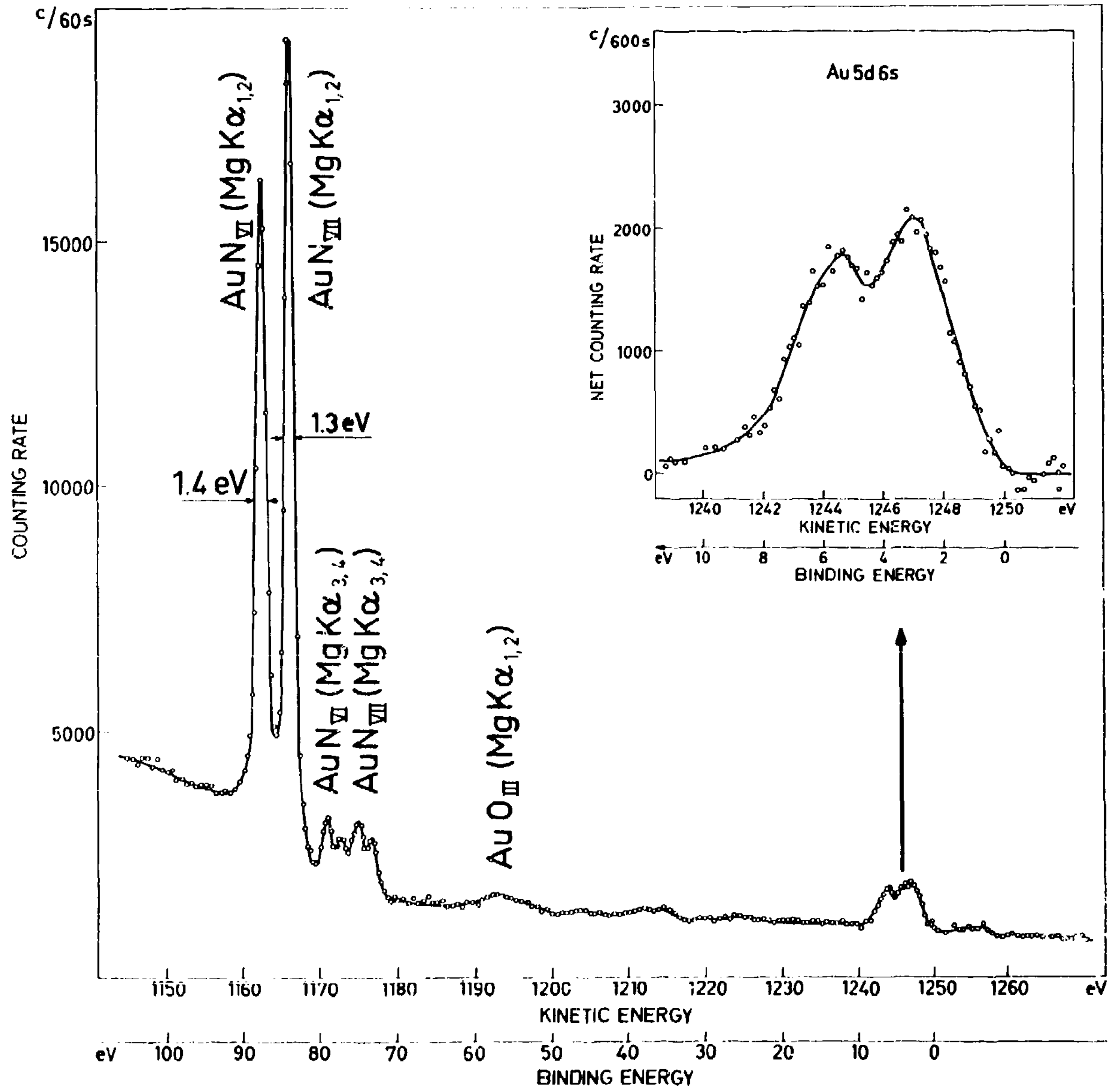

Fig. 1:7. ESCA spectrum of the outer levels of gold. The strong N_{VI}, N_{VII} spin doublet is completely resolved into two sharp lines. The conduction band is displayed separately and shows two maxima. See also Chapter IV.

two maxima in the electron distribution. Likewise, the electronic level structure of an insulator can be studied by ESCA, all the way out to the valence band. Thus, the electron spectrum of Fig. 1:8 shows the electron levels of NaCl from zero binding energy at the Fermi level to the sodium $2p$ level at binding energy 30 eV. The narrow valence band (chlorine $3p$) is situated about 5 eV below the Fermi level.

A favourable feature of the relatively high photon energies that are employed in the ESCA method is that the energy of the photoelectrons is of such a magnitude that slight surface contamination is not

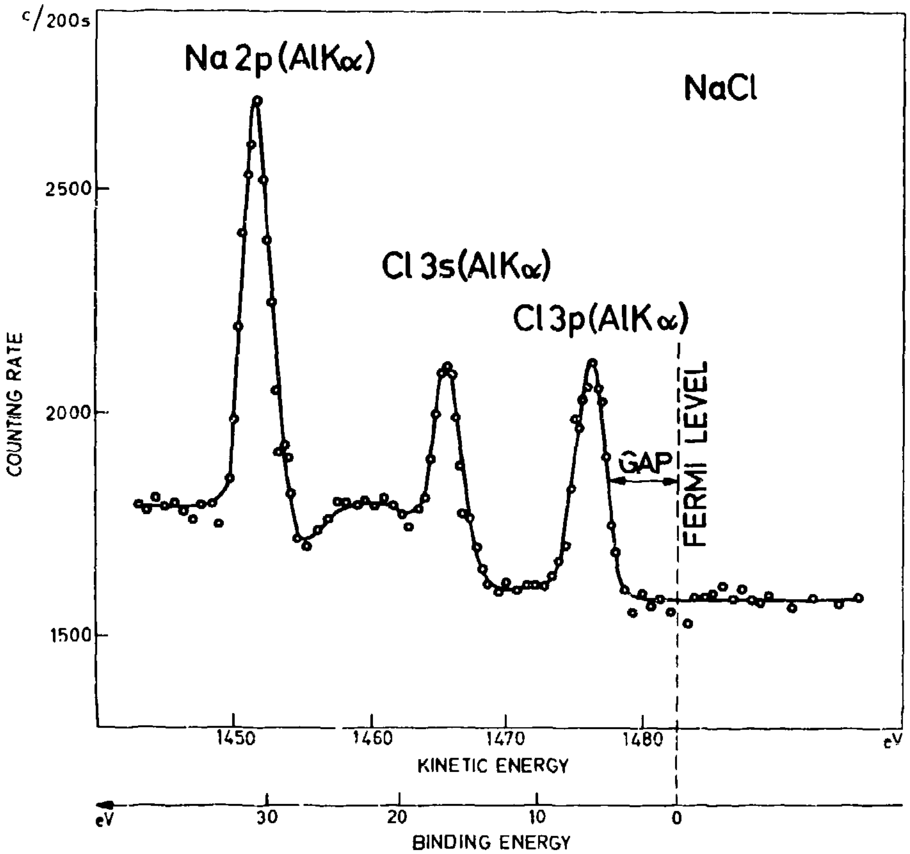

Fig. I:8. Electron spectrum from NaCl. This is an insulator with a gap of 8 eV between the valence and the conduction bands. The electron spectrum shows a marked decrease in intensity at about 5 eV below the Fermi level. See also Fig. IV:1.

detrimental since the electrons can pass such a layer without distortion of the spectrum.

As an analytical method, ESCA can be applied over the whole periodic system. It is well known that X-ray fluorescence spectroscopy used in other analytical contexts is not straightforward for elements lighter than sodium because of the rapidly decreasing fluorescence yield for low atomic numbers, see Fig. II:4. For the light elements, as for example carbon, nitrogen and oxygen, ESCA gives excellent signals, see Fig. I:9.

The sensitivity of ESCA is high. Only a very thin surface layer of around 100 Å of the sample is utilized for the analysis. Photoelectrons emitted from atoms further down in the source lose energy and are therefore removed from the electron line. Gases adsorbed on the surface of a foil yield spectra of good intensity. In this way, we have measured the atomic levels of the rare gases like argon and xenon which are difficult to study by X-ray emission spectroscopy.

Oxide films formed at the surface of most metals are seen in ESCA spectra, both as an oxygen line and as a shifted line situated near the line from the unoxidized metal. The latter effect will be discussed further in Section V:1. Corrosion and surface reaction kinetics are thus obvious fields for ESCA as indicated by its surface sensitivity. It is possible that free radicals may also be studied.

The sensitivity of ESCA to surface changes is demonstrated by the carbon line from the diffusion pump oil which grows rapidly in intensity if no precautions are taken to prevent this, by using, for instance, an ionic or a molecular pump (Section V:7). We have made

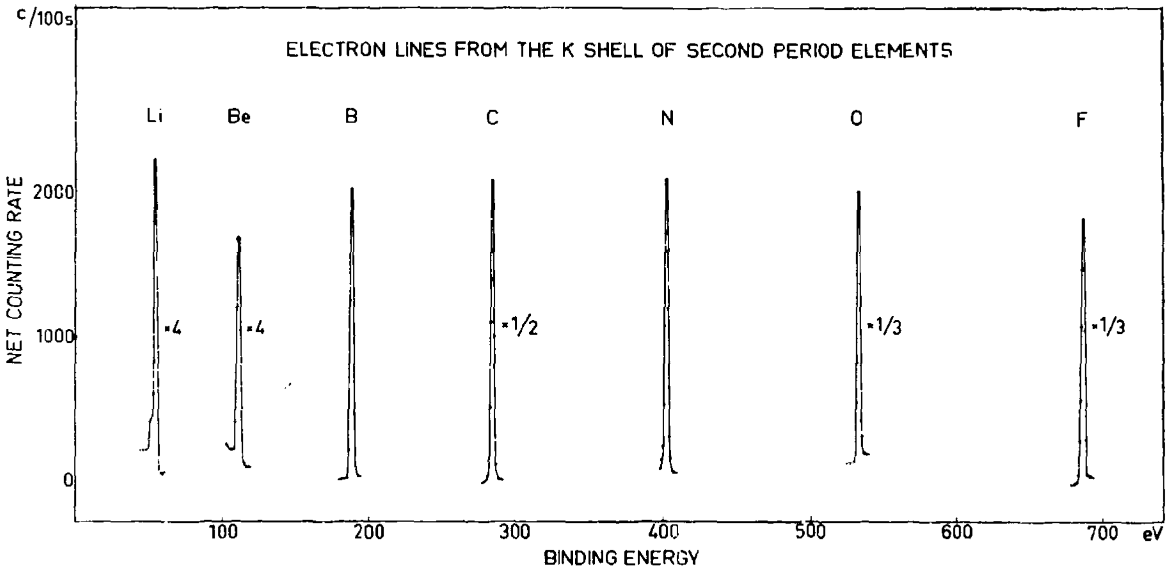

Fig. I:9. Electron spectrum from the *K* shells of the second period elements, obtained with Al*K*α radiation. See also Sections III:1 and III:2.

a special study of the surface sensitivity of ESCA by preparing a monomolecular layer of an iodine substituted stearic acid and recording the iodine spectrum (Section V:6). High intensity was obtained from the iodine although the amount of iodine was only some thousandths of a microgram. This means that only minute quantities of material are required, provided that the source area can be made sufficiently large, i.e. a few mm².

Other examples of the sensitivity are found in large molecules like vitamin B_{12}, or insulin. Vitamin B_{12} contains only one cobalt atom among 180 atoms of other elements[118], see Fig. I:10. A 100 Å layer of vitamin B_{12} thus contains very few cobalt atoms. Nevertheless we could easily observe the cobalt in the electron spectrum from vitamin B_{12}, see Fig. I:11, furthermore, its valence state can be determined. Insulin has a molecular weight of about 6000 and contains 51 amino acids with three disulfide bridges, two of which bind the two peptide chains together[288], see Fig. I:12. There is approximately one sulfur atom for every 140 other atoms. A good signal was recorded from sulfur, see Fig. I:13, and the binding energy obtained was consistent with the value for simple disulfides. The relative intensity was in accordance with the known content of sulfur.

ESCA can thus be used for elemental analysis, i.e. for determining the proportions of constituent elements in chemical compounds, see Section V:7. We have studied the relative intensities of the electron

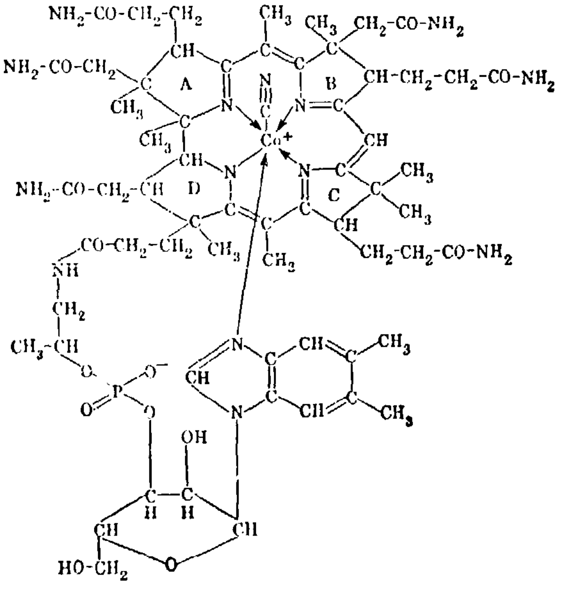

Fig. I:10. The vitamin B_{12} molecule.[118] There is one cobalt atom among 180 atoms of other elements.

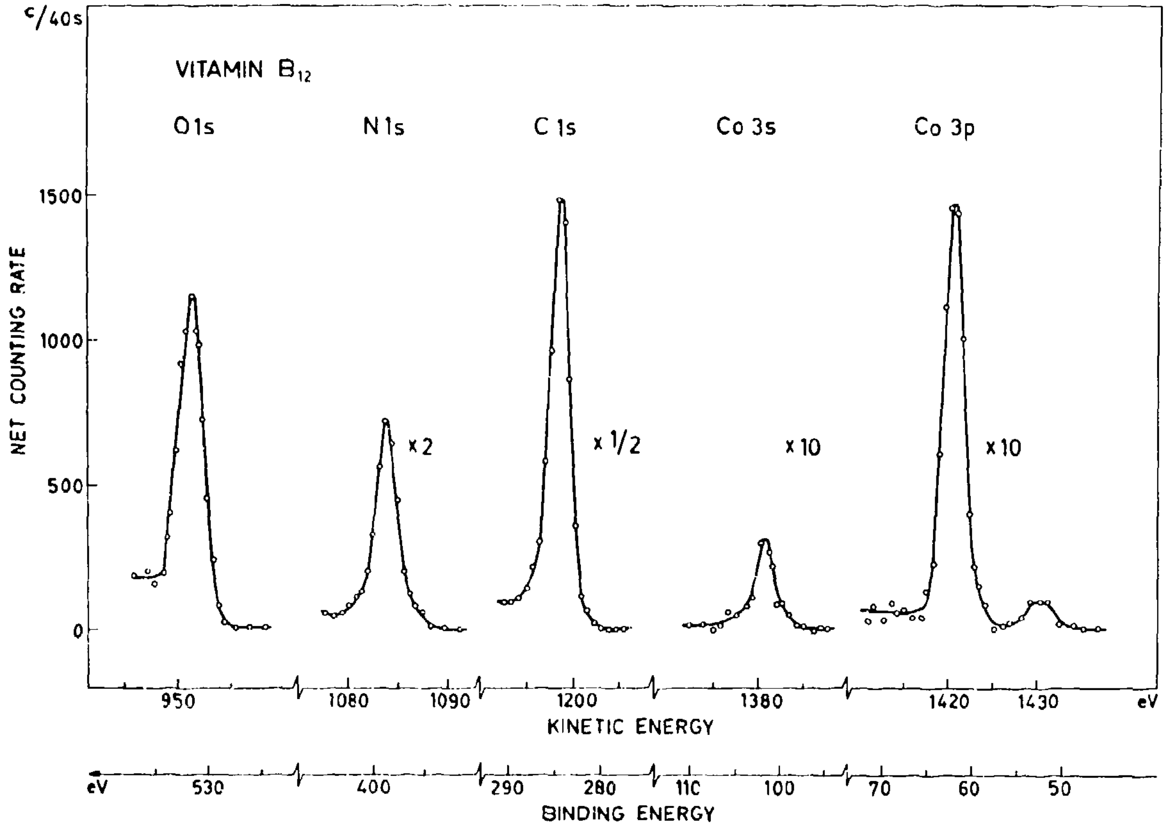

Fig. I:11. Electron spectrum from vitamin B_{12} with electron lines from oxygen, nitrogen, carbon and cobalt.

lines in a number of cases as, for instance, in chloro substituted aromatic sulfur compounds with chlorine and sulfur in various proportions. The relative intensities of the electron lines were found to agree with the known empirical formulae.

From an analytical point of view it is noteworthy that ESCA yields more information than can be gained from stoichiometric relationships. It also gives information about the valence state. This is connected with the chemical shift effect which will be discussed below and which can be used for the study of charge on atoms, oxidation state, bond character or chemical structure.

The results from the study of vitamin B_{12} have demonstrated that ESCA is sensitive for heavy metals in large molecules, and it may therefore provide a method for investigating the charge of metal ions in for instance enzymes and similar compounds. Since ESCA also yields information on the oxidation state of atoms, it may for instance, be used to study the breaking up of the disulfide bridges in insulin by oxidation processes, see Section V:5b.[91]

A number of problems should be studied in more

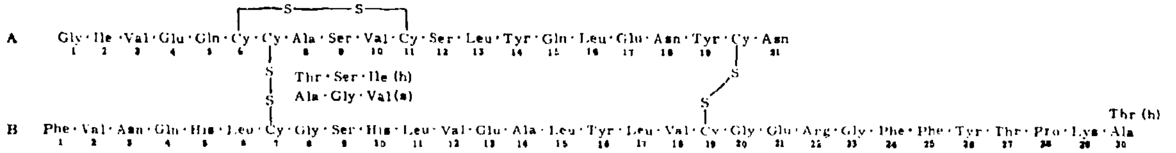

Fig. I:12. The insulin molecule.[288] It consists of 51 amino acids with three disulfide bridges, two of which bind the two peptid chains together.

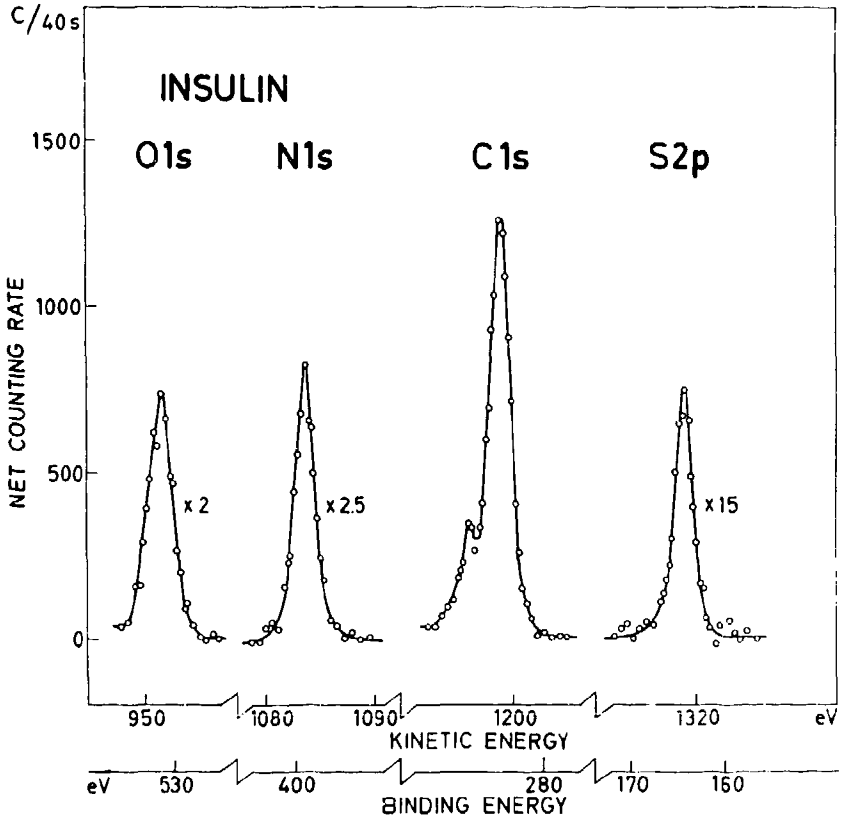

Fig. I:13. ESCA spectrum of insulin. Electron lines are obtained from oxygen, nitrogen, carbon, and sulfur.[91] See also Sections V:5b and V:7.

detail before ESCA is used for routine work. Thus further information on the behaviour of unstable compounds, which might gradually decompose under the combined action of X-radiation and vacuum is required. We have found freezing techniques very useful in such cases. In fact, ESCA can be applied not only to solid material but also to liquids and gases by means of a simple freezing technique. Fig. I:14 shows an ESCA spectrum from solidified benzene obtained using the freezing technique. Aluminum $K\alpha$ radiation was used for expelling electrons from the benzene molecules on the cooled source backing. At a kinetic energy of 1200 eV, a narrow line (half-width 1.5 eV) is observed. This corresponds to the atomic $1s$ level in carbon. Since the X-radiation also contained the satellite lines $K\alpha_3$ and $K\alpha_4$, the same atomic level is again seen as two electron lines at a kinetic energy of ca. 1210 eV. Electron binding energies are around 280 eV. It is of interest to note that the continuous background is small and in particular that the low-energy electron veil is negligible. The current in the X-ray tube was lowered to 6 mA (if necessary, it could be raised to a much higher value, say 100 mA) and still, as can be seen, the intensity in the electron spectrum is high.

A group of lines is observed with binding energies between five and twenty eV. These lines in the ESCA spectrum cannot be attributed to any atomic levels in carbon or hydrogen. Instead they correspond to molecular orbitals in the solidified benzene molecule.

It had already been observed in the early twenties, that the position of emission lines and absorption edges in X-ray spectroscopy was not solely an atomic property but was also to a small extent dependent on the chemical state of the atom.[106,119] Not only the peripheral atomic levels which could be expected to be influenced by chemical binding were affected but also the inner levels, for example the K level. Much work has been devoted to the task of interpreting this chemical effect on X-rays and thereby improving our understanding of the chemical bond. Progress has been hampered,

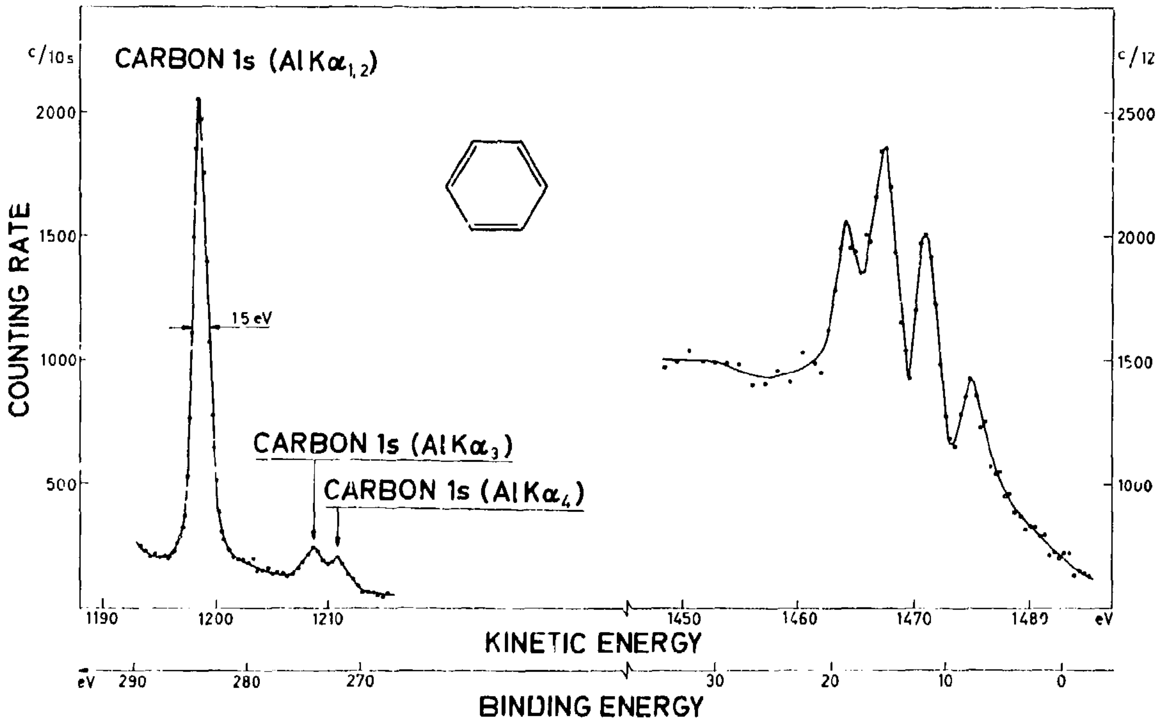

Fig. I:14. Electron spectrum from carbon in solidified benzene using the freezing technique. The 1*s* electron line has a width of 1.5 eV. The right part of the spectrum shows electron lines from the molecular orbitals. See also Fig. VIII:52.

for two main reasons: the chemical shifts in X-ray emission spectra are generally very small (of the order of tenths of an eV) and furthermore they are difficult to interpret theoretically. In X-ray absorption spectra, the chemical shifts are larger but, on the other hand, the effects are much more difficult to study because of the edge structures, which are often further complicated by additional structures on the high energy sides. Faessler[120] in his review of this field concludes that in spite of the small effects in X-ray emission spectroscopy, from the experimental point of view this approach is definitely to be preferred to X-ray absorption studies. Early attempts made by Robinson and coworkers[121] to study chemical displacements in X-ray produced electron spectra were not sufficiently rewarding to make this type of spectroscopy useful for the study of chemical structure problems.

After having developed high resolution electron spectroscopy, our first attempt to study the chemical effects was made in 1957 on copper and its oxides.[14] It was found that electron spectroscopy was particularly well suited for this field of research for the following reasons: (a) the sensitivity is high, (b) the chemical effects are relatively large and can be studied separately for each individual level, (c) the precision is high even in complicated cases because of the line character of ESCA spectra. We have found a particularly rewarding field among the light elements in the Periodic System, i.e. elements like carbon, nitrogen, and oxygen[75,76,81] which are of special importance in organic chemistry and biochemistry. X-ray emission spectra from these elements have a serious limitation in the fact that the X-ray lines are not sharp since the broad valence band is involved in the X-ray transitions. Although the inherent width of the *K* level is itself very small, it is impossible to make use of it in X-ray emission spectroscopy. In ESCA, however, the *K* electron spectra of these light elements are easily excited giving very sharp lines of high intensity, as was shown in Fig. I:9. Since the inherent widths of the *K* levels of the lightest elements are of the order of some tenths of an electron volt, the main contribution comes from the inherent width of the exciting X-ray line, if Mg*K*α or Al*K*α radiation is used this is still less than 1 eV (Section II:5). Including the finite resolution of the spectrometer, the *K* electron lines from the light elements have widths of 1.3—1.5 eV, and in the following a few examples are discussed.

In the electron spectrum of acetone, the carbon line is split into two well-resolved lines, see Fig. 1:15. The distance between the two lines is 2.7 eV. The intensity ratio is 2 : 1, which shows that the left line corresponds to the carbon bound to oxygen and the right line to the carbon in the methyl groups. This spectrum was not recorded with the above mentioned freezing technique. Instead, acetone vapour was allowed to flow into the source compartment and the vapour was irradiated with aluminum X-radiation. Thus the electron spectrum shown in Fig. 1:15 was obtained from free acetone molecules. A great number of similar spectra recorded from compounds both in the gaseous and the solid phase, have shown that we have here found a general method to distinguish atoms with different valence states. For example, ethyl trifluoroacetate is a molecule with four carbon atoms having different valence states and as shown in Fig. 1:16 the carbon electron spectrum from this molecule reflects each of these valence states. The lines corresponding to the different carbon atoms in the molecule appear in the same order from left to right as do the carbon atoms in the structure that has been drawn in the figure. The different valence states of atoms of the same element may also be resolved in more complicated molecules.

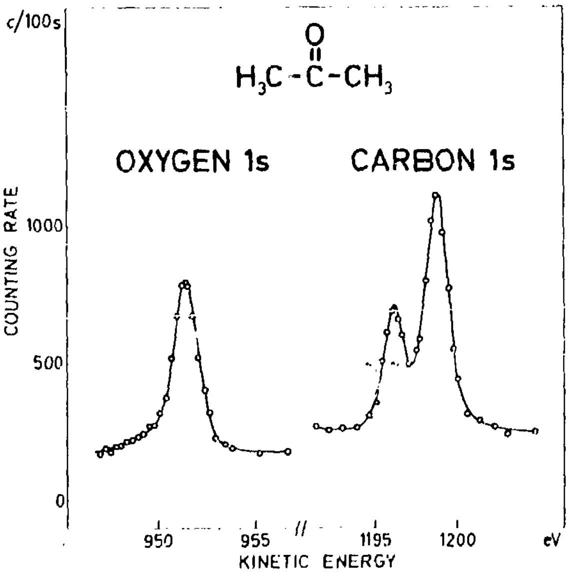

Fig. 1:15. Electron spectrum of acetone with two carbon lines corresponding to differently bound carbon atoms. See also Sections V:1 and V:5c. This spectrum was recorded from acetone vapour irradiated with Al*K*α radiation.

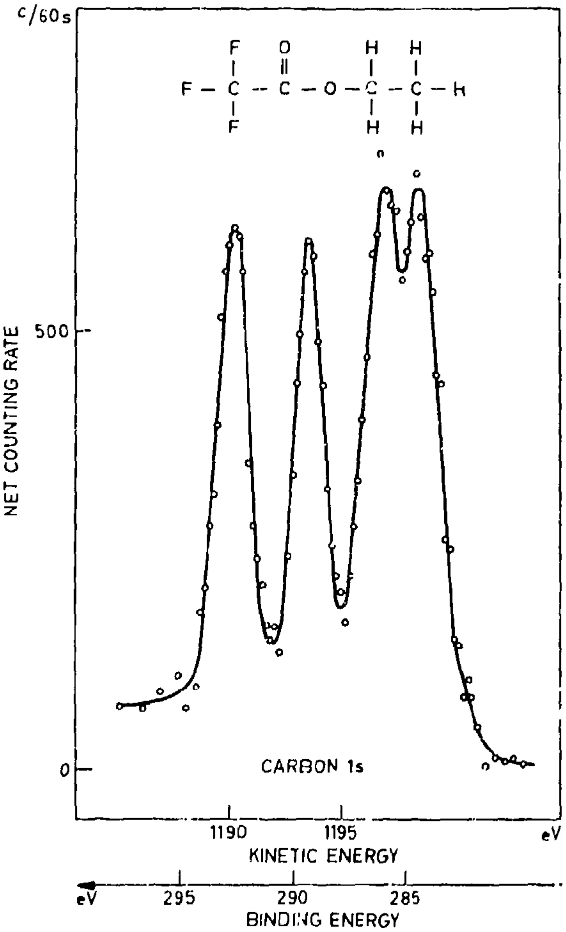

Fig. 1:16. Electron spectrum from carbon in ethyl trifluoroacetate. All four carbon atoms in this molecule are distinguished in the spectrum. The lines appear in the same order from left to right as do the corresponding carbon atoms in the structure that has been drawn in the figure.

We have recently studied an extensive series of organic nitrogen compounds[76,81] of which some examples

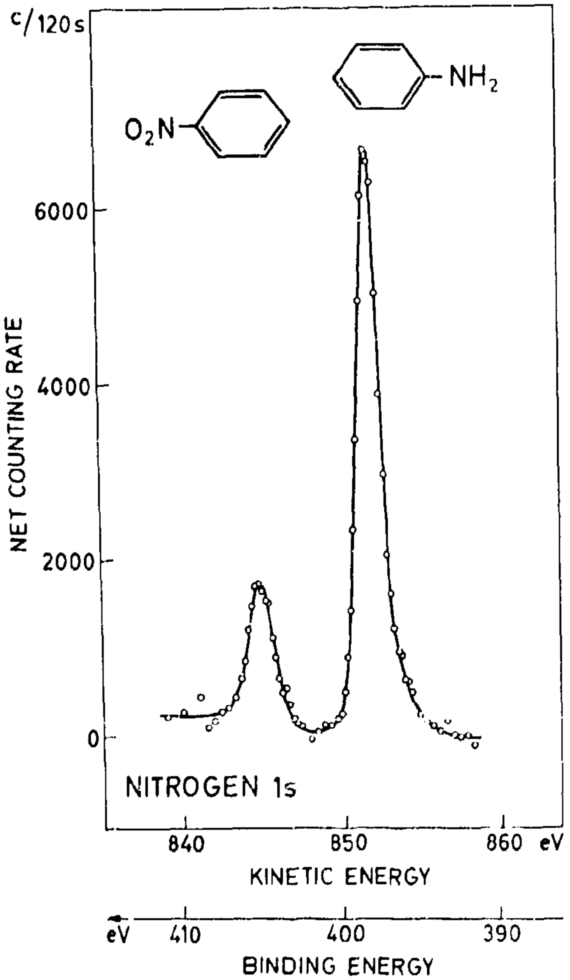

Fig. I:17. Nitrogen 1*s* lines from a 1:1 mixture of aminobenzene and nitrobenzene, both of which are liquids at room temperature.[78,81] The energy separation is 7.0 eV. See also Section V:5a.

will be given here. Fig. I:17 shows the 1*s* nitrogen lines from a 1:1 mixture of

aminobenzene

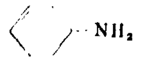

and

nitrobenzene

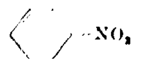

both of which are liquids at room temperature. The separation of the nitro- and the amino nitrogen lines is appreciable, being 7.0 eV. The intensity ratio depends on the partial vapour pressures of the two compounds in the mixture.

Fig. I:18 shows the nitrogen spectrum from the molecule

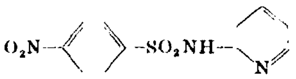

The nitrogen is here split into three lines. The line of lowest kinetic energy can easily be shown to correspond to NO_2 whereas the interpretation of the other two lines is more difficult. However, in a separate study it was established that the pyridine nitrogen corresponds to the electron line of highest kinetic energy. The energy difference between NO_2 and NH is 5.4 eV and between the NH and pyridine nitrogen is 2.1 eV.

Oxygen and other elements are also subject to chemical shift effects in their ESCA spectra.

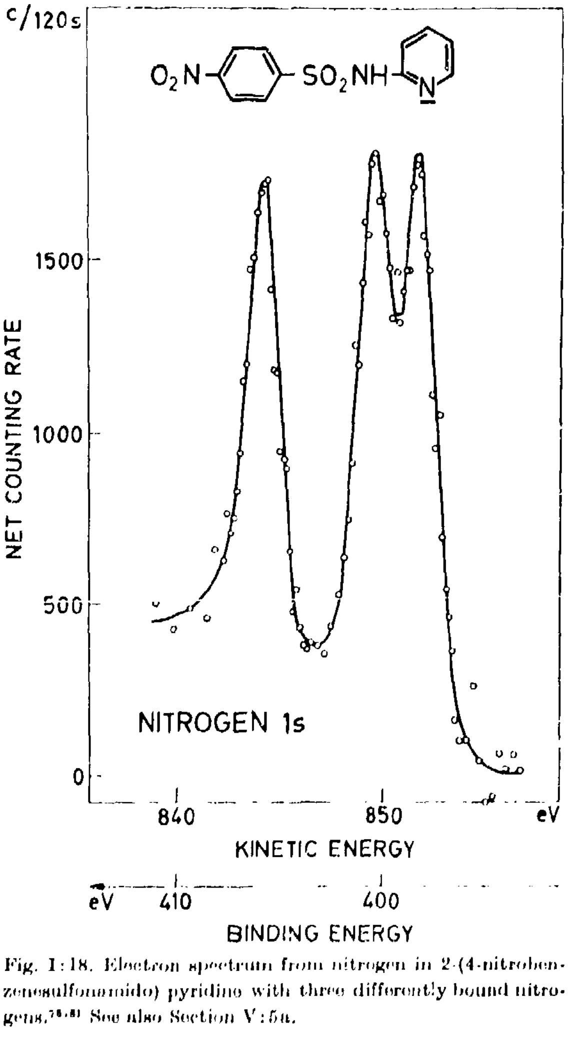

Fig. I:18. Electron spectrum from nitrogen in 2-(4-nitrobenzenesulfonamido) pyridine with three differently bound nitrogens.[78,81] See also Section V:5a.

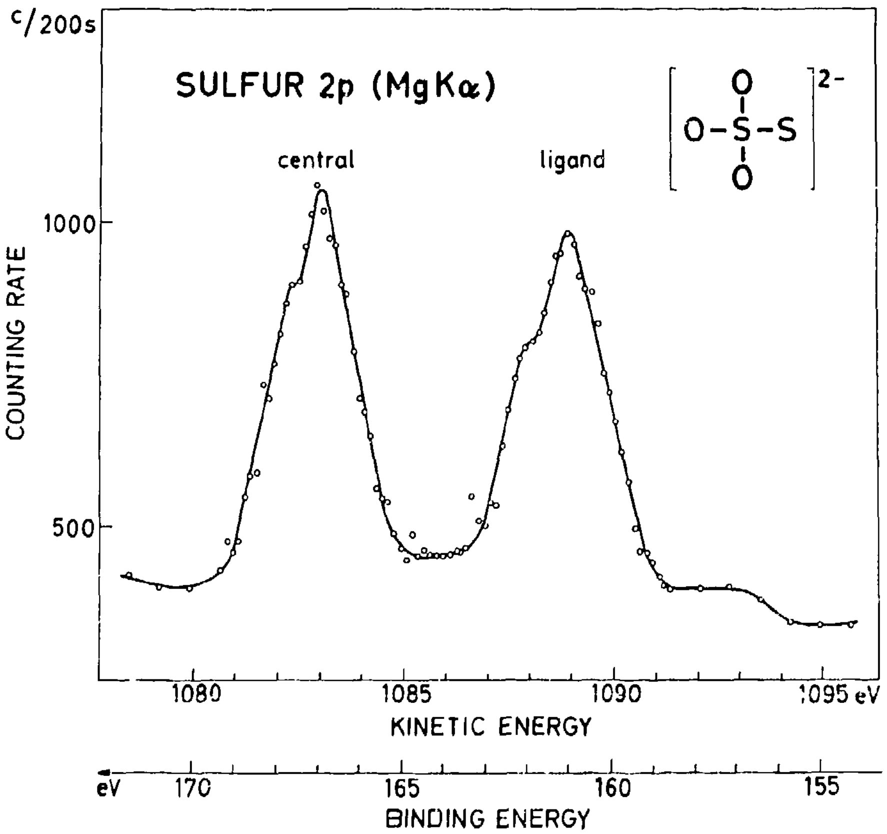

Fig. I:19. Electron spectrum of the $2p$ subshell of sulfur in sodium thiosulfate, $Na_2S_2O_3$. The chemical shift is 6.0 eV. The lines are asymmetric due to the spin doublet splitting $2p_{1/2}$ and $2p_{3/2}$. See also Section V:5b.

The chemical binding effect can be followed from shell to shell. In the third row of the periodic system where the $L_{II,III}$ shells are sharply defined in energy, one finds elements like phosphorus, sulfur and chlorine which can occur in a variety of valence states. Fig. I:19 shows the splitting of the sulfur $2p$ line in sodium thiosulfate, $Na_2S_2O_3$. The two sulfur atoms have different oxidation numbers, namely 6+ and 2 −. The chemical shift in the $2p$ level is 6.0 eV. Similarly, we have found a shift of 7.0 eV in the $1s$ level. Thus the splitting is large and is easy to measure with considerable precision (≈ 0.1 eV). In X-ray emission, the chemical shifts in sulfur have been given particular attention.[120] The shifts encountered are, however, almost an order of magnitude smaller than in ESCA and, furthermore, expose only the difference between the shifts in the K and L levels, not the total shifts of each level. The shifts between different sulfur compounds generally amount in X-ray emission spectra to only a few tenths of an eV, i.e. to a small fraction of the inherent line width of the $K\alpha$ line. Also, since the sulfur $K\alpha$ line is an unresolved doublet owing to the large inherent line widths compared to the small doublet separation, the interpretation of the X-ray chemical shifts is further complicated in this case. In X-ray absorption spectroscopy on the other hand, as pointed out by Faessler,[120] the uncertainties can be demonstrated by the fact that for some time it was thought that the sulfur K absorption edge derived from thiosulfate was composed of three instead of two different components.

The examples given so far of chemical shifts in electron spectra were obtained in the K and L shells. Fig. I:20 is an example of the chemical binding effect in the M shell. It demonstrates the chemical influence on the M_{IV} and M_{V} levels in iodine in the two com-

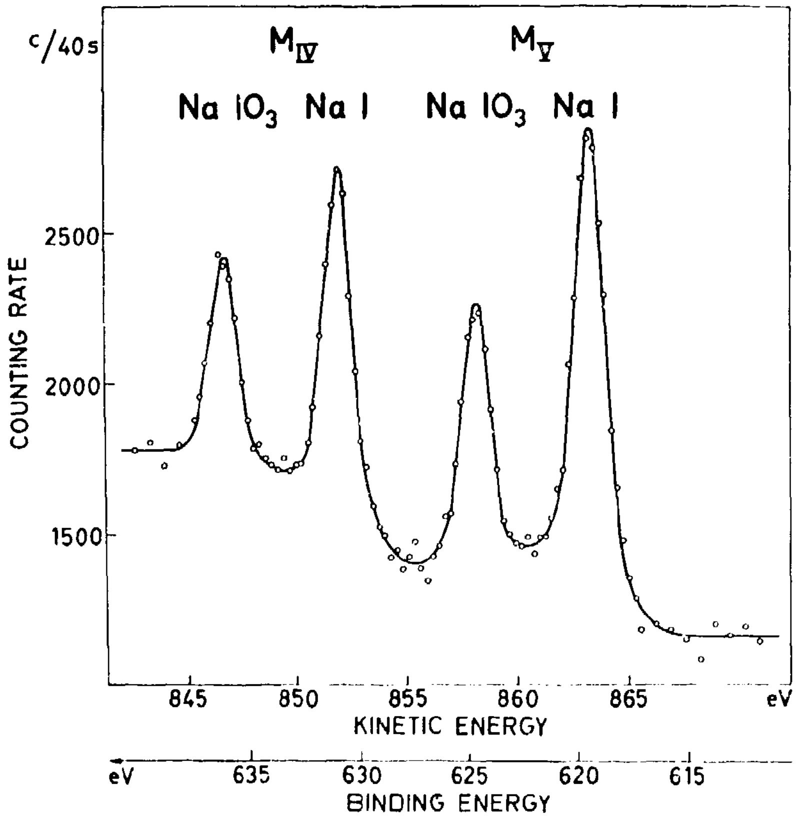

Fig. I:20. Electron spectrum from a mixture of NaI and $NaIO_3$. The chemical shift of the iodine *M* levels is about as large as the difference between the M_{IV} and M_V levels themselves.

pounds NaI and $NaIO_3$. The spectrum was taken from a powder mixture of the two compounds. The powder mixture was pressed to form a pellet in much the same way as IR sources are made. It is interesting to note that the chemical shift is about as large as the difference between the M_{IV} and M_V levels themselves in iodine.

Chemical shifts in the *N* shell, finally, are exemplified in Fig. I:21 and Fig. I:22. Fig. I:21 shows the shifts of the platinum N_{VI} and N_{VII} levels in metallic Pt compared to K_2PtCl_6, and Fig. I:22 shows the same levels in bismuth. The latter spectrum was obtained from evaporated bismuth and reveals that the sample had been partly oxidized. Each of the levels N_{VI} and N_{VII} are split in two, one from metallic bismuth and one from bismuth in oxide form.

We have found that all elements studied so far exhibit in their compounds chemical structure effects which, in many cases, can be more closely investigated by ESCA. For instance, metals like Li, Be, Al, Cu, Fe, Mn, Cr etc. and their oxides, all give easily measurable shifts. Non-metallic elements like C, N, O, S, P, Cl, I etc. behave in the same way.

The question arises whether the observed chemical shifts can be fitted into a consistent theoretical picture. This can be done providing one takes into account that the formation of a chemical bond influences the distribution of electric charge in the outer orbitals and therefore causes a change in the screening of the core electrons. In this model, the position of an electron line from an element can be used as a measure of the effective atomic charge on the element in the molecular or solid state structure. The shifts can be calculated quantum mechanically as described in Section V:3, and by comparison with observed shifts one can make a semi-empirical determination of the effective atomic charge, from which some estimate concerning the character of bonds can be made. One example can be mentioned here. In the third period of the Periodic System partial double bond character through contribution from higher orbitals has been invoked to explain the character of sulfur-oxygen bonds. We have therefore recently

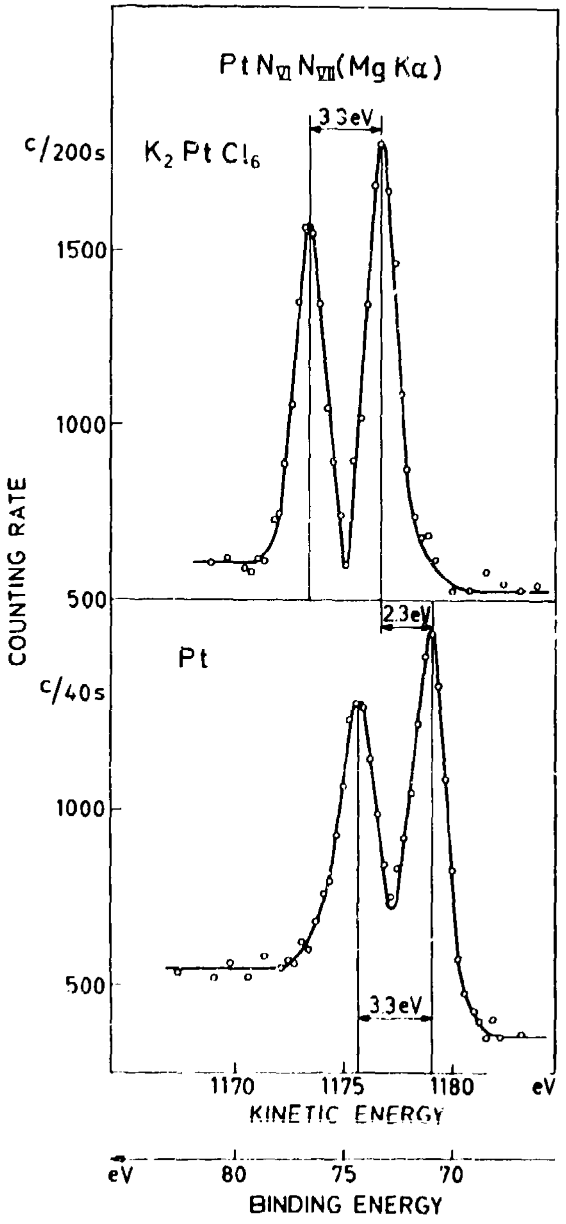

Fig. 1:21. Electron spectra from metallic Pt and K_2PtCl_6 showing the shifts of the platinum N_{VI} and N_{VII} levels.

studied the sulfur-oxygen bond in an extensive series of organic sulfur compounds[83] (Section V:5b).

For more comprehensive series of compounds we have used the simple electronegativity concept in the discussion of the influence of valence on chemical shifts, see Section V:4. Concepts like valency or oxidation number have also been used for correlating chemical shifts but are too crude for a detailed discussion and more sophisticated concepts must be used for this purpose.

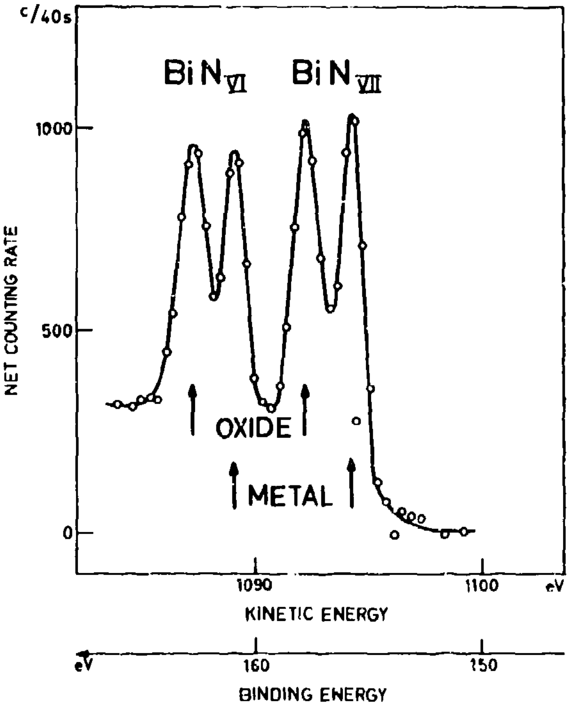

Fig. 1:22. Electron spectrum from vacuum evaporated bismuth. The metallic source was covered by a thin layer of oxide when exposed to air. The chemical shift between the metal and the oxide is about 2 eV.

Chemical effects are also important in other types of spectroscopy as, for instance, in nuclear magnetic resonance spectroscopy (NMR), electron spin resonance spectroscopy (ESR), and in the isomeric shifts in Mössbauer spectroscopy. In NMR and ESR, however, it is the magnetic interactions of the electron distribution that exposes the chemical structure. In NMR the effective magnetic field at the nucleus is modified by the surrounding electron distribution and the magnetic energy is also dependent on the spin-spin interaction with neighbouring nuclei. Isomeric shifts in Mössbauer spectroscopy are caused by the Coulomb interaction between the nucleus and the surrounding electrons that penetrate the finite nuclear volume. A change in valence causes a change in *s* electron density at the nucleus and therefore a change in the Coulomb interaction, which results in a shift of the nuclear

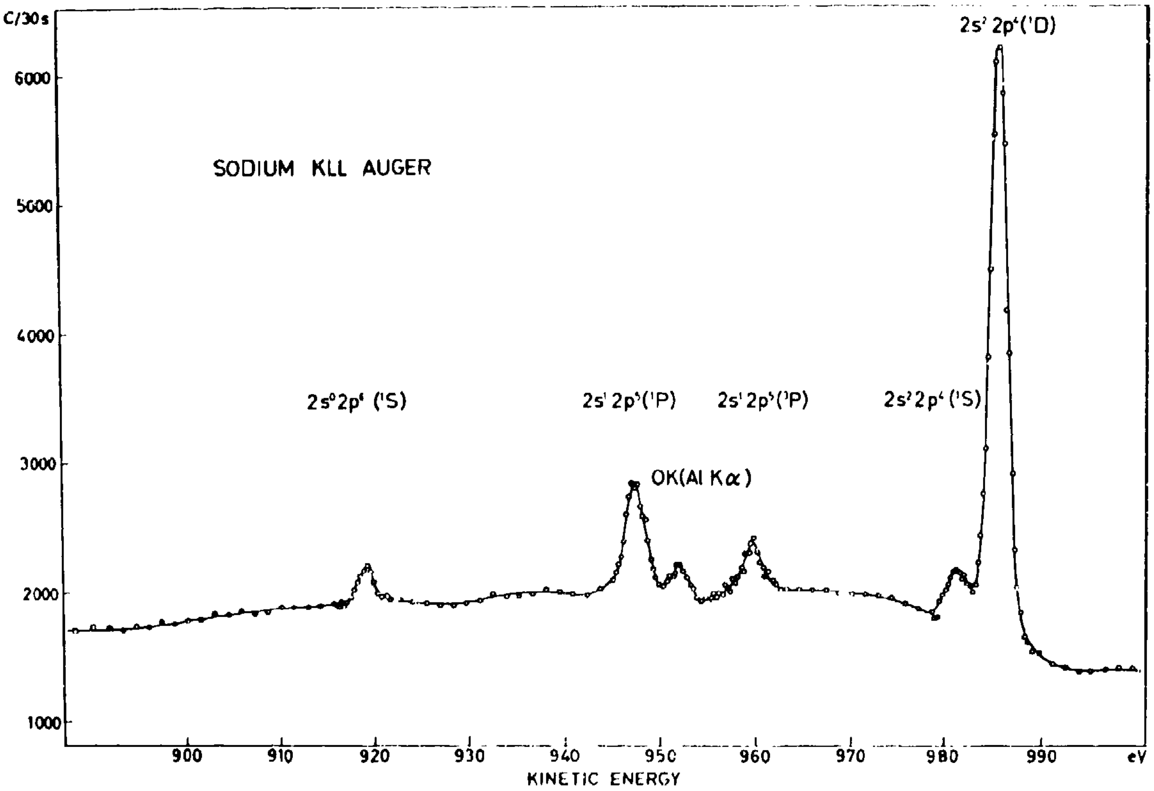

Fig. 1:23. *KLL* Auger spectrum of sodium. It contains five Auger lines from sodium plus one photoelectron line from oxygen.[55] See also Chapter VI.

levels. ESCA shifts are also caused by changes in Coulomb interaction, but unlike NMR and isomeric shifts, they are not of the h.f.s. type. The spectacular resolution of h.f.s. resonance methods, like NMR and Mössbauer spectroscopy is not attainable by ESCA because of the natural limitations caused by the inherent widths of the atomic levels. ESCA does, however, provide fairly direct information on the charge distribution associated with chemical interactions, and generally any constituent element of a molecule can be selected for study, regardless of its nuclear properties such as spin and magnetic moments. It should therefore be a valuable complement to these other methods in the study of chemical structure.

From the application of ESCA to different chemical structures we have seen that chemical effects cause considerable shifts, and that the technique provides a method for the study of charge distribution in bonds. ESCA will therefore be particularly suitable for elucidating problems which are directly connected with the charge distribution in molecules. There are relatively few other methods available for a direct estimation of charge on an atom. X-ray diffraction can be used for this purpose but is often tedious. Charge distribution in bonds can be estimated from dipole moments,[174] but a serious drawback is the vector character of this quantity, which requires exact knowledge of the geometry of molecules, and even if it is known it may be difficult to determine the signs of the moments which constitute the resultant moment. In symmetrical molecules, the resultant moment can be zero. In such molecules, the bond moments or partial ionic character of bonds can be estimated by ESCA, because the individual atoms can be studied directly and independently.

The concepts of partial ionic character of bonds and partial double bond character are aspects of the charge distribution in bonds, see Section V:4. These are connected with bond lengths and vibrational force constants. Since exact bond lengths cannot be determined on non-crystalline material and vibrational spectra sometimes may be difficult to interpret, ESCA may also be a useful complement to X-ray crystallography and IR and Raman spectroscopy.

Charge is also an important parameter in quantum chemistry and often depends on the choice of other independent parameters, some of which often have to be estimated empirically. The fact that ESCA shifts reflect the charge distribution therefore implies that charges from ESCA can be useful for correlation with data calculated by quantum mechanical procedures.

When an electron from one of the inner shells is ejected from the atom the vacancy is filled by successive electronic transitions from outer shells. There is an associated emission of X-rays in well-defined wavelengths. Alternatively, the atom can emit so called Auger electrons, by radiationless transitions, see Section II:2. Thus, the excitation energy is converted into kinetic energy of electrons, which are characteristic for a given atom. The Auger electron lines are independent of the primary radiation and defined solely by the element concerned and its chemical environment. In addition to the photoelectron lines, we can record these Auger electron spectra in ESCA at high resolution and with a good intensity. Auger spectra are particularly easy to excite for the elements at the beginning of the Periodic System, in contrast with the X-ray fluorescence spectra (see Section II:2). This provides another means for the chemical analysis of light elements.

The most important Auger electron line group for an element involves transitions between the K and L shells. The selection rules are quite different from those for X-ray transitions and the number of lines in the KLL group varies from five for the lighter elements to nine for medium Z elements. Fig. I:23 shows an electron spectrum of the KLL transitions in sodium,[58] containing five Auger lines plus one photoelectron line from oxygen. The existence of nine Auger lines for medium Z was first demonstrated for zirconium[33] (Z 40). Auger electron lines are also excited in radioactive decay, either in electron capture or the internal conversion in gamma decay. However, for light elements the probability of internal conversion is very small and the cases of electron capture are few. The Auger spectra have therefore been studied mostly among medium and large Z elements. In ESCA the Auger lines, including those for the lighter elements, are easily excited.

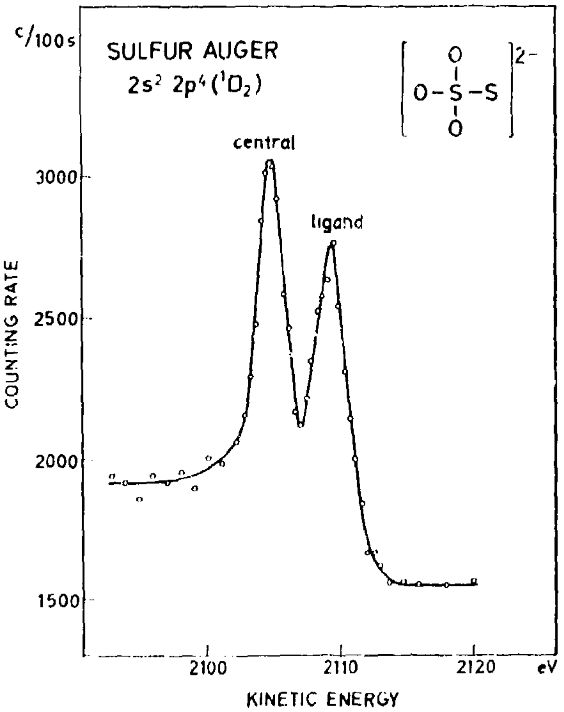

Fig. I:24. Chemical effect on the sulfur $2s^2 2p^4(^1D_2)$ Auger transition in sodium thiosulfate $Na_2S_2O_3$.[55] The energy separation between the two lines is in agreement with the observed shifts in the photoelectron spectra of the $1s$ shell and the $2p$ subshell.

We have mapped out part of this field, and have established semi-empirical energy relationships in different parts of the Periodic System[33, 35] so that different lines in the Auger electron spectra can be identified (see Appendix 4). Using the general computer program, Appendix 3, for the SCF calculation of atomic binding energies, described in Section III:9, we have made new calculations on the Auger effect[73] aimed at obtaining more accurate theoretical values of energies and intensities in Auger spectra (Chapter VI).

There are some other interesting features which we have observed in connection with the studies of Auger spectra. For instance, continuous electron distributions on the low energy sides of such electron lines indicate the emission of electrons from multiply ionized atoms. Another effect which we have observed in the case of

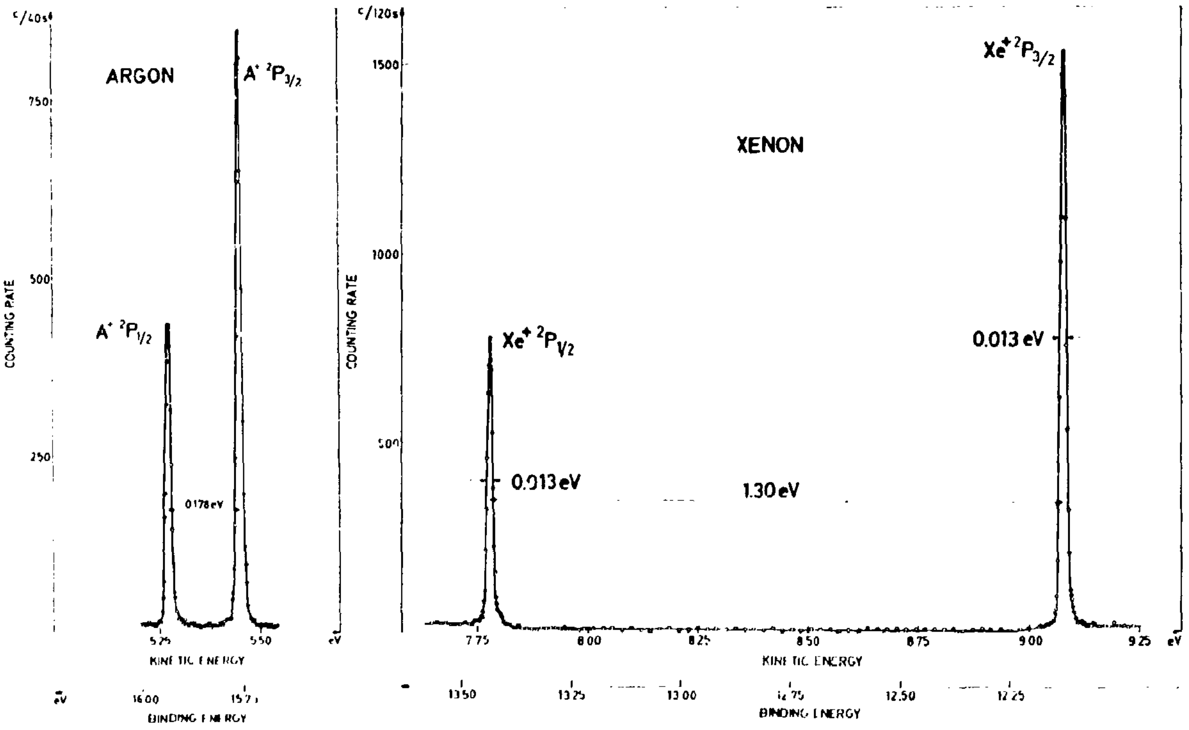

(*a*) (*b*)

Fig. 1:25. Electron spectrum of argon (*a*) and xenon (*b*) showing the spin-orbit splitting of the $3p^5(^2P)$ term and $5p^5(^2P)$ term, respectively. The spectra were excited by helium radiation and the line widths are as small as 0.013 eV.

for example, K and Cl is the existence of additional electron lines which indicate an extra atomic excitation of several eV.[59]

We have also studied chemical effects on Auger electron lines.[11,14,62] The chemical shifts in the photoelectron spectra refer to each separate level and a characteristic feature is that the shifts for the *K* and *L* shells are of about the same magnitude. This explains the small shifts (usually well inside the natural line widths) of the *Kα* X-ray emission lines, which are transitions between the *K* and *L* shells. For Auger electron lines from ESCA, both the *K* and the *L* shells are involved but, unlike the X-ray emission lines, the *L* shell occurs twice in the transition. Therefore, approximately the full level shift can be expected. We have made a study of this problem and have confirmed this behaviour. Fig. 1:24 shows the chemical shift of the KL_2L_3 line in sodium thiosulfate. The distance between the two lines, corresponding to the 6+ and 2− oxidation states, is found to be 4.7 eV. We had before observed a shift of 7.0 eV in the *K* shell and 6.0 eV in the *L* shell for the photoelectron lines. The calculated Auger line shift would thus be $\Delta E = \Delta E_K - 2\Delta E_L = -5.0$ eV, i.e. in agreement with the direct measurement shown in the figure.

Molecular orbital levels with binding energies of some eV can also be seen in ESCA spectra. In such compounds as water, benzene and other organic molecules, we have complemented our measurements of the inner levels by additional studies of outer molecular levels, see Fig. 1:14. Using our high resolution experimental equipment for ESCA and ultraviolet light for exciting the spectra these levels can be resolved in considerable detail. For this purpose, a helium light source has been designed.

The UV excitation of the electron spectra of gases at low pressures in the energy region around 10 eV has yielded line widths as small as 0.01 eV. In these cases vibrational structures are widely separated and the rotational sub-structure is within reach. This field has

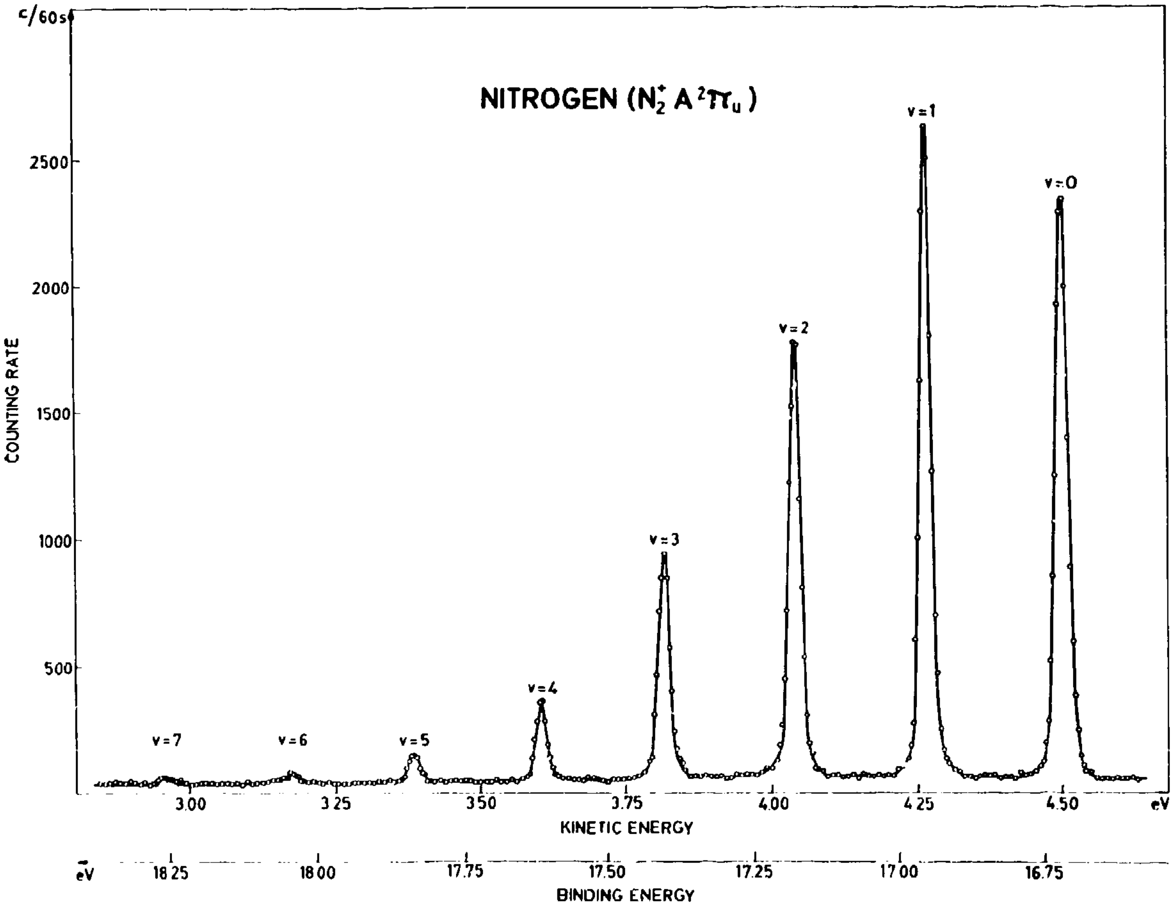

Fig. 1:26. Electron spectrum of nitrogen showing 8 vibrational levels of the molecule ion in the $A^2\Pi_u$ state. Excitation of the spectrum was made by helium radiation.

been studied, in particular by groups in England and Germany.[122 126] Fig. 1:25 shows UV excited electron spectra from gaseous argon (1:25a) and xenon (1:25b), recorded recently by our present equipment at a pressure of 0.05 torr. Fig. 1:26 shows the electron spectrum of the $A^2\Pi_u$ state of the N_2^+ molecule ion. Eight vibrational levels are seen in this group. Some other spectra are shown in Section VIII:5.

Excitation by electrons is also of interest, and the equipment has been provided with facilities for such studies. With this equipment we have produced Auger electron spectra from neon, krypton, and some organic molecules. For neon, the KLL spectrum was recorded and for krypton, the $M_{4,5}NN$ spectrum. In the latter, the line widths observed were 0.15 eV which means that the Auger transition energies can be measured to within a few millielectronvolt. Part of this spectrum is shown in Fig. 1:27. For a more complete discussion see Chapter VI.

ESCA can be further improved technically. The basic requirement is high resolution, but in practice the speed and reliability of the recording of data are additional important factors. The scope is wide and in order to make full use of the potentialities of the method, further instrumental development work is desirable. It is also possible to increase the resolving power still more and improve the intensity and the signal-to-background ratio in the spectra.

Our present equipment consists of: (1) An improved version of our original instrument,[62] (2) A newly built

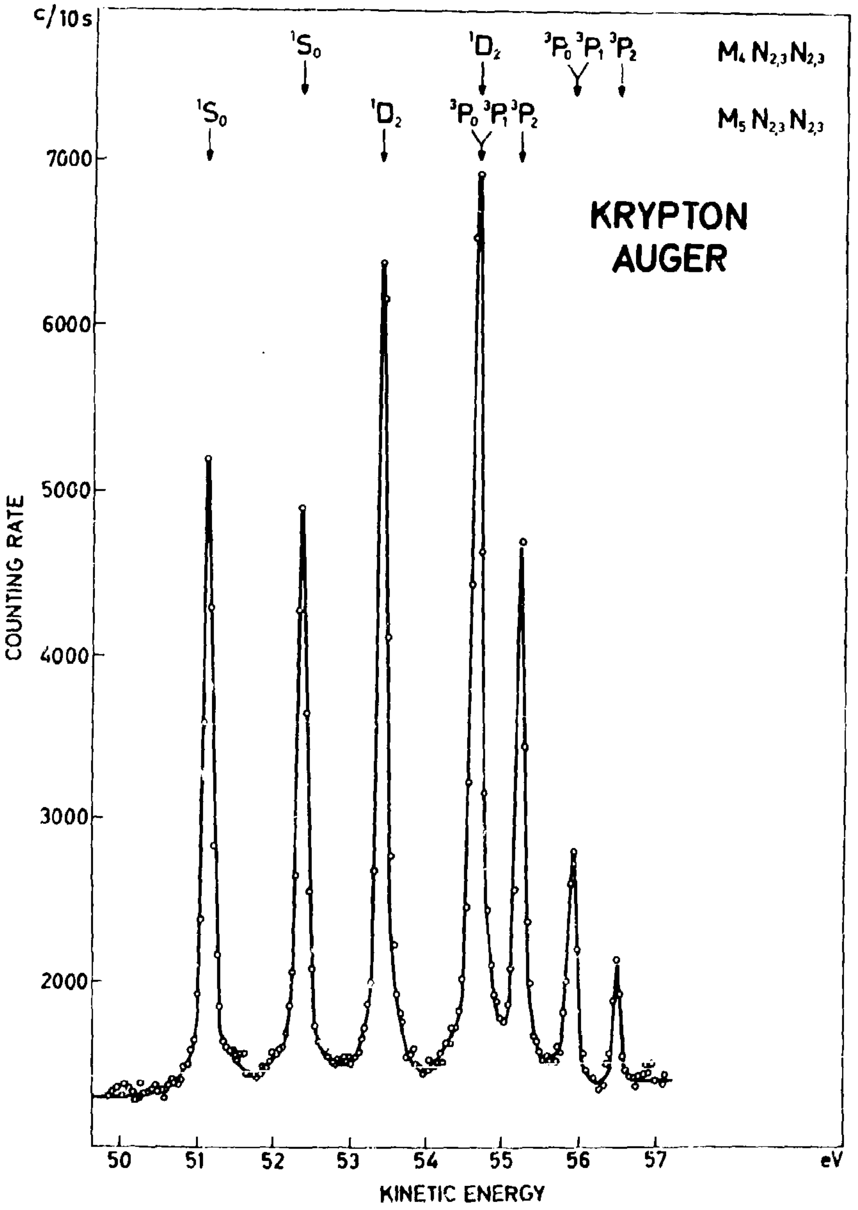

Fig. I:27. Part of $M_{4,5}NN$ Auger spectrum krypton of krypton excited by electron impact. The whole spectrum, containing some 40 lines, is shown and discussed in Chapter VI.

30 cm radius magnetic double focussing instrument with improved coil design in which emphasis has been placed on ease of handling, e.g. better access to source and counter arrangements,[86] (3) An electrostatic double focussing device of the sector type with a radius of 36 cm.[87] This is the first of its kind, being capable of a resolution of a few parts in 10^4. It is provided with a cryostat with which the sources can be cooled to liquid nitrogen or liquid helium temperatures and it is equipped, in addition, with the above-mentioned alter-

native arrangements for exciting electron spectra with UV light and electrons. The instrument can be used for solid, liquid, and gaseous sources. When gases or liquids are studied they can also be solidified by means of the cryostat arrangement. (Cryostats have now also been incorporated with instruments 1 and 2.) UV light or electron excitation is used mostly for the study of gases at low pressure. (4) A combination of a curved crystal monochromating X-ray system and a permanent magnet, homogeneous field electron spectrometer with photographic recording.[64] To scan the plates, an automatized TV microdensitometer[71,80] has been developed, which counts individual tracks in the emulsion. (5) Furthermore, a large, 50 cm radius, high resolution magnetic double focussing instrument, previously used for radioactive work[46], has been redesigned[93] for ESCA work. This instrument is characterized by high dispersion and is provided with facilities to use extended sources without sacrificing resolution. A multidetector system [illegible] ituated in the focal plane of the spectrometer. In this way the intensity will be greatly enhanced and a larger part of the spectrum can be recorded simultaneously. The instruments will be described in some detail in Chapter VIII.

II. SOME BASIC PRINCIPLES

II:1. Photoelectric Effect in ESCA and in X-ray Absorption Spectroscopy

In Chapter I, we pointed out the much overlooked fact that electron spectroscopy is a powerful alternative to X-ray spectroscopy for the study of atomic structure. It was shown that the electron spectra appear as line spectra when studied in modern high-resolution instruments and that the electron lines are just as narrow as the X-ray emission lines. In developing ESCA, we have so far employed mostly the photoelectric effect for producing electron spectra. An X-ray absorption spectrum is also obtained as a result of the photoelectric effect. The experimental layout for the ESCA method and the X-ray absorption method is shown in Fig. II:1. In ESCA, the sample is irradiated with an X-ray beam, and the ejected photoelectrons are analysed in a magnetic or in an electrostatic spectrometer. In the X-ray absorption method, the sample is also irradiated with X-rays, but here the absorption of the X-ray beam is measured as a function of the X-ray energy.

The atomic processes that yield the photoelectron part of the ESCA spectrum and the X-ray absorption spectrum, are also illustrated in Fig. II:1. In the photoelectric process utilized by the ESCA method (left-hand side of figure), a bound electron, in the figure an electron in the K shell, is promoted to a free state outside the sample. Its kinetic energy is well defined, and any lack of definition of its energy is solely due to the natural width of the level from which the electron has been ejected (the level and band profiles have been marked on the right hand side of the figure) and to the lack of definition of the energy of the incident characteristic X-ray beam.

An X-ray absorption edge arises when a bound electron is promoted to the first unoccupied level which is allowed according to the relevant selection rules. For a metallic sample this will be a level in the conduction band, at or just above the Fermi level. For an insulator it will be a level at the bottom of the conduction band. When the energy of the X-ray beam increases, the excitation involves higher regions of the conduction band and the course of the absorption curve will to a great extent be determined by the structure in the outer, unoccupied bands. This complicates the interpretation and evaluation of the positions of the levels being investigated.

The gross features of a photoelectron spectrum and the corresponding X-ray absorption spectrum are shown in Fig. II:2. A diagram for the levels present in the element studied is given at the top of the figure.

II:2. Auger Electrons and X-ray Quanta

If a vacancy is created in an inner electron shell, by electron bombardment, X-ray irradiation or some other method, the excited atom will revert to the ground state by emitting characteristic X-ray radiation or alternatively by radiationless transitions, the so-called Auger transitions, as illustrated in Fig. II:3. Thus both processes are initiated by the excitation resulting from the ejection of an electron from an inner shell (the K shell in the figure). However, the subsequent de-excitation takes place in different ways in the two processes. In the X-ray case, the vacancy is filled by an electron from an outer shell (the L_{III} shell in the figure) and the energy released is emitted as electromagnetic radiation in an X-ray quantum. In the Auger case, the energy released is instead transferred to another electron in one of the outer shells (the L_{I} shell in the figure). This electron is then released and leaves the atom. The simplest notation for the Auger transition illustrated in the figure is $KL_{\mathrm{I}}L_{\mathrm{III}}$.

When the primary vacancy is created in one of the inner subshells of the $L, M, \ldots$ shells, the excitation energy is often sufficient to bring about a process in which one of the two final vacancies lies in an outer subshell of the primary vacancy's shell. Radiationless transitions of this type, for example $L_{\mathrm{I}}L_{\mathrm{III}}M_{\mathrm{V}}$, are called Coster-Kronig transitions.

For a long time the Auger process was ignored, both by experimentalists and theoreticians. However, the

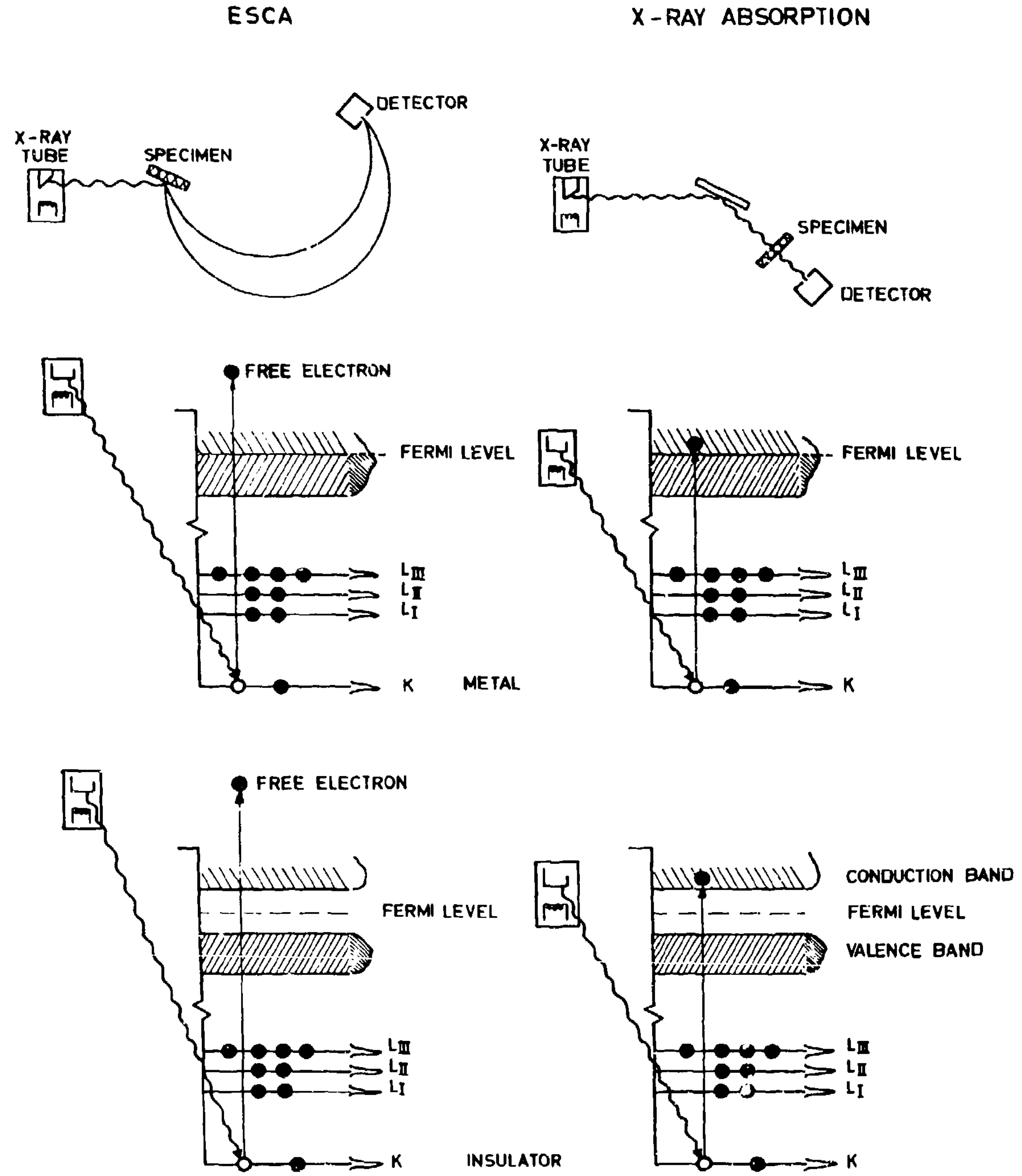

Fig. II:1. The experimental set-up and the atomic processes in the cases of the ESCA method and the X-ray absorption method. The atomic processes are illustrated in level diagrams for metallic samples and for samples of an insulator or an intrinsic semiconductor. Solid circles indicate electrons and open circles indicate vacancies created when electrons have been excited to higher levels by the incident X-ray beam.

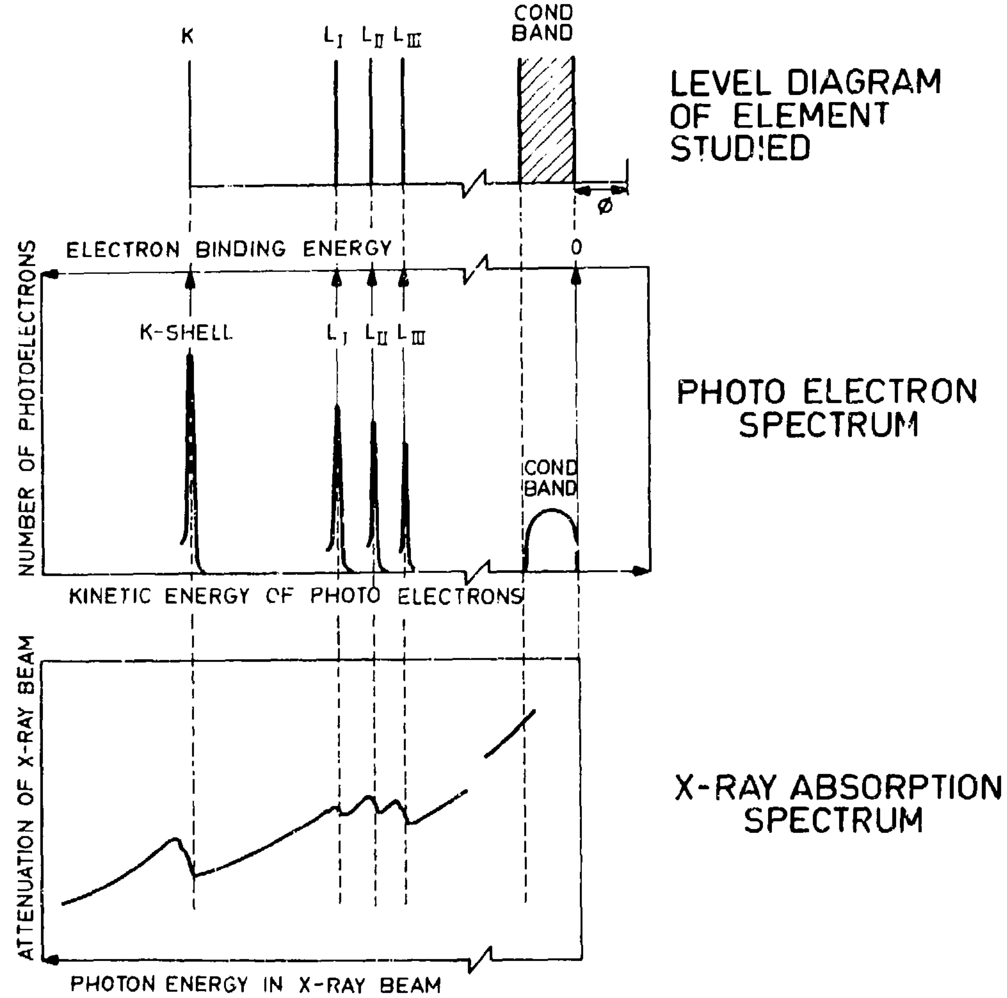

Fig. II:2. Principle features of the photoelectron spectrum (ESCA spectrum) and the X-ray absorption spectrum for a given substance. With the ESCA method an electron spectrum is obtained which directly maps out the electronic structure. Sharp lines are obtained from the inner shells and broader distributions from the bands. The edges in an X-ray absorption spectrum are dependent upon the structure in the band to which the electron is excited.

radiationless de-excitation of an excited atom by emission of electrons is often more probable than the radiative de-excitation by emission of X-ray quanta. This has been the disappointing experience of those working in the field of X-ray fluorescence analysis. Thus the X-ray fluorescence yields decrease with decreasing atomic number and become very low for the lightest elements. This is shown for K shell vacancies in Fig. II.4, which gives a graphical representation of the K fluorescence yield ω_K according to the following semi-empirical relation by Hagedoorn and Wapstra.[127]

$$\frac{\omega_K}{1-\omega_K} = (-6.4\cdot 10^{-2} + 3.40\cdot 10^{-2}Z - 1.03\cdot 10^{-6}Z^3)^4$$

A low fluorescence yield corresponds to a high yield of Auger electrons, since the sum must equal unity. Thus, as the X-ray fluorescence yield diminishes at low atomic numbers so the Auger yield increases. This offers interesting possibilities for utilizing the Auger part of the ESCA spectra as well, for the study and analysis of the light elements.

II:3. Principles for the Calculation of Binding Energies from ESCA Spectra

Conservation of energy in the photoelectric process of a free atom requires that the kinetic energy E'_{kin} of the photoelectron is given by

$$E'_{\text{kin}} = E_{\text{X-ray}} - E'_b - E_r \tag{1}$$

Here $E_{\text{X-ray}}$ is the quantum energy of the X-ray photon, E_b is the energy of liberation for the electron and E_r is the recoil energy. By applying the law of conservation of momentum for the case when the recoil is in the direction of the incoming photon, we obtain as an upper limit for the recoil energy

$$E_r \quad E_{\text{X ray}} \frac{m}{M}\left[\frac{E'_{\text{kin}}}{E_{\text{X-ray}}} + \left(\frac{2E'_{\text{kin}}}{mc^2}\right)^{\frac{1}{2}} + \frac{E_{\text{X-ray}}}{2mc^2}\right] \tag{2}$$

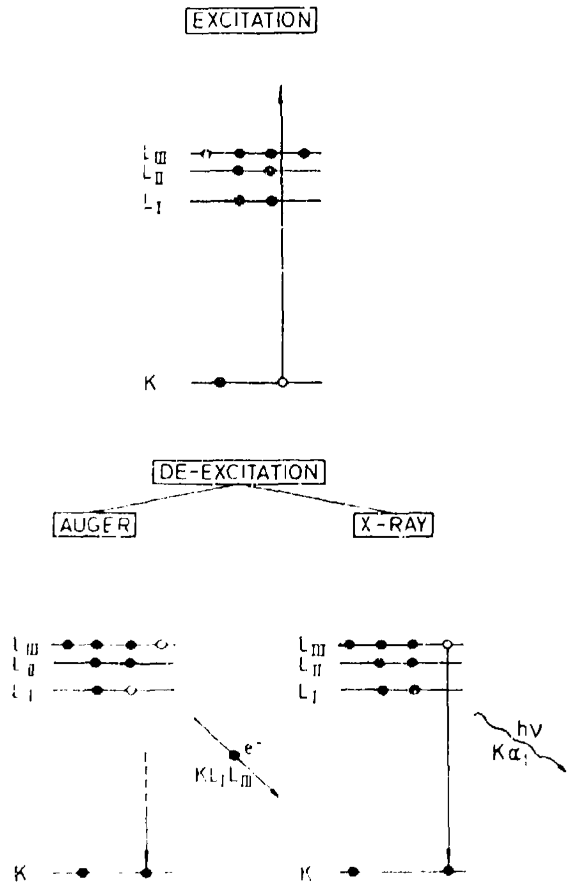

Fig. II:3. Two alternative modes of atomic de-excitation which follow upon a creation of an inner shell vacancy.

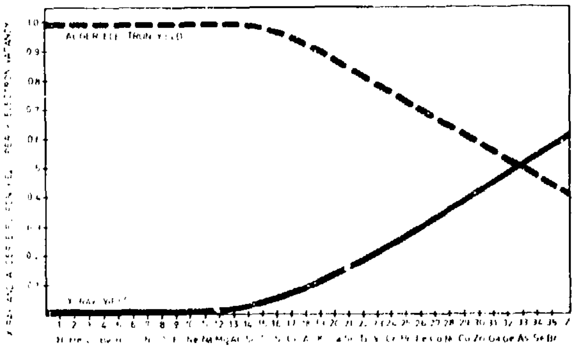

Fig. II:4. X-ray fluorescence yield and Auger electron yield in the K shell as a function of atomic number Z for the light elements in the Periodic System.

M and m are the masses of the recoiling atom and the photoelectron, respectively, and a non-relativistic calculation is assumed to be valid. Table II:1 gives the maximum recoil energy calculated from eq. (2) for some elements in the first group of the Periodic Table. Calculations are made for three different X-radiations, namely silver, copper, and aluminum $K\alpha$. The maximum recoil energy for the photoelectric ejection of a valence electron is calculated.

Table II:1 Maximum recoil energies (eV)

	Ag$K\alpha$	Cu$K\alpha$	Al$K\alpha$
H	16	5	0.9
Li	2	0.8	0.1
Na	0.7	0.2	0.04
K	0.4	0.1	0.02
Rb	0.2	0.06	0.01

It is, in most cases, less than one electron volt in magnitude, and with proper choice of X-radiation the recoil energy becomes negligibly small in our measurements. The term E_r in eq. (1) will, therefore, hereafter be disregarded. Instead, we have to modify eq. (1) when we consider the solid state aspects of the experimental arrangement for measuring the electron binding energy. This is illustrated in Fig. II:5.

In general, there exists a small electric field in the space between the source and the entrance slit to the spectrometer even if both are grounded. This is so because grounding the source and the spectrometer material means that their Fermi levels are the same. Any difference in work function of the source material

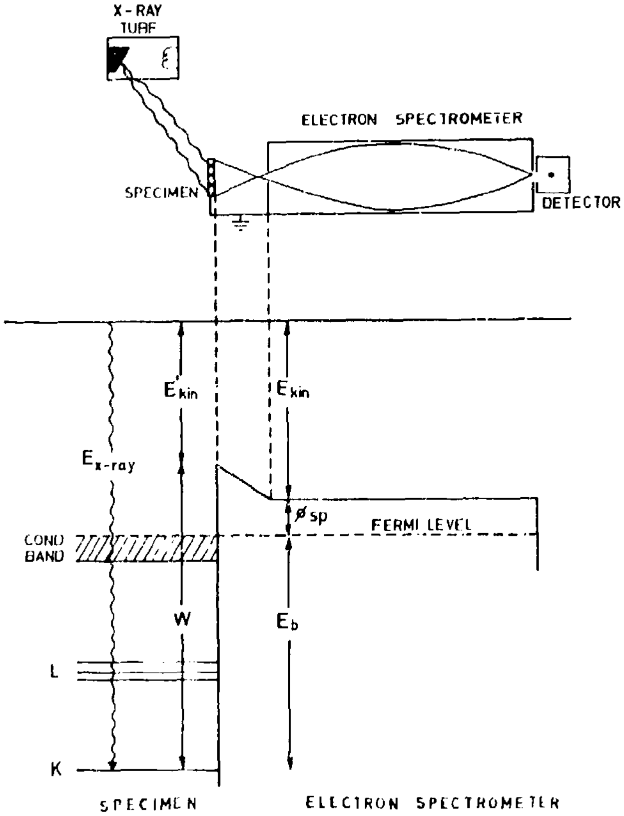

Fig. II:5. Principles for the calculation of binding energies from electron spectra. The specimen has been assumed to be metallic and in electrical contact with the spectrometer.

and the spectrometer material thus gives a difference in macro-potential[16,18] (i.e. a contact potential) and an electric field in the space between source and spectrometer chamber. The kinetic energy E_{kin} of the electron when it enters the spectrometer chamber is thus slightly different from the energy E'_{kin} which it has on emerging from the source. It is the kinetic energy E_{kin} that is measured. If we choose the Fermi level as a reference level for the electron binding energies, i.e. if we have zero binding energy at the Fermi level, conservation of energy requires that

$$E_b = E_{X\text{-ray}} - E_{kin} - \phi_{sp} \qquad (3)$$

Here E_b is the electron binding energy and ϕ_{sp} is the work function of the spectrometer material. It should be noticed that the term ϕ_{sp} in eq. (3) does not depend on the source material and as long as it does not vary with time, one and the same work function correction can be applied to all the measurements. The choice of zero binding energy at the Fermi level has been made not only in electron spectroscopy but also in X-ray spectroscopy.

In Fig. II:5, the source material is assumed to be metallic. The same result is obtained if the specimen is non-metallic. However, a sufficient number of free charge carriers must be present in the specimen so that the Fermi level can adjust to the thermodynamical equilibrium state. It has been found that electrically insulating materials can also be studied by the ESCA method, since a sufficient number of free charge carriers are formed during X-ray irradiation of the specimen.

II:4. Modification of Level Diagram Due to Double Layers and Electric Fields

Electric double layers may develop on the surface as a result of adsorbed atoms. A double layer also develops at the surface to retain electrical quasi-neutrality when the crystal departs from periodicity at the surface. Electrons from the interior that move towards the surface with an energy that is too small to allow them to escape, proceed to a small distance outside the rigid crystal lattice before returning. This again is equivalent to a dipole layer at the surface. The dipole layer that is the result of these different effects gives a potential step at the surface that can be either positive or negative in sign, i.e. the macro-potential in the interior of the crystal is different from the macro-potential in the surrounding vacuum (the vacuum level). The level diagram of a metal is modified as shown in Fig. II:6.

If the metal is placed in an electric field, the macro-potential outside the metal will slope but otherwise no change occurs in the level scheme of Fig. II:6 for reasonably small fields (i.e. the Schottky effect is negligibly small). If, instead, we have a semiconductor or an insulator the electric lines of force will penetrate to some depth, a space charge develops, and a bending of the bands and inner levels will occur as shown in Fig. II:7.

An electric field that causes this effect is produced by the Volta potential (contact potential) between the semiconductor or insulator and the walls of the container or any other material from which it is separated by the vacuum. If the distance between the two materials is decreased, the electric field increases and so does the bending of the energy levels. However, this tends to decrease the Volta potential and in the limiting case when the two materials are brought in contact with each other, the Volta potential is zero. One then has a change in macro-potential due to bending of the levels that is approximately the same as the Volta potential at infinite separation, i.e. a few tenths of an electron volt in most cases. This is the situation when two different materials are brought into contact with each other in semiconductor devices.

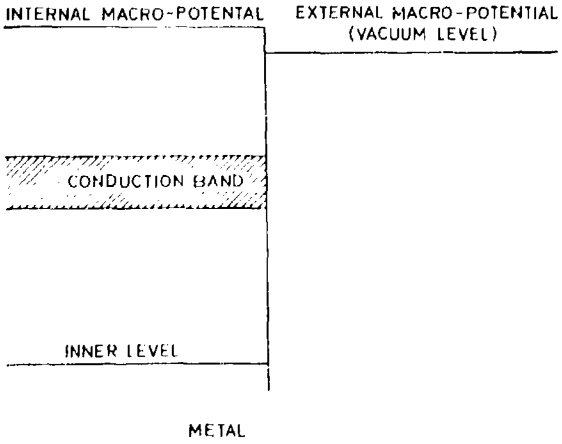

Fig. II:6. Modification of level diagram for a metal due to double layers. The macro-potential in the crystal is different from the macro-potential in the surrounding vacuum.

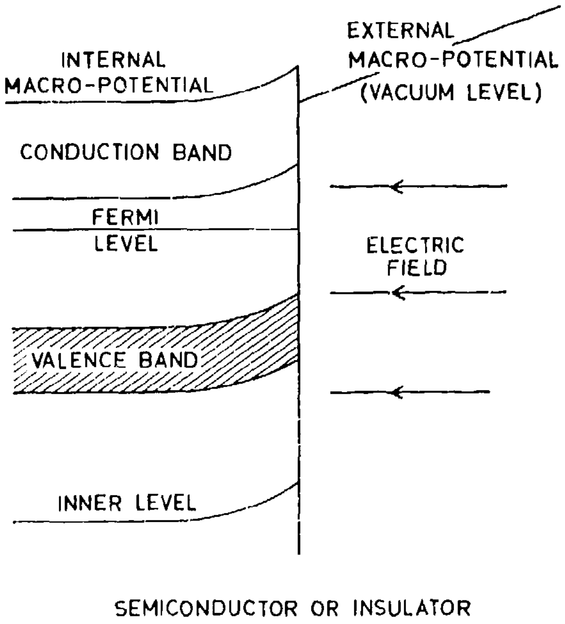

Fig. II:7. Modification of the level scheme for a semiconductor or an insulator due to an electric field. A space charge develops and a bending of the bands and inner levels will occur.

The situation is different for a sample used as an electron source for ESCA studies. Assuming that the sample is thick enough, then electrons expelled from the interface between the sample and its backing are not studied in the electron spectrum. Level bending in this interface may therefore be neglected. Instead, there is a bending of levels in the surface region that faces the vacuum. However, since the baffle plate of the entrance slit to the spectrometer is situated at a distance of about 5 mm from this surface, the electric field due to the Volta potential is so small as to make the level bending negligibly small.

Bardeen[128] in 1947 introduced the concept of surface states. Surface states can exist in the otherwise forbidden gap of a semiconductor and can be filled as high up as to the Fermi level of the material. If this occurs, a region depleted of electrons is formed under the surface. The electric field between electrons in the surface

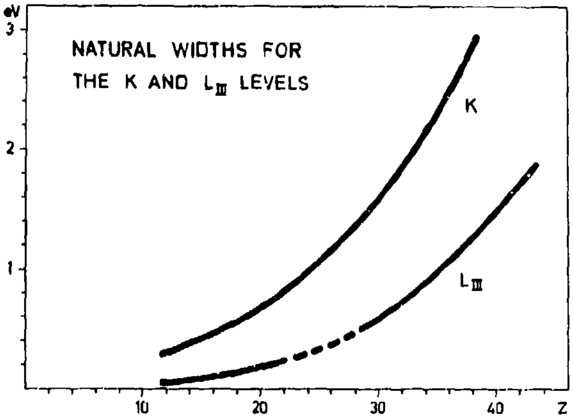

Fig. II:8. Inherent widths of K and L_{III} levels versus atomic number Z. The diagram has been drawn up with the aid of data for level widths which have been published by Parratt.[130]

states and the now unscreened positive ions in the depleted region produces a bending of the levels in this region. The bending is no larger than the energy difference between the top of the valence band and the Fermi level. Level bending due to surface states has so far been of minor concern in ESCA spectra.

II:5. Inherent Widths and Energy Separations

When an inner electron shell is ionized, the vacancy is filled by outer electrons within a time interval of the order of 10^{-16} seconds. According to the uncertainty principle, this finite life for a level corresponds to a lack of definition in the energy level of the order of a few electron volts. This is the inherent or "natural" width of the level, which defines an upper limit for the accuracy with which atomic level energies can be measured. With the ESCA method this limit can actually be reached.

As is seen from the diagram in Fig. II:8, the width of each level decreases with decreasing atomic number. For aluminum, both the K and the L_{III} widths are only a few tenths of an electron volt. In certain cases when radiationless de-excitations of the Coster–Kronig type take place the life of a vacancy in an electron shell is considerably shortened. The width of each level then increases according to the uncertainty principle, and in this way, there is a greater broadening for the L_I level in certain parts of the Periodic System.[129]

The X-ray line $K\alpha_1$ corresponds to an electron transition from the L_{III} shell to a vacancy in the K shell. The "natural" width of this line is made up of the widths for the two levels. Fig. II:9 shows the natural width of the $K\alpha_1$ line as a function of atomic number Z. Some of the anode materials used in the ESCA method are indicated in the diagram. The diagram shows that the $K\alpha_1$ line from aluminum is approximately half an electron volt, i.e. five times sharper than, for instance, the $K\alpha_1$ line from copper. This constitutes one of the advantages of using aluminum radiation instead of copper radiation. A further advantage is that the lower energy of aluminum radiation, 1.5 keV, gives photoelectron spectra of lower energy. These can therefore be analysed with greater absolute accuracy, since the relative resolving power of the electron spectrometer is constant. The large width of the $K\alpha_1$ line from the transition elements of the fourth period is combined with the fact that the line is assymmetrical in this area.

The presence of the $K\alpha_2$ line does not normally inconvenience the recording of ESCA spectra with, for example, copper radiation. If this should be the case, however, it is possible to utilize crystal monochromatization or to use the $K\beta$ line, although this line has a considerably lower intensity, or to use an L emission line from some other anode material. The energy gap between the $K\alpha_1$ and $K\alpha_2$ lines is given in Fig. II:10 on a logarithmic scale, and we see that it decreases rapidly at low atomic numbers. Thus, if the precision in the measurements needs to be increased for levels with low binding energies by using lighter elements as the

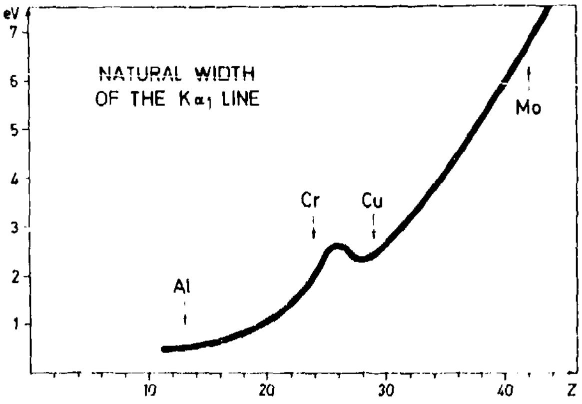

Fig. II:9. Inherent width of X-ray line $K\alpha_1$ versus atomic number Z. Some of the anode materials used in the ESCA method are indicated in the diagram.

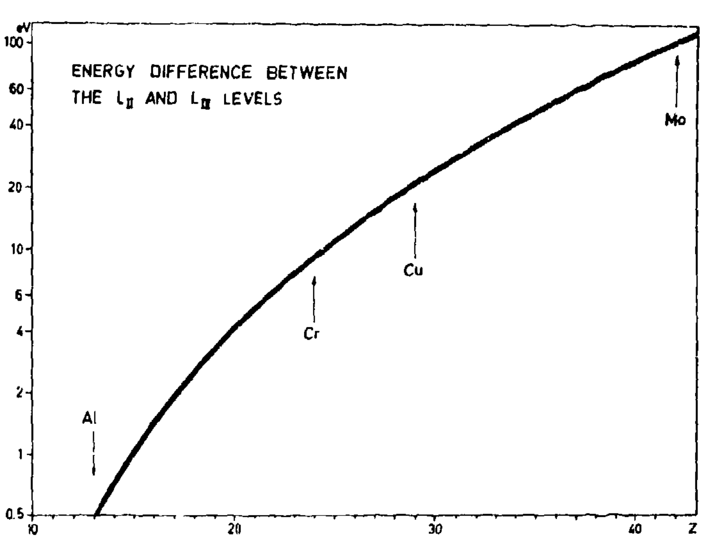

Fig. II:10. Energy separation in the X-ray $K\alpha$ doublet versus atomic number Z.

anode material, the complication arises that the $K\alpha_2$ line comes too near the $K\alpha_1$ line. However, if lighter elements such as aluminum or magnesium are chosen, the distance shrinks to such a degree that the doublet separation is comparable with the natural width of the $K\alpha$ lines. Thus, the $K\alpha$ doublet can here be considered as one line, with a width that is approximately one electron volt. This makes aluminum and magnesium suitable as anode materials for low-energy ESCA spectra.

A recorded profile* of the X-ray $K\alpha_1-K\alpha_2$ doublet in aluminum is seen in Fig. II:11. It is found to have a total width of 1.0 eV, which is in agreement with the value to be expected from the diagrams of line widths and doublet separations. A graphical analysis has been carried out, which shows the two components to have an intensity ratio of 2:1, as expected, and a half-width of approximately 0.7 eV each.

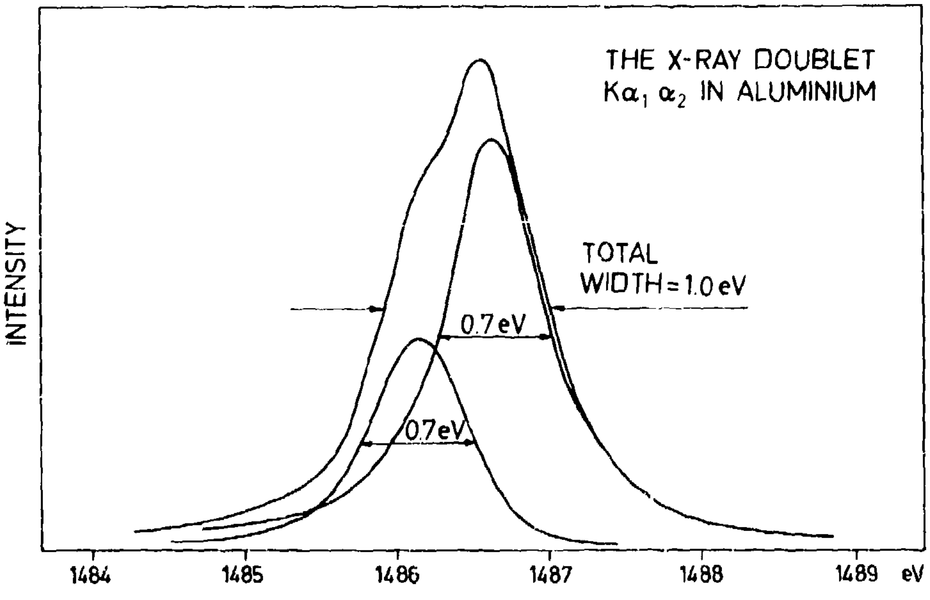

Fig. II:11. The X-ray $K\alpha_1$-$K\alpha_2$ doublet in aluminum. Corrections have been made for the spectrometer broadenings.

---

* The recording was carried out by Docent Erik Noreland at this Institute.

III. BINDING ENERGIES OF ATOMIC ELECTRONS

III:1. Scope

Knowledge of atomic level energies has previously been based solely on the information which can be obtained from emission and absorption spectra in the X-ray and optical region. In order to determine the levels for an element, it has been necessary to first select one level as reference, for light elements up to $Z \approx 30$ usually the K level, and for heavier elements the L_{III} level. The energy of the reference level has been obtained from the relevant X-ray absorption edge. The outer levels have then been evaluated with the help of X-ray emission data for transitions between the reference level and the other levels. As a result, the uncertainty in the determination of the energies of the X-ray absorption edges is relayed to each level in the element.

ESCA provides a new method for the accurate determination of all levels, from the K level to the Fermi level, directly from the photoelectron spectrum. Metals, semiconductors, and insulators may all be studied. We have measured in all ca. 300 levels, distributed over practically all the elements in the Periodic System and tables of electron binding energies, based on these measurements have been published.[38,131] The table of binding energies in Appendix 1 includes our most recent electron spectroscopic data and is recalculated with the new values for the X-ray emission lines published by Bearden,[115] and with a wavelength-energy conversion factor of $E\lambda_s =$

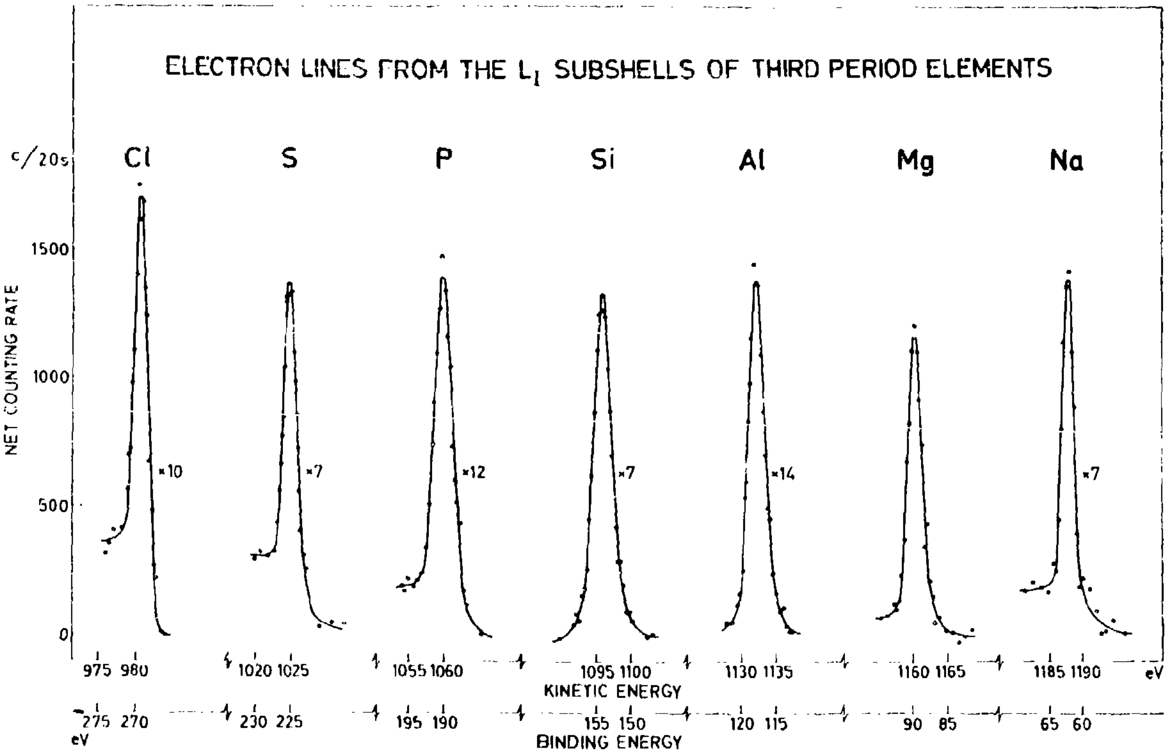

Fig. III:1. Electron lines from the L_I subshells of third period elements (sodium to chlorine) excited with magnesium $K\alpha$ radiation.

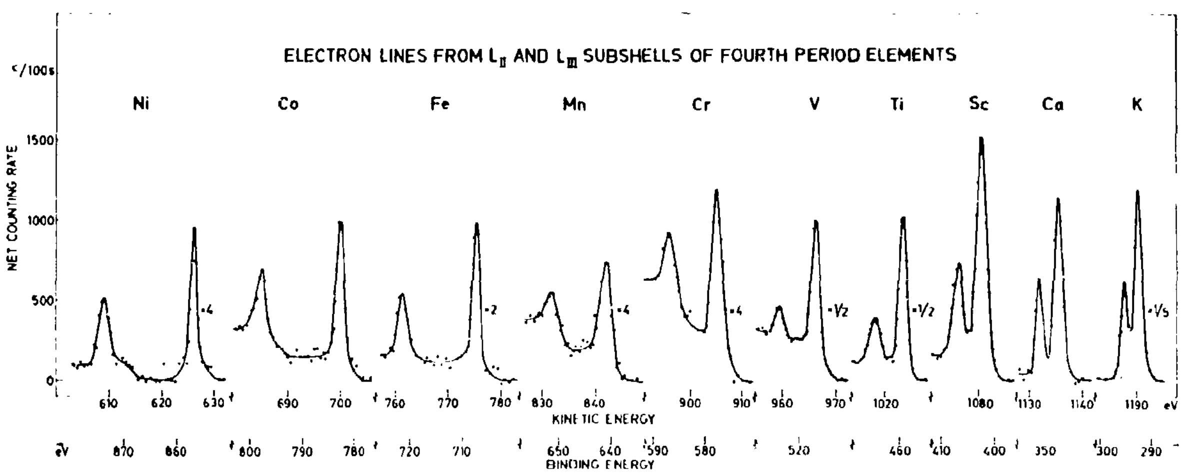

Fig. III:2. Electron lines from the L_{II} and L_{III} subshells of fourth period elements (potassium to nickel) excited with aluminum *Ka* radiation.

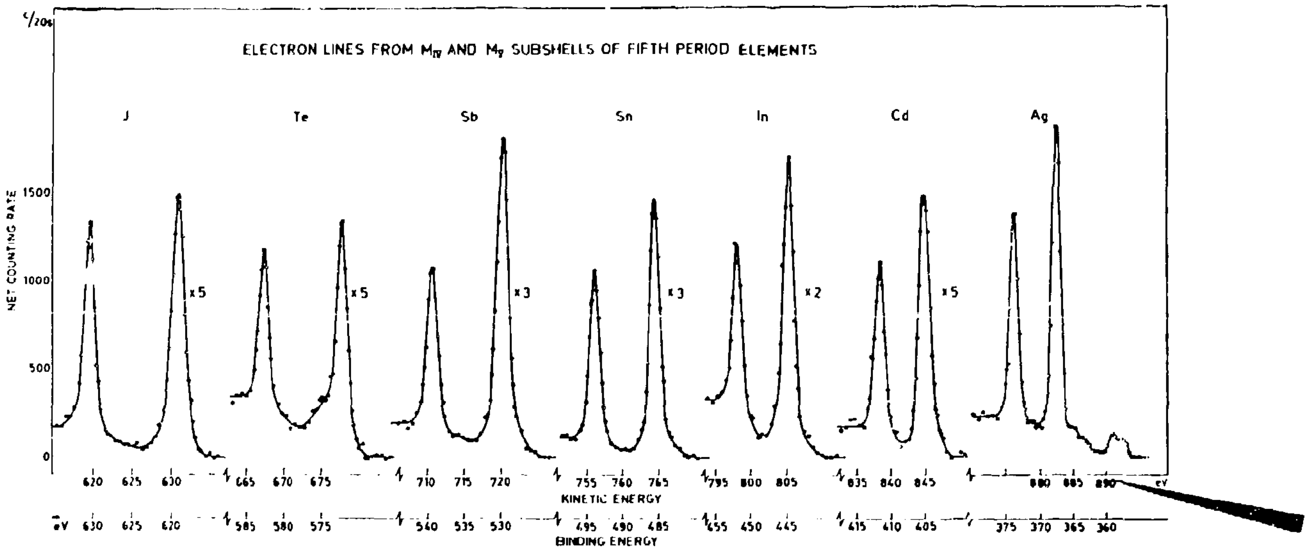

Fig. III:3. Electron lines from the M_{IV} and M_{V} subshells of fifth period elements (silver to iodine) excited with magnesium *Ka* radiation. In the silver spectrum the electron lines excited with the X-ray satellites $K\alpha_{3,4}$ are included.

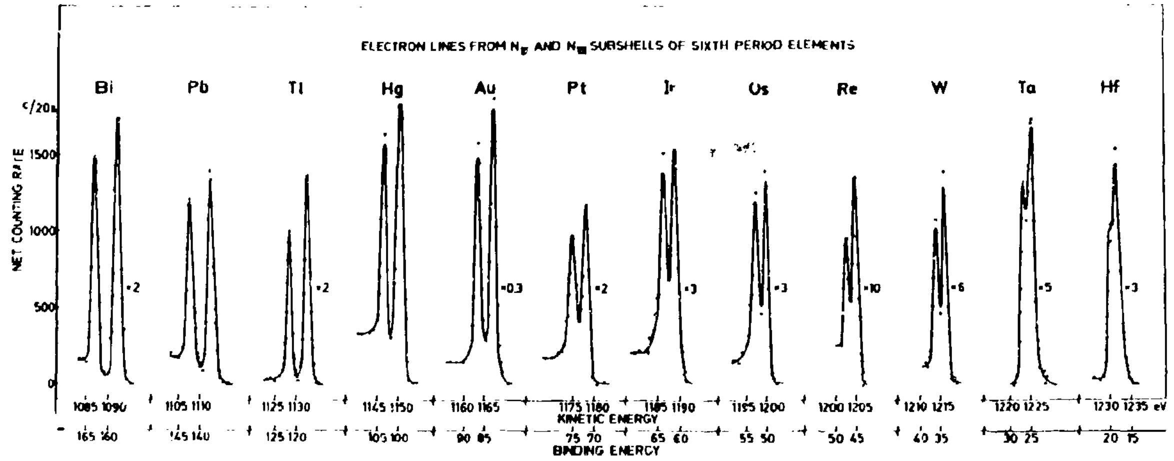

Fig. III:4. Electron lines from the N_{VI} and N_{VII} subshells of sixth period elements (hafnium to bismuth) excited with magnesium *Ka* radiation.

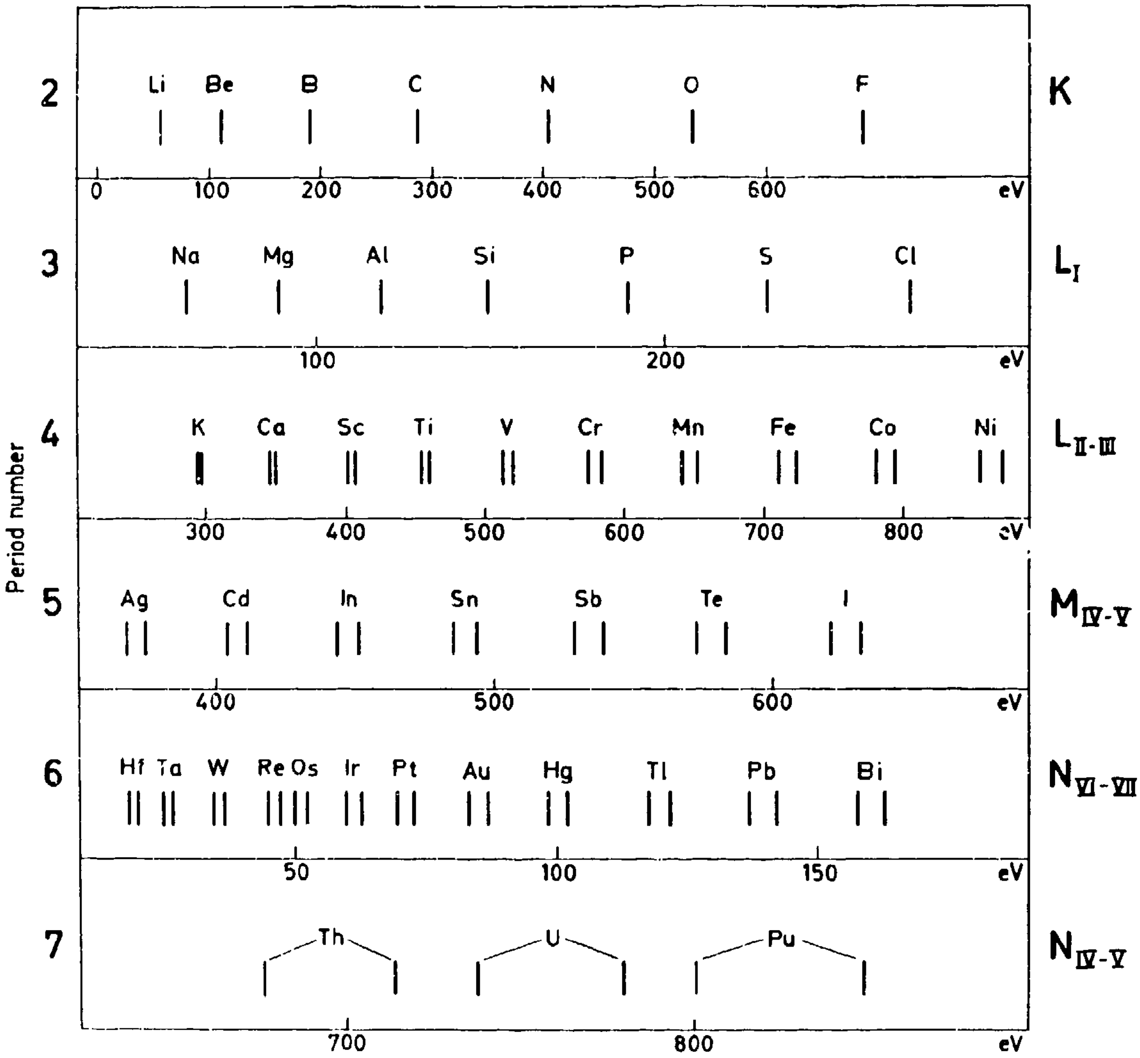

Fig. III:5. Atomic level energies obtained from the electron spectra of Figs. I:9, III:1–III:4, III:13–III:15, and III:19 The chemical compounds from which these electron spectra were obtained are listed in Table III:1.

(12372.42 ± 0.13) xu · keV. Many of the levels for which binding energies have been measured by the new precision method have not been observed in X-ray absorption spectra.

An illustration of the atomic level structure as revealed by high resolution electron spectra is given in Figure I:9. Some more examples are given in Figs. III:1–III:4. Each of these figures represents one row of elements in the Periodic Table. We have chosen sublevels in different electronic shells, from the K shell (in Fig. I:9) to the N shell. The electron spectra were excited by magnesium $K\alpha$, and in some cases by aluminum $K\alpha$ radiation. The time used to record an electron line was in no case more than 30 minutes and often as little as 5–10 minutes. The line widths are from 1 to 3 eV, which means that the spin-doublets $L_{\mathrm{II,III}}$, $M_{\mathrm{IV,V}}$, and $N_{\mathrm{VI,VII}}$ can be resolved in most cases. The energy of each level can be determined from the electron lines with a precision of a few tenths of an eV, which is about the same as the inherent width of the levels, as determined by the uncertainty relation.

In Fig. III:5, the energies of the atomic levels obtained from the electron spectra in Figs. I:9 and III:1–III:4 are displayed. Seventy-eight atomic levels are shown here, including the $N_{IV,V}$ levels of the elements thorium, uranium, and plutonium in the seventh period. These energies are obtained from the electron spectra shown in Section III:3. The chemical compounds from which the electron spectra were obtained are listed in Table III:1.

We shall now discuss in some detail these and other electron spectra from which electron binding energies can be obtained.

III:2. Light Elements ($Z < 30$)

Photoelectric cross sections as well as fluorescence yields decrease with decreasing atomic number. However, despite this decrease in the photoelectric cross section, the electron spectra that we obtain from low-Z elements are at least as good as those obtained from heavier elements. The electron lines in Fig. I:9 were obtained from the very light elements lithium ($Z = 3$) to fluorine ($Z = 9$) of the second row of the Periodic Table. Samples containing these elements were irradiated with aluminum X-radiation and electrons obtained by photoelectric conversion of Al*K*α in the *K* shell of the elements were recorded. The lines are narrow with a halfwidth less than 2 eV. The Li*K*(Al*K*α) and the Be*K*(Al*K*α) lines have a doublet structure which is discussed in Section V:1. The carbon line consists of 15 points, each with a counting time of 20 seconds. This line was thus obtained in five minutes. The horizontal scale of Fig. I:9 gives the electron binding energy, and the line positions indicate the approximate Z^2 dependence of the *K* level energy.

Electron spectra have also been recorded for the *L* shells in light elements. X-ray absorption spectra of the *L* shells are scarce in this region and the L_I energies available were mostly interpolated values. Our electron spectroscopic measurements showed that previously accepted values for the L_I energies had to be corrected by up to 50 % in some cases.[51] L_I electron lines of the third period elements sodium ($Z = 11$) to chlorine ($Z = 17$) are shown in Fig. III:1 and the $L_{II,III}$ lines of the same elements are shown in Fig. III:6. In the latter spectrum, one can see how the $L_{II,III}$ levels begin to appear as a doublet at around $Z = 15$.

Table III:1. Chemical compounds from which the electron spectra in Figs. I: 9, III: 1–4, III: 13–16, and III: 19 were obtained.

Element	*Z*	Compound
Lithium	3	Li evaporated
Beryllium	4	Be evaporated
Boron	5	HBO_2
Carbon	6	C graphite
Nitrogen	7	$NaNO_2$
Oxygen	8	MgO
Fluorine	9	LiF evaporated
Sodium	11	NaCl evaporated
Magnesium	12	MgO
Aluminum	13	Al_2O_3
Silicon	14	H_2SiO_3
Phosphorus	15	NaH_2PO_4
Sulfur	16	S sublimed
Chlorine	17	KCl evaporated
Potassium	19	KCl evaporated
Calcium	20	$CaCl_2$
Scandium	21	Sc_2O_3
Titanium	22	TiO_4
Vanadium	23	V_2O_5
Chromium	24	$K_3[Cr(CN)_6]$
Manganese	25	$K_3[Mn(CN)_6]$
Iron	26	$K_4[Fe(CN)_6]$
Cobalt	27	$K_3[Co(CN)_6]$
Nickel	28	$K_2[Ni(CN)_4]$
Silver	47	Ag evaporated
Cadmium	48	$CdCl_2$
Indium	49	In evaporated
Tin	50	SnO_2
Antimony	51	Sb evaporated
Tellurium	52	Te evaporated
Iodine	53	NaI
Hafnium	72	HfO_2
Tantalum	73	Ta lump
Tungsten	74	WO_3
Rhenium	75	Re lump
Osmium	76	Os lump
Iridium	77	Ir evaporated
Platinum	78	Pt evaporated
Gold	79	Au evaporated
Mercury	80	Hg on gold
Thaliium	81	TlCl
Lead	82	$PbCl_2$
Bismuth	83	BiO
Thorium	90	Th evaporated
Uranium	92	U evaporated
Plutonium	94	Pu oxide

At very low *Z* values, i.e. for the second row elements, the L_I subshell becomes broadened due to solid state effects. It can still be seen in the electron spectra, however, although the uncertainity in the energy is greater and the intensity less than in the *K* shell. This

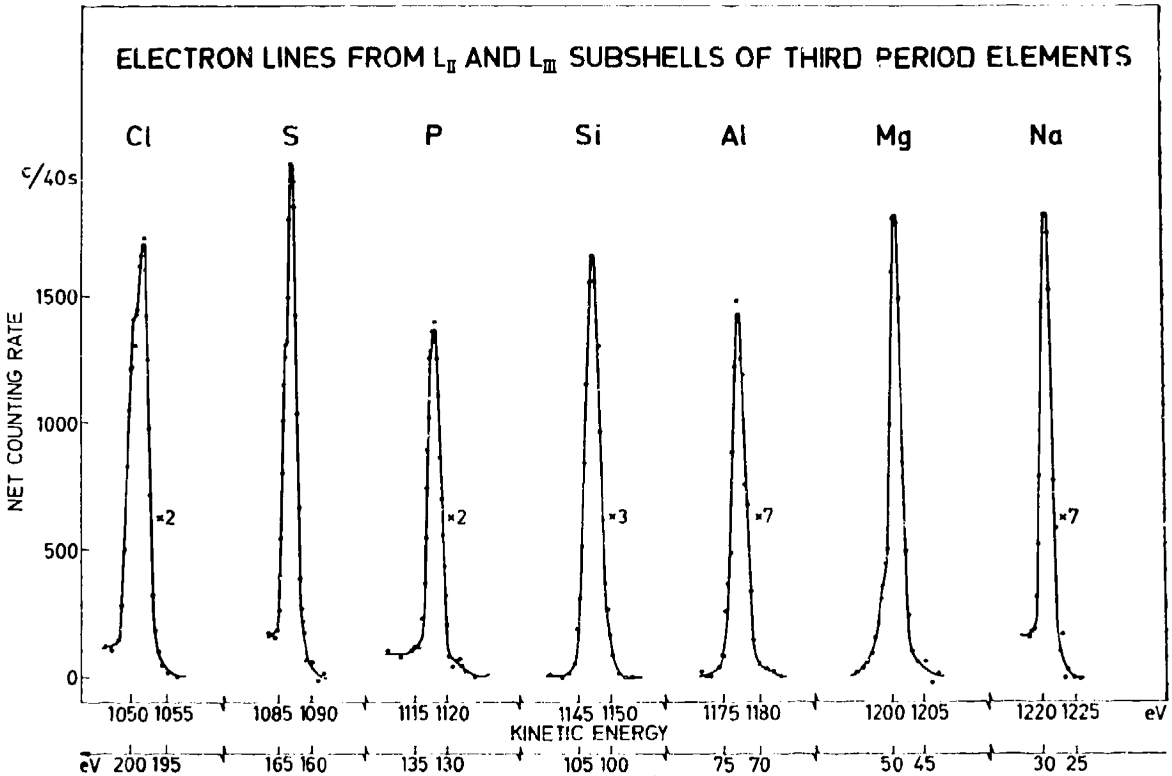

Fig. III:6. Electron lines from the L_{II} and L_{III} subshells of third period elements (sodium to chlorine), excited by Mg$K\alpha$ radiation.

is shown in Fig. III:7 and Fig. III:8 for the elements oxygen ($Z=8$) and carbon ($Z=6$), respectively. The lack of definition becomes even larger for the $L_{II,III}$ levels and is, of course, also found in the X-ray emission spectra of the lightest elements.

Apart from hydrogen and helium, lithium is the lightest element. When exploring the range of elements that can be studied by ESCA, we therefore tried to excite electron spectra from lithium even before aluminum and magnesium had been used as X-ray anode materials. An early lithium spectrum excited by chromium radiation is shown in Fig. III:9. The figure also shows that the surface layer contains oxygen, owing to adsorption and oxidation. From this combination of electron lines, situated within a small energy interval, it is possible to obtain an accurate comparison between different atomic energy levels in various elements and shells.

In the transition elements of the fourth period, the L electron spectra can be excited by soft X-radiation, for example Al$K\alpha$, see Fig. III:2. The K shell has to be studied with harder radiation, and Cu$K\alpha$ is an obvious choice. In fact, the harder copper and chromium radiations have been also used for the L_I subshell of the heavier transition elements. The use of soft X-radiation leads to a decrease in the intensity of the L_I electron lines of these elements relative to L_{II} and L_{III} with increasing Z. The L_I level also becomes increasingly broadened with increasing Z (Fig. III:10). An electron spectrum of the three L subshells of titanium ($Z=22$), excited by aluminum $K\alpha$, is shown in Fig. III:11 (see also Fig. VII:2 for vanadium). One can see here that the L_I level is considerably broader than the L_{II} and L_{III} levels and that the relative photoelectric yield in the L_I subshell is quite low (cf. Chapter VII).

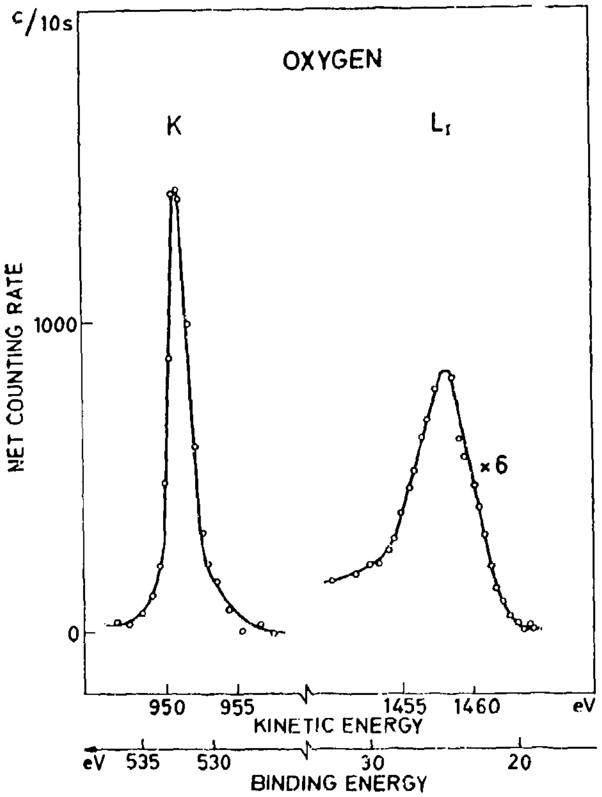

Fig. III:7. Comparison of electron lines from the K and L_I levels of oxygen (in frozen acetone). The electron distribution of the L_I subshell is much broader than that of the K shell.

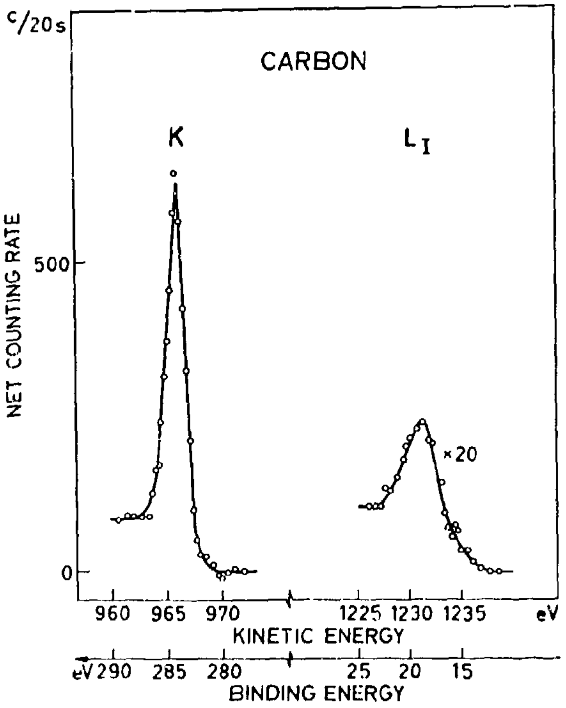

Fig. III:8. Comparison of electron lines from the K and L_I levels of carbon in graphite. A similar broadening as in Fig. III:7 is seen for the L_I electron distribution in comparison with the K electron line.

Fig. III:9. Electron spectrum from lithium oxide excited by chromium X-radiation. Lithium and oxygen lines are seen in the spectrum. A comparison with Fig. I:9 shows that the photoelectric cross section in Li is much larger for Al$K\alpha$ radiation than for Cr$K\alpha$ radiation, see Appendix 7.

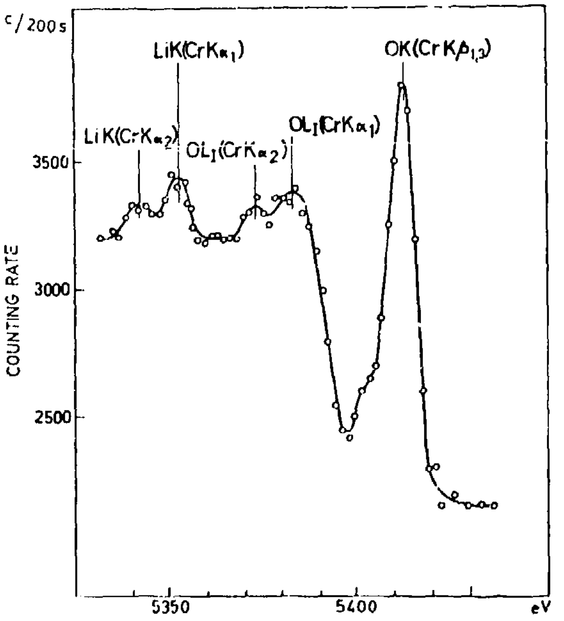

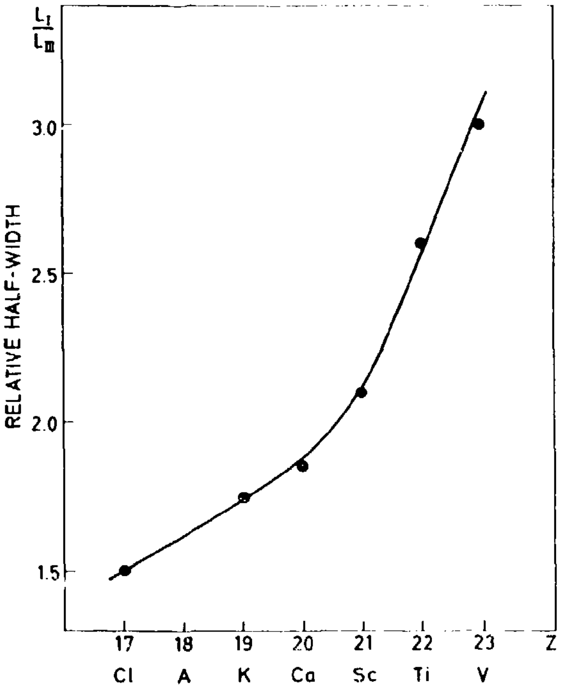

Fig. III:10. Relative half-width of the L_I and L_{III} lines of the elements chlorine to vanadium obtained from ESCA spectra excited by Al*Kα* radiation. Widths were not corrected for instrumental broadening and width of exciting X-radiation.

It is possible to make a comparison of optical transitions and electron spectroscopic data for the *L* shell of light elements. In Fig. III:12, we have plotted the transition energies (open circles) of the optical doublet $2s2p^6\ {}^2S_{\frac{1}{2}} \rightarrow 2s^22p^5\ {}^2P_{\frac{1}{2},\frac{3}{2}}$ as given by Edlén in the Encyclopedia of Physics.[132] Energies for the same transitions can be obtained from our electron spectroscopic measurements as the difference $L_I - L_{II,III}$, and are plotted with crosses. According to Hertz' rule for screening doublets[133], and with the assumption that the level energies increase with atomic number as Z^2 (see Section III:5), one would expect a linear relationship. A slight deviation from linearity is obtained with the electron spectroscopic data. Similar departures from Hertz's rule have been observed in other *Z*-regions.[21,31,43] The optical transitions are studied in highly ionized free atoms which correspond more closely to the idealized system for which the Hertz's rule is valid. The number of elements for which these optical transitions can be obtained is very limited, mainly because of the extremely high degrees of ionization that are necessary at higher *Z* values. (The calcium lines have been obtained from eleven times ionized calcium.)

The plot of the $L_I - L_{II}$ and $L_I - L_{III}$ energy differences (filled circles) obtained from previously accepted values for the level energies[39,134] illustrates the vast improvement obtainable by measuring the *L* energies of the light elements by electron spectroscopy.

We have also made quantum mechanical self-consistent-field calculations of electron binding energies in the light elements. This will be discussed further in Section III:9 and Appendix 2.

III:3. Heavy Elements ($Z > 70$)

The electron spectroscopic method for measuring binding energies of atomic electrons can be employed equally well for heavy elements. One is, of course,

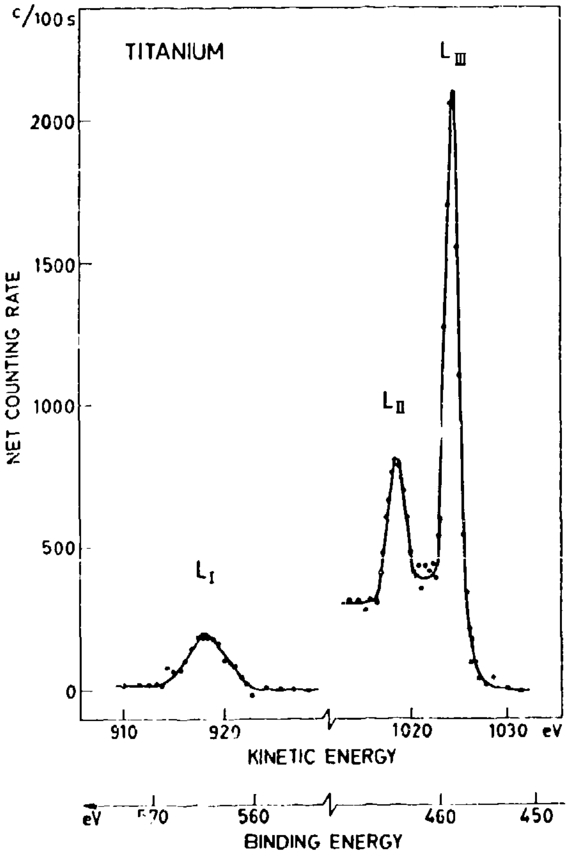

Fig. III:11. Electron lines from the *L* subshells of titanium excited by aluminum *Kα* radiation.

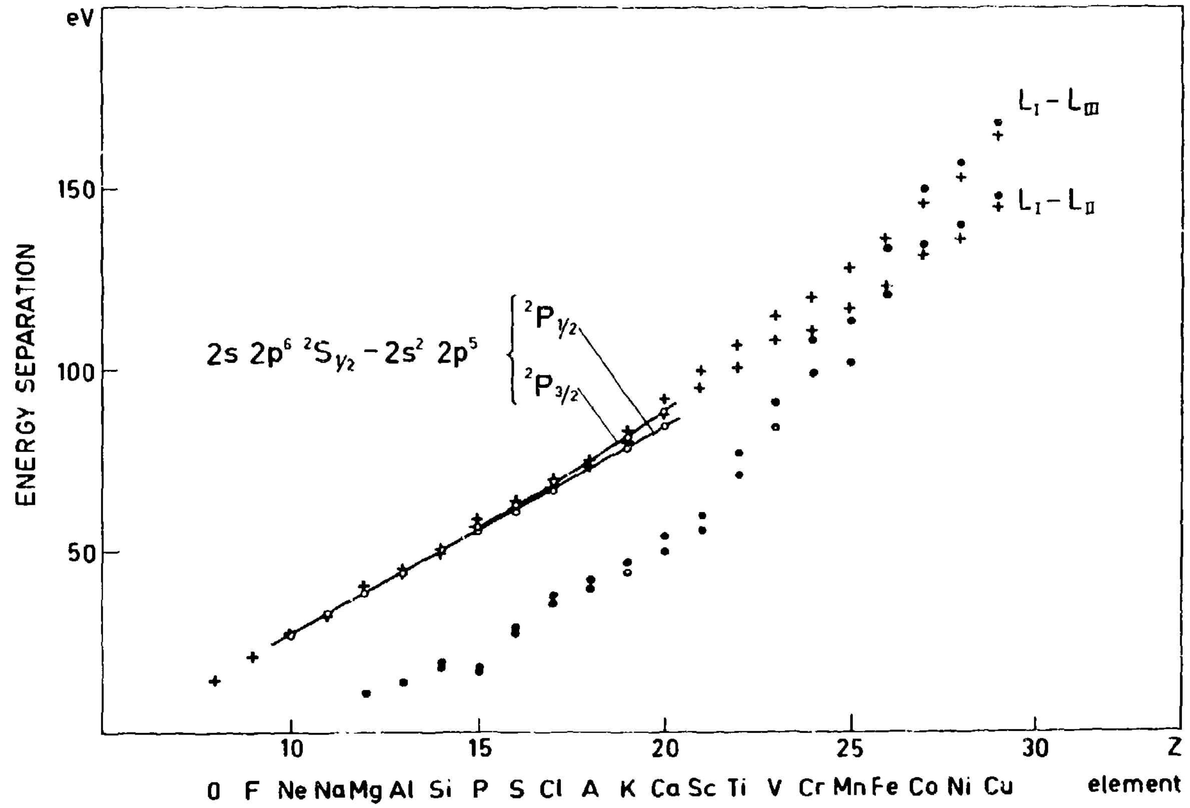

Fig. III:12. Comparison of optical transitions and electron spectroscopic data for the L shell of light elements. Energy differences from ESCA measurements[51,56] are plotted with crosses, optical data[133] with open circles, and previously accepted values[31,134] for the L level energies with filled circles.

limited to some extent by the anode materials that can be used in the X-ray tube. As one approaches the region of very heavy elements, there is no characteristic X-radiation that can conveniently be used for producing photoelectrons from the K shell. This does not mean, however, that electron spectra from heavy elements are poor. On the contrary, there are many subshells outside the K shell from which photo- and Auger electrons can be obtained. Fig. III:13 and Fig. III:14 show electron lines from the L, M, N, and O shells of thorium ($Z = 90$) and Fig. III:15 shows the corresponding spectrum from uranium ($Z = 92$). The atomic levels that are mapped out by these spectra have binding energies from 17,000 eV down to zero binding energy at the Fermi level. By using different X-radiations for different shells, it is possible to cover the whole energy region and at the same time work with a high resolution. However, at the time when the uranium spectrum was recorded[19] we had not yet made use of Al and Mg radiation so the electron lines from the outer N subshells shown in Fig. III:15 are not as well resolved as they could be. Better resolution was obtained in the spectrum shown in Fig. III:16 which was recorded more recently. Al$K\alpha$ was used for exciting this spectrum which displays the structure of the levels of uranium in considerable detail down to 400 eV below the Fermi level.

Another example of high resolution electron spectra in the heavy element region was given in Fig. III:4 for the $N_{VI,VII}$ levels of the elements hafnium ($Z = 72$) to bismuth ($Z = 83$). The energy separations of these two levels, obtained from the spectra in Fig. III:4, are plotted in Fig. III:17 as a function of atomic number. The Z^4 dependence of a spin-doublet, pre-

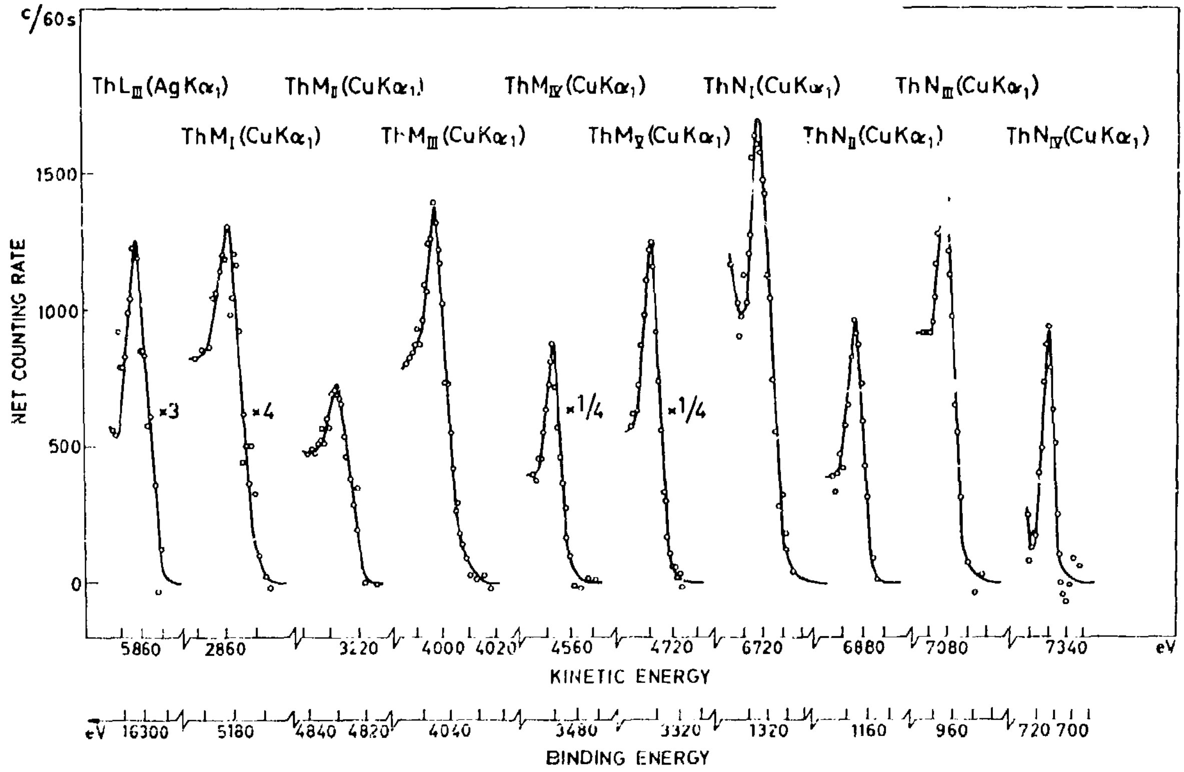

Fig. III:13. Electron spectrum from thorium[45] excited by $AgK\alpha_1$ and $CuK\alpha_1$ radiations.

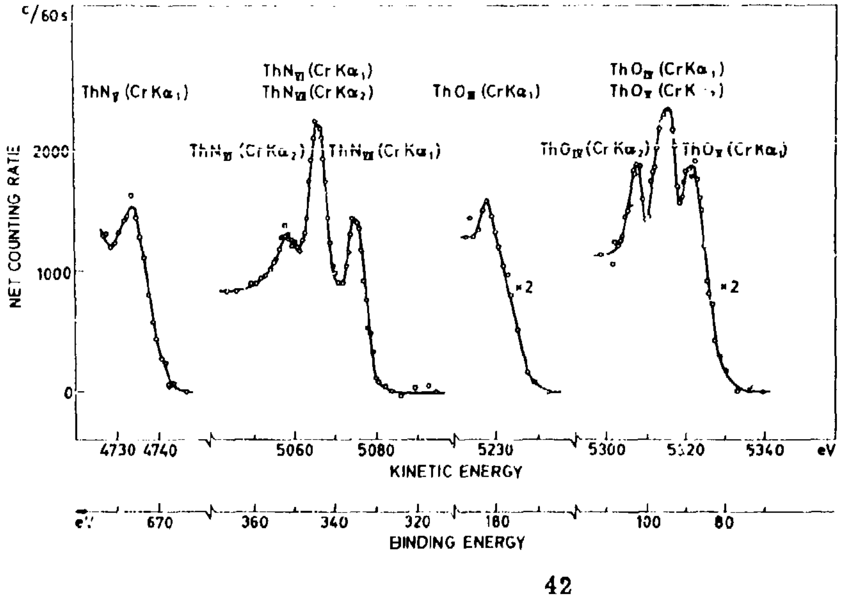

Fig. III:14. Electron spectrum from thorium[45] excited by $CrK\alpha$ radiation.

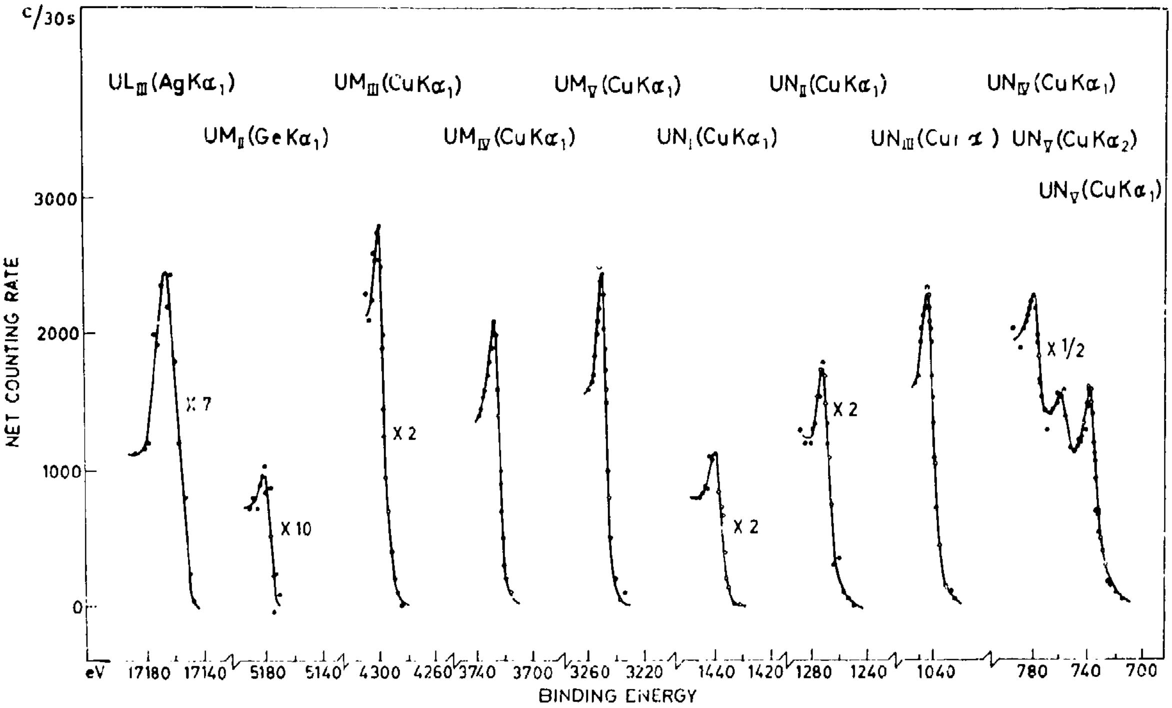

Fig. III:15. Electron spectrum from uranium[19] excited with AgKα, GeKα and CuKα radiations.

dicted by the Dirac-Sommerfeld theory[135,136] (see Section III:5), gives a slight curvature to the graph. A more detailed comparison of the experimental data with the Dirac-Sommerfeld theory can be made, which yields the screening constant for the $N_{VI,VII}$ subshells. This has been done for several spin-doublets in various regions of the Periodic System.[21,31,43]

The $O_{II,III}$ and $N_{VI,VII}$ subshells of the elements in the sixth period have similar energies. The O levels of the first elements in the period have the highest

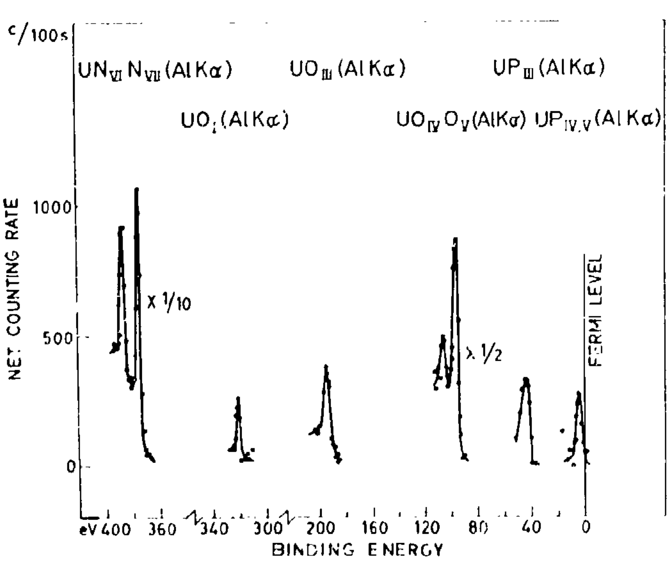

Fig. III:16. Electron spectrum from uranium excited by aluminum Kα radiation.

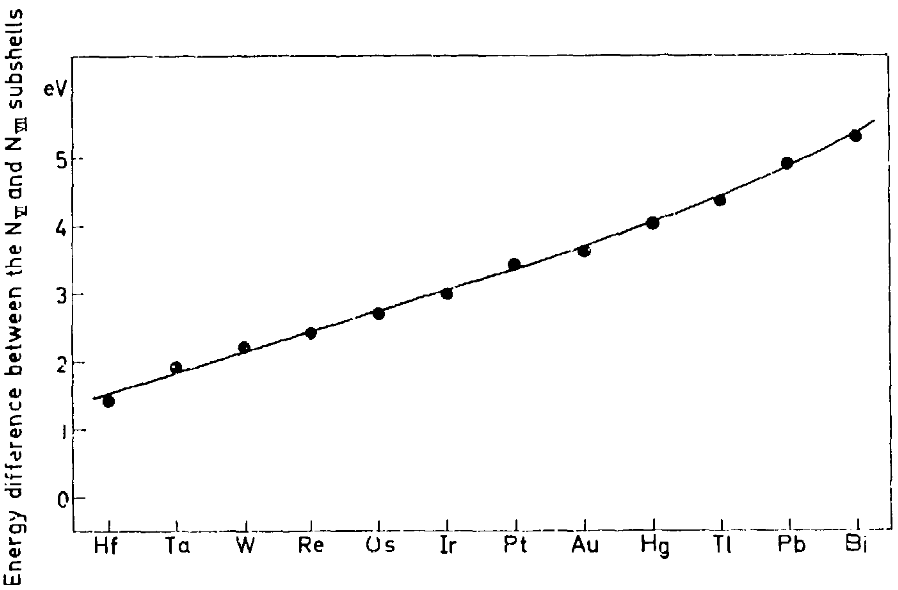

Fig. III:17. Energy separation of the N_{VI} and N_{VII} levels of sixth period elements. The separation values are obtained from the electron spectrum shown in Fig. III:4.

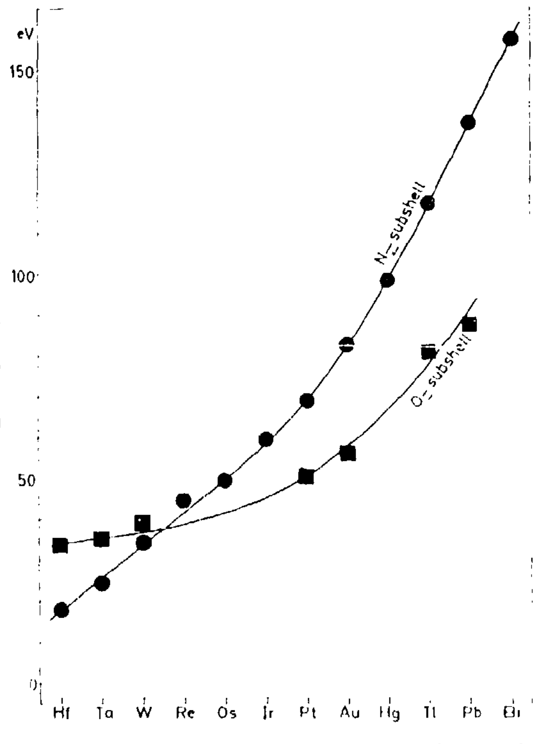

Fig. III:18. Binding energies of N_{VII} and O_{III} electrons for sixth period elements.

binding energy, but at the end of the period the situation is reversed. It is difficult to establish the positions of these levels from X-ray spectra and the O_{III} level was therefore measured by electron spectroscopy in addition to the N levels shown in Fig. III:4. An energy versus Z plot of the O_{III} and N_{VII} levels as obtained from these measurements is shown in Fig. III:18.

The quantity of material that is required for ESCA is very small (see Section V:6) and is less than that normally required for X-ray spectroscopy. Because of this, and also from the radiation protection point of view, the transuranic elements can be more conveniently studied by electron spectroscopy than by X-ray spectroscopy. Much work remains to be done in this region and so far only the elements neptunium ($Z = 93$),[137] plutonium ($Z = 94$)[57] and americium ($Z = 95$)[138] have been studied. Fig. III:19 shows some electron lines obtained from a plutonium oxide sample made by electroplating plutonium on a platinum foil. The amount of material that was deposited in this way was about 1 μg. Cu $K\alpha_1$ and Cr $K\alpha_1$ radiations were used to excite the plutonium lines; the use of softer X-radiation available with our present apparatus would improve the spectra considerably.

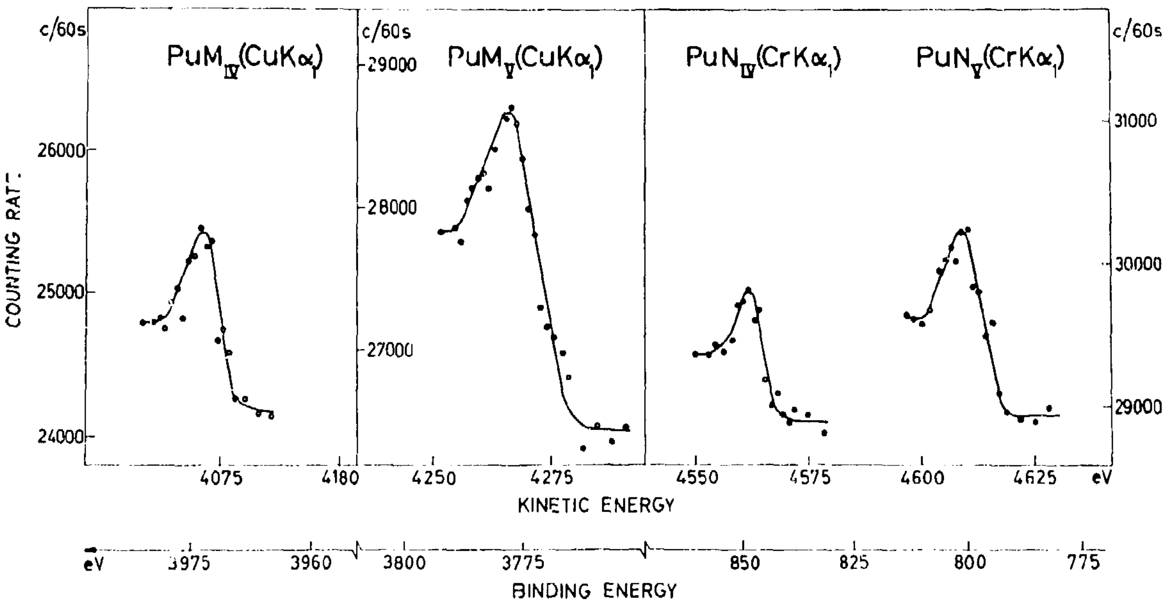

Fig. III:19. Electron lines from the M and N shells of Pu. The sample consisted of plutonium oxide.[57]

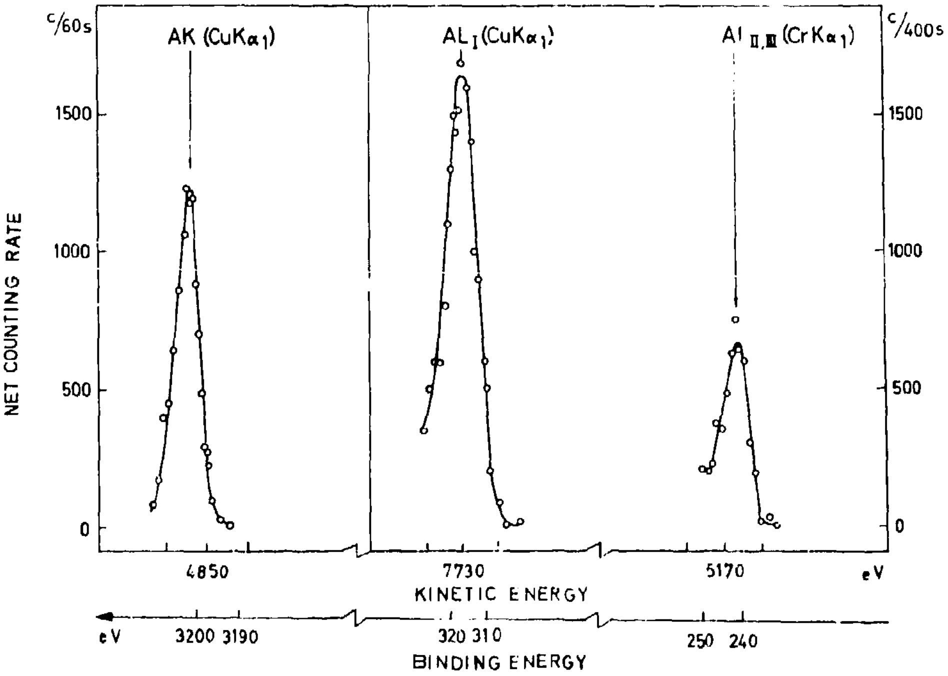

Fig. III:20. Electron spectrum from argon. An argon sample was made by loading a metallic foil with argon ions accelerated in a gaseous discharge. See also Fig. I:26.

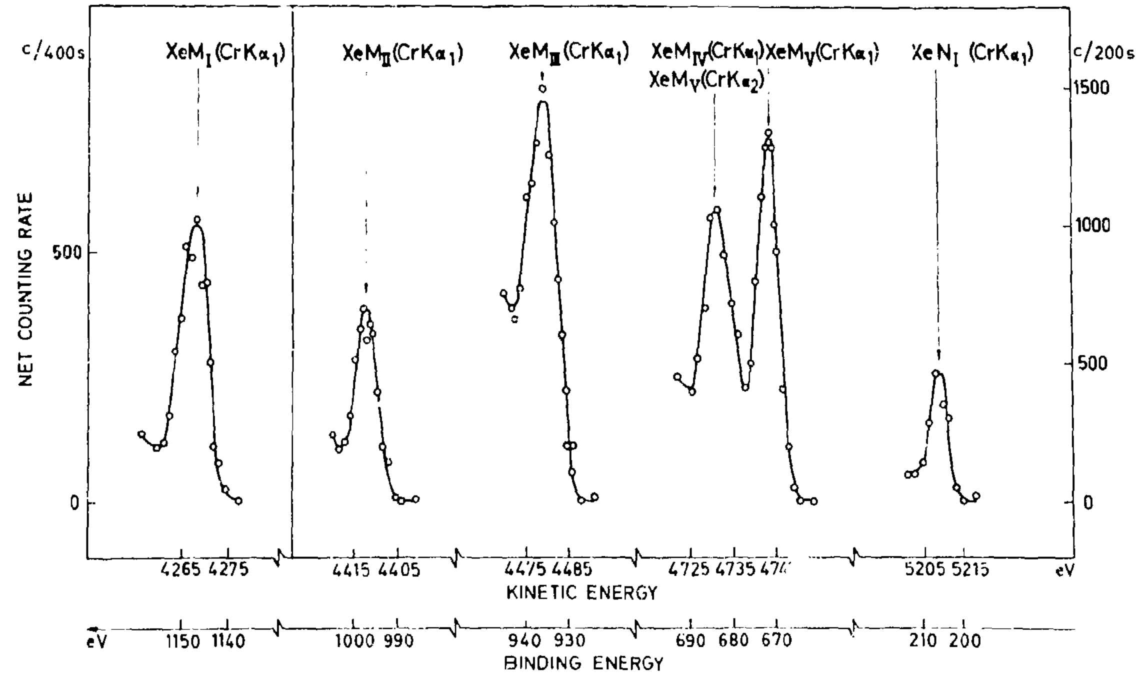

Fig. III:21. Electron spectrum from xenon. The sample was made by the procedure described in Fig. III:20.

III:4. Noble Gases

Photoelectron spectra from gaseous samples are difficult to produce by X-rays, and the noble gases cannot easily be studied by the freezing technique. To prepare sources from the noble gases we saturated the surface of a metallic foil with noble gas atoms in a gaseous discharge. This was accomplished by making the foil the negative electrode on which the noble gas ions of the discharge were collected. Fig. III:20 and Fig. III:21 show electron spectra of the noble gas elements argon and xenon, obtained from sources prepared in this way. Naturally, the amount of gas deposited on the backing was very small. Nevertheless, electron spectra of high quality could be obtained.

From argon, electron lines from the K,L_I, and $L_{II,III}$ shells were obtained. In the investigation of xenon, recordings were made of the five M levels plus the N_I level. The binding energies in xenon vary from ca. 1150 eV for the M_I level down to ca. 200 eV for the N_I level. These are only preliminary results from our studies on gases by the ESCA method, cf. Chapter I and VIII.

III:5. Rare Earths

For a long time the X-ray transition energies and atomic level energies of the rare earth elements were much less accurately known than for most other elements. This gap in the experimental data was partly filled when Bergvall[139] made precision measurements of the $K\alpha$ lines of the rare earth metals, and later, together with Hagström, measured the L level energies by electron spectroscopy.[21] The instrument used in these latter measurements was that described in Section VIII:2, and was at the time operated manually. The results are shown in Fig. III:22 in which electron lines from the L_I subshell for the entire series of rare earth elements are seen.

The Dirac theory gives the following expression for the energy levels of hydrogenic atoms:[140]

$$E = -\frac{\mu Z^2 e^4}{8\varepsilon_0^2 h^2 n^2}\left[1 + \frac{Z^2\alpha^2}{n}\left(\frac{1}{j+\frac{1}{2}} - \frac{3}{4n}\right)\right] \quad \text{(SI units)} \qquad (1)$$

For many-electron atoms, the expression must be modified to take into account electron-electron interaction. Sommerfeld[135] did this by replacing the nuclear

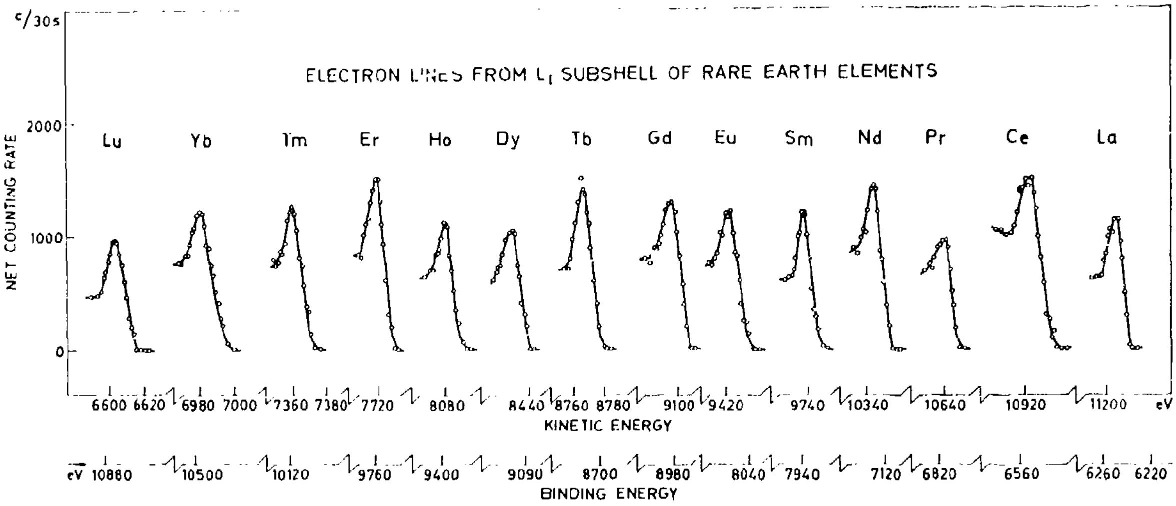

Fig. III:22. Electron lines from the L_I subshells of the rare earth elements.[24]

charge Z with an effective charge $(Z-d)$, where d is a screening number. With the reduced mass of the electron-nucleus equal to the electron mass and using atomic units, i.e. with $\mu = e = \hbar = 4\pi\varepsilon_0 = 1$, the binding energy of an electron in a many-electron atom is then given by

$$E_b = \frac{(Z-d)^2}{2n^2}\left[1+\frac{(Z-d)^2\alpha^2}{n}\left(\frac{1}{j+\frac{1}{2}}-\frac{3}{4n}\right)\right] \text{(a.u.)} \qquad (2)$$

Thus as a first approximation, the square root of the electron binding energy is a linear function of atomic number Z.

The square root of the experimental electron binding energies or X-ray transition energies may therefore be conveniently plotted against atomic number giving so-called Moseley diagrams.[141] To obtain a more expanded scale in such plots, Idei[142] subtracted a linear function of the atomic number from the square root of the energy. Such a modified Moseley diagram is shown in Fig. III:23 for the L_I energies of the rare earth elements as obtained from the electron spectrum in Fig. III:22.

Hagström[37] took the fourth power term in Z into account by repeating the procedure once more, i.e. by plotting the quantity

$$\sqrt{\sqrt{E_b}-aZ-b}-cZ$$

as a function of Z. A Moseley diagram, modified in this way, is shown in Fig. III:24 for the L_I energies of the rare earths. This diagram reveals the scatter of the experimental energies to within a fraction of an eV, although the binding energies in question span an energy range of several thousand eV. The simplified

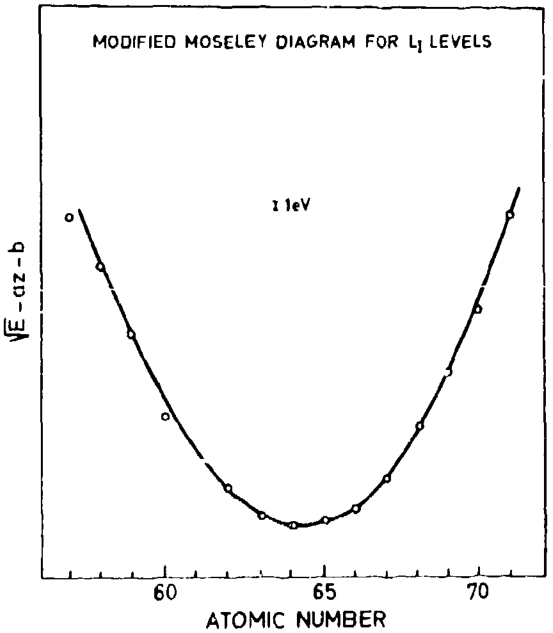

Fig. III:23. Modified Moseley diagram for the L_I energies of the rare earth elements as obtained from the electron spectrum shown in Fig. III:22.[24]

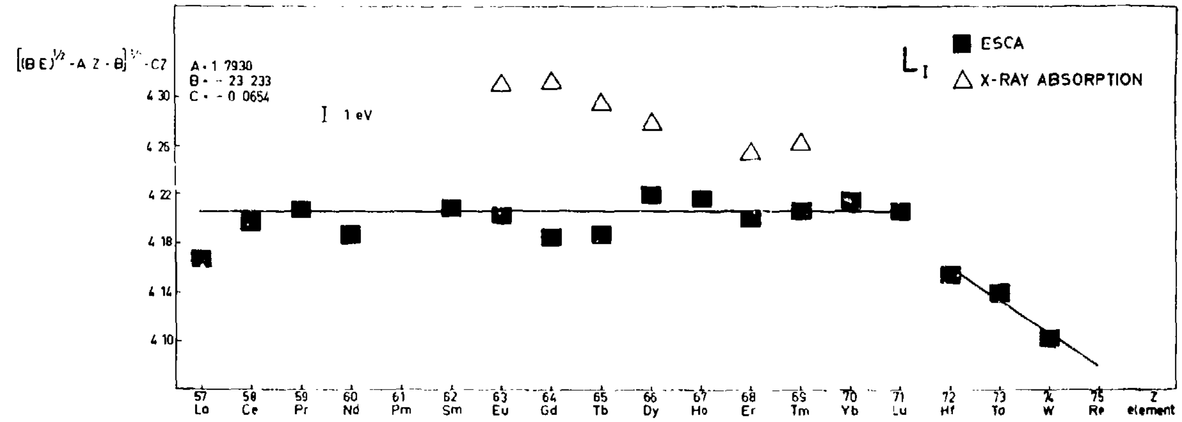

Fig. III:24. Moseley diagram modified according to Hagström[37] for the L_I energies of the rare earth elements.

theory from which the linear function in the diagram may be deduced cannot however be expected to describe the course in detail and the scatter of experimental points is much larger than the error in the measurements. L_I energies obtained by Sakellaridis[113] from X-ray absorption spectra are also plotted in the diagram.

It is interesting to note that the X-ray absorption method yields higher energies than the electron spectroscopic method for the L_I energies of the rare earths. This indicates that the quantity measured is not the same. The X-ray absorption process is limited by selection rules to a much larger extent than the photoelectric ejection of electrons to states in the continuum. One should also bear in mind that the electron binding energies are not entirely an atomic

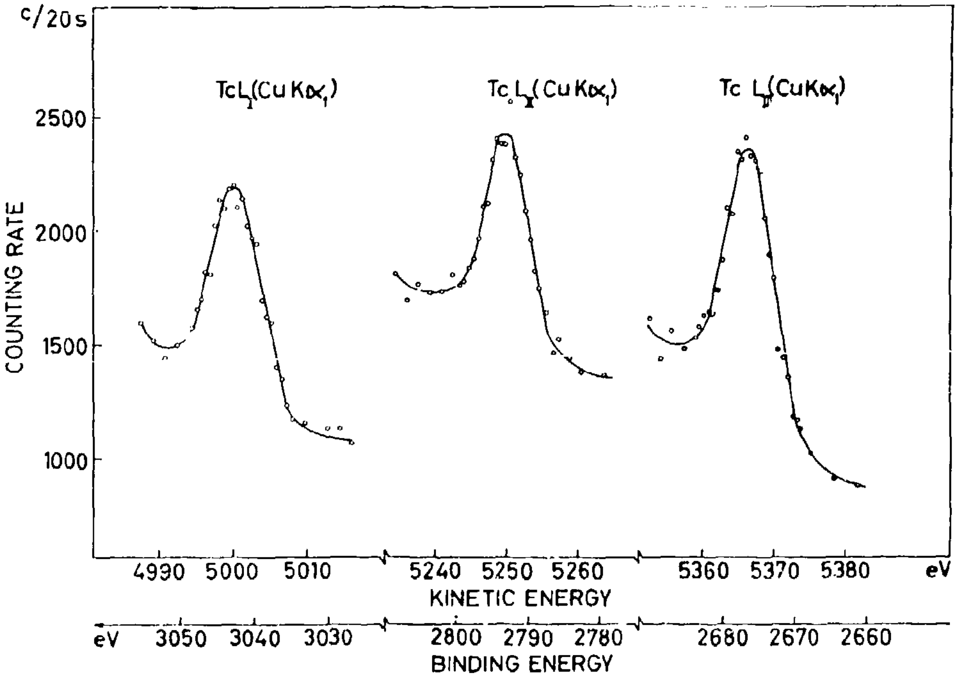

Fig. III:25. Electron lines from the L subshells of technetium excited by copper $K\alpha_1$ radiation.[31] This is another example of electron lines from an element that does not occur naturally. See also Fig. III:19.

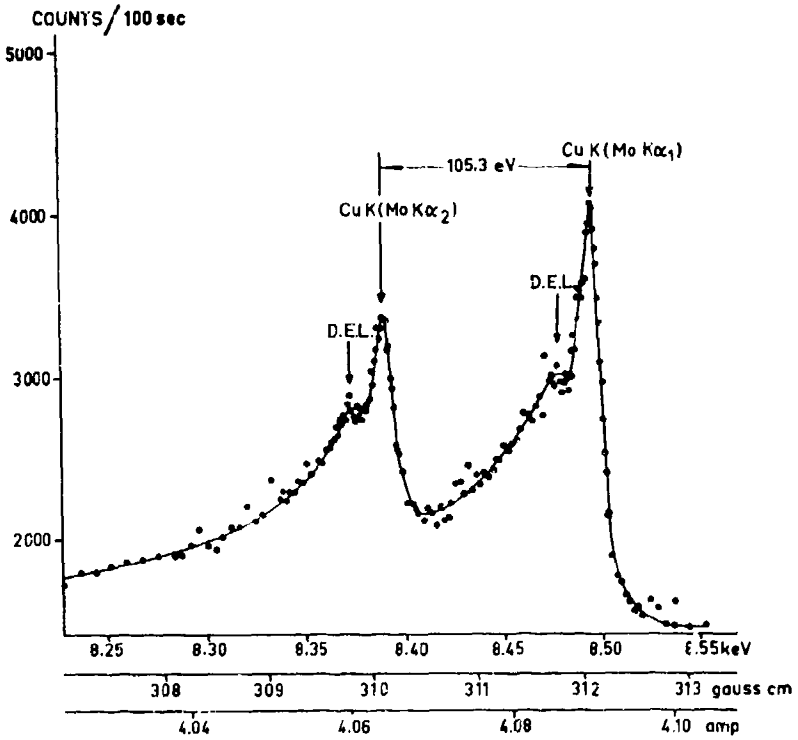

Fig. III:26. Electron spectrum from the copper K shell excited by molybdenum $K\alpha$ radiation.[8] The figure shows the important fact that electrons on their way out of the specimen lose energy in discrete amounts. The separation of the main peaks in the spectrum corresponds to the energy difference between the L_{II} and L_{III} levels in molybdenum. The ESCA spectrum thus gives information also on energy levels of the X-ray anode material.

property but to some extent dependent on the chemical environment and may differ for one and the same element in different compounds (see Section V:1).

In their electron spectroscopic measurements of the binding energies in the L subshells of the rare earths Bergvall and Hagström[21] could also make a comparison with the theoretical predictions given by Sommerfeld[135] for the $L_{II,III}$ spin-doublet splitting

$$E_{L_{II}} - E_{L_{III}} = \frac{1}{2\alpha^2}\{[4-\alpha^2(Z-d)^2]^{1/2} - [2+2(1-\alpha^2 \times (Z-d)^2)^{1/2}]^{1/2}\} \quad \text{(atomic units)} \quad (3)$$

A quantitative estimate of the influence of the finite nuclear size on the fine structure was discussed in terms of the Christy-Keller[114] correction to the Sommerfeld-Dirac[135, 136] expression. The anomalous moment of the electron was taken into account by the Bethe-Longmire factor.[145] One thus obtains:

$$E_{L_{II}} - E_{L_{III}} = \left\{\frac{1}{2\alpha^2}\left\{[4-\alpha^2Z^2]^{1/2} - [2+2(1-\alpha^2Z^2)^{1/2}]^{1/2}\right\} - \alpha^2Z^3f(\alpha Z) + BZ^2 - C\alpha^4Z^5\right\}\left(1+\frac{\alpha}{\pi}\right) \quad \text{(atomic units)} \quad (4)$$

III:6. Miscellaneous

As was mentioned previously electron binding energies have been measured for practically all elements by ESCA, including some that do not occur naturally,[31, 57] see Fig. III:19 and Fig. III:25. The first element that we studied was copper and Fig. III:26 shows the copper spectrum that was published in our first report in 1957.[8] A thin evaporated layer of copper was irradiated with an X-ray beam from a molybdenum anode. As a result of the photoelectric absorption of the $K\alpha_1$ and $K\alpha_2$ radiation from molybdenum in the K shell of copper, the two electron lines shown in the figure were obtained. The right-hand line, CuK(Mo$K\alpha_1$), corresponds to electrons which have been ejected by the photoelectric absorption of Mo$K\alpha_1$, and the left-hand line, CuK(Mo$K\alpha_2$), to electrons ejected by Mo$K\alpha_2$. The energy difference between the two lines is exactly that expected from the splitting of the molybdenum $K\alpha$ X-ray doublet, i.e. the energy difference between the L_{II} and L_{III} levels in molybdenum. Thus, the electron spectrum also indicates the energy levels of the X-ray anode material. On the

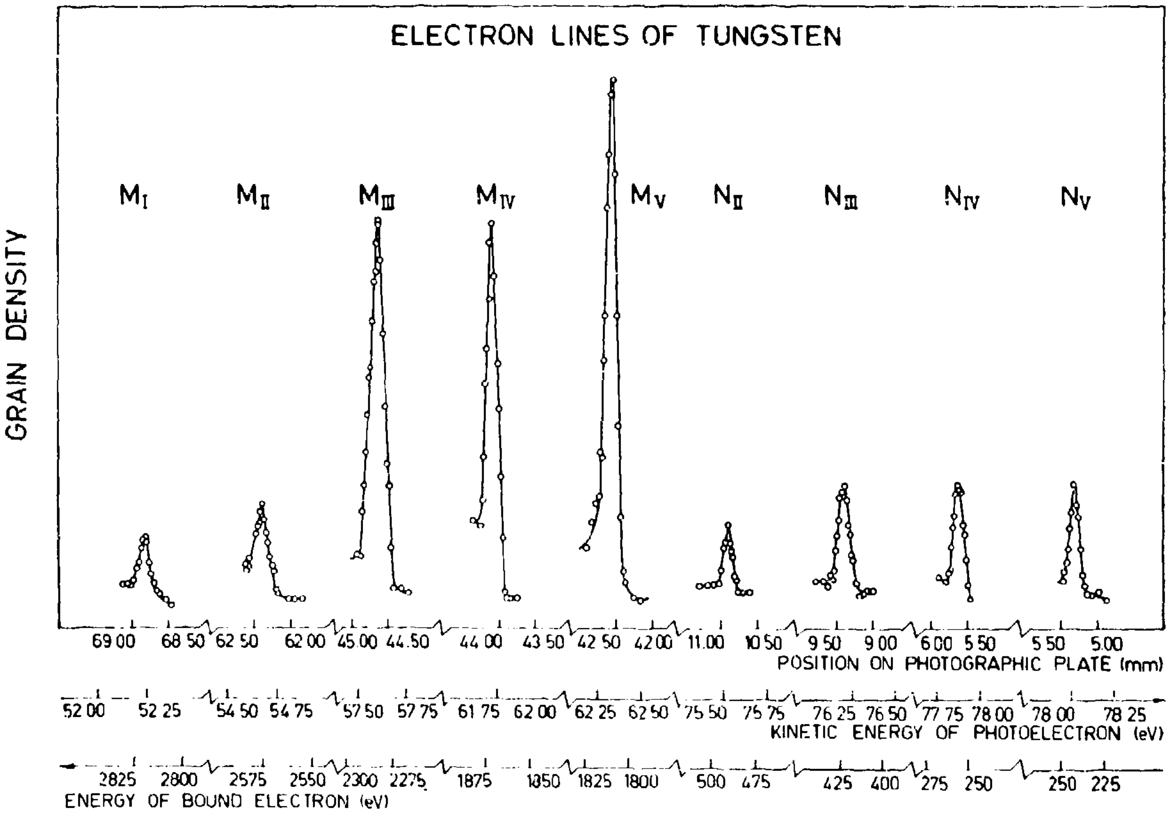

Fig. III:27. Electron lines from tungsten excited by Cu$K\alpha_1$ radiation.[64] The energy analysis of these electrons was performed in the semicircular homogeneous field spectrograph with photographic detection. The lines were obtained with the track counting technique.

low-energy side of each line a satellite structure can be seen, labelled D.E.L., derived from electrons which have lost energy on their way out of the specimen. The important observation to be made here is that the energy losses occur in discrete amounts. The position of the principal line is therefore not affected by the distribution of retarded electrons. A prerequisite for this is, of course, a sufficiently high resolution of the electron spectrometer.

It is of interest to note that even the classical instrument for beta-ray spectroscopy, namely the semicircular homogeneous field spectrograph, can be used for ESCA.[64] An instrument of this type is described in Section VIII:3 and was used for recording the tungsten spectrum in Fig. III:27. Thus the detection of the electrons was carried out photographically and the result was analysed by the method of track counting.[65] Electron lines from all five M subshells plus four N subshells were obtained on the same plate.

Photographic detection was used by Robinson in his early studies of X-ray produced electrons. However, the experimental techniques and equipment available at the time were insufficient to produce electron spectra that could be used for any detailed analysis of atomic or molecular structure. Fig. III:28 shows an electron spectrum of gold, recorded by Robinson in 1925.[103] Several subshells in the M and N shells of gold can be identified in the photometric recording of the plate but the resolution is insufficient to distinguish all subshells and a true line spectrum was not obtained. For example, the N_{VI}, N_{VII} and O levels appear together as a hump in the photometric recording. The energy difference between the N_{VI} and N_{VII} levels in gold is 3.7 eV which would correspond to a distance less than

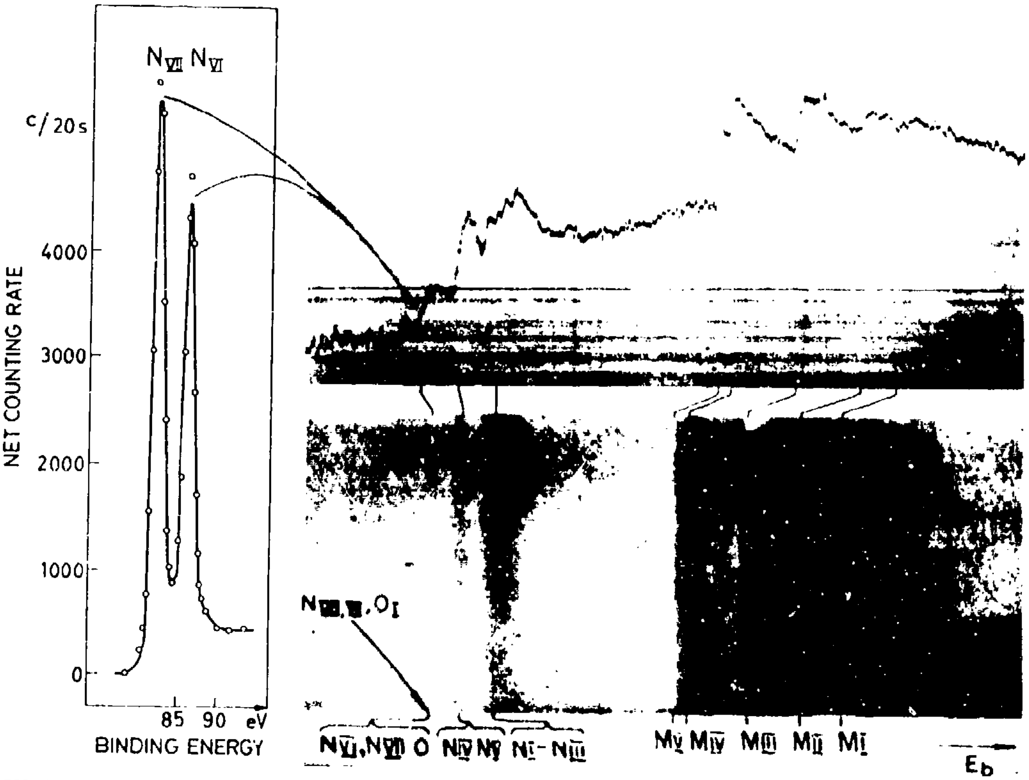

Fig. III:28. Electron spectrum of gold recorded by Robinson in 1925.[103] (Reproduced by due permission from Taylor & Francis Ltd., London). For comparison a part of a recently recorded spectrum of gold is shown to the left in the figure. The N_{VI}, N_{VII} levels are seen as two completely resolved lines in this spectrum whereas the N_{VI}, N_{VII} and O levels appear together as a hump in the photometric recording by Robinson and are only barely visible on the photographic plate. The energy distance between the two peaks N_{VI} and N_{VII} in the ESCA spectrum, to the left in the figure, would correspond to less than 0.1 mm in Robinson's spectrum. (Energy scales of photographic plate and photometric recording are not the same. An indication of corresponding points is made in the figure).

0.1 mm in the photographic recordings made by Robinson. For comparison the gold N_{VI}, N_{VII} electron lines recorded with our present day techniques are also shown. The lines are completely resolved, each having a full width at halfmaximum intensity of 1.3 eV.

Several examples have been given of how electron

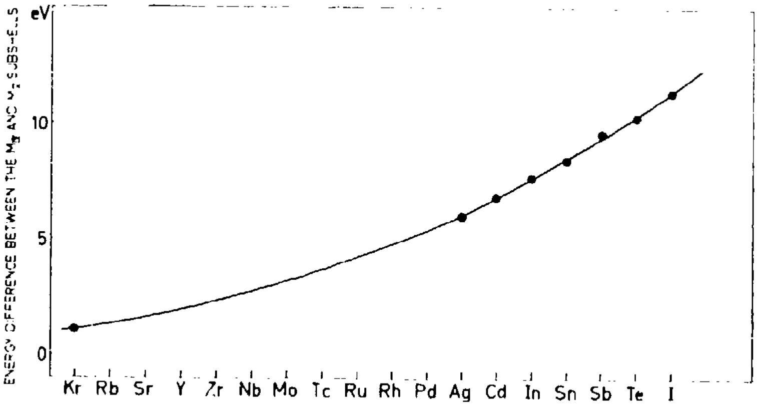

Fig. III:29. The M_{IV}-M_V energy difference for elements in the fifth period.

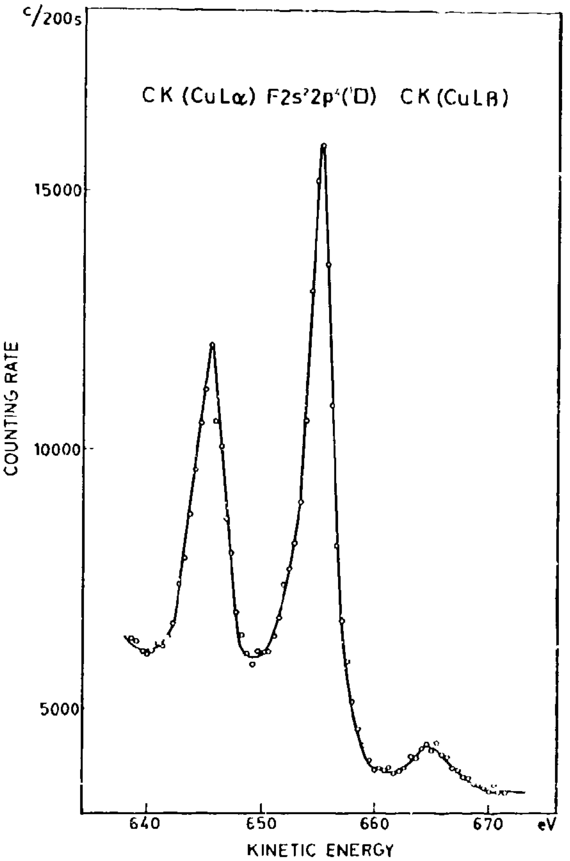

Fig. III:30. Electron spectrum of fluorine and carbon excited by copper L emission lines. The carbon lines were used for energy calibration of the fluorine $2s^22p^4(^1D)$ Auger line.

binding energies and energy differences can be displayed as a function of atomic number. One more such example is given in Fig. III:29 which shows the $M_{\mathrm{IV}}-M_{\mathrm{V}}$ energy difference versus atomic number for elements in the fifth period. The $M_{\mathrm{IV,V}}$ spin doublet splitting of the elements silver ($Z=47$) to iodine ($Z=53$) was obtained from the photoelectron spectra in Fig. III:3 and for krypton ($Z=36$) from the $M_{4,5}NN$ Auger spectrum shown in Fig. I:27. One would not anticipate any difficulties in measuring the $M_{\mathrm{IV,V}}$ levels in the remaining elements $Z=37$ to $Z=46$ by ESCA.

In producing ESCA spectra, we have utilized not only the characteristic $K\alpha$ radiation, but also the $K\beta_{1,3}$ line and emission lines of the L and M series. This is illustrated by the spectra shown in Figs. III:9, III:30, and III:31.

Great improvement was achieved by using aluminum $K\alpha$ radiation for the production of electron spectra in addition to the harder molybdenum, copper, etc. radiations. One naturally looks for high intensity X-ray emission lines of still lower energy and smaller inherent width (cf. Section II:5). Fig. III:32 shows an electron spectrum from sodium, obtained with magnesium $K\alpha$ radiation. The energy of the magnesium $K\alpha$ is 1250 eV and the K photoelectron line of sodium then has an energy of only 175 eV. The sodium K binding energy can therefore be determined with considerable precision. The $KL_2L_3(^1D)$ Auger line comes out excellently in this case. The production of electron spectra by means of magnesium radiation has now become a standard procedure in our work.

Another element with low atomic number suitable as

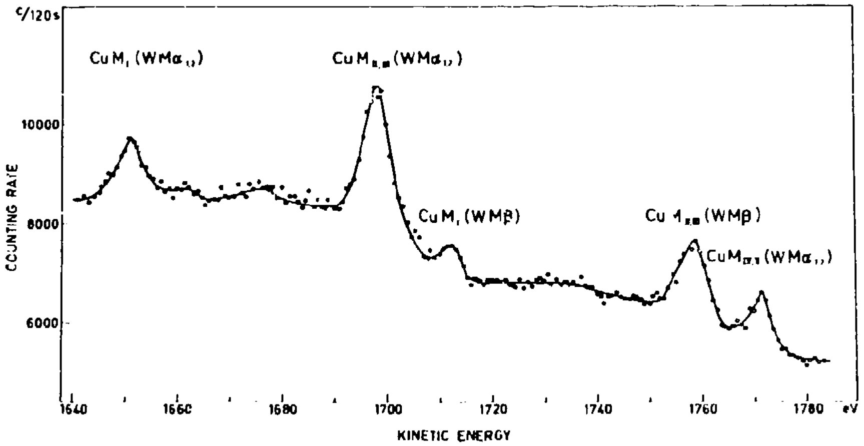

Fig. III:31. Electron spectrum of copper excited by tungsten M emission lines.

an X-ray anode is sodium. At still lower Z-values, however, the $K\alpha$ X-ray lines become broadened due to solid state effects. One does not, therefore, improve the resolution of the electron spectra by utilizing elements in the second row of the Periodic Table. If sodium is to be used in the X-ray anode, it has to be in the form of an alloy or a compound. We have done some preliminary work to produce a suitable X-ray anode with a high sodium content. Fig. III:33 shows an electron spectrum which was obtained with sodium $K\alpha$ radiation from an anode consisting of the alloy Au_2Na, which has a melting point of 1000° C. We have also used NaCl and NaF as anode materials; however, these compounds rapidly evaporated from the metallic base on which they had been deposited.

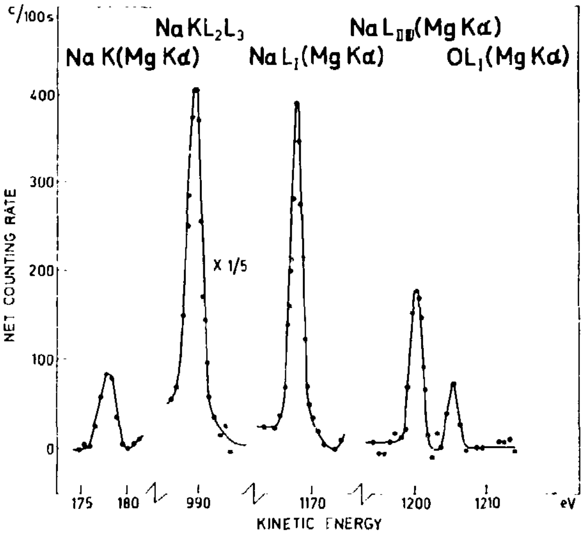

Fig. III:32. Electron spectrum from Mg$K\alpha$ irradiated sodium oxide.

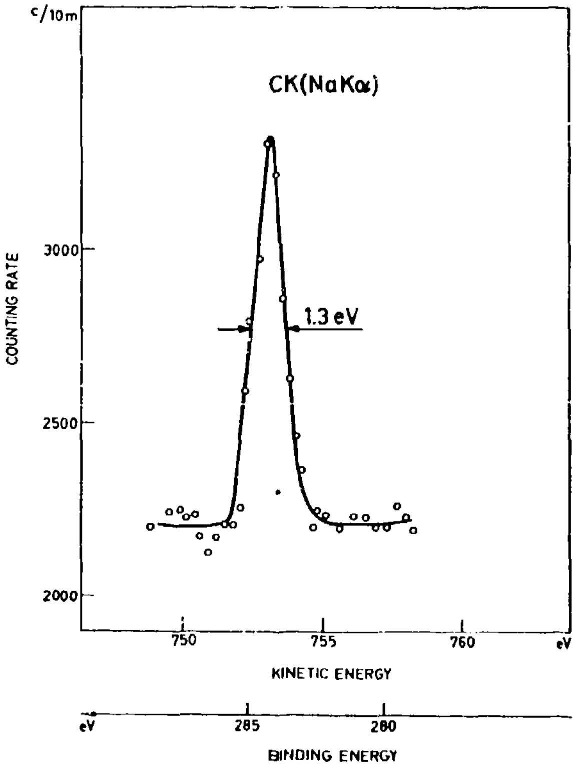

Fig. III:33. A K electron line from carbon excited by sodium ($Z = 11$) $K\alpha$ radiation.

III:7. Basic Energy Calibration of the Electron Spectra

The energy scale of an electron spectrum is usually established by comparison with an electron line of known energy. If the electron spectrum is recorded in an iron-free magnetic spectrometer, the calibration is made assuming a linear relationship between the momentum p of the focussed electrons and the spectrometer current I:

$$p = k \cdot I \qquad (5)$$

The kinetic energy T corresponding to momentum p is then obtained from the relation:

$$T = E_0\left[\sqrt{\left(\frac{pc}{E_0}\right)^2 + 1} - 1\right] \qquad (6)$$

where E_0 is the rest mass energy of the electron.

If the spectrum is recorded in an electrostatic spectrometer, there is a similar relation between the kinetic energy of focussed electrons and the spectrometer voltage U:

$$T = kU\left(1 + \frac{T}{2E_0 + T}\right) \qquad (7)$$

The term $T/(2E_0 + T)$ is the relativistic correction to the simple linear relation $T = kU$ which holds in the nonrelativistic limit.

The calibration line can be obtained by accelerating

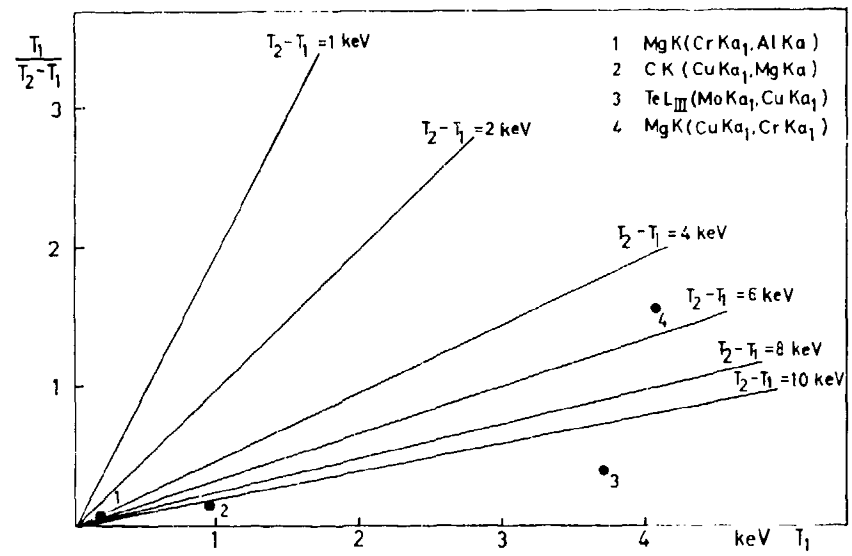

Fig. III:34. Diagram for comparison of different combinations of photoelectron lines in order to minimize the weighting factor in eq. (8).

thermionic electrons to a well-defined electric potential. This requires an accurate measurement of the accelerating voltage and the focussing current or voltage. Moreover, the electron-optical properties, for example, the effective source position, may be slightly different for the different sources used for the calibration line and the photoelectron or Auger lines. Although the method is attractive in that the energies are obtained directly in eV it has not yet been used for high precision measurements. Instead the calibration lines used in β-ray spectroscopy and atomic electron spectroscopy are related to X-ray spectroscopy measurements and are thus based on the X-unit.

An electron spectrum, recorded in an iron-free instrument, can be calibrated in terms of X-ray transition energies if the energy difference between two lines in the spectrum corresponds to an X-ray transition of known energy. In β-spectroscopic work, this is the case when internal conversion lines from two different shells are recorded for the same γ-transition. The energies of the two conversion lines can then be calculated from the known energy of the X-ray transition between the shells. This transition might be forbidden by selection rules, but often, especially for heavy elements, it can be obtained by combinations of allowed transitions. In this way several conversion lines in the thorium $B+C$ spectrum were determined by Siegbahn and Edvarson.[5] A slightly different approach was made by Nordling[18] for calibrating ESCA spectra. Conversion of monochromatic electromagnetic radiation in two different shells of an element was not utilized in this case. Instead, by using two different elements in the X-ray anode, photoelectron lines due to conversion of the $K\alpha_1$ radiations in the same atomic shell were recorded. The energies of these two photoelectron lines could be deduced from the known energies of the X-ray transitions without knowing the electron binding energy or the work function of the spectrometer material. Other electron lines, used for the calibration of ESCA spectra, have since been related to these lines. In the described calibration procedures it is essential that the source is made thin. This precaution should be undertaken because we have found that insulating sources can be charged (see Section VIII: 1) and that this effect depends on the thickness of the source. For thin sources placed on a conducting backing the charging of the source becomes negligibly small.

The relative accuracy in making a calibration from the known energy difference between two electron lines can be estimated from the following nonrelativistic relation:

$$\frac{\Delta T_2}{T_2}=\frac{\Delta h/e}{h/e}+\frac{\Delta\nu}{\nu}+\frac{T_1}{T_2-T_1}\cdot\frac{\Delta\alpha}{\alpha} \qquad (8)$$

T_1 and T_2 are the kinetic energies of the two electron lines ($T_1 < T_2$), ν is the corresponding X-ray frequency or frequency difference, and α is the ratio between the squares of the focussing currents for the two electron lines in a magnetic spectrometer or the ratio of the focussing voltages in an electrostatic instrument.

There are thus three sources of error, namely the uncertainty of the fundamental constant combination h/e, the X-ray data, and the relative position of the two lines in the electron spectrum. The relative error in α is weighted by a factor $T_1/(T_2-T_1)$ and the experimental parameters should be chosen so as to make this factor small. It is shown graphically in Fig. III:34 as a function of T_1 for several energy differences (T_2-T_1). Each combination of photoelectron lines for calibration purposes defines a point in the diagram and the diagram can thus be used as a guide for comparing different combinations. Some combinations are plotted in Fig. III:34.

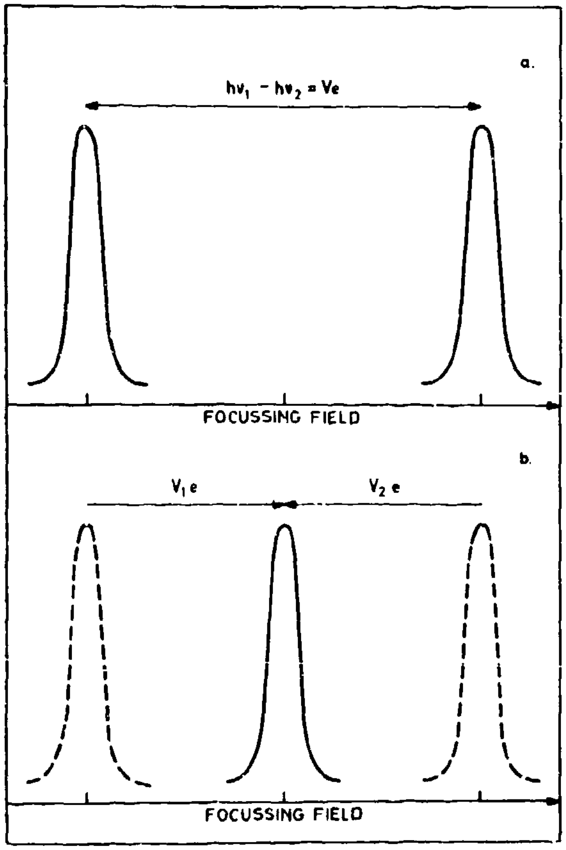

Fig. III:35. *a*) Electrons expelled by two different X-radiations. *b*) By accelerating the electrons of lower energy by V_1 volt and retarding the electrons of higher energy by a voltage V_2, the two lines can be focussed at the same spectrometer field. The energy difference between the two X-radiations is then $e(V_1 + V_2)$ electron volt.

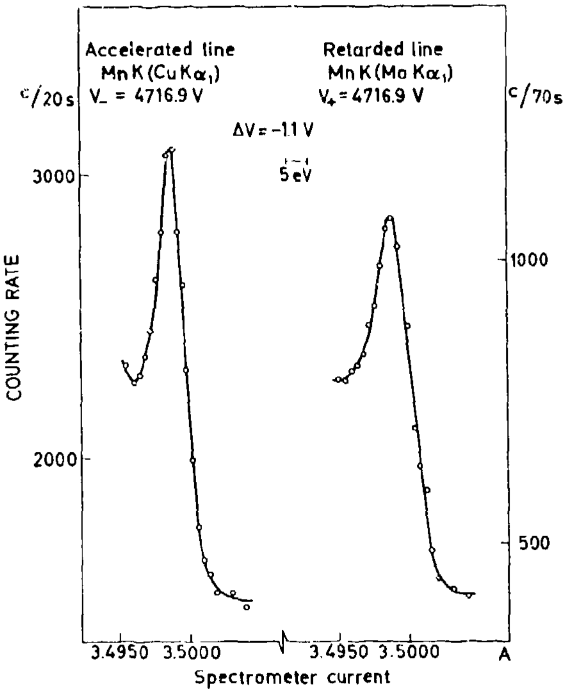

Fig. III:36. Two photoelectron lines focussed by acceleration and retardation at nearly the same spectrometer current.[32]

III:8. A Method for Measuring Atomic Energy Level Differences in Electron Volt

The quantum energy of a photon can be measured in electron volt only by converting the photon energy into kinetic energy of a charged particle. Bridging the gap between the microscopic scale of energies in terms of X-ray wavelengths and the macroscopic scale of energies to which the electron volt is tied has provided a challenging problem over the years. The ESCA method opens a new approach to this problem, see Fig. III:35. Thus it is assumed that photoelectrons are expelled from an atomic K shell by two different X-rays with photon energies $h\nu_1$ and $h\nu_2$ (Fig. III:35a). The low-energy electron line is focussed in the spectrometer and a potential is then applied to the source so that the electrons are retarded before the energy analysis. For a certain value of the retarding potential the

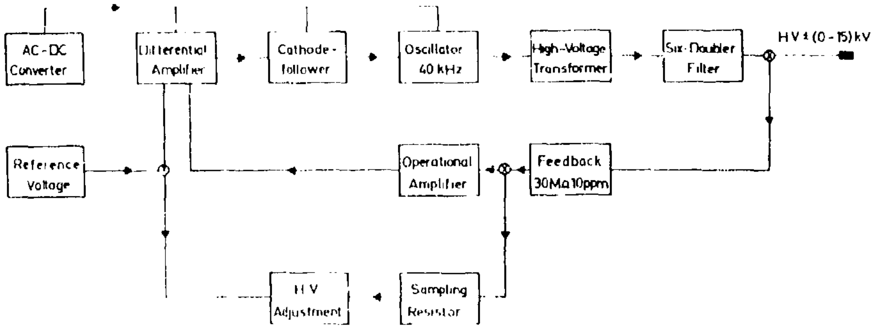

Fig. III:37. Block diagram of the high voltage supply for "absolute" energy calibrations and h/e-measurements.

high energy line comes into focus. If this occurs at a retarding voltage V the following relation holds:

$$h\nu_1 - h\nu_2 = eV \tag{9}$$

The spectrometer can also be set to focus electrons of energy somewhere between the two lines. These are then brought to focus by successively applying a retarding potential V_1 and an accelerating potential V_2, such that $V_1 + V_2 = V$ (Fig. III:35b). Inasmuch as the frequencies ν_1 and ν_2 are known from X ray spectroscopy, a measurement of the voltage V provides a means of determining the fundamental constant combination h/e. This is true for conducting sources and thin sources of nonconducting materials placed on a conducting backing. For thick sources of insulating materials we have found that the displacements of the electron lines upon acceleration or retardation may not correspond to the applied voltage.

X-rays are measured by their wavelengths rather than by their frequencies, so that when solving eq. (9) for h/e, one should introduce wavelengths λ_1 and λ_2 instead of frequencies ν_1 and ν_2:

$$h/e = \left(\frac{\lambda_1\lambda_2}{\lambda_1 - \lambda_2}\cdot V\right)\cdot\frac{\Lambda}{c}\cdot 10^{-10} \tag{10}$$

λ_1 and λ_2 are expressed in the X unit, and Λ is the dimensionless conversion factor between mÅ and xu. Other quantities are given in SI units. Fig. III:36 shows two electron lines, MnK(Cu$K\alpha_1$) and MnK-(Mo$K\alpha_1$), that are focussed at approximately the same current in one of our magnetic spectrometers. One line has been accelerated by 4716.9 V and the other has been retarded by the same amount. These measurements gave the value (12372.9 ± 1.5) keV·xu for the quantum energy conversion factor ($E\lambda_s$) (the quantity in parenthesis in eq. (10)), and the value (4.1356 ± 0.0006)·10^{-15} Vs for h/e.[32]

The ratio h/e has been determined by many different experimental methods. The results of these experiments have, however, always tended to yield values that are inconsistent with the bulk of data on the fundamental constants.[148] This "h/e discrepancy" is partly due to the uncertainty in the wavelength conversion factor. The method that we have developed offers a direct and high precision route for establishing atomic energy-level differences, measured in the electronvolt unit and without need for introducing any X-ray data or X-ray wavelength conversion factors. Instead of two different X-radiations undergoing photoelectric absorption in one and the same shell of the target atoms one can let X-radiation of one frequency undergo photoelectric absorption in two different shells. In both cases one produces two photoelectron lines for which the energy difference is known in terms of the frequencies of X ray transitions and measured in terms of electron volt.

The sector focussing electrostatic instrument has the great advantage in these investigations that the acceleration of the electrons can take place in an environment free from magnetic fields. Additional contributions to the improved accuracy include a new construction of the high tension generator and a further development of the apparatus for measuring the voltage. This makes it possible to carry out an absolute determination of the acceleration voltage (or retardation voltage) with an error which is $< 10\cdot 10^{-6}$.*

* Docent Stig Hagström, now at CTH in Göteborg, contributed much to the construction of this equipment.

calculation is considerably more complicated. Firstly, the binding energy is normally referred to the Fermi level, which implies that a correction for the mostly unknown work function of the source material has to be applied before a comparison with calculated atomic binding energies can be made. Secondly, the neighbouring atoms perturb the atomic orbitals in a very complicated manner. Fortunately, both these effects are comparatively small for inner shells, with which this section is mainly concerned, and, as a first approximation, the calculations can be confined to isolated atoms or ions. For a more accurate comparison between experimental and theoretical values, however, it is necessary to consider various solid-state effects. These effects will be briefly discussed at the end of this section and also in connection with the calculation of "chemical shifts" in the binding energies in Section V:3.

In SCF methods, the electrons are assumed to move independently of each other in the average field caused by the nuclei and the other electrons. For free atoms or ions, this field is furthermore usually assumed to be spherically symmetrical. In the simplest SCF method (the Hartree method), the wave function for an N-electron atom (the following refers equally well to atoms as to ions) is of the form

$$\psi = \phi_1(1)\phi_2(2)\ldots\phi_N(N) \qquad (11)$$

where ϕ_i is a single-electron wave function including a spin dependence (spin-orbital) and the number in parenthesis represents the four coordinates of the electron. The spin-orbitals are then solutions of the single-electron Schrödinger equation (in atomic units)*

$$[-\tfrac{1}{2}\Delta_1 + V(r_1)]\phi_i(1) = \varepsilon_i\phi_i(1) \qquad (12)$$

and are of the form

$$\phi_i(r,\theta,\varphi,\sigma) = \frac{1}{r}P_i(r)\,Y_i(\theta,\varphi)\chi_i(\sigma), \qquad (13)$$

where Δ_1 is the Laplacean operator and other symbols have their usual meaning. The potential in eq. (12) becomes

$$V_i(r_1) = -\frac{Z}{r_1} + \sum_{j \neq i}\left\{\frac{1}{r_1}\int_0^{r_1} P_j(r_2)^2 dr_2 + \int_{r_1}^{\infty}\frac{1}{r_2}P_j(r_2)^2 dr_2\right\}, \qquad (14)$$

where Z is the nuclear charge and r_1 and r_2 the electron-nuclear distances. The N equations (12) are coupled through the potential in eq. (14) and can therefore be solved only by iterative methods.

The Hartree method does not take into account the equivalence of the electrons (exclusion principle). In the more refined method, Hartree-Fock (HF), antisymmetrized wave functions are used (Slater determinants)

$$\psi = \frac{1}{\sqrt{N!}}\begin{vmatrix} \phi_1(1)\phi_1(2)\ldots\phi_1(N) \\ \phi_2(1)\phi_2(2)\ldots\phi_2(N) \\ - \quad - \quad - \quad - \quad - \quad - \\ \phi_N(1)\phi_N(2)\ldots\phi_N(N) \end{vmatrix}. \qquad (15)$$

The variational principle then leads to the general Hartree-Fock equations

$$\left(-\frac{1}{2}\Delta_1 - \frac{Z}{r_1}\right)\phi_i(1) + \sum_j \int \phi_j(2)^* \frac{1}{r_{12}} \times$$
$$\times [\phi_i(1)\phi_j(2) - \phi_j(1)\phi_i(2)]dv_2 = \varepsilon_i\phi_i(1), \qquad (16)$$

where r_{12} is the inter-electron distance. Here the spin-orbitals are quite general and not restricted to the type (13). These equations can at present be solved only for atoms with closed electron shells. Atoms with open shells are treated in an approximative way, assuming a spherical symmetry as for closed shells ("restricted" or "conventional" HF). The general HF functions give by definition the lowest energy of all wave functions expressed as a single Slater determinant. The conventional HF functions give the lowest energy of all similar functions, where the spin-orbitals are of the form in eq. (13).

Even if the conventional HF method is tractable for all atoms with modern computers, a simplified method, called Hartree-Fock-Slater (HFS),[illegible] is of great interest. Here the exchange part of eq. (16)

$$-\sum_j \int \phi_j(2)^* \frac{1}{r_{12}} \phi_j(1)\phi_i(2)\,dv_2$$

is approximated by a "localized" potential term

$$V_{ex}(r_1)\phi_i(1) = -\left[\frac{81\varrho(r_1)}{32\pi^2 r_1^2}\right]^{1/3}\phi_i(1), \qquad (17)$$

where $\varrho(r)$ is the radial electron density

$$\varrho(r) = \sum_j P_j(r)^2. \qquad (18)$$

This reduces eq. (16) to the same simple form as the Hartree equation (12)

$$[-\tfrac{1}{2}\Delta_1 + V(r_1)]\phi_i(1) = \varepsilon_i\phi_i(1), \qquad (19)$$

where

---

* Atomic units are used in this section unless stated otherwise, i.e. $e = m = \hbar = 4\pi\varepsilon_0 = 1$, which implies that the energy unit (Hartree unit) is 1 H = $2hcRy$ = 27.2107 eV.

The high tension generator (Fig. III:37) has been constructed with double feedback according to a method which is partly new. One line feeds back the slow variations via an operational amplifier. The other is direct feedback of the rapid variations to the differential amplifier of the high tension generator. The first gives the generator a stability of $< 5 \cdot 10^{-6}$ for two hours, and since the recording of one electron line in these measurements takes less than 30 minutes this stability is adequate. In addition, it is possible to check and correct the voltage continuously with an accuracy of $1 \cdot 10^{-6}$. This makes it possible to determine the voltage to better than $5 \cdot 10^{-6}$. The other feedback reduces the ripple considerably, and the remainder is filtered off as much as possible. The ripple is approximately $50 \mu V$. However, this does not affect the measurements to any great extent, but only produces a broadening of the lines.

In order to check and measure the voltage in absolute volts, a very accurate potential divider and a series of absolute calibrated and temperature stabilized standard cells are used. The potential divider consists of thirty-four selected highly stable resistors from Julie Research Laboratories Inc. The relative stability of the resistors is better than $5 \cdot 10^{-6}$ per annum and their temperature coefficients are $< 2 \cdot 10^{-6}$ deg^{-1}. We have measured all the resistors in the potential divider relative to the first with an accuracy of $1 \cdot 10^{-6}$. We have also measured the temperature coefficients and found that the temperature coefficients are $< 1.5 \cdot 10^{-6}$ deg^{-1}.

The potential divider has been constructed so that a minimum of current leakage is obtained. It is particularly important that no corona discharges should take place from the resistors, since such discharges would cause an error in the measurement of the voltage.

Our standard cell unit consists of twelve standard cells. Four of these (manufactured by Weston Instrument Div.) have been calibrated at N.B.S. (National Bureau of Standards). The accuracy of the calibration is $0.6 \cdot 10^{-6}$ relative to their reference unit, which forms one of the world's four official voltage standards. (The transport from N.B.S. to our laboratory took place under special control, so that the cells were not subjected to any thermal or vibrational shocks). The standard cells are stored in a box which is temperature-stabilized to within a few thousandths of a degree. It is particularly important that there should be no temperature gradient between the two electrodes of a standard cell. They have therefore been placed in a special metal block, and any gradient over this can be measured. The remaining eight standard cells have been calibrated against the four which we obtained from N.B.S.

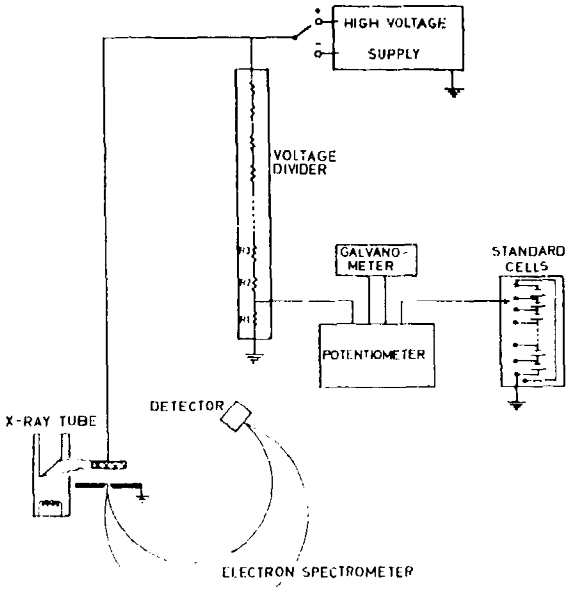

Fig. III:38. The principle of voltage measurement for "absolute" energy calibrations and h/e measurements.

In order to compare the voltage, as measured by the potential divider with the absolute voltage from the standard cells, a potentiometer is required which can measure μV; in this case we have used a Tinsley potentiometer type 5203A.

The principle of the measurement is shown in Fig. III:38.

III:9. Calculation of Electron Binding Energies

Self-consistent-field methods

The binding or ionization energy of an electron in a free atom or ion is defined as the work required to remove the electron from its orbit to infinity. By means of self-consistent-field (SCF) methods[149, 150] and modern data techniques this quantity can be calculated with good accuracy. In the solid state the corresponding

$$V(r_1) = -\frac{Z}{r_1} + \sum_j \left\{ \frac{1}{r_1}\int_0^{r_1} P_j(r_2)^2 dr_2 + \int_{r_1}^{\infty} \frac{1}{r_2} P_j(r_2)^2 dr_2 \right\} + V_{ex}(r_1). \tag{20}$$

There are two essential differences, however. Firstly, in the HFS method, an approximate correction for the exchange effect is included and, secondly, the potential is the same for all electrons, which makes the spin-orbitals exactly orthogonal. This method has been applied by Herman and Skillman[152] to all atomic ground states in the range $Z = 2$ to $Z = 103$.

The exchange correction (17) is derived by use of a free-electron gas model[151] and does not necessarily give the "best" central potential for a particular atom. It has been shown by one of us (I.L.) that the HFS wave functions can be considerably improved by a slight modification of the Slater correction[54, 55]

$$V'_{ex}(r_1) = -C\left[\frac{81}{32\pi^2}\right]^{1/3} r_1^{n/3-1} \varrho(r_1)^{m/3}. \tag{21}$$

C, n and m are here adjustable constants (equal to unity in the Slater approximation), which are determined by minimization of the total energy. It will be shown below, that the wave functions obtained in this way are remarkably close to those obtained by the much more involved HF method. It will also be shown that the parameters need not be determined separately for each element, degree of ionization, configuration etc., but the same combination may be used over large regions of the Periodic Table.

Recently, Kohn, Sham, and Tong [153, 154] and Cowan *et al.*[155] have suggested an exchange potential, equal to two-thirds of Slater's potential (i.e. $C = 2/3$, $n = m = 1$). This modification represents a definite improvement over the original Slater method, but the approximation is inferior to the optimized potential above (21). This will be illustrated for some typical cases below (Tables III:3 and III:4).

The optimized potential (21) has also a principle interest of its own, since it offers the best (central) approximation in terms of localized potential for the non-localized HF-potential. Localized potentials are particularly useful in solid-state application, where approximations of the Slater type are used extensively at present.

The HFS method can also be applied in relativistic SCF calculation, where the Schrödinger equation (12) is replaced by the corresponding Dirac equation. Such calculations have recently been performed by Liberman and Waber[156, 157] at Los Alamos Scientific Laboratory and by Nestor *et al.*[158] at Oak Ridge National Laboratory. We have applied the conventional as well as the modified HFS method for relativistic calculations on a large number of atoms, and some results are given in the tables below and in Appendix 2.[54, 55, 72, 73, 78]

Calculation of the total energy

The total electronic energy of an atom described by the wave function (15) is

$$E(\text{atom}) = \sum_i \langle i|f|i\rangle + \sum_{i<j} \langle ij|g|ij\rangle, \tag{22}$$

where

$$\langle i|f|i\rangle = \int \phi_i(1)^* \left[-\tfrac{1}{2}\Delta_1 - \frac{Z}{r_1} \right] \phi_i(1)\, dv_1$$

and

$$\langle ij|g|ij\rangle = \iint \phi_i(1)^* \phi_j(2)^* \frac{1}{r_{12}} \times [\phi_i(1)\phi_j(2) - \phi_j(1)\phi_i(2)]\, dv_1\, dv_2.$$

When the spin-orbitals are solutions to equations of the type (19), the total energy can be written

$$E(\text{atom}) = \sum_i \varepsilon_i + \sum_i \left\langle i \left| -\frac{Z}{r} - V(r) \right| i \right\rangle + \sum_{i<j} \langle ij|g|ij\rangle, \tag{23}$$

where ε_i is the eigenvalue in eq. (19)

$$\varepsilon_i = \langle i| -\tfrac{1}{2}\Delta + V(r)|i\rangle. \tag{24}$$

Now the last term in eq. (23) cancels approximately half the second term, and it is therefore convenient to write this equation

$$E(\text{atom}) = \sum_i \varepsilon_i + \frac{1}{2}\sum_i \left\langle i \left| -\frac{Z}{r} - V(r) \right| i \right\rangle + \frac{1}{2}\sum_i \delta\varepsilon_i \tag{25}$$

where $\delta\varepsilon_i$ is a small correction

$$\delta\varepsilon_i = \left\langle i \left| -\frac{Z}{r} - V(r) \right| i \right\rangle + \sum_j \langle ij|g|ij\rangle. \tag{26}$$

In earlier applications of the HFS method[152, 157] the correction term $\frac{1}{2}\sum_i \delta\varepsilon_i$ was omitted. As shown in Table III:3 the correction is comparatively large, considerably larger than the difference in the total energy between different approximations considered here. Therefore, any comparison between various methods is meaningless, unless the energy is calculated in the proper way.

The parameters in eq. (21) have been determined in a number of cases by minimizing the total energy calculated according to eq. (22). It has been found

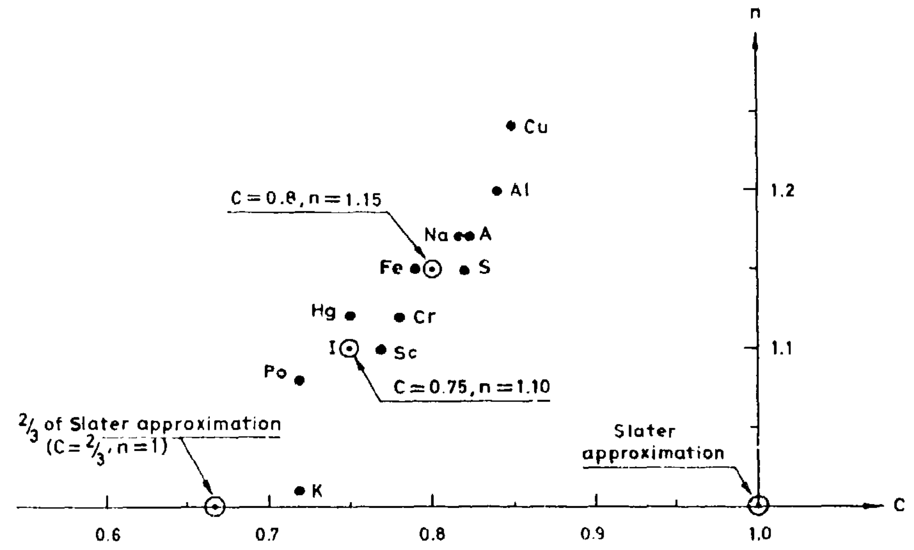

Fig. III:39. Parameters of optimized exchange potential. In all cases $m = 1$. Parameters defined in eq. (21).

that for practical purposes it is sufficient to vary two parameters. In a few cases all three parameters have been varied, but the improvement is very small. The optimum values are collected in Table III:2. Some values obtained in relativistic calculations for medium-heavy and heavy elements are also included in this table. When the values are plotted in a diagram (Fig. III:39), one sees that they fall in a narrow band in the C-n plane, i.e. there is a strong correlation between the two constants, as could be expected. The energy surface is such that the slope is very much smaller along this band than perpendicular to it. Therefore, the absolute values of the two parameters are not critical as long as a combination in this band is chosen. It is then possible to find parameter sets which to a good approximation yield the optimum exchange potential over large regions. The region Na($Z = 11$) to Kr ($Z = 36$) has been most extensively investigated, and it has been found that the combination

$$C = 0.80, \quad n = 1.15, \quad m = 1 \qquad (27\,\text{a})$$

is a good compromize, much better than the combination $C = 2/3$, $n = m = 1$. For heavier elements the investigation made so far is less complete, but the optimum values seem to be grouped around the combination

$$C = 0.75, \quad n = 1.10, \quad m = 1 \qquad (27\,\text{b})$$

(see Table III:2 and Fig. III:39). Further calculations are now in progress in this region.

Table III:2. Parameters of optimized potential.

(Parameters defined in eq. (21). In all cases $m = 1$)

Z	Atom	C	n
Non-relativistic			
11	Na	0.82	1.17
13	Al	0.84	1.20
16	S	0.82	1.15
18	A	0.82	1.17
19	K	0.72	1.01
21	Sc	0.77	1.10
24	Cr	0.78	1.12
26	Fe	0.79	1.15
29	Cu	0.85	1.24
Relativistic			
53	I	0.75	1.10
80	Hg	0.75	1 12
84	Po	0.72	1.08

Calculation of binding energies

When an electron is removed from its atomic orbit, the atom is (for some time) left in an excited state. The binding energy, which is the work done on the system, is then the difference in energy after and be-

Table III:3. Comparison between total atomic energies calculated by different methods. (Hartree units).

(Weighted average for the ground configuration)

Non-relativistic (The values in parenthesis are the differences to the HF value)

Atom	Conv. HFS uncorr. Snow *et al.*[157]	Conv. HFS corr. (eq. 25)	Modified HFS			HF Froese[161]
			$C = 2/3$ $n = m = 1$	$C = 0.8,$ $n = 1.15, m = 1$	optimized potential	
Na	160.582	161.781	161.837	161.846	161.846	161.860
	(1.278)	(0.079)	(0.023)	(0.014)	(0.014)	
Al	240.271	241.789	241.848	241.859	241.860	241.877
	(1.606)	(0.088)	(0.029)	(0.018)	(0.017)	
S	395.386	397.368	397.436	397.456	397.456	397.479
	(2.093)	(0.111)	(0.043	(0.023)	(0.023)	
A	524.404	526.689	526.771	526.792	526.793	526.818
	(2.414)	(0.129)	(0.047)	(0.026)	(0.025)	
K	596.571	599.027	599.140	599.142	599.144	599.165
	(2.594)	(0.138)	(0.025)	(0.023)	(0.021)	
Sc	756.842	759.580	759.701	759.709	759.709	759.737
	(2.895)	(0.157)	(0.036)	(0.028)	(0.028)	
Cr	1039.839	1042.986	1043.131	1043.143	1043.143	1043.177
	(3.338)	(0.191)	(0.046)	(0.034)	(0.034)	
Fe	1258.641	1262.076	1262.239	1262.254	1262.254	1262.292
	(3.651)	(0.216)	(0.053)	(0.038)	(0.038)	
Cu	1634.922	1638.705	1638.870	1638.912	1638.914	1638.953
	(4.031)	(0.248)	(0.083)	(0.041)	(0.039)	

Relativistic

Atom	Conv. HFS uncorr. Snow *et al.*[157]	Conv. HFS corr. (eq. 25)	Modified HFS	
			$C = 2/3$ $n = m = 1$	optimized potential
K	598.931	601.385	601.501	601.505
Cu	1649.474	1653.193	1653.197	1653.406
Ga	1938.158	1942.211	1942.507	
Br	2599.82	2604.73	2604.97	2604.99
Kr	2783.46			2788.82
In	5872.92		5880.48	5880.49
Te	6785.64	6793.41	6793.81	6793.82
I	7107.70	7115.51		7115.93
Xe	7438.66			7447.05
W	16148.06	16157.82	16158.47	16158.49
Pt	18427.46	18437.75	18438.43	18438.46
Hg	19642.10	19652.59	19653.31	19653.33[a]
Tl	20268.46	20279.08	20279.82	20279.83
Bi	21560.36			21571.94
Po	22226.25	22237.14	22237.91	22237.92
Rn	23598.97		23610.78	23610.79
U	28057.88		28069.70	28069.71
Am	30494.42			30506.05

fore the ionization process (the former, of course, before any transition takes place). If an SCF calculation has been performed for the ground state, the total energy can be calculated for that state as described above (eq. 22–26). The removal of one electron does not change the field inside the atom appreciably, and we can therefore to a first approximation assume that the spin-orbitals of the other electrons remain unchanged during the ionization process ("frozen" orbitals). The total energy of an atom with one electron hole (electron k missing) is then

$$E(\text{atom} - k) = \sum_{i \neq k} \langle i|f|i\rangle + \sum_{\substack{i<j \\ i,j \neq k}} \langle ij|g|ij\rangle, \tag{28}$$

and the binding energy

$$E_b(k) = E(\text{atom} - k) - E(\text{atom}) = -\langle k|f|k\rangle - \sum_j \langle kj|g|kj\rangle. \tag{29}$$

In the general HF scheme this quantity is (with re-

---

[a] Hartree–Fock value is 19653.70[162]. The difference between this value and the optimized HFS value is mainly due to numerical errors. A smaller integration step will increase the HFS values several tenths of a Hartree unit. However, all HFS calculations are made in exactly the same way and therefore the relative error is much smaller.

Table III : 4. Comparison between binding

Non-relativistic

Atom	Shell	Conv. HFS uncorr. Herman-Skillman[152]	Conv. HFS corr. (eq. 30)	Modified HFS $C = 2/3$ $n = m = 1$	Modified HFS $C = 0.8$, $n = 1.15$, $m = 1$	Modified HFS optimized potential	HF Froese[161]
Na	1*s*	1061.9	1087.8	1104.0	1100.4	1099.9	1101.5
	2*s*	64.3	71.5	77.4	75.9	75.7	76.1
	2*p*	36.5	36.6	42.8	41.2	41.0	41.3
	3*s*	5.14	4.79	5.03	4.97	4.96	4.96
S	1*s*	2447.5	2485.9	2508.0	2503.1	2501.9	2503.7
	2*s*	224.6	236.8	248.1	244.7	244.1	245.2
	2*p*	171.8	173.0	185.2	181.8	181.1	182.0
	3*s*	20.8	22.0	25.6	24.3	24.0	24.0
	3*p*	10.29	9.86	12.55	11.68	11.52	11.60
A	1*s*	3163.8	3207.5	3232.0	3226.7	3225.7	3227.5
	2*s*	311.1	324.9	338.3	334.5	334.0	335.3
	2*p*	247.7	249.4	263.8	259.9	259.3	260.4
	3*s*	28.7	31.8	36.5	34.9	34.6	34.8
	3*p*	14.5	13.4	17.4	16.1	15.9	16.1
Fe	1*s*	7017.8	7083.0	7117.4	7110.6	7111.5	7112.2
	2*s*	829.3	850.1	873.2	867.2	867.9	867.0
	2*p*	722.2	726.0	750.5	744.4	745.1	746.0
	3*s*	98.9	105.7	117.0	113.4	113.7	113.5
	3*p*	66.5	67.0	78.1	74.6	74.9	74.6
	3*d*	13.09	9.76	18.74	15.98	16.23	17.61
	4*s*	7.42	6.10	7.63	7.12	7.17	7.02
Cu	1*s*	8839.4	8912.1	8953.5	8945.1	8944.3	8946.7
	2*s*	1063.3	1086.6	1116.9	1109.0	1107.4	1110.7
	2*p*	939.0	943.9	975.6	967.7	966.2	969.2
	3*s*	117.5	126.2	142.0	137.0	135.7	135.4
	3*p*	77.6	80.6	96.0	91.1	89.8	90.5
	3*d*	10.11	5.24	17.60	13.85	12.79	13.41
	4*s*	6.93	5.83	7.43	6.87	6.67	6.44

versed sign) according to Koopmans' theorem[159] equal to the one-electron eigenvalue ε_k However, this is not the case in other approximations such as HFS. There the binding energy becomes[54,55]

$$E_b(k) = -\varepsilon_k - \delta\varepsilon_k, \tag{30}$$

where $\delta\varepsilon_k$ is the correction defined in eq. 26. In previous applications of the HFS method, e.g. by Herman and Skillman[152] and relativistically by Liberman *et al.*[156], the correction due to the nonvalidity of Koopmans' theorem was not considered. We have found that the agreement with the more accurate HF values is considerably improved when this correction is applied. This is true non-relativistically as well as relativistically as illustrated in Table III:4 above, where the binding energies obtained by various methods are compared for a few typical cases.[72,73,78] The very good agreement between the optimized HFS and the HF methods for Hg is quite remarkable.

So far it has been assumed that the spin-orbitals are unchanged by the ionization process. This can be assumed to be a good approximation, if the process is very rapid compared to the time required for the spin-orbitals to find their equilibrium in the new atomic field (relaxation time). In the other case, where the relaxation time is comparatively short, another method should be used. Then the energy of the ionized state should be calculated by use of spin-orbitals in equilibrium, i.e. a separate SCF calculation for the ionized state. We shall here refer to this more elaborate method as method B and the conventional method with atomic ("frozen") spin-orbitals (eq. 29) as method energies calculated by different methods (eV).

		Relativistic				
		Conv. HFS uncorr. Liberman *et al.*[154]	Conv. HFS corr. (eq. 30)	Modified HFS		HF Coulthard[162]
Atom	Shell			$C = 2/3$ n $m = 1$	optimized potential	
Hg	1*s* 1/2	83403	83617	83707	83704	83704
	2*s* 1/2	14834	14912	14984	14980	14980
	2*p* 1/2	14255	14265	14340	14336	14336
	2*p* 3/2	12286	12316	12389	12384	12384
	3*s* 1/2	3539	3576	3628	3623	3624
	3*p* 1/2	3275	3287	3342	3336	3337
	3*p* 3/2	2837	2852	2904	2898	2899
	3*d* 3/2	2395	2383	2438	2433	2433
	3*d* 5/2	2300	2291	2345	2340	2341
	4*s* 1/2	788.3	806.5	838.7	834.3	834.4
	4*p* 1/2	673.6	682.8	715.2	710.8	710.9
	4*p* 3/2	567.1	577.7	607.9	603.7	603.7
	4*d* 3/2	378.2	376.7	406.8	402.6	402.6
	4*d* 5/2	358.1	357.1	286.6	382.4	382.3
	4*f* 5/2	113.3	97.2	125.9	121.8	121.6
	4*f* 7/2	108.8	93.2	121.6	117.4	117.2
	5*s* 1/2	125.9	127.5	142.2	139.5	138.9
	5*p* 1/2	87.4	85.6	99.3	96.7	96.3
	5*p* 3/2	68.2	68.0	80.1	77.7	77.3
	5*d* 3/2	15.88	10.95	19.68	17.94	17.69
	5*d* 5/2	13.82	9.35	17.52	15.90	15.63
	6*s* 1/2	9.49	7.00	9.78	9.25	8.93

A. Previously method A has been used almost exclusively, but we have found that method B gives systematically better agreement with experiments as far as inner electrons are concerned.[54,55,72,73,78] For outer electrons in heavy elements method A seems to yield somewhat better results.[72,73,78] This tendency is quite natural from a superficial point of view, since the relaxation time should be much shorter for inner electrons due to their much higher "revolution frequency". However, further calculations are here required before any definite conclusions can be drawn.

The difference between the two methods of calculating the binding energy is illustrated in a simple way in Fig. III:40, where the energy is schematically drawn as a function of a single-parameter wave function. The energy minimum represents the "true" wave function, which in this context can be assumed to be the HF function. When atomic orbitals are used for the excited state, the energy minimum is not obtained. This means that if the orbitals are allowed to relax, the energy is reduced. Method A should therefore give larger binding energy than method B, which has been found to be the case in all numerical examples (see also Fig. III:41). It is furthermore seen from Fig. III:40 that method A is quite sensitive to small changes in the wave function, unlike method B. This property has also been verified in the numerical calculations, and some results for Hg are shown in Table III:5. Therefore, in calculating the binding energies for inner electrons by use of method B it is not important that the very best wave function is used. The HFS and particularly the optimized HFS method is quite sufficient for practical purposes. In other words, one obtains better results by using a simpler wave function and the more elaborate method B than by using a more exact wave function and the approximative method A. This fact does not seem to have been generally appreciated previously.

Comparison with experiments

In Appendix 2, a number of calculated binding energies are compared with the corresponding experi-

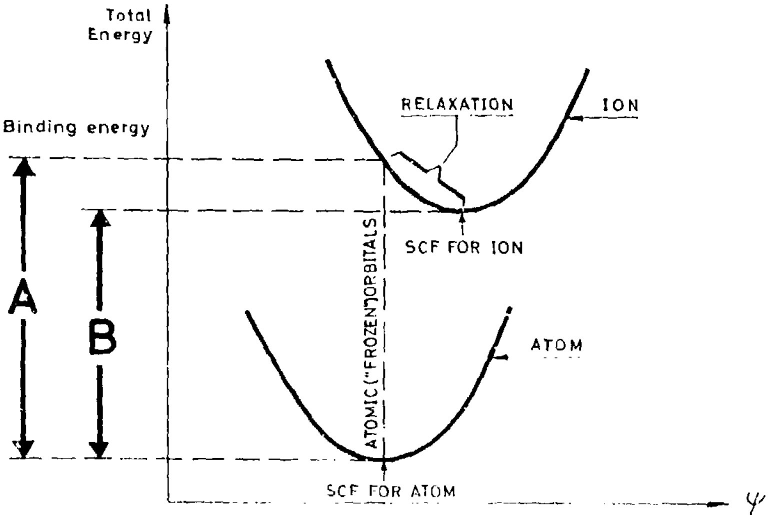

Fig. III:40. Comparison of the two methods A and B for calculating electron binding energies.

mental values. All theoretical values are obtained by the previously described relativistic Hartree-Fock-Slater method with optimized exchange correction. Most of the experimental determinations have been made on solids and the binding energy is referred to the Fermi level. Since the theoretical calculations are made on free atoms, the zero level of the energy scale is at a finite distance. Therefore, the experimental results have been corrected for the work function.

From the comparison in Appendix 2, some systematic observations can be made. Method A ("frozen" orbitals for the ion) gives in most cases, particularly for inner shells, binding energies which are significantly too large. The results in method B (self-consistent orbitals for the ion) are, as previously noted, consistently lower and for inner shells in much better agreement with experiments. For light elements, up to copper, say, the discrepancy between theory and experiment is for the K shell at most about 15 eV and considerably less for other shells. For heavier elements, on the other hand, the discrepancy becomes relatively larger, as much as 500 eV or 0.6 % for the K shell in Hg.

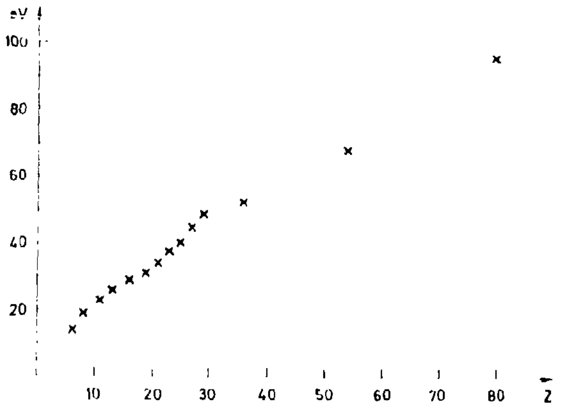

Fig. III:41. The difference in binding energy for the 1*s* electron of some elements calculated according to the methods A and B, respectively.

We shall now try to analyze the possible explanations for the residual discrepancy between the experimental and theoretical binding energies. As previously mentioned method B is very insensitive to changes in the spin-orbitals. Therefore, the difference between the optimized HFS method used here and the more accurate HF method is quite negligible, much smaller than the numerical uncertainties. There are then two possible sources of errors, namely

(a) approximations in the conventional HF method for free atoms,

(b) solid-state effects.

Table III : 5. Binding energy for the 1*s* electron in Hg (eV).

	Method A	Method B
Conventional HFS	83617	83610.4
Optimized HFS	83704	83610.7
Difference	97	0.3

The approximations in the conventional HF method are essentially the following

(1) the electrons are assumed to move independently of each other, i.e. correlations effects are neglected

(2) all electrons in the same shell (same *nl* values) are assumed to have the same radial distribution.

The correlation effects could be expected to increase with the number of electrons and therefore one would expect the energy of the atomic state to be reduced more than the energy of the ionic one, when correlation is considered. This would consequently enhance the discrepancy between theory and experiments.

For Hg the atomic state contains only closed shells, and hence there is no difference between the general and the restricted HF methods. For the ionic state (e.g. with a *K* hole) on the other hand, there is an appreciable deviation from symmetry. Here the general or unrestricted HF method would lead to different exchange potentials and consequently to different radial distributions for electrons with "spin-up" and "spin-down", respectively. This would reduce the energy of the ionic state and therefore also the binding energy. Whether this effect could account for most of the discrepancy of 500 eV between theory and experiment remains uncertain without quantitative calculations. Conolly[160] has recently suggested an "unrestricted Hartree Fock-Slater" method, which seems appropriate in this case. Calculations of this type for Hg and other elements are now in progress.

For lighter elements there is probably a competition between the above-mentioned effect due to limitations of the Hartree Fock method and solid-state effects. In a solid the spin-orbitals differ from those in a free atom or ion due to perturbation from the neighbouring atoms or ions. The effect on the inner electrons could probably be estimated by use of a perturbing potential, which represents the crystal field. Calculations of this kind are also in progress.

Comparison between theoretical and experimental binding energies for the noble gases is of special interest, since these experiments are performed on essentially free atoms. As seen in Appendix 2, the agreement between theory and experiment is not considerably better for these gases than for surrounding elements. From this comparison one can estimate the solid-state effects to be less than 5–10 eV for the inner shells in light and medium heavy elements.

For outer electrons, data are in some cases available from ESCA or X-ray measurements on solids as well as optical measurements on free atoms. (In Appendix 2 the optical results are marked with +). The difference is usually of the order of 3–5 eV, which gives an idea of the solid-state effect in the outer shells. In most cases where such a comparison can be made the optical data agree better with the calculated values than do the data obtained from solid sources. It should be noted that the measurements on solids are in Appendix 2 corrected for the work function and thus referred to the same zero level as the optical results. Therefore, the difference should, besides experimental uncertainties and uncertainties in the work function, be due mainly to deformation of the atomic orbitals in the solid state or to relaxation effects.

IV. BAND STRUCTURE OF SOLIDS

Over the last few years, much information on the band structure of metals has been obtained from photoemission measurements[163] and from the study of optical properties in the region extending from the infrared to the ultraviolet region.[164] Progress in the field has been facilitated by the rapidly growing computer techniques, and both theory and experiment have developed at a rapid pace[165–167].

Special techniques have been developed for the experimental study of the Fermi surface of metals and degenerate semiconductors. The most powerful of these methods are based on de Haas van Alphen effect,[168] magneto-acoustic resonance[169] and cyclotron resonance.[170] However, the nature of the electronic states throughout the bands and in those deeper levels that retain their atomic character cannot be evaluated by these techniques.

The photon energies of X-ray transitions are high enough to permit a study of the entire band structure, and X-rays have been used for both emission and absorption solid-state spectroscopy. X-ray emission band spectra reflect the occupied electronic states and X-ray absorption spectra reflect the empty states. A prerequisite for obtaining from X-ray spectra any detailed information on the density of states throughout the conduction and valence bands is a small inherent width of the inner level in the X-ray transition. This means that one usually works in the soft X-ray region, i.e. with wavelengths larger than 10 Å, with an associated increase in the experimental difficulties. Nevertheless, X-ray spectroscopy has been used with considerable success for band structure studies.[117,171]

Electromagnetic radiation interacts with all bound electrons that have binding energies less than the photon energy to give photoelectric effect. Upon irradiation with monochromatic X-rays, a solid sample

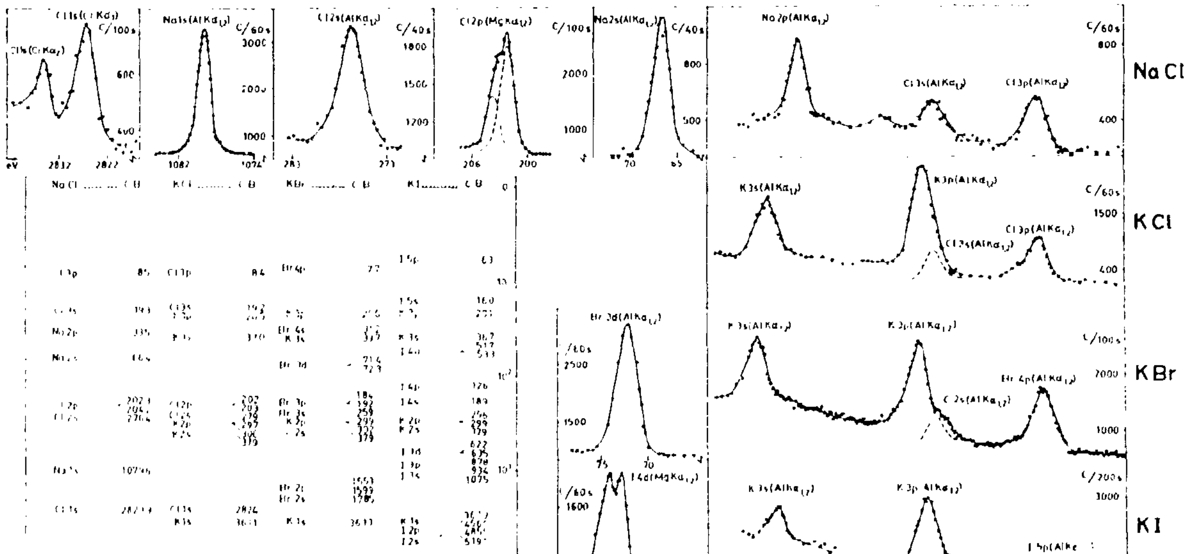

Fig. IV:1. Electron spectra of NaCl, KCl, KBr and KI. For sodium chloride the entire electron spectrum was recorded from the Cl1s level to the band structure. All levels between 100 eV binding energy and the Fermi level were recorded in KCl, KBr and KI. Complete level diagrams of the four alkaline halides are given in the figure.

emits photoelectrons with an energy distribution that reveals not only the atomic levels but also the solid state band structure below the Fermi level.

It is therefore also of interest to delineate ESCA spectra in the region immediately below the energy of the exciting X-radiation. We have recently made preliminary studies on some alkali halides (NaCl, KCl, KBr, and KI) from this angle.[85] Single crystals were used and clean surfaces, obtained by splitting the crystals, were exposed to the X-radiation. Electron spectra were recorded from which electron binding energies could be determined for all filled levels in sodium chloride. In KCl, KBr, and KI, all levels down to 100 eV binding energy were recorded. The electron spectra obtained in these measurements are shown in Fig. IV:1. All the levels shown in these spectra can be reached by Mg$K\alpha$ and Al$K\alpha$ radiations, with the exception of the chlorine K level for which Cr$K\alpha$ was utilized. With Mg$K\alpha$ as the X-ray probe the spin-doublet $L_{II,III}$ ($2p_{1/2,3/2}$) in chlorine and $N_{IV,V}$($4d_{3/2,5/2}$ in iodine could be partly resolved in the electron spectra. Of particular interest in the present context is that even the most peripheral electronic states can be studied without difficulty. Thus, the valence bands of all four ionic crystals are easily identified in the electron spectra.

The valence band of each ionic crystal was utilized for the energy calibration of the entire spectrum. Zero binding energy was then defined as the energy at the bottom of the conduction band. The high-energy side of the valence band, corrected for estimated instrumental broadening and inherent width of the X-radiation, was assigned an energy equal to the gap width. The energy of the forbidden gap was taken from the literature.[289]

Complete diagrams of the levels for the four alkaline halides are given in Fig. IV:1. Of the fifty-nine energy levels, about one-third could be determined from the electron spectra shown in the figure. Many have previously been measured by ESCA, and the remaining ones were calculated from X-ray emission data. None of these should be difficult to measure with high precision in electron spectra, with the possible exception of the iodine $1s$ level which would require an X-radiation with shorter wavelength than we have used up to now.

Knowledge of the exact structure of the levels in ionic crystals is essential for the study of different electronic processes which occur when the crystals are irradiated with monochromatic ultraviolet radiation or X-radiation. Many attempts have been made to establish the energy levels from X-ray emission and absorption spectra,[130-172] but there is a great need for other techniques. The electron spectra shown in Fig. IV:1 indicate that ESCA may be another valuable tool in the field. For example, ESCA may serve as a guide for the interpretation of X-ray absorption spectra which often have a complicated structure.

In Chapter I, we showed an ESCA spectrum of the outer levels of metallic gold (Fig. I:7). Gold belongs to group Ib in the Periodic System. There are two more elements in this sub-group, namely copper and silver. The electron configurations of the group Ib elements are:

Cu: $\ldots 3s^2 3p^6 3d^{10} 4s$
Ag: $\ldots 4s^2 4p^6 4d^{10} 4f^0 5s$
Au: $\ldots 4f^{14} 5s^2 5p^6 5d^{10} 6s$

All three elements are metals with d and s symmetry of the conduction band electrons. Fig. IV:2 and Fig. IV:3 show the outer levels of copper and silver, respectively, recorded with Al$K\alpha$ radiation. There are no sharp and intense f electron lines in these spectra, as was the case in the gold spectrum of Fig. I:7 (the (the $N_{VI,VII}$ lines). Instead we observe the broader s and p electron distributions. The height of these relative to the distribution of conduction electrons is smaller in the silver spectrum. In gold only the $5p_{3/2}$ distribution (O_{III}) was observed and was of even less relative intensity. The conduction band in copper is obtained as a line of half-width 2.5 eV and the conduction band of silver as a line with a half-width of 3.6 eV. The conduction band of gold that was shown in Fig. I:7 (recorded with Mg$K\alpha$) has a doublet structure with a total half-width of 5.5 eV and a distance of 2.3 eV between the peaks. This structure is due to spin-orbit interaction in the d band.

The large width observed for the s and p subshells in all three noble metals compared to the $4f$ levels of gold cannot be ascribed to band broadening. A more reasonable explanation would be that the inherent widths are increased due to transitions of the Coster Kronig type.[129] Such transitions cannot occur from the $4f$ levels of gold.

Alloys of silver and gold may be expected to have

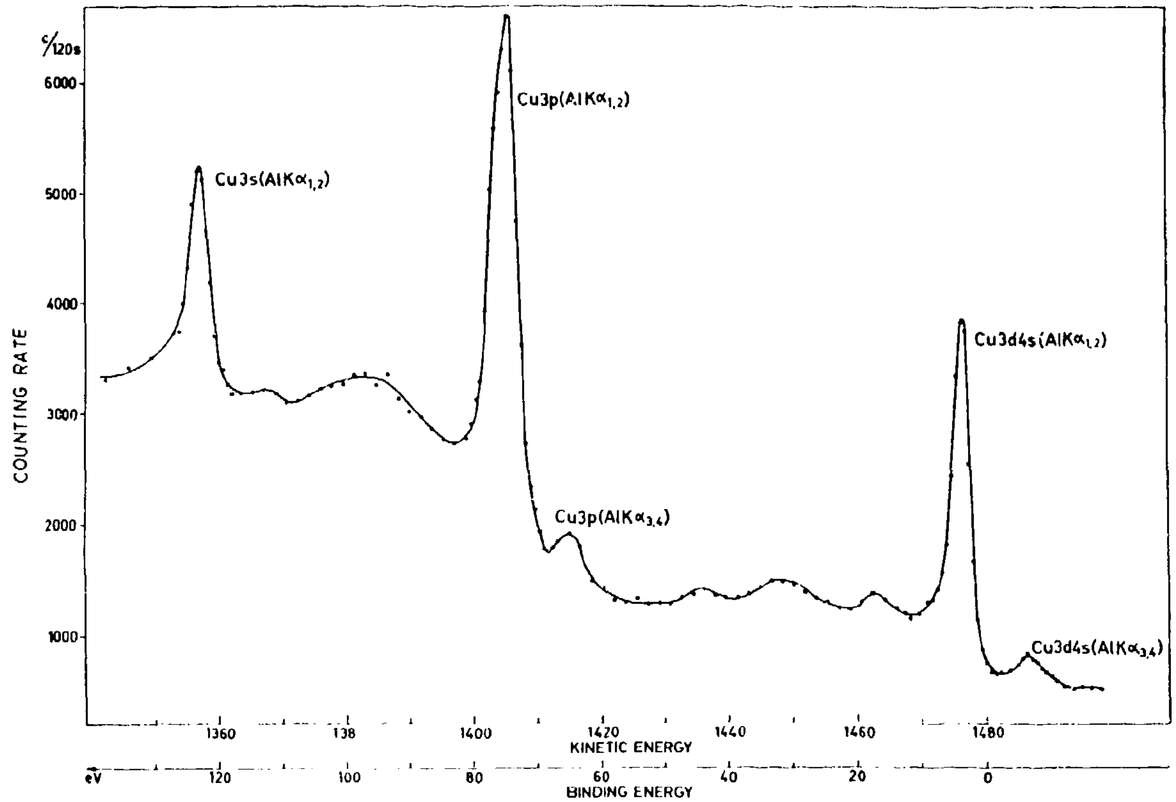

Fig. IV:2. Electron spectrum of copper recorded with aluminum *Kα* radiation. The 3*s* level and the 3*p* spin-doublet level are shown. The conduction band (3*d*4*s*) is obtained as one line of half width 2.5 eV.

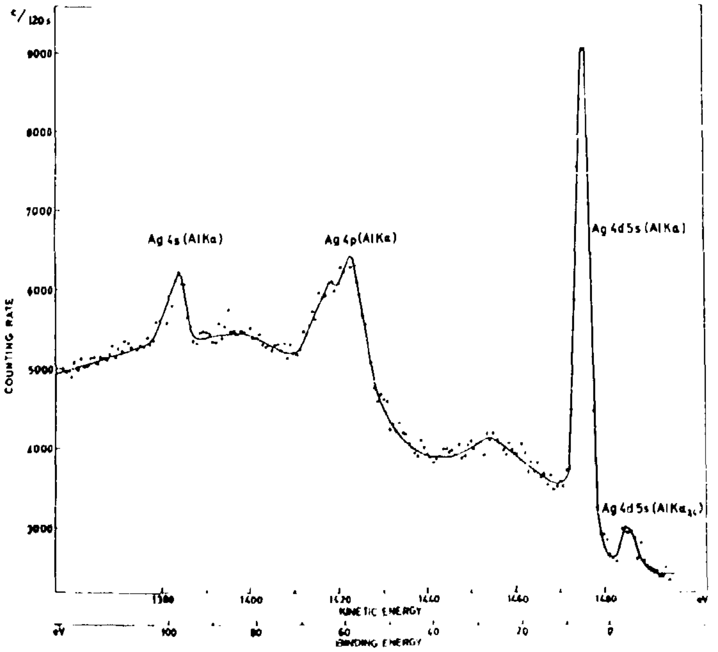

Fig. IV:3. Electron spectrum of silver recorded with aluminum *Kα* radiation. The distributions of 4*s* and 4*p* electrons are broad. The conduction band (4*d*5*s*) appears as one peak with a half width of 3.6 eV.

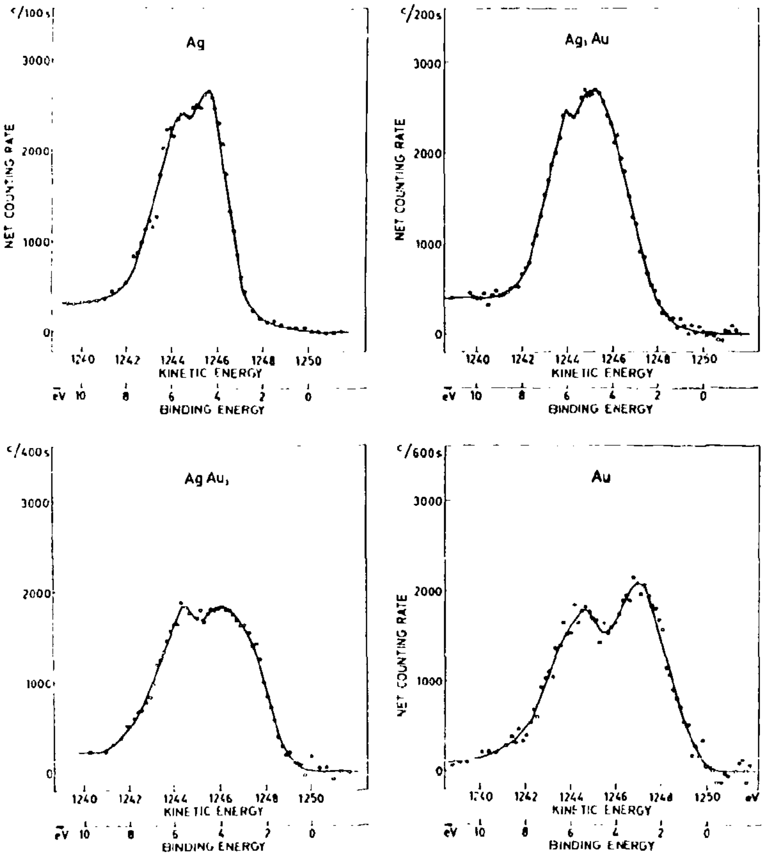

Fig. IV:4. Conduction band spectra of metallic silver, the three alloys Ag_3Au, AgAu, $AgAu_3$, and metallic gold recorded with magnesium $K\alpha$ radiation. The widths of the distributions change gradually from metallic silver with two unresolved peaks of total half width 3.6 eV to the broad distribution of metallic gold with two nearly resolved peaks of total half width 5.5 eV and a distance of 2.3 eV between the peaks.

conduction band distributions that are intermediate between those of the pure metals. Gold-silver alloys in the proportions 3:1, 1:1, and 1:3 were prepared by heating the metals in an atmosphere of noble gas and carefully rocking the crucible containing the melt to obtain a homogeneous alloy. Foils were made of the alloys and the electron spectra of the conduction bands were recorded from these and from foils made from the pure metals. The five conduction band spectra obtained in this way are shown in Fig. IV:4. The spectra were recorded with $MgK\alpha$ radiation and the resolution was sufficient to reveal the substructure in the conduction band of all five samples. It is found that the band structures of Ag, Ag_3Au, AgAu, $AgAu_3$, and Au change gradually from the narrow distribution of metallic silver to the comparatively broad distribution of metallic gold. The density of *d* symmetry states in the conduction band is much higher than the density of *s* symmetry states and the photoelectric cross section is larger for the *d* electrons. The shape of the conduction band spectra are therefore determined mainly by the *d* states. However, the existence of states above the *d* part of the band is indicated by the position of the zero point for the binding energy, which corresponds to the Fermi level (Section II:3). In metallic silver, the Fermi level is situated several eV above the *d* part of the conduction band as can be seen in Fig. IV:4.

V. ELECTRON SPECTROSCOPY FOR CHEMICAL ANALYSIS

V:1. Chemical Shifts in Electron Spectra

In Chapter III, we discussed several examples of electron spectra that can be utilized for a study of the electronic structure of atoms, in particular for precision measurements of binding energies of the core electrons. However, much evidence has been obtained from ESCA spectra that these energies are not a property solely of the atom but also of its chemical environment, i.e. of the molecular structure. The change in the charge distribution in the valence shell which occurs when an atom changes its valence state is relayed to all the core electrons and revealed in the electron spectra. In quoting electron binding energies of an element to within a fraction of an eV, which is possible from ESCA measurements, one therefore has to specify the chemical compound in which the measurements were made. This is illustrated by the three electron spectra of beryllium,[84] shown in Fig. V:1. Metallic beryllium was evaporated at a pressure of 10^{-5} torr onto an aluminum backing. The sample was irradiated by Al$K\alpha$ and photo-emitted $1s$ electrons were studied in order to determine the $1s$ electron binding energy in beryllium. The spectrum in Fig. V:1a was then obtained which had two lines of about the same intensity, and with an energy separation of (2.9 ± 0.1) eV. The most plausible explanation for the existence of two lines instead of one is that the metal had been oxidized to some extent and that the two $1s$ lines in the electron spectrum correspond to beryllium in metallic form and in oxide form, respectively. To check this explanation, the sample was heated in air until it could be assumed that all the beryllium had become oxidized, and its electron spectrum was again recorded. This time only one $1s$ line was obtained as can be seen in Fig. V:1b. Its position coincides with the line of lower kinetic energy in Fig. V:1a. This line should then correspond to beryllium in oxide form. Further evidence was obtained by making a vacuum evaporated beryllium sample under the action of zirconium as a reducing agent. This sample yielded the electron spectrum of Fig. V:1c. Although both lines are seen in this spectrum, the oxide line is much reduced in intensity. In view of these experiments it seems safe to ascribe to metallic beryllium the line of higher kinetic energy and to beryllium as its oxide the line of lower kinetic energy. This means that the higher state of oxidation corresponds to a 2.9 eV higher binding energy for the beryllium $1s$ core electrons.

If beryllium is instead bound to fluorine as in BeF_2 it is brought to a still higher state of oxidation, although represented by the same oxidation number (2+) as in BeO. This is due to the extremely high electronegativity of fluorine (see Appendix 13). One may thus expect the electron lines from fluorine in BeF_2 to be shifted even more than in BeO. This is exemplified in Fig. V:2 which shows the experimental line positions for metallic beryllium, beryllium oxide, and beryllium fluoride. As will be discussed later the binding energies of the core electrons generally increase with increasing state of oxidation.

Chemical effects can be seen not only in electron and X-ray spectra from the atomic core but also in the decay of radioactive atomic nuclei. A change of valence state has an exceedingly small effect on nuclear transitions but can be observed as an isomeric shift in Mössbauer spectra or as a small change in the decay constant. The change of the atomic $1s$ wave function at the nucleus due to oxidation of beryllium has been observed in this latter way.[173]

The fact that the electron spectrum of an element is modified by the nature of the attached atoms in the molecular structure has obvious potential applications in a more refined qualitative analysis. We first observed chemical shifts in the electron spectra of copper in metallic form and in its oxides[11] and later also in tin and cadmium.[17] As the experimental techniques were developed interest became focussed on elements of importance in organic chemistry. Special importance is then attached to the element carbon and we have recently shown that the electron spectra of carbon are indeed modified by the molecular environment.[75]

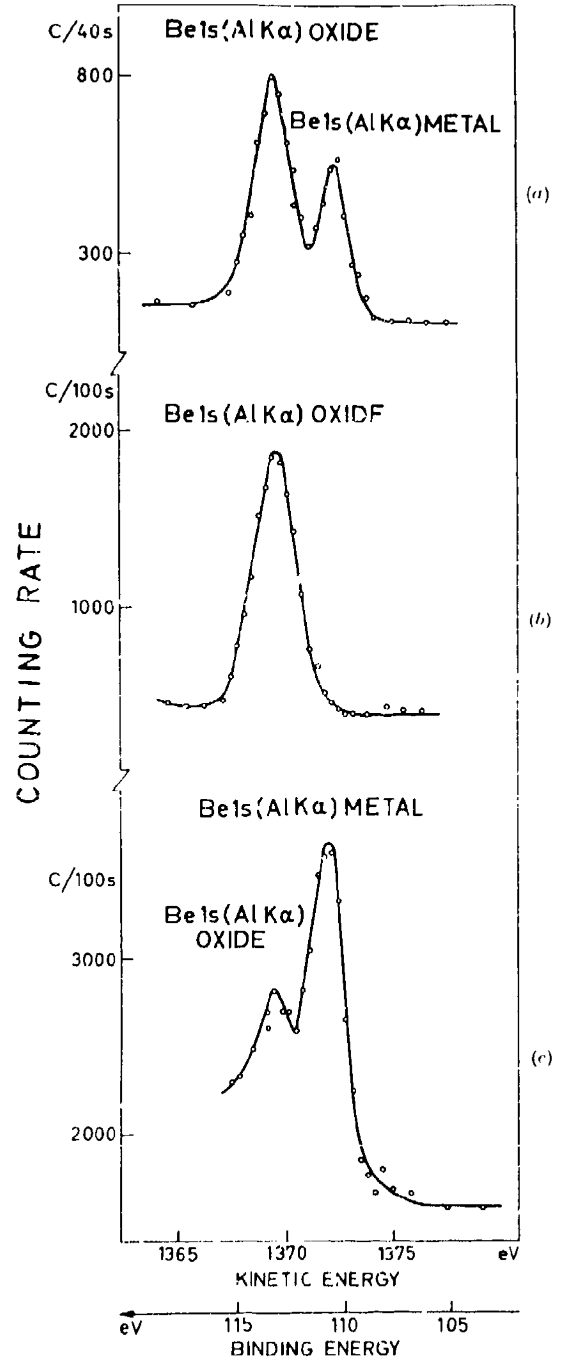

Fig. V:1. Electron spectra of beryllium.

(*a*) Spectrum obtained from vacuum evaporated metallic beryllium.

(*b*) Spectrum obtained from the same sample after being being heated in air.

(*c*) Spectrum obtained from vacuum evaporated beryllium under the action of zirconium as a reducing agent.

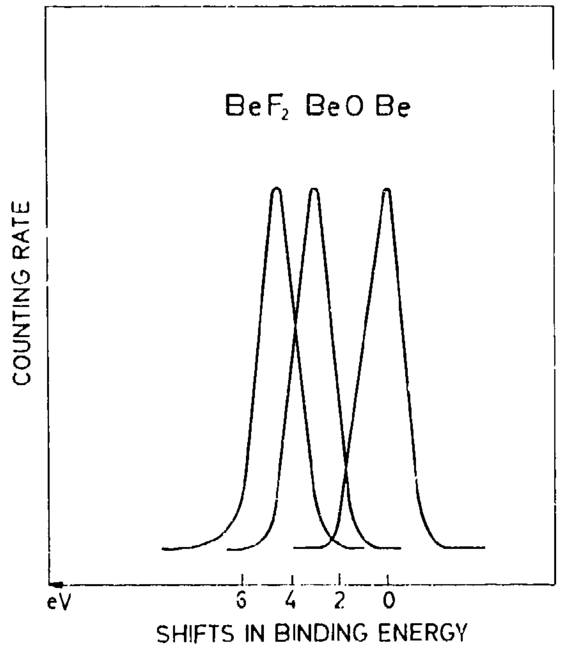

Fig. V:2. Line positions of metallic beryllium, beryllium oxide and beryllium fluoride illustrating the shift in the 1*s* level energy of beryllium between the compounds.

Fig. V:3 shows electron spectra from the three aromatic compounds 1,2,4,5-benzenetetracarboxylic acid, 1,2-benzenedicarboxylic acid, and sodium benzoate. All the substances contain six carbon atoms in a benzene ring, which is substituted with a varying number of carboxyl carbons. Photo- and Auger electron lines from the constituent elements sodium, oxygen, and carbon are seen in the spectra. The counting rates are high although the elements all have low atomic numbers and therefore small photoelectric cross sections. The line widths are essentially the inherent widths of the atomic levels. The most striking observation is that carbon gives two well separated lines. The relative intensities of the lines are about 4:6, 2:6, and 1:6, and it is therefore natural to associate the two lines with the carboxyl carbon and the benzene carbon, respectively. A small excess of intensity in the benzene

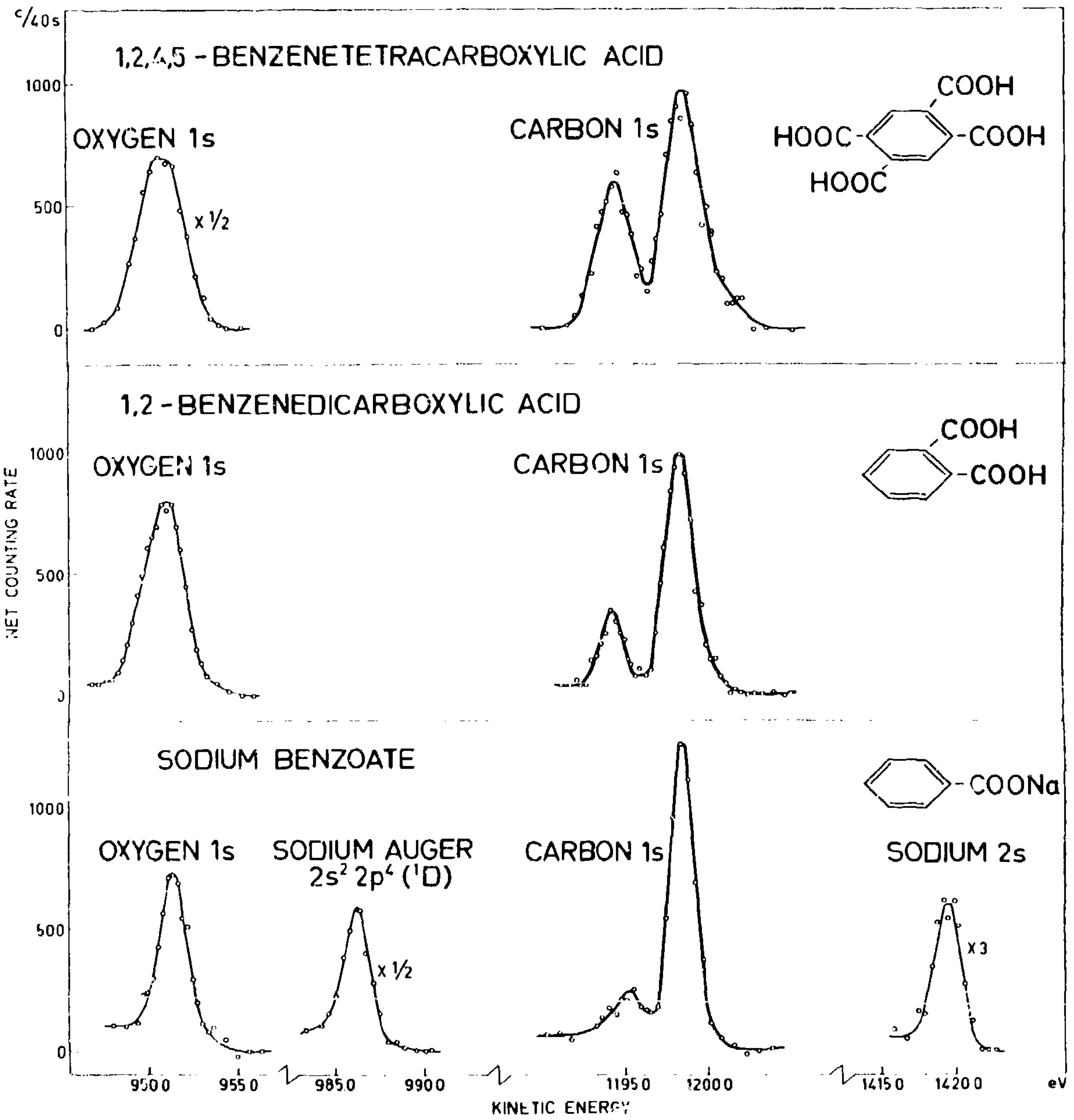

Fig. V:3. Electron spectra from 1,2,4,5-benzenetetracarboxylic acid, 1,2-benzenedicarboxylic acid and sodium benzoate. Two well separated carbon lines are seen in each spectrum corresponding to benzene carbon and carboxyl carbon, respectively.

carbon line is accounted for by traces of pump oil and other impurities containing carbon that are present in the moderate vacuum at which the recordings were made.

The fact that the carboxyl line has lower energy in the electron spectrum is consistent with the differences in electronegativity between the elements in question, see Section V:4 and Appendices 13 and 14. The benzene carbons are bound to carbon and hydrogen and the carboxyl carbons are bound to carbon and oxygen.

Oxygen has an electronegativity that is considerably higher than the electronegativities of carbon and hydrogen. Therefore there will be less negative charge within a certain atomic distance around the carbon nucleus in a carboxyl group than within the same distance around a carbon nucleus in the benzene ring. Electrostatic shielding of the 1*s* electron is therefore smaller for the carboxyl carbon and the binding energy of the 1*s* electrons becomes larger, as seen in the electron spectrum.

Fig. V:4 shows carbon 1*s* electron spectra from the sodium salts of the first four fatty acids. In sodium formiate one only sees the carboxyl carbon line after the line from the carbon containing layer that develops on the surface has been deducted. In the higher homologues, which contain additional CH_2 groups a carbon line, which is shifted 3.5 eV towards higher kinetic energy appears with increasing intensity. The increase in intensity corresponds to the number of additional CH_2 groups. The fact that the carbon containing surface layer can be corrected for indicates that it is very thin and consists of only a few molecular layers. This will be discussed further in Sections V:6 and V:7 where it will also be shown that a monomolecular layer of stearic acid, which is number eighteen in the homologous series of fatty acids, absorbs a large fraction of photoelectrons produced by aluminum radiation.

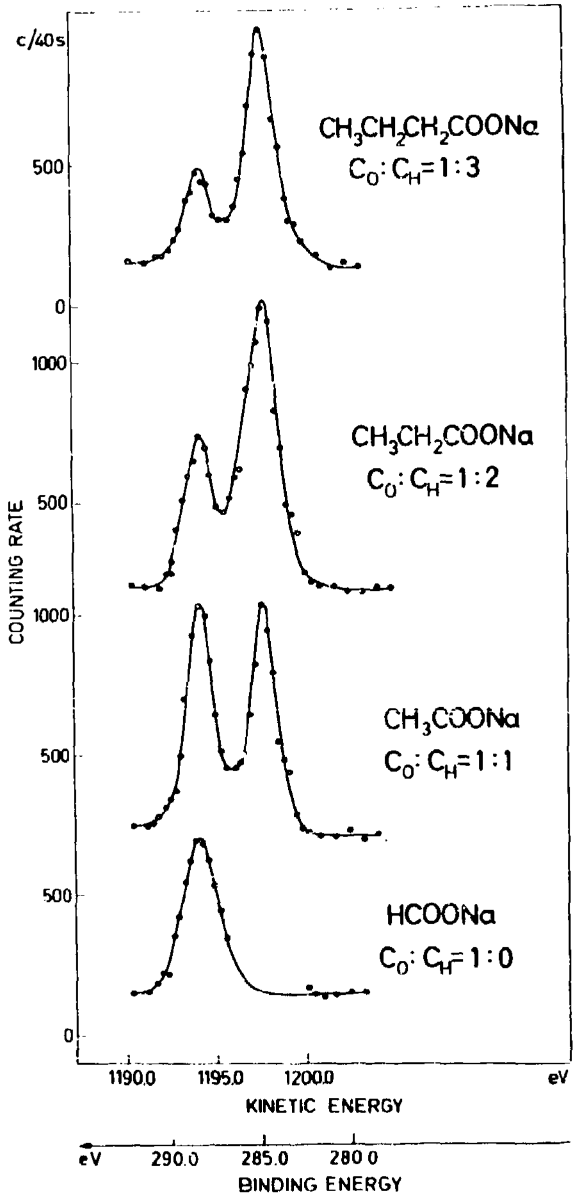

Fig. V:4. Electron lines from carbon in the sodium salts of the first four fatty acids. The carbon lines correspond to hydrocarbon and carboxyl carbon, respectively.

V:2. A Simple Model for Interpreting ESCA Shifts

It has already been indicated that the chemical shifts of the binding energies of core electrons can be explained by the redistribution of electric charge that occurs in peripheral orbitals when a chemical bond is formed. The observed chemical shifts can be interpreted in terms of an ionic model[80] which may be described as follows.

The atomic valence electron orbitals define a spherical "valence shell" of electric charge and the inner electrons, for instance the 1*s* electrons, reside inside this charged shell. If charge is added to or removed from the valence shell, as is the case when the atom is bound to other atoms in a molecule or a crystal, the electrical potential inside the valence shell is changed. If, for instance, q electronic charges are removed from the valence shell and brought to infinite distance the potential energy of the inner electrons is lowered by the amount (in atomic units $m = e = \hbar = 4\pi\varepsilon_0 = 1$)

$$\Delta E = \frac{1}{r} q \qquad (1)$$

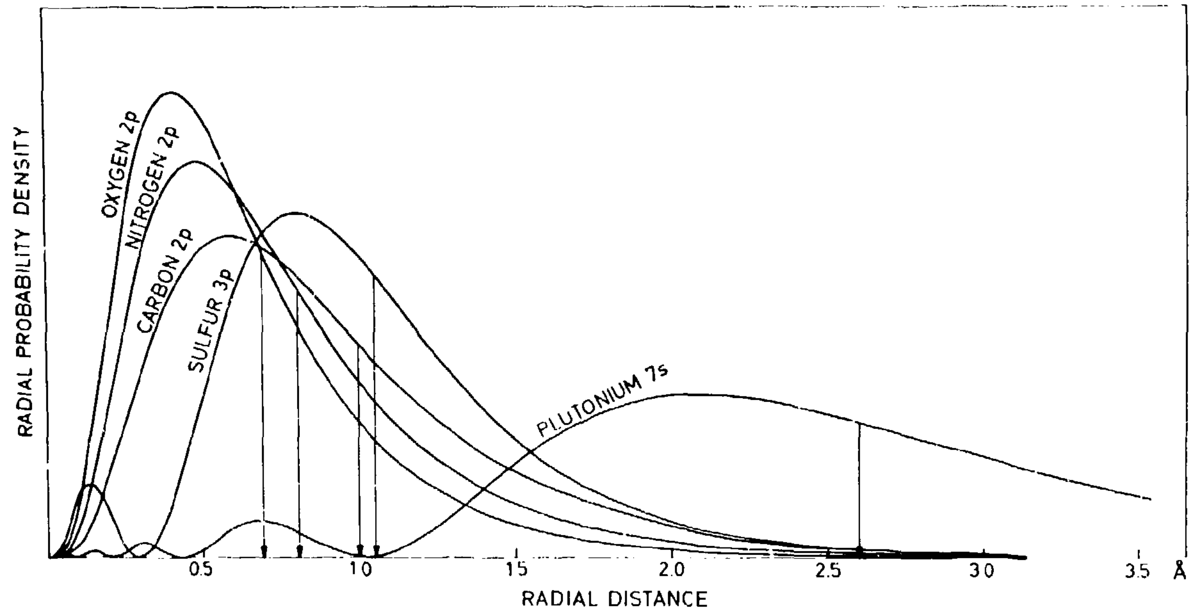

Fig. V:5. Radial probability distribution of valence electrons in carbon ($Z = 6$) nitrogen ($Z = 7$), oxygen ($Z = 8$), sulfur ($Z = 16$), and plutonium ($Z = 94$). Arrows indicate mean radii.

where r is the radius of the valence shell. The binding energy of an inner electron, i.e. the energy required to transfer it to infinite distance from the atom is then increased by the same amount. To calculate the energy shift according to equation (1) we must find a value for the valence shell radius r. Ionic radii have been tabulated for many elements[174] but these represent the distances at which the ions come into contact, i.e. the distances at which the wave functions of neighbouring atoms start to overlap, and the repulsive forces become exceedingly high. As a more realistic value for the valence shell radius in our model we could choose the mean radius for the valence electron orbitals according to the wave functions of atomic electrons. Fig. V:5 shows the radial probability distribution of valence electrons for the elements carbon ($Z = 6$), nitrogen ($Z = 7$), oxygen ($Z = 8$), sulfur ($Z = 16$) and plutonium ($Z = 94$). The mean radius is in all cases of the order of 1 Å (1 Å ≈ 2 a.u.) and the corresponding shift in binding energy of inner electrons per unit charge removed from the valence shell becomes $\Delta E = \frac{1}{2}$ a.u. ≈ 14 eV. The observed shifts are all smaller than this and therefore correspond to a charge transfer of less than one unit in the valence shell. Used so far, in its simplest form, the model may be described as a "free-ion" model.

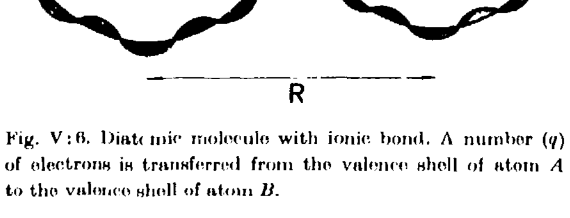

Fig. V:6. Diatomic molecule with ionic bond. A number (q) of electrons is transferred from the valence shell of atom A to the valence shell of atom B.

We can improve the free-ion model to take into account the fact that valence electrons are not transferred to or from infinite distance when a chemical bond is established. In an ionic bond between two atoms A and B, electrons are transferred from the valence shell of the atom A to the valence shell of the atom B, see Fig V:6. If the internuclear distance for

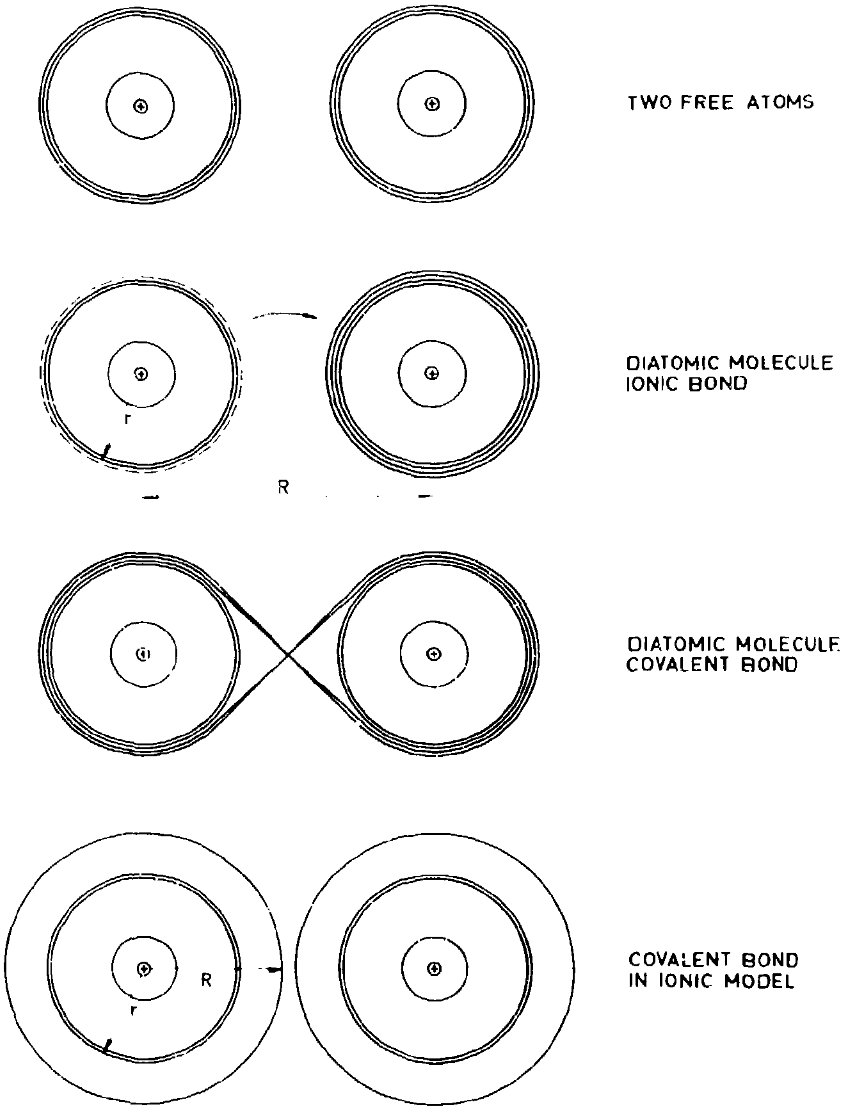

Fig. V:7. The ionic model for ionic and covalent bonds. The radius r is the mean radius of the valence shell and R represents the average distance to which charge is transferred when a chemical bond is established. For an ionic bond this is the internuclear distance. A covalent bond can be represented by a partial expansion of the valence shell to radius R.

the two atoms is R, the energy shift of the core electrons becomes

$$\Delta E = \left(\frac{1}{r} - \frac{1}{R}\right) q \tag{2}$$

and with opposite sign for the two atoms; q is the number of electrons transferred.

When the ions A^{+q} and B^{-q} are arranged in a lattice to form a crystal one has to calculate the Coulomb interaction of a core electron in one atom with all the ions in the lattice. This is essentially the same problem as one has in calculating the lattice energy of ionic crystals. Eq. (2) is modified by the Madelung constant α:[175]

$$\Delta E = \left(\frac{1}{r} - \frac{\alpha}{R}\right) q \tag{3}$$

(In a more general structure, α would be the contribution to the Madelung constant from the particular atom that one is studying.) Madelung constants have been calculated for many different crystal structures, and their values are generally around 1.7 for diatomic crystals when based on unit charges and referred to the nearest neighbour distance. Nearest neighbour distances in these structures are generally around 5 a.u. Thus, very roughly, the expected shift per degree of ionization, calculated from eq. (3) becomes $\Delta E \approx 5$ eV, which, although smaller than the shift calculated from eq. (1), is still of considerable magnitude.

A third term, due to electronic (and nuclear) relaxation in the solid, could be added to eq. (3). This contribution to the energy shift can be expressed in terms of the dielectric constant and is independent of the charge q.

For higher states of oxidation, i.e. when more electrons are removed from the valence shell, the valence shell should contract (r decreases). Thus, according to our model the shift per degree of oxidation should increase as the state of oxidation increases.

As long as the valence electrons do not penetrate into the atomic core, the model predicts the same shift for all core electrons. However, if there is a penetration of valence electrons into the core one would expect to find different shifts for different core electrons. Since ESCA spectra map out the inner as well as the outer core levels one could expect these spectra to yield information also on the electron configuration in the valence shell. Information of this sort is often needed in Mössbauer spectroscopy for the interpretation of isomeric shifts.[176] ESCA spectra and Mössbauer spectra thus complement each other in this respect.

Very few, if any, crystals have pure ionic binding. Instead, there is a continuous range between the covalent and ionic limits. We can still use our ionic model, however, providing we estimate the amount of ionic character of the bonds. Even for a completely covalent bond there is a redistribution of charge, which may be accounted for. The transfer of electrons to bonding orbitals then corresponds to the transfer of charge from the valence shell to some other spherical shell, centered on the atom of interest. The radius of this shell will be larger than the radius r of the valence shell since electrons that move in molecular orbitals will on the average have a larger distance to the parent nucleus than when moving in the atomic orbitals of the valence shell. If the larger sphere radius is R the "covalent" shift is given by eq. (2), see Fig. V:7. This could, for example, be the shift in core electron binding energy between an element in the gaseous state and in the solid state. (Zero potential energy in both cases when the electron is completely removed from the system, i.e. at the vacuum level of the solid.)

The free ion contribution to the chemical shift, which was written as $(1/r)q$ in eq. (3), can be calculated quantum mechanically with the same self-consistent-field method, developed by one of us (I.L.),[54,55] as was used for the calculation of electron binding energies. The crystal energy contribution, i.e. the negative term in eq. (3), can be obtained from calculations of Madelung constants. However the contributions to the Madelung constant from the different atoms in the unit cell are not often reported in the literature. In the following section, we shall describe the more detailed calculations of the free-ion contribution and the crystal field contribution. We shall then in Section V:4 discuss the ESCA shifts from the chemist's standpoint in order to correlate the observed shifts with such parameters as can easily be derived from simple structural concepts.

V:3. Calculation of Chemical Shifts in Electron Binding Energies

In a pure covalent bond, an electron pair is evenly distributed between two atoms. If the atoms have different electronegativities (see Appendix 13), the bond can be regarded as partly ionic, and the electrons in the bond have different probabilities of being found in the neighbourhood of each of the two atoms. As a quantitative measure of this probability one may use an "effective charge" of the atoms, which can be defined as the total charge within a certain volume around the nucleus. Of course, it is not possible to draw any definite border-line between the atoms in a molecule, and the effective charges are therefore only crude measures of the electron distribution. Nevertheless, as a first approximation, this quantity has proved to be a valuable concept, and it is believed that it also has some significance in molecules with covalent bonds. The effect of the electron distribution on the inner electrons can presumably be described adequately with such a simple ionic model.

In the ionic model the shift in the binding energy of the inner electrons has mainly two components (cf. Section V:2):

I. the "free-ion shift" and

II. the "crystal-field shift".

The free-ion shift is defined as the shift in binding energy between a free, neutral atom and a free ion with a certain charge. The crystal-field shift is the effect of the surrounding atoms (ions) on the binding energies.

Calculations of free-ion shift

The free-ion shift can be calculated by self-consistent-field methods in the same way as binding energies described in Section III:9. It was shown in that section that for inner electrons considerably better agreement between the observed and calculated values is obtained by the more elaborate method B, where the binding energy is calculated as the difference between the total energy of two states, obtained by separate SCF calculations. Therefore, the chemical shifts are calculated by the same method here, and results of the simpler method A are only used for comparison.

In Table V:1a, some different methods of calculating ionic shifts are compared in a few typical cases. The calculation of binding energies using method A is dependent on the approximations assumed whereas with method B this is not the case to the same extent. There is furthermore an appreciable difference between the results obtained by the two methods, e.g. for fluorine about 4 eV or more than 20 %. It is believed that method B is the more accurate one. This comparison shows that there is little to be gained by using a more elaborate method, such as Hartree–Fock, for this type of calculation. In method A, the results are unreliable irrespective of the approximation and in method B almost identical results are obtained with other approximations, such as Hartree-Fock-Slater. In Table V:1b, some binding energies for sulfur obtained by various relativistic and non-relativistic methods are compared. This shows that the relativistic effect is quite negligible for sulfur.

Table V:1a. Comparison between different methods of calculating ionic shifts ($1s$ level) (eV).*

Element	q	Method A			Method B	
		HFS	OHFS	HF	HFS	OHFS
F	−1	−16.9	14.9	−15.1	−19.2	−19.3
Na	1	9.6	9.1	7.6	9.4	9.2
S	−1	−10.2	−9.2	−9.1	−11.2	−11.3
	1	13.1	12.3	12.0	13.8	13.8
Cl	−1	−11.4	−10.3	−10.3	−12.4	−12.4
K	1	7.2	7.3	6.0	7.2	7.1

* All shifts in Tables V:1 and V:2 are related to the free, neutral atom in its ground configuration.

A:	Atomic orbitals for atom as well as ion, i.e. use of Koopmans' theorem (with the appropriate correction, see Section III:9)
B:	Separate self-consistent-field orbitals for atom and ion
HFS:	Hartree-Fock-Slater
OHFS:	Hartree-Fock-Slater with optimized exchange correction
HF:	Hartree-Fock

Table V:1b. Relativistic effect on the ionic shift ($1s$ level) (eV).

Element	q	Method A		Method B	
		non-rel.	rel.	non-rel.	rel.
S	1	12.32	12.30	13.76	13.77
	2	27.07	27.04	29.82	29.89

The binding energies of inner electrons in a free ion depend not only on the degree of ionization but also on the configuration of the outer electrons. It is, of course, difficult to determine the configuration of the free ion that, in this model, best corresponds to the actual situation in the molecule. As a first approximation, one can use the ground-state configuration of the ion. Fortunately, it is found that the choice of configuration is in many cases not critical. If e.g. a $3s$ electron in sulfur is raised to the $3p$ state, the binding energy of the inner electrons is shifted by only 0.6 eV, compared with 14 eV when the electron is completely removed.

In most of the elements investigated here, the bonds are mainly of the sp^3 hybrid type. In order to investigate the effect of such a hybridization on the binding energies, the energies are calculated for different configurations and the results weighted in such a way that the outer electrons have 75 % p character and 25 % s character. As an example, we can take singly ionized sulfur S^+, which has five outer electrons. By weighting the configuration $3s^2 3p^3$ and $3s3p^4$ in the proportions 1:3, a configuration of sp^3 character ($s^{1.25}p^{3.75}$) is obtained. Since the difference in binding energy between the different configurations is small in this

Table V:2a. Ionic shift in the $1s$ level (eV).

Element	q	A	B	B sp^3-hybr.	B sp^3d-hybr.
C	1	15.3	18.8	17.1	
	2	35.4	42.4	39.1	
N	1	17.4	20.7	19.5	
	2	39.8	46.3	43.3	
O	−1	−13.0	−17.5	−17.2	
F	−1	−14.9	−19.3	−19.3	
Na	1	10.1	9.2	9.2	
S	−1	−9.2	−11.3	−10.8	1.0
	0	0	0	0.8	7.4
	1	12.3	13.8	14.8	19.7
	2	27.1	29.8	30.9	34.3
	3	44.0	48.1	49.0	51.2
	4	62.9	68.5	69.0	
	6	109.1	115.0	115.0	
Cl	−1	−10.3	−12.4	−12.4	
	0	0	0	0.4	9.7
	1	13.4	14.9	15.6	21.7
	2	29.2	32.2	32.9	37.2
	3	47.2	51.5	52.2	
	5	89.2	96.4	96.5	
	7	141.0	148.4	148.4	
K	1	7.7	7.1	7.1	

Table V:2b. Ionic shift in the $2s$ level (eV).

Element	q	A	B	B sp^3-hybr.	B sp^3d-hybr.
C	1	11.7	12.7	14.9	
	2	26.0	27.8	21.5	
N	1	13.5	14.5	16.6	
	2	29.7	31.4	33.7	
O	−1	−11.0	−13.4	−12.6	
F	−1	−12.7	−15.2	−15.2	
Na	1	8.7	8.8	8.8	
S	−1	−9.1	−11.1	−10.7	
	0	0	0	0.7	6.0
	1	12.0	13.3	14.1	17.6
	2	26.3	28.5	29.3	31.4
	3	42.4	45.6	46.2	47.3
	4	60.3	64.4	64.8	
	6	101.5	106.4	106.4	
Cl	−1	−10.2	−12.1	−12.1	
	0	0	0	0.3	8.0
	1	13.1	14.4	14.9	19.1
	2	28.3	30.7	31.3	33.9
	3	45.5	48.9	49.4	
	5	84.9	90.2	90.1	
	7	130.9	136.9	136.9	
K	1	7.5	7.0	7.0	

case, this simple method should be sufficient for the present purpose.

However, for elements in the third period, the d electrons are supposed to participate significantly in the bonds. Thus, for example, in sulfur compounds, configurations of the type $3s3p^33d^2$ may play an important role.[177-180] Such hybrids have been found to influence the binding energies of the inner electrons much more than the sp hybrid discussed above. When a $3s$ or $3p$ electron in sulfur is raised to the $3d$ state, the binding energy of the inner electrons is increased by as much as 3-5 eV, compared to 0.6 eV for the $3s-3p$ excitation. The reason for this is, of course, that the $3d$ orbital is further removed from the nucleus than the $3p$ orbital. Consequently, the participation of d electrons is a critical factor in these interpretations. Now, the atomic $3d$ orbitals are too diffuse to take any significant part in the bonding. Craig and Zauli[177] have found that the sulfur $3d$ orbital in SF_6 contracts to about one half of the free atom size. Such a contraction evidently reduces the influence of d admixture on the binding energy of inner electrons. This effect can be estimated quantitatively using a slight modification of the SCF program, which was briefly described in connection with the discussion of solid-state effects on the binding energies in Section III:9. If a fixed potential, representing the crystal field and the electron clouds of the neighbouring atoms, is superimposed upon the SCF potential, more realistic orbitals could be obtained. Such calculations are now in progress. At present we shall treat the d contribution in the same approximate way as the sp hybridization outlined above. In the absence of more accurate descriptions of the orbitals, we may compensate for the contraction of the d orbitals by using a somewhat smaller admixture of atomic d orbitals in the bonds than is expected on other grounds. Hybrids of the sp^3d type then probably represent an upper limit to d orbital participation. Again, the binding energies of such hybrids are obtained by appropriate weighting of different configurations. Hence by weighting the configurations s^2p^4, sp^5 and sp^4d of neutral sulfur in the relation 1 : −2 : 6 a configuration of sp^3d character $(s^{1.2}p^{3.6}d^{1.2})$ is obtained.

Tables V:2 a–e give the ionic shifts in the $1s$, $2s$, and $2p$ levels, and in the $K\alpha$ radiation for certain ele-

Table V:2c. Ionic shift in the $2p$ level (eV).

Element	q	A	B	B sp^3- hybr.	B sp^3d- hybr.
C	1	13.3	14.1	12.4	
N	1	15.2	15.9	14.5	
	2	33.6	35.0	32.4	
O	−1	−12.7	−14.3	−14.3	
F	−1	−14.4	−16.1	−16.1	
Na	1	8.7	9.0	9.0	
S	−1	−9.1	−11.0	−10.5	
	0	0	0	0.9	6.0
	1	12.0	13.2	14.4	18.1
	2	26.2	28.4	29.7	31.9
	3	42.3	45.5	46.7	48.0
	4	60.1	64.2	65.4	
	6	102.6	107.6	107.6	
Cl	−1	−10.2	−12.1	−12.1	
	0	0	0	0.5	8.3
	1	13.0	14.3	15.1	19.6
	2	28.2	30.7	31.6	34.4
	3	45.4	48.8	49.9	
	5	84.8	90.1	91.0	
	7	132.3	138.3	138.3	
K	1	7.5	7.0	7.0	

ments using different methods of calculation and different hybridizations. The results are illustrated in Figs. V:8–V:13. In all cases modified Hartree-Fock-Slater wave functions are used (see Section III:9).

Calculation of crystal field shift

In the previous section we have considered the shift in the binding energy of inner electrons when outer electrons are excited or removed. The atom or ion is in these cases considered to be free, i.e. the effect of surrounding atoms is ignored. This means that when the atom is ionized, the electron is supposed to be removed to infinity. In a solid, normally only smaller rearrangements of electric charge, between neighbouring atoms take place. Therefore, the free-ion shifts become much larger than the real shifts for reasonable values of the effective charge, or reversely the charges deduced from the experimental shifts become unreasonably small.[68] The theoretical ionic shifts are of the order 10–20 eV per unit charge while the experimental shifts are usually of the order of 5 eV or less. The reason is, of course, that the neighbouring atoms receive charge of the opposite sign, which counteracts the free-ion shifts. This effect is qualitatively described in

Table V:2d. Shift in $K\alpha$ radiation (eV).

Element	q	A	B	B sp^3- hybr.	B sp^3d- hybr.
C	1	2.0	4.7	4.8	
N	1	2.2	4.8	5.1	
	2	6.2	11.3	11.0	
O	−1	−0.3	−3.2	−2.9	
F	−1	−0.5	−3.2	−3.2	
Na	1	1.4	0.3	0.3	
S	−1	−0.1	−0.3	−0.3	
	0	0	0	−0.1	1.3
	1	0.3	0.5	0.4	1.6
	2	0.9	1.4	1.2	2.3
	3	1.7	2.7	2.3	3.2
	4	2.8	4.2	3.6	
	6	6.5	7.4	7.4	
Cl	−1	−0.2	−0.4	−0.4	
	0	0	0	0.5	1.4
	1	0.4	0.6	0.5	2.1
	2	0.9	1.5	1.3	2.8
	3	1.8	2.7	2.4	
	5	4.2	6.3	5.5	
	7	8.8	10.0	10.0	
K	1	0.2	0.1	0.1	

Section V:2. In this section we shall try to evaluate the effect more quantitatively.

As far as inner electrons are concerned, the neighbouring ions can, as a first approximation, be regarded as point charges, since the overlap is negligibly small. Therefore, in order to evaluate the direct effect of the crystal field on the binding energy we have only to perform a summation of potentials from point charges similar to the calculation of the crystal energy and the Madelung constants.

In the point-charge model, the crystal potential at the nucleus of atom i becomes

$$V_i = \sum_j \frac{q_j}{r_{ij}} \text{ a.u.} = 27.2 \sum_j \frac{q_j}{r_{ij}} \text{ volt}, \tag{4}$$

Table V:2e. Ionic shifts for some configurations with two d electrons (eV).

Element	q	config.	$1s$	$2s$	$2p$	$K\alpha$
S	0	sp^3d^2	12.9	9.7	10.2	1.8
	1	sp^2d^2	23.8	20.4	20.9	2.9
Cl	0	sp^4d^2	12.9	10.3	10.9	2.0
	1	sp^3d^2	25.3	21.5	22.2	3.2

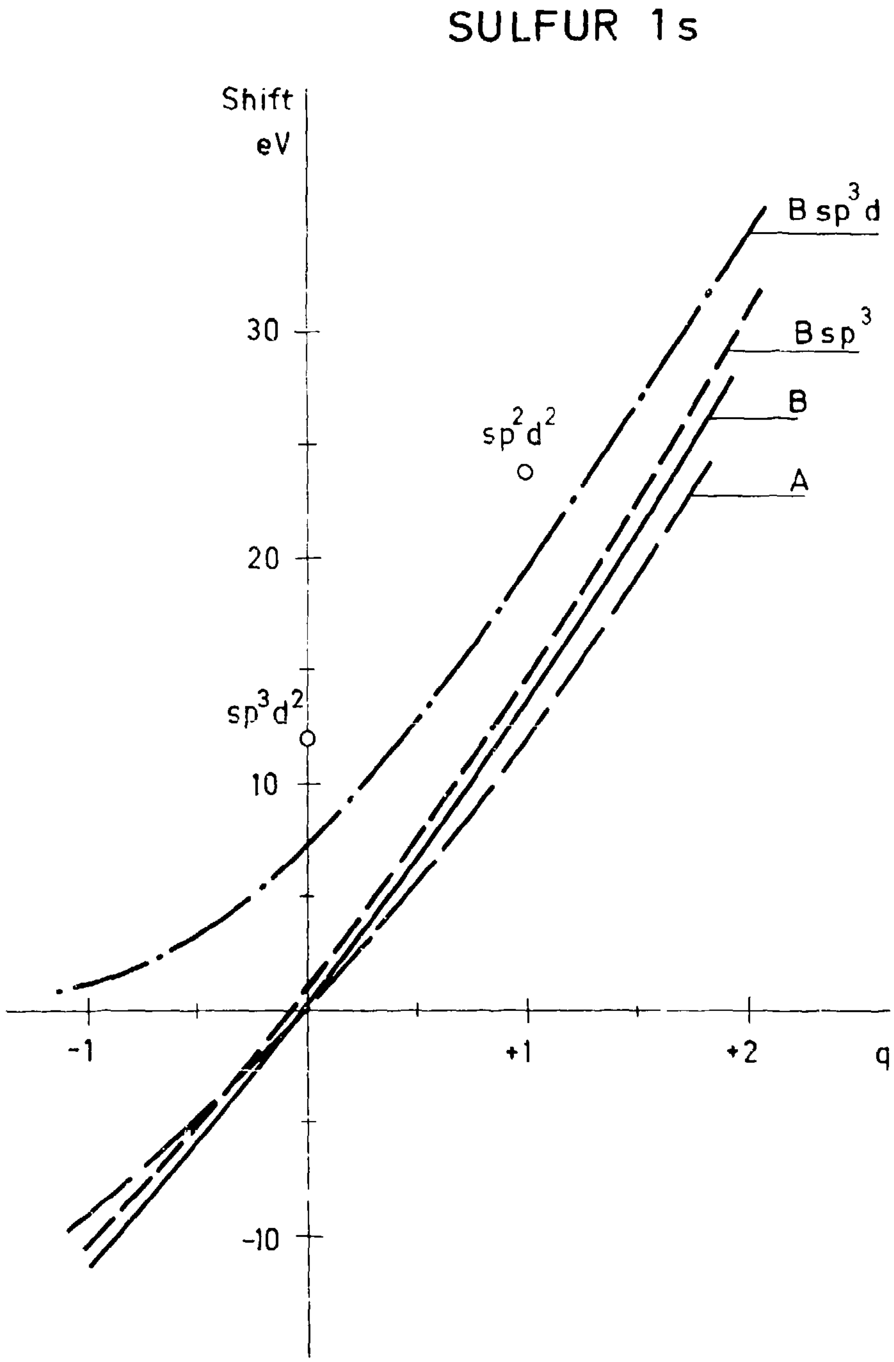

Fig. V:8. Shift in 1s level of sulfur calculated by use of different methods and different hybridizations.

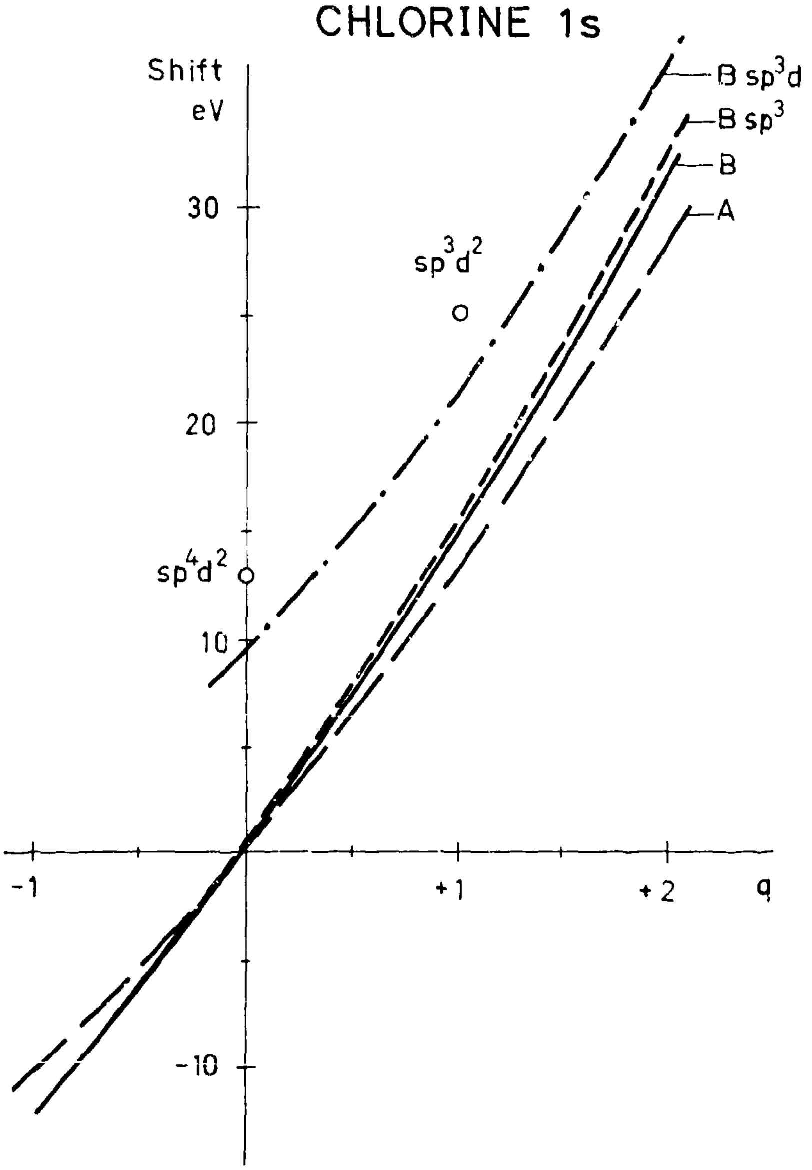

Fig. V:9. Shift in 1*s* level of chlorine calculated by use of different methods and different hybridizations.

where q_j is the charge on ion j and r_{ij} is the inter-atomic distance. The total electrostatic energy of the crystal then becomes

$$E_c = \frac{1}{2}\sum_i q_i V_i = \sum_{i<j} \frac{q_i q_j}{r_{ij}} \mathrm{H} = 27.2 \sum_{i<j} \frac{q_i q_j}{r_{ij}} \mathrm{eV}. \qquad (5)$$

Crystal energies and Madelung constants are calculated for a large number of crystals, but these data cannot be used to evaluate the individual potentials (eq. 4) in the general case. Therefore, we have made a computer program for evaluating the crystal sums above and applied it to some crystals of particular interest here.

There is one specific difficulty in evaluating the

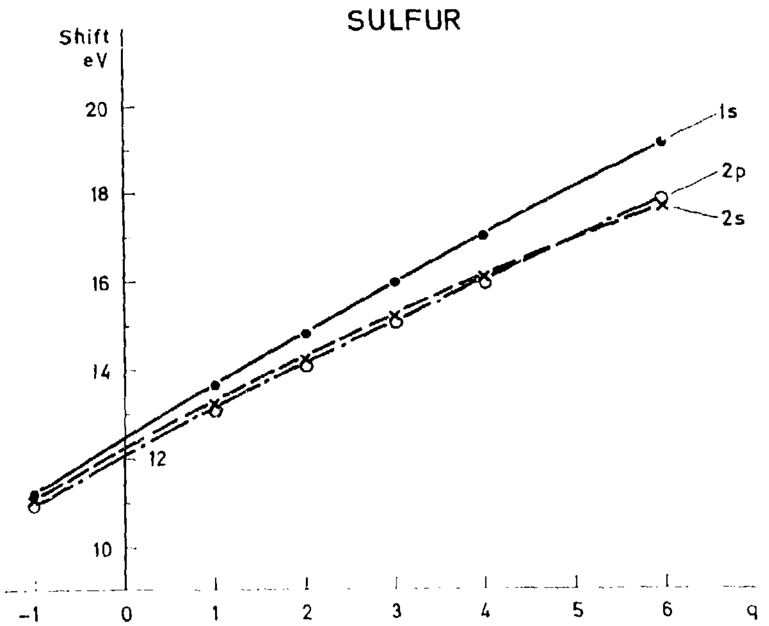

Fig. V:10. Shift per unit charge in the inner levels of sulfur calculated by use of method B (no hybridization).

crystal potential, which to some extent is also encountered in the calculation of the total energy. If a crystal is constructed from a unit cell possessing a given dipole moment, each half of the surface will acquire charge of opposite sign, and the crystal as a whole will exhibit a large dipole moment (as illustrated in Fig. V:14). This dipole moment gives rise to an electric field at the center, which approaches a constant value, as the dimensions of the crystal are increased. Therefore, one cannot avoid this problem by extending the summation over a sufficiently large volume. One effect of such a dipole is that equivalent atoms in dif-

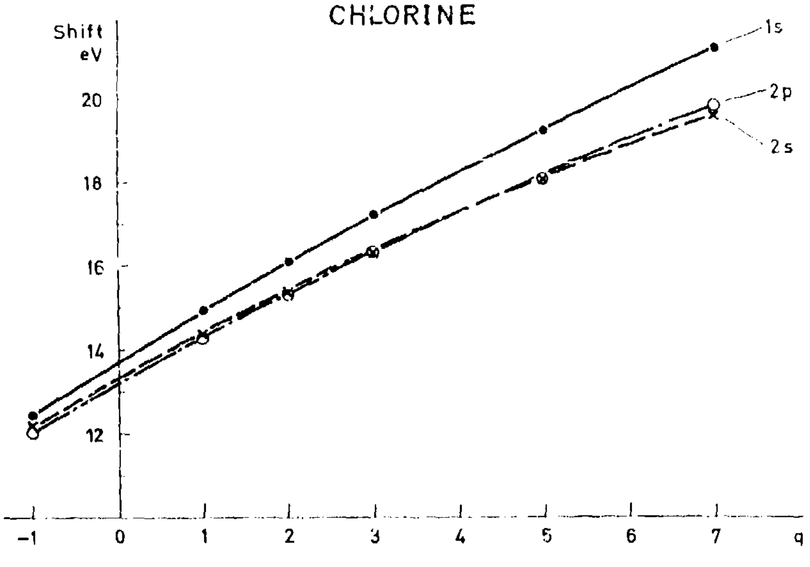

Fig. V:11. Shift per unit charge in the inner levels of chlorine calculated by use of method B (no hybridization).

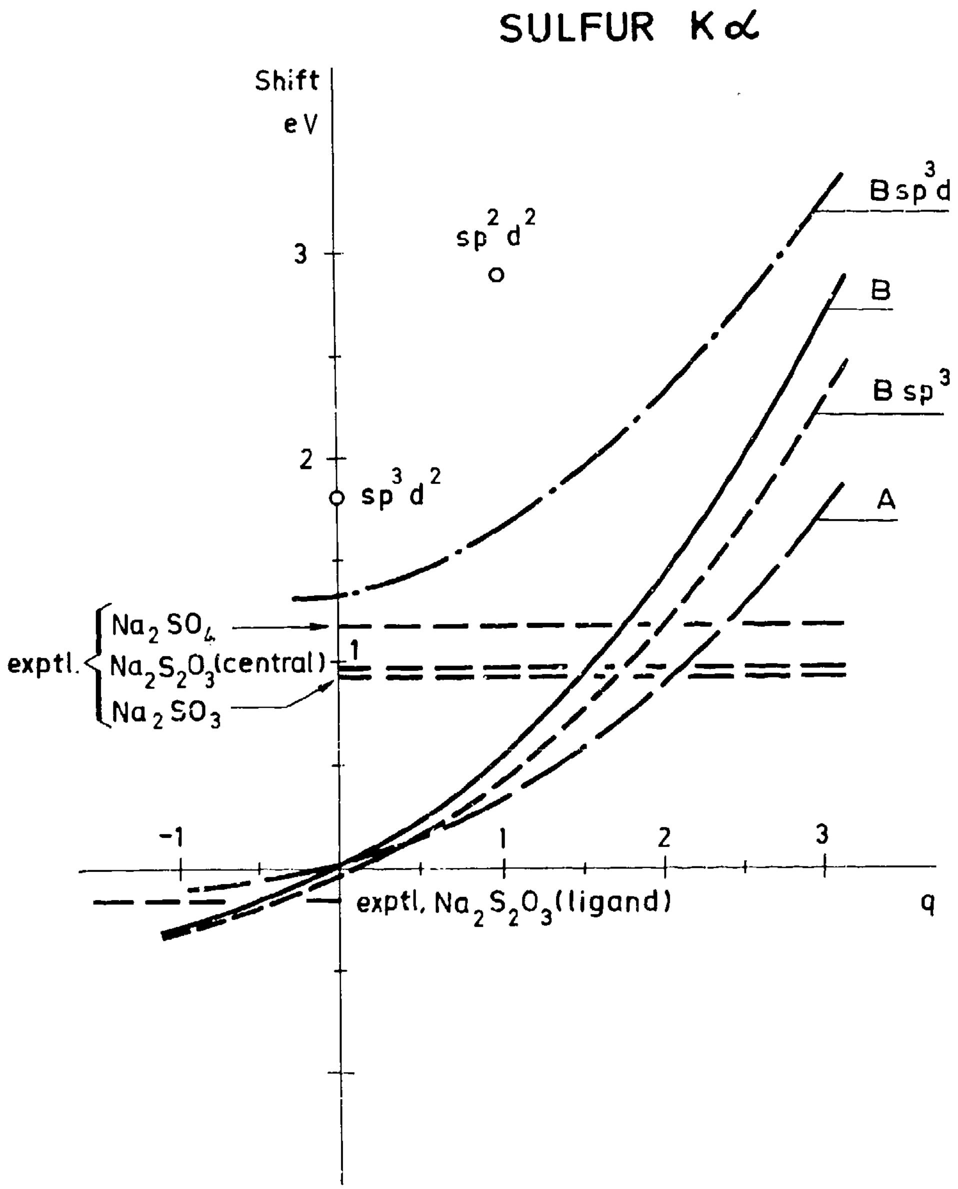

Fig. V:12. Shift in *Kα* radiation of sulfur calculated by use of different methods and hybridizations.

ferent molecules acquire quite different potentials. For each atom, however, the summation converges and the effect is therefore not revealed if the calculations are restricted to one molecule. When a cell with no dipole moment is used, equivalent atoms have the same potential. This is illustrated in Table V:3 for Na_2SO_3. The total energy is also affected by the dipole moment but to a less extent than the potentials at the individual atoms, since the molecule is electrically neutral and therefore the positive and negative contributions compensate each other.[181]

In Table V:4, we have given the calculated potentials as well as total electrostatic energies for a number of crystals. The crystal structures are taken from

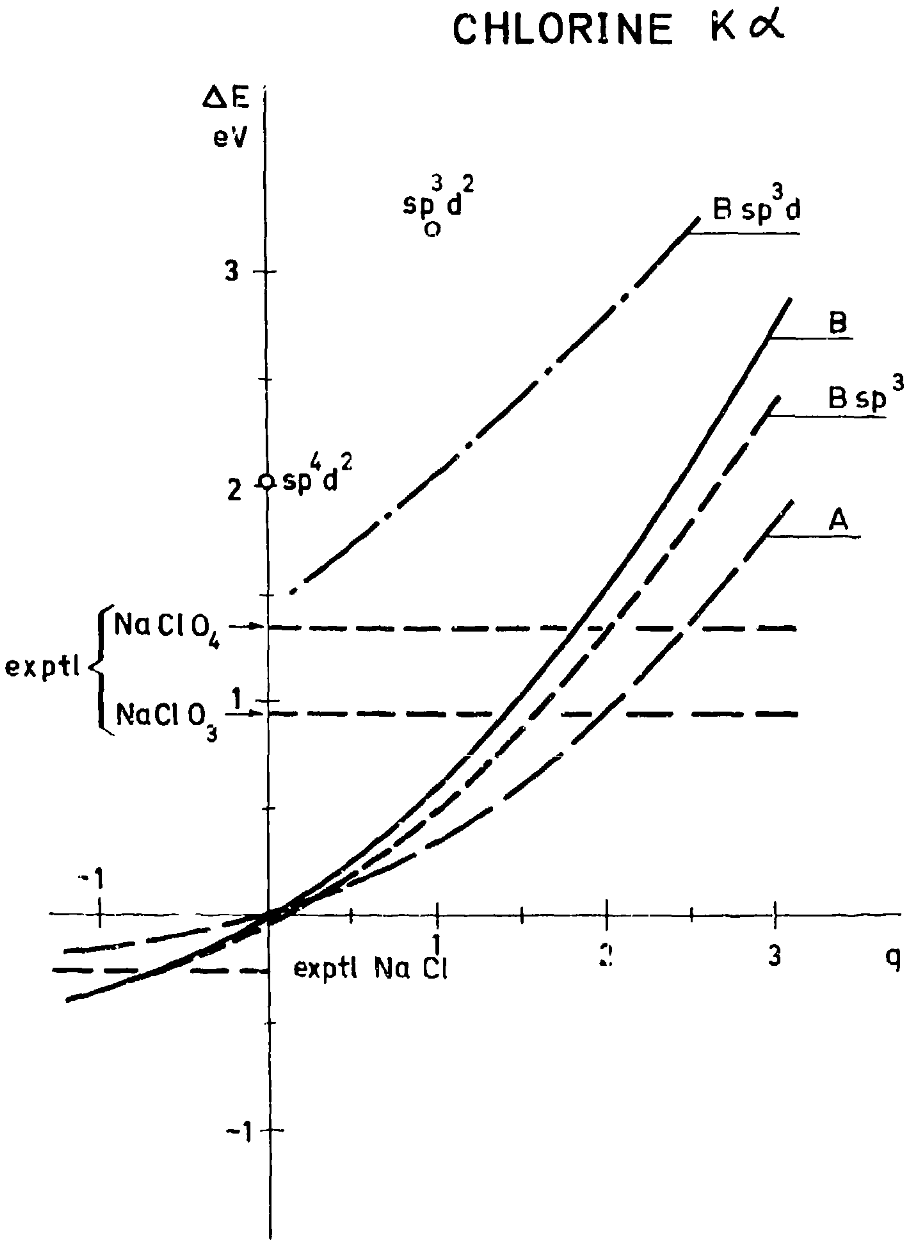

Fig. V:13. Shift of *Kα* radiation of chlorine calculated by use of different methods and hybridizations.

Wyckoff's tables.[182] In all cases a unit cell without dipole moment is chosen. Wood's[181] values for K_2SO_4, presumably calculated using the dipole moment of the unit cell, are also included in the table for comparison.

Crystals of some different nitrogen compounds have also been studied, but the calculations are not yet complete. For the nitrites, it does not seem possible to choose a unit cell without dipole moment owing to the low symmetry of the nitrite ion. Therefore, the results become so uncertain that a comparison with experimental data is difficult.

It should be emphasized that most of our results in Table V:4 are only preliminary, since owing to lack of time they have not always been cross-checked (by use of different unit cells etc.) to the extent that would have been desirable.

The total chemical shift in the binding energy between a crystal and a free atom can now be calculated by adding the ionic shift (ΔE_{ion}) and the crystal field shift (ΔE_{cryst}) with the effective charges as parameters

$$\Delta E_{\text{calc}} = \Delta E_{\text{ion}} + \Delta E_{\text{cryst}}. \tag{6}$$

(The value of ΔE_{cryst} in eV is equal to the crystal potential in volt given in Table V:4). By fitting the calculated shift to the experimental value, one can in principle determine the effective charges. However, the experimental values are related to the Fermi level, while the theoretical values are related to the potential at infinity. Therefore, eq. (6) has to be corrected for the work function

$$\Delta E_{\text{calc}} = \Delta E_{\text{ion}} + \Delta E_{\text{cryst}} - \phi. \tag{7}$$

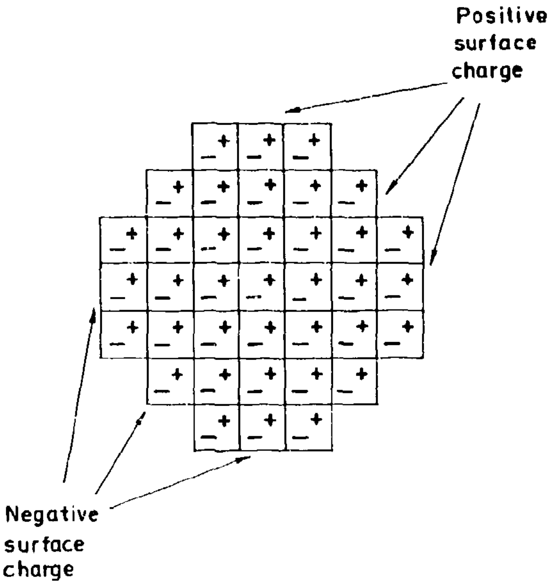

Fig. V:14. A unit cell with dipole moment leads to a surface charge on the crystal.

A comparison between, for instance, the different sulfates in Table V:4 shows that the potential on corresponding atoms may be quite different. The

Table V:3. Crystal potentials in Na_2SO_3 (volt)

Unit cell ***with*** dipole moment

Atom	q	Molecule 1	Molecule 2	q	Molecule 1	Molecule 2
Na	1	−12.2	−15.2	1	−13.0	−16.0
Na	1	−14.7	−9.1	1	−16.8	−11.3
S	0	−11.0	−14.0	2	−32.0	−35.0
O	−2/3	2.8	−1.7	−4/3	14.4	10.0
O	−2/3	3.1	−1.8	−4/3	14.8	9.8
O	−2/3	0.6	0.7	−4/3	12.2	12.3
Energy (eV)		−15.6	−11.2		−74.5	−70.2

Unit cell ***without*** dipole moment

Atom	q	Molecule 1	Molecule 2	q	Molecule 1	Molecule 2
Na	1	−14.8	−14.8	1	−15.6	−15.6
Na	1	−14.7	−14.7	1	−16.8	−16.8
S	0	−13.6	−13.6	2	−34.7	−34.7
O	−2/3	−0.5	−0.5	−4/3	11.1	11.1
O	−2/3	−0.5	−0.5	−4/3	11.2	11.2
O	2/3	−0.5	−0.5	−4/3	11.1	11.1
Energy (eV)		14.2	14.2		−73.2	−73.2

Table V:4. Crystal potentials (volt).

Atom	q	V	q	V
	Na_2S			
Na	1/4	−0.5	1/2	−1.0
Na	1/4	−0.5	1/2	−1.0
S	−1/2	5.9	−1	11.8
Energy (eV)		−1.6		−6.4
	$Na_2S_2O_3$			
Na	1	−7.5	1	−6.8
Na	1	−7.3	1	−6.5
S	0	−3.7	2	−20.3
S	−1/2	5.1	−1	12.9
O	−1/2	5.6	−1	17.9
O	−1/2	5.9	−1	14.4
O	−1/2	5.7	−1	16.8
Energy (eV)		−13.0		−58.0
	Na_2SO_4 mod. III			
Na	1	−9.6	1	−8.9
Na	1	−9.4	1	−10.0
S	0	−6.5	2	−25.2
O	−1/2	4.0	−1	14.4
O	−1/2	4.0	−1	14.4
O	−1/2	3.7	−1	14.0
O	−1/2	3.7	−1	14.0
Energy (eV)		−13.3		63.0
	K_2SO_4			
K	1	−13.1	1	−12.4
K	1	−12.9	1	−13.2
S	0	−11.8	2	−31.1
O	−1/2	−2.1	−1	8.2
O	−1/2	−1.2	−1	9.1
O	−1/2	−1.5	−1	9.2
O	−1/2	−1.5	−1	9.2
Energy (eV)		−11.4		61.7
	$NaCl$			
Na	1	−8.9		
Cl	−1	8.9		
Energy (eV)		−8.9		
	$NaClO_3$			
Na	1	4.2	1	8.2
Cl	0	8.8	2	−6.3
O	−1/3	15.3	−1	32.1
O	−1/3	15.3	−1	32.1
O	−1/3	15.3	−1	32.1
Energy (eV)		−5.5		−50.5

Atom	q	V	q	V
	Na_2SO_3			
Na	1	−14.8	1	−15.7
Na	1	−14.7	1	−16.8
S	0	−13.6	2	−34.7
O	−2/3	−0.5	−4/3	11.1
O	−2/3	−0.5	−4/3	11.1
O	−2/3	−0.5	−4/3	11.1
Energy (eV)		−14.2		−73.2
	$Na_2S_2O_3$			
Na	1	−7.1	1	−6.4
Na	1	−7.7	1	−6.9
S	0	−4.2	2	−20.9
S	0	2.6	−1/2	10.4
O	−2/3	6.6	−7/6	19.0
O	−2/3	6.4	−7/6	15.0
O	−2/3	7.3	−7/6	18.4
Energy (eV)		−14.1		−60.7
	Na_2SO_4 mod. V.			
Na	1	−13.6	1	−13.6
Na	1	−13.6	1	−13.6
S	0	−11.3	2	−30.3
O	−1/2	−0.6	−1	10.0
O	−1/2	−0.6	−1	10.0
O	−1/2	−0.6	−1	10.0
O	−1/2	0.6	−1	10.0
Energy (eV)		13.0		−63.9
	K_2SO_4 Wood(2)			
K	1	−8.0	1	−7.6
K	1	−7.8	1	−8.4
S	0	−6.4	2	−25.9
O	−1/2	3.6	−1	13.7
O	−1/2	3.8	−1	13.8
O	−1/2	3.7	−1	13.5
O	1/2	3.7	−1	13.5
Energy (eV)		−11.6		−61.2
	$NaClO_4$			
Na	1	7.2	1	−7.5
Cl	0	−2.9	2	−20.3
O	−1/4	3.4	−3/4	13.0
O	−1/4	3.4	3/4	13.0
O	−1/4	3.5	−3/4	13.6
O	1/4	3.0	−3/4	13.6
Energy (eV)		−5.2		−44.0

effective charges and therefore also the ionic shifts can be assumed to be very similar in these cases, and consequently one would expect the differences in the crystal potentials to appear in the binding energies. Experimentally, however, no such variations have been found. The experimental binding energies are the same within one electron volt in these cases. This apparent discrepancy could be explained by variations in the reference level, which almost completely compensates for the variation in the crystal potential.

By comparing the results for the different sulfates in Table V:4, one finds that the potentials are shifted by nearly the same amount for all atoms. In other words, the relative potentials are almost the same for all the sulfates. Therefore, it is believed that the relative potentials have more physical significance than the absolute ones. If the calculated shifts are always referred to the potential at the cation, the problem with the unknown zero level (and therefore also with the work function) is eliminated. Since the experimental variation in the binding energy of the cation is small (usually less than 1 eV), it need not be considered here, although, it is easy to correct for this variation, if a more accurate comparison is required. One could, in principle, also use oxygen as a reference. However, since the effective charge, and therefore also the ionic shift, of the oxygens may differ from compound to compound, it is less suitable for this purpose.

Application to sulfur compounds

The most interesting sulfur compound for the present investigation was thiosulfate, which has two sulfur atoms in different positions. The difference in binding energy between these two atoms is independent of the work function, and the problem with the reference level discussed above vanishes. Figs. V:15 and V:16 show the difference in the ionic, crystal and total shifts for different hybridizations of the central sulfur. (The ligand sulfur is assumed to have a configuration of sp^3 character.) In Fig. V:15, it is assumed that the charges on the ligand sulfur and the oxygens are the same. Due to the difference in electronegativity, the oxygens should be more negative, and Fig. V:16 shows the corresponding results assuming a charge difference of 2/3 units. In both figures, the experimental shift (6.0 eV) is marked.

With no charge difference between oxygen and ligand sulfur (Fig. V:15), sp^3 hybridization gives an effective charge of about 1.9 on the central sulfur and about -1.0 on the ligand sulfur. The corresponding values with sp^3d hybridization are 1.4 and -0.85, respectively. With a charge difference of 2/3 units between the oxygen and the ligand sulfur, the charge on the central sulfur increases by about 0.5 units.

The effective charges obtained above are numerically somewhat larger than those deduced in Section V:5b. When this comparison is made, the following should be remembered. Firstly, the effective charge cannot be exactly defined and, therefore, the quantity used here need not be precisely the same as that in Section V:5b. Secondly, there are appreciable uncertainties in both estimations. Figs. V:15 and V:16 show clearly that the two contributions, the ionic and the crystal shift, tend to counteract each other, which makes the total shift one order of magnitude smaller than the main contributions taken separately. Therefore, a relatively small error in one of those may affect the result seriously. Furthermore, the unknown contributions from *d* orbitals to the bonds makes an interpretation difficult. In spite of this, some qualitative conclusions can be drawn. As mentioned previously, the atomic *d* orbitals used in the calculations here, exaggerate the effect of the *d* orbitals, and, therefore, it should be sufficient to include one *d* electron. It may be deduced that the effective charge on the central sulfur lies between 1.5 and 2.0 and hence a value considerably than less 1.5 is difficult to explain on these grounds.

For other sulfur compounds with only one sulfur atom, the comparison with experimental values is more difficult. The best way is probably to use the cations for reference purposes as described previously. In ionic compounds, where the cation always has the same charge, this method should be fairly reliable.

In $Na_2S_2O_3$, the potential at the central sulfur with a charge of $+2$ is about -14 V relative to the cation. In Na_2SO_3, the corresponding value is -19 V and in Na_2SO_4 -16 to -17 V. Experimentally, the shifts in these compounds are 0.8 eV and $+0.5$ eV, respectively, relative to the central sulfur in $Na_2S_2O_3$. From this one can conclude that the effective charges on the sulfur in sulfate and sulfite should be nearly the same, being both somewhat larger than on the central sulfur in thiosulfate. Owing to the uncertainties involved, it does not seem possible to draw any more precise conclusions from the available data.

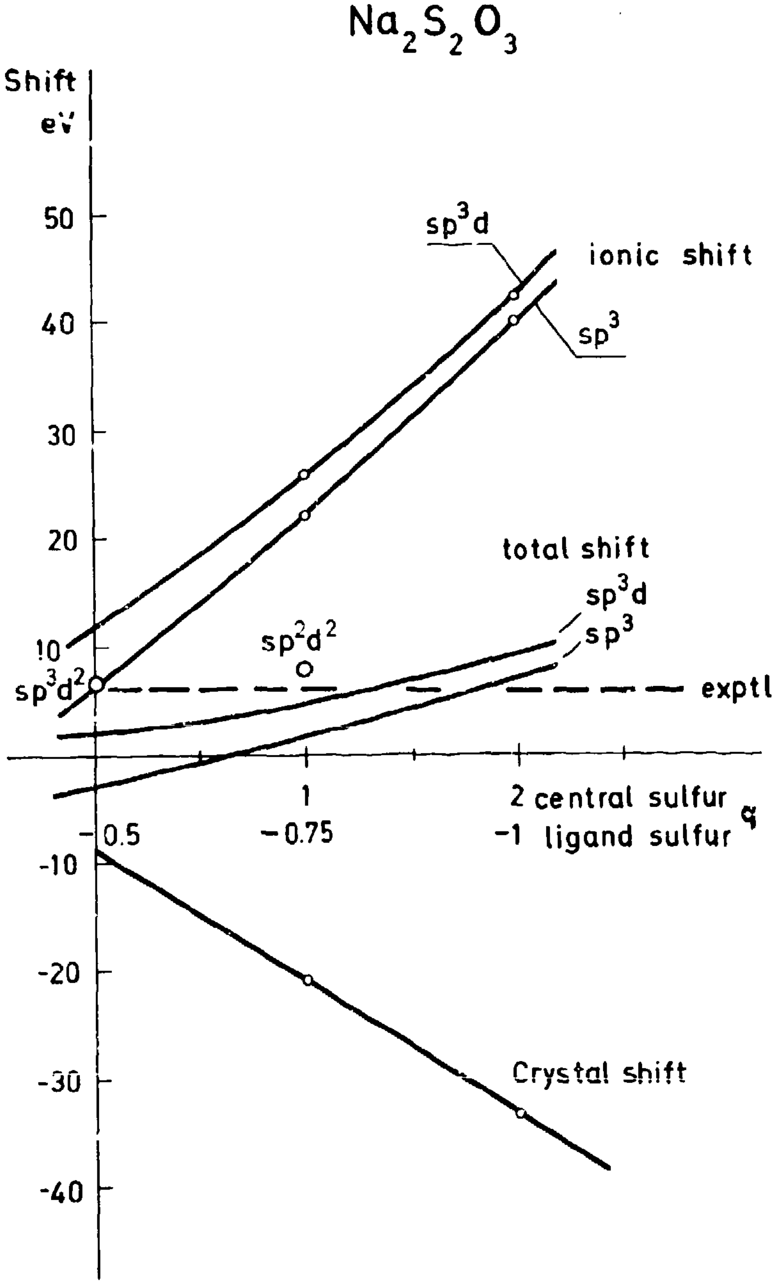

Fig. V:15. Shift in 2*p* level between the two sulfur atoms in $Na_2S_2O_3$. No charge difference between oxygen and ligand sulfur.

Application to chlorine compounds

The measurements on chlorine compounds are based on NaCl (see Section V:4). Since the structure of this latter compound can be treated theoretically with some accuracy, a comparison with theory can be made. As before we use the cation as reference, and the theoretical shift for $NaClO_3$ and $NaClO_4$ relative to NaCl is as shown in Fig. V:17. Assuming sp^3 hybridization, this yields

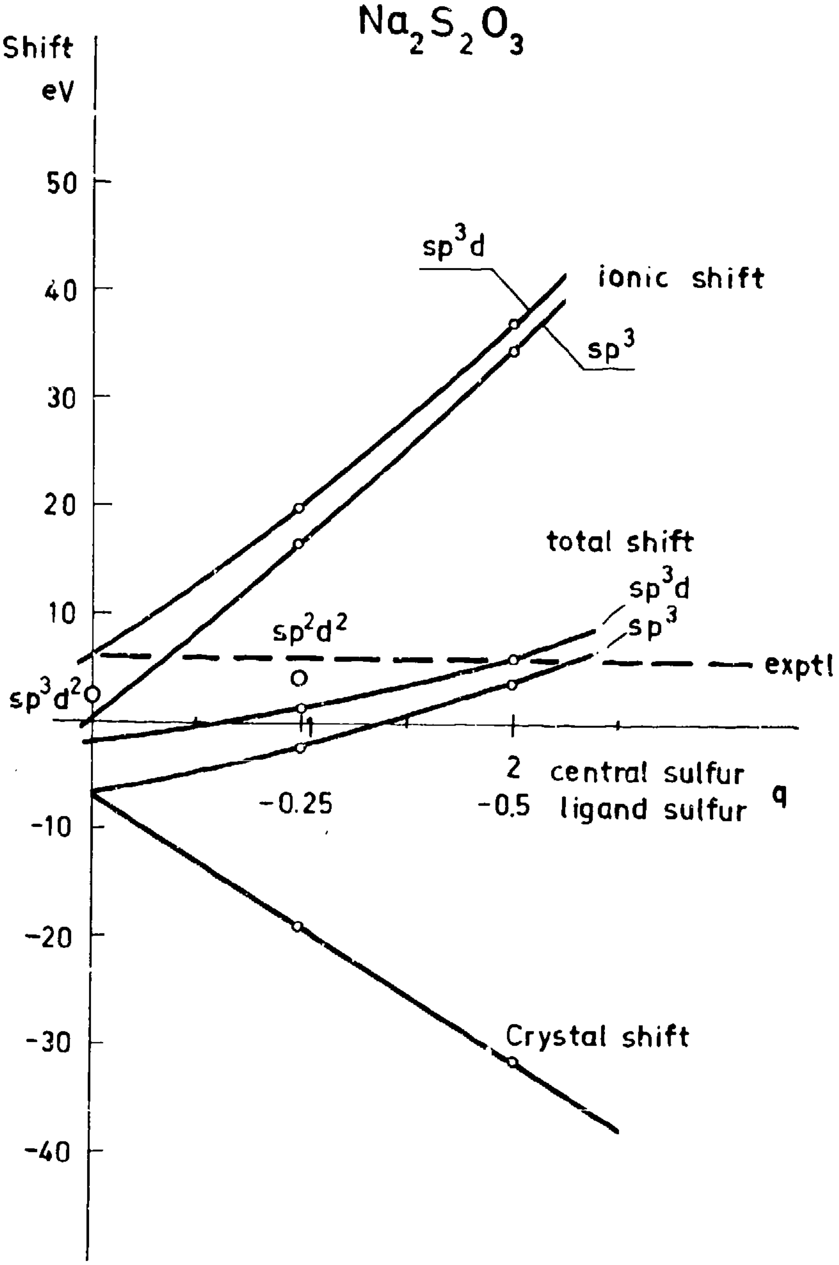

Fig. V:16. Shift in $2p$ level between the two sulfur atoms in $Na_2S_2O_3$. Charge difference of 2/3 units between oxygen and ligand sulfur.

effective charges of 1.2 and 1.3, respectively. If the possible contributions from *d* orbitals are considered, the charges become considerably smaller. NaCl is presumed to be purely ionic. However, an admixture of e.g. 10 % covalent character would change the shift by only a few tenths of an eV and thus be of little consequence to the present discussion. Also, a moderate degree of covalency in the $Na-ClO_4$ and $Na—ClO_3$ bonds would be unimportant.

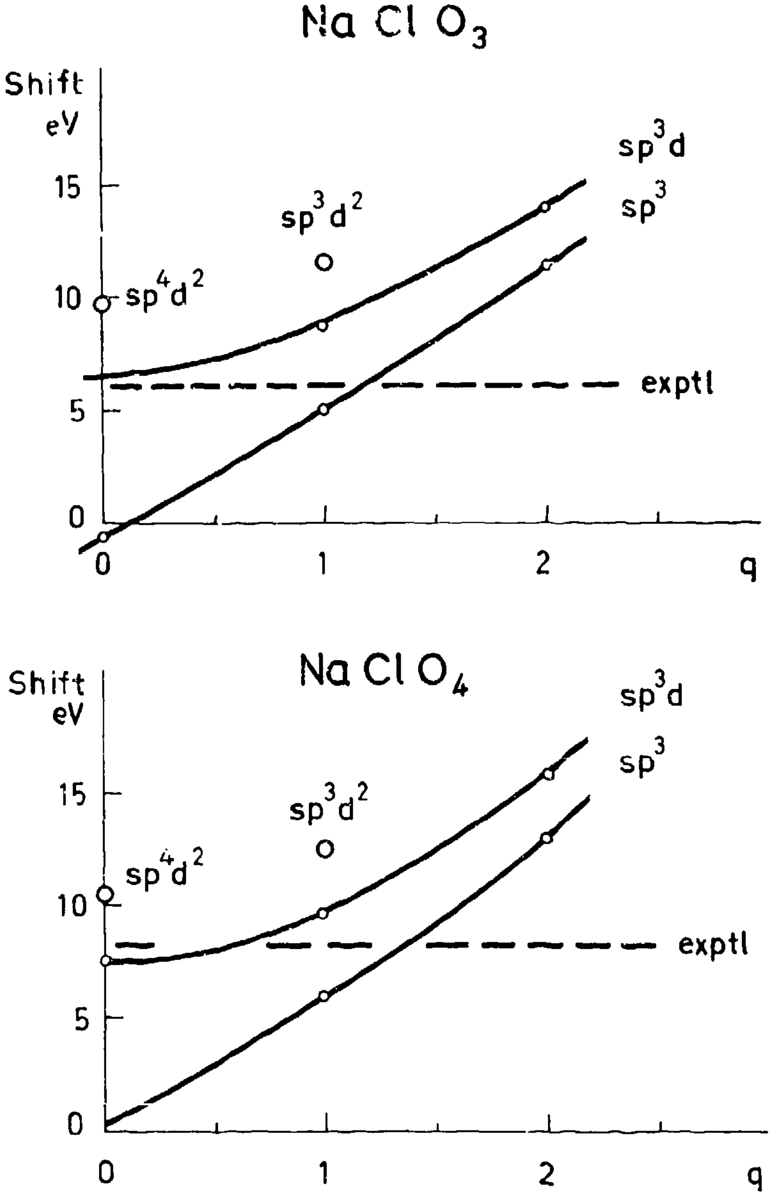

Fig. V:17. Total shift in $2p$ level of chlorine in NaClO$_3$ and NaClO$_4$ relative to NaCl. The cation is used as a reference in the calculation.

Interpretation of chemical shifts in X-ray emission lines

Chemical effects on the emission lines in X-ray spectra have been studied for several decades (see e.g. Refs. 105, 106, 120, 183, 282) and different interpretations have been suggested[184-186]. Since the energy of the emission line is essentially the energy difference between two inner electron states, one can assume that the crystal field has only a small effect. In the simple model for the crystal field used above, the energies of all inner electron states are shifted by the same amount, and consequently the emission lines are unaffected. Some free-ion shifts in the $K\alpha$ radiation are given in Table V:2d and the results for sulfur and chlorine are illustrated in Figs. V:12 and V:13, where some experimental shifts are also marked. When these figures are compared with Figs. V:8 and V:9, showing the corresponding shifts in the binding energies, one finds that the shifts in the emission lines depend much more on the method of calculation and on the assumptions made concerning the hybridization. The main reason for this is, of course, that the shifts in the emission lines are one order of magnitude smaller than the shifts in the binding energies.

Assuming an sp^3 hybridization for sulfur, the effective charges for SO_3^{2-}, SO_4^{2-}, and $S_2O_3^{2-}$ (central atom) are in the range 1.7 – 2.0 and for the ligand sulfur in $S_2O_3^{2-}$ about – 0.5 (see Fig. V:12). These values are in good agreement with those obtained from the shifts in the binding energies above. With sp^3d hybridization the calculations of effective charge do not give reasonable values.

Qualitatively, the same results are obtained for chlorine (Fig. V:13). Here the charges deduced from the shifts in the emission lines assuming sp^3 hybridization are somewhat larger than the corresponding values obtained from the shifts in the binding energies. sp^3d hybridization again yields quite unreasonable values.

The fact that the shifts in the emission lines calculated with a configuration of sp^3d type are significantly larger than the experimental shifts has two possible explanations. The calculated shifts are related to free atoms in their ground state (no hybridization), while the experimental values are, in the cases considered here related to elemental sulfur in solid form and chlorine in NaCl, respectively. If there is a considerable admixture of *d* electrons in these reference substances, the theoretical shifts would be reduced to more reasonable values. Elemental sulfur might have such admixture[232] but hardly NaCl. Therefore, a more probable explanation is that a configuration of sp^3d character with free-atom orbitals exaggerates the effect of *d* admixture in the sulfur and chlorine bonds. If this conclusion is correct then together with the previous conclusions on the shifts in the binding energies, some limits can be determined for the effective charges. However, it should be remembered that the relative uncertainty in the theoretical line shifts is considerable and, therefore, no definite conclusion should be drawn at the present stage.

Further investigations

As mentioned previously, the calculations presented here are only at a preliminary stage, and further investigations are now in progress. Some calculations have been made on elements in the second period (C, N, O), but they are not yet complete. In these cases the contribution from *d* orbitals is supposed to be small and, hence, one of the main obstacles facing the interpretation of sulfur and chlorine data would be absent. A further approach to this latter problem involves calculations of the distortion of the atomic orbitals by surrounding atoms or ions. We hope that it will be possible to derive more realistic wave functions particularly for the excited states in this way and make more definite statements about elements in the third period.

V:4. Correlation of ESCA Chemical Shifts with Valence

One of the many ways in which ESCA can contribute to the solution of chemical problems is to be found in the study of the chemical bond. This is a large and important field in organic chemistry. Since organic chemistry is based on the element carbon, and since carbon is versatile from the point of view of chemical binding, the number of combinations between carbon and other light elements in organic chemistry is very great. Of these the elements hydrogen, oxygen, nitrogen, phosphorus, sulfur, and the halogens are the most common ones. For the study of the reaction mechanisms in organic chemistry an understanding of the nature of the chemical bond is of great importance. Electron spectra have been shown to depend on valence in chemically combined elements and the chemical shifts reflect the charge distribution in molecules, see Chapter I and Section V:1. Electron spectroscopy should therefore be particularly well suited for the study of chemical bonding.

The application of ESCA to structural problems in organic chemistry appears to have great potential value. Electron spectra of an element are sensitive to such structural variations that involve changes in the oxidation state, or more generally in the valence state. The method is thus of value for the study of isomeric structures in which elements are involved in different oxidation states. (An example will be given in Section V:5b.)

7 – 671163 *Nova Acta Reg. Soc. Sc. Ups., Ser IV. Vol. 20. Impr.* $^{20}/_{11}$ *1967*

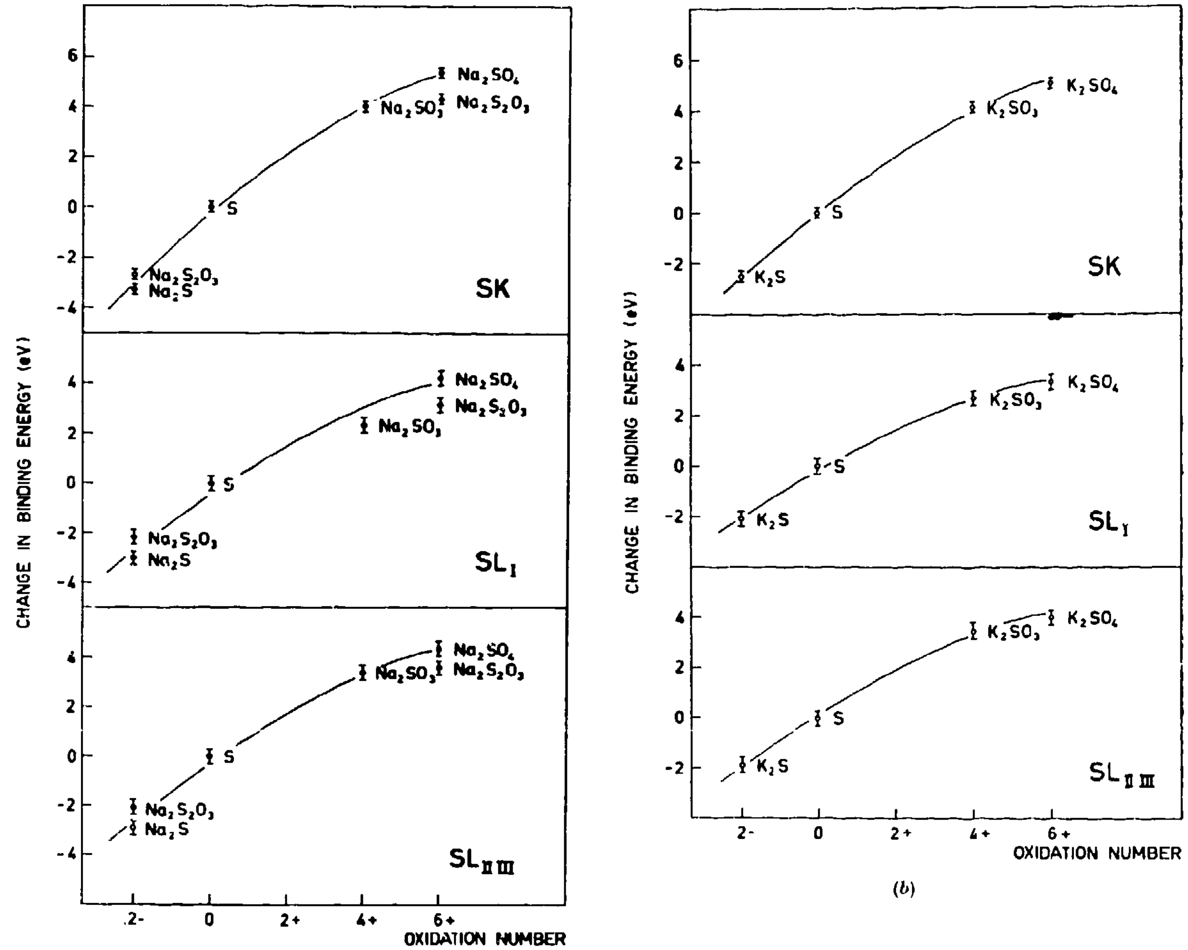

(a)

(b)

Fig. V:18. Chemical shifts in the K and L shells of sulfur versus oxidation number in a series of inorganic compounds with sodium (a) and potassium (b) as cations.[60]

The ESCA shifts used for the discussion in this section are taken mainly from early measurements on sulfur[60] and chlorine[61] in a series of compounds representing widely differing valence states.

Correlation of shifts with oxidation number

In previous papers[60,61] the shifts have been correlated with conventional oxidation numbers for series of different compounds, e.g. sodium and potassium salts of sulfur compounds and sodium salts of chlorine compounds (Figs. V:18 and V:19).

The investigation of shifts has now been extended to some organic sulfur compounds[83] (Table V:5) and to the 2s subshell of chlorine (Table V:6). The sulfur shifts do not fit well into the correlation previously obtained with inorganic sulfur compounds (dashed line in Fig. V:20). This is mainly due to the rather arbitrary character of the definition of oxidation number (Appendix 11), which approximates every bond between elements of different electronegativity to a fully ionized bond.

In certain compounds it may be doubtful which of the bonded atoms is the more electronegative. The carbon-sulfur bond is an example of this. On the electronegativity scale (Appendix 13) carbon and sulfur have the same electronegativity. Because alkyl groups possess a positive inductive effect (p. 206, Ref. 187) they are usually treated as electron donors in relation to sulfur. Thus sulfonic acid sulfur is assigned an oxidation number +4 whereas organic sulfide sulfur is assigned an oxidation number −2.

The oxidation number is defined as the charge, that is left on the central atom, when all ligands are removed with or without the bonding electrons, depending on their electronegativity. The oxidation number highly exaggerates the charge on atoms because it ignores the covalent character of the bonds. When the bonds have little ionic character, the concept of formal charge (Appendix 11) which approximates every bond to a fully covalent bond is a better representation of the real charge distribution.[188]

Correlation of shifts with a modified oxidation number

When ESCA shifts are subsequently correlated with oxidation states for the various sulfur compounds listed in Table V:5, better results are obtained, when the electrons are assigned as follows: for large electronegativity differences, $|\chi_A - \chi_B|$, the electrons are assigned according to oxidation number rules and for small electronegativity differences according to the rule for formal charge. From a consideration of the relation between electronegativity and amount of partial ionic character, I, of single bonds (Appendix 14) an electronegativity difference of 0.5 has been chosen as a limit for the two ways of assigning electrons. Thus when the electronegativity difference is >0.5 the assignment is made according to the rules for oxidation number and when it is <0.5 according to the rule for formal charge. In this section the quantity thus defined is called "modified oxidation number". The correlation between the ESCA shifts for the sulfur compounds and their modified oxidation numbers obtained in this way is shown in Fig. V:21. An improvement resulting from this modification is that both odd and even oxidation numbers become occupied. With the unmodified oxidation number scale elements in odd groups in the Periodic System mostly occupy odd numbers and elements in even groups even numbers.

A further example of the difficulty in applying the concept of oxidation number to complex molecules, is provided by the thiosulfate ion, in which the sulfur atoms are usually assigned the oxidation numbers +6 and −2 respectively by analogy with the sulfate ion (Fig. V:22a,b). The central sulfur atom with its formal positive charge will be more electronegative than the ligand sulfur atom and a more meaningful allocation would then be the one shown in Fig. V:22c. If rule No .3 in Appendix 11 is applied, the assignation shown in Fig. V:22d follows. With the modified oxidation number, the last assignation is unambiguous.

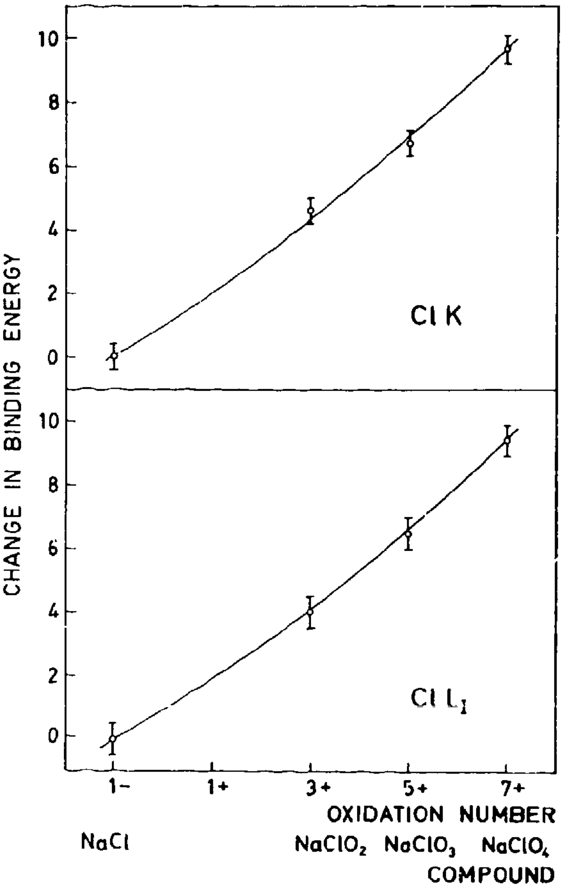

Fig. V:19. Chemical shifts in the K and L_I shells of chlorine in a series of inorganic compounds.[41]

The chemical shifts may be regarded as measures of the atomic charges in molecules or crystals, see Sections V:2 and V:3. From the observed shifts and by making the appropriate self-consistent field calculations in the free-ion model, the degree of ionization could in an earlier paper[68] be related to valence (defined as oxidation number) by a single coefficient in such a way that a consistent correlation between degree of ionization and shifts was obtained. Since the degree of ionization can be regarded as an idealized representation of charge, this is an indication that the chemical shifts reflect the charge distribution in mole-

Table V:5. Chemical shifts in the 1*s* level of sulfur and correlation data for sulfur compounds. (See also Figs. V:20, V:21, and V:27).

No.	Compound	Shift eV	Oxidation number	Modified ox. number	$\|\chi_A - \chi_B\|$	I %	Charge
1	Sulfur	0	0	0	0	0	0
2	Na_2S	−2.0	2	−2	1.6	47	−0.94
3	Na_2SO_3	+4.5	+4	+4	1.0	22	+0.88
4	$Na_2S_2O_3$	+5.3 1.7	+6 −2	+5 −1	1.0 0	22 0	+0.99 −0.50
5	Na_2SO_4	+5.8	+6	+6	1.0	22	+1.32
6	K_2S	−2.6	−2	−2	1.6	47	−1.02
7	K_2SO_3	+4.6	+4	+4	1.0	22	+0.88
8	K_2SO_4	+5.4	+6	+6	1.0	22	+1.32
9	$HS\,CH_2CH(NH_3Cl)COOH$	+0.1	−2	−1	0.4	0.4	−0.04
10	Penicillin	+0.3	2	0	0	0	0
11	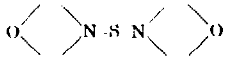	+1.4	+2	+2	0.5	6.5	+0.13
12	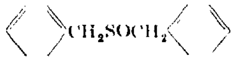	+3.0	0	+2	1.0	22	+0.44
13	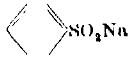	+4.2	+2	+3	1.0	22	+0.66
14	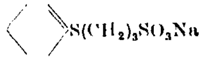	+5.3 +0.4	+4 −2	+5 0	1.0 0	22 0	+1.10 0
15	Heparin	+6.3	+6	+6	1.0 0.5	22 6.5	+1.25
16	$DextranOSO_3Na$	+5.6	+6	+6	1.0	22	+1.32

cules. Because of the simplicity and usefulness of this concept we have adopted it as a preliminary working hypothesis. We have, however, seen that the oxidation number highly exaggerates the charges on atoms. An attempt has therefore been made to derive a more satisfactory scale for the correlation of shifts with "valence state" expressed in terms of a calculated charge.

Table V:6. Chemical shifts in the 2*p* level of chlorine and correlation data for chlorine compounds. (See Fig. V:28).

Compound	Shift eV	Oxidation number	$\|\chi_A - \chi_B\|$	*I* %	Charge
NaCl	0	−1	2.1	67	0.67
$NaClC_4H_4O_2S$	1.8	−1	0.5	6.5	−0.07
$NaClO_2$	3.8	+3	0.5	6.5	+0.20
$NaClO_3$	7.1	+5	0.5	6.5	+0.33
$NaClO_4$	9.5	+7	0.5	6.5	+0.46

Correlation of shifts with charge

Estimation of charge based on the concept of electronegativity and the theory of resonance.—The estimation of charge distribution in molecules is a difficult problem. In certain systems it can be calculated by quantum mechanical methods. For some of the simplest compounds charge distributions calculated by means of quantum chemical methods are available, but since the methods and choice of parameters for these calculations have differed, the results are not comparable.

Recent developments in the electronegativity concept, have led to relatively simple methods for the estimation of charge distribution in molecules or groups.[189–193] These are based on the principle of equalization of electronegativity upon bond formation and operate with orbital-, bond-, and group-electronegativities (Appendix 16). Unfortunately, in the case of the higher oxidation states of, for example, sulfur or chlorine, they fail because of the lack of fundamental data for estima-

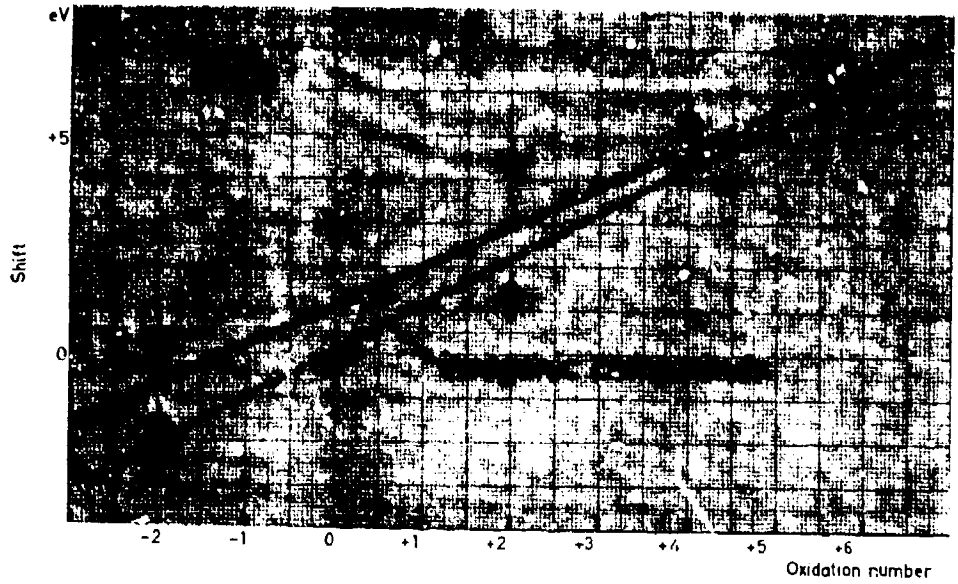

Fig. V:20. Chemical shifts in the 1s shell of sulfur versus oxidation number.

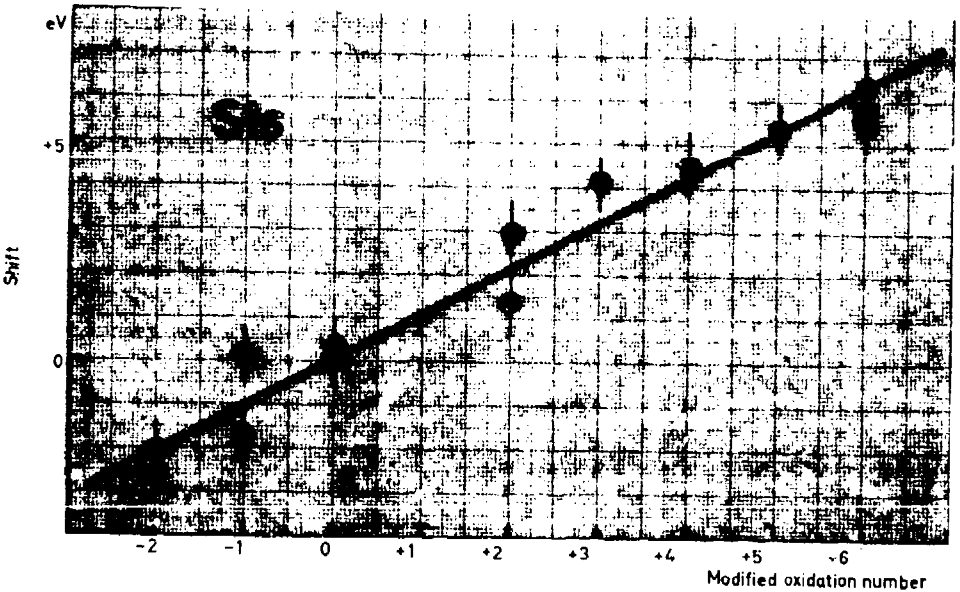

Fig. V:21. Chemical shifts in the 1s shell of sulfur versus modified oxidation number

tion of the electronegativity of the *d* orbitals involved in bond formation.

However, by employing a modification of the procedure used by Pauling for estimation of charges on atoms in molecules,[193] based on the original concept of electronegativity as an invariant atomic property, we have derived a method for calculating charge, which can also be used for the higher oxidation states involving *d* orbitals.

The procedure of Pauling is based on the concept of partial ionic character of bonds (Appendix 14). For this treatment knowledge of the exact bond lengths in molecules and of the pure single, double and triple bond lengths of the bonds under consideration is re-

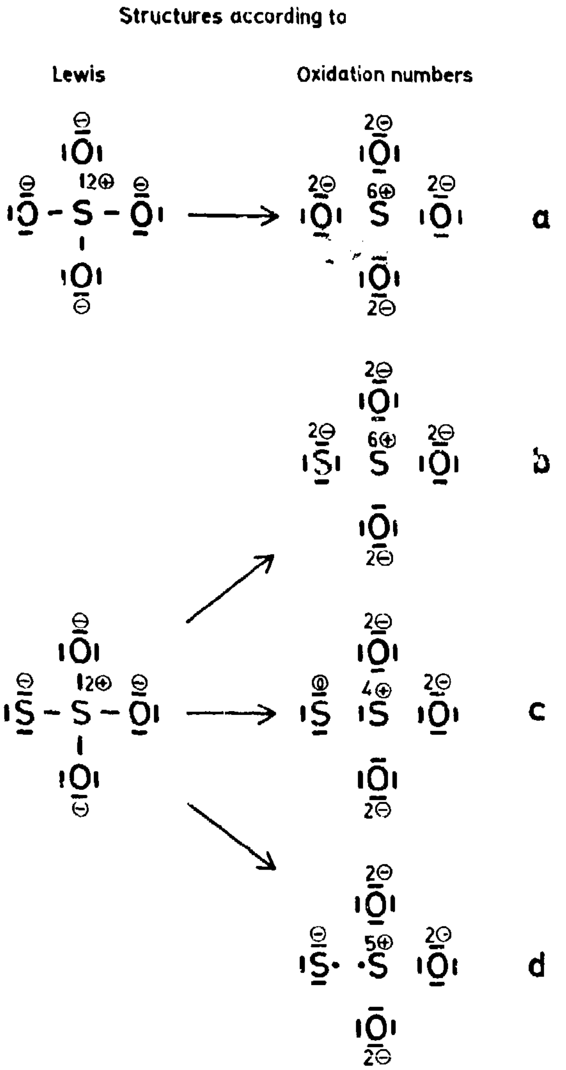

Fig. V:22. Derivation of oxidation numbers for the sulfate and thiosulfate ions.

quired. The bond lengths are used to estimate the bond number, n, which represents the total degree of covalent bonding between atoms. The basis for the calculation of this quantity is given in Appendix 15.

Here we shall only illustrate the use of n for calculation of charge by giving Pauling's calculation of charge on the sulfur atom in the sulfate ion (p. 322, Ref. 193):

The bond number of the sulfate ion calculated from bond lengths is 1.83. This means that an extra electron pair from each oxygen in the Lewis structure is shared

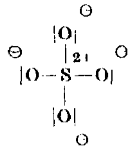
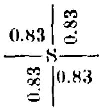

between oxygen and sulfur to a degree of 83 per cent: The charge on the sulfur then becomes $+6-4-4\cdot 0.83=-1.32$. Each bond is assumed to have the amount of ionic character corresponding to the electronegativity difference between the two atoms, 22 per cent. (Appendix 14). As a result of this partial ionic character the sulfur loses $4\cdot 1.83\cdot 0.22=1.61$ of its share of electrons to the oxygen, and the residual charge on sulfur becomes $-1.32+1.61=+0.29$.

Unfortunately accurate bond lengths are only available for a limited number of molecules. We have, however, made approximate estimations of bond numbers as follows. In the resonance theory (Appendix 12) there are certain rules for estimating the relative weight of each of the structures contributing to a resonance hybrid.[194] The most stable structures contribute most. According to the principle of electroneutrality (pp. 172, 273, Ref. 193) the most stable structures are those in which there is a minimum of charge separation. Structures with charges of the same sign on adjacent atoms are less stable and make small contributions. (Adjacent charge rule p. 270, Ref. 193). In charged structures, the structures with negative charges on the most electronegative atoms are the most stable. Selecting the structures which best comply with these requirements we have estimated approximate bond numbers for calculation of charges. Allowing for d_π bonding in sulfur compounds, the structures in which the central sulfur atom is formally neutral have been chosen. We shall illustrate the procedure by three examples, the sulfate, and the thiosulfate ions and sodium sulfide:

1. Starting with the Lewis[195] structure (I) electron pairs from the oxygen atoms are shared with the central sulfur atom in order to neutralize the formal charge on the sulfur atom:

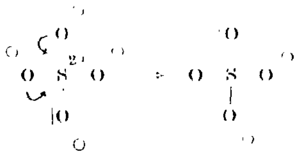

I II

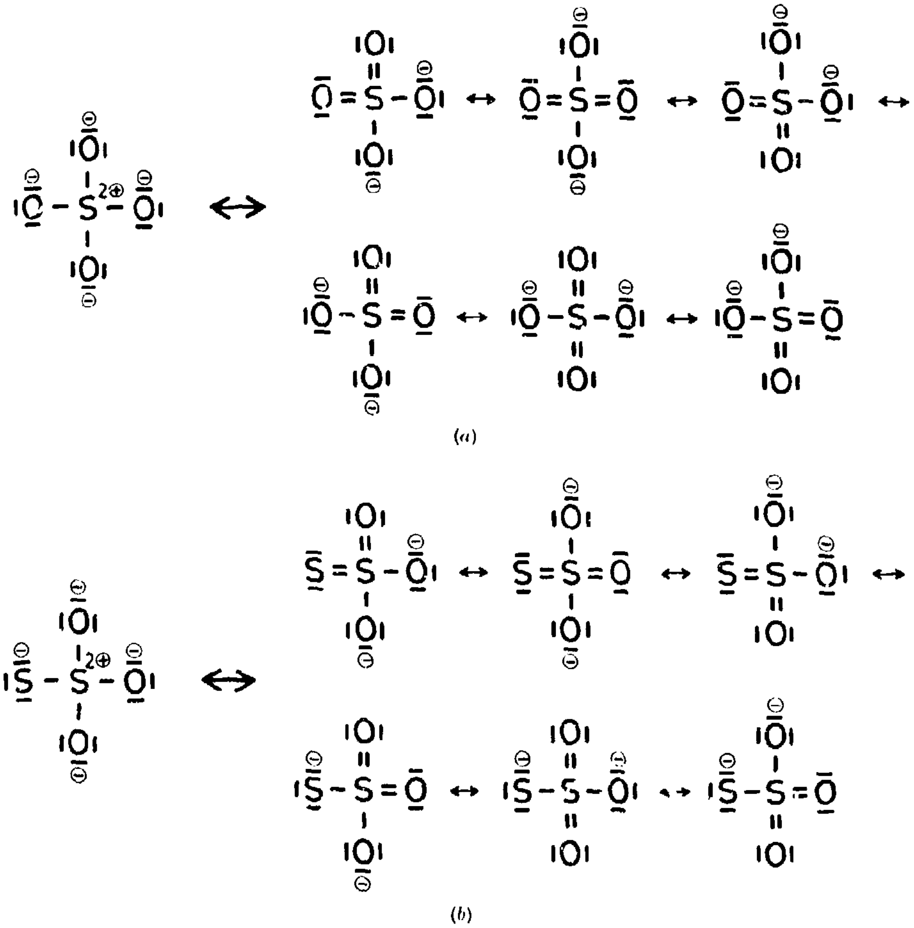

Fig. V:23. Resonance structures for the sulfate (*a*) and thiosulfate ions (*b*).

A structure obtained in this way (II) contains only covalent bonds.

The number of bonds is determined by the position of the central atom in the Periodic Table. Six different structures of type II can be drawn (Fig. V:23a). In these every sulfur-oxygen link is three times a single bond and three times a double bond. These structures are assumed to make the predominating contributions to the resonance hybrid. If the contributions of other less important structures are neglected, n becomes $(3 \cdot 1 + 3 \cdot 2)/6 = 9/6 = 1.5$. This is equivalent to saying that as a result of the resonance the six bonds in the type II structure are distributed equally over the four ligands, thus $n = 6/4 = 1.5$. The 50 per cent double bond character neutralizes the formal charge on the sulfur atom. The electronegativity difference transfers $+4 \cdot 1.5 \cdot 0.22 = +1.32$ to the sulfur atom, which leaves a total residual charge of $+1.32$. This approximation is a better representation of the real charge distribution than the oxidation number ($+6$).

2. The resonance structures for the thiosulfate ion are shown in Fig. V:23b. The bond number, n, for the sulfur-oxygen bonds is $(3 \cdot 1 + 3 \cdot 2)/6 = 1.5$. These bonds transfer $+3 \cdot 1.5 \cdot 0.22 = +0.99$ to the central sulfur atom. The bond number for the ligand sulfur atom is $(3 \cdot 1 + 3 \cdot 2)/6 = 1.5$ and the charge $= (3 \cdot (-1) + 3 \cdot 0)/6 = -0.5$.

3. Sodium sulfide may be represented as follows:

$$\text{Na}-\text{S}-\text{Na}$$

$n = 1$, charge $= -2 \cdot 1 \cdot 0.47 = -0.94$.

In the same way charges have been calculated for the

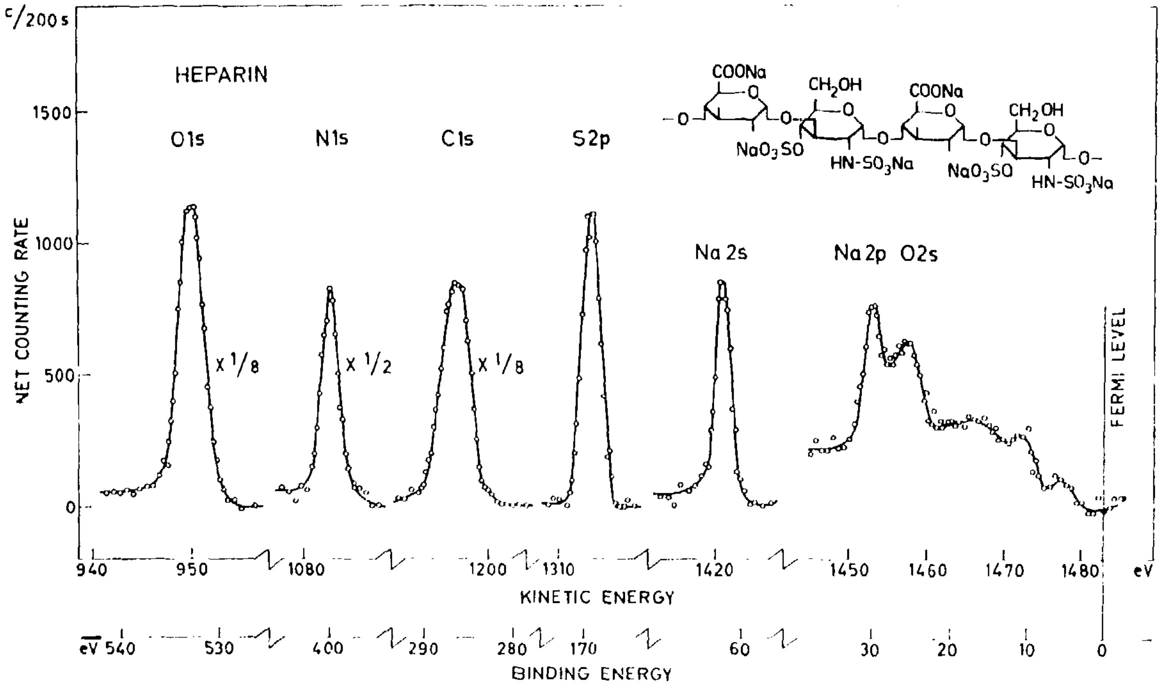

Fig. V:24. Electron spectrum of heparin excited with Al$K\alpha$ radiation.

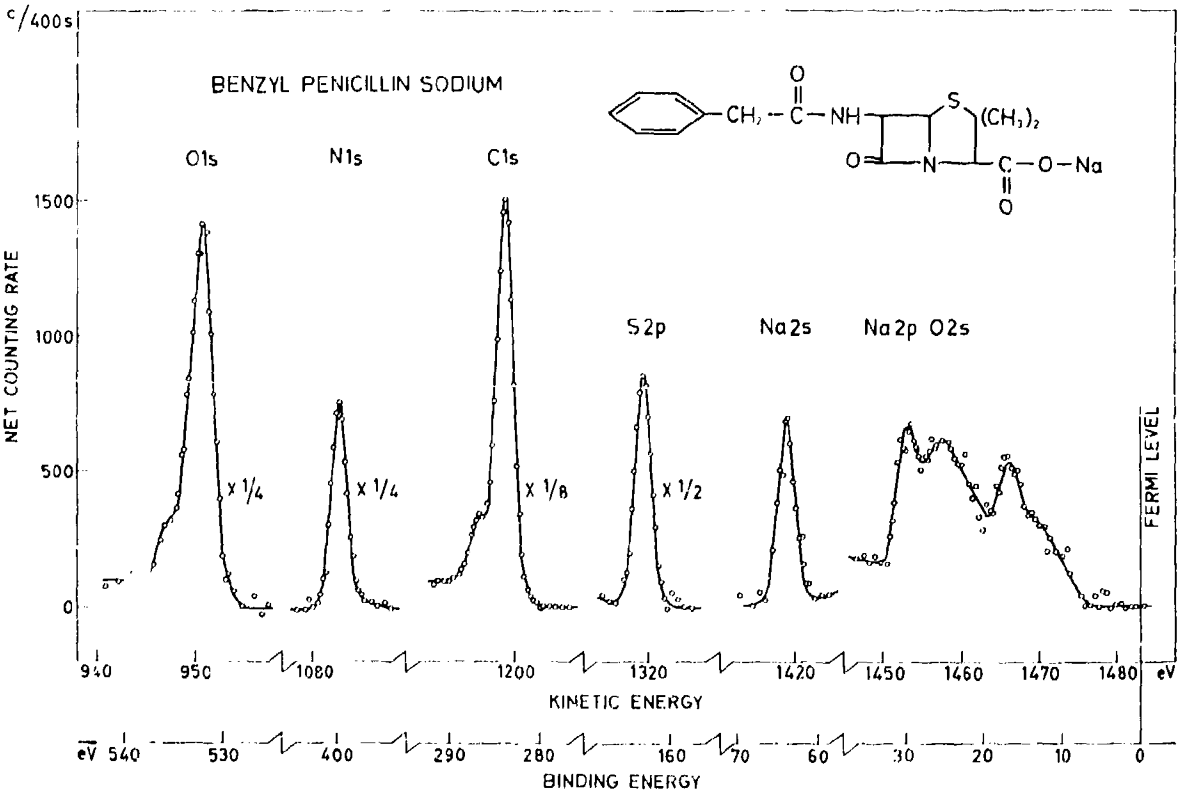

Fig. V:25. Electron spectrum of benzyl penicillin sodium excited with Al$K\alpha$ radiation.

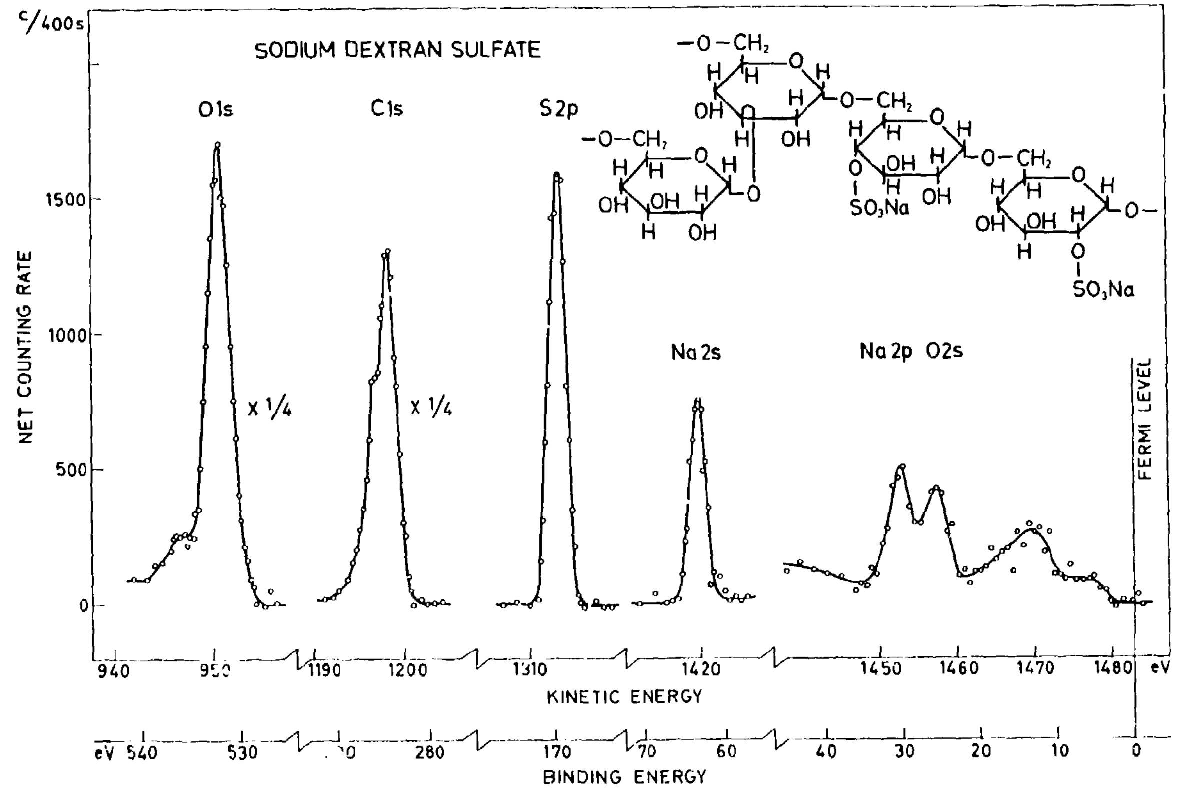

Fig. V:26. Electron spectrum of sodium dextran sulfate excited with Al$K\alpha$ radiation.

compounds listed in Tables V:5 and V:6. The quantity thus calculated can be regarded as a measure of "valence state" in terms of charge, and should be distinguished from charges calculated by more exact quantum chemical methods or from experimental shifts.

Spectra of some of the compounds in Table V:5 are shown in Figs. V:24, V:25, and V:26. In the large penicillin molecule as well as in the sulfated polysaccharides heparin and dextran sulfate, the sulfur lines are as sharp and distinct as in smaller molecules.

Correlation of shifts with charge for sulfur and chlorine compounds. -The relationship between calculated charge and chemical shifts for the sulfur compounds is plotted in Fig. V:27. The slope of the regression line agrees well with the slope obtained from compound No. 14, in Table V:5 containing two different covalent sulfur atoms in the same molecule. This correlation scale distinguishes between 13 "valence states" compared with 5 and 8 in Figs. V:20 and V:21 respectively.

The relationship between calculated charge and chemical shifts for some chlorine compounds is shown in Fig. V:28. With the sulfur compounds an approximately rectilinear plot was obtained, Fig. V:27, whereas the plot with the chlorine compounds in Fig. V:28 is curvilinear. There is no reason to anticipate a linear shift-charge plot. The free-ion model predicts an increasing shift per degree of ionization (Section V:2 and V:3).

Compared with other calculations which allow for d_π bonding the charges obtained for sulfur in the higher oxidation states seem high. The charge on sulfur in the sulfate ion calculated by the more exact bond length treatment of Pauling is for instance +0.29. From a calculation based on the equalization of electronegativity (Appendix 16) the charge +0.19 is obtained.[196] In a recent quantum chemical calculation using the Wolfsberg-Helmholz approximation the charge obtained on sulfur in the sulfate ion ranges from +0.16 to

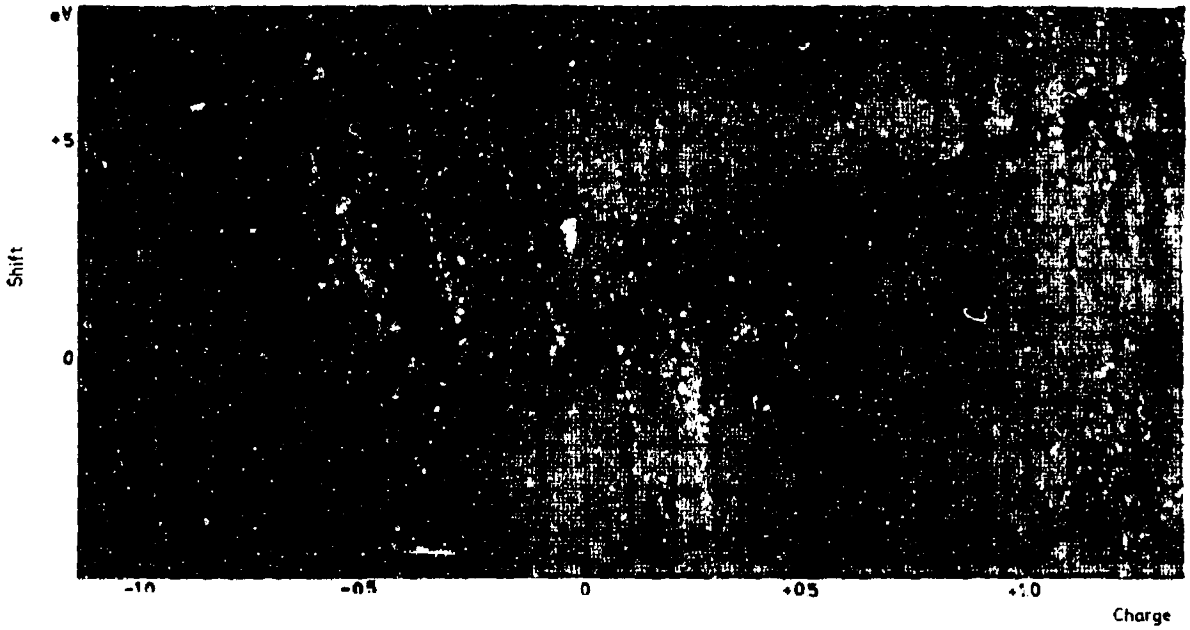

Fig. V:27. Chemical shifts in the 1*s* shell of sulfur versus calculated charge.

+0.52 when *d* orbitals are included and from +0.49 to +1.36 when *d* orbitals are excluded[197]. A molecular orbital calculation on the sulfite ion including *d* orbitals has given the charge +0.59 on the sulfur atom[198]. Another calculation using an approximate MO-LCAO-SCF method without empirical parameters and not allowing for d_π bonding, gives higher charges on the sulfur in the sulfate, +1.79, thiosulfate, +1.54 (−0.96), and sulfite, +0.93, ions.[233]

For the chlorine-oxygen compounds in which the

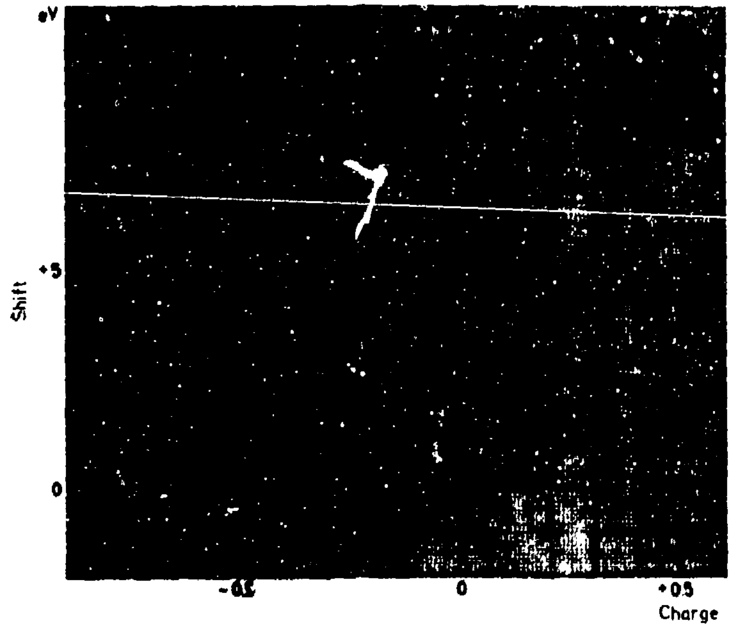

Fig. V:28. Chemical shifts in the 2*p* shell of chlorine versus calculated charge.

electronegativity differences are smaller than in the case of sulfur-oxygen compounds the simplified resonance treatment for derivation of bond number seems to give better results for the Cl—O bonds than for the S—O bonds, compared with data calculated from bond lengths.

For the chlorite ion, for example, $n = (1 \cdot 1 + 1 \cdot 2)/2 = 1.5$

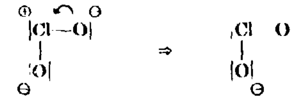

and the charge $q = +2 \cdot 1.5 \cdot 0.065 = +0.20$. Bond length data give bond number 1.37 and charge +0.38 (p. 324, Ref. 193).

When comparing charges obtained with the present treatment with charges from other sources it should be kept in mind that the atomic electronegativity scale ignores the influence of bonding on electronegativity. The electronegativity of different kinds of orbitals differs more or less from the average atomic electronegativity. Thus, for a bond involving atoms with a relatively large difference in electronegativity and a considerable contribution from higher orbitals, as for instance the *d* orbitals in sulfur-oxygen bonds, the use of the average atomic electronegativity probably causes greater errors in calculated charges than when the electronegativity differences are smaller, as for example in chlorine-oxygen compounds.

Another factor causing errors is the influence of charge on electronegativity. Corrections can be made for this (Appendix 13), but because of the approximate character of charges calculated from electronegativity differences, especially when *d* orbitals are involved, we have ignored it in this section.

For reasons obvious from the discussion in this section the proposed correlations must be regarded as tentative and liable to further modification and refinement.

Discussion

The Pauling treatment is mainly concerned with bond lengths and interprets bond shortening as being solely due to a higher degree of bonding. Some objections have been raised over the preponderating double bond character that this treatment assigns to sulfur-oxygen bonds.[199] This may be an indication that bond numbers calculated on this basis are uncertain and in the case of sulfur-oxygen bonds too high. For some sulfur-oxygen compounds for which bond lengths are known, calculation of charge fails when based on the bond length treatment. In fact, an earlier development by Pauling assigned bond number 1.54 to the S—O bond in the sulfate ion[200] (cf. present value 1.83, p. 321, Ref. 193). It is also of interest to note that bond numbers calculated by Siebert using force constants from Raman spectra[201] correspond very closely to the bond numbers of the structures with formally neutral sulfur, see Table V:7.

Table V:7. Bond numbers obtained from Raman spectra[201] and calculated by the present method.

	Ref. 201	Calc.
SO_4^2	1.53	1.50
$S_2O_3^2$ S−O	1.57	1.50
$S_2O_3^2$ S−S	1.46	1.50
SO_3^2	1.29	1.33

The same applies to calculations on various sulfur compounds based on IR data.[202] As long as the interpretation of bond shortening remains controversial it therefore seems justified to base the calculation of bond numbers for correlation purposes on the simple treatment involving resonance between valence-bond structures and a minimum of formal charges.

The present approach is mainly concerned with charges, and because of the lack of better simple methods our estimation of charges on atoms has been based on the proposed simplification of the Pauling treatment using bond numbers. However, the uncertainty in the bond numbers affects the calculation of charges. The absolute values of the charges calculated by the present treatment should therefore be regarded as very approximate. They should only be used for comparing bonding effects in series of similar compounds, i.e. only their relative values are significant.

The correlation of chemical shifts with independently estimated charges constitutes an interesting contribution to the discussion of the character of bonds. Provided that the ESCA shifts reflect the atomic charge in molecules in a consistent manner, agreement of a calculated charge with the general pattern implies that the structure on which the calculation of charge has been based is correct. Deviations from the general

Table V:8. Electronegativity values of elements involved in nitrogen bonds.

The electronegativities of elements with formal charge have been corrected according to Pauling (p. 65, Ref. 174).

Element	Electro-negativity	Element	Electro-negativity
H	2.1	$N^{\oplus}$	3.3
C	2.5	O	3.5
$C^{\ominus}$	2.2	$O^{\ominus}$	3.2
N	3.0	S	2.5
$N^{\ominus}$	2.7		

correlations would mean that the structure chosen for the calculation has been incorrect. Deviations can therefore serve to single out interesting cases for study, and may provide useful information on chemical structure.

It should be noted that this approach differs in principle from calculation of charges from observed shifts (see Section V:3). The latter approach is based on the assumption that a definite relationship exists between shifts and charge distribution. The former approach instead poses the question whether the shifts really reflect the charge distribution in molecules. A combination of these two approaches is therefore highly desirable.

The correlation of chemical shifts with independently estimated charges promises to be of value for the study of, for instance, sulfur-oxygen bonds. In spite of having been intensely investigated by chemists for several decades, the true character of these bonds is still a subject of debate.

The conclusions that can at present be drawn from this discussion are:

1. The relationship between valence defined as oxidation numbers and ESCA shifts has little real physical meaning, although it may be very useful as a guide for handling shift data.

2. The relationship between independently estimated charge on the atoms and ESCA shifts appears to be more meaningful, but at present only approximate estimations of charge have been made for extended series of complex molecules.

3. The dependence of ESCA shifts on charges on individual atoms in molecules provides a new basis for the study of the character of bonds in complex molecules.

V:5. Chemical Binding and Molecular Structure Studied by ESCA

V:5a. ESCA shifts of nitrogen

Since nitrogen belongs to the second period it obeys the octet rule and cannot expand its valence shell by the use of *d* orbitals like for instance sulfur. The complications caused by the expansion of the valence shell in the estimation of the bond number necessary for the calculation of atomic charge from electronegativity differences and partial ionic character of bonds (Section V:4) are therefore absent in nitrogen. When in the study of ESCA shifts use is made of the absolute value of the calculated charges (as for instance in comparison with charges from other sources) nitrogen is consequently more suitable than sulfur. We have made fairly extensive measurements of ESCA shifts in nitrogen compounds. Thirty-nine organic compounds were studied and the nitrogen 1*s* level was measured from the electron spectra.[76,81] Both solid and liquid samples were investigated in an effort to cover a reasonably wide range of calculated charge on the nitrogen.

Calculation of charge

In compounds with formal charges the electronegativities were corrected for the effect of electric charge. According to Pauling,[174] one unit of formal charge changes the electronegativity value of an element by approximately two thirds of the electronegativity difference between the actual element and the next element in the Periodic Table (see Appendix 13). The electronegativities, χ, of the most important atoms in nitrogen organic chemistry are listed in Table V:8. The partial ionic character, I, of the various bonds in

Table V:9. Partial ionic character for bonds, derived from the relationship by Pauling.[174]

The signs refer to the calculation of charge on nitrogen.

Bond	Partial ionic character	Bond	Partial ionic character
N – H	– 0.18	N – O	+ 0.06
$N^{\oplus}$ – H	– 0.30	N – $O^{\ominus}$	+ 0.01
N – C	– 0.06	$N^{\oplus}$ – O	+ 0.01
N – $C^{\ominus}$	0.15	$N^{\oplus}$ – $O^{\ominus}$	≈ 0.00
$N^{\oplus}$ – C	– 0.15	N – S	– 0.06
$N^{\oplus}$ – N	– 0.02	$N^{\oplus}$ – S	0.15
$N^{\oplus}$ – $N^{\ominus}$	– 0.09		

which nitrogen is involved, calculated according to Pauling's empirical equation (Appendix 14), is listed in Table V:9. The calculation procedure will here be illustrated by two examples, aniline and nitrobenzene.

Fig. V:29 shows the structures of aniline and nitrobenzene. The electronegativities and charges are given in the figure. The charge, q, has been obtained as the sum of the formal charge, Q, and the partial ionic character, I, of the bonds in which nitrogen is involved: $q = Q + \Sigma I$. The sign of the electronegativity difference of the elements involved in the bond determines the sign on I. With this treatment the charge on the nitrogen in a nitrogen containing group becomes the same for aliphatic and aromatic compounds, e.g. $q = -0.42$ for an amino group.

In the qualitative resonance theory the chemical properties of aniline and nitrobenzene are accounted for by contributions from resonance structures of the type shown in Fig. V:30. These structures are due to the M effect (resonance or mesomeric effect) of the groups.[203, p. 212 Ref. 187] When a group with a strong M effect is conjugated with a substituent possessing an M effect of opposite sign, the effect of the conjugated resonance structures on the charge cannot be ignored.

The effect of resonance on the charge on the amino nitrogen atom is also observed in unsubstituted aniline, and the measured binding energy has been used to estimate the contribution of the conjugated structures to the resonance hybrid.

The calculations do not take into account the effect of the partial ionic character of a bond on other bonds, and is thus only strictly applicable to singly bonded diatomic molecules.[196] Nevertheless it can be used as a first approximation also for complex molecules.

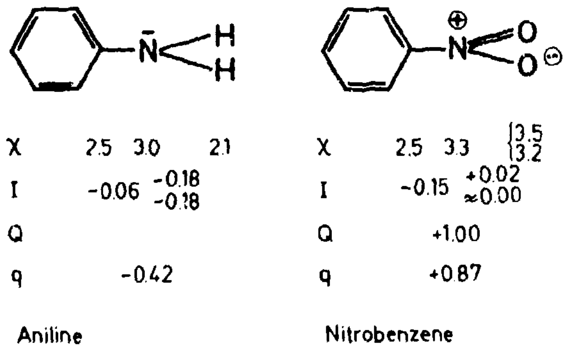

Fig. V:29. Calculations of charge on nitrogen in aniline and nitrobenzene using data from Tables V:8 and V:9.[81]

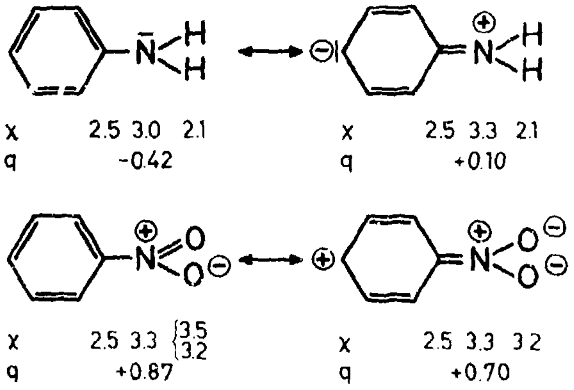

Fig. V:30. Effect of conjugation on the charge on nitrogen in aniline and nitrobenzene.[81]

The NH_3^+-group is a case where the mutual influence of the partial ionic character of the NH bonds cannot be ignored, Fig. V:31. With the electronegativity corrected for the formal charge on nitrogen, the partial ionic character of the bonds causes all the positive charge to reside in the hydrogens, leaving no positive charge on the nitrogen. Thus the need for a correction is eliminated and the charge on the nitrogen then becomes $q = +0.39$. In this case we have therefore calculated a charge on the nitrogen which takes the mutual effect of the partial ionic character of the bonds into account. The charge obtained in this way is $q_0 = +0.27$. Because of the approximate character of electronegativities and calculations based on them, no corrections for the effect of partial ionic character on electronegativity were applied except in this extreme case.

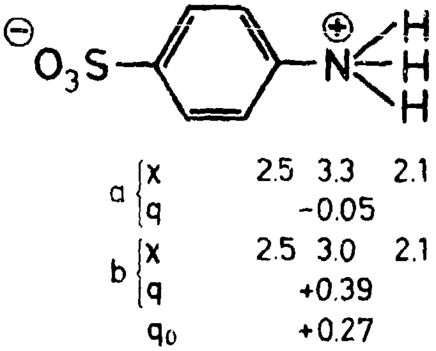

Fig. V:31. Calculations of charge on nitrogen in the NH_3^+-group a) with and b) without correction of electronegativity for formal charge on nitrogen.[81]

Table V:10. Comparison of charges calculated from electronegativity and by the MO-LCAO-method according to Del Re *et al.*[205,206]

Group	q MO-LCAO-method	q Present method
NH_3	−0.75	−0.54
RNH_2	−0.54	−0.42
R_2NH	−0.36	−0.30
R_3N	−0.20	−0.18
$RN^{\oplus}H_3$	+0.13	+0.27

The calculated charges have been compared for some important groups with the corresponding literature values calculated by a semiempirical MO-LCAO-method for saturated organic molecules. This MO-LCAO-method uses an approximation proposed by Del Re *et al.*[205,206] and the values are listed in Table V:10. They compare remarkably well and the use of the simplified electronegativity treatment for the calculation of charge when correlating shifts in binding energy therefore seems justified.

In order to cover as much of the charge scale as possible a series of compounds with widely varying structures was used. This made more elaborate methods for the calculation of charge impractical in the initial stage of this investigation. Charge calculations using an extended Hückel molecular orbital method are in progress.*

Results

Twenty-seven of the compounds studied in this investigation are listed in Table V:11. It gives the measured nitrogen 1*s* binding energies, E_b, the calculated charge for the nitrogen, and the number of measurements made on each compound, *n*.

The spectra, obtained from compounds which contain nitrogen atoms, all with the same calculated charge, only show one peak, while compounds containing nitrogen atoms with different calculated charges give spectra with more than one peak. Hexamethylenetetramine (compound No. 7) is of the first type and its spectrum is shown in Fig. V:32. Sodium azide (compound No. 1) is an example of the second type and its spectrum is shown in Fig. V:33. Of the three nitrogen atoms in the azide ion, the central atom has a calculated charge of +0.64 according to the structural formula in Fig. V:33 and the other two nitrogen atoms both have a lower oxidation state, characterized by a charge $q = -0.72$. The electron spectrum is in accordance with this and shows two nitrogen 1*s* lines of which the one of higher kinetic energy has twice the intensity of the other line. Another example of a spectrum from a nitrogen compound with different calculated charges is given in Fig. I:18. Fig. I:17 shows a chemical shift of the 1*s* core electrons in nitrogen for the sample consisting of two different compounds, aniline and nitrobenzene. These are both liquids at room temperature and a target for the X-rays was made from a mixture of the two compounds by the freezing technique described in Section VIII:5.

In Fig. V:34 the measured binding energies have been plotted against calculated charge for nitrogen.

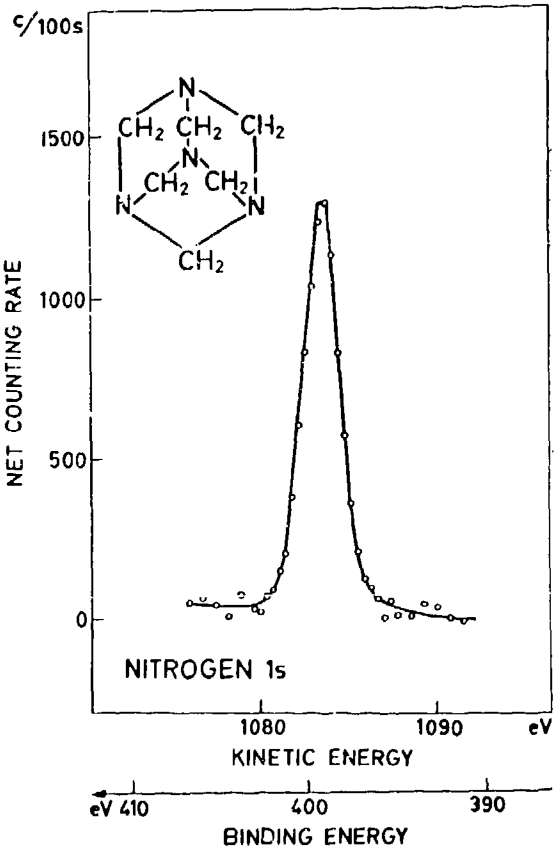

Fig. V:32. Nitrogen 1*s* electron spectrum from hexamethylenetetramine.[81] The molecule contains four nitrogen atoms all of which have the same calculated charge.

---

* We thank Fil.lic. Rolf Manne for providing the computer program.

The curve in the figure has been fitted to all the points except Nos. 1, 2, 15 and 16 by the method of least squares. If one considers that the charge parameter has been obtained by an approximate method and that the series under study is composed of compounds with widely varying structures, the correlation can be regarded as good. In the molecules containing oxygen and sulfur the O 1*s* and S 2*p* levels have also been measured and will be dealt with in Sections V:5b and V:5c.

From Table V:11 and Fig. V:34 it can be seen that the binding energies of nitrogen in various nitro compounds fall within a small range. The substituent effects do not seem to affect the binding energies of nitrogen in the nitro groups to any great extent, and the binding energy 405.2 eV can thus be taken as characteristic of an aromatic nitro group.

In Table V:12, data obtained for compounds in which resonance affects the charge distribution have been listed, and the correlation in Fig. V:34 has been used to estimate the contribution of conjugated or resonance structures as discussed below.

The binding energy for the nitrogen 1*s* electrons in aniline, compound No. 28, is higher than could be expected from a non-conjugated structure. The charge assigned to the nitrogen atom in this molecule by the correlation, - 0.14, means 54 % contribution of conjugated structures.

In compound No. 29 the peak representing the nitrogen in the amino- and azo-groups, Fig. V:35, has been resolved graphically under the assumption that the two nitrogens of the azo group have equal binding energies. The structural formula and charges are given in Fig. V:36. This assigns a charge to the amino group which leads to 94 % contribution of the conjugated structure. If the binding energies of the nitrogens in the azo group are assumed to be unequal, the same distribution of intensities in the spectrum would only be obtained if the binding energy of the amino group nitrogen were equal to that of one of the azo group nitrogens. With this assumption the binding energy of the amino group nitrogen should be about equal to that of the aniline nitrogen. This is unlikely for two reasons. Firstly, since the amino group is conjugated with a strong *M* substituent, one would expect that the contribution from the conjugated structure should be higher than in aniline. Secondly, the auxochromic character of the substituents and the colour of the compound also indicate a high contribution from the conjugated structure. For reasons mentioned below, no definit conclusions can be made about the conjugation from the values for the nitro group.

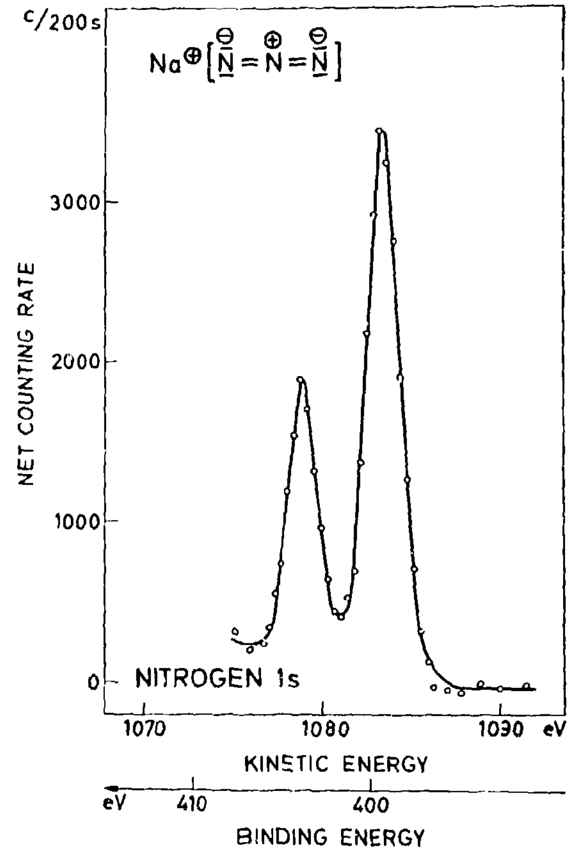

Fig. V:33. Nitrogen 1*s* electron spectrum from sodium azide.[81] The peaks corresponding to the positively and negatively charged nitrogen atoms are identified from the line intensities.

In compounds Nos. 9, 22, 23, and 30, Tables V:11 and V:12, the binding energies of the nitrogen in the sulfonamido groups are significantly higher than that of an ordinary aliphatic amino group. This is consistent with the known high electron attracting power of the sulfonyl group which can be represented by the resonance structures:

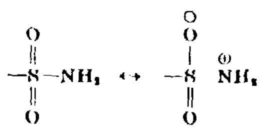

$$-\overset{\overset{O}{\|}}{\underset{\underset{O}{\|}}{S}}-NH_2 \leftrightarrow -\overset{\overset{\overset{\ominus}{O}}{|}}{\underset{\underset{O}{\|}}{S}}\ \overset{\oplus}{N}H_2$$

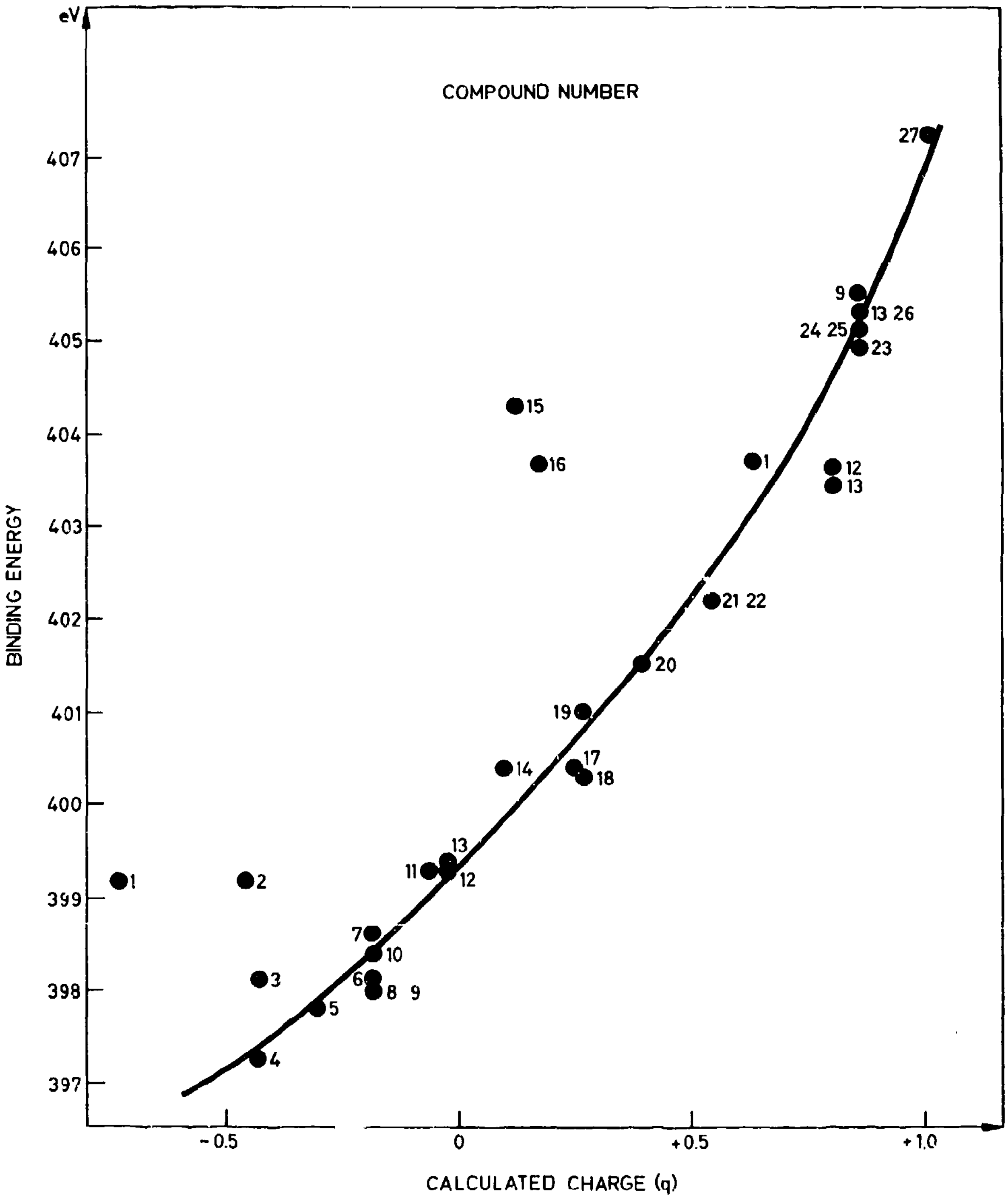

Fig. V:34. Binding energy for the nitrogen 1s electrons versus calculated charge.[81]

Table V:11. Calculated charges and measured binding energies (E_b) for a series of nitrogen containing compounds.

The nitrogens to which the given data refer are given with bold symbols. *n* refers to the number of measurements.

Nr	COMPOUND	n	Calculated charge	E_b N1s
1	$[\overset{\ominus}{N}=\overset{\oplus}{N}=\overset{\ominus}{N}]Na^{\oplus}$	2	-0.72	399.2
2	$[N\equiv\overset{\ominus}{C}]K^{\oplus}$	2	-0.45	399.2
3	$\begin{smallmatrix}H\\H\end{smallmatrix}{>}\bar{N}-CH_2CH_2CH_2CH_3$	5	-0.42	398.1
4	$\begin{smallmatrix}H\\H\end{smallmatrix}{>}\bar{N}-CH_2COO^{\ominus}Na^{\oplus}$	1	-0.42	397.3
5	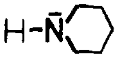	3	-0.30	397.8
6	$n\text{-}H_9C_4-\bar{N}\begin{smallmatrix}C_4H_9\text{-}n\\C_4H_9\text{-}n\end{smallmatrix}$	6	-0.18	398.1
7	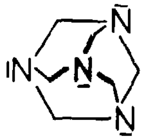	2	-0.18	398.6
8		3	-0.18	398.0
9	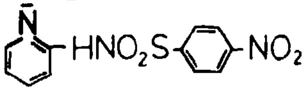	3	-0.18	398.0
10	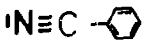	4	-0.18	398.4
11	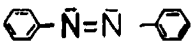	2	-0.06	399.3
	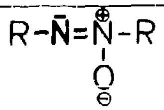		-0.02	
12	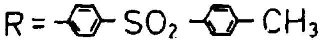	2		399.3
13	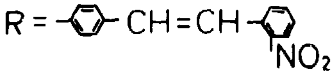	5		399.4
14		2	+0.10	400.4
15	$[O=\bar{N}-\overset{\ominus}{O}]Na^{\oplus}$	1	+0.13	404.3

Table V : 11. *(Cont.)*

Nr	COMPOUND	n	Calculated charge	E_b N1s
16	$O{=}\bar{N}{-}O{-}(CH_2)_4\ CH_3$	2	+0.18	403.7
17	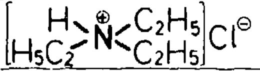	3	+0.25	400.4
18	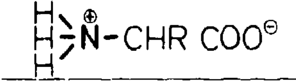 [1]	10	+0.27	400.3
19	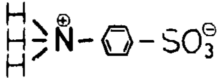	3	+0.27	401.0
20		3	+0.40	401.5
21	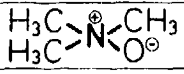	2	+0.55	402.2
22	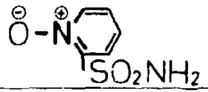	2	+0.55	402.2
1	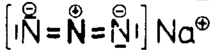 $[\overset{\ominus}{N}{=}\overset{\oplus}{N}{=}\overset{\ominus}{N}]Na^{\oplus}$	2	+0.64	403.7
	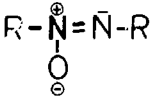		+0.81	
12	R = 12	2		403.6
13	R = 13	5		403.4
	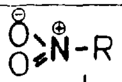		+0.87	
23	R = 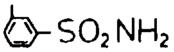	2		404.9
24	R = 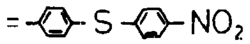	2		405.1
25	R = 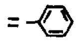	10		405.1
26	R = 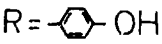	3		405.3
13	R = 13	5		405.3
9	R = 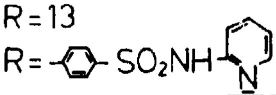	3		405.5
27	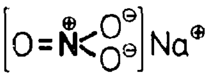	2	+ 1.02	407.2

[1] Mean from 10 amino acids.

Table V:12. Estimation of the amount of conjugation or resonance structures in some nitrogen containing compounds.

Nr	COMPOUND	n	Calculated charge	Charge from correlation curve	E_b N1s	Conjugation %
28	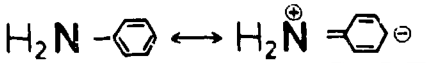	4	-0.42 +0.10	-0.14	398.6	54
29	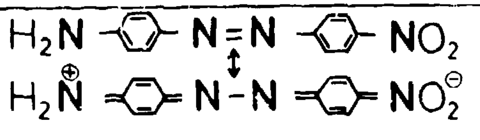	4	-0.42 +0.10	+0.07	399.6	94
			-0.06 -0.12	-0.10	398.8	(67)
			+0.87 +0.70	+0.86	405.0	
	$RHNSO_2R' \leftrightarrow RH\overset{\oplus}{N}=SO_2^{\ominus}R'$					
30	R = H R' = 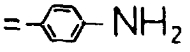		-0.37 +0.28	-0.06	399.0	48
22	R = H R' = 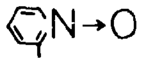		-0.37 +0.28	-0.12	398.7	38
23	R = H R' = 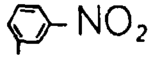		-0.37 +0.28	-0.12	398.7	38
9	R = 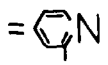 R' = 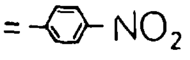		-0.26 +0.42	+0.14	400.1	59
31	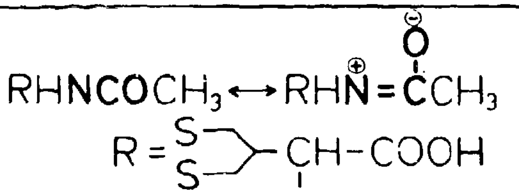 $RHNCOCH_3 \leftrightarrow RH\overset{\oplus}{N}=\overset{\overset{\ominus}{O}}{C}CH_3$		-0.30 +0.25			
		2		+0.08	399.7	70

The correlation assigns q −0.12 to the sulfonamido nitrogen in compounds Nos. 22 and 23, which means contribution of 38 % by the charged structure. For compounds 9 and 30 the charges from the correlation are +0.14 and −0.06 which means a contribution of 59 % and 48 % by the charged structures respectively. Similarly there is a contribution of 70 % from the charged structure in amide No. 31. This is in agreement with IR data, which show that the oxygen bond has relatively less double bond character in amides than in sulfonamides as compared with sulfones and ketones[207] and this result indicates that the carbon-nitrogen link in amides has a considerable double bond character.

In compound No. 30, Fig. V:37, the peak representing the two amino groups has the same half width as a single nitrogen line. This shows that the binding energies are equal for the amino and sulfonamido nitrogens. This also means that the sulfonamido group does not show any significant −*M* effect, which is in accordance with the general behaviour of sulfonyl substituents.[208]

During this investigation, some anomalies occurred which could be explained as radiation effects. With *para*-aminonitrobenzene and *para*-diethylamino-nitrobenzene, Nos. 32 and 33 in Table V:13, a double peak appeared immediately instead of the single peak expected for the nitro group, Fig. V:38 a, and the sample became discoloured. One component in the spectrum has about the same binding energy as the oxygen-carrying nitrogen in the azoxy group in the compounds Nos. 12 and 13. This would indicate that an azoxy compound is rapidly formed on the surface of the sample upon irradiation. There is evidence in the lit-

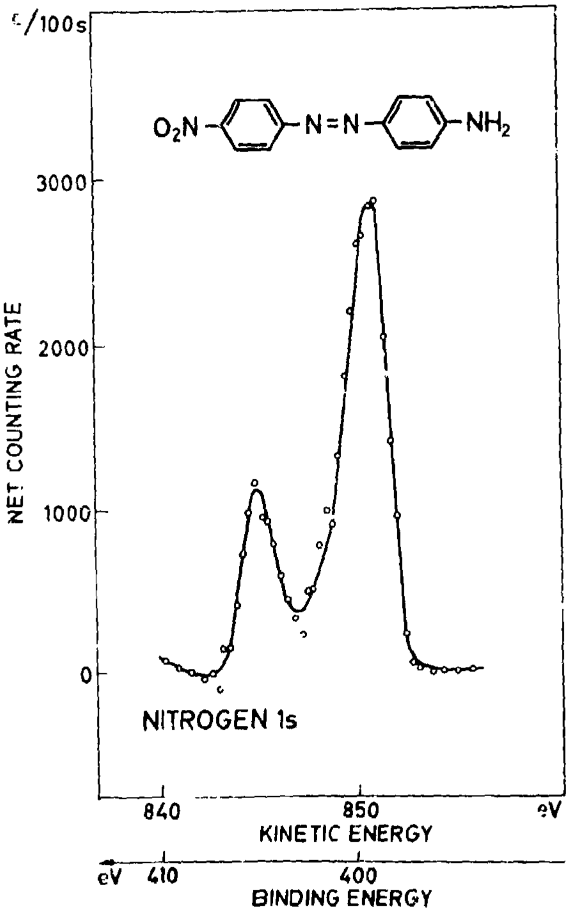

Fig. V:35. Nitrogen 1*s* electron spectrum from 4-amino-4'-nitroazobenzene.[81]

terature that azoxy compound can be formed from certain nitro compounds by means of radiation.[294] 3-nitrobenzenesulfonamide, Fig. V:38b, is an example of a molecule containing both a nitro and an amino group in which the nitro group is unaffected upon irradiation.

Some unstable compounds gave peaks with expected binding energies but beside the main peaks extraneous peaks were observed, which most probably were due to decomposition. These compounds are listed in Table V: 13, Nos. 34–39.

Tetraethylammonium iodide, No. 34, gave an extra peak of low binding energy in the region of the binding energy of triethylamine, probably due to decomposition. This compound (34) is also known to be sensitive to light. Some of the alkylammonium chlorides showed a tendency to lose hydrogen chloride in the high vacuum, and ammonium chloride evaporated too quickly to allow any measurements to be made.

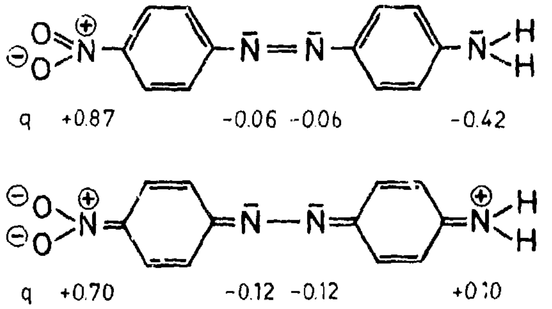

Fig. V:36. Effect of conjugation on the calculated charges for the nitrogen atoms in 4-amino-4'-nitroazobenzene.[81]

The results plotted in Fig. V: 34 were all taken from compounds for which no changes were observed in

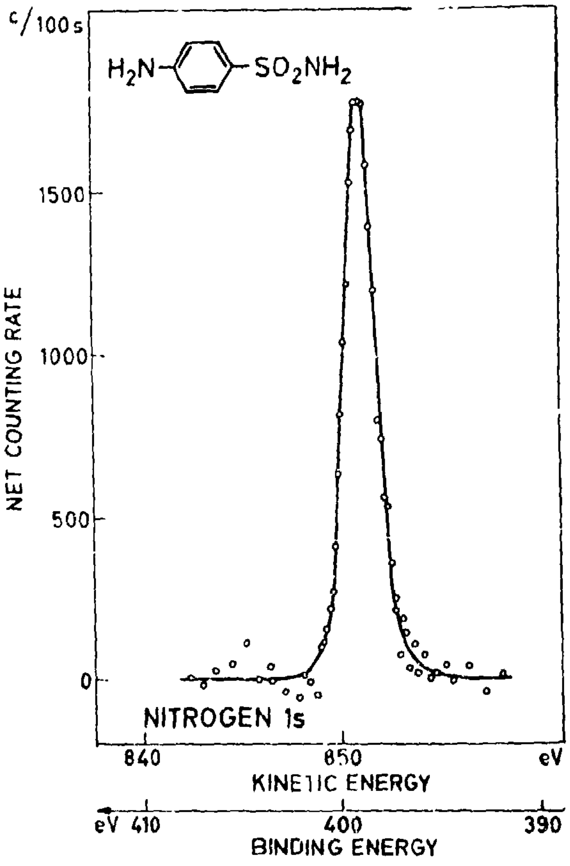

Fig. V:37. Nitrogen 1s electron spectrum from *p*-aminobenzene sulfonamide.[81]

Table V : 13. Compounds showing anomalies due to irradiation.

Nr	COMPOUND	Calculated Charge	E_b N1s
32	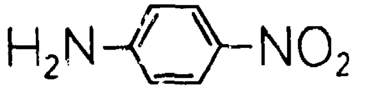	- 0.42 + 0.87	398.7 404.4 406.0
33	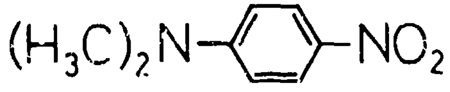	- 0.18 + 0.87	398.3 403.8 405.2
34	$(Et)_4\overset{\oplus}{N}\overset{\ominus}{I}$	+ 0.40	397.1 402.3
35	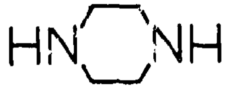	- 0.30	398.5
36		- 0.30 + 0.10	400.0 401.7
37	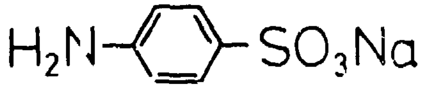	- 0.42	398.1
38		+ 0.87 - 0.42	405.5 399.1
39	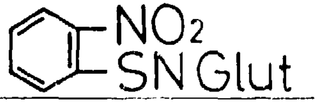	+ 0.87 - 0.31	405.1 398.8

the samples during the measurements. Deviations from the general correlation in the figure may have the following explanations:

1. *Uncertainties in the calculation of charges.* As has been pointed out on page 109 the calculation of partial ionic character is only strictly valid for singly bound diatomic molecules. In fact the electronegativities of atoms are affected not only by charge but also by the kind of orbitals utilized for bond formation, see Appendix 16. The electronegativities used are average electronegativities for all types of bonds. This means that charges calculated for bonds greatly differing in type of bonding are not strictly comparable. A closer inspection of Table V: 11 from this point of view reveals that compounds with widely varying types of hybridization on the nitrogen atoms have been used for establishing the correlation. The uncertainties in the electronegativities caused by different types of bonding do therefore not seem to be of sufficient magnitude to explain any large deviations, except possibly in points Nos. 1 and 2 which represent types of bonding greatly differing from that of the other compounds.

2. *Crystal effects.* – As was discussed in Sections V: 2 and V:3 there is a considerable contribution from the crystal potential to the energy shifts of core electrons between a free atom and an atom in a chemical compound. If the degree of ionicity of the bonds is large and if the bond distances are very different for the same element in different chemical compounds the crystal potential contribution may obscure the correlation between atomic charge and binding energy of a core electron. In fact it is rather sur-

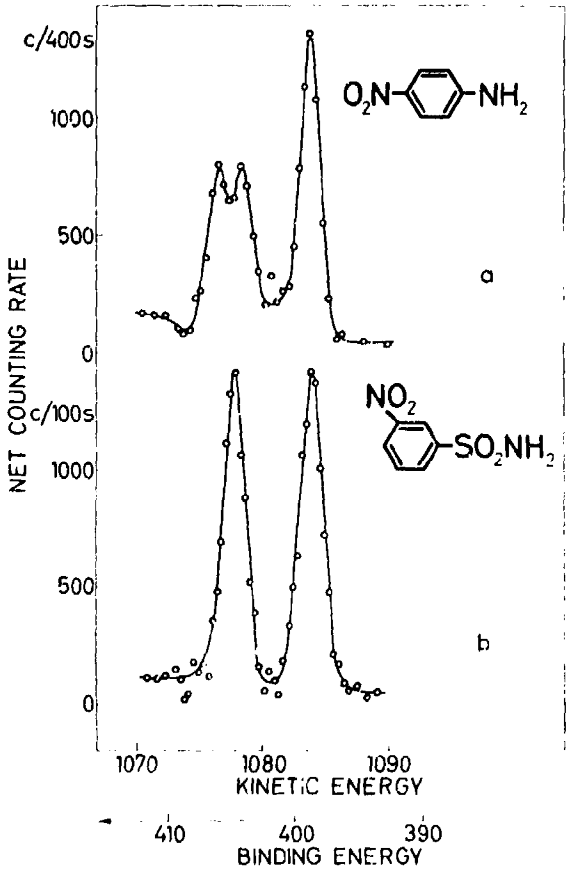

Fig. V:38. Nitrogen 1*s* electron spectra from (*a*) *p*-aminonitrobenzene and (*b*) 3-nitrobenzenesulfonamide. In (*a*) the nitro group nitrogen gives a double peak, probably due to photochemical reactions, while in (*b*) the nitro group is unaffected.

prising that as good a correlation as that of Fig. V:31 can be established. Here we shall only draw attention to the fact that compounds Nos. 15 and 16, a salt and a neutral ester, having the same oxidation state of nitrogen, both show a large and similar deviation. If the deviation had been due solely to the crystal potential, one should have expected a significant difference between these compounds*.

Electronic relaxation in the solid may also obscure the correlation, although the contribution to the energy shifts from electronic polarization around the atom with an inner shell vacancy is usually negligible.[225]

V:5b. ESCA shifts of sulfur

Since the character of the bonds between sulfur and other elements, especially carbon, nitrogen, oxygen and halogens is an important subject in organic chemistry and biochemistry, electron spectroscopic measurements on a large number of organic sulfur compounds are now in progress with the aim of establishing a charge-binding energy correlation for the study of sulfur bonds with particular emphasis on the sulfur-oxygen bond. In this section we shall mainly report the results of the measurements made to date and correlate them with the charge parameter previously used. Some relevant results obtained by the use of this correlation will also be briefly discussed, but the detailed study of the special problems in sulfur bonding will be more fully dealt with in future papers.

A discussion of the correlation of ESCA chemical shifts with valence based on earlier data from measurements on inorganic and some organic sulfur compounds has already been given in Section V:4. These measurements were made on the sulfur 1*s* shell with Cu$K\alpha_1$ radiation.[60] It has subsequently proved more advantageous to make the measurements in the sulfur 2*p* shell with Al$K\alpha$ or Mg$K\alpha$ radiation. The measurements on the sulfur compounds with which we are now concerned have been performed in this shell.[83]

The setting up of the binding energy versus charge correlations has been based on the simple estimation of charge, using the concepts of electronegativity and partial ionic character of bonds according to Pauling, as discussed in Section V:4. Some refinements in the estimation of charge which are based on the experience gained in the study of the nitrogen compounds, Section V:5a, have been introduced.

Calculation of charge. – For nitrogen and other elements in the second period of the Periodic Table, which obey the octet rule, the estimation of charge is simple and straightforward. The smooth correlation obtained between binding energy and charge for a large series of nitrogen compounds[81], indicates that the calculated charge reflects the influence of valence on the binding energy in a meaningful and useful manner.

In the case of sulfur, the calculation of charge becomes more complicated because of the possible contribution of higher orbitals to the bonding, thereby exceeding the octet rule. There also remains the controversy about the role of sulfur *d* orbitals in for in-

---

* *Note added in proof:* When charge is calculated with the extended Hückel method (see page 110) and plotted versus binding energy we obtain a rectilinear correlation. This method also assignes charges for compounds Nos. 1, 2, 15 and 16 that make them fit the curve

stance sulfur-oxygen bonds. In the discussion in Section V:4 of the shifts of electron binding energies in the sulfur 1s shell a fairly good correlation between binding energy and calculated charge was obtained on the assumption that the bond number in sulfur compounds was governed by the electroneutrality principle. In order to make a straightforward and consistent application of the electroneutrality principle, the calculation of bond number was based on simple valence bond structures with formally neutral sulfur. The same procedure has been used in this section, but the calculation of charge has been improved by correcting the electronegativities for formal charge as described for the nitrogen compounds.[81] The electronegativities of the elements involved in the sulfur bonds concerned are given in Table V:14 and the partial ionic character for the bonds has been listed in Table V:15.

Charge—binding energy correlation

The results from the measurements on the S 2*p* shell of a number of organic sulfur compounds, taken from various series of compounds under investigation, as well as results from some inorganic compounds are given in Tables V:16 - V:18. (Some results obtained for the nitrogen and oxygen 1*s* shells are also listed in these tables.) In Table V:19, the average binding energies for compounds representing the same sulfur structures, and to which the same calculated charges consequently are assigned, have been summarized. The binding energy versus charge relationship for these structures is shown in Fig. V:39 (Filled points). An excellent rectilinear correlation, similar to that which was obtained for the S 1*s* shell, is the result. The point for sodium sulfide (No. 1) falls outside the general pattern. Too much importance must not be attached to this, since the application of the charge calculation to predominantly ionic bonds in a crystal lattice is doubtful. In all other compounds the sulfur is involved in predominantly covalent bonds, to which the application of the calculation of charge is simple and straightforward.

Table V:14. Electronegativity values of elements involved in sulfur bonds.

The electronegativities of elements with formal charge have been corrected according to Pauling.[174]

Element	Electronegativity	Element	Electronegativity
H	2.1	S	2.5
C	2.5	S	2.2
N	3.0	S^+	2.8
N^+	3.3	S^{2+}	≈ 3.1
O	3.5	Cl	3.0
O	3.2	F	4.0
O^+	3.8	Na	0.9

Table V:15. Partial ionic character for bonds, derived from the relationship by Pauling.[174]

The signs refer to the calculation of charge on sulfur.

Bond	Partial ionic character	Bond	Partial ionic character
S—Na	− 0.47	$^+$S—O	+ 0.12
S—H	− 0.04	$^{2+}$S—O	+ 0.04
S—C	0	$^+$S—O^-	+ 0.04
$^+$S—C	− 0.02	$^{2+}$S—O^-	≈ 0.00
$^{2+}$S—C	− 0.09	S—Cl	+ 0.06
S—N	− 0.06	$^+$S—Cl	+ 0.01
S—N^+	+ 0.15	$^{2+}$S—Cl	≈ 0.00
$^+$S—N	+ 0.01	S—S	0
$^{2+}$S—N	≈ 0.00	S—S^-	− 0.02
S—O	+ 0.22	S—S^+	+ 0.02
S—O^-	+ 0.12	S—S^{2+}	+ 0.09
S—O^+	+ 0.35	S—S^{2+}	+ 0.18
		S—F	+ 0.43

Also included in Fig. V:39 are some measurements on liquids and gases (open points). These were investigated using the freezing technique, see Chapter VIII.

More positive charges than those represented by the filled points in Fig. V:39 can be obtained by attaching fluorine to the sulfur, and we are now extending the correlation by measurements on compounds with sulfur-fluorine bonds. As the first compound in this series we have chosen SOF_2 in which the calculated charge on sulfur ($q = 1.30$) is still about the same as the highest charge represented by sulfur-oxygen compounds. We then found that if the flow of SOF_2 gas into the source housing was increased the oxygen signal disappeared and a new and broad sulfur line was observed at a considerably higher binding energy. Graphical resolution of this line in two, each with the width normally observed, yielded sulfur 2*p* binding energies $E_b = 173.0$ eV and $E_b = 175.0$ eV. If the correlation is extrapolated towards higher binding energies (dashed line) the corresponding charge values are $q = 2.1$ and $q = 2.5$, respectively (see Fig. V:39). This indicates that the SOF_2 contained also some S_2F_{10} and SF_6 (calculated charge $q = 2.15$ and $q = 2.58$). Sulfurhexafluoride has been

Table V : 16. Calculated charges (q) and measured binding energies for a series of sulfur compounds. The sulfur to which the given data refer is given with bold symbols.

No	Compound	q	S2p	O1s
1	$Na_2\mathbf{S}$	-0.60	160.8	530.7
3 1	$H-\mathbf{S}-CH_2CH(NH_3^{\oplus})COO^{\ominus}$	-0.04	161.8	530.6
2	$H-\mathbf{S}-CH_2CH(NH_3^{\oplus}Cl^{\ominus})COOH$		162.2	530.9
4a 1	$H_3C-\mathbf{S}-(CH_2)_2CH(NH_3^{\oplus})COO^{\ominus}$	0	162.1	530.6
2	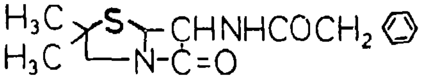		161.9	530.9
3	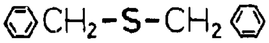		162.4	
4	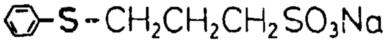		162.8	531.3
5	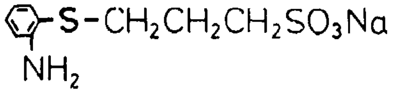		162.5	531.8
6	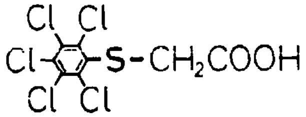		161.5	532.0
4b 1	$^{\ominus}OOC(NH_3^{\oplus})CHCH_2-\mathbf{S}-\mathbf{S}-CH_2CH(NH_3^{\oplus})COO^{\ominus}$	0	162.7	530.3
2	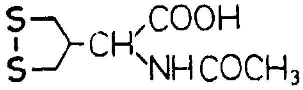		162.7	531.8
3			162.8	
4c	$\mathbf{S}_8$	0	162.2	
6 1	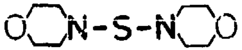	+0.13	162.5	531.8
2	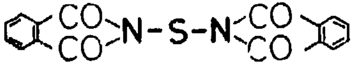		164.3	531.7
10 1	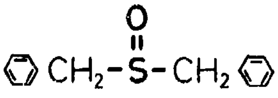	+0.44	164.9	530.5
2			164.9	531.4
3			165.0	530.9

Table V : 16. (*Cont.*)

No	Compound	q	S2p	O1s
12 1 2	 	+0.56	165.4 165.5	530.9 531.2
16	$Na_2^{\oplus}[SO_3]^{2\ominus}$	+0.68	165.8	531.3
25a	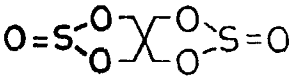	+0.88	167.0	531.5
25b 1	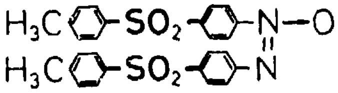	+0.88	167.2	531.6
26a 1 2	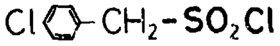 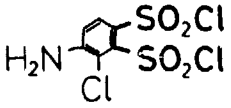	+0.95	167.3 167.3	531.5 531.4
26b 1 2	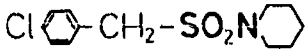 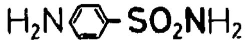	+0.95	167.2 167.3	531.7 531.9
27 1 2 3	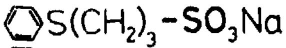 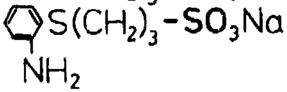 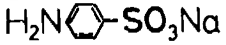	+1.00	167.1 167.5 167.0	531.3 531.8 531.6
32 1 2 3	$Na_2^{\oplus}[SO_4]^{2\ominus}$ $Fe^{2\oplus}[SO_4]^{2\ominus}$ $(Fe)_2(SO_4)_3$	+1.12	167.7 168.0 168.3	531.6 531.8 531.1
36	Dextran$-OSO_2\overset{\ominus}{O}Na^{\oplus}$	+1.22	168.7	531.4
38a	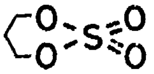	+1.32	168.6	532.5
62	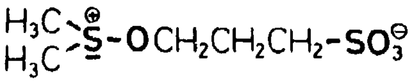	+1.07	167.6	531.3

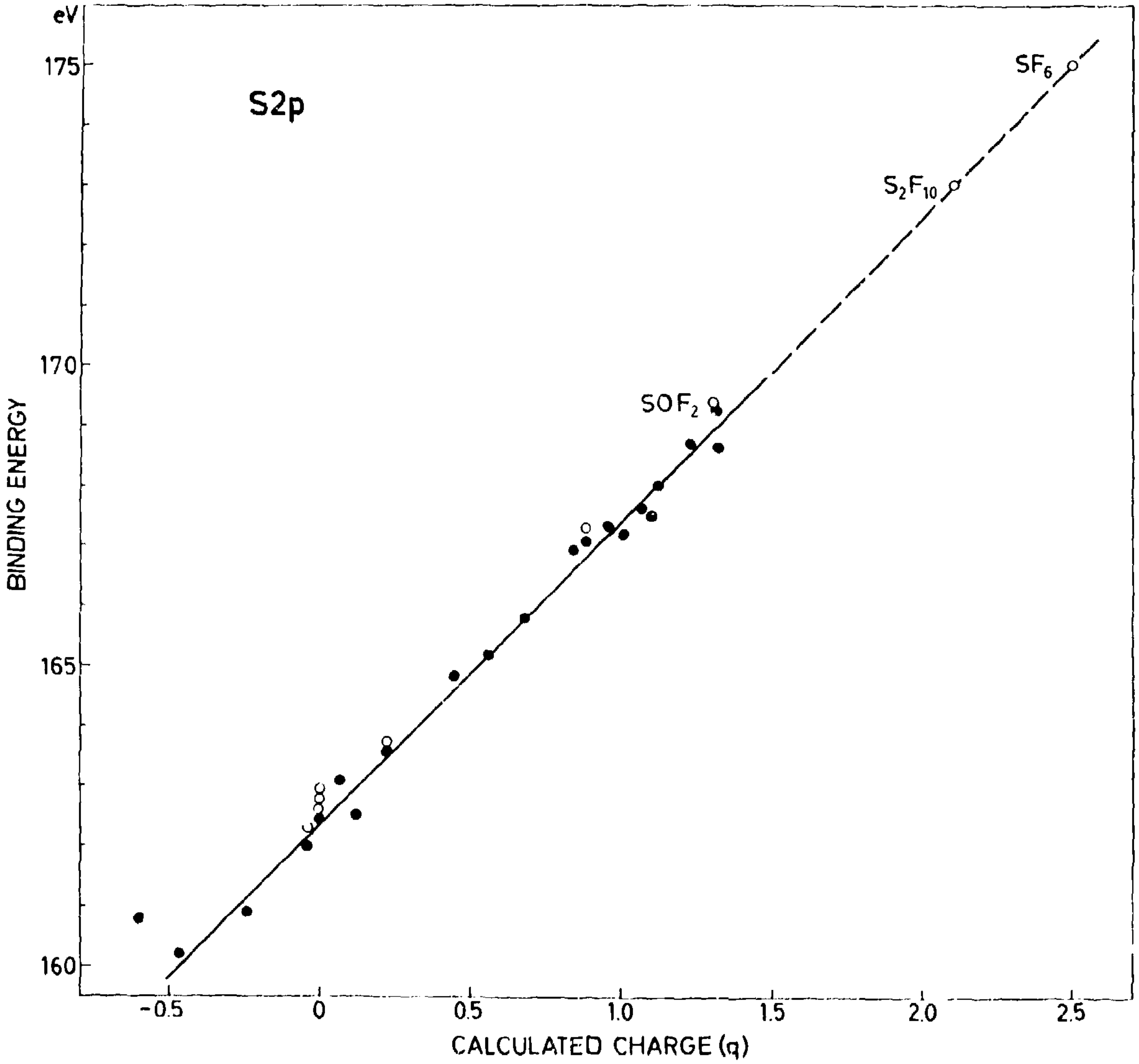

Fig. V:39. Binding energy for the sulfur $2p$ electrons versus calculated charge. The correlation is obtained from more than eighty compounds. Filled points indicate averages from compounds studied in the solid phase at room temperature. Open points represent liquids and gases studied with the freezing technique.

studied recently in Berkeley and the preliminary results for the $2p$ binding energy seem to agree with the extrapolated value in Fig. V:39.[293]

Nitrophenyl substituted sulfur compounds. — In establishing the correlation between binding energies and calculated charge in the nitrogen series it was necessary to use a very inhomogeneous series of compounds in order to cover a wide charge range. Because of the chemical versatility of sulfur a large range of the charge scale can be covered with a much more homogeneous series, and for various reasons a series of nitrophenyl substituted sulfur compounds has been chosen for special study, see Table V:17 and Fig. V:40.

Since the carbon $1s$ line from the pump oil is used for calibration, this may be affected to some degree by the carbon components in the compound under study. For a refined treatment, it is therefore of impor-

Table V:17. Calculated charges (q) and measured binding energies for a series of nitrophenyl substituted sulfur compounds.

No	Compound	q	S2p	O1s	N1s
4a 7	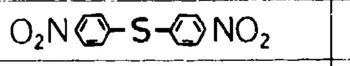	0	162.6	532.3	405.0
7	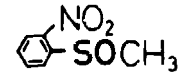	+0.22	164.2	532.6	
12 3	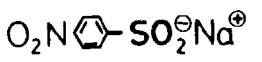	+0.56	165.2	530.9 532.9	404.9
4	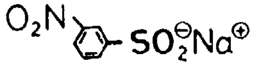		164.9	530.8 532.1	
5	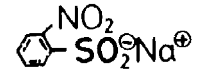		165.1	531.0 532.8	
25b 2	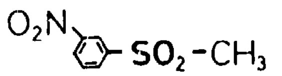	+0.88	167.1	531.9	405.0
3	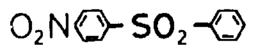		166.9	531.9	405.2
4	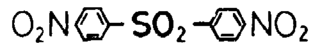		167.0	531.9	404.8
26a 3		+0.95	166.8	531.6	404.9
27 4		+1.00	167.1	531.7	405.5
31	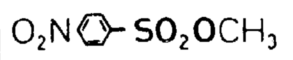	+1.10	167.5	532.1	405.2
51	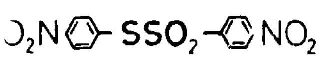	0 +0.88	163.3 167.3	532.1	405.0

tance that the carbon components in the compounds compared are identical. Such a carbon reference is provided by the nitrophenyl group in the nitrophenyl substituted compounds shown in Table V:17. Although the list is not yet complete, the binding energy v. charge plot for the compounds measured to date is given in Fig. V:41. In this figure, the binding energies for the nitrogen in the nitro group have also been included.

The nitro substituent was included in order to investigate whether any substituent effects from the various sulfur groups on the nitro group could be detected in the binding energy of nitrogen. It can be seen from the figure that if any such effect is present, it is very slight. This result is well in accordance with the results obtained for the nitro group in the nitrogen series, see Table V:11.

The filled points in Fig. V:41 represent compounds for which the calculation of charge is based on unequivocal structures, and the unfilled points represent uncertain structures under study. If the charge assigned to the sulfur in the *ortho*-nitrobenzenesulfenic ester (No. 7) is based on structure I, this point deviates considerably from the correlation. The observed binding energy, which corresponds to a charge of +0.4, agrees with Structure II, for which there is evidence in the literature based on X-ray diffraction measurements.[209]

In the thiolsulfonate (No. 51b.4) the divalent sulfur

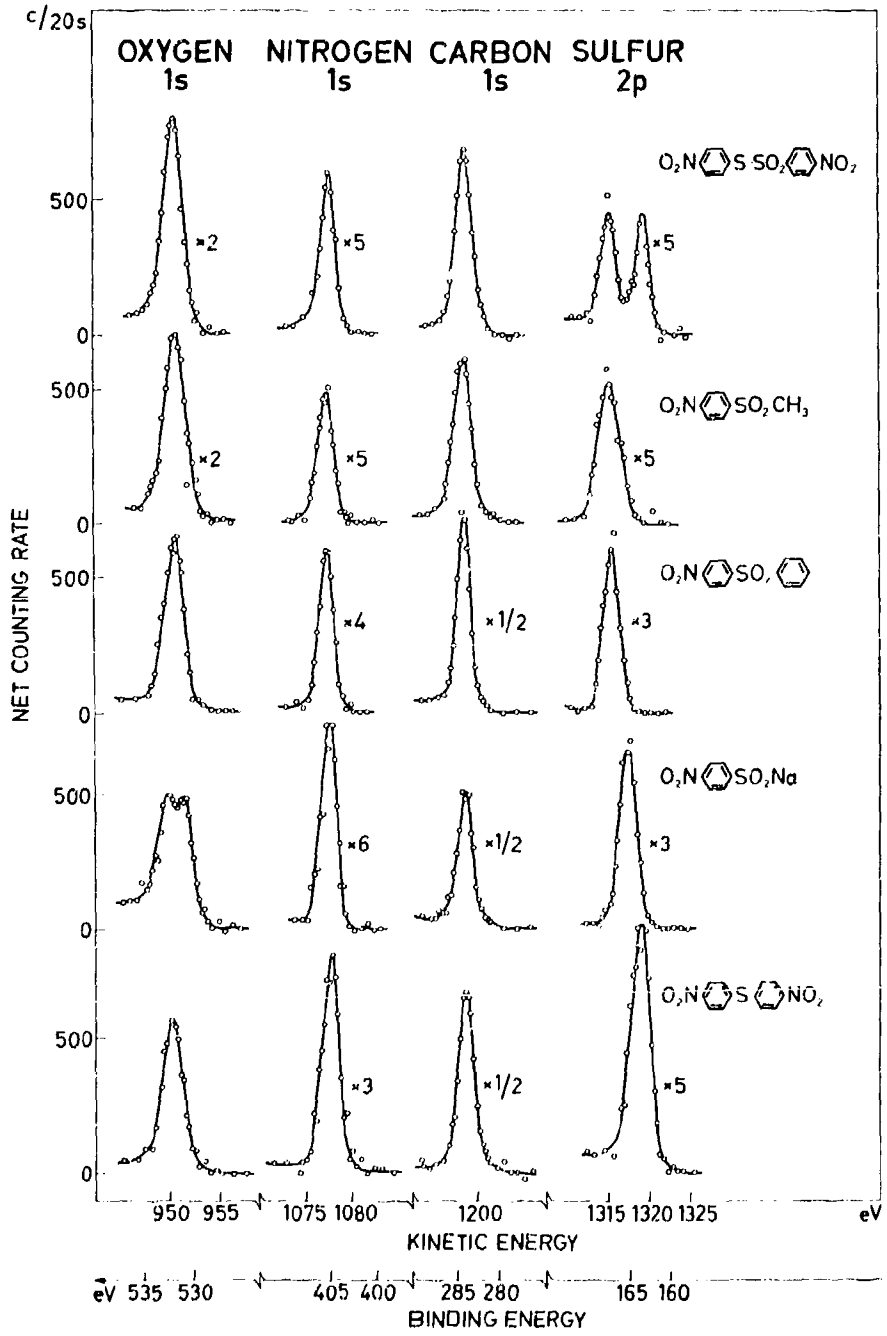

Fig. V: 40. Electron spectra of some nitrophenyl substituted sulfur compounds excited by Al*K*α.

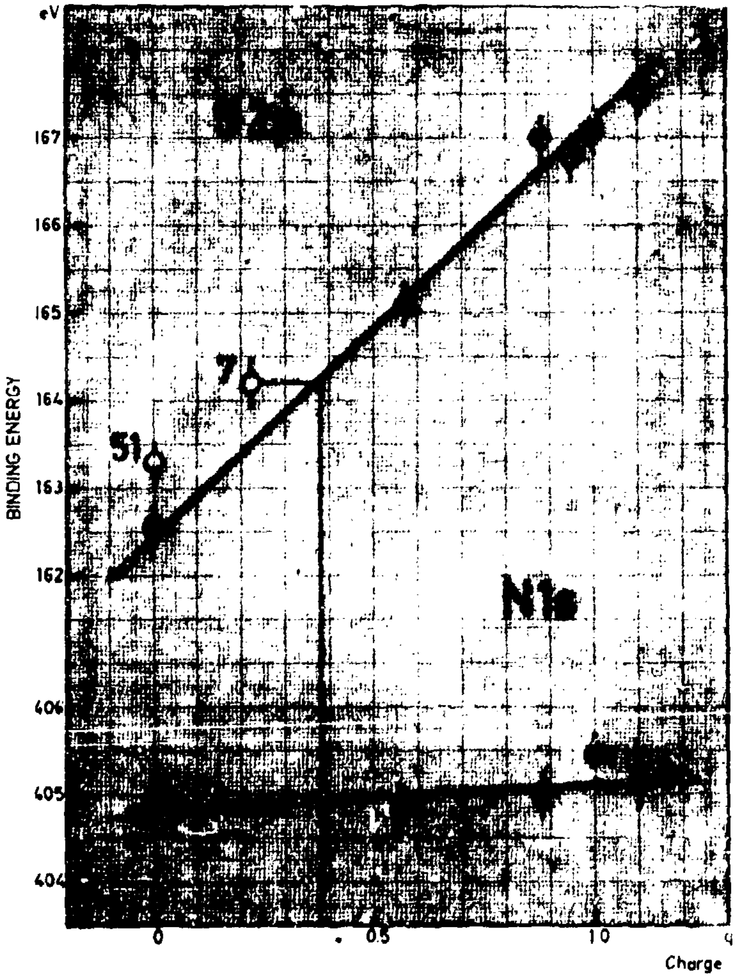

Fig. V:41. Binding energy for the sulfur $2p$ electrons and nitrogen $1s$ electrons versus calculated charge in a series of nitrophenyl substituted sulfur compounds.

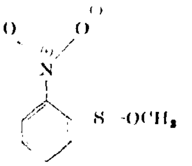
I
q +0.22

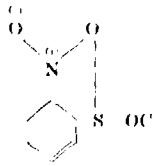
II
q +0.44

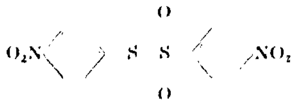
III
q 0.00, +0.88

is directly attached to an electron attracting sulfonyl group. It could therefore be expected to have a higher binding energy than the sulfur in bisnitrophenyl sulfide (No. 4a.7). This also seems to be the case and could be explained in terms of contributions from Structure IV to the resonance hybrid.

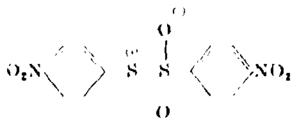
IV
q +0.94, +0.60

Table V : 18. Calculated charges and measured binding energies for a series of sulfur compounds with sulfur of different oxidation states in the same molecule. The sulfur to which the given data refer is given with bold symbols.

No		q	S2p	O1s
50	$[\mathbf{S}\text{-}SO_3]^{2\ominus}\ Na_2^{\oplus}$	-0.24	160.9	531.0
51a 1	$^{\ominus}OOC(NH_3^{\oplus})CH\,CH_2\text{-}\mathbf{S}\text{-}SO\text{-}CH_2CH(NH_3^{\oplus})COO^{\ominus}$	0	162.1	530.4
3	⌬$CH_2\text{-}\mathbf{S}\text{-}SO\text{-}CH_2$⌬		162.7	531.9
2	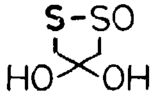		162.1	531.1
51b 1	$^{\ominus}OOC(NH_3^{\oplus})CH\,CH_2\text{-}\mathbf{S}\text{-}SO_2\text{-}CH_2CH(NH_3^{\oplus})COO^{\ominus}$	0	162.5	530.4
3	⌬$CH_2\text{-}\mathbf{S}\text{-}SO_2\text{-}CH_2$⌬		162.9	532.6
4	O_2N⌬$\text{-}\mathbf{S}\text{-}SO_2\text{-}$⌬$NO_2$		163.3	532.1
2	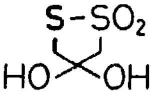		162.7	531.4
51c	Cl⌬$CH_2\text{-}\mathbf{S}\text{-}SO_3^{\ominus}Na^{\oplus}$	0	162.8	531.8
52a 1	$^{\ominus}OOC(NH_3^{\oplus})CH\,CH_2\text{-}\mathbf{OS}\text{-}S\text{-}CH_2CH(NH_3^{\oplus})COO^{\ominus}$	+0.44	164.4	530.4
3	⌬$CH_2\text{-}\mathbf{OS}\text{-}S\text{-}CH_2$⌬		165.2	531.9
2	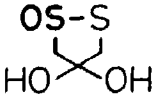		164.8	531.1
53	$Na^{\oplus}[^{\ominus}O_2\mathbf{S}\text{-}SO_3^{\ominus}]Na^{\oplus}$	+0.56	<167.5	532.0
54	$[O_3\mathbf{S}\text{-}S]^{2\ominus}\ Na_2^{\oplus}$	+0.84	166.9	531.0
55a 1	$^{\ominus}OOC(NH_3^{\oplus})CH\,CH_2\text{-}\mathbf{O_2S}\text{-}S\text{-}CH_2CH(NH_3^{\oplus})COO^{\ominus}$	+0.88	167.1	530.4
3	⌬$CH_2\text{-}\mathbf{O_2S}\text{-}S\text{-}CH_2$⌬		167.2	532.6
2	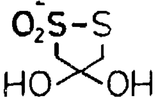		166.9	531.4
56a	$Na^{\oplus}\,^{\ominus}O_3\mathbf{S}\text{-}\mathbf{S}\text{-}CH_2$⌬Cl	+1.00	167.8	531.8
56b	$Na^{\oplus}[^{\ominus}O_3S\text{-}SO_2^{\ominus}]Na^{\oplus}$	+1.00	>167.5	531.0

Considering the great difference between the calculated charges on the divalent sulfur in the two structures, the contribution from Structure IV seems, however, to be very small.

Thiolsulfonates and some related compounds. — Thiolsulfinates and thiolsulfonates are being studied in connection with the problem, why oxidation of thiolsulfinates invariably yields thiolsulfonates and never disulfoxides. Some results are shown in Table V:18 together with results from some related com-

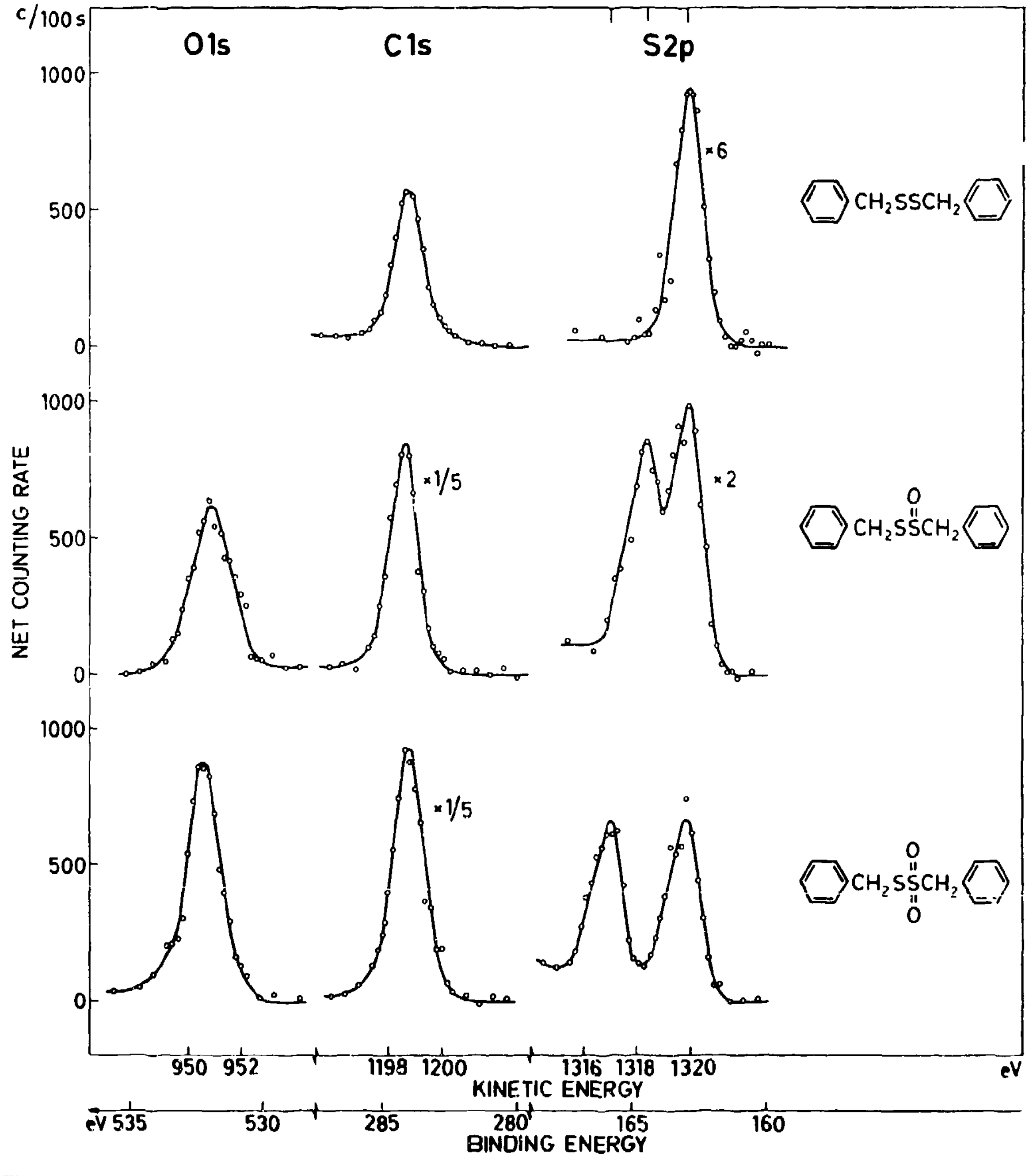

Fig. V:42. Electron spectra of dibenzyldisulfide and the corresponding thioisulfinate and thiolsulfonate. The shift in binding energy upon oxidation of sulfur is shown for the $2p$ level of sulfur.

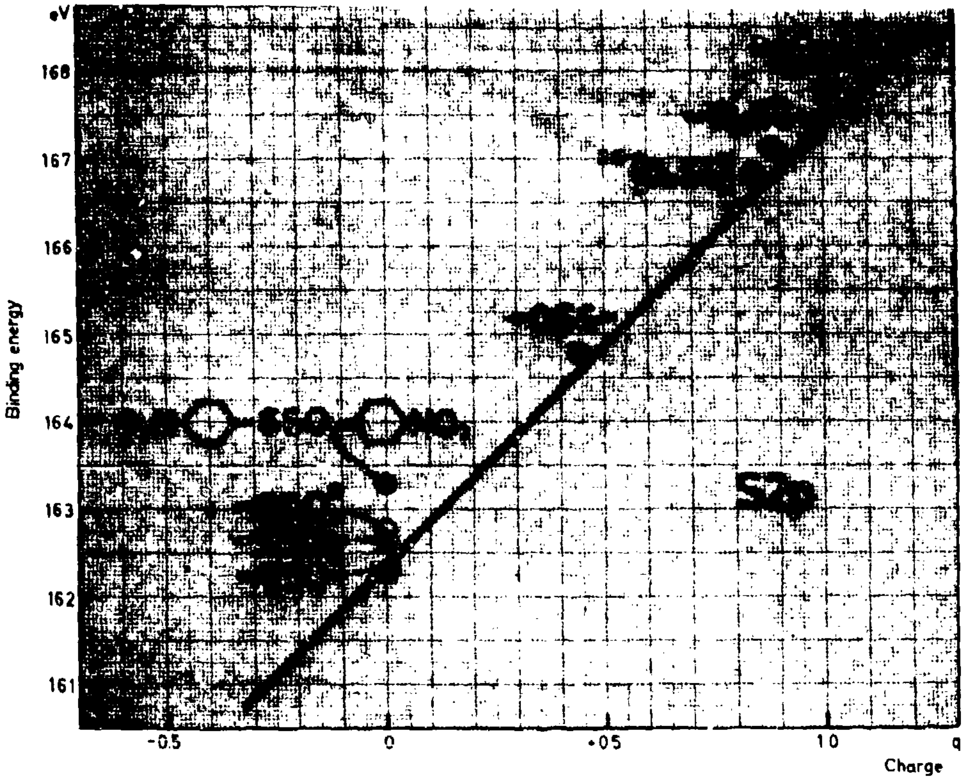

Fig. V:43. Binding energy for the sulfur $2p$ electrons versus calculated charge in a series of sulfur compounds containing S-S bonds.

pounds in which divalent sulfur is directly attached to an oxygen-carrying sulfur. These results are also summarized in Table V:19 and have been plotted against calculated charge in Fig. V:43, where the correlation line is that from Fig. V:39. All the values for the oxygen-carrying sulfur fit the correlation, whereas an increase in the number of oxygens attached to the oxygen-carrying sulfur adjacent to the divalent sulfur results in an increased binding energy for the divalent sulfur moiety. In the nitro substituted thiolsulfonate, this effect may probably be significantly enhanced by the substituent effect of the nitro group. The divalent sulfur moiety in a Bunte salt (Nos. 51c, 56a), included for comparison shows an analogous behaviour.

The ESCA spectra of compounds 4b.3, 51a.3, and 51b.3 are shown in Fig. V:42.

The structure of pyrosulfite. -- For the pyrosulfite ion (Nos. 53, 56b) the two structures V and VI are possible. Structure V has been proved by X-ray diffraction measurements.[210] The electron spectroscopic result is in full accordance with this structure. The spectrum is shown in Fig. V:44. An unresolved broadened sulfur line was obtained. The broadening corresponds to a difference of 1.9 eV between the binding energies of the two sulfur atoms and a charge difference of 0.38. The calculated charge difference is 0.44 for Structure V. The mean binding energy, 167.6 eV, seems somewhat high in relation to the mean charge. This could possibly be due to a contribution from Structure VIIa, for which the mean charge is higher:

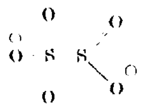

V

VI

	V	VI
q	+ 1.00, + 0.56	+ 0.78, + 0.78
q_{mean}	+ 0.78	+ 0.78
Δq	0.44	0.00
$E_{b\,mean}$	166.2	166.2

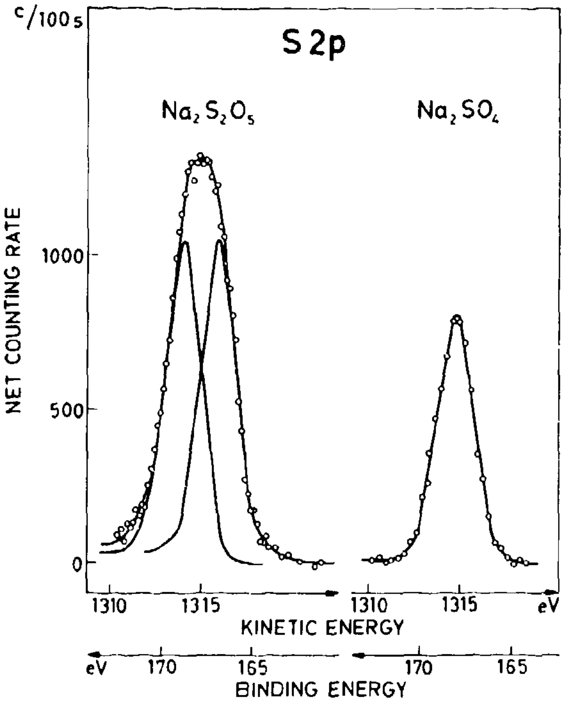

Fig. V:44. The sulfur $2p$ electron line in sodium pyrosulfite compared with the sulfur $2p$ electron line in sodium sulfate.

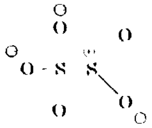

VII a

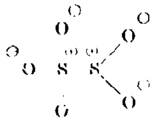

VII b

	VII a	VII b
q	+ 0.73, + 1.23	+ 1.32, + 1.08
q_{mean}	+ 0.98	+ 1.20
Δq	0.50	0.24
$E_{b\,\text{mean}}$	167.2	168.3

However, considering that the contribution from structures of type IV is small in the thiolsulfonate and related compounds discussed above, a large contribution from Structure VIIa seems unlikely. Since the binding energy of the divalent sulfur in compound 51c, in which it is attached to a sulfinate group, is only about 0.5 eV above the normal value, it seems unlikely that the more electronegative sulfur in the thionite moiety in V should increase its binding energy more by attachment to the thionate group than does the divalent sulfur in 51c. The experimental binding energy indicates a high positive charge on both sulfurs. Moreover, a structure containing two adjacent high positive charges seems to be consistent with the greater length of the S—S bond in the pyrosulfite[211] as compared with the length of a normal single S—S bond and indicates a preponderance of Structure VIIb. A 50% contribution of Structure VIIb and a 50% contribution of V, gives a calculated charge difference and a binding energy in good agreement with the experimental values:

	q_{mean}	Δq	$E_{b\,\text{mean}}$
0.50 V 0.50 VII b	+ 0.99	0.34 (0.38 found)	167.3 (167.6 found)
V	+ 0.78	0.44	166.2
VII b	+ 1.20	0.24	168.3

The sulfur-oxygen bond. — The character of the sulfur-oxygen bond in sulfoxides is an interesting problem in organic chemistry. There is a large relative charge difference between the two possible Structures VIII and IX.

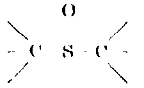

VIII

$q + 0.44$

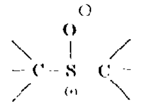

IX

$q + 0.99$

The sulfoxides measured to date have exactly the same binding energy (Nos. 10.1–3). This binding energy is well in accordance with Structure VIII. The nearest point in the correlation belongs to the sulfinate group, to which the Structure X has been assigned.

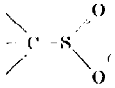

X

$q + 0.56$

It has recently been shown that this structure is consistent with IR data.[212] Thus, in the region where the sulfoxide is expected the correlation is well established, and from the data at present available, considerable double bond character must be ascribed to the sulfoxide bond.

The character of sulfur-oxygen bonds can be further explored by measuring the oxygen binding energies. Investigations in progress substantiate the previous conclusions. A further very interesting observation, relevant to this problem, can be obtained from compound No. 62, in which the sulfonate group serves as an internal standard. Two different structures can be

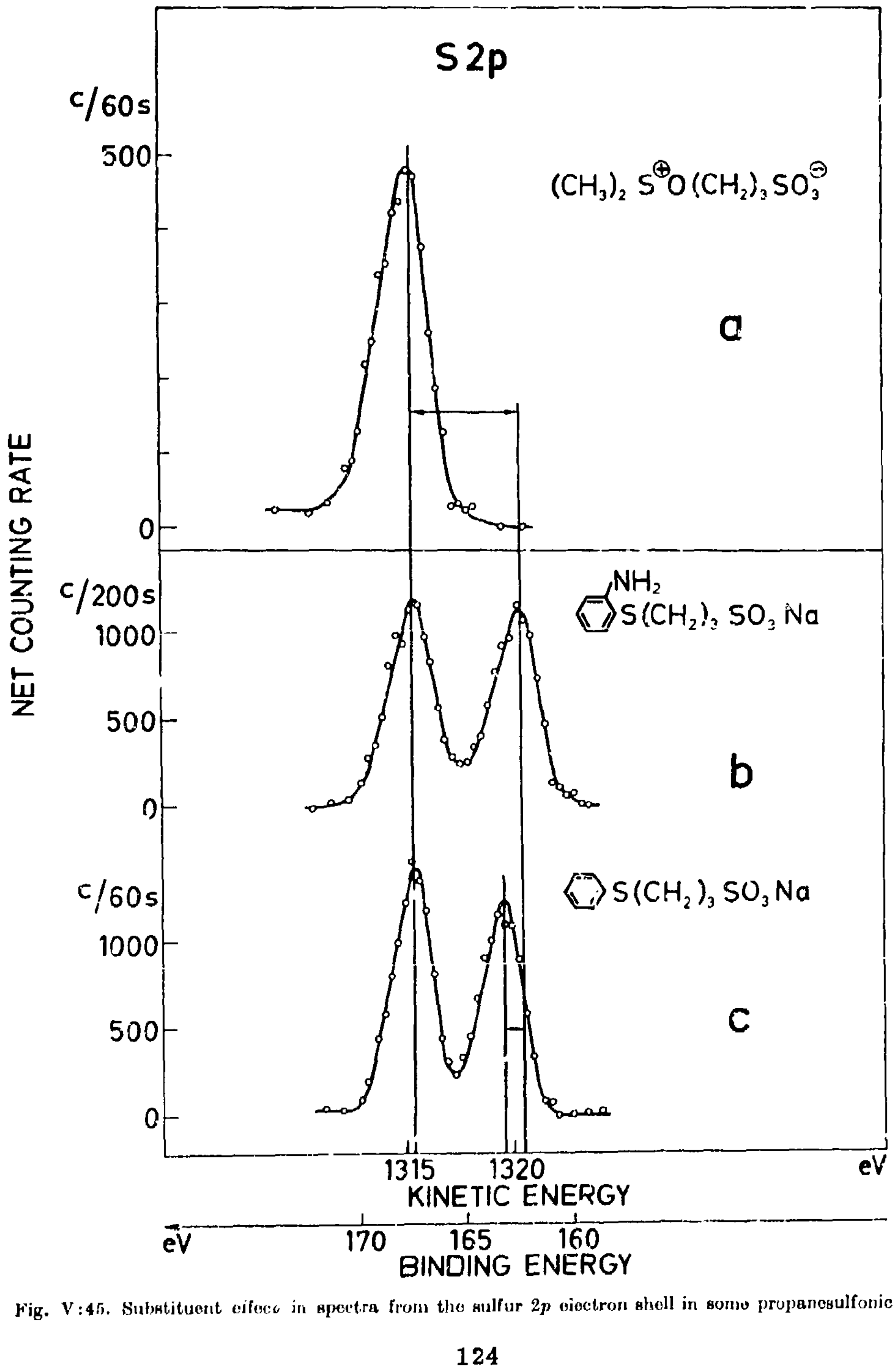

Fig. V:45. Substituent effect in spectra from the sulfur $2p$ electron shell in some propanesulfonic acid derivatives.

assigned to this compound (XI and XII). It is unlikely that the oxonium structure contributes substantially to the resonance hybrid because of the high electronegativity of oxygen. The charge on the sulfonium sulfur must therefore be near to + 1 or almost the same as that calculated for the sulfonate group assuming a large contribution of double bond character to the sulfur-oxygen bonds (XIII).

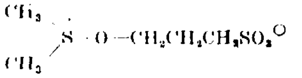

$$(CH_3)_2\dot{S}{-}O{-}CH_2CH_2CH_2SO_3^{\ominus}$$

XI

q + 1.07 + 1.00

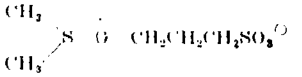

$$(CH_3)_2\dot{S}\;O\;CH_2CH_2CH_2SO_3^{\ominus}$$

XII

q + 0.70 + 1.00

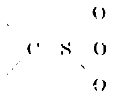

XIII

q + 1.00

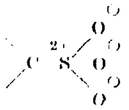

XIV

q + 1.92

If a Lewis structure is assumed for the sulfonate group (XIV) the charge becomes twice as large as in Structure XIII (= XI), and a shift of at least 5 eV would be expected between the sulfonium sulfur and the sulfonate sulfur. The spectrum of compound No. 62 is shown in Fig. V:45a. It consists of an unresolved sulfur line showing relatively little broadening. The binding energy of the sulfonate sulfur is thus close to that of sulfonium sulfur and consequently it carries a charge similar to that of sulfonium sulfur. Since the maximum charge which can be assigned to the sulfonium sulfur is + 1.07, this result is inconsistent with a Lewis structure for the sulfonate sulfur, which gives a charge close to + 2. This favours the use of structures with a large double bond contribution for the calculation of charge.

In Table V:19, charges calculated from Lewis structures have also been included and the binding energy v. charge plot using these charges is shown in Fig. V:46. In this plot the points are concentrated around integral values of charge, except the point for compound No. 62 which falls completely out of the pattern.

Thus only by assigning substantial double bond character to the sulfur-oxygen bonds is a consistent binding energy—charge correlation obtained with the simple method adopted here for the calculation of charge. This result supports in our opinion a contribution of d_π-p_π bonding to the sulfur-oxygen link. Regardless of their exact interpretation the results definitely show that charge on the sulfur tends to be neutralized in sulfur-oxygen compounds.

In addition to this it can be mentioned that in the case of sulfonamides, results have been obtained, which can well be explained in terms of contributions from structures where the nitrogen is double bonded to sulfur.[81] This could hardly be expected for nitrogen, if it did not also occur for oxygen.

Substituent effects on divalent sulfur

A further example of the substituent effect on divalent sulfur of the type discussed for the thiolsulfonates and related compounds can be found in compounds Nos. 6.1 and 6.2, the spectra of which are shown in Figs. V:47a and V:47b, respectively. The attachement of the electron attracting amide group to divalent sulfur evidently has a large effect on the binding energy of sulfur. This effect can best be explained in terms of a large contribution of Structure XVb to the resonance hybrid.

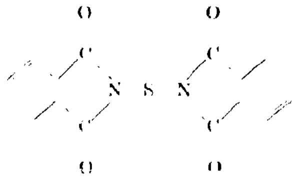

XV a

q_S + 0.12
q_N − 0.18

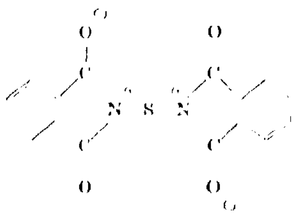

XV b

q_S + 0.30
q_N + 0.45

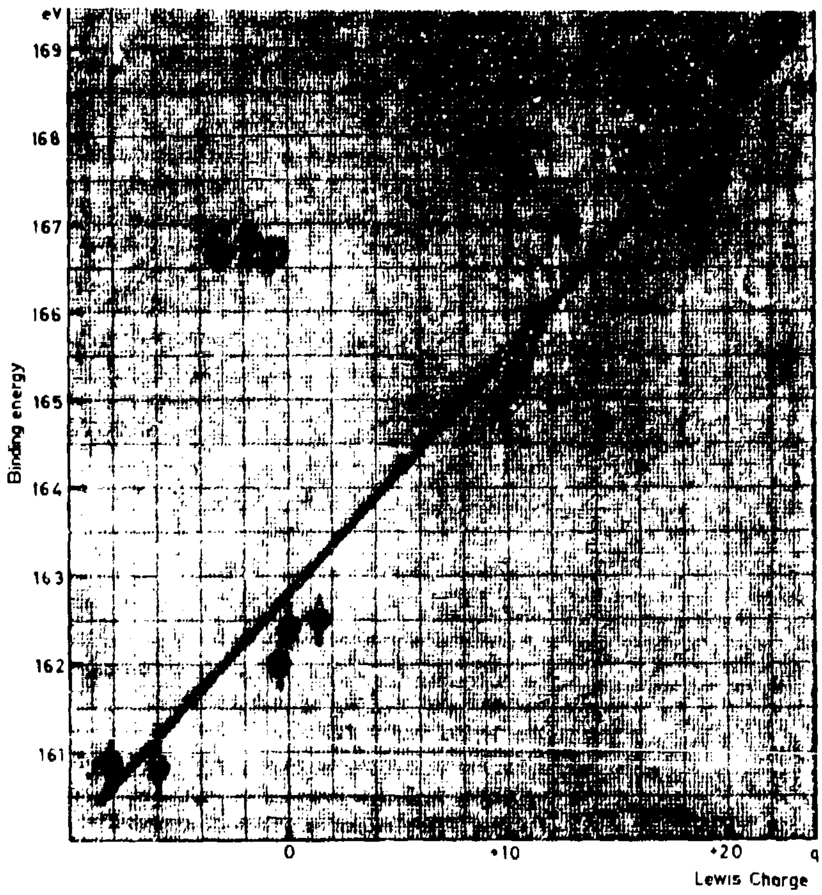

Fig. V:46. Binding energy for the sulfur $2p$ electrons versus charge calculated from Lewis's structures for a series of sulfur compounds.

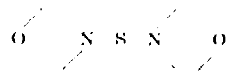

XVI

q_S +0.12
q_N 0.18

		XV	XVI	Δ
E_b	N 1*s*	399.5	398.5	1.0 ± 0.6
	S 2*p*	164.3	162.5	1.8 ± 0.6

In compounds Nos. 4a. 4,5; 27.1,2 with the sulfonate group as an internal sulfur standard, the difference between the binding energies of the two peaks in the spectra, which are shown in Figs. V:45b and V:45c, can be very accurately measured. The substituent effects of substituents in the benzene ring on the binding energy of the divalent sulfur can therefore be readily observed although they are small. The substituent effect of the *ortho*-amino group on the binding energy of the sulfide sulfur (referred to the sulfonate as a standard) is 0.7 eV. This is well in accordance with the known electron donating character of an aromatic *o*- or *p*- amino group.

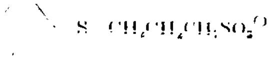

X	S	$SO_3^{(-)}$	$\Delta_{S-SO_3^{(-)}}$	Δ
o-NH_2	162.5	167.4	4.9	−0.7 ± 0.2
H	163.0	167.2	4.2	0

Applications to structural problems

In addition to the structural studies based on the quantitative estimation of charge mentioned above, some studies based on qualitative aspects of the electron spectra, such as the shape and relative intensities of the electron lines, have been made.

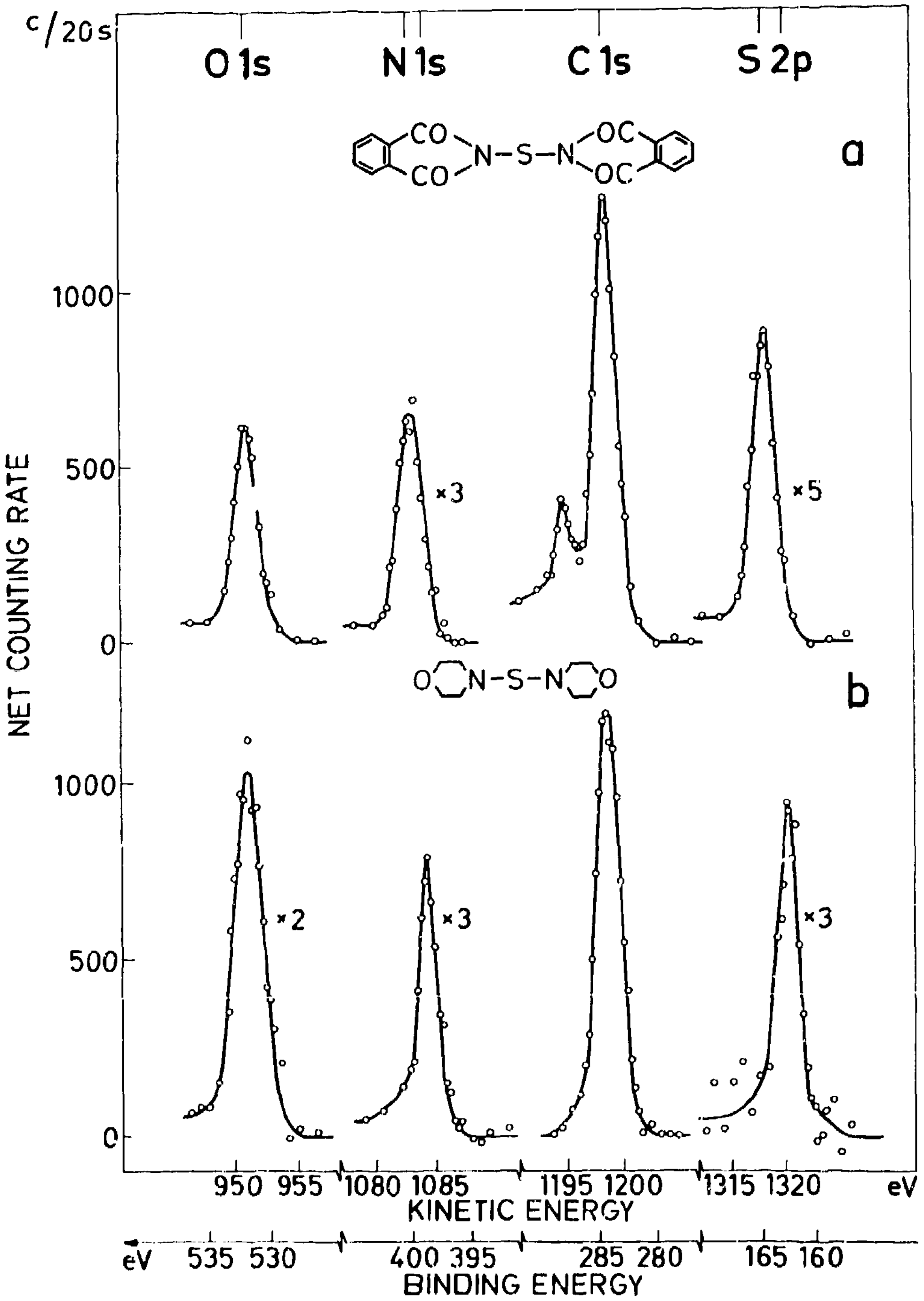

Fig. V:47. Electron spectra of N,N′-thiodiphtalimide and N,N′-thiodi-4-morpholine showing a substituent effect on divalent sulfur.

Table V:19. Summary of the data given in Tables V:16–18 giving the average ding energy of various sulfur structures.

No		q	q_{Lewis}	S2p
1	Na_2S	−0.60	−0.60	160.8
3	R-S-H	−0.04	−0.04	162.0
4a	R-S-R	0	0	162.3
b	R-S-S-R			162.7 } 162.4
c	S_8			162.2
6	$R_2N\text{-}S\text{-}NR_2$	+0.13	+0.13	162.5
7	R-S-OR	+0.22	+0.22	164.2
10	$R_2S{=}O$	+0.44	+0.99	164.9
12	$R\text{-}SO_2^{\ominus}$	+0.56	+1.05	165.4
16	$SO_3^{2\ominus}$	+0.68	+1.12	165.8
25a	$(RO)_2S{=}O$	+0.88	+1.28	167.0 } 167.1
b	$R\text{-}SO_2\text{-}R$		+1.83	167.1
26a	$R\text{-}SO_2Cl$	+0.95	+1.92	167.3 } 167.3
b	$R\text{-}SO_2N<$			167.3
27	$R\text{-}SO_3^{\ominus}$	+1.00	+1.92	167.2
31	$R\text{-}SO_2OR$	+1.10	+1.96	167.5
32	$SO_4^{2\ominus}$	+1.12	+2.02	168.0
36	$RO\text{-}SO_3^{\ominus}$	+1.22	+2.05	168.7
38	$(RO)_2SO_2$	+1.32	+2.09	168.6
50	$[S\text{-}SO_3]^{2\ominus}$	−0.24	−0.82	160.9
51a	R-S-SO-R	0	0	162.3
b	$R\text{-}S\text{-}SO_2\text{-}R$			162.8
c	$R\text{-}S\text{-}SO_3^{\ominus}$			162.8
52	R-OS-S-R	+0.44	+0.99	164.8
54	$^{2\ominus}[O_3S\text{-}S]$	+0.84	+1.83	166.9
55	$R\text{-}O_2S\text{-}S\text{-}R$	+0.88	+1.83	167.1
56	$^{\ominus}O_3S\text{-}S\text{-}R$	+1.00	+1.92	167.8

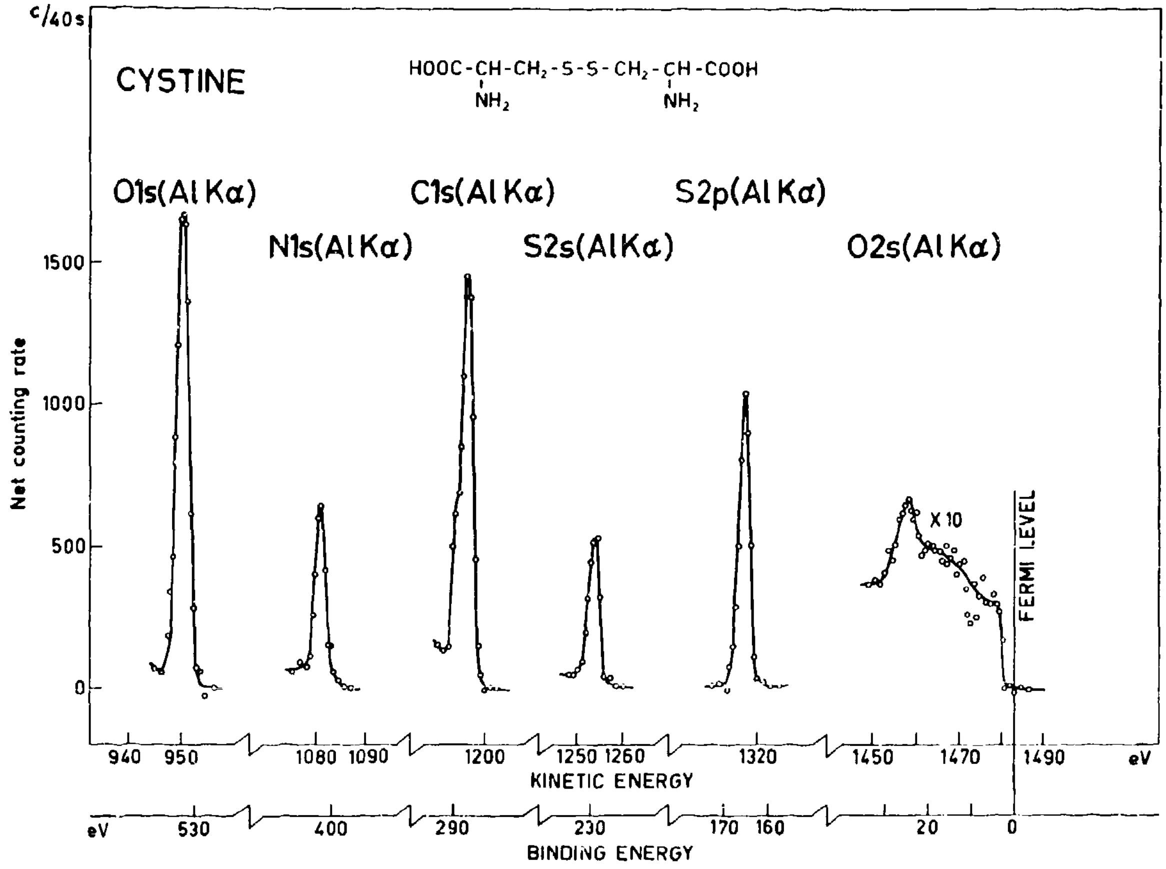

Fig. V:48. Electron spectrum of cystine.[77]

In the case of cystine dioxide some controversy about the structure has existed. We have confirmed the thiolsulfonate structure by utilizing the fact that two sulfur peaks occur in the electron spectrum.[77]

In insulin selective oxidative cleavage of the interchain disulfide bridges can be effected. We have followed this cleavage by observing the changes in the relative intensities of the sulfur electron lines upon oxidation.[91]

The thiolsulfonate structure of cystine S-dioxide. — The structure of disulfide dioxides has been the subject of recurrent investigations ever since the first compounds of this type were prepared and examined.[213-215] The two possible structures of the disulfide dioxides, i.e. the disulfoxide (I) and the thiolsulfonate (II) structures, have both received support. Modern evidence based on IR spectra favours the thiolsulfonate structure.[215] For certain disulfide dioxides this structure has also been proved by chemical evidence[216] and by evidence obtained from NMR spectra,[217,218] and the thiolsulfonate structure is now generally accepted.[219]

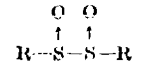
$$\mathrm{R-\overset{\overset{O}{\uparrow}}{S}-\overset{\overset{O}{\uparrow}}{S}-R}$$

(I)
α-Disulfoxide

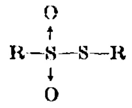
$$\mathrm{R-\underset{\underset{O}{\downarrow}}{\overset{\overset{O}{\uparrow}}{S}}-S-R}$$

(II)
Thiolsulfonate

However, in the case of cystine S-dioxide there has been some controversy. Utzinger claims to have

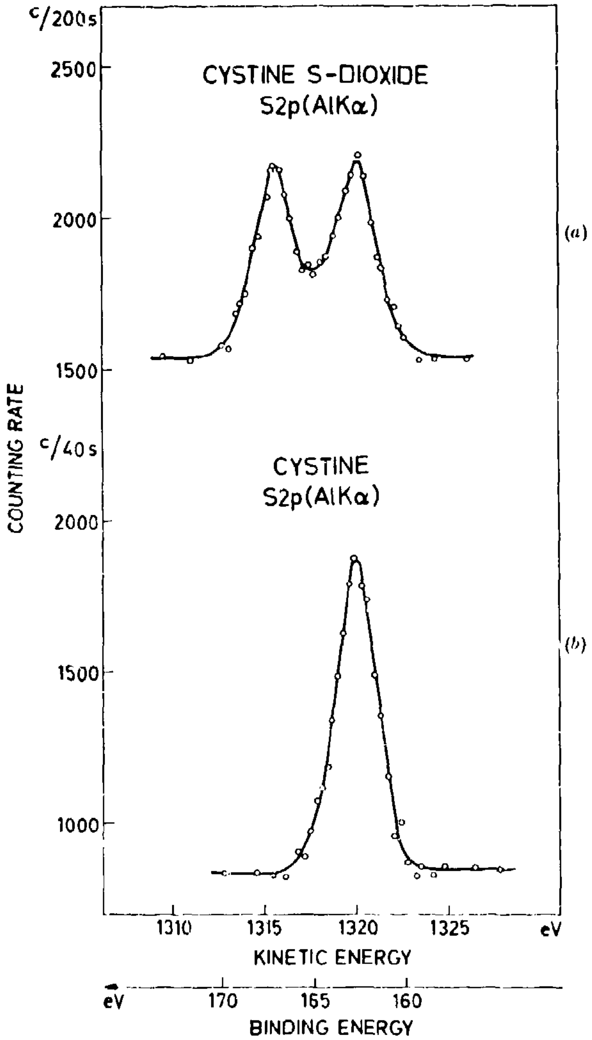

Fig. V:49. Electrons from the $2p$ shell of sulfur in cystine S-dioxide (a) and cystine (b). The two lines in (a) give evidence of a thiolsulfonate structure of cystine S-dioxide. The valence states of the sulfur atoms can be determined from the spectra.[77]

isolated both forms I and II, by using different methods of oxidation.[220] The assignment of structure to the two products was based on IR spectra. However, re-investigation of his oxidation methods has shown that one of them yields a mixture of cystine S-dioxide, cystine S-monoxide, and cystine.[221] The interpretation of the IR spectrum of the pure product to which was assigned the disulfoxide structure has recently been criticized by Block and Weidner, who made an extensive reinvestigation into the general problem of the structure of disulfide S-dioxides using IR and Raman spectra.[222] According to their interpretation of Utzinger's data, his spectra are consistent with a thiolsulfonate structure. They recommend that spectral evidence in literature for the disulfoxide structure of disulfide S-dioxides should be scrutinized.

The cystine molecule contains two equivalent sulfur atoms:

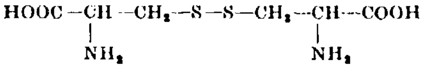

$$\underset{\displaystyle NH_2}{HOOC-\underset{|}{CH}}-CH_2-S-S-CH_2-\underset{\displaystyle NH_2}{\underset{|}{CH}-COOH}$$

Fig. V:48 shows the electron spectrum of L(-)-cystine obtained with aluminum $K\alpha$ radiation. All elements in the compound, except hydrogen, are seen in the spectrum which has been recorded between 940 eV and 1490 eV kinetic energy.

The spectrum shows only photoelectron lines since the Auger transitions of the elements in question have energies outside the interval shown in the figure.

At zero binding energy, i.e. at the Fermi level, the intensity has decreased. The decrease in intensity occurs at the top of the valence band where no more electrons are available for the photoelectric process (see Chapter IV). Since the specimen is in this case an electrical insulator the decrease in intensity occurs at a distance of a few eV from the Fermi level. The sulfur $2p$ subshell is observed as one single line, which has a full width at half-maximum intensity of 2.5 eV. This is consistent with the equivalence of the two sulfur atoms in the cystine molecule.

In the disulfide dioxide in which two oxygens are attached to sulfur, two different structures may be formulated. If one oxygen is attached to each of the two sulfur atoms (I), the resulting symmetry with equivalent sulfur atoms would give rise to single lines in the electron spectra of the sulfur atoms. If both oxygens are attached to one of the sulfur atoms, i.e. if the disulfide dioxide has the thiolsulfonate structure (II), the two sulfur atoms having non-equivalent structural positions, would give rise to two different lines in the electron spectra of the sulfur atoms. This is actually the case. Fig. V:49 shows the electron spectrum of the $2p$ subshell of sulfur in L(-)-cystine S-dioxide, recorded with aluminum $K\alpha$. Instead of one single line as in the symmetrical L(-)-cystine, two lines are now obtained from the $2p$ subshell in sulfur. One of the lines has approximately the same energy as the cystine S line and the other line has an energy 4.0 eV lower. Each line has a halfwidth of about 2.5 eV. The separation is of the same order of magnitude as the shifts previously observed for sulfur atoms with comparable differences in the oxidation states.

The electron spectrum of cystine S-dioxide obtained by ESCA therefore gives conclusive evidence for the thiolsulfonate structure:

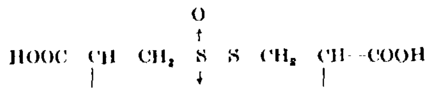

$$\mathrm{HOOC\;\;\underset{\displaystyle NH_2}{\underset{|}{CH}}\;\;CH_2\;\;\overset{\displaystyle O}{\overset{\uparrow}{\underset{\displaystyle O}{\underset{\downarrow}{S}}}}\;\;S\;\;CH_2\;\;\underset{\displaystyle NH_2}{\underset{|}{CH}}{-}COOH}$$

This evidence is more direct than that which can be obtained from IR, Raman, and NMR spectra, since the electron spectrum of the substance contains lines from the element sulfur that can be studied separately.

Oxidation of Insulin. — Insulin was oxidized according to a method which has been claimed to cleave the two interchain disulfide bonds by oxidation to the sulfonate stage while the disulfide bond of the A chain (see Fig. I:12) remains intact.[224] Fig. V:50 shows the sulfur $2p$ electron line from different sources of insulin. (The total spectrum from one of the samples was shown in Chapter I, Fig. I:13). The sulfur $2p$ spectrum from unoxidized insulin (Fig. V:50a) has one narrow peak as expected from the common character of the three disulfide links in the cystine components (see Fig. I:12). Oxidation by iodate caused a strong shift of the sulfur electron line as seen in Fig. V:50b. It was expected that this shift would concern two-thirds of the sulfur atoms, since the method employed has been claimed to oxidize selectively the sulfur of the two bridges between the chains thus leaving the intrachain bridge intact. The relative intensity of the sulfur lines, which showed that the amount of oxidized sulfur was 2.1 times the amount of the unconverted form, is in satisfactory accordance with the postulated selective oxidation. A sulfur spectrum from a source of pork insulin, which was oxidized only by a fraction of the amount of oxidant needed to achieve the oxidation of two of the three disulfide links is shown in Fig. V:50c. In this spectrum the relative heights of the sulfur peaks is accordingly reversed. The fact that the sulfur shifts in Figs. V:50b and V:50c are approximately the same as the shifts between the disulfide and sulfonate oxidation states of sulfur supports the postulated mode of oxidation.

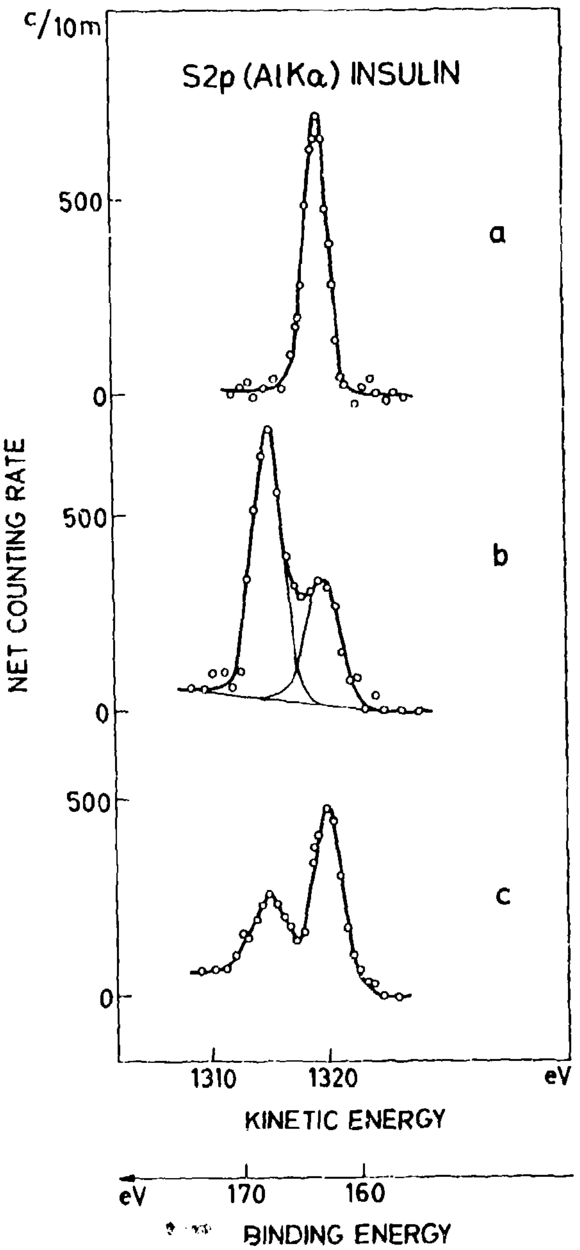

Fig. V:50. The sulfur $2p$ electron line from different sources of insulin, (*a*) unoxidized, (*b*) oxidized and (*c*) partly oxidized.

V:5c. ESCA shifts of carbon and oxygen

Work is in progress to establish charge-binding energy correlations for the elements carbon and oxygen and to apply ESCA to structural problems involving these elements.

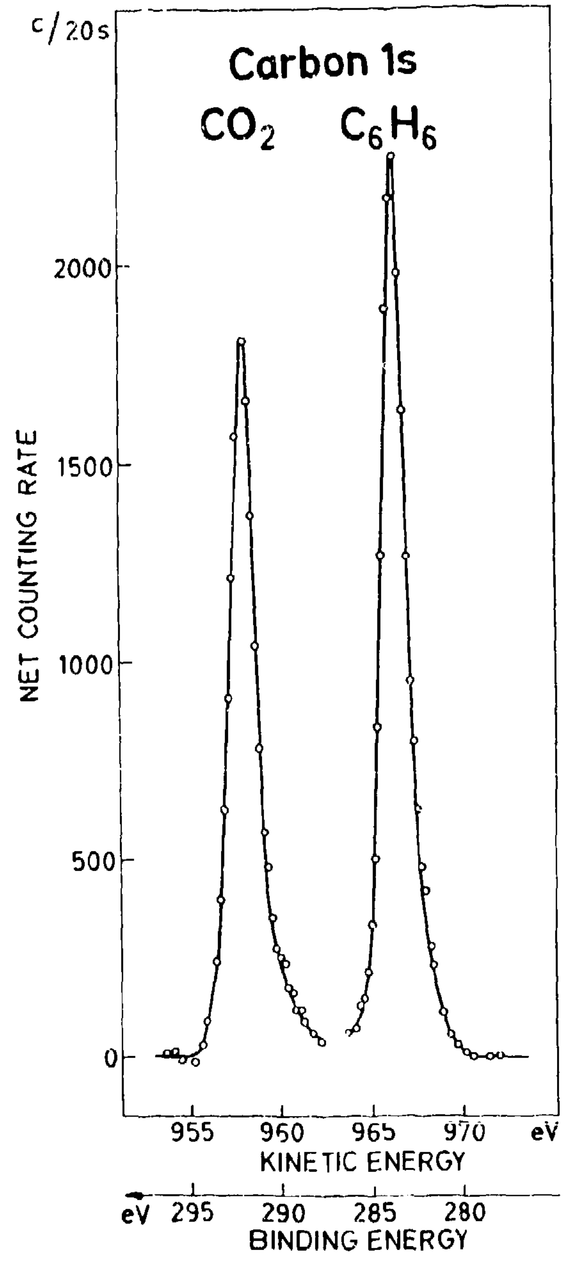

Fig. V:51. The carbon 1*s* line in carbon dioxide and benzene.

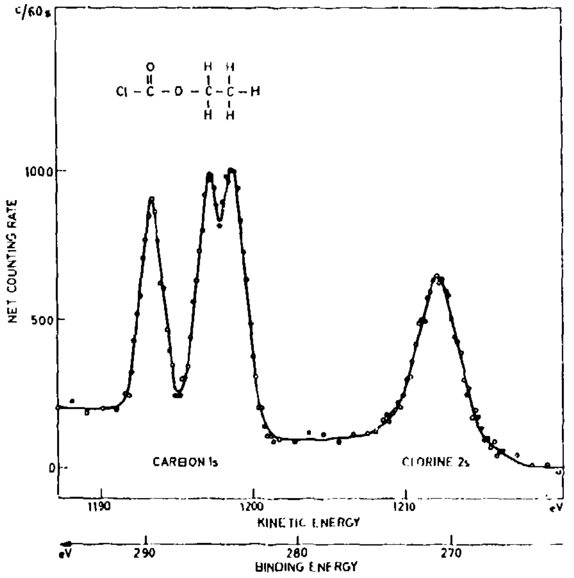

Fig. V:52. Electron spectrum from ethyl chloroformiate. Three lines are obtained in the carbon 1*s* spectrum which appear in the same order from left to right as the carbon atoms in the structure that has been drawn in the figure. The different valence states of carbon in this molecule are thus reflected in the ESCA spectrum. The chlorine 2*s* line is also seen. It is much broader than the carbon 1*s* lines because of the large inherent width of the chlorine 2*s* level.

Carbon.—In a series of carbon containing compounds chemical shifts of the same order of magnitude as in other elements have been observed. Fig. V:51 shows the carbon 1*s* level shift between solidified carbon dioxide and solidified benzene. Fig. V:52 shows an electron spectrum from ethyl chloroformiate. The different valence states of the three carbon atoms in this molecule are reflected in the ESCA spectrum and the broad 2*s* level of chlorine is also seen. It is interesting to compare this spectrum with those of ethyl trifluoroacetate (Fig. I:16) and acetone (Fig. I:15). The largest shift, 8.2 eV, was observed between the trifluoromethyl carbon and methyl carbon in ethyl trifluoroacetate. Chlorine as a substituent in ethyl chloroformiate causes a 0.6 eV larger shift between the oxycarbonyl carbon and methyl carbon than does the trifluoromethyl substituent in ethyl trifluoroacetate. The shift in carbonyl carbon in acetone falls between the shifts of carboxyethyl carbon and oxymethylene carbon. This sequence of shifts is in accordance with the group electronegativities of the ligands.

There also seems to be a shift between elemental carbon in the forms of graphite and diamond. This could either be due to crystal effects or to the different types of hybridization in graphite and diamond or to both.

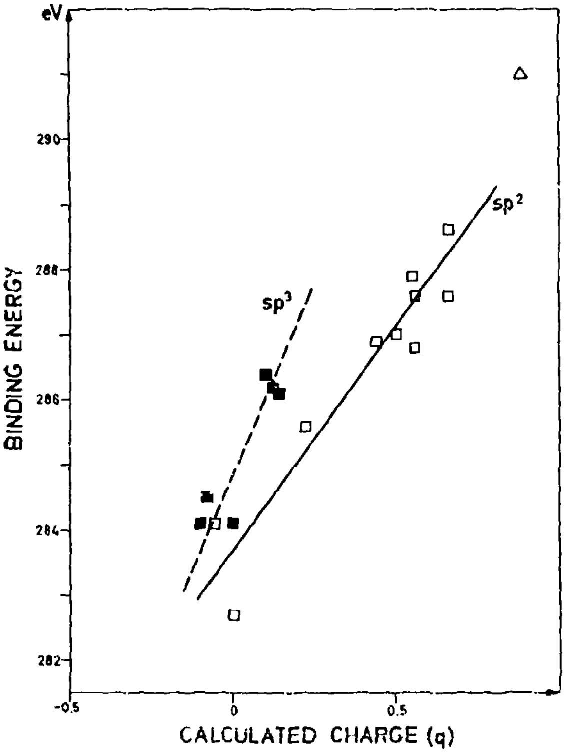

Fig. V:53. Binding energy for the carbon 1*s* electrons versus calculated charge for sp^2- and sp^3- hybridized carbon.

A preliminary charge-binding energy correlation for carbon is shown in Fig. V:53. With the charge calculation based on average electronegativities one distinguishes two rectilinear correlations, one for sp^2-hybridized carbon (open squares) and one for sp^3-hybridized carbon (filled squares). When the orbital electronegativities of Hinze and Jaffé[169] (see Appendix 16) are employed these lines tend to coalesce to one.* It is thus obvious that the differences in electronegativity caused by hybridization are reflected in the electron spectra, and carbon seems to be a suitable element for the study of the effects of hybridization.

Oxygen.—ESCA data are also being collected for oxygen (see Tables V:16–V:18), but we have not yet made any attempts to cover a large range of charge. However, shifts of the same order of magnitude per charge unit as in other elements have also been observed in oxygen. An example of an oxygen shift is given in Fig. V:54, which shows the electron lines from oxygen in sodium *para*-nitrobenzene sulfinate (No. 12.3 in Table V:17). The sulfinate oxygen has by comparison with the spectra of unsubstituted sodium benzenesulfinate and nitrobenzene been shown to be the most negatively charged of the two oxygens. This is in accordance with what could be expected from the usual charge calculation.

V:6. ESCA—a Surface Method

Electrons with energies of a few keV or less penetrate only very thin layers of solid matter. Range-energy curves for electrons in the keV region are about the same for different materials[226] when the range is expressed as mass per unit area; for electrons with kinetic energy 600 eV it is 10^{-5} g cm^{-2}. Thus a thickness of aluminum of 400 Å will totally absorb the energy. Photoelectrons produced by, for example, aluminum $K\alpha$ emerge from a surface layer of a few hundred atomic layers. The fraction that emerges without energy loss becomes exceedingly small as this depth is approached. The average depth at which those electrons are produced that one observes in the electron lines may be only a few tens of Å. This is illustrated in Fig. V:55 which shows an electron line from iodine obtained from three multilayer samples of different thickness. It is possible to build up multilayers of many long-chain

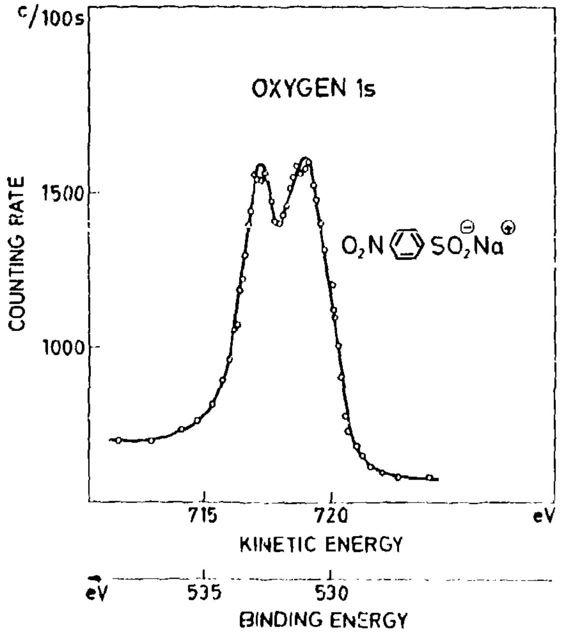

Fig. V:54. The 1*s* electron line of oxygen from sodium *para*-nitrobenzene sulfinate. The energy shift between the nitro and sulfinate oxygen is 2.0 eV.

---

* *Note added in proof:* When applying the extended Hückel method for calculation of charge we obtain one rectilinear correlation.

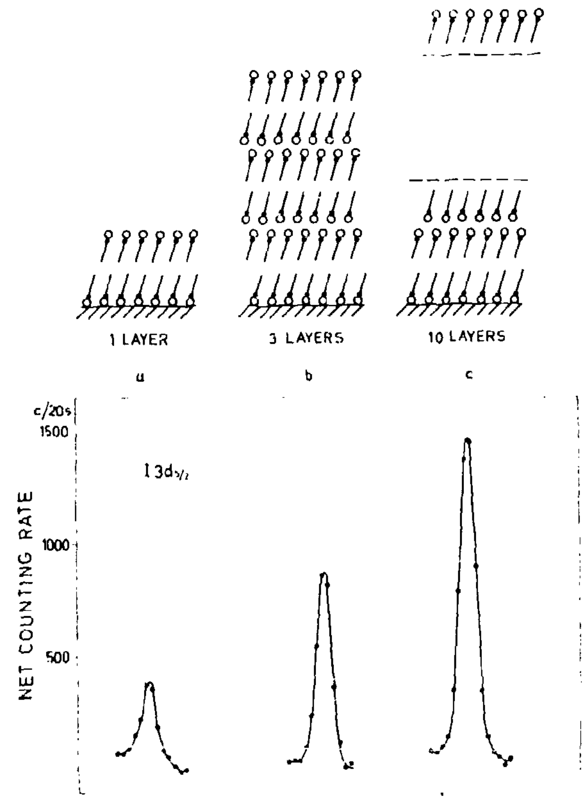

Fig. V:55. The $3d_{5/2}$ electron line from iodine in three different multilayer samples. They consist of 1, 3, and 10 double-layers of α-iodostearic acid, respectively.

compounds on solid surfaces from monolayers deposited on water[227-229], and it has been shown that, for example, a replacement of methyl groups in fatty acids by bromine or iodine atoms does not generally influence the molecular arrangement in the solid state. The samples in Fig. V:55 were made from a monolayer of very pure iodostearic acid, dispersed on a water surface. Multilayers were built up from this monolayer on chromium plated brass slides by dipping them in the water*. The samples consisted of one, three, and ten molecular double layers, respectively, see Fig. V:55. Each double layer was 40 Å thick and contained one iodine atom over an area of ten square Ångström. The total amount of iodine was less than 10^{-8} g in sample (a) but was sufficient to give a net counting rate of 20 counts per second at the peak of the iodine $3d_{5/2}$ electron line (aluminum $K\alpha$ radiation), which illustrates the sensitivity of the method.

As the number of double layers was increased from one to three (sample (b)) the counting rate increased, but not by a factor of three. When the number of layers reached ten (sample (c)) the intensity had only increased by a factor of 3.5. This indicates that the electrons of the ESCA line were emitted from an average depth of less than 100 Å.

Since the general features of the molecular packing in fatty acid layers can be determined by X-ray diffraction methods, physical methods for examining the

---

* We thank Docent Kåre Larsson, Dept. of Medical Biochemistry, Göteborg, for making the multilayer samples for us.

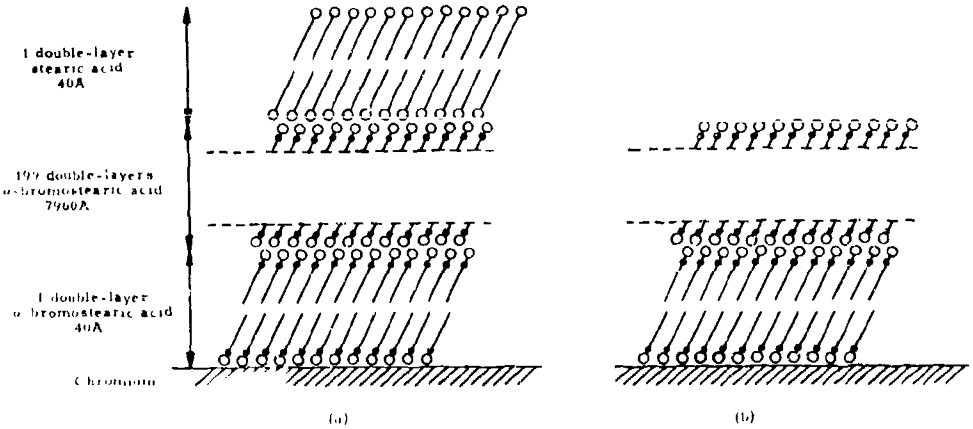

Fig. V:56. Two multilayer samples with 200 molecular layers of DL-α-bromostearic acid. Two layers of "unlabelled" stearic acid are deposited on one of the samples (a).

molecular packing in phase boundaries can be tested using multifilms of fatty acids as models.

Another experiment to study molecular layers by ESCA was made on two multilayers that were "labelled" with bromine.[74] Two samples with 200 molecular layers of DL-α-bromostearic acid were built up on chromium plated brass slides, and two layers of "unlabelled" stearic acid were deposited on one of them. The long-spacings of the multifilms were determined by X-ray diffraction using Cu$K\alpha$ radiation. The molecular packing in the surface films according to the X-ray analysis is illustrated in Fig. V:56. Photoelectrons expelled by Al$K\alpha$ radiation from the 1s shell of carbon and the 3d shell of bromine were studied.

No signal was obtained from the chromium backing but well-defined bromine lines were recorded from both samples showing that a film of 8000 Å thickness gives complete shielding whereas atoms covered with about 50 Å of organic material can be detected by ESCA. The most interesting result, however, was the relative intensities of the bromine and carbon signals from the two samples. As seen in Fig. V:57, the ratio of the bromine to carbon signals was three times smaller for the slide where the α-bromostearic acid was covered with two layers of stearic acid (sample (a)). The bromine line was also shifted towards lower kinetic energy by about 1 eV. This could be a crystal field effect (Section V:2) if convergence of the Madelung constant requires more than a few Ångström of length. Such a surface correction has been suggested by Fadley *et al.*[204,225] Electron spectra like those of Fig. V:57 can be very useful for the study of molecular packing and the occurrence of defects in monomolecular layers. A larger part of the bromine spectrum from sample (b), including some Auger transitions, is shown in Fig. V:58.

ESCA is thus a surface method in the sense that it yields information on the atomic and molecular structure to a depth, say, of 100 Å. It is not limited to the first few ångströms as is, for example, the LEED method (Low Energy Electron Diffraction), although one can by ESCA obtain information even from a monoatomic surface layer. These features of ESCA are obviously of special interest in the physics and chemistry of surfaces.

Earlier attempts to use X-ray photoelectron spectra for the study of built-up films reported by Steinhardt and Serfass[230] gave little information since their resolution was insufficient to yield a true line spectrum. Similar studies have also been reported by Henke.[231]

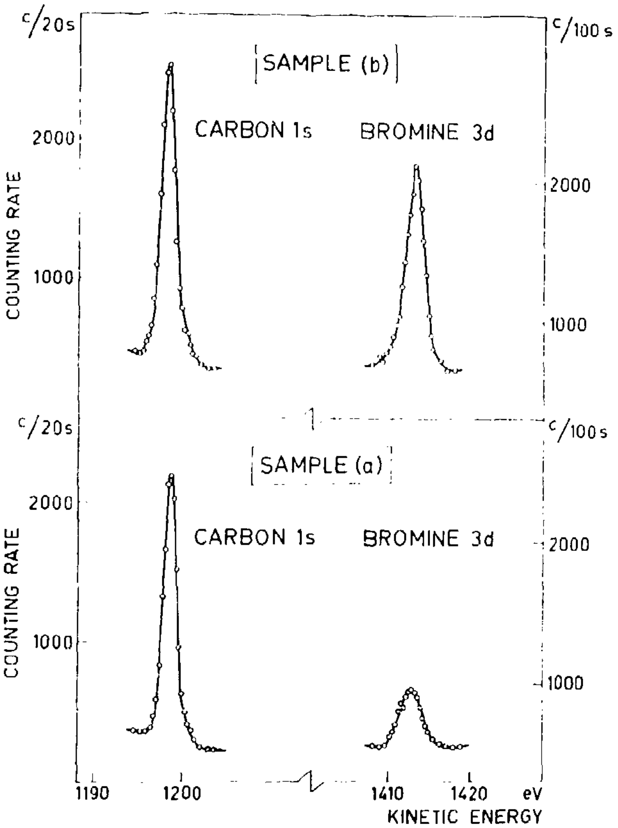

Fig. V:57. Electron lines from carbon and bromine in the samples shown in Fig. V:56. The relative intensity of the bromine line to the carbon line is three times smaller when the α-bromostearic acid is covered with two layers of stearic acid.[74]

V:7. Elemental Analysis

Each element in a chemical compound makes a characteristic contribution to the electron spectrum. It is therefore possible to make a qualitative elemental analysis from the positions of the lines in the electron spectrum. We have also found that a quantitative elemental analysis of a compound can be made from the intensities of the lines in the electron spectrum. Fig. V:59 shows some of the electron spectra that were recorded in our first attempt to study quantita-

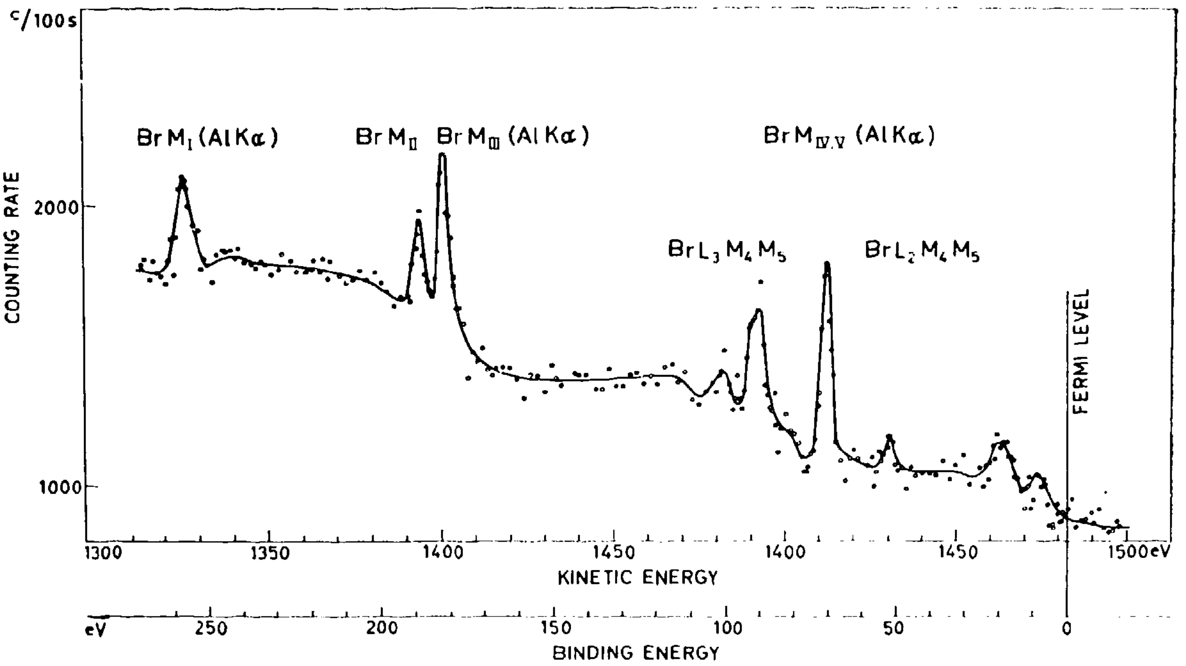

Fig. V:58. Electron spectrum from sample (*b*) in Fig. V:56, showing both photoelectron and Auger electron lines from bromine.

tively the elemental composition of a sample.[48] Sodium sulfate, sodium carbonate, and silicon carbide were chosen as test substances and electron spectra were produced by chromium and copper X-radiation. The observed line intensities had to be corrected for the following effects:

(*a*) *Z-dependence of photoelectric cross section*

Empirically it has been found[278] that the attenuation cross section can be written as

$$\mu = cZ^4\lambda^3 + b \qquad (8)$$

Here the first term in the expression can be identified with the photoelectric absorption and the second term with the scattering if the latter is assumed to be independent of wavelength. The Z^4-dependence for the photoelectric part of the cross section will "favour" elements of high atomic number. (The exponent in the Z-dependence has not been exactly established; the value given in eq. (8) is merely chosen as a mean of several suggested values. The approximate variation of the mass absorption coefficient with Z for a number of radiations frequently used in ESCA measurements is given in Appendix 7.)

(*b*) *Energy dependence of attenuation for electrons emerging from the irradiated sample*

On emerging from the sample, the electrons suffer energy losses. Since these losses occur in discrete amounts, some electrons leave the sample without any loss of energy. These electrons form the lines on which the measurements are made. The fraction of electrons that fall outside the recorded lines increases with decreasing kinetic energy of the electrons. This will tend to favour elements of low atomic number in the photoelectron spectra.

(*c*) *Detector efficiency*

In our first measurements, we used GM-detection without postacceleration and the window cut-off thus put a lower limit of around 3 keV to the electron energies that could be detected. For a given characteristic X-radiation, and for a photoelectric effect in, say, the K shell, there is then an upper limit for Z above which the detector efficiency becomes zero The fall of detector efficiency down to zero occurs over several atomic numbers.

The corrections (a)-(c) for the observed line intensities were determined empirically from a set of com-

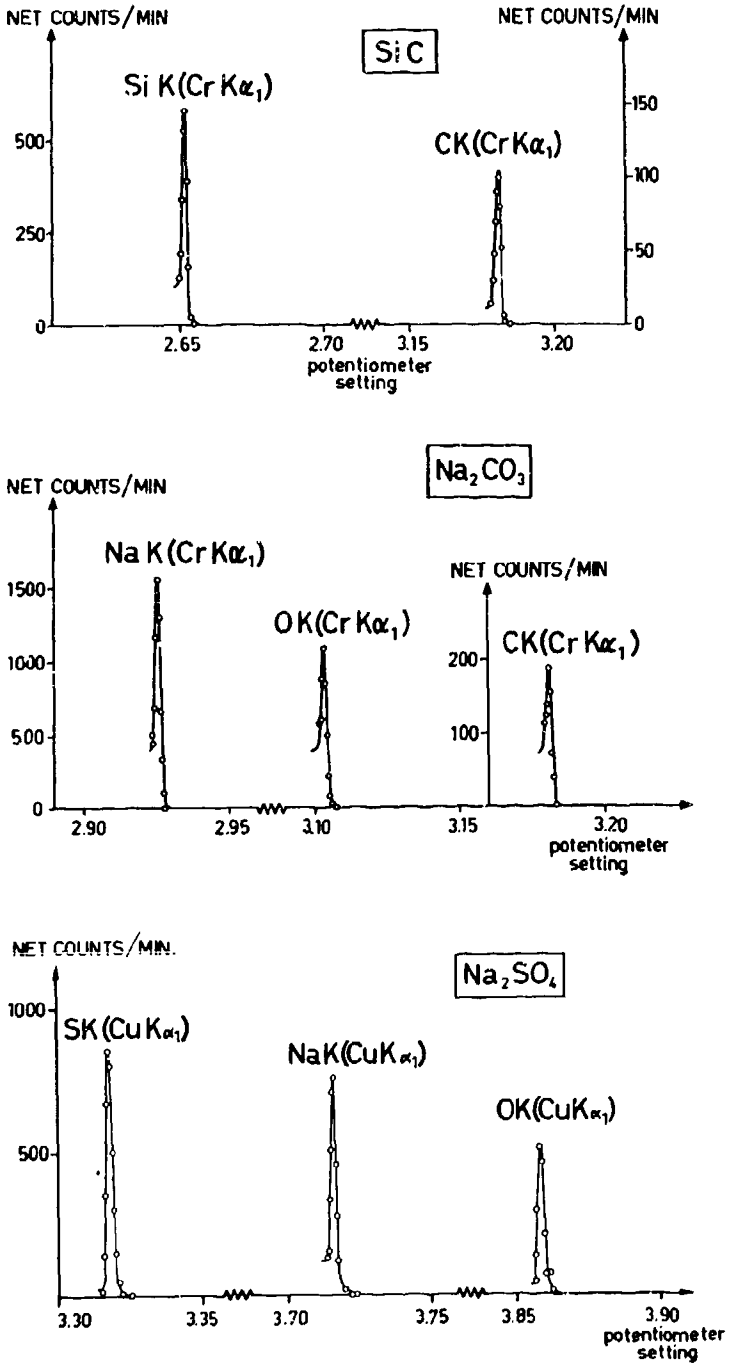

Fig. V:59. Electron spectra from SiC, Na_2CO_3 and Na_2SO_4.[48] A quantitative elemental analysis of the compounds can be made from the intensities.

Table V:20. Relative amounts of carbon, chlorine and sulfur as obtained from the ESCA spectra of some organic compounds.

Compound		Observed relative amounts			
Number	Empirical formula	C_O	C_H	Cl	S
1	$C_{O_0}C_{H_6}H_4ClSO_2Na$	0	6	1	1
2	$C_{O_0}C_{H_7}H_6ClS_2O_3Na$	0	7.1 ± 0.7	0.98 ± 0.08	2
3	$C_{O_0}C_{H_7}H_6Cl_2SO_2$	0	7.6 ± 0.7	1.95 ± 0.16	1
4	$C_{O_1}C_{H_7}H_3Cl_5SO_2$	1.0 ± 0.1	6.9 ± 0.7	4.86 ± 0.30	1

pounds of known composition, and the calibration curve obtained was then used to evaluate the relative amounts of the constituent elements in the test samples. The result of the analysis was correct to within 5 to 10 %. An excess amount of oxygen was found that was probably due to surface absorption of oxygen and to traces of humidity left in the sources.

In Table V:20 and Table V:21 some other data showing the potentialities of ESCA for quantitative elemental analysis have been collected. The electron spectra from which the data for these tables were obtained are shown in Figs. V:60, V:61, and V:62.

Fig. V:60 shows the electron spectra obtained from a series of organic compounds, all containing a benzene ring substituted in different positions with various numbers of sulfur and chlorine atoms. Sources were prepared by pressing the powdered compounds onto a copper mesh. The figure shows electron lines from the 1*s* shell of carbon and the 2*p* shell of sulfur and chlorine, obtained with aluminum *Kα* radiation. The intensities are adjusted so that the heights of the sulfur lines are all unity.

In compounds with an increased number of chloro substituents, the chlorine line increases proportionately in intensity. The chlorine atoms are bound to carbon atoms in the benzene ring and core electron binding energies of the chlorine atoms are the same in different compounds. Compound 3 in Table V:20 is an exception in which one chlorine is bound to sulfur in a sulfonyl group instead of benzene carbon. This is reflected in the electron spectrum as a broadening of the chlorine line. A larger chemical shift effect is observed in Compound 2 which contains two sulfur atoms in different oxidation states. Two well-resolved sulfur lines of equal height are obtained in this case. It is also of interest to notice how the oxidation states of sulfur in different compounds are reflected in the positions of the sulfur lines. Compound 4 contains a carboxyl group and the carboxyl carbon is observed as a separate line in the electron spectrum.

Geiger counter detection with post-acceleration was used in the recording of these spectra, and there is little difference in window absorption for the different lines (see point (c) above). The kinetic energy of the different lines is between 1.2 keV and 1.3 keV and the observed difference in intensity between the carbon, chlorine, and sulfur lines that cannot be ascribed to differences in elemental composition are mainly a result of the different X-ray absorption coefficients for these elements (see point (a) above and Appendix 7). Thus the observed relative intensity of the chlorine line in compound 1 is 1.28, which is exactly the value calculated from eq. 8. The relative intensity of the carbon line cannot be calculated as easily from this equation since the constant *c* assumes different values for absorption in the 1*s* and 2*p* shells. Compound 1 has therefore been used as a standard for obtaining the relative elemental composition from the electron spectra of compounds 2–4.

The result of this elemental analysis is shown in Table V:20 where the relative amounts of carboxyl

Table V:21. Elemental analysis of insulin and five amino acids by ESCA.

Compound		Observed relative amounts					
Name	Empirical formula	C_O	C_H	C	N	O	S
Glycine	$C_{O_1}C_{H_1}H_5NO_2$	1	1	2	1	2	0
Alanine	$C_{O_1}C_{H_2}H_7NO_2$	0.99	1.95	2.94	1	1.87	0
Glutamic acid	$C_{O_2}C_{H_3}H_9NO_4$	1.96	3.05	5.01	1	3.60	0
Cysteine	$C_{O_1}C_{H_2}H_7NO_2S$	0.97	2.02	2.99	1	1.90	1
Methionine	$C_{O_1}C_{H_4}H_{11}NO_2S$	0.99	3.98	4.97	1	1.90	0.87
Insulin	$C_{O_{61}}C_{H_{193}}H_{450}N_{65}O_{75}S_6$	61	205	271	65	66	5.7

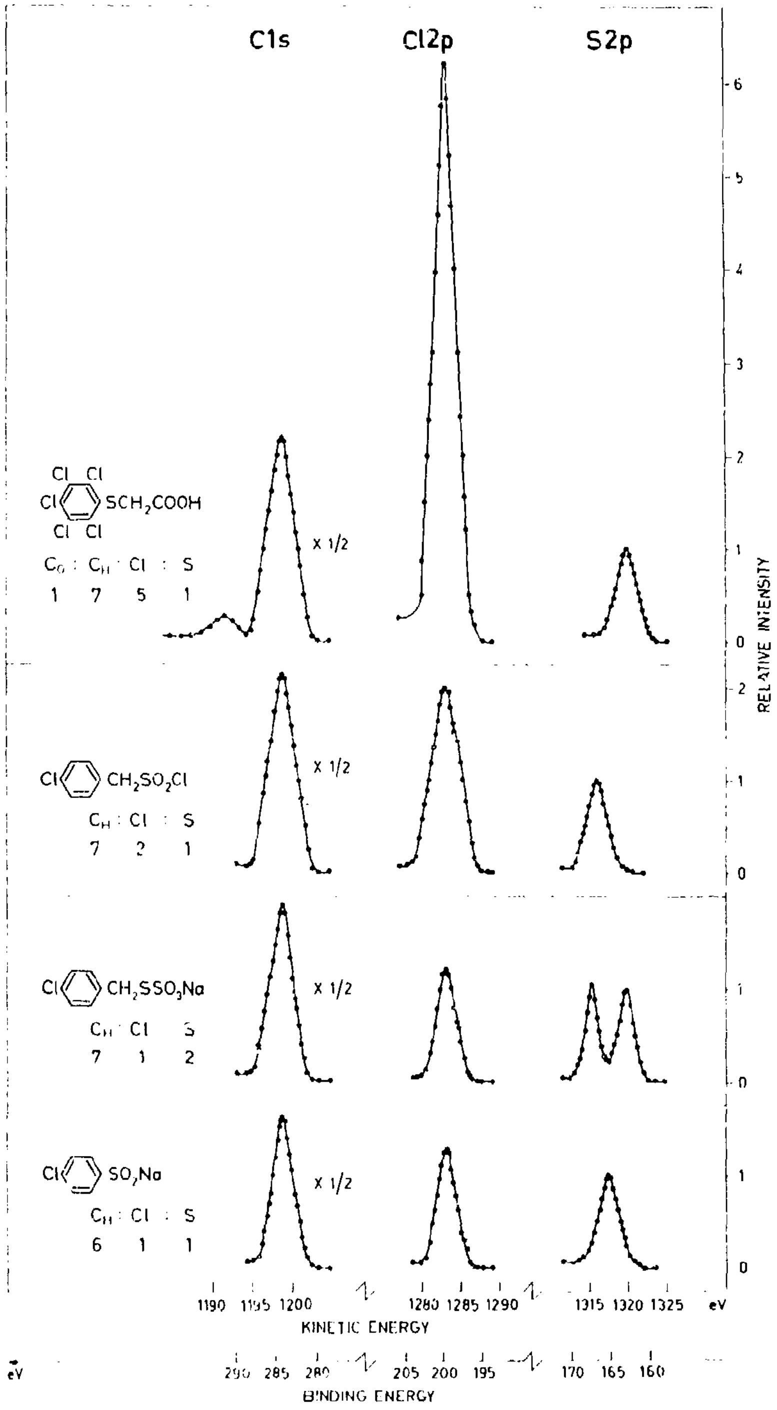

Fig. V:60. Electron spectra from a series of organic compounds all containing a benzene ring substituted with various numbers of chlorine and sulfur atoms. The intensities are related to the height of the sulfur $2p$ line as unity.

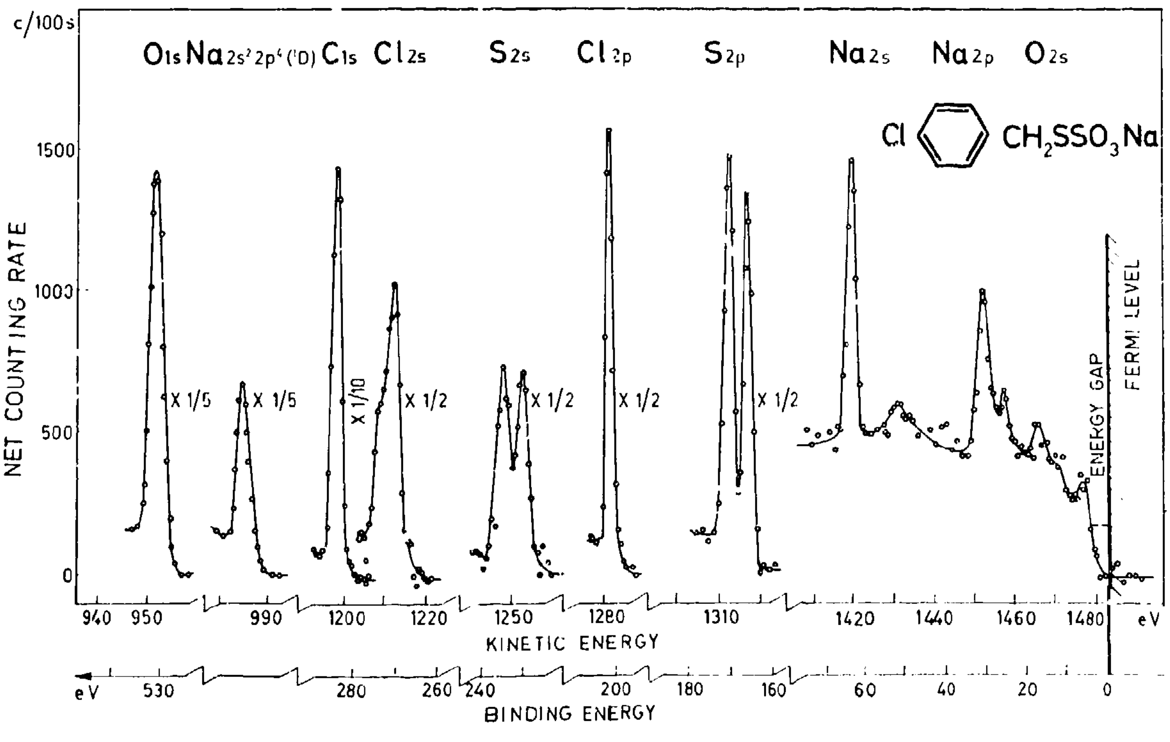

Fig. V:61. ESCA spectrum from one of the substances in Fig. V:60. All constituent elements, except hydrogen, show up in the spectrum.

carbon (C_O), benzene and CH_2 carbon (C_H), chlorine, and sulfur, obtained from the electron spectra, are compared with the empirical formulae of the different compounds. The precision of these preliminary measurements, defined as the maximum deviation from the mean of two or more measurements, is indicated in the table. As seen from this table, the relative amounts of C_O, C_H, Cl, and S are reproduced with an accuracy of better than 5 % in the electron spectra. The entire spectrum recorded from one of the substances (compound 2) is shown in Fig. V:61. All constituent elements, except hydrogen, are represented in this spectrum, both as photoelectron and as Auger electron lines. The spectrum extends to zero binding energy at which there is a marked decrease in intensity.

Fig. V:62 shows the electron spectra of five amino acids and insulin which consists of two polypeptide chains cross-linked by two disulfide bridges, see Fig. I:12. All constituent elements, except hydrogen, were recorded; oxygen, nitrogen, and carbon are represented by their 1*s* photoelectron lines, and sulfur by its 2*p* photoelectron lines. The intensity scale is adjusted in this case so that the heights of the nitrogen lines are all unity. Glycine is the simplest amino acid and contains one carboxyl carbon and one CH_2 carbon. These are seen in the electron spectrum as two lines of which the carboxyl carbon line has lower kinetic energy. The excessive height of the CH_2 carbon line is accounted for by the presence of a small amount of extraneous organic material on the surface (cf. Section V:1). If this is corrected for, the glycine spectrum can be used for calibration when deducing the elemental composition of other amino acids from their electron spectra. The result of such an elemental analysis for the other four amino acids and insulin is given in Table V:21.

The result of a determination of the relative amounts of copper and zinc in brass is shown in Fig. V:63. Five samples with different compositions were analysed. With one of the alloys used as a standard, the analysis of the other four could be made with an accuracy better than two per cent. The electron spectrum recorded from a sixth sample is shown in Fig. V:64.

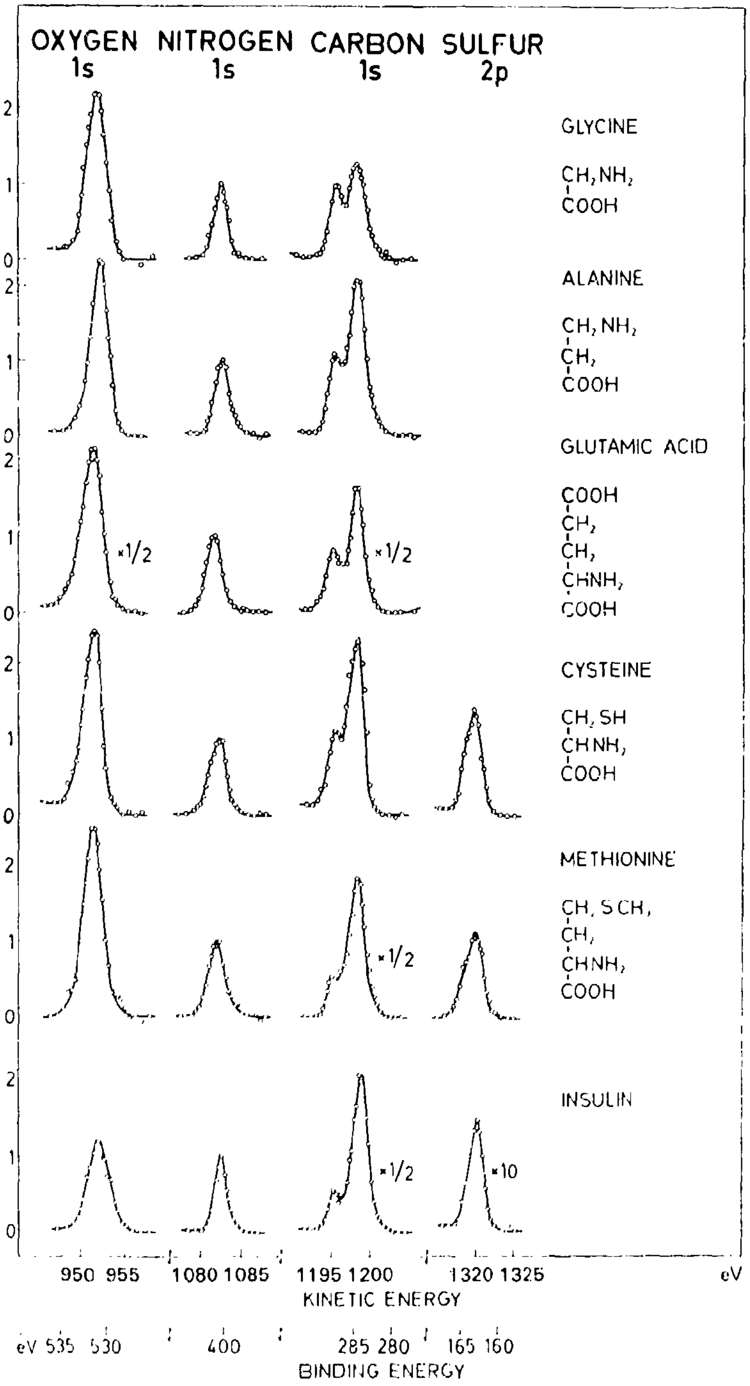

Fig. V:62. Electron spectra from five amino acids and from insulin. The lines are related to the nitrogen 1s line as unity.

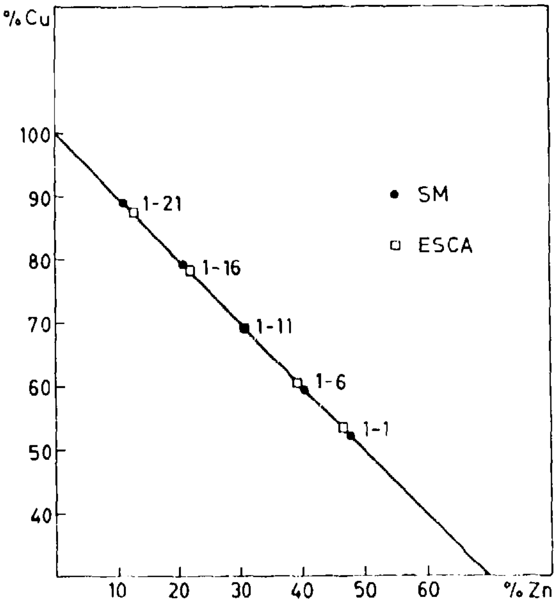

Fig. V:63. The relative amount of copper and zinc in some brass alloys as measured by ESCA. The results are compared with data (SM) given by the factory, Svenska Metallverken.

This contained small amounts of other metals, e.g. 0.68 % tin and 0.82 % lead. The tin $M_{\text{IV,V}}$ signal is weak but the $N_{\text{VI,VII}}$ electron lines from lead are so intense that they had to be reduced in height by a factor of five when plotted in the figure. It thus seems as if heavy elements, which are favoured by the Z^4-dependence of the photoelectric cross section, can be analysed by ESCA even in small proportions among several other elements.

Although this line of research has not yet been developed to the accuracy and precision necessary for the determination of empirical formulae for (unknown) complex compounds, the results obtained so far suggest that this should in principle be possible. The relative proportions of carboxylic carbon and other carbons obtained in the series of amino acids and in the series of carboxylic acids (Section V:1) suggest that ESCA could be applied to quantitative group analysis.

ESCA is in most cases a non-destructive analytical tool but decomposition of the sample sometimes occurs under the combined action of vacuum and electromagnetic radiation. If the decomposition takes

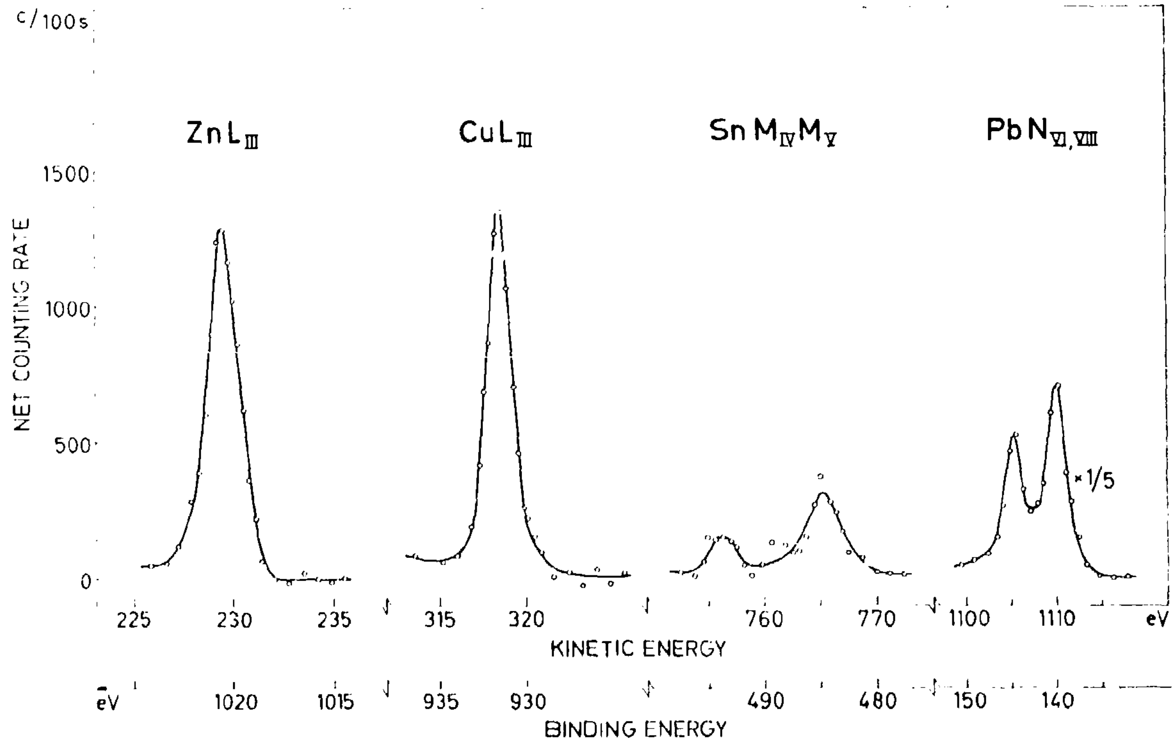

Fig. V:64. An electron spectrum from a brass alloy containing small amounts of lead and tin.

place over a period of minutes or hours, it may be possible to follow the process in the ESCA spectrum. This is illustrated in Fig. V:65, which shows the intensities of the chlorine $2p$ and sulfur $2p$ electron lines (produced by Al$K\alpha$) of an organic compound as a function of time. The extrapolated intensity at $t = 0$ of chlorine relative to sulfur is around 1.6 and this ratio decreases to 1.1 after about 2 h, thereafter remaining constant. This indicates that on the average one chlorine atom per molecule is removed from the surface region when the specimen has been kept in a vacuum and exposed to X-radiation for two hours.

Unless special precautions have been taken to maintain a clean vacuum, there is always a small deposit of carbon-containing material on the samples. The contaminating layer is probably due to hydrocarbons from the pump oil. This is a surface effect of quite trivial nature which may be a nuisance when the element carbon is being studied since the carbon line from the contaminating film overlaps the carbon spectrum from the sample. In most cases, however, we have

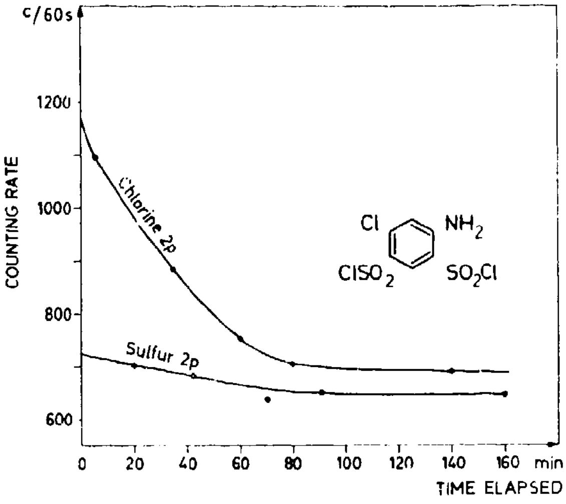

Fig. V:65. Intensities of the chlorine $2p$ and sulfur $2p$ lines as a function of elapsed time in an organic compound which decomposes under the action of vacuum and radiation.

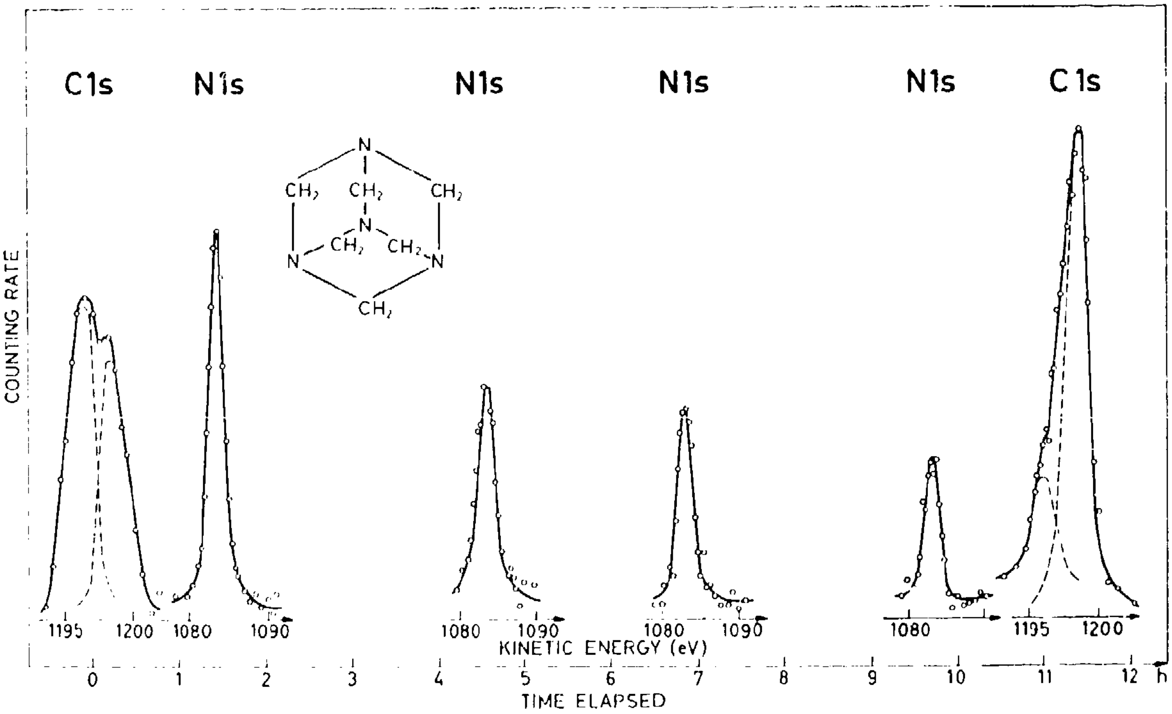

Fig. V:66. Successive recordings of carbon and nitrogen from a hexamethylene tetramine sample. The surface layer of pump oil increases with time. This is reflected in the spectrum by an increase in the intensity of the line from carbon in the contaminating layer.

found the carbon 1*s* line from the pump oil ideally suited for use as a calibration line. In fact, there is usually no difficulty in distinguishing this line from the rest of the spectrum since its relative intensity increases with time. This is illustrated in Fig. V:66 which shows successive recordings of carbon and nitrogen lines from a hexamethylenetetramine sample. The sequence was made such that the carbon 1*s* line was first recorded; then four recordings were made of the nitrogen 1*s* line, and finally the carbon 1*s* line was recorded again. The carbon atoms in the compound itself all have the same valence state and therefore give only one carbon line in the ESCA spectrum. The other carbon line is due to carbon in the surface film. The two lines are resolved graphically in the figure. From the graphical analysis, it is seen that one of the carbon lines has increased in intensity by a factor of two over a period of 10 h, whereas the other line has decreased in intensity by almost a factor of three. It is therefore evident that the former is due to the pump oil and the latter is due to the hexamethylenetetramine. The thickness of the surface layer and the intensity of the carbon line increases with time at the expence of intensities of both carbon and nitrogen lines from the compound under study. However, even after 8 h, the nitrogen line from the hexamethylenetetramine could be recorded without difficulty and the energy determination could be made with the "surface" carbon line as a reference.

Although much work remains to be done before the applicability of ESCA to quantitative elemental analysis has been fully explored both for the photoelectron and Auger electron spectra, we should in the following like to draw attention to some general features of ESCA as a quantitative analytical method.

ESCA is a purely physical method and, provided that the samples are not decomposed by the radiation used, a non-destructive method. In principle it permits a total analysis of all elements except hydrogen in one operation without disturbing interferences between the constituent elements. In this respect ESCA is rather unique compared with other quantitative methods and allows any sample or homogeneous mixture to be analysed for any element without chemical pretreatment or separations.

Quantitatively ESCA is a relative method, but it should in principle also be possible to use it for absolute determinations using standard addition techniques.

We have seen that the absolute sensitivity of the method is high, provided the sample is applied as a thin coherent film of a certain minimum area. For certain applications such a film need not consist of more than a monomolecular layer. It should therefore be possible to adapt ESCA to the ultramicro scale.

The limits for the relative sensitivity, i.e. the smallest proportion of an element that can be determined with adequate accuracy, remains to be investigated, but the results obtained for cobalt in vitamin B_{12}, sulfur in insulin, and lead in brass show that elements occurring in a small proportion among several other elements can be satisfactorily determined. A relative sensitivity in the p.p.m. region, which is sometimes required in analytical chemistry, does not seem to be within immediate reach.

To sum up, the following virtues of ESCA may be mentioned that recommend it as a useful analytical tool:

1. Heavy and light elements may all be studied alike by ESCA.

2. The absolute sensitivity is high, i.e. the amount of material required for obtaining an ESCA spectrum is small (less than 10^{-8} g).

3. Amorphous as well as crystalline samples may be studied by ESCA.

4. ESCA is in most cases a non-destructive method.

5. The spectral position of an ESCA line depends on the valence state of the corresponding atom. This suggests a more refined qualitative analysis, e.g. the determination of the oxidation states of metals or the quantitative distinction between different organic groups (quantitative group analysis).

VI. ELECTRON EMISSION FROM EXCITED ATOMS

An atom with an inner shell vacancy can be de-excited in two different ways as illustrated in Fig. II:3. The radiationless de-excitation process in which the atom is left with two vacancies is known as the Auger effect. If one of the final state vacancies lies in the same shell as the primary vacancy (although not in the same subshell) the radiationless transition is referred to as a Coster–Kronig transition. Other modes of radiationless de-excitation may also occur; for example, the number of electrons that are emitted in a radiationless transition can be more than one and electrons may be emitted from atoms with multiple primary vacancies. An accurate study of these processes was for many years hampered by experimental difficulties. The theoretical treatment of the electron spectra from highly excited atoms was also far from satisfactory. During the last decade, improved experimental techniques have facilitated the study of the Auger effect and related effects and the necessary experimental basis now exists for more comprehensive theoretical treatments. The *KLL* Auger spectra (see Section II:2) have been of particular interest and in what follows we shall mostly confine ourselves to these Auger transitions. For a detailed discussion the reader is referred to review articles in the field.[38,246]

KLL Auger spectra in intermediate coupling

In 1957, the Auger spectrum of copper was studied at Uppsala[9] in a search for a more complex spectrum than that predicted by *jj* or *LS* coupling theory. The following year, a theoretical treatment of the Auger effect based on intermediate coupling was made by Asaad and Burhop.[234] Semiempirical energies and calculated relative intensities of the *KLL* Auger lines were given for five elements, viz. $Z = 25$, 30, 37, 47, and 80. Intermediate coupling theory gives a nine-line *KLL* Auger spectrum as opposed to seven lines in pure *LS* and six lines in *jj* coupling. In 1962, a full nine line *KLL* Auger spectrum was established for elements in the region around $Z = 40$ using X-radiation for production of K vacancies[33] and also by use of K-capture and internal conversion.[238] The Auger line energies predicted by Asaad and Burhop[234] were found to be considerably in error for the elements between $Z = 38$ and $Z = 47$ whereas the predicted line separations within the spectra were in good agreement with the experimental values. From the experimental data, it was possible to improve the semiempirical relations for the energies of the different Auger lines.[33] Auger line energies calculated from these new expressions showed good agreement with experimental values for elements of low and intermediate Z. For heavier elements, the semiempirical expressions were later modified to give better agreement with experiment.[35] Auger energies calculated from these two sets of expressions are listed in Appendix 4. A major part of the electron binding energies which are used in these calculations are obtained from ESCA measurements, see Appendix 1.

A more straightforward calculation of Auger energies has now been made.[73] The relativistic self-consistent-field method, described in Section III:9, was applied to the calculation of *KLL* Auger energies of a free atom or ion. Separate calculations of the total energy of the atom in its initial state with a vacancy in the K shell, and in its final, doubly ionized, state were performed. The kinetic energy of the emitted electron, i.e. the Auger energy, was obtained as the difference in total energy between the final and initial states (Method B, Section III:9). In the computer program only the weighted average of the configuration was calculated. To obtain all nine *KLL* Auger energies, the term splitting had to be calculated in intermediate coupling. Electrostatic and exchange integrals have already been calculated in the self-consistent-field program to obtain the total energy of the atom. Applying the theoretical treatment of intermediate coupling given by Condon and Shortley[214] the following expressions are obtained for the *KLL* Auger energies:

$$E_{KL_1L_1}(^1S_0) = E_{L_1L_1} - E_K$$

$$E_{KL_1L_2}(^1P_1) = E_1 - \tfrac{1}{4}\zeta - \sqrt{(G_1 - \tfrac{1}{4}\zeta)^2 + \tfrac{1}{2}\zeta^2}$$

$$E_{KL_1L_2}(^3P_0) = E_1 + G_1 - \zeta$$

$$E_{KL_1L_3}(^3P_1) = E_1 - \tfrac{1}{4}\zeta + \sqrt{(G_1 - \tfrac{1}{4}\zeta)^2 + \tfrac{1}{2}\zeta^2}$$

Table VI:1. Calculated and measured *KLL* Auger energies (eV) in magnesium, potassium and copper.

Final State	Element					
	12 Mg		19 K		29 Cu	
	a^{73}	b^{58}	a^{73}	b^{41}	a^{73}	b^{15}
$KL_1L_1(^1S_0)$	1088	1101	2801	2809	6736	6744
$KL_1L_2(^1P_1)$	1123	1135	2878	2878	6880	6872
$KL_1L_3(^3P_0)$	1137	1150	2902	2904	6911	6914
$KL_1L_3(^3P_1)$			2903		6920	
$KL_1L_3(^3P_2)$			2905		6932	
$KL_2L_2(^1S_0)$	1165	1175	2954	—	7016	7011
$KL_2L_3(^1D_2)$	1171	1180	2967	2972	7044	7040
$KL_3L_3(^3P_0)$	1175		2973	— —	7060	7068
$KL_3L_3(^3P_2)$			2976	— —	7073	

[a] Calculated using the relativistic self-consistent-field method.

[b] Experimentally obtained energies.

$$E_{KL_1L_3}(^3P_2) = E_1 + G_1 + \tfrac{1}{2}\zeta$$

$$E_{KL_2L_3}(^1S_0) = E_2 - \tfrac{5}{2}F_2 - \tfrac{1}{2}\zeta - \sqrt{(\tfrac{15}{2}F_2 - \tfrac{1}{2}\zeta)^2 + 2\zeta^2}$$

$$E_{KL_2L_3}(^1D_2) = E_2 + 2F_2 + \tfrac{1}{4}\zeta - \sqrt{(3F_2 + \tfrac{1}{4}\zeta)^2 + \tfrac{1}{2}\zeta^2}$$

$$E_{KL_2L_3}(^3P_0) = E_2 - \tfrac{5}{2}F_2 - \tfrac{1}{2}\zeta + \sqrt{(\tfrac{15}{2}F_2 - \tfrac{1}{2}\zeta)^2 + 2\zeta^2}$$

$$E_{KL_2L_3}(^3P_2) = E_2 + 2F_2 + \tfrac{1}{4}\zeta + \sqrt{(3F_2 + \tfrac{1}{4}\zeta)^2 + \tfrac{1}{2}\zeta^2}$$

where

$E_1 = \tfrac{1}{3}(E_{KL_1L_2} + 2E_{KL_1L_3})$

$E_2 = \tfrac{1}{15}(E_{KL_2L_2} + 8E_{KL_2L_3} + 6E'_{KL_3L_3})$

$\zeta = \tfrac{2}{3}(E_{L_2} - E_{L_3})$

$F_2 = F_2(21,21) = \tfrac{1}{25}F^2(21,21)$

$G_1 = G_1(21,20) = \tfrac{1}{3}G^1(21,20)$

$E'_{KL_iL_j} = E_{L_iL_j} - E_K$

$E_{L_iL_j}$ The total energy of the atom with a vacancy in each of the L_i and L_j shells (Weighted average of configuration).

E_X The total energy of the atom with a vacancy in the X shell. $X = K, L_1, L_2$ or L_3. (Weighted average of configuration).

KLL Auger line energies were calculated for the elements magnesium ($Z = 12$), potassium ($Z = 19$) and copper ($Z = 29$). The energies are given in Table VI:1 and compared to those obtained experimentally.

The experimental values have the Fermi level as a reference level (see Section II:3), i.e. a work function correction for the spectrometer material has been added to the measured kinetic energies of the Auger electrons. The theoretical value, on the other hand, is referred to the vacuum level for a free atom or ion. To obtain a fair comparison between these results a correction of about 5 eV should therefore be subtracted from the experimental values. Table VI:1 then shows quite good agreement between experimental and theoretical data. The remaining discrepancies are probably due to electron electron correlation and configuration interaction.

Interconfiguration interaction

Although the Auger theory was greatly improved by the consideration of intermediate coupling[234], the calculated intensities were not in accordance with the observed finer details of the *KLL* Auger spectra of the light and heavy elements. For the heavy elements this discrepancy may to a large extent be explained by relativistic effects.[235,236]

A new theoretical approach to the Auger effect was made in 1965 by Asaad[237] who introduced interconfiguration interaction into the calculations. In this treatment, the interaction between the $J = 0$ states of the $2s^02p^6$ and $2s^22p^4$ configurations leads to an increase in the intensity of the latter configuration at the expense of the former. The $2s^02p^6$ configuration has only one term ($^1S_0$) whereas one finds two terms, ($^1S_0$) and ($^3P_0$), with $J = 0$ in the $2s^22p^4$ configuration. The intensity of the ($^3P_0$) term depends on the spin doublet splitting which is very small for low Z elements and even taking into account the new interaction, the $1s(^2S_{1/2}) \to 2s^22p^4(^3P_0)$ transition becomes very weak. Thus, for low Z elements, the strength of the $2s^22p^4(^1S_0)$ line increases markedly at the expense of the $2s^02p^6(^1S_0)$ line. Furthermore, since the absolute intensity of the $2s^02p^6$ configuration is decreased by this coupling, the intensity ratio of the $2s^12p^5$ and the $2s^02p^6$ configuration will also increase. A closer study of the Hamiltonian matrix shows that this effect will become of less importance with increasing Z.[237] The calculated intensity ratios will then approach those obtained using the unmodified intermediate coupling theory.

By taking the interconfiguration interaction into

Table VI:2. Relative intensities in the *KLL* Auger spectrum of magnesium.

	Relative intensities			
		Theory		
Final State	Experiment $Z = 12$[58]	$Z = 12$[237, 239]	$Z = 12$[237, 239, 241]	$Z = 10$[239, 242]
$KL_1L_1(^1S_0)$	1.0	1.00(1.00)	1.00(1.00)	1.00
$KL_1L_{2,3}(^1P_1)$	4.6 ± 0.5	2.08(5.29)	1.24(2.32)	6.48
$KL_1L_{2,3}(^3P_{0,1,2})$	1.3 ± 0.3	0.65(1.75)	0.40(0.74)	
$KL_{2,3}L_{2,3}(^1S_0)$	1.8 ± 0.5	0.52(3.05)	0.17(1.15)	3.83
$KL_{2,3}L_{2,3}(^1D_2)$	18.4 ± 1.8	4.98(13.29)	0.75(1.39)	34.14

The values given in parantheses are obtained using an earlier L_I binding energy obtained from X-ray spectroscopy work. By ESCA measurements[51] this binding energy has later been proved to be much in error. The values given without parantheses are obtained using the new L_I binding energies.

account, Asaad obtained a better agreement between theory and experiment for the Auger intensities of light elements.[237] However, the very limited amount of experimental data that was available at the time did not allow an accurate comparison. We therefore performed an experiment in which the X-ray produced *KLL* Auger spectra of sodium ($Z = 11$) and magnesium ($Z = 12$) were studied.[58] In this region of low atomic number, the three final states ($^3P_2$), ($^3P_1$), and ($^3P_0$) of the $2s^12p^5$ configuration have almost identical energies and can therefore not be resolved. Furthermore, the transition rates for the ($^3P_0$) and ($^3P_2$) states of the $2s^22p^4$ configuration are very low compared with other final states not excluded by selection rules. A five-line *KLL* Auger spectrum can therefore be expected and was in fact observed for both elements,[58] see Figs. I:23 and VI:1. The theoretical transition rates for the three configurations of the magnesium *KLL* spectrum have been calculated by Asaad[237] using the Auger transition probabilities derived by Archard. A comparison between the experimental values and these theoretical values gave good agreement. The agreement was, however, coincidental. The Hamiltonian contains average values for the energies of the two configurations $2s^02p^6$ and $2s^22p^4$.[237] Asaad calculated these average energies using tabulated L_I and L_{II} electron binding energies and matrix elements of the electrostatic and spin-orbit interactions. We have since shown that the tabulated L_I binding energies for light elements were much in error, sometimes by as much as 50 %.[51] (see Section III:2). Since the intensity change between the $2s^02p^6$ and $2s^22p^4$ configurations is very dependent on the difference between the average values for the energies of the two configurations quite different results are obtained when our L_I energies are used. This is exemplified in Table VI:2 where our experimental values for the element magnesium ($Z = 12$) are compared with those calculated.[237,239] The values given in parentheses are obtained using the previously accepted value for the L_I binding energy of magnesium.

A comparison between theory and experiment thus gives an unsatisfactory agreement for $Z = 12$. This is also the case for other light elements.[240] Relative intensities calculated by Mehlhorn and Asaad[239] using transition probability amplitudes computed by Callan[241] ($Z = 12$) and Krause *et al.*[242] ($Z = 10$) are also given in Table VI:2. The large difference between these results may indicate that the inconsistencies between theory and experiment are to a large extent caused by erroneous transition probability amplitudes and wave functions.

Excitation lines and multiple ionization in KLL Auger spectra

In a study of the *KLL* Auger spectrum of potassium in potassium oxide, we observed a structure on the low energy side of the Auger lines.[51] This broadening of the lines was so conspicuous as to necessitate further investigation. Experiments were therefore also performed on other compounds containing potassium.[59] In Fig. VI:2 the result obtained from potassium chloride, KCl, is shown.

As can be seen in part (a) of the figure a line of comparatively high intensity is observed on the low

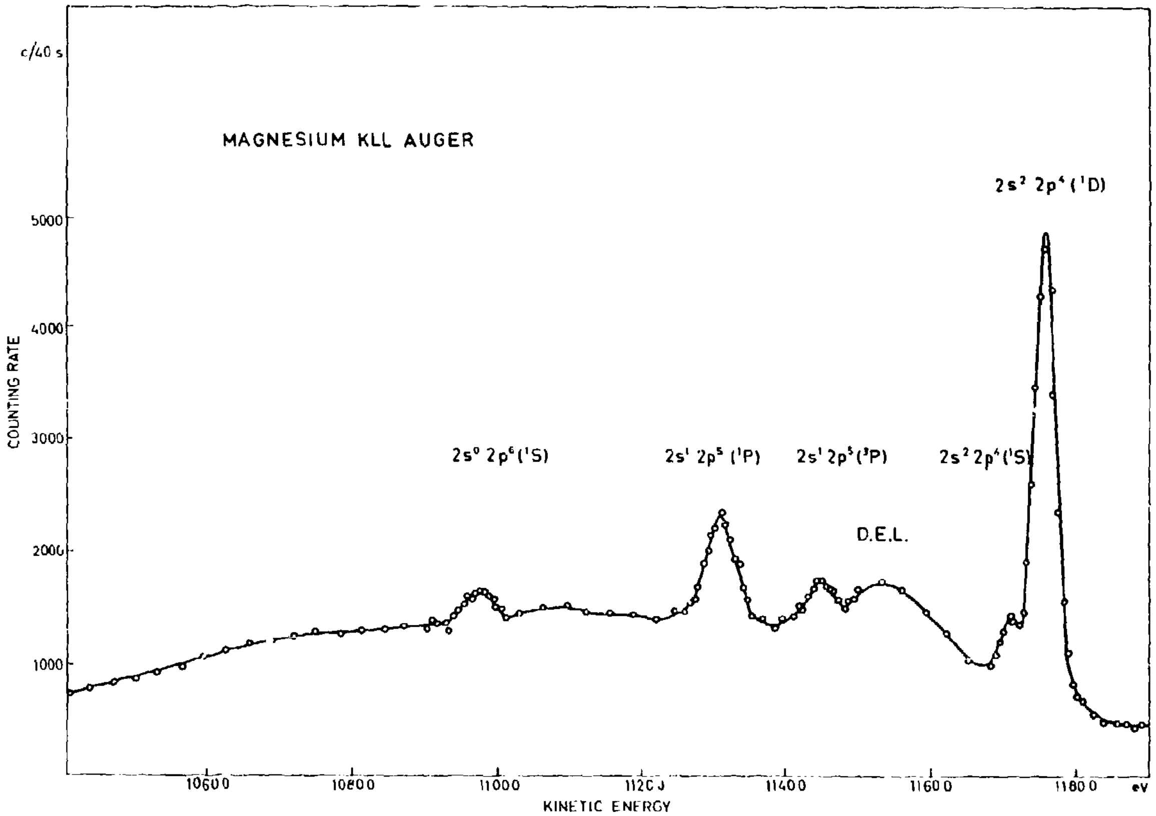

Fig. VI:1. *KLL* Auger spectrum of magnesium.[58] All five lines predicted in extreme *LS* coupling theory are resolved.

energy side of the intense $KL_2L_3(^1D_2)$ line of potassium. The satellite line does not have the energy nor the intensity of any Auger line predicted by theory. The same satellite structure was observed with other lines in the *KLL* Auger spectrum of potassium. This is exemplified for the $KL_1L_2(^1P_1)$ line in Fig. VI:3. The structure cannot be explained by chemical effects or discrete energy losses because these effects should have been observed in the photoelectron spectrum of potassium. This was not the case as can be seen in part (b) of Fig. VI:2. The satellite line and the excessively large number of energy degraded electrons can be explained in terms of a double Auger process in which either one Auger electron leaves the atom and an outer electron is promoted to an excited state (the line) or two electrons leave the atom by the Auger process (the continuous distribution). Another possible explanation would be a shake-off process during the ionization of the atom.[215]

Excitation lines are also observed in the chlorine Auger spectrum, see part (c) of Fig. VI:2. The energy separation of the $KL_2L_3(^1D_2)$ Auger line and the satellite line is not the same in chlorine as in potassium. We have also studied other compounds containing potassium or chlorine. In Fig. VI:4, part of the *KLL* Auger spectrum of potassium in K_2SO_4 is shown. A satellite structure is observed close to the $KL_2L_3(^1D_2)$ line. The energy separation is only 4.1 eV as opposed to 5.0 eV in KCl. Such a chemical dependence is, of course, likely to exist.

In Fig. VI:5 the *KLL* Auger spectrum of chlorine in sodium chloride is shown. X-radiation from silver was used for production of *K* vacancies in a thin evaporated film of sodium chloride. Silver was particularly suitable as a radiation source in this experiment since all *L* X-radiation quanta of silver are capable of producing a *K* vacancy in a chlorine atom. The photoelectric cross section for the process is com-

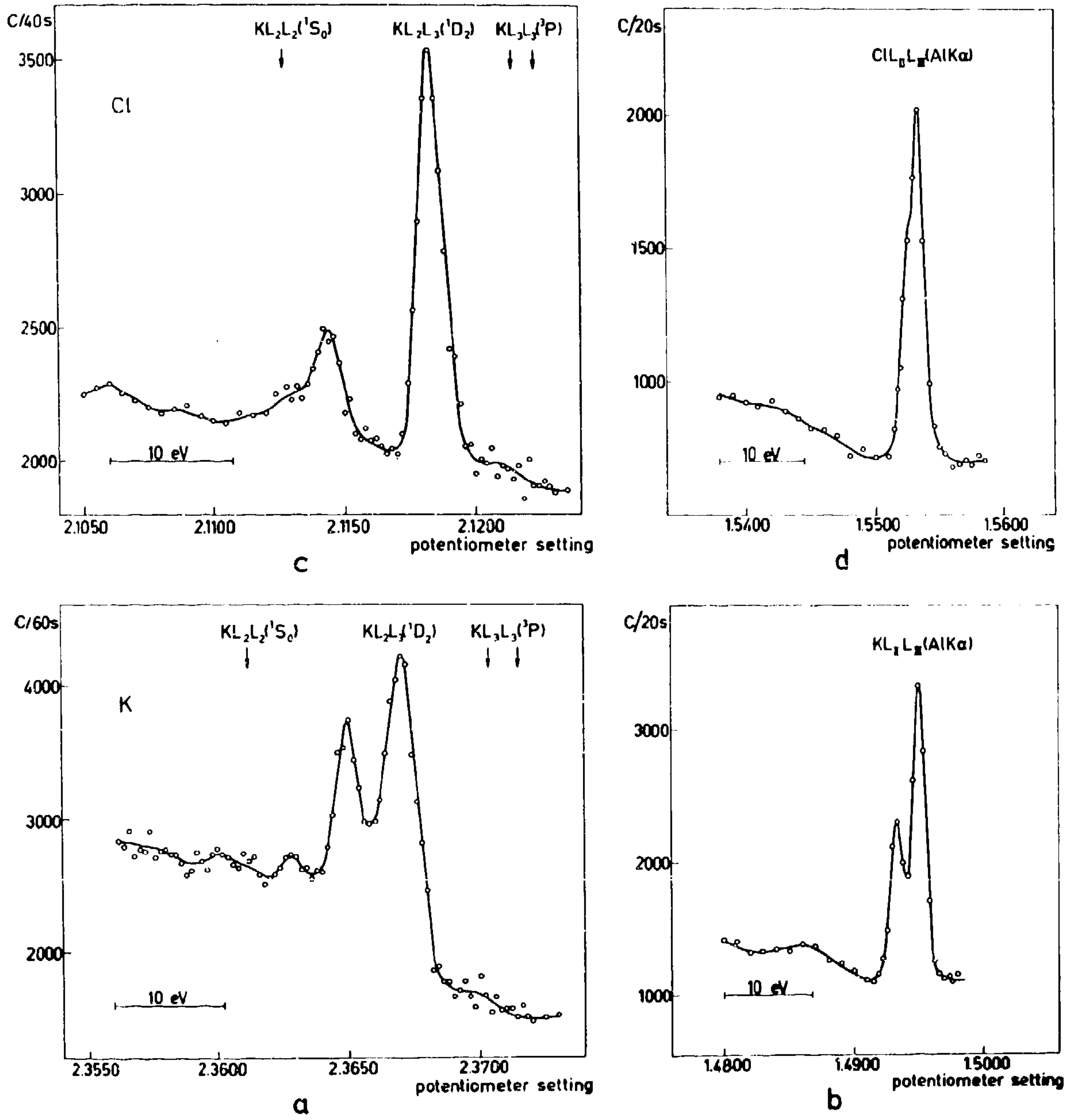

Fig. VI:2. Auger and photoelectron spectra of potassium and chlorine in KCl.[59] In the Auger spectra one finds a line that does not correspond to a normal Auger transition.

paratively large (see Appendix 7) because the differences between the photon energies and the K level energy of chlorine are small. Also in this spectrum a satellite line is observed at the low energy side of the intense $KL_2L_3(^1D_2)$ line. The separation is ≈9.5 eV. No satellite line was observed in the sodium Auger spectra recorded from the same specimen.

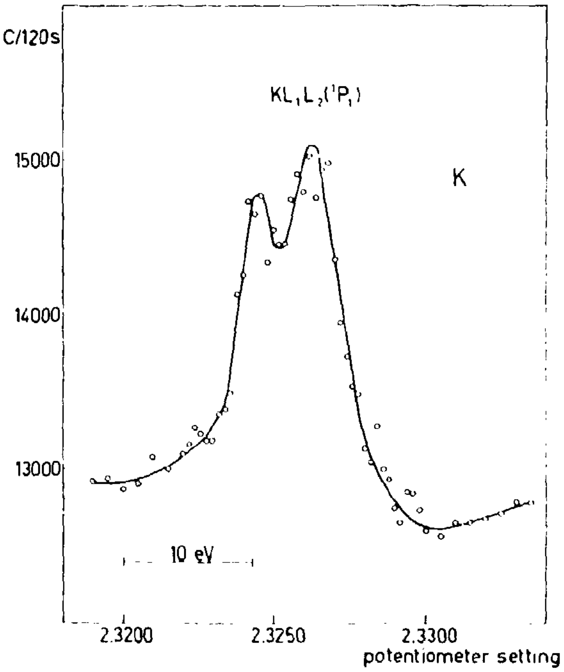

Fig. VI:3. Extra lines are found not only for the $KL_2L_3(^1D_2)$ transition as in Fig. VI:2, but also for other Auger lines as demonstrated for the potassium $KL_1L_2(^1P_1)$ transition in KCl.[59]

Electron emission from free atoms and molecules

In the Auger studies on solids discussed above, X-radiation was used for the production of primary vacancies. For gaseous targets, it is more convenient to use an electron beam for this purpose. This mode of excitation is now used in one of our spectrometers (see Section VIII:5). As an example of a spectrum produced by electron impact, Fig. VI:6 shows a KLL Auger spectrum from neon ($Z = 10$). In the spectrum one observes more than ten lines, five of which are due to ordinary KLL Auger transitions. The other lines can be identified as Auger transitions from an atom with two primary vacancies, one in the K shell and the other in one of the L subshells. Neon has previously been studied by Körber and Mehlhorn,[210] although with lower signal-to-background ratio.

An Auger spectrum from a free molecule is shown in Fig. VI:7. The spectrum is recorded from carbon in methane, CH_4. The L electrons of carbon are involved in the chemical binding which complicates the interpretation of the spectrum. We have also studied the KLL carbon Auger spectrum in other organic compounds, for example, benzene. These spectra are characteristic for the compound under study which shows that information on molecular structure can be obtained from such Auger spectra, although their interpretation is still not straightforward.

We have calculated the KLL Auger energies of neon using the RHFS method described above. The results are given in Table VI:3 together with the measured Auger energies. The agreement between theory and experiment is very good for the relative energy separations within the KLL Auger spectrum, except for the $KL_1L_1(^1S_0)$ transition; the calculated absolute energies are in general a few eV higher than the experimental ones. The Auger lines corresponding to the $KL_{2,3}L_{2,3}(^3P_0)$ and $(^3P_2)$ transitions were not seen in the neon spectrum. These transitions are partly forbidden in pure LS coupling. A description of the atomic structure of neon in the LS scheme should be valid because the spin orbit coupling energy is less than 1 % of the coulomb interaction energy. We have also calculated Auger energies for a neon atom with two primary vacancies. The data are given in Table VI:4 together with energies obtained from the spectrum shown in Fig. VI:6. The agreement between theory and experiment is rather good although the calculated energies are consistently some eV higher than the measured ones.

Although it is the KLL Auger spectrum that has

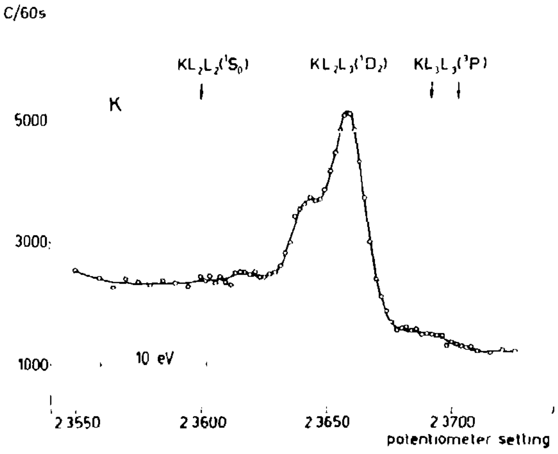

Fig. VI:4. Excitation lines are found in compounds other than KCl. This is part of the Auger spectrum of potassium in K_2SO_4.[59] The energy separation from the $KL_2L_3(^1D_2)$ line in potassium is 0.9 eV less in this compound than in KCl.

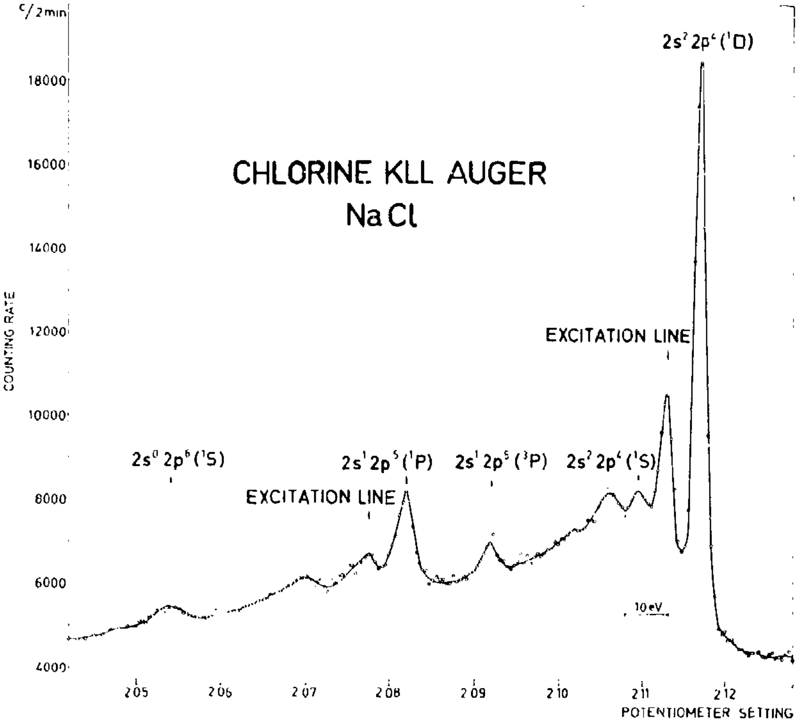

Fig. VI:5. *KLL* Auger spectrum of chlorine in NaCl. Satellite lines are observed on the low energy side of the ordinary Auger lines.

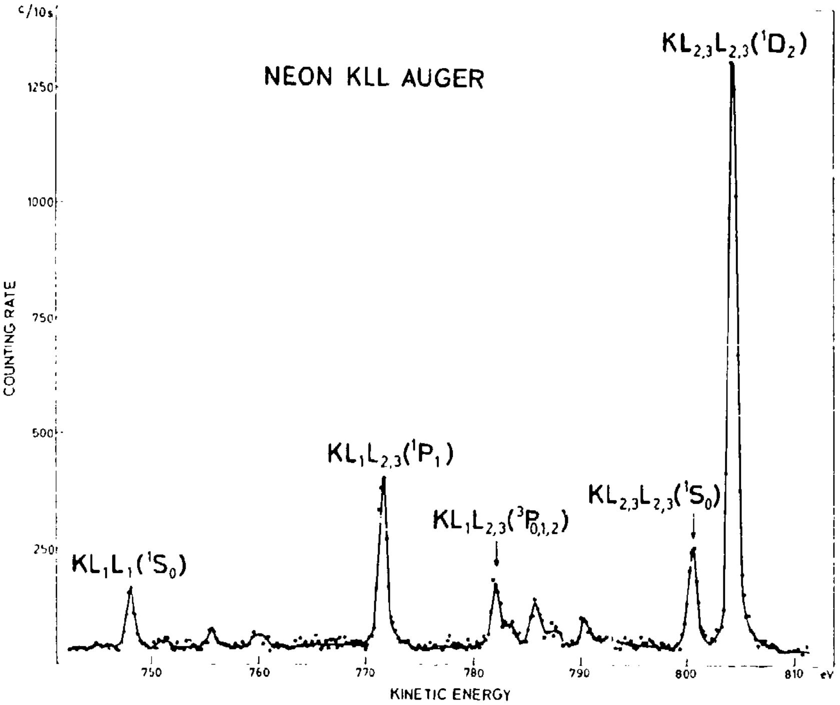

Fig. VI:6. *K* Auger spectrum of neon ($Z = 10$) excited by electron impact. More than ten lines are observed in the spectrum, five of which are due to ordinary *KLL* Auger transitions. The other lines are identified as transitions from an atom with two primary vacancies.

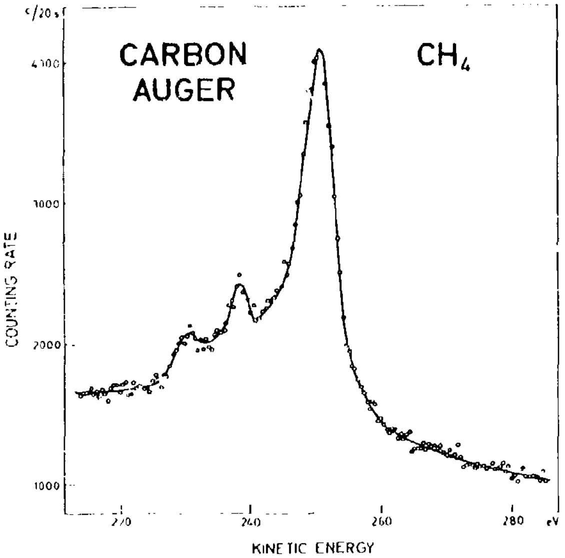

Fig. VI:7. K Auger spectrum of carbon in methane, CH_4. This spectrum was excited by electron impact.

Table VI:3. Calculated and measured KLL Auger transition energies of neon (Z 10).

Transition	Energy (eV)		Relative energies (eV)	
	Calculated (RHFS)	Measured	Calculated (RHFS)	Measured
$KL_1L_1(^1S_0)$	748.13	748.1 ± 0.1	−60.39	−56.0
$KL_1L_{2,3}(^1P_1)$	775.81	771.6 ± 0.1	−32.71	−32.6
$(^3P_0)$	786.30	781.9 ± 0.1	−22.22	−22.2
$(^3P_1)$	786.34		−22.18	
$(^3P_2)$	786.44		−22.08	
$KL_{2,3}L_{2,3}(^1S_0)$	804.47	800.5 ± 0.1	−4.05	−3.7
$(^1D_2)$	808.52	804.15*	0	0
$(^3P_0)$	811.13		+2.61	
$(^3P_2)$	811.27		+2.75	

* The energy of this transition was obtained from optical data and was used for calibration of the spectrum.

been the object of most investigations, we have also studied L and M Auger spectra. In Fig. VI:8, part of a recently recorded MNN Auger spectrum of krypton is shown (see also Fig. I:27). Electron impact was used for the ionization of the M shells in the gaseous target. In the part of the spectrum shown in the figure, ≈ 40 lines from the M_4 and M_5 Auger spectrum can be identified in the energy region between 20 and 60 eV. More than half of them are due to transitions in an atom with two primary vacancies. The half-widths of the Auger lines are as small as 0.10 eV.

A krypton Auger spectrum has previously been recorded by Mehlhorn with lower resolution which permitted energies and relative intensities to be determined for 22 lines in the $M_{4,5}$ Auger spectrum.[246]

The identification of the lines in the spectrum is in most cases made by using optical data.[213,217] KrIII is the final state for Auger transitions from a krypton

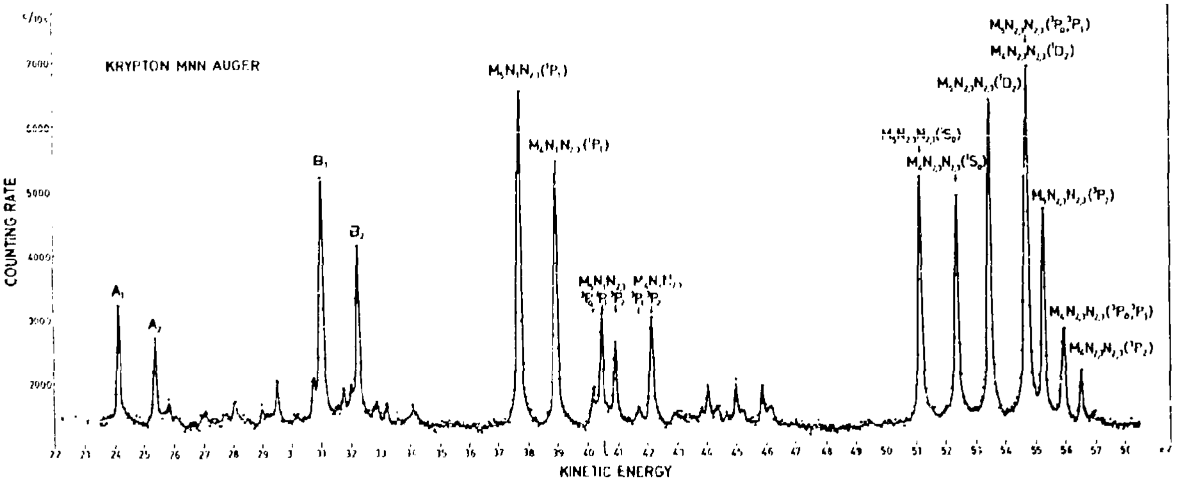

Fig. VI:8. $M_{4,5}$ Auger spectrum of krypton (Z 36). About 40 lines in the M_4 and M_5 Auger spectrum are seen in the figure in an energy region between 20 and 60 eV. The half widths of the lines are as small as 0.10 eV. More than half the lines are due to transitions in an atom with two primary vacancies.

Table VI:4. Calculated and measured KL-LLL transition energies of neon ($Z = 10$).

Initial state	Final state	Energy (eV)	
		Calculated (RHFS)	Measured
$KL_{2,3}(^2P)$	$L_{2,3}^3(^4S)$*	794.90	
	(^2D)	790.85	785.8 ± 0.5
	(^2P)	788.15	783.1 ± 0.5
	$L_1L_{2,3}^2(^4P)$	775.12	
	(^2D)	767.13	760.0 ± 0.5
	(^2S)	763.08	
	(^2P)	759.25	
	$L_1^2L_{2,3}(^2P)$	731.62	
$KL_{2,3}(^1P)$	$L_{2,3}^3(^4S)$*	797.70	
	(^2D)	793.65	790.2 ± 0.5
	(^2P)	790.95	787.6 ± 0.5
	$L_1L_{2,3}^2(^4P)$*	777.92	
	(^2D)	769.93	
	(^2S)	765.88	
	(^2P)	762.06	755.7 ± 0.5
	$L_1^2L_{2,3}(^2P)$	734.42	
$KL_1(^3S)$	$L_1L_{2,3}^2(^4P)$*	802.72	
	(^2D)	794.73	792.6 ± 0.5
	(^2S)*	790.68	
	(^2P)	786.85	
	$L_1^2L_{2,3}(^2P)$	758.92	
$KL_1(^1S)$	$L_1L_{2,3}^2(^4P)$*	808.48	
	(^2D)	800.49	
	(^2S)*	796.44	
	(^2P)	792.61	
	$L_1^2L_{2,3}(^2P)$	764.68	

* Transitions which are forbidden in LS-coupling.

Table VI:5. Term energy separations of krypton III according to Moore.[247]

Configuration	State	Relative energy (eV)
$4s^24p^4$	$^3P_2$	0
	$^3P_1$	0.56
	$^3P_0$	0.66
	$^1D_2$	1.82
	$^1S_0$	4.10
$4s4p^5$	$^3P_2$	14.37
	$^3P_1$	14.80
	$^3P_0$	15.07
	$^1P_1$	17.59

atom with one primary vacancy. The term separations of KrIII give the energy separations of Auger transitions having the same initial state, see Table VI:5. It is not, however, possible to identify the $M_4N_1N_1(^1S_0)$ and $M_5N_1N_1(^1S_0)$ transitions using optical data because the energy of the final state $N_1N_1(^1S_0)$ is not known. Two doublets in the spectrum, labelled A_1,A_2 and B_1,B_2, show an energy splitting which may correspond to a transition from an M_4 and M_5 vacancy, respectively to the N_1N_1 $(^1S_0)$ state. In the paper by Mehlhorn[246], it is proposed that the doublet B_1,B_2 would correspond to the $M_{4,5}N_1N_1(^1S_0)$ transitions. The assignment was based on measurements on neon ($Z = 10$) and argon ($Z = 18$). We have calculated the energies of the $M_{4,5}NN$ Auger spectrum of krypton for identification purposes. The calculated energies and the experimental ones are given in Table VI:6. A comparison between the two sets of data shows that the calculated energies are ≈ 2 eV larger than the experimental ones for transitions with the final state configuration $4s^24p^4$ and ≈ 2 eV smaller for transitions with the final state configuration $4s^14p^5$. The agreement between the calculated and measured energies of these transitions is thus rather good. For the $M_{4,5}N_1N_1(^1S_0)$ transition, the situation is still uncertain. The calculated energies are 7.5 eV smaller than the energies of the doublet labelled

Table VI:6. Calculated and measured $M_{4,5}NN$ Auger transition energies of krypton ($Z = 36$).

Transition	Energy (eV)	
	Calculated (RHFS)	Measured
$M_5N_1N_1(^1S_0)$	16.56	23.94*
$M_4N_1N_1(^1S_0)$	17.86	25.19*
$M_5N_1N_{2,3}(^1P_1)$	34.14	37.66
$M_4N_1N_{2,3}(^1P_1)$	35.44	38.88
$M_5N_1N_{2,3}(^3P_0)$	39.68	40.13
$M_5N_1N_{2,3}(^3P_1)$	39.95	40.42
$M_5N_1N_{2,3}(^3P_2)$	40.43	40.85
$M_4N_1N_{2,3}(^3P_0)$	40.98	41.31
$M_4N_1N_{2,3}(^3P_1)$	41.25	41.67
$M_4N_1N_{2,3}(^3P_2)$	41.73	42.1[illegible]
$M_5N_{2,3}N_{2,3}(^1S_0)$	52.12	51.15
$M_4N_{2,3}N_{2,3}(^1S_0)$	53.42	52.41
$M_5N_{2,3}N_{2,3}(^1D_2)$	54.50	53.44
$M_5N_{2,3}N_{2,3}(^3P_{0,1})$	54.75	54.69
$M_4N_{2,3}N_{2,3}(^1D_2)$	55.80	54.69
$M_5N_{2,3}N_{2,3}(^3P_2)$	56.42	55.26
$M_4N_{2,3}N_{2,3}(^3P_{0,1})$	57.05	55.94
$M_4N_{2,3}N_{2,3}(^3P_2)$	57.72	56.51

* These values correspond to the interpretation suggested on p. 160.

Table VI:7. Calculated $M_{4,5}N$–NNN transition energies of krypton ($Z = 36$).

Initial configuration	Final configuration	Energy (eV)
$M_5N_{2,3}$	$N_1^2N_{2,3}$	7.30
$M_4N_{2,3}$	$N_1^2N_{2,3}$	8.60
M_5N_1	$N_1^2N_{2,3}$	27.00
M_4N_1	$N_1^2N_{2,3}$	28.30
$M_5N_{2,3}$	$N_1N_{2,3}^2$	27.69
$M_4N_{2,3}$	$N_1N_{2,3}^2$	28.99
$M_5N_{2,3}$	$N_{2,3}^3$	44.93
$M_4N_{2,3}$	$N_{2,3}^3$	46.23
M_5N_1	$N_1N_{2,3}^2$	47.39
M_4N_1	$N_1N_{2,3}^2$	48.69
M_5N_1	$N_{2,3}^3$	64.63
M_4N_1	$N_{2,3}^3$	65.93

A_1,A_2 and 14.3 eV smaller than the energies of the doublet B_1,B_2. Although it seems as if the energy contribution from the 4*s* electrons is overestimated in the calculations, it is less probable that this error would amount to 14 eV. It would therefore seem more likely that the doublet A_1,A_2 corresponds to the transitions $M_{4,5}N_1N_1(^1S_0)$. The energy of the $4s^04p^6(^1S_0)$ term in KrIII would then be 69.86 ± 0.05 eV.

The Auger transitions which have KrIII as initial state and KrIV as final state are more difficult to identify from optical data because the energies of the initial states as well as the energies of some of the final states are not known. Some of the missing final state energies can be extrapolated from data on the neighbouring elements bromium, selenium, and arsenic.[246] Another complication in the interpretation of the spectrum is due to the intermediate coupling scheme which has to be used for the assignments of allowed Auger transitions in the krypton spectrum. Many transitions which are forbidden in the *LS* coupling scheme (selection rules for the system atom plus Auger electron are: $\Delta L = \Delta S = \Delta H = 0$) will become allowed due to the mixing of wave functions of the final states. We have calculated the energies of Auger transitions for a krypton atom with two primary vacancies in the same manner as for neon. The energies which are given in Table VI:7 were calculated for each configuration only. A detailed analysis of the spectrum shown in Fig. VI:8 has not yet been made and further discussion is therefore postponed to a forthcoming paper.[92]

Chemical effects in Auger spectra

Already in our first studies of X-ray produced Auger spectra from copper we observed that the lines were shifted upon oxidation of the sample.[10] Chemical effects can be expected in Auger spectra for the same reasons as in the photoelectron spectra. A calculation of the chemical shifts in Auger spectra can be made in the same two steps as for the photoelectron spectra, i.e. first a calculation of the free-ion shift and then a calculation of the crystal energy contribution (see Sections V:2 and V:3).

The calculated free-ion shift of sulfur is shown in Table VI:8. Only the results for the KL_1L_1 transition are given since the energy shifts of the other *KLL* Auger electrons from a free ion will be nearly the same. The effect of hybridization on the Auger energies can be included in the calculations in the approximate way described in Section V:3. As can be seen in Table VI:8, the effect of hybridization is very small in the singly ionized case and practically zero in the doubly ionized case. The Auger energies for different $3p_{1/2}^i\,3p_{3/2}^k$ ($i = 0,1,2$; $k = 0,1,2,3,4$; $i + k = 2,3,4$) configurations have also been studied and it was found that the energy shift between different con-

Table VI:8. Calculated KL_1L_1 Auger energies and KL_1L_1 Auger shifts for a free sulfur ion with various degrees of ionisation in the valence shell.

Degree of ionisation of the valence shell	Configuration of the valence shell	KL_1L_1 Auger energy (eV)	Approximate KL_1L_1 Auger energy for an sp^3-hybrid (eV)	KL_1L_1 Auger shifts (eV)
0	$3s^23p^4$	1970.39		
1	$3s^23p^3$ $3s^13p^4$	1954.93 1954.73	1954.87	15.52
2	$3s^23p^2$ $3s^13p^3$	1938.11 1938.10	1938.11	32.28

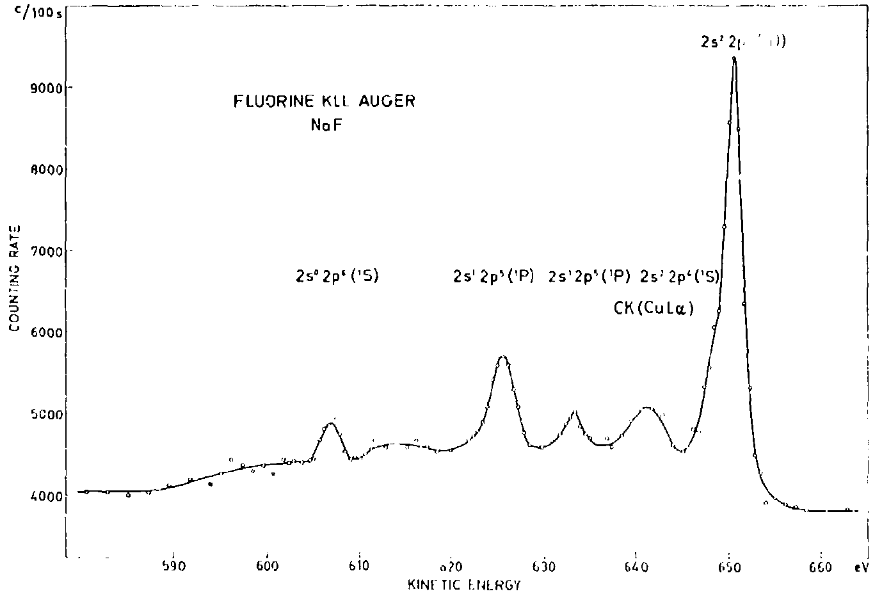

Fig. VI:9. *KLL* Auger spectrum of fluorine in sodium fluoride, NaF.[82]

figurations was 0.03 eV for sulfur, which is negligibly small.

The calculated free-ion shifts are of course much larger than the experimentally observed shifts from solids.[62] Fig. I:24 illustrates the chemical effect on Auger electron energies obtained experimentally for sulfur in $Na_2S_2O_3$ in which compound sulfur is present in two different chemical states. For gases, the free-ion model is valid and the calculated Auger shifts for ionized atoms should therefore show a better agree-

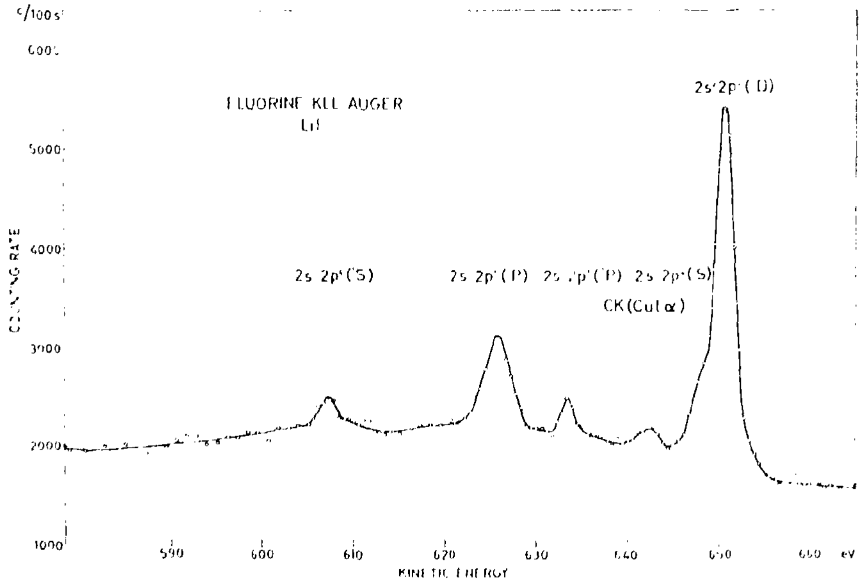

Fig. VI:10. *KLL* Auger spectrum of fluorine in lithium fluoride, LiF.[82]

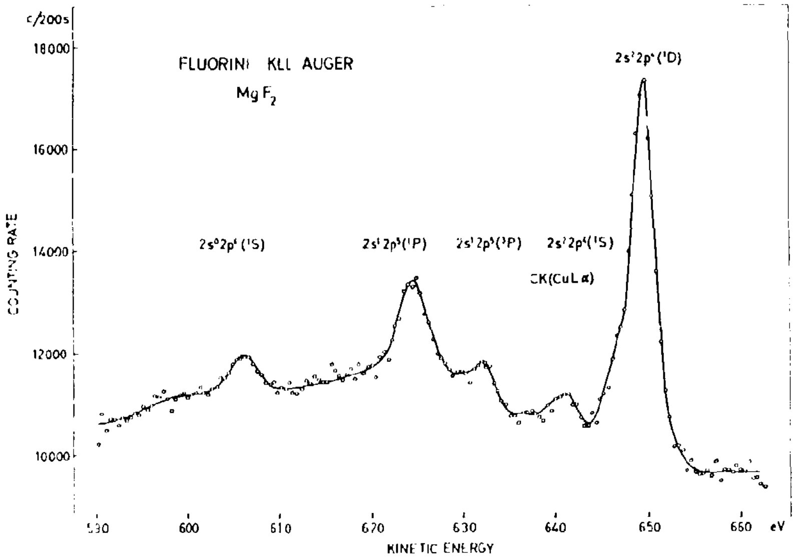

Fig. VI:11. *KLL* Auger spectrum of fluorine in magnesium fluoride, MgF_2.[82]

ment with the experimentally measured ones. This is in fact the case as shown by the calculations of Auger transition energies for ionized neon and krypton, see Tables VI:4 and 7 and Figs. VI:6 and 8.

Elements in the Periodic System with an atomic number below ten have an incomplete *L* shell. For these elements, the *L* electrons are directly involved in the chemical binding and a chemical dependence of the Auger spectrum would therefore be expected. We have investigated experimentally the cation dependence of Auger electron transitions for some fluorine (Z 9) salts.[82] Fluorine Auger spectra were recorded from NaF, LiF, and MgF_2 and the spectra are shown in Figs. VI:9 11.

The NaF and LiF bonds are ≈ 90 % ionic and the MgF_2 bond is ≈ 8 % ionic; thus it is reasonable to assume that the fluorine *L* shell is completely occupied and that the states available as final states for the Auger transitions are those listed in the figures. Relative intensities are the same in the three spectra within experimental error except for the $2s^12p^5(^1P)$ transition which has a higher relative intensity in LiF and MgF_2 than in NaF. This discrepancy may be explained by photoelectron lines coinciding with the Auger line. These lines are excited by fluorescent fluorine $K\alpha$ radiation from the source and the expelled electrons are 1*s* core electrons of lithium (LiF) and 2*p* core electrons of magnesium (MgF_2) respectively. The chemical effect on relative intensities in the different compounds is thus, if any, small.

A cation effect is, however, found for the energies of the Auger electrons. The measured energies of the fluorine Auger transitions are 1.5 eV and 1.1 eV larger in NaF and LiF respectively, than in MgF_2. This trend

Table VI.9. KLL Auger energies of fluorine

Final state	Energies (eV)			
	Measured (NaF)	Measured (LiF)	Measured (MgF_2)	Calculated (Z 9) (Appendix 4)
$2s^02p^6(^1S)$	609.6 ± 0.4	609.1 ± 0.4	608.3 ± 0.4	610.2
$2s^12p^5(^1P)$	628.7 ± 0.4	628.1 ± 0.4	627.1 ± 0.4	626.8
$2s^12p^5(^3P)$	637.0 ± 0.4	636.5 ± 0.4	635.2 ± 0.4	638.2
$2s^22p^4(^1S)$	651.7 ± 0.5	651.5 ± 0.5	650.4 ± 0.5	350.4
$2s^22p^4(^1D)$	654.6 ± 0.4	654.4 ± 0.4	653.3 ± 0.4	654.2

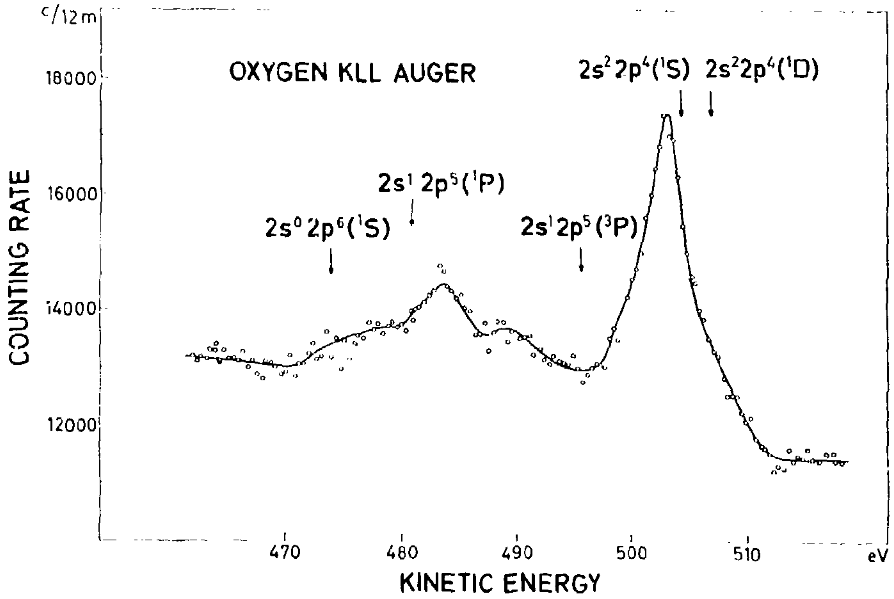

Fig. VI:12. *KLL* Auger spectrum of oxygen in titanium oxide, TiO_2. Arrows in the figure indicate energies calculated using semiempirical formulae, see Appendix 4.

is consistent with the electronegativities 0.9 (Na), 1.0 (Li) and 1.2 (Mg) of the three cations (see Appendix 13). The partial ionic character will be largest for the NaF bond and smallest for the MgF_2 bond. The amount of negative charge within a certain distance from the fluorine nucleus will therefore decrease in the order NaF, LiF, MgF_2, and the fluorine electron binding energies will increase in the same order (see Section V:2). The Auger transition energies will consequently decrease in the same order because they are obtained to the first approximation as the difference between the energies of one *K* electron and two *L* electrons. The energy shift is expected to be nearly the same for all core electrons and the relative energies should therefore agree for all three compounds. This is also the case as seen in Table VI:9.

Although the intensities of the Auger lines do not seem to be influenced by the difference in chemical binding for the three cations, we observed an effect on the widths of the Auger lines. The fluorine Auger lines of LiF and MgF_2 were ≈ 0.2 eV and ≈ 0.7 eV broader respectively than the Auger lines of NaF.

The fluorine Auger lines not only have different widths in different compounds but they are all broader than the Auger lines of the element sodium (atomic number $Z = 11$).[58] This trend becomes even more pronounced in the Auger spectrum of oxygen ($Z = 8$) which has been the subject of preliminary studies in several solids. An example of an Auger spectrum obtained from a solid containing oxygen is shown in Fig. VI:12. The spectrum was recorded from TiO_2. The assignment of final states is made under the assumption that the bonds are completely ionic. Arrows in the figure indicate the energies calculated according to semiempirical formulae (see Appendix 4).

If the oxygen did not receive any electrons from the titanium it would have three electron vacancies in the initial state configuration and four vacancies in the final state configuration of the Auger transition and many more states would be available. The difference in electronegativity between oxygen and titanium corresponds to a ~50 % ionic character of the bonds. This implies a more complex Auger spectrum than the assignment in Fig. VI:12. One way to estimate the influence of the increased complexity on the observed line widths would be to study the Auger spectrum of gaseous oxygen. It is however likely that the major part of the broadening will find an explanation in solid state effects (see Section III:2).

VII. PHOTOELECTRIC CROSS SECTIONS

In the photoelectric process, the energy of a radiation quantum is transferred to an atomic electron which is liberated from a bound state. The probability for the process depends on the wavelength λ of the radiation and the atomic number Z of the element. Many electron spectra resulting from the photoelectric process of X-rays have been shown in the preceding chapters, in which we have discussed mainly the information that is obtained from the energy determinations of electron lines in ESCA spectra. Another interesting aspect of ESCA spectra was dealt with in Section V:7, where it was shown that the intensity of electron lines can be used for quantitative elemental analysis. From intensity measurements one can also obtain information about the probability for the photoelectric effect and we shall now discuss briefly the information on photoelectric cross sections that can be obtained from ESCA spectra.

Experimental studies of photoelectric cross sections performed in recent years have almost exclusively been confined to high radiation energies and heavy elements.[218] Theoretical work has mainly dealt with the elements lead and uranium.[218-250] For radiation energies comparable to the electron binding energies and for light elements the calculations become more complicated and are very scarce. The theoretical treatment of the photoeffect in this region emanates from the early 1930's.[251] Expressions for photoelectric cross sections and angular dependence of emitted electrons were then calculated by a number of workers using hydrogenic wave functions.[252-254] The treatment was far from complete but is believed to reflect generally the angular dependence of the emitted electrons. Only the contribution from the inner shell electrons to the photoelectric cross section was taken into account in these calculations.

The limited interest, which has been paid to the calculation of photoelectric cross sections for low radiation energies, may to some extent be due to the lack of accurate experimental data. The high resolution and precision which are attained in ESCA offer a new means for the measurements of relative photoelectric cross sections.

The contribution from the different atomic subshells to the total photoelectric cross section for an element depends very much on the radiation energy. This is illustrated in Fig. VII:1 which shows ESCA spectra from silver recorded with three different radiation energies: Al$K\alpha_{1,2}$ (a), Cr$K\alpha_1$ (b) and Cu$K\alpha_1,\alpha_2$ (c). The angle between the photon direction and the direction of analysed electrons was 90° in all cases. Crystal monochromatized radiation was used in the recording shown in Fig. VII:1b whereas the two other spectra were recorded with unfiltered X-radiation. The lines in the spectra are due to electrons expelled from the N_I ($4s$), N_{II} ($4p_{1/2}$), and N_{III} ($4p_{3/2}$) subshells in silver, and to electrons expelled from the conduction band of silver. The conduction band consists of $4d$ and $5s$ states. The $4d$ band is much narrower than the $5s$ band, see Chapter IV. The peak close to binding energy zero in each spectrum is therefore to a large extent due to d electrons. In the three spectra, we thus observe essentially the dependence of photoelectric cross section on photon energy for $s(N_I)$, $p(N_{II}, N_{III})$ and d (N_{IV}, N_V) electrons having binding energies which are small compared to the photon energy.

As can be seen from the figures, the three spectra look quite different. The intensities of the N_I and $N_{II,III}$ lines relative to the intensity of the line associated with the conduction band increase with increasing radiation energy. The effect is relatively larger for the N_I electron line.

The above spectra illustrate the strong dependence of relative subshell photoelectric cross sections on the radiation energy. The dependence on atomic number is also very pronounced. This is demonstrated in Fig. VII:2 where the L_I, L_{II}, and L_{III} electron lines of sodium ($Z = 11$) and vanadium ($Z = 23$) are shown. The radiation used for exciting the spectra was aluminum $K\alpha$. The intensity ratio between the L_I electron line and the $L_{II} + L_{III}$ electron lines is 2.5 for sodium, whereas, it is only 0.20 for vanadium.

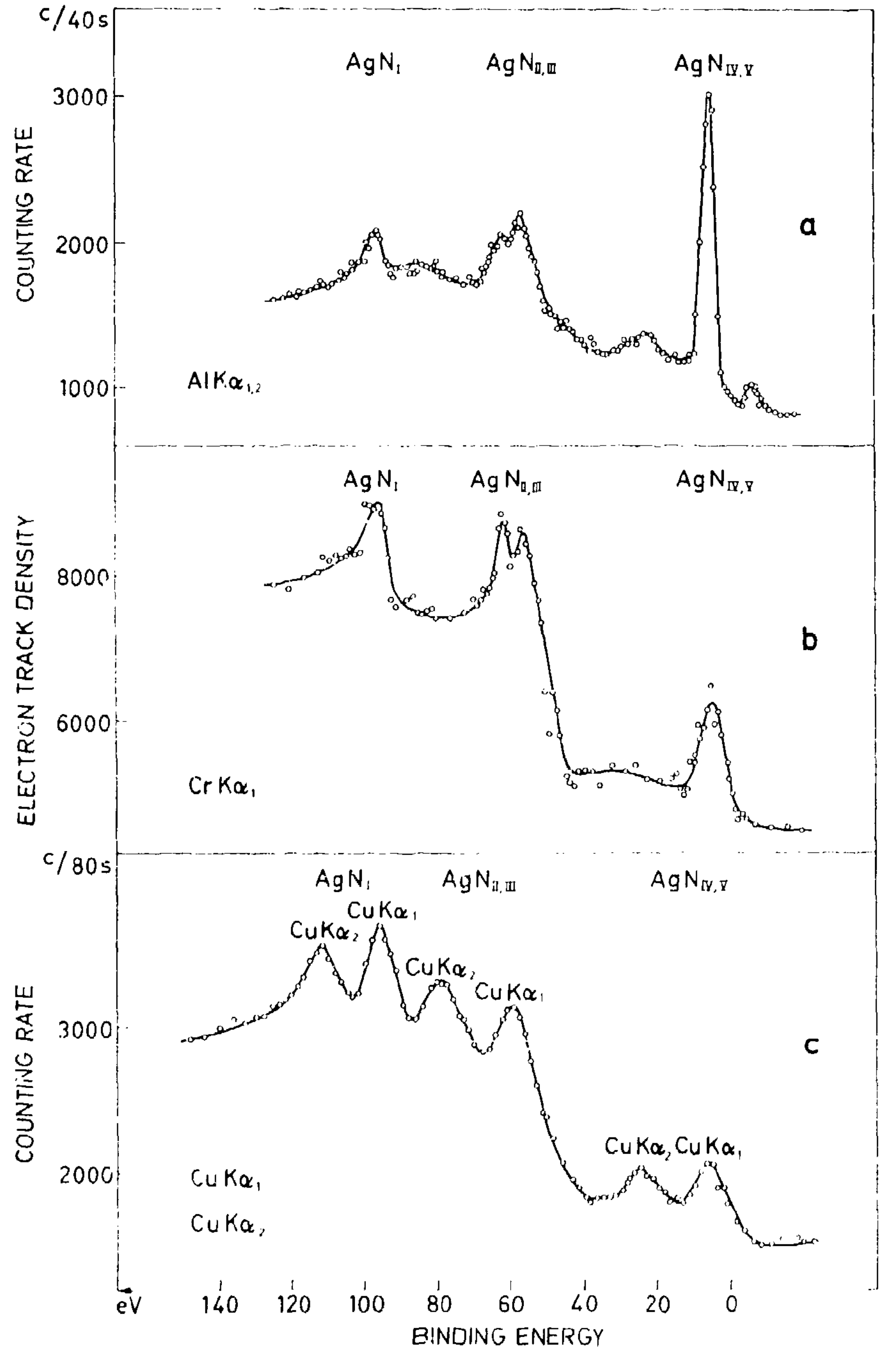

Fig. VII:1. Electron spectrum of silver recorded with three different radiation energies, Al$K\alpha_{1,2}$ (a), Cr$K\alpha_1$ (b) and Cu$K\alpha_1,\alpha_2$ (c). The spectra show the dependence of photoelectric cross section on photon energy for the N_I–N_{III} subshells and the conduction band ($N_{IV,V}$) of silver. ($\theta = 90°$).

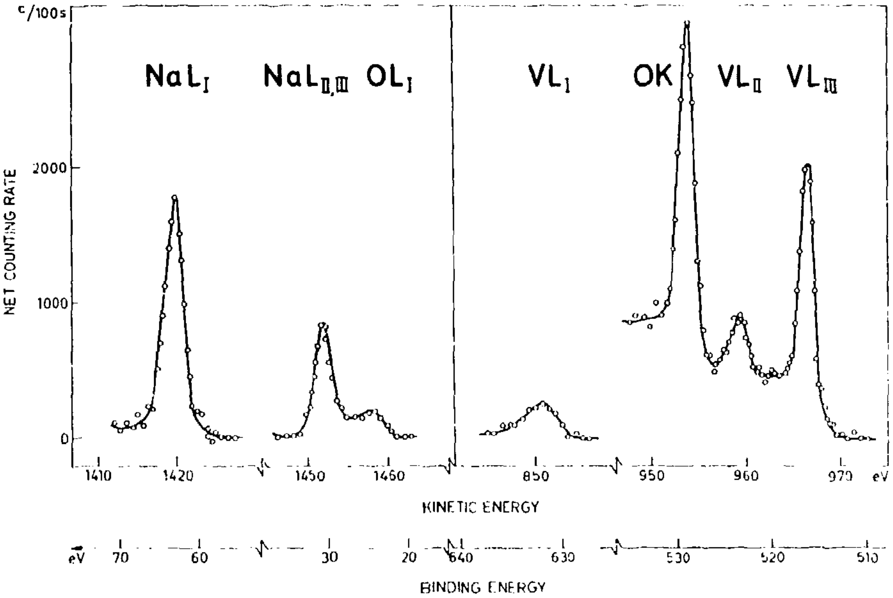

Fig. VII:2. Electron spectrum of sodium and vanadium recorded with Al$K\alpha$ radiation. The relative intensities of the L_I and L_{II}, L_{III} electron lines are quite different for sodium ($Z = 11$) and vanadium ($Z = 23$). Since the spectrum of vanadium was recorded from vanadium oxide, electron lines from oxygen were also obtained. The oxygen line seen in the spectrum can therefore be used for comparing the photoelectric absorption in the K shell of oxygen with that of the L subshells of vanadium. ($\theta = 90°$).

In Fig. VII:3 we have plotted the experimentally determined $L_I/(L_{II}+L_{III})$ intensity ratios for a number of elements from sodium to vanadium. The ratios were deduced from spectra obtained in the measurements of L level energies in this Z-region. The radiations used were Al$K\alpha$, Cr$K\alpha_1$, and Cu$K\alpha_1$. A curve has been fitted to the experimental points for each radiation. Extrapolation of these curves gives a result similar to that obtained from Fig. VII:1. The ratio between the photoelectric cross sections for the $2s(L_I)$ and $2p(L_{II}+L_{III})$ electrons in an element increases with increasing photon energy. For a certain photon energy it decreases with increasing atomic number. The same trends are is obtained from the analytical expressions.

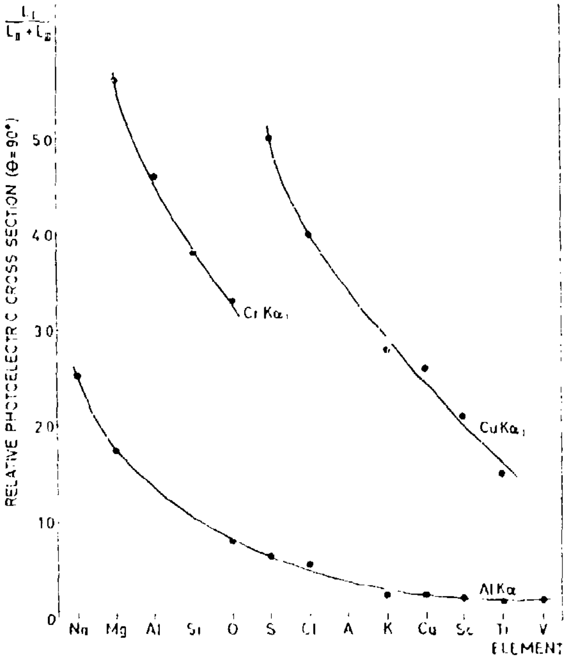

Fig. VII:3. The figure shows the experimentally determined $L_I/(L_{II}+L_{III})$ intensity ratio for a number of elements from sodium to vanadium. The radiations used were Al$K\alpha$, Cr$K\alpha_1$, Cu$K\alpha_1$. A curve has been fitted to the experimental points for each radiation. The data show the rapid decrease in the ratio between the photoelectric cross section for the $2s(L_I)$ and $2p(L_{II}+L_{III})$ electrons with increasing atomic number. ($\theta = 90°$).

According to Schur[253] the angular distribution of photoelectrons emitted from the L_I subshell can be written, omitting a constant, as

$$J_{L_I}(\theta,\varphi) \propto \sin^2\theta \cos^2\varphi + \frac{4v}{c} \sin^2\theta \cos^2\varphi \left(1 - \frac{I_L}{h\nu}\right) \quad (1)$$

while that of the L_{II} and L_{III} electrons is written as

$$J_{L_{II+III}}(\theta,\varphi) \propto \frac{I_L}{h\nu + 3I_L}\left[1 + \frac{8I_L}{h\nu} \sin^2\theta \cos^2 \varphi \right.$$
$$\left. + \frac{2v}{c} \cos \theta \left(1 + 2 \sin^2\theta \cos^2 \varphi \left(1 + \frac{11 I_L}{h\nu}\right)\right)\right] \quad (2)$$

where

θ = angle between the direction of the incident radiation quantum and of the emitted electron.
φ = angle of polarization of the radiation.
$h\nu$ = quantum energy.
I_L = mean value of the ionisation energies of the L sub-shells.

The energy I_L is expressed in terms of the atomic number Z and a screening factor S_2 for the L electrons[255] and is written as

$$I_L = \frac{(Z - S_2)^2}{4} 13.6 \quad (3)$$

expressed in eV.

After integration over the polarization angle φ and using the appropriate angle θ, which is equal to 90° in the experiments quoted, we have calculated the $L_I/(L_{II} + L_{III})$ intensity ratios from eqs. (1)-(3). The same trend as in the experiments is observed but the ratio is approximately twice as large as the experimental value for each element and radiation. The difference in kinetic energy for the L_I and $L_{II} + L_{III}$ electrons favours the L_{II} and L_{III} electrons lines somewhat, see Section V:7. However, the energy difference is small compared to the kinetic energy in most cases and cannot be the explanation for the discrepancy.

In Fig. VII:2 one observes another electron line in the vanadium spectrum besides the L lines. It is identified as the K electron line of oxygen in V_2O_5. This line can be used for comparing the photoelectric absorption in the K shell of oxygen with that of the L subshells of vanadium. It is thus possible to determine from ESCA spectra, relative photoelectric cross sections, not only within an element but also between different elements.

VIII. INSTRUMENTS AND EXPERIMENTAL TECHNIQUES

VIII:1. Experimental Conditions for ESCA

In order to find the optimal conditions for ESCA a variety of possible experimental arrangements must be considered. The basic requirement is *high energy resolution*. In order to obtain useful information about atoms and molecules from ESCA, the line widths generally have to be of the order of the inherent widths of the atomic levels. For example, the chemical structure effects that one wishes to study are often of this order of magnitude, i.e. some eV or less. As pointed out in Chapter I, the ESCA line width is determined by the spectrometer aberrations, the widths of the spectrometer slits (i.e. the entrance slit, defining the effective source width, and the detector slit), the inherent width of the X-ray line which is used to excite the electron spectrum, and the inherent width of the atomic level under study.

In other types of charged particle spectroscopy, for example mass spectroscopy, the ions are all accelerated in a selected direction. The situation is similar in the study of discrete energy loss spectra of electrons. The electrons to be analysed in ESCA are emitted more or less isotropically from a broad source. This is the case for Auger electrons and also, to some extent, for photoelectrons, which, however, are preferentially emitted perpendicular to the incoming X-ray beam.[252] For this reason it is desirable that the incident X-ray beam should be perpendicular to the electron-optical axis.

Since electrons are emitted to a high degree isotropically from the irradiated sample and the total intensity from the outermost layer is rather low, it becomes a quite delicate operation to balance resolving power and luminosity in the electron analysing instrument. Two-directional focussing in magnetic or electric fields, is then of special interest. By this means, the dispersion, and with it the irradiated area of the specimen, can be increased without either a loss in resolving power or of intensity in the beam of focussed electrons. The larger the dimensions of the spectrometer the larger becomes the luminosity, defined as source area times transmission. For an optimally adjusted system the factors that limit the resolution, i.e. source width, detector slit, and spherical aberrations, should all contribute equally. A retarding electric field could be employed to reduce the energy of the electrons before the analysis in the spectrometer. This would reduce the resolving power required in the dispersive system, whether this be magnetic or electric in nature. Such arrangements have been used in, for example, mass spectroscopy.[256] We have used a pre-retarding (and pre-accelerating) electric field for the electron spectroscopic determination of h/e, described in Section III:8. It was then found that a retarding field decreased the luminosity of the total system whereas an accelerating field increased the luminosity.[32] This is in accordance with the Lagrange-Helmholtz law[27]:

$$\alpha \cdot S \cdot E^{\frac{1}{2}} = \text{const.} \tag{1}$$

α angle of divergence of the beam
S - beam size
E energy

which is valid both for photon- and electron-optical systems. It is thus quite generally true that the pre-retarding electric field acts as a defocussing lens or gives an intermediate image (virtual or real) that is larger than the object. In both cases the acceptance angle of the spectrometer has to be made larger if the aforementioned optimal adjustment is to be accomplished. Provided that the required field can be attained over the larger volume that results from this larger acceptance angle, there is no loss of intensity for a given size of the spectrometer. The most convenient size of spectrometer is of course open to discussion. Small dimensions mean somewhat smaller manufacturing costs, a smaller vacuum recipient and a compensating system for external magnetic fields that requires less space. Larger dimensions offer the advantage of larger total luminosity. As a convenient size we have chosen a central orbit radius of around 30 cm in our later instrument designs. The dimensions are to some extent dictated by the type of work that one plans to do.

As an alternative to the electric field, discussed above, it should be possible to use a magnetic condensor lens to capture a larger solid angle from the irradiated sample. One has in this case also to consider the total effect of the combined system taking into account the Lagrange-Helmholtz relation.

The high resolution magnetic double focussing 30-cm instrument[5] that was first constructed for ESCA (see Section VIII:2 and Appendix 8) proved to be a very suitable instrument. Basic experience of ESCA was acquired using this instrument and many new design features were incorporated as the experiments proceeded.[63] A new instrument was finally designed (Section VIII:4) resembling in its basic features the original one but also incorporating a number of improvements, especially in the coil design,[86] see Fig. VIII:1.

Instead of analysing the electron spectrum in a magnetic field, it is possible to use an electric field. Two-directional focussing can also be attained in this case and the theory for this has been described in the literature,[258,52] (see Appendix 9). However, no instrument of this kind had been built that approached the performance required for ESCA work. The advantage with this type of spectrometer is primarily that it can more easily be designed for sector focussing than a magnetic instrument, since the disturbing fringing fields at the boundaries of the spectrometer field can more easily be controlled.[259,260] For example, one can completely eliminate all fields at the source, both of electric and of magnetic origin. This is a great advantage particularly when excitation is made with an electron beam. The electrostatic sector focussing instrument[87] described in Section VIII:5 was constructed for this particular type of experiment. A drawing of this instrument (not exactly to scale and with many details left out) is shown in Fig. VIII:2. To attain the high resolution required, the mechanical construction and the adjustments demand the utmost precision. On the other hand, this instrument is in many respects convenient to operate. Resolution and transmission are about the same as for the magnetic instruments.

The two spectrometer principles mentioned above can be considered the basic types for ESCA. In addition to these, there are other modifications to which some mention may be made here, since they are the subject of a closer study by our group and have been employed in some cases. The sector focussing

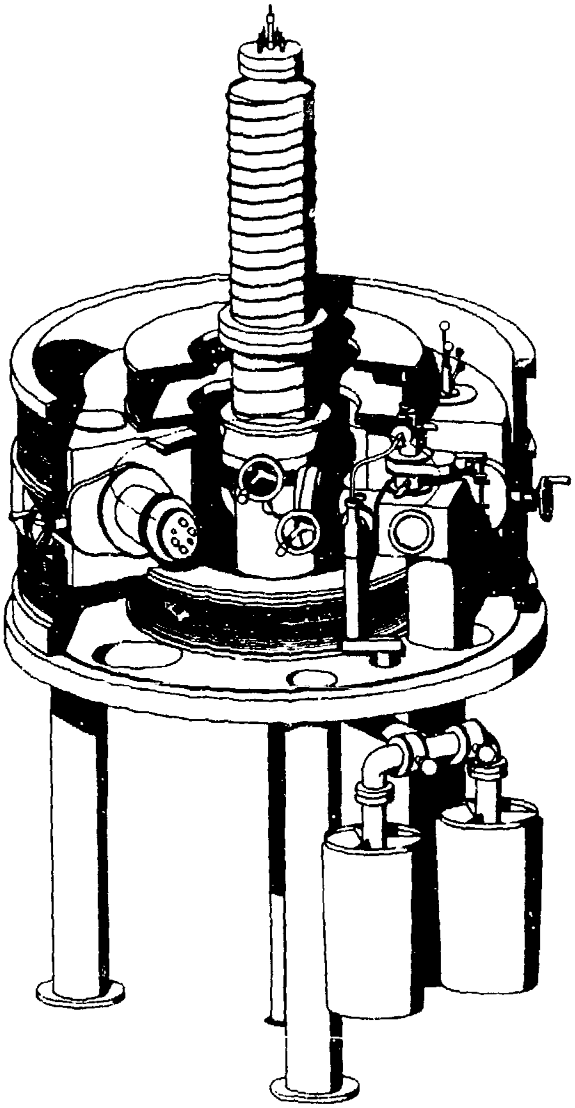

Fig. VIII:1. Cut-away view of the new magnetic spectrometer.

magnetic instrument incorporates two-directional focussing, either by means of an air-cored *coil system* or by means of an iron-yoke magnet, see Fig. VIII:3. In the former case one has to take the effect of the fringing field into account when calculating the coil dimensions and the calculations are relatively complicated for optimal performance. Like other iron-free instruments it must have an extra coil system for eliminating the earth's magnetic field and other exter-

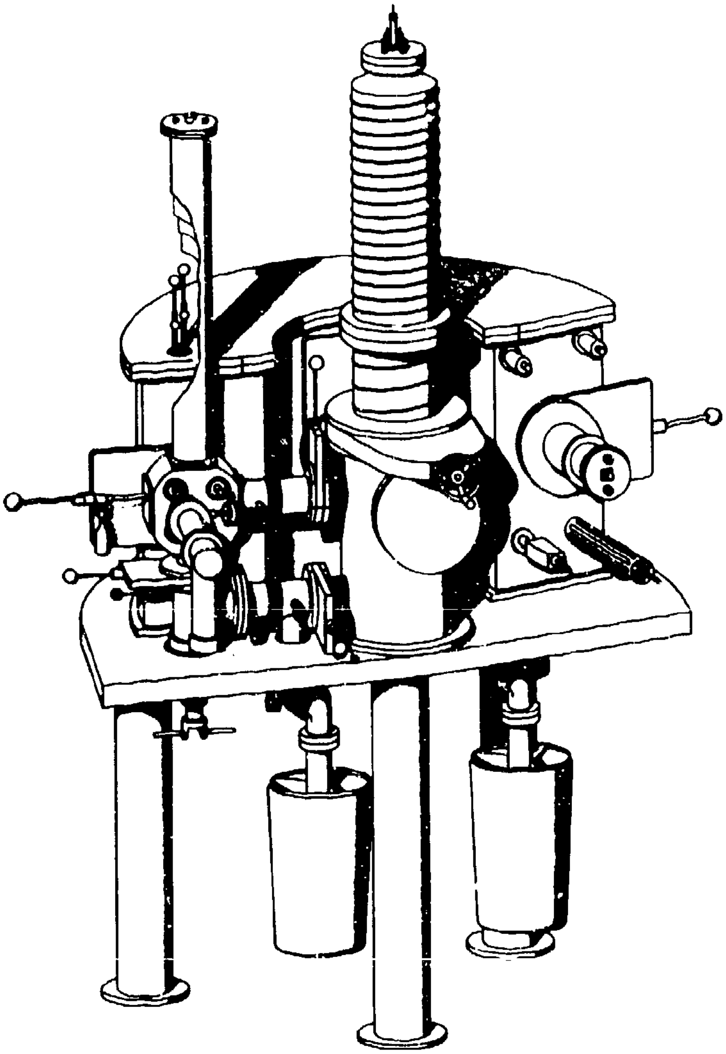

Fig. VIII:2. Schematic view of the electrostatic instrument.

nal magnetic fields. However, with such an arrangement one has the advantage of strict linearity between spectrometer current and magnetic rigidity of the focussed electrons.

A magnetic sector instrument with pole-pieces of iron is of interest because it is easier to construct and also because it does not require a compensating system, since external magnetic fields could be almost totally eliminated by the iron yoke. The existence of magnetic boundaries in such a magnet means that one has one more degree of freedom that can be utilized to improve the resolution and transmission. Altogether it is easier to attain the desired field over a larger volume by means of iron-cored magnets than by means of air-cored coils. The non-linearity between current and magnetic rigidity of focussed electrons can be accepted in many cases. Some uncertainty is introduced as to the constancy of the expansion coefficients of the field at different energies, particularly at low fields. If this problem can be overcome, the use of curved pole boundaries in the iron yoke sector magnet would permit an increase in the luminosity. Theoretically, it should be possible to attain two-directional focussing and second order focussing at the same time[52] (aberra-

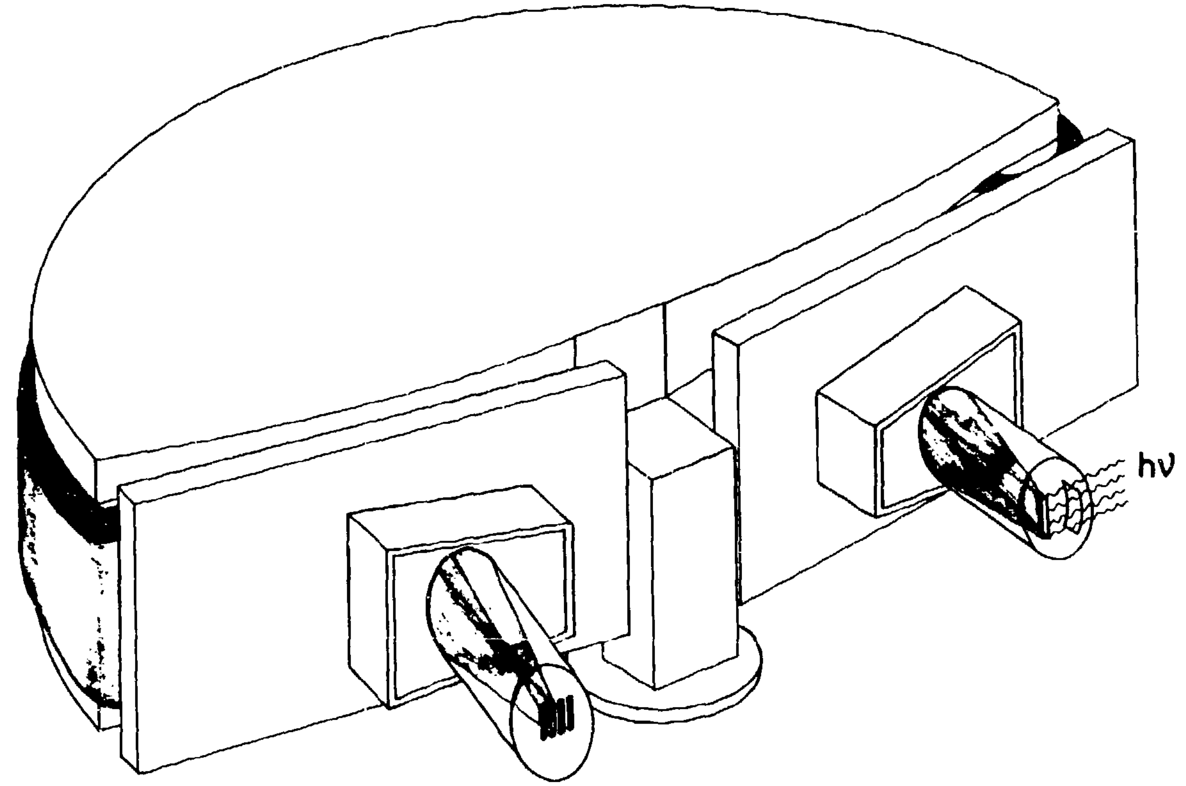

Fig. VIII:3. A sector focussing magnetic instrument with twodirectional focussing being designed for ESCA measurements.

tion coefficients of φ_0^2 and ψ_0^2 vanish simultaneously, φ_0 and ψ_0 are the radial and axial angles of departure, respectively). This necessitates a very careful shimming of the pieces.

The dispersion of the magnetic as well as the electrostatic double focussing field is twice that of the homogeneous magnetic field.[112,52] Furthermore, one can increase the dispersion by increasing the size of the spectrometer without loss of transmission because of the two-directional focussing. This cannot be done in the homogeneous field. All three fields focus different energies in well-defined focal planes so that a broad region of the electron spectrum can be recorded simultaneously. The homogeneous field is superior to the non-uniform fields in this respect, since the energy interval that is focussed is much larger for the homogeneous field. From this point of view, it is often advantageous to use the semicircular focussing principle in spite of its low transmission. The natural detector for the electrons is in this case the photographic plate. Photographic detection does not involve any particular difficulties as long as electron energies are larger than 10 keV; at lower energies, however, there have been difficulties in using this type of detection. The use of photographic detection in ESCA is therefore not straightforward, since ESCA spectra generally have energies below 10 keV. For example, copper *Kα* radiation yields electron energies below 8 keV and the magnesium *Kα* radiation yields electron energies below 1.2 keV. To investigate the possibilities of utilizing the semicircular focussing principle for ESCA, the homogeneous field permanent magnet spectrometer described in Section VIII:3 was constructed.[64]

It is not usually necessary to have strictly monochromatic X-radiation for the excitation of photoelectron spectra since the magnetic or electrostatic field also resolves the electron spectrum with respect to the different X-ray components. Of these the *Kα*

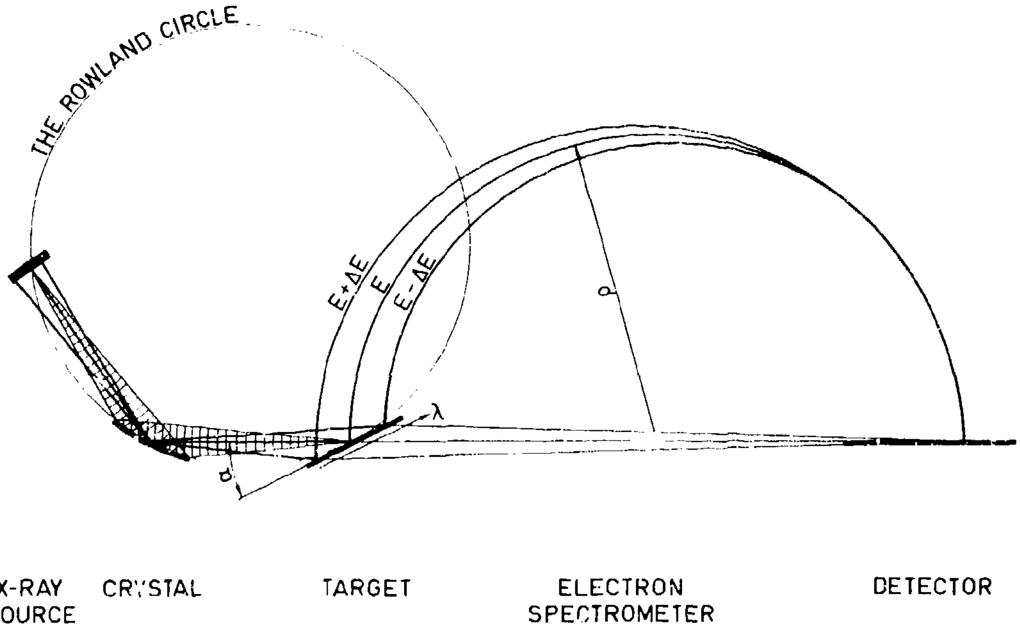

Fig. VIII:4. The principle of combined crystal and magnetic focussing for eliminating inherent width of X-radiation.

lines are one order of magnitude stronger than any other characteristic X-radiation and are therefore the most convenient lines for exciting the electron spectra. The energies of the $K\alpha$ lines of copper and chromium are sufficient to permit the photographic detection of the X-ray produced electrons; however, the separation between the α_1 and α_2 components is quite small for these elements and the corresponding doublet structures in the electron spectra can sometimes complicate the interpretation, particularly when chemical effects are studied. To avoid this and to reduce the background of electrons that have been excited by the continuous radiation and by harder components in the characteristic radiation (with subsequent decrease in energy), a combination of crystal monochromatization of the X-rays and magnetic analysis of the electrons has been tried.[64] The sample is attached to a thin wire ($\phi = 0.05$ mm) and the monochromator is adjusted so that the $K\alpha_2$ component is suppressed and only the $K\alpha_1$ line strikes the wire. In this way, the desired conditions are attained, although with a considerable reduction in intensity. The crystal monochromator focusses the X-radiation on the source wire which constitutes the object in the electron-optical system, but two factors resulting in a reduction in intensity are introduced at the same time. These are the reflectivity of the crystal and the effective aperture angles of the X-ray optical system. An additional factor is the low luminosity of the semicircular focussing of the electrons. The electron spectrum produced by this arrangement is of low intensity and long exposure times are required. To compensate for this we have developed a rapid technique for retrieving all the information that is stored in the photographic emulsion.[65] This technique has made it possible to delineate line profiles and measure line intensities accurately even in cases when the lines are so weak as to be invisible to the eye. It has also been applied to the low electron energies that are obtained with the Mg and Al radiations. The instrument by which this analysis is made may be described as an automatic television microdensitometer.[71,80] It is discussed in some detail in Section VIII:8. It may be added that this photometric technique for weak spectra can also be applied to optical spectra, mass spectra etc.[65,71]

From the combination of crystal dispersion (of the X-radiation) and magnetic dispersion (of the electrons) the possibility arises of eliminating the contribution of the X-ray line width to the total width of the observed electron line. The principal arrangement is shown in

Fig. VIII:4 where we have chosen a semicircular spectrometer for the magnetic dispersion. After Bragg reflexion in the crystal the X-ray spectrum will be distributed over the target in such a way that each point on the target corresponds to a certain wavelength. This is valid even for the different wavelengths of one and the same X-ray line provided that the crystal is perfect, i.e. if its diffraction pattern (rocking curve) is much narrower than the natural width of the X-ray line. A higher energy photon hits the target to the right (in the beam direction) of a lower energy photon as depicted in the figure and the photoelectrons produced by the higher energy photon have a larger trajectory radius in the electron spectrometer. The target is tilted an angle α with respect to the incoming X-radiation and the angle α can be adjusted so that photoelectrons emerging from different parts of the target are brought to a common focus which is independent of the X-ray wavelength. The condition that the crystal and magnetic field dispersions should cancel out is

$$\tan\alpha = \frac{E \cdot D}{\varrho} \qquad (2)$$

E photoelectron energy
ϱ radius of electron trajectory
D crystal dispersion $dx/d(h\nu)$ (x is direction of emitted photoelectrons)

The angle α calculated from eq. (2) is 5°–20° for systems that are convenient to use. A further analysis of the arrangement is given in Appendix 10. Experiments have shown that it is possible to use this technique, but strict requirements are placed on the quality of the crystal. It would be possible to combine the crystal dispersion with electron spectrometers that have higher transmission, for example, an electrostatic or a magnetic double focussing instrument. The above condition then has to be modified owing to the different dispersion of these electron focussing devices.

A reduction of the wavelength interval of the exciting X-radiation beyond the inherent width of the X-ray transition could in principle be attained by successive Bragg reflexions in two flat crystals. If the crystals are placed in the (n, n) position, the radiation reflected from the second crystal comprises a wavelength interval that is defined by the diffraction pattern of the crystal. For perfect crystals this wavelength interval would be considerably smaller than the inherent width of an X-ray line. However, this improvement of the monochromatization could be attained only at the expense of intensity.

Since the potentialities of the ESCA method are dependent on the ultimate line widths which can be attained, in particular in studies of chemical shifts, it is worth-while to discuss in some detail the factors limiting the resolution. Let us consider the case where soft X-rays are used to excite the electron spectra. According to Fig. II:11, the inherent width of the $K\alpha$ radiation of Al is determined both by the spin doublet splitting and the inherent width of each line in the doublet. The total width (at half maximum intensity) amounts to about 1.0 eV. Since the doublet splitting increases with Z^4,[135] a valuable reduction in width can be gained by going from Al to Mg. A reasonable estimate of this width would be 0.7–0.8 eV. If Na anodes can be developed which can sustain a sufficiently high dissipation of power, a further reduction in line width can be expected. Still lower Z elements, like carbon, can be used but the inherent width is much larger since the L levels involved in the transition are appreciably broadened due to band structure effects. The variation of the inherent widths of the levels with Z is depicted in Fig. II:8 for the K and L_{III} levels. Since the chemical shifts are about the same for different shells it is preferable to study the chemical effect on levels that have minimum band broadening and also minimum Heisenberg broadening (due to the uncertainty principle). Thus in the third and fourth period, the $L_{\mathrm{II,III}}$ levels are suitable for this purpose; in the second period which contains the elements carbon, nitrogen and oxygen, the K level is the most suitable one. In these cases, the internal widths are a few tenths of an electronvolt. Disregarding for a moment the possibilities to reduce the width of the exciting X-radiation, we arrive at a minimum width of ESCA lines of ≈ 1.0 eV. Since it is highly desirable to approach this width, the contribution from the finite resolution of the electron spectrometer should be kept at a minimum. In some cases, we have been able to record ESCA lines with a width of 1.3 eV (see for example Figs. I:5 and I:7) which is close to the ultimate limit.

An improved energy resolution would be achieved if the crystal dispersion—magnetic dispersion could be further developed or if two flat crystals could be used for monochromatization of the X-rays, as mentioned above. The contribution from the spectrometer aberration, which is already small in the magnetic double focussing instrument, can be further reduced without loss of intensity (rather with a gain in intensity) by inserting an electrostatic corrector for the spherical aberration. Such a device was suggested by Bergkvist[261] who applied it to an iron yoke instrument.[262] The arrangement is more easily adapted to an ironfree magnetic instrument because of the constancy of the expansion coefficients of the field. A corresponding corrector for an electrostatic instrument cannot be so easily incorporated.

The X-ray unit should be constructed to meet the following requirements: The anode should be situated as close to the sample as possible so that a maximum solid angle of X-radiation is established. It should be efficiently cooled to permit maximum loading of the X-ray tube, and the anode should be exchangeable. Evaporation of tungsten from the filament on the anode should be kept at a minimum. This is of particular importance when excitation is made with soft X-radiation. Even a slight contamination of the anode surface then means a considerable decrease of intensity in the ESCA spectrum and a relatively large intensity of parasitic lines from the tungsten. In the most effective arrangement, the anode is not in a direct line with the cathode filament; the electron beam then has to be focussed on the anode by special electrode arrangements, see Section VIII:4. If water is used as a cooling agent for a magnesium anode it is preferable to apply the magnesium on a copper base since magnesium dissolves under prolonged action of the water. Both magnesium and aluminum can be applied in excellent thermal contact with a copper base by a special spraying technique. To obtain extremely high X-ray intensities, one can introduce a rotating, water cooled anode, see Fig. VIII:29 and Appendix 10.

The source compartment must be well separated from the X-ray unit; otherwise one obtains an excessively high background of scattered electrons. The X-radiation is allowed to pass through a thin window, usually aluminum. The choice of window material and thickness of the window is determined by the filtering action on the X-rays that one wishes to employ. X-ray absorption coefficients for different elements as a function of X-ray energy have been compiled in graphical form in Appendix 7 and can be used for finding the best filter in each case. One purpose of the X-ray filter is to prevent low-energy radiation from causing undesirable radiation effects in the sample.

Sources can be prepared in different ways. The quality of an ESCA electron spectrum is not particularly dependent on the preparation technique that is utilized, nor on the thickness of the source or on the degree of vacuum in the spectrometer. The radiation should strike the sample surface at an angle of 45°; however, the angle of incidence is not very critical. Since ESCA is a method by which a surface layer of around 100 Å is analysed, one should avoid surface contamination. Oil vapours from the vacuum pumps should be avoided since these give a carbon line which increases in intensity with time at the expense of intensity in the spectrum under study (see Section V:7). We have used this characteristic carbon line as a convenient calibration line in many cases but its presence is sometimes disturbing, particularly when organic compounds are studied. We have therefore provided one instrument with non-magnetic ion pumps and sorption roughing pumps instead of oil diffusion pumps and rotary roughing pumps. Reference lines can then be obtained by evaporating an extremely thin film (only a few atomic layers) on the sample surface, preferably of some electrically conducting material, or by mixing the sample under study with a substance that has suitable calibration lines. In these and other cases the sample is pounded and can then be pressed into a disc using the same technique as for IR samples. One can also place the finely pulverized sample on a copper mesh alternatively scatter it on Scotch tape. Electro-spray technique can also be used.[263] Vacuum evaporation is often the most convenient technique for substances that do not decompose during evaporation. For liquids and gases we have found continuous deposition on a cryostat cooled sample holder during the measurements to be very convenient. By this technique ESCA can also be used for a large number of chemical compounds, particularly organic compounds, that at room temperature exist in the gaseous or liquid state. Several compounds have been studied by this technique; see for example Fig. I:14 and Fig. I:15.

If adequate arrangements are made for differential pumping around the source (using only the narrow source slit for evacuating the source housing) liquid sources can be studied by ESCA. When evaporation from the liquid can be kept at a convenient level there appears to exist interesting opportunities to study chemical solutions. We have already used this technique on liquid mercury with good results and, no doubt, it could find a more general application to liquids with higher vapor pressures, provided the above-mentioned precautions are taken.

Samples that are electrical insulators could become positively charged during irradiation with X-rays since electrons are continuously emitted. However, the sample is surrounded by a large number of secondary electrons that tend to neutralize any surface charges and furthermore the electrical conductivity of the sample may increase during irradiation to the extent that sufficiently rapid charge transport is provided through the specimen. To allow this latter process to take place the sample must be quite thin so that a considerable part of the incident X-rays can pass through all the sample. As seen in Appendix 7 the half-thickness for Al$K\alpha$ radiation is of the order of 1 mg/cm^2. In some cases when thick insulating samples are used, we have found a small charge effect ($\approx$ 1 V). In such cases it is important to find a reference line for which the shift due to the charging effect is identical with that for the spectrum under study. This can be accomplished by mixing the sample to be studied with a substance that has suitable reference lines as mentioned above, or even better by using an electron line from another atom in the same molecule.

When the line positions of two samples are compared one must be able to reproduce the source position exactly. This is difficult to achieve if the sample itself constitutes the electron-optical source. For this and other reasons it is appropriate to have a fixed narrow slit a few mm in front of the irradiated sample, to define the electron-optical source of the spectrometer. This arrangement gives a high reproducibility of the line positions (see p. 10) provided that the measurements are made after thermal equilibrium has been attained. The irradiated area on the sample should be of such dimensions that the beam of expelled electrons after passage through the slit fills the solid angle accepted by the spectrometer. The exact position of the source is then not critical. However, in cases where crystal focussing is used for the X-rays the sample itself defines the source position.

In one of our instruments (see Section VIII:6) we are investigating the possibility of increasing the intensity by a multi-source arrangement. Several fine wires or narrow strips which are covered with the source material are mounted vertically a short distance apart. By applying small potential differences between the wires one can compensate for the differences in radii of the electron trajectories from the different source wires to the detector. Such a system has previously been utilized with good results for radioactive sources in the same spectrometer[79] and resulted in an increase of intensity that was approximately proportional to the number of wires or strips. The arrangement is basically the same as that developed by Bergkvist for an iron-yoke double focussing β-spectrometer.[261,262]

For a double focussing magnetic spectrometer with central orbit radius ϱ, the contribution to the base-resolution R from the source slit s and detector slit w is given by

$$R = \frac{s + w}{4\varrho_0} \tag{3}$$

For a 30-cm instrument, this means that a momentum resolution, defined as the relative half-width of an electron line, of $2 \cdot 10^{-4}$ can be obtained only if $s \approx w \lesssim$ 0.25 mm. Thus, at an energy of 1 keV, which is about the kinetic energy of electrons expelled by Mg or Al $K\alpha$ radiation, the total contribution to the energy resolution is 0.4 eV from the source and detector widths $s = w = 0.25$ mm. At present, we are using slits of this width in our spectrometers, but smaller slits can be used without detrimental loss of intensity, if one wishes to improve the resolution. In order to adjust the opening angle of the electron beam in the spectrometer to different slit widths, the so-called iso-aberration curves of the spectrometer have been measured so that the beam-limiting baffle can be made to correspond to the chosen slits. The procedure has been described in detail elsewhere[271,52]; it is in principle applicable also to the electrostatic instrument.

For a long time, the detection of electrons in the low energy region where ESCA spectra are measured constituted a difficult problem. Until recently we used GM detection. Although the formvar windows of the counters were extremely thin, a post-acceleration of 4–5 kV was necessary for the detection of electrons with kinetic energy around 1 keV. A new type of detector, the continuous channel electron multiplier, has completely eradicated these difficulties.[264,63] This type of detector, now available commercially, may be described as a windowless electron multiplier with continuous multiplication. Instead of a system of dynodes, the interior of a small glass tube is covered with a semiconducting layer from which secondary electrons are expelled. Multiplication is achieved by applying a voltage of about 4 kV over the length of the tube. There are several reasons for using a continuos channel electron multiplier as detector in preference to a Geiger counter for detecting electrons in the low-energy region. Its volume is small, the inner diameter of the tube is 2 3 mm or less, and the counter therefore has a low background. The delicate task of making windows with a thickness less than a micron is avoided and no acceleration of the primary electrons is needed. The small size of the detector makes it possible to use an array of detectors in the focal plane of the spectrometer (see Sections VIII:4 and VIII:6).

ESCA was originally developed for excitation by means of X-radiation, whereby electron spectra encompassing the whole range of atomic energy levels, from the core outwards could be obtained. The technique afforded non-destructive analysis of solid samples. As was discussed in Chapter V, the observed chemical shifts of inner electron levels are related to the charge distribution in the peripheral orbitals participating in the chemical bond. These shifts are therefore primarily of interest as a phenomenon in molecular physics. The outermost energy levels in the molecules, in the range between 0 and 20 eV, can be excited by UV radiation which has the advantage of very small inherent line widths. Studies on the energy losses of the electrons expelled from gaseous samples represents another approach; such work has been reported from some laboratories.[122-126,265-267,296] By baking the source and the spectrometer chamber so as to eliminate even monoatomic layers on the source surface and by working at pressures below 10^{-9} torr, it has also been possible to use UV radiation for the study of the conduction band in metals.[167,268,269]

The high resolution that characterizes the ESCA apparatus would seem to provide a sound basis for achieving a valuable improvement in the analysis of gases by UV irradiation. Thus the electrostatic instrument has been furnished with a helium lamp emitting the resonance radiation at 21.22 eV (584 Å), see Section VIII:5. The helium radiation passes through a capillary tube, which has a simple arrangement for differential pumping, down into a small metal cylinder. This cylinder has a gas inlet with a needle valve. Photoelectrons expelled from the gas leave the cylinder through a narrow vertical slit and enter the spectrometer in a direction perpendicular to the helium radiation. A molecular beam arrangement seems to offer some interesting further possibilities as an alternative to the collision chamber.

Electron spectra can also be excited by electrons. This method of excitation suffers from the disadvantage that solid samples easily decompose during irradiation with electrons. This is one reason why X-ray analysis is currently based on fluorescence radiation rather than on radiation derived from electron impact. However, we shall disregard this limitation and consider the various ways in which electron spectroscopy by means of electron excitation can be attained. In one system, the electron beam is directed at the sample either along the electron-optical axis of the spectrometer or (approximately) perpendicular to it. The former arrangement is used to study the discrete energy losses of an electron beam passing through matter. This is a widely explored field in which full advantage has been taken of the very small angle of deviation of those electrons in the beam which have suffered discrete energy losses. The line width and the precision depend on the degree to which the primary electron beam is monokinetic. So far experimental difficulties have prevented the study of inner levels by this technique. For ESCA the second alternative seems particularly attractive. Electrons are expelled from inner shells by means of the interaction caused by the rapidly varying electric field from a beam electron as it passes the atom. It is a process that can be visualized as an impact in which the incoming electron, the reflected electron, the expelled electron and the atom are involved. This is a more complicated situation than ordinary X-ray photoelectric emission which results in essentially monokinetic electrons (apart from the level widths and the atomic recoil energies). Monokinetic electron beam impact will result in a continuous electron spectrum for each atomic level with at best a fairly well defined peak at its upper limit, dependent on the geometrical conditions. The Auger process, however, results in monoenergetic electrons independent of the energy of the incoming electrons and only subject to the same inherent broad-

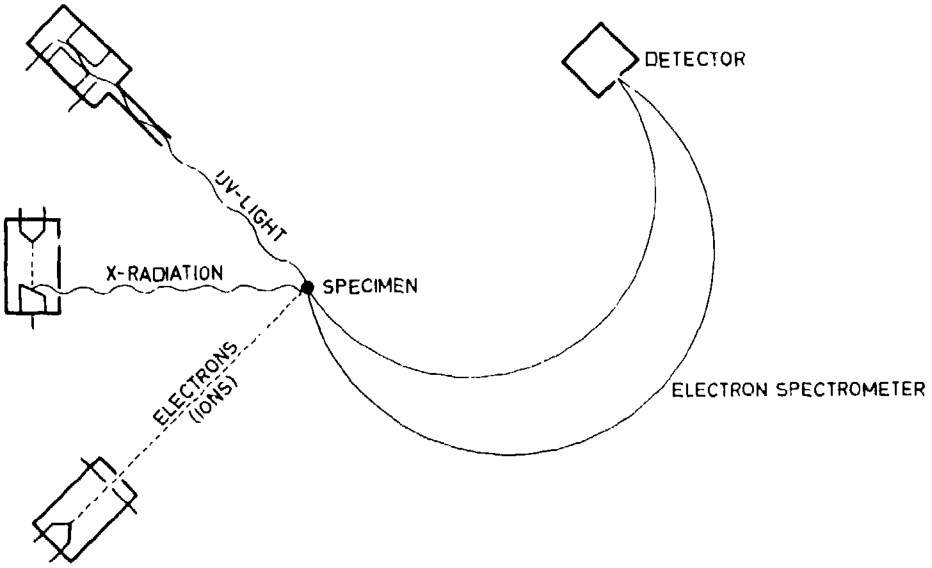

Fig. VIII:5. Different modes of excitation of electron spectra recorded in high resolution instruments.

enings as ordinary X-ray produced Auger electrons. If one furthermore restricts oneself to the study of gases, the effect of the destruction of the sample upon electron impact can be eliminated by a slow flow of the gas. The same equipment can be used as before except that the He lamp is replaced by an electron gun. The electron beam, of small diameter and with an energy of a few keV, is directed vertically into the same cylinder as before. In this case the electrostatic instrument is very convenient since the electron beam passes a completely fieldfree space before entering the cylinder.

We have thus employed three different modes of excitation of electron spectra, namely by X-rays, by ultraviolet light, and by electrons. There are specific virtues of each of these modes; so far we have mostly employed X-rays, for which the scope seems to be the widest. Fig. VIII:5 is a sketch of the basic experimental arrangement when all three modes of excitation are included. One could think of other modes than those mentioned above. Excitation by heavier particles than electrons, for example protons, would reduce the background of scattered electrons and could also yield electron spectra from fragmented molecules.

Special precautions for the stabilization and stepwise regulation of currents (for the magnetic instrument) and voltages (for the electrostatic instrument) are required in order to achieve high precision. The required long time stability at anyone field setting of $1 \cdot 10^{-5}$ is somewhat difficult to achieve for an automatic system, for which a reliable and rapid response to a programmed change in field is also essential. Block diagrams of the data recording systems that we have built for the different instruments are shown in the following sections. Instead of recording the ESCA spectra point by point, whether manually or automatically, one can use a repeated sweep technique over a limited region of the spectrum, for example a closely spaced line group. A sufficiently fast sweep eliminates any intensity variations and, furthermore, the continuous growth of the spectral lines can be followed on the screen of a multichannel analyser. This system can be used with one detector or with an array of several detectors.

VIII:2. The First Instrument

In connection with the rapid development of nuclear spectroscopy, a series of successively more refined instruments for the analysis of electron spectra from radioactive nuclei were constructed during the 1940's and 1950's. The principle of two-directional magnetic focussing was introduced, first in iron yoke instruments[112] and then in air-cored spectrometer magnets.[5] This latter type is well suited for high precision work in the energy region below 10 keV, and our first instrument for ESCA was constructed utilizing a beta-ray

12 − 671163 *Nova Acta Reg. Soc. Sc. Ups., Ser IV. Vol. 20. Impr.* $^{29}/_{11}$ *1967*

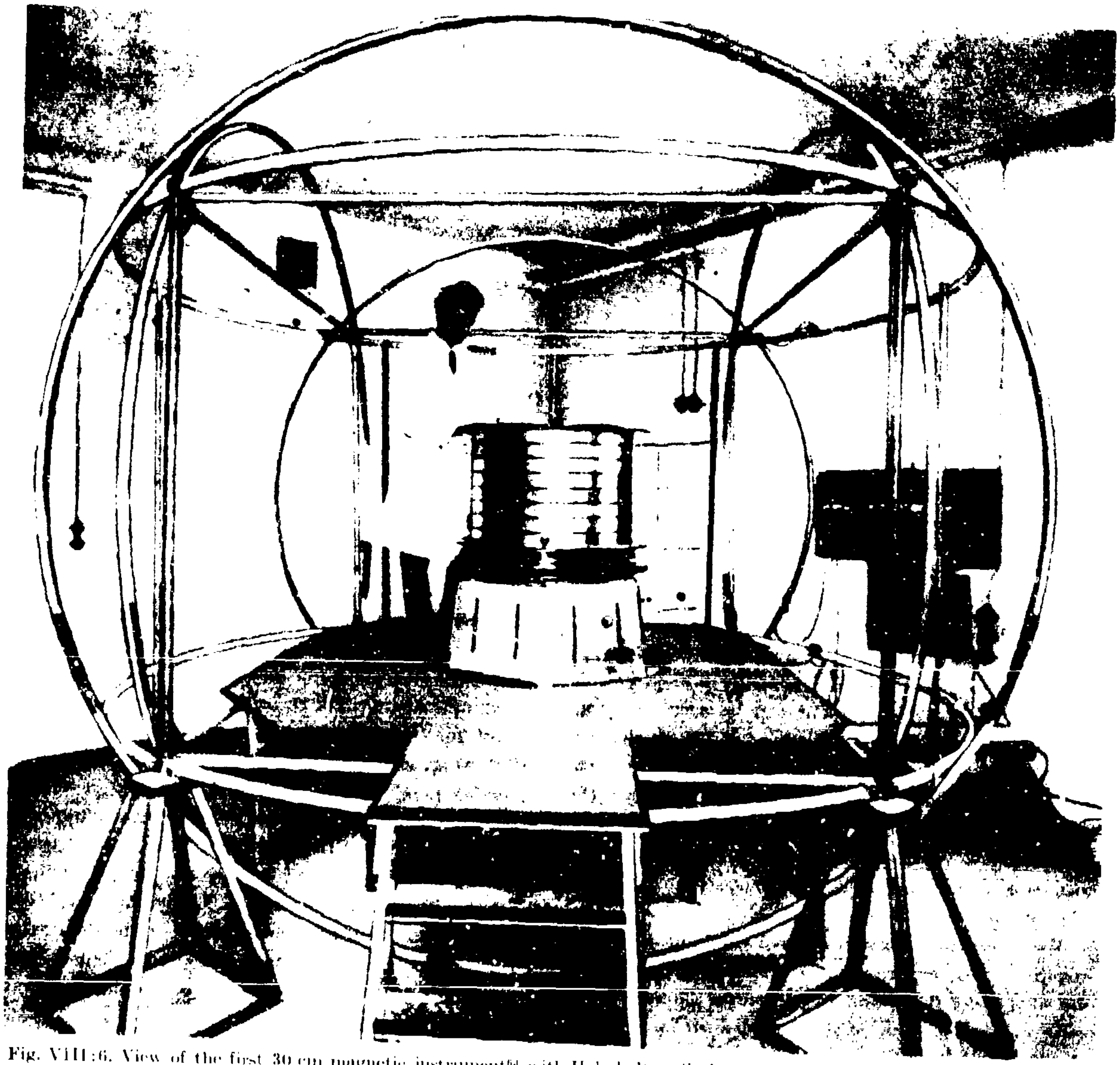

Fig. VIII:6. View of the first 30 cm magnetic instrument[64] with *Helmholtz* coils for compensation of external magnetic fields. For the new instruments more compact compensating systems have been designed with quadratic coils for the horizontal field components, see Section VIII:7, so that the instruments can stand on the floor at a *convenient* level.

spectrometer of this type for the analysis of X-ray produced electron spectra.[8] For many years, this was the only instrument available for ESCA work. It has, however, been redesigned and improved over the years to the extent that only the magnet coils remain the same as in the original version of the instrument.[63]

The physical arrangement of the spectrometer and the Helmholtz coil system for eliminating the earth magnetic field and other stray fields is shown in Fig. VIII:6.

Electron source and X-ray generator

The X-ray source and the electron source are built into a common source housing as shown in Fig. VIII:7. The X-ray anode, mounted on the top of the source house, is grounded and can easily be changed if

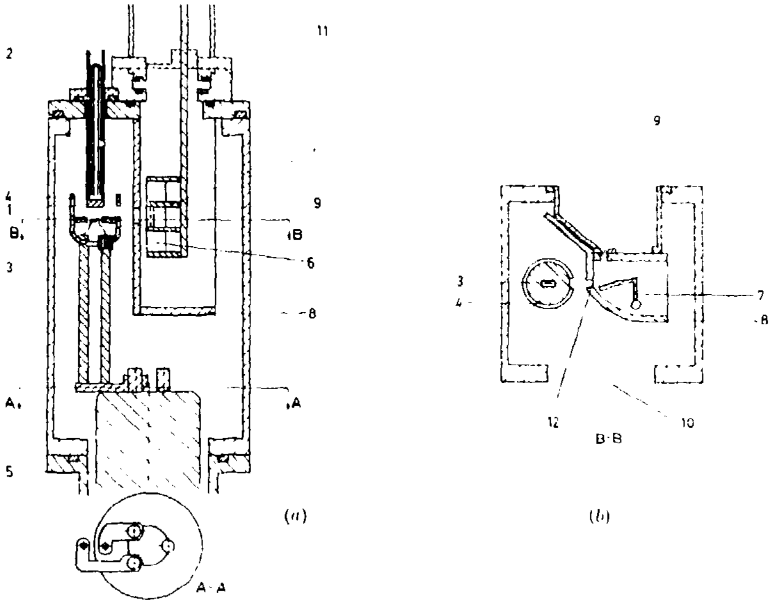

Fig. VIII:7. (a) Vertical section of the source housing. (b) Horizontal section of X-ray source and electron source.[63]
1. Anode. 2. Cooling water. 3. Cathode filament. 4. Focussing electrode. 5. High voltage feed-through. 6. Electron source backing. 7. Source holder. 8. Wall separating X-ray and electron source compartments. 9. Entrance slit to spectrometer. 10. To pumping system. 11. Air lock. 12. X-ray window.

required. Water is used as a cooling agent. Two copper pins, mounted on an insulating base at the bottom of the source housing, hold the cathode filament and a focussing electrode. The anode projects axially into this electrode. X-radiation from the anode emerges through an opening in the cylindrical electrode. High voltage and filament current are supplied to the cathode by a Philips PW 1010 X-ray power supply. Voltage is stabilized to 0.1 % and emission current to 0.1 % in this equipment at a maximum mains voltage fluctuation of ± 10 %. Maximum voltage is 54 kV and maximum emission current is 36 mA.

The electron source is mounted in a separate compartment of the source housing and is lowered into this compartment through an air lock. It has three sections that can be exposed individually to the X-radiation (a cryostat has recently been incorporated). Fig. VIII:8 is a photograph of the air lock and source holder with an aluminum strip as the source backing. The entrance slit to the spectrometer is placed at a distance of approximately 5 mm from the source backing and, being only 0.25 mm wide, it constitutes the electron-optical source of the instrument.

The electron source compartment is evacuated through the spectrometer vacuum chamber, whereas the X-ray compartment is evacuated by separate pumps to a pressure of 10^{-6} torr.

Spectrometer magnet and current supply

The spectrometer magnet consists of two co-axial, cylindrical, copper coils of mean radii 24 cm and 36 cm, respectively and of equal height, 48 cm. Both coils are wound on copper bobbins. The inner coil has 357 turns and the outer coil 75 turns connected in series with the inner coil. This system produces a magnetic field in the space between the coils that has a form very close to the theoretical form

$$B(\rho) = B(\rho_0) \cdot (\rho_0/\rho)^{\frac{1}{2}} \tag{4}$$

of a double focussing field.

External fields are compensated by three pairs of circular coils, see Section VIII:7. The coil diameters are 3.2 m. The three pairs of coils are connected in parallel to a power supply with a variable resistance in series with each coil. The power supply gives an

Fig. VIII:8. Air lock and source holder with an aluminum strip as a source backing.[63]

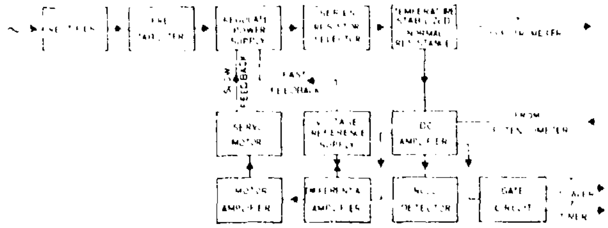

Fig. VIII:9. Block diagram of the current supply.[63]

output voltage from 0 V to 36 V with a long time stability of $2\cdot10^{-5}$. With this compensating system the residual magnetic field is less than $\pm 2\cdot10^{-4}$ gauss in the central electron orbit. The compensation of external fields is measured by a magnetometer which has a sensitivity of 10^{-5} gauss. The laboratory building contains no ferromagnetic material in its basic construction and is therefore well suited for housing an instrument of this type.

The power of the spectrometer magnet as given by

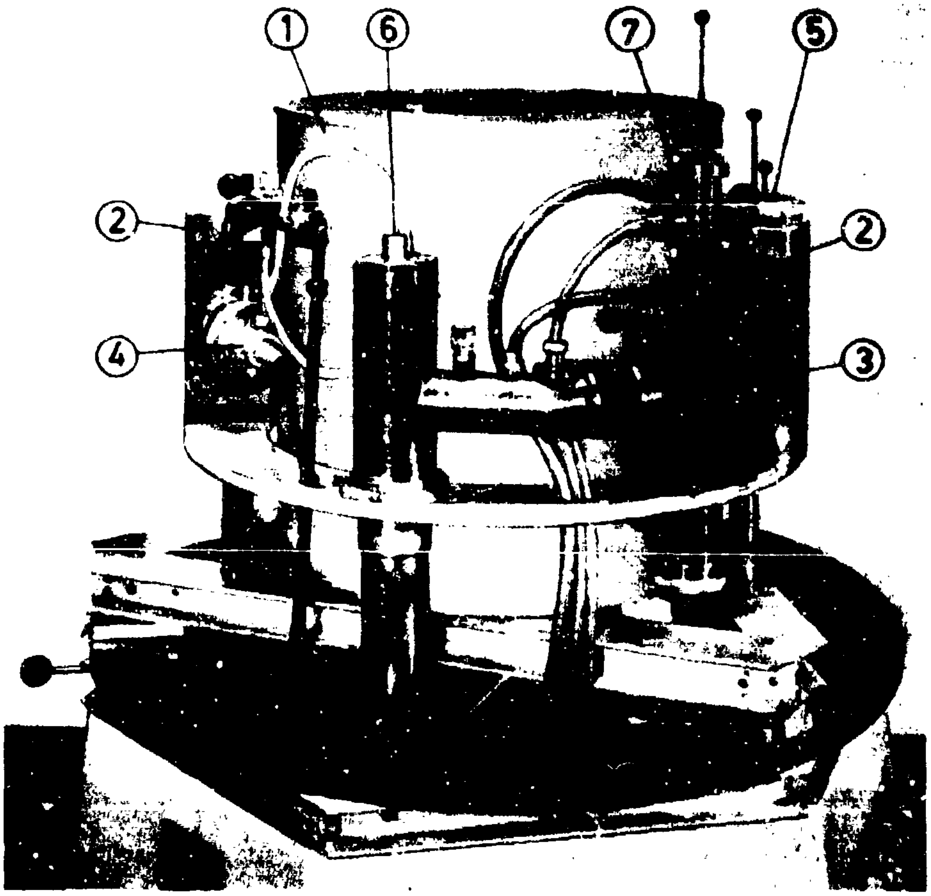

Fig. VIII:10. Photograph of the electron spectrometer with outer coil removed to show the spectrometer chamber and the source and detector arrangements.[63] 1. Inner coil of spectrometer magnet. 2. Sector shaped spectrometer chamber. 3 Source housing with X-ray tube. 4. Channel electron multiplier or Geiger counter with post-acceleration. 5. Spectrometer baffle shafts. 6. Liquid air trap. 7. Air lock.

the ratio of magnetic rigidity of focussed electrons to spectrometer current is approximately 76.3 Gcm/A. Since the instrument is used in the energy range 0.1 keV–10 keV and with momentum resolution down to the order of $1\cdot10^{-4}$, the current supply should be capable of delivering from 0.5 A to 5 A into the 0.65 Ω magnet coils with a stability of a few parts in 10^6. A current supply to meet these specifications was built after much the same design as that reported by Bäckström *et al.*[270] for an iron yoke instrument. It is operated automatically. Fig. VIII:9 is a block diagram of the current supply for the spectrometer.

Spectrometer chamber and baffle system

The instrument has a free space of 10 cm between the outer and inner coils. To provide maximum space at the source and detector positions the spectrometer vacuum chamber, made of aluminum, is sector shaped as shown in Fig. VIII:10. The source housing and detector are mounted on the vertical end-walls of the chamber. Evacuation of the spectrometer chamber is made by an oil diffusion pump made of stainless steel and a rotary pump which is placed outside the compensating system. In addition to the liquid air traps on the diffusion pumps for the X-ray compartment and the electron source compartment there is a liquid air cooled aluminum plate between the source and the electron-optical baffles. With this arrangement the deposit of pump oil and other contaminations of the sample surface is much reduced.[82]

Aperture defining baffles are placed at an azimuthal position of 48° from the electron-optical source. Each baffle consists of a rectangular aluminum plate with an aperture of appropriate shape and size. The baffle plate is held by a shaft that extends through a cover plate to open air and by which the baffle can be moved into position. Two baffles can be accommodated in this way, and including a fixed baffle with maximum aperture, one can choose one of three apertures without breaking vacuum. The shapes and sizes of the apertures were obtained from iso-aberration curves. These curves were obtained by a procedure that has been described elsewhere.[271] The baffle aperture that has been used mostly corresponds to a spectrometer aberration of 0.05 % in momentum (full base width) and a solid angle of 0.06 % of 4π.

Fig. VIII:11. Photograph of the detector (Mullard Experimental Channel Multiplier).

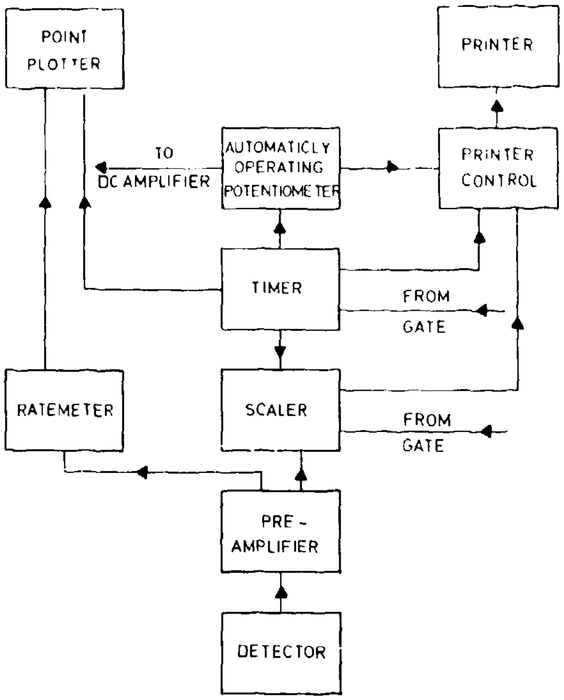

Fig. VIII:12. Block diagram of the data recording system.[83]

Detector and data recording system

Detection was up till recently made by Geiger counter technique. Formvar was used as a window material and a post-acceleration system was built for detection of electrons below 2 keV kinetic energy. However, we have found the continuous channel electron multiplier to be a more convenient detector since it is an open detector which counts electrons with high efficiency down to very low energies (below 1 eV). We have found it to be very reliable in operation and it is sufficiently small to allow for an array of detectors to be placed in the focal plane of a spectrometer (see Section VIII:4). A photograph of the detector (Mullard Expe-

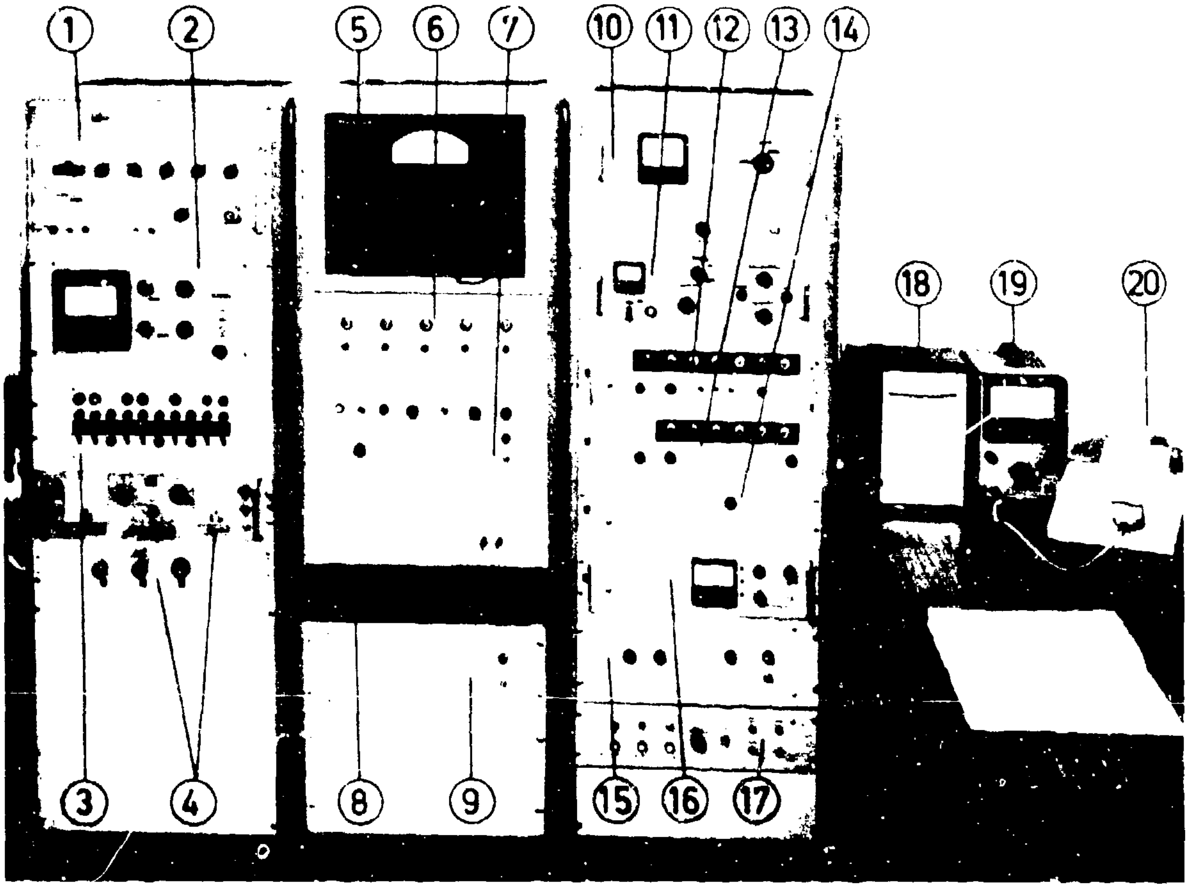

Fig. VIII:13. The electronic equipment.[63] 1. High voltage supply for the channel electron multiplier and for the Geiger counter with post-acceleration. 2. Potential divider for the post-acceleration system. 3. Control panel for pumps, cooling water, and temperature of standard cell and standard resistor. 4. Power supply and series resistors for Helmholtz coils. 5. Magnetometer for measurement of residual field. 6. Automatically operating potentiometer. 7. Resistor network and step length selector. 8. Adjustment of current in resistor network. 9. Power supply for the potentiometer electronics. 10. Current range selector. 11. Current supply for the spectrometer coils. 12. Scaler. 13. Timer. 14. Printer control. 15. Gate circuit. 16. Ratemeter. 17. Point plotter control. 18. Point plotter. 19. Null detector. 20. Printer for the potentiometer setting and number of counts.

rimental Channel Multiplier) is shown in Fig. VIII:11.

Recording of data (number of counts and spectrometer current) is made automatically as shown by the block diagram of Fig. VIII:12. Commercially available equipment is used for the scaler, timer, ratemeter, point plotter, and printer.

The automatic stepping potentiometer has five decadic resistor sets. High precision manganin resistors are used and the total resistance is 50,000 Ω. The linearity of the potentiometer is $1 \cdot 10^{-5}$ for spectrometer currents from 0.5 A to 5 A. Ledex rotary relays are used to step the potentiometer. Step lengths from 0.1 mA up to 800 mA can be chosen for the spectrometer current. The potentiometer setting (spectrometer current) is shown by nixie read-out on the panel of the potentiometer unit. If preferred, the instrument can be operated manually. A photograph of the electronic equipment is shown in Fig. VIII:13.

VIII:3. The Permanent Magnet Instrument

Semicircular focussing of electrons in a homogeneous magnetic field has been invaluable in β-ray spectroscopy ever since it was suggested by Danysz in

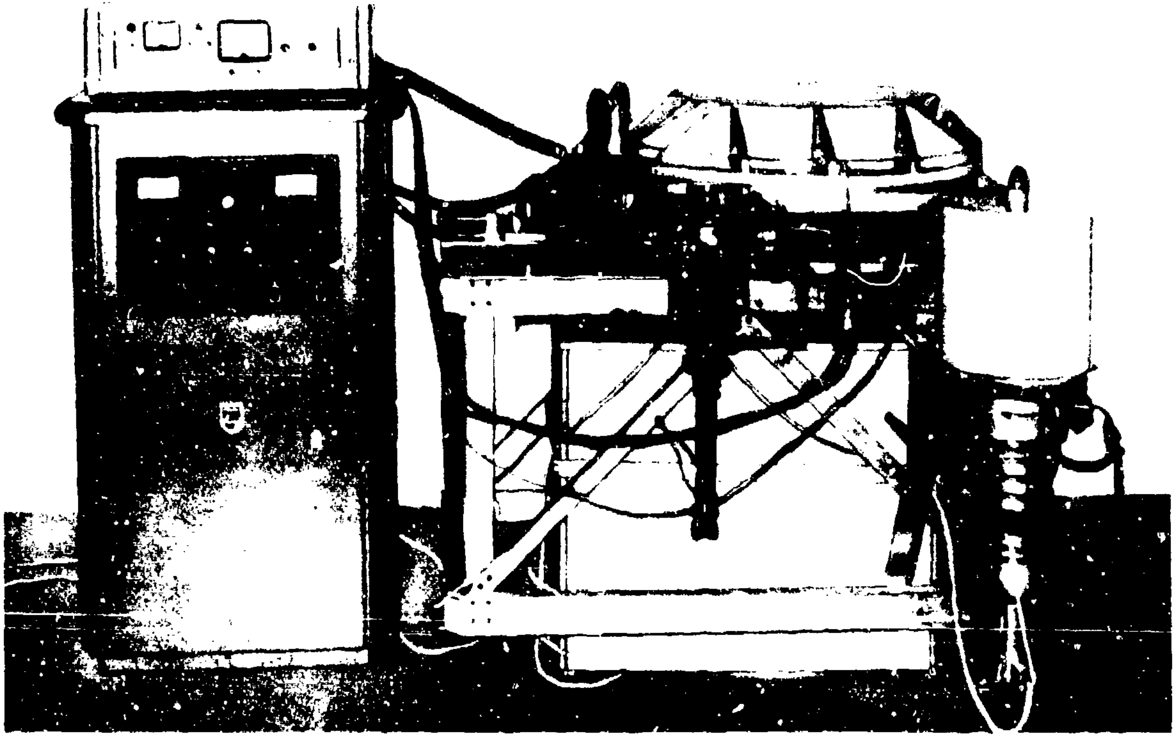

Fig. VIII:14. View of the permanent magnet instrument.[64]

1912.[272,273] To investigate the possibilities of utilizing semicircular focussing for ESCA, we have constructed an instrument in which the electrons are analysed in a permanent magnet, homogeneous field spectrograph[64] (cf. Section VIII:1). In this instrument a crystal monochromator is used for the X-radiation. Detection of the electrons is made photographically and track counting is used in preference to conventional photometric methods for scanning the photographic emulsion[65]. The physical arrangement of the instrument is shown in Fig. VIII:14.

Magnet and vacuum chamber

The vacuum chamber of the spectrograph also serves as an iron yoke for the magnetic return flux as shown in Fig. VIII:15. The vacuum chamber consists of a cylindrical shell *1* and two circular plates *2* (numbers refer to Fig. VIII:15). The cylindrical wall has six openings which afford good access to the pole gap. Owing to the large diameter of the spectrograph, special precautions had to be taken in order to reduce any displacement of the iron plates when the spectrograph was evacuated. Two aluminum plates *3* were therefore made and glued on the iron plates of the vacuum chamber. The aluminum plates were specially designed in order to withstand the atmospheric pressure. After the plates were glued, the iron discs were machined to within 0.007 mm. The total weight of the vacuum chamber is 150 kg. Although the spectrograph was intended to be used for analysing photoelectrons with fairly low energies (3-10 keV), it was decided that adaptation of the instrument for nuclear spectroscopy would be of value. It was therefore designed to yield a maximum magnetic field of about 250 gauss, which allows the focussing of electrons up to the 1 MeV region.

The magnetic steel is made into cylindrical sections

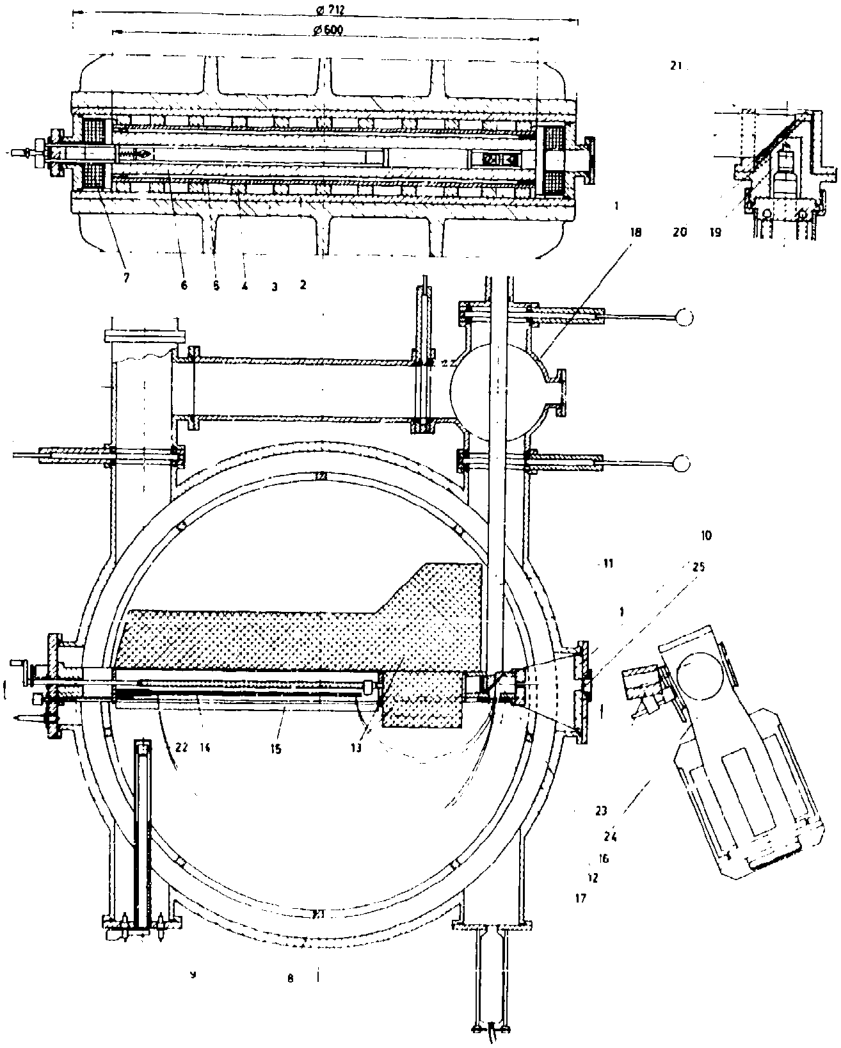

Fig. VIII:15. Vertical and horizontal section of the permanent magnet spectrograph.[64] 1. Cylindrical wall of the vacuum chamber. 2. Bottom plate of the vacuum chamber. 3. Aluminum plate glued to the bottom plate. 4. Permanent magnets. 5. Iron disc (thickness: 5 mm) placed on the magnet pieces. 6. Pole pieces so placed that a gap of 4.5 mm exists between them and the thin iron discs. 7. Magnetization coils. 8. Bars soldered to the coil bobbin. 9. Vacuum tight feed-through. 10. Guiding system for the plate holder. 11. Source holder. 12. Beam defining baffles. 13. Lead shields. 14. Photographic plate. 15. Movable doors. 16. Source ring. 17. Cavity for collection of unconverted X-radiation. 18. Evaporation chamber. 19. Evaporation unit. 20. Tungsten boat. 21. A slit which defines the source width. 22. A coil for approximate measurement of the magnetic field in the gap. 23. Monochromator. 24. X-ray tube shield. 25. Beryllium window.

4 and are machined to within 0.01 mm. They are placed upon the iron plates of the vacuum chamber, each layer containing 73 sections. The permanent magnet sections are kept in position by an aluminum matrix (Fig. VIII:16). On each layer, a circular iron disc *5* is placed. The discs are made of soft iron. The pole pieces *6* are made of the same quality of iron as the thin discs and are mounted so that they form a gap of 4.5 mm with the thin iron discs. These extra gaps have been inserted in the magnetic circuit in order to increase the homogeneity of the magnetic field. The air gap between the pole pieces, in which the electrons are analysed, is 29.0 mm. The two pairs of iron discs have been ground flat to within 0.007 mm and the variation in thickness over the plates is less than 0.005 mm.

The radius of curvature in the spectrograph varies between 10 cm and 24 cm so that electron energies below 10 keV correspond to a low magnetic field, < 20 G. Obviously, it is more difficult to obtain a high relative homogeneity with low magnetic field strengths than with higher strengths. Great efforts have therefore been made to overcome this difficulty. In addition to carefully machining and aligning the parts constituting the magnetic circuit, we have inserted in the circuit two extra air gaps. These extra air gaps are believed to have had a substantial effect on the homogeneity of the field. As seen in Fig. VIII:17 the area over which there is little field variation is quite extensive even for the low field of 17 G. During the initial magnetization procedures it was found that the permanent magnet pieces had to be carefully demagnetized before they were inserted in the spectrograph. Otherwise the variation in the field in the air gap became serious at fields around 25 G and lower. This lack of uniformity could not be eliminated by the normal demagnetization procedure after installing the magnet pieces in the spectrograph. This demagnetization is performed by sending DC current of decreasing strength and alternating direction through the magnetization coils of the spectrograph.

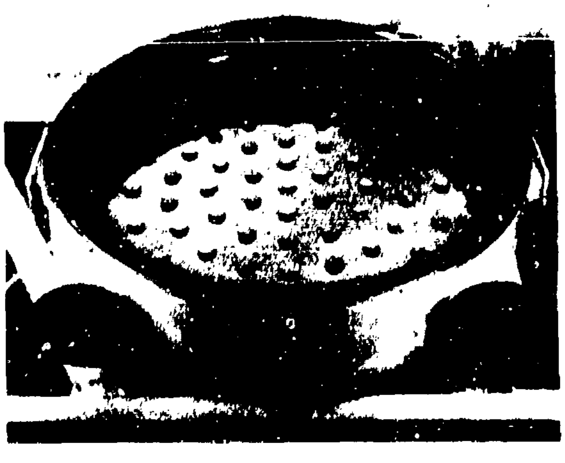

Fig. VIII:16. The lower part of the spectrograph.[64] The permanent magnets are placed upon the bottom plate of the vacuum chamber. They are kept in position by an aluminum matrix. The magnetization coils are also seen in the figure.

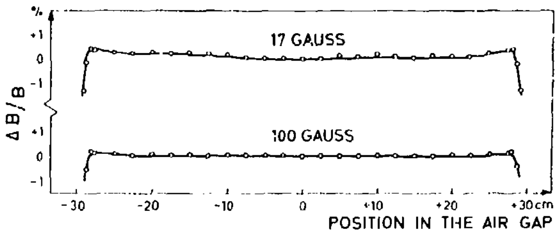

Fig. VIII:17. Field variation along a diameter in the pole gap for two different magnetic fields.[64]

In order to obtain high precision in the measurements, the permanent magnets are maintained at constant temperature. A hard plastic cover has thus been made for each of the two reinforcing aluminum plates (see Fig. VIII:14) and temperature controlled air is allowed to circulate in the system.

Since the vacuum chamber also serves as an iron yoke for the magnetic return flux, it has been necessary to place the magnetization coils in high vacuum. The coils *7* each contain 64 windings of cotton covered copper wire wound in 8 layers with an average radius of 323 mm. For the excitation of the coils a power supply, which gives a maximum DC current in the coils of 90 A, has been constructed. This power supply is also used for heating the filament in the evaporation chamber as described below.

Plate holder and source arrangement

The plate holder is shown in Figs. VIII:15 and VIII:18. It is introduced into the spectrograph through a hole in the cylindrical shell of the vacuum chamber and is pushed into a well defined position in the guiding system *10* which is located inside the opposite hole of the vacuum chamber.

Through a hole in the back of the plate holder, the source holder *11* may be pushed towards a stop (see Fig. VIII:15). The position of the source holder relative to the plate holder is fixed by a three point guiding system. In front of the source and in the same plane as the photographic plate, two movable baffles of brass *12* are located. These define the width of the electron beam. Between the source position and the photographic plate, a lead shield *13* has been inserted in the plate holder. This shield protects the emulsion from direct irradiation by X-rays or by γ-rays from a radioactive source.

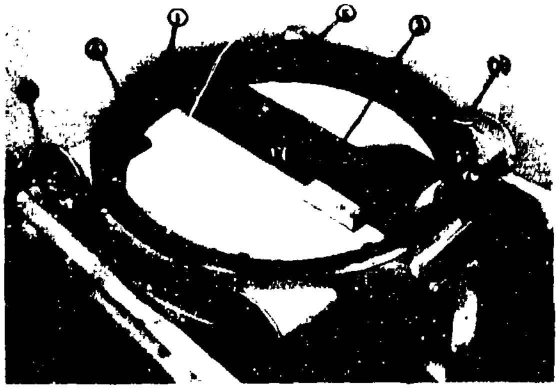

Fig. VIII:18. The lower half of the magnet with the plate holder.[64] The plate holder is introduced into the pole gap through one of the openings (1) in the cylindrical shell. It is pushed into a guiding system (2) positioned in the opposite hole. A lead shield (3) is placed behind the plate holder. A small coil (4) is placed in the pole gap. The coil can be rotated from outside the vacuum chamber, and the field strength can be measured by a fluxmeter. The magnetization coils (5) are electrically connected to a vacuum tight feed-through (6).

The photographic plate *14* which has the dimensions 17 × 300 mm^2 is placed in a light excluding casset. The casset has two movable shutters *15*, which can be operated individually from outside the spectrograph. They can either be closed, half-open or open.

The source, 12 mm long, is mounted on a brass ring *16*. The alignment of the source on the ring is made by means of a mark on the ring and is checked with a microscope. Either thin wires or aluminium strips have been used as backing materials. A hollow brass rod *17* is used to introduce the source into the spectrograph. The position of the rod during an exposure is seen in Fig. VIII:15. Experiments have shown that the reproducibility in positioning the source relative to the photographic plate is within 0.03 mm.

An evaporation chamber *18* is attached to the spectrograph which makes it possible to introduce a source to the spectrometer without exposing it to air.

X-ray equipment

For the production of X-radiation, Philips' fine focus X-ray diffraction tubes are employed. The apparent line focus at the anode seen from the window of this type of tube is 0.02 × 8 mm^2. The tubes are connected to a Philips PW 1009 DC X-ray diffraction generator, which delivers a maximum power of 1 kW. The high tension and the tube current are continuously variable, 0–55 kV and 0–40 mA, respectively.

After reflection in the crystal, the radiation passes a 0.15 mm thick beryllium window which separates the vacuum in the spectrograph from the atmospheric pressure. Between the window and the source position, a slit is placed which prevents scattered radiation from reaching the analysing region of the spectrometer.

Three crystals are available which are bent for Cr$K\alpha$, Cu$K\alpha$, and Mo$K\alpha$ radiation, respectively. The monochromators are bent-quartz asymmetric crystals of the Jagodzinski design[274] with reflecting plane (1011), supplied by R. Seifert and Company, Hamburg. The monochromator *23* is mounted on the X-ray tube shield *24*, (see Figs. VIII:15 and VIII:19). It permits an almost complete separation of the $K\alpha_1$ radiation when the monochromator is set for maximum reflection of that particular wavelength.[275]

The photographic plates and the delineation of spectra

One of the features of the permanent magnet semicircular spectrograph is that it enables a large part of the energy spectrum to be analysed in one operation. Photographic detection is thus very suitable for this type of instrument. Line intensities are determined by counting, by means of a microscope, the electron tracks in a nuclear research emulsion. This method appears to give accurate results and it also reduces the exposure time required. For example, it is not necessary to expose the emulsion until the electron lines become visible. The number of grains per electron track is very small, ≲ 3, and it is difficult to distinguish true electron tracks from the single grain tracks formed by handling and cosmic radiation. It is therefore important to use an emulsion having a very low intrinsic background. We have used a nuclear research emulsion, Ilford K5, and prepared the photographic plates ourselves in order to reduce the inherent background.[61]

The photographic plate is analysed by counting the number of individual electron tracks per unit area on the plate in a microscope with a magnifying power of × 1250. Electrons with energies < 10 keV only penetrate the photographic emulsion slightly and the tracks appear as more or less circularly shaped black points when observed in the microscope. Since these electron tracks are less than a few microns from the surface of

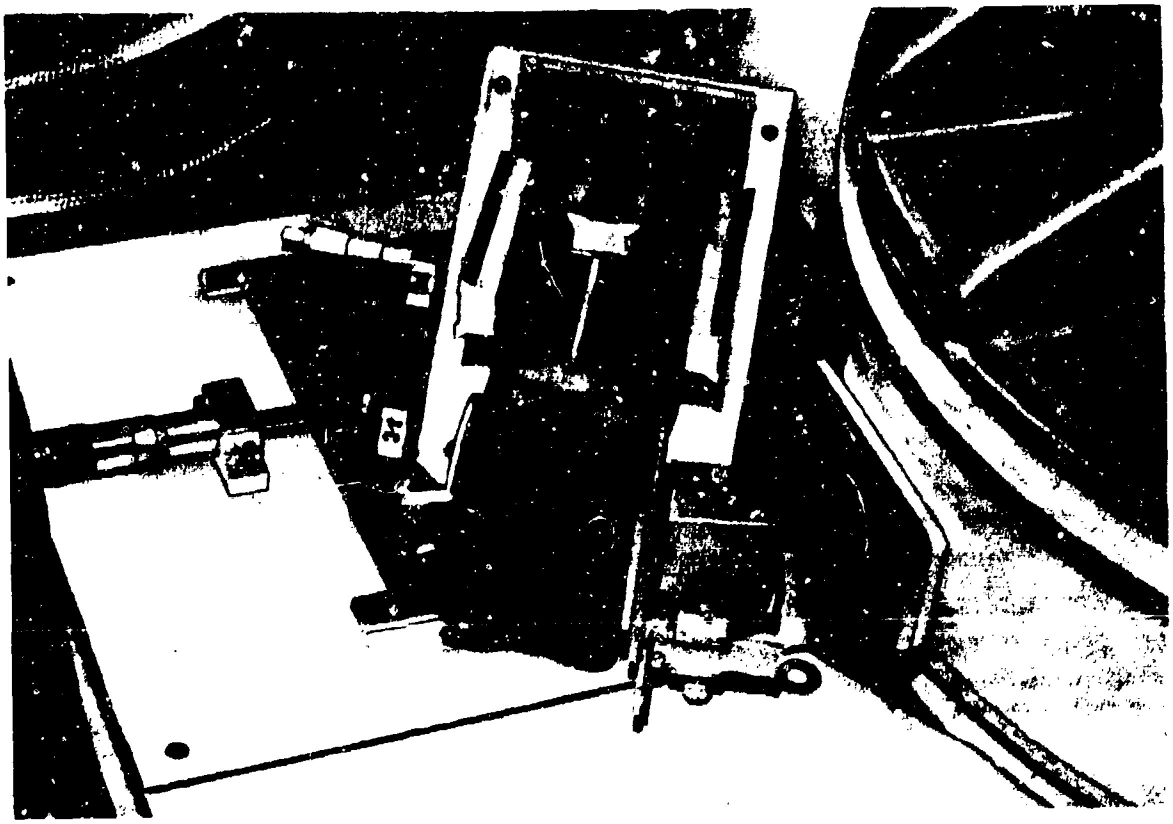

Fig. VIII:19. X-ray tube and monochromator. The reflected X radiation can be directed by means of precision screws which fix the position of the X ray tube relative to the source position.

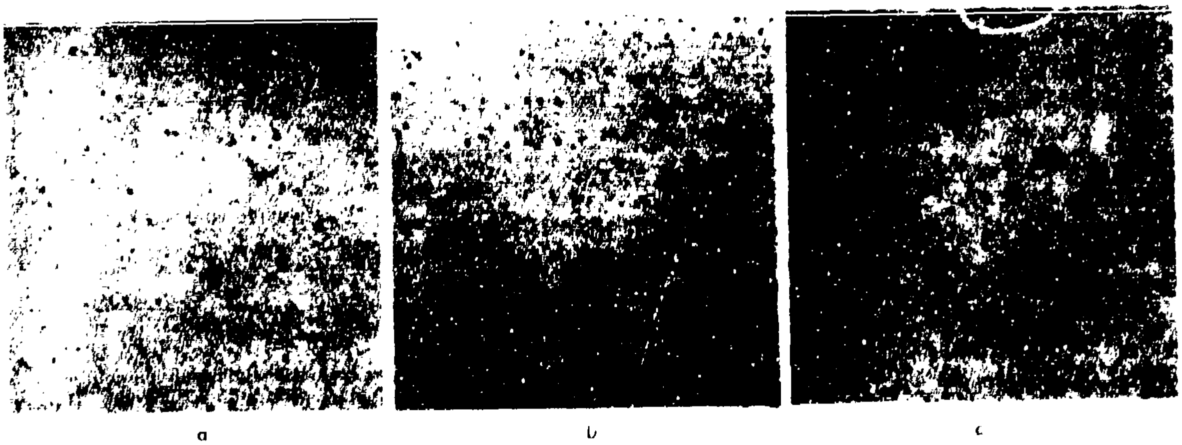

Fig. VIII:20. A 5 keV electron track distribution as seen in the microscope.[51] In (*a*) the background on the high energy side of an electron line is shown. In (*b*) part of the background and the high energy slope of the electron line is shown and in (*c*) the microscope is focussed on the peak of the line.

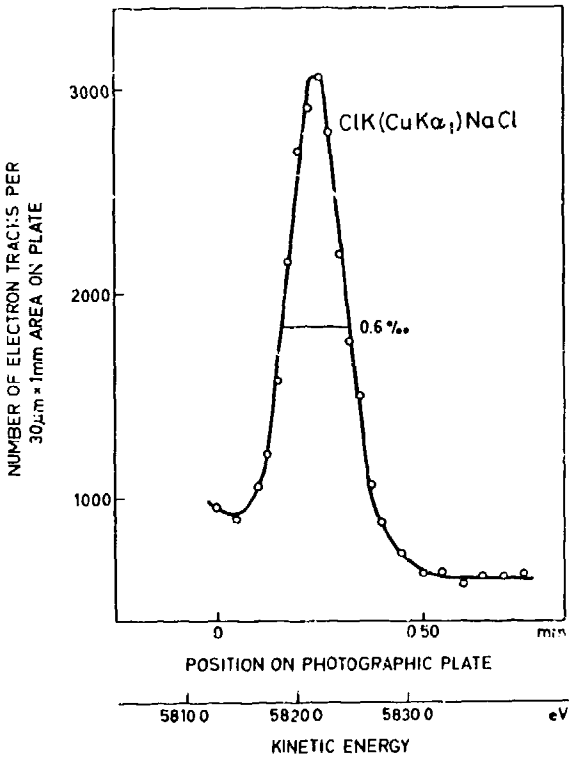

Fig. VIII:21. The electron line ClK(Cu$K\alpha_1$)NaCl.[44] This line was obtained by counting the electron tracks shown in Fig. VIII:20.

the emulsion, it is easy to distinguish them from tracks formed by electrons of higher energies.

A typical electron track distribution for 5 keV electrons in a 10 μm thick Ilford K5 emulsion as seen in the microscope is shown in Fig. VIII:20. The pictures are taken during an analysis of an electron spectrum of sodium chloride. They show three parts of the electron distribution of chlorine K electrons expelled by copper $K\alpha_1$ radiation. Exposure time was 40 h. On the high energy side (a) of the electron line only a few tracks are found consisting mainly of the original single grain background in the emulsion. The next picture (b) shows the beginning of the high energy side of the electron line profile. Finally, in the third picture (c), the electron track density has reached its maximum. The pictures correspond to an area on the plate of approximately 50 × 50 μm^2. The electron spectrum of the corresponding energy interval is shown in Fig. VIII:21. It is obtained by counting the electron tracks over an area on the plate of 1 mm × 30 μm.

Fig. VIII:22 and Fig. VIII:23 show two more examples of ESCA spectra that have been recorded in the semicircular permanent magnet spectrograph, and delineated by the track counting technique.

Fig. VIII:22 shows an electron spectrum from sodium chloride using a monochromatic X-ray beam, so that only one electron line, originating from copper $K\alpha_1$ radiation, is obtained for each level in NaCl. As a result of mono-energetic radiation it is possible to distinguish smaller maxima on the low-energy side of the electron lines. These are formed by electrons which have lost energy during their passage out of the specimen. The energy loss (D.E.L.) takes place in discrete amounts (cf. Chapter I) and two such energy losses can be seen on the low-energy side of the chlorine K electron line.

Fig. VIII:23 shows an electron spectrum of hepa-

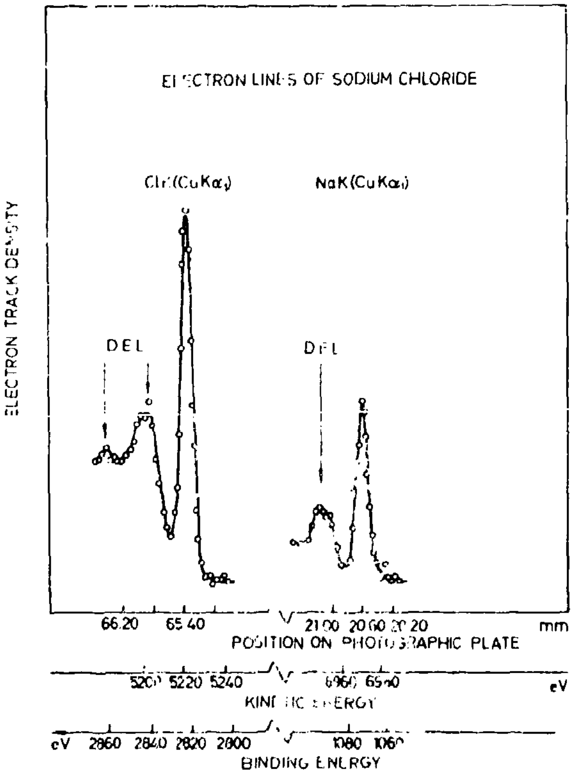

Fig. VIII:22. Electron lines of sodium and chlorine in NaCl excited by Cu$K\alpha_1$ radiation. Discrete energy losses (D.E.L.) are seen on the low-energy side of the lines

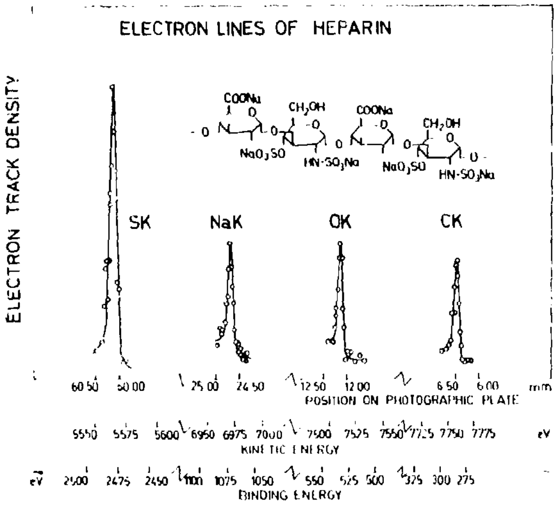

Fig. VIII:23. Electron spectrum of heparin excited with $CuK\alpha_1$ radiation.[40]

rin. The spectrum contains one *K* shell electron line from each of the constituent elements sulfur, sodium, oxygen, and carbon.

The plates were *originally analysed manually* by means of the microscope, but experiments soon showed that the counting procedure could be automatized by means of a television camera provided with necessary electronic equipment. This "Television Micro Densitometer"[71,80] is described in Section VIII:8.

VIII:4. The New Instrument with Magnetic Focussing

The first instrument that we used for ESCA employed an iron-free double focussing beta-ray spectrometer[5] for the analysis of the electron spectra (see Section VIII:2). The energy (or rather, momentum) analysis was thus made by an instrument that was initially built for an entirely different purpose, namely nuclear spectroscopy. It had been used for the investigation of a problem which later attracted a growing interest in the field of nuclear structure research and which may be outlined thus:—How will the interaction between the atomic nucleus and the electron envelope depend upon the fact that the nucleus cannot be considered as a point but has a finite radius, and what conclusions about the structure of the nucleus can be drawn from the observed effects?[7] The instrument was very well suited for this type of work which required high resolution and precision but less of space at and access to the source. However, it was not ideally suited for ESCA work since the space available for special source and detector arrangements was quite small. The new instrument with magnetic focussing[86] has been constructed exclusively for ESCA and therefore differs in many ways from the instrument described in Section VIII:2.

Spectrometer magnet

A new type of current sheet coils, coupled in series, are used for the spectrometer magnet, see Fig. VIII:24. As with the instrument described in Section VIII:2, we have used two coaxial cylindrical coils; however, each coil is now split in two sections, an upper section and a lower section. There are two reasons for making such a coil design. One is the much improved access to the spectrometer that is obtained through the open gap between the upper and lower sections. The other is the further improvement in the magnetic field that can be attained since one now has more design parameters for the optimal adjustment of the field.

Calculation of the optimal coil parameters was made on an IBM 1620 and a CDC 3600 computer.[86] The magnetic field in the plane of symmetry was obtained by numerical integration of the elliptical integrals deduced from basic electromagnetic theory:

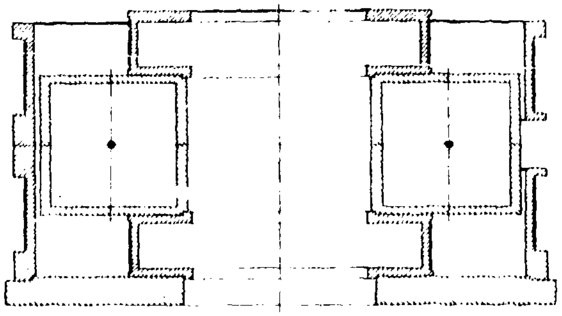

Fig. VIII:24. Coil arrangement in the new magnetic instrument. The bobbins for the outer coil and for the lower section of the inner coil stand on the base plate. The spectrometer chamber is placed between the two sections of the inner bobbin.

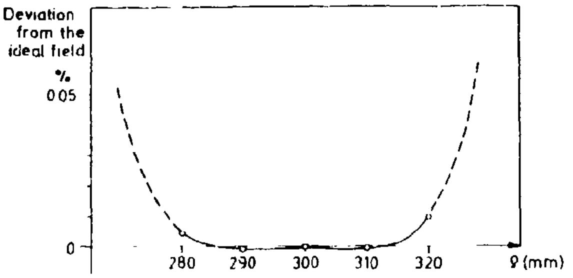

Fig. VIII:25. Deviation from the ideal magnetic field plotted versus distance, ϱ, from the spectrometer axis.

$$B_z(0,\varrho) = 0{,}4\,\lambda h \times$$
$$\times \int_0^{\pi/2} \frac{2R(R+\varrho-2\varrho\sin^2\psi)\,d\psi}{[(R+\varrho)^2-4R\varrho\sin^2\psi][h^2+(R+\varrho)^2-4R\varrho\sin^2\psi]^{\frac{1}{2}}} \tag{5}$$

ϱ distance from spectrometer axis
λ number of ampereturns per unit length
$2h$ coil height
R coil radius
ψ azimuthal angle of current element

With some of the design parameters fixed, the others could be adjusted so that the three first coefficients of the Taylor expansion of the calculated field at the central orbit radius (30 cm) were those of an optimum field (see Appendix 8). Fig. VIII:25 shows the calculated field form in the vicinity of the central orbit. Deviation from the ideal field is plotted versus distance, ϱ, from the spectrometer axis. The calculations show that electrons emitted in the symmetry plane with a radial angle of emission less than $\pm 3°$ will never experience a field which deviates more than $1 \cdot 10^{-4}$ from the ideal field and electrons emitted with a radial angle of emission less than $\pm 5°$ will never experience a field which deviates more than $1 \cdot 10^{-3}$ from the ideal field.

Only one layer of enamelled copper wire (ϕ = 2.6 mm) is used for the coils in which the position of each wire is defined by a precision machined groove in the coil bobbin. One extra turn is provided on each coil section. By sending a current through one or several of these extra windings, one can make minor adjustments to the magnetic field.

The coil bobbins, the spectrometer chamber and the base plate are made of aluminum. The bobbin for the two sections of the outer coil and the bobbin for the lower section of the inner coil stand on the base plate. Their positions are defined by grooves and flanges in the base plate and the bobbins. Likewise, the position of the spectrometer chamber is defined by a groove in the bobbin on which it stands (see Fig. VIII:24). Finally, the inner upper bobbin fits on top of the spectrometer chamber. By this arrangement of the coils and the spectrometer chamber, one can take the whole instrument apart and reassemble it in a short time without loss of coil adjustment. The physical arrangement of the spectrometer is shown in Fig. VIII:26. Fig. VIII:27 is a photograph of the spectrometer when the outer coils have been removed. Drawings of the spectrometer are shown in Fig. VIII:28.

For the elimination of the earth's magnetic field the instrument is equipped with one pair of circular coils for compensation of the vertical component and two pairs of quadratic coils for the horizontal components. For further details see Section VIII:7.

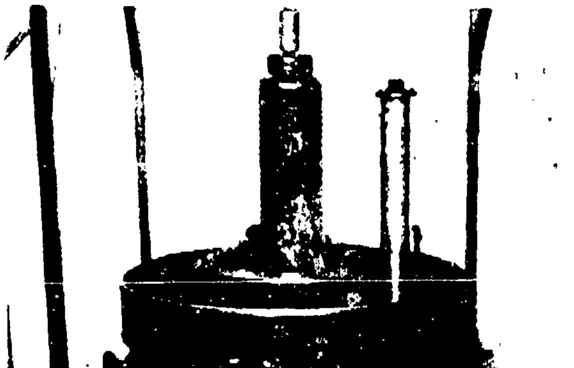

Fig. VIII:26. Physical arrangement of the new magnetic spectrometer.

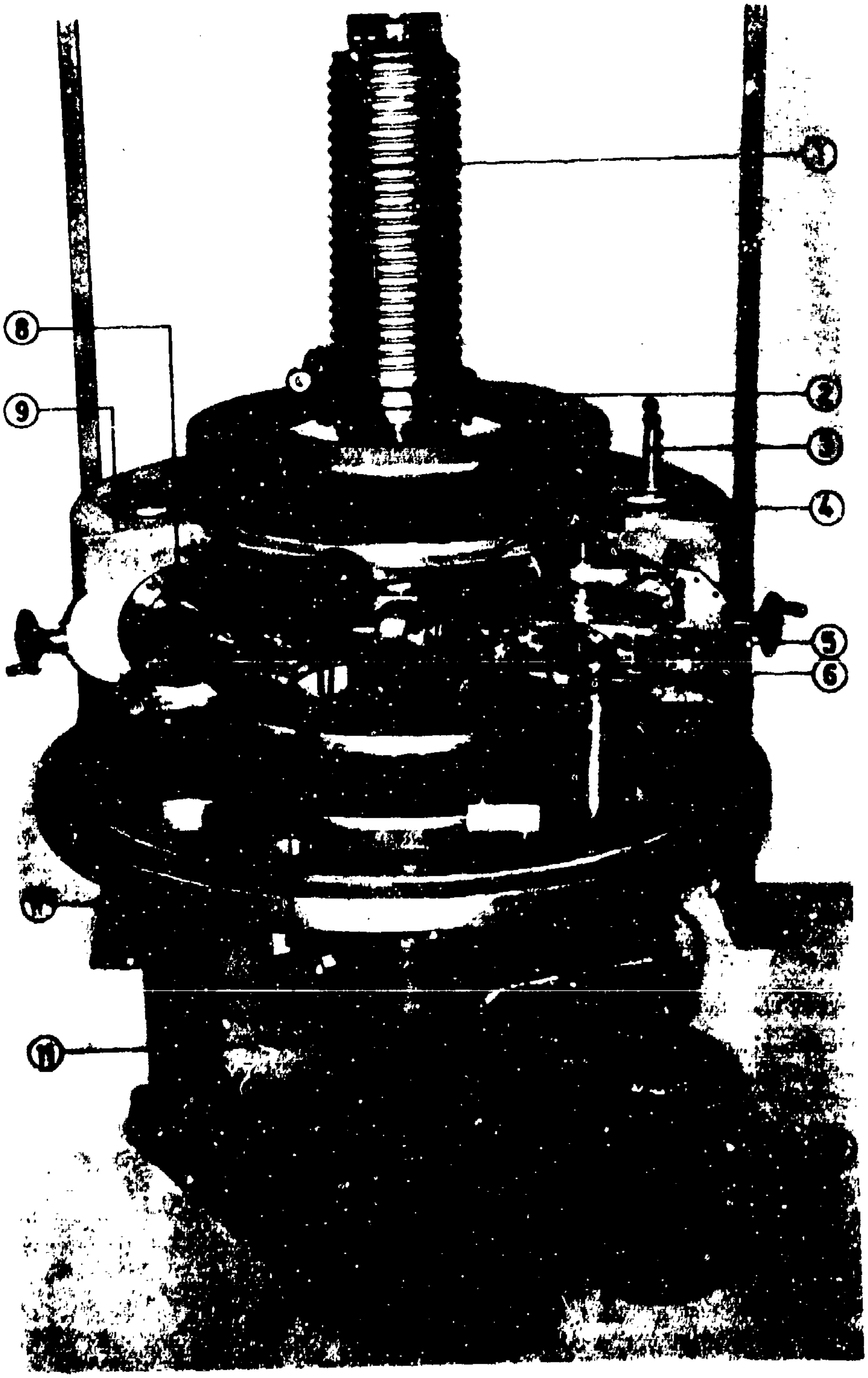

Fig. VIII:27. The new magnetic spectrometer with bobbin for the outer coil removed. 1. Ionisation pump. 2. Upper part of the inner bobbin. 3. Spectrometer baffle shafts. 4. Air lock for the source. 5. Turnable X-ray anode. 6. Inspection window. 7. Sorption pumps. 8. Detector housing. 9. Spectrometer chamber. 10. Base plate. 11. Lower part of the inner bobbin.

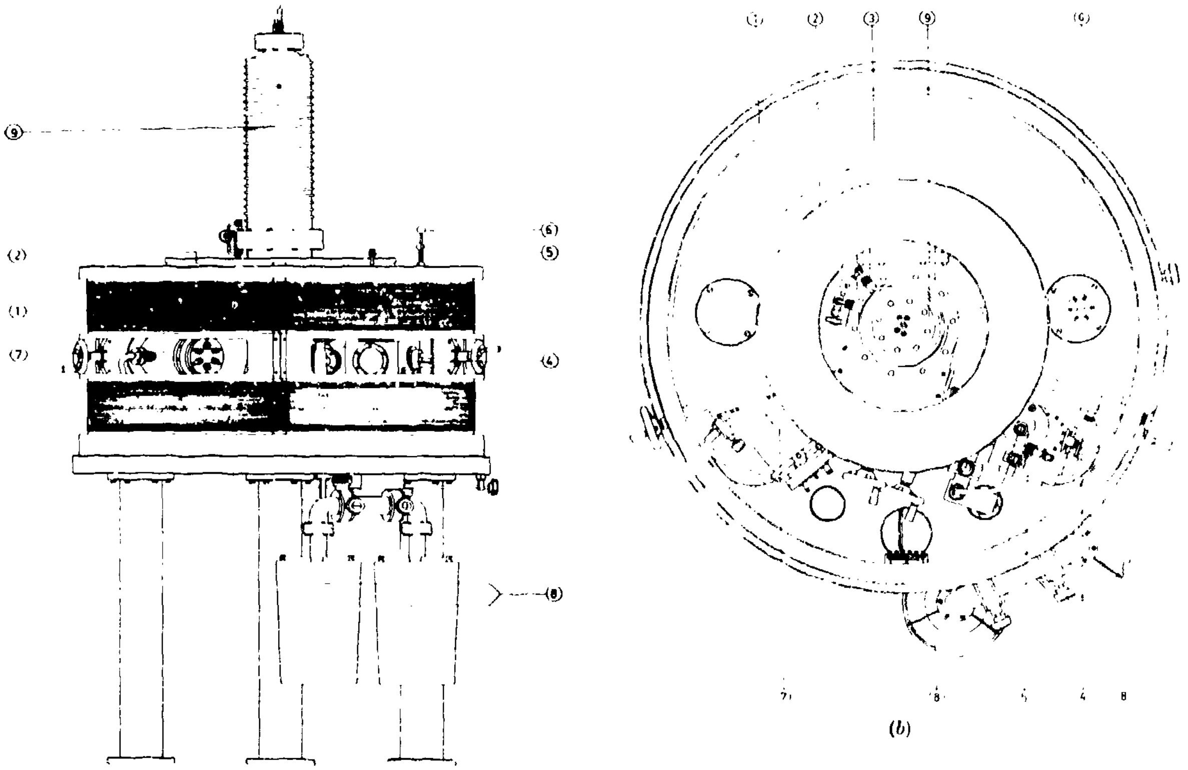

(*a*)

(*b*)

Fig. VIII:28. Drawing of the new magnetic spectrometer (*a*) as seen from the side, (*b*) as seen from above. 1. Outer coil bobbin. 2. Upper section of the inner coil bobbin. 3. Sector shaped spectrometer chamber. 4. Turnable X-ray anode. 5. Upper part of the source holder. 6. Spectrometer baffle shafts. 7. Detector housing. 8. Sorption pumps. 9. Ionisation pump.

Source—spectrometer chamber—detector

The distance between inner and outer coils is 17 cm, the open gap between the outer coil sections is 10 cm and between the inner coil sections 25 cm, and the dimensions of the end walls of the sector shaped spectrometer chamber are 26 cm × 26 cm. Corresponding data for the first instrument, described in Section VIII:2 are: distance between coils = 10 cm, open gap = 0 cm, end wall area 25 cm × 10 cm. The new spectrometer thus provides much more space for the source and detector arrangements that are used in ESCA work. Of the three modes of excitation that were shown in Fig. VIII:5 we now use the X-ray mode. However, the other two modes of excitation can also be incorporated in the instrument.

When soft X-radiation is used for the production of ESCA spectra, the intensity decreases with time owing to evaporation of tungsten from the filament on the anode in the X-ray tube. This problem has been eliminated in the new magnetic instrument. The anode is not in a straight line with the filament; instead, the acceleration takes place in an electron gun combined with an electrostatic lens. The electron beam is then deflected by an electrode so as to hit the anode which is retracted from the initial path of the electron beam. Adjustment of the focal point on the X-ray anode is made electrically by changing the electrode potentials and mechanically by pivoting the electron gun. Both types of adjustment are made without breaking the vacuum. A window is provided for visual inspection of the anode and other details in the interior of the source housing. The tip of the anode has four sections which can be covered with different anode materials. A change of target materials is made, either by changing the anode, or by turning it through 90° so as to have a new section of the tip exposed to the electron beam. This latter operation can be made without breaking the vacuum.

When exceptionally high radiation density is required use can be made of a rotating anode in the X-ray tube. Such a device has been designed, see Fig. VIII:29.

The X-ray power supply is a Philips PW 1010. However, this is not built for soft X-rays and a power supply which gives higher current at lower voltage is now being incorporated with the instrument.

The samples to be studied are lowered into the source housing through an air lock. The source compartment has one opening to the electron spectrometer and one to the X-ray compartment. The former is a slit, defining the electron-optical source. Different widths can be chosen for this slit, corresponding to different resolutions at which the electron spectra are recorded. The opening to the X-ray compartment is covered by a suitable X-ray filter (see Appendix 7). In order that the sample subtends a large solid angle of radiation from the X-ray anode, the sample and the anode are only 10 mm apart. It is, however, difficult to avoid heating of the source compartment by electron bombardment from defocussed electrons in the electron gun and by secondary electrons and heat radiation from the anode. Cooling of the source compartment is therefore provided and, furthermore, the beam of electrons from the gun is limited by a cooled baffle. In addition to this, provisions are made for cryostat cooling of the specimen.

An exploded view of the present source arrangement is shown in Fig. VIII:30; drawings of the same are shown in Fig. VIII:31.

As can be seen in Fig. VIII:27, the source housing is mounted on one of the vertical end walls of the spectrometer chamber, and the detector on the other end wall. Aperture defining baffles are mounted on vertical shafts that project through a plate that covers a 10 cm diameter hole in the top of the spectrometer chamber. Evacuation of the system is made by an ionisation pump and sorption pumps, by a Turbo molecular pump and rotary pump, or by an oil diffusion pump and rotary pump.

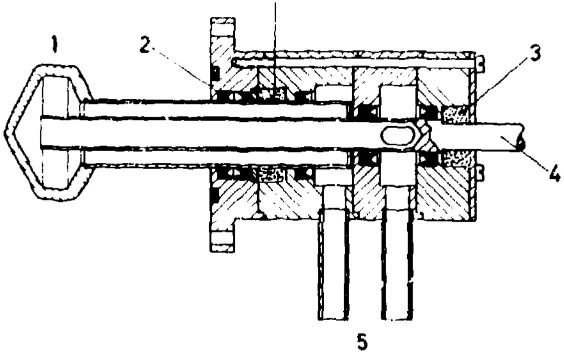

Fig. VIII:29. Drawing of a rotating anode arrangement. 1. Anode. 2. Vacuum seal. 3. Self-greasing bearing. 4. Driving-shaft. 5. Water connections.

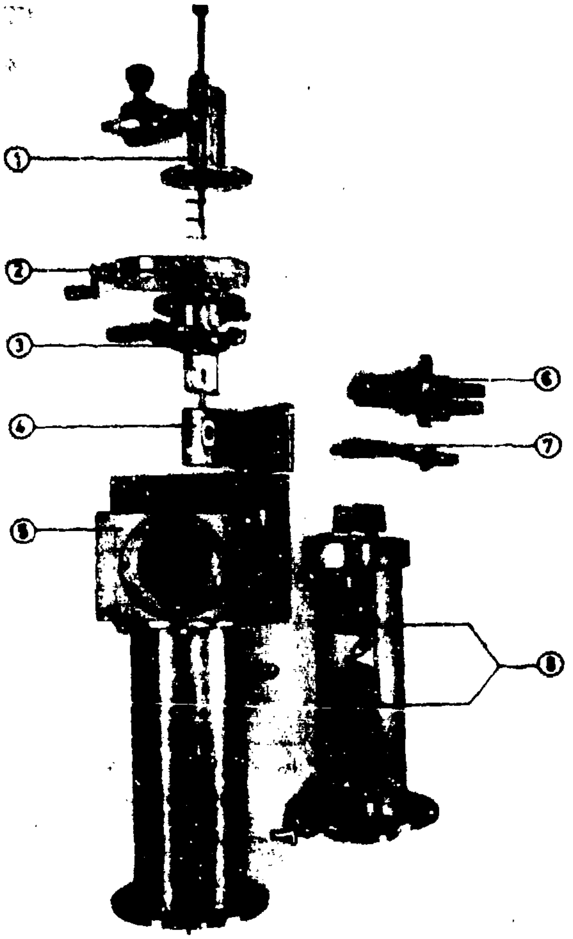

Fig. VIII:30. Exploded view of the X-ray tube and the source arrangement. 1. Air lock for the source. 2. Valve. 3. Water cooled source compartment. 4. Source housing. 5. Housing for the X-ray tube. 6. Turnable X-ray anode. 7. Water-cooled diaphragm. 8. Electron gun and high voltage feed-through.

Detection is made either photographically (see Fig. VIII:32) or by a channel electron multiplier. Photographic detection has the advantage over detection by a counter that variations in the irradiation intensity of the sample become unimportant. It has only recently been incorporated in the instrument but may turn out to be a valuable complement to the other mode of detection, especially since the plates can be scanned in the TMD[71,80] (see Section VIII:8). However, it is also possible to reduce the effect of variations in the intensity when detection is made by a counter. Instead of a single detector one can use an array of several detectors with the corresponding reduction in counting time, see Fig. VIII:33. There is also the possibility of accumulating counts from many repeated scans, each of short duration. A device for doing this is incorporated in the instrument and will be described in the following paragraph.

Recording of spectra

Automatic recording of the spectra is made in all our instruments and work is continuously in progress to develop the electronic equipment in order to attain better performance and greater versatility. Two methods for recording spectra are presently used with the new 30-cm magnetic instrument.

The first method is similar to the system used with the instrument described in Section VIII:2. A block diagram is shown in Fig. VIII:34; a photograph of the electronic equipment for the instrument is shown in Fig. VIII:35. A program unit is being constructed by which six different current intervals can be selected for study. Each interval, defined by pre-set "start" and "stop" values of the potentiometer, is scanned with a step length and a counting time per point according to pre-set values.

The power supply for the spectrometer magnet is fully transistorized. It has a long-time stability at any one field setting of $2 \cdot 10^{-6}$ and a ripple of less than $1 \cdot 10^{-4}$. The voltage drop over a temperature controlled precision resistor, coupled in series with the spectrometer, is balanced against the voltage obtained from the precision potentiometer. A slow feedback (servo motor) and a fast feedback (electronic) is provided to maintain balance.

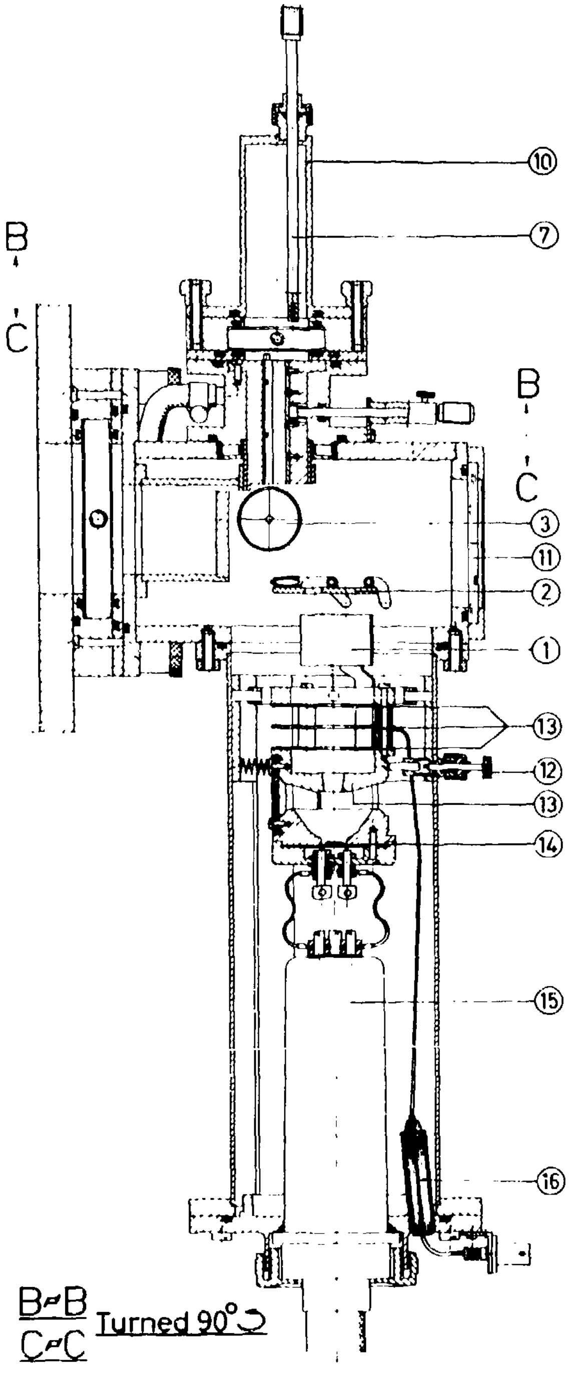

(*a*)

Fig. VIII:31. Drawings of the X-ray tube and the source arrangements. 1. Electrode for deflecting the electron beam. 2. Water-cooled diaphragm. 3. Turnable anode. 4. X-ray window. 5. Wall separating the X-ray and the electron source compartments. 6. Spectrometer entrance slit. 7. Source holder. 8. Cooling water connection. 9. To vacuum pump. 10. Air lock. 11. Glass window. 12. Screw for mechanical pivoting of the electron gun. 13. Focussing electrodes. 14. Electron gun filament. 15. High voltage feed-through. 16. Focussing voltage feed-through.

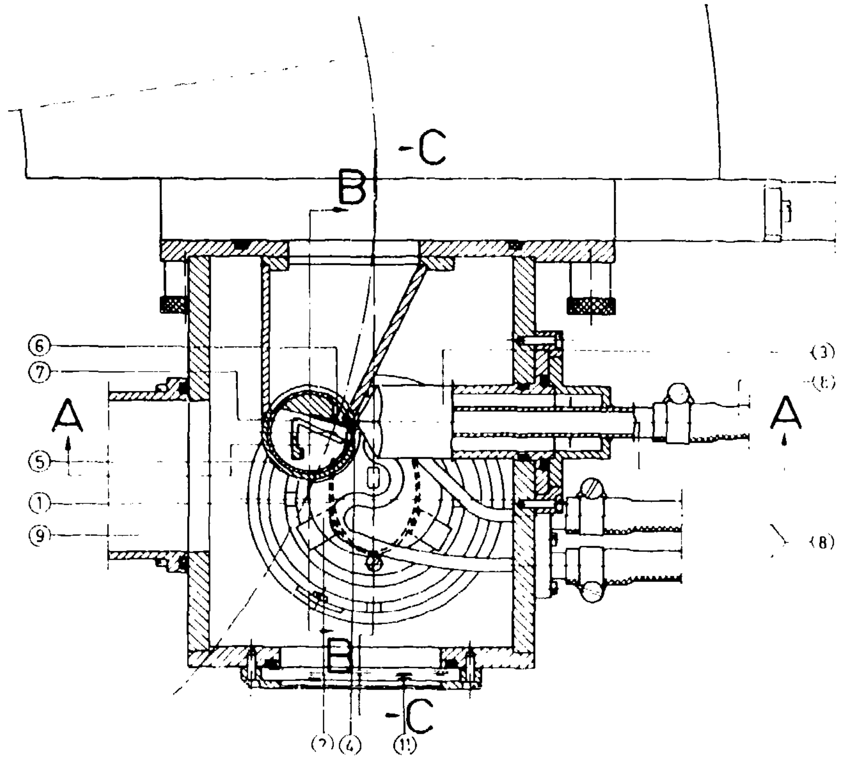

(b)

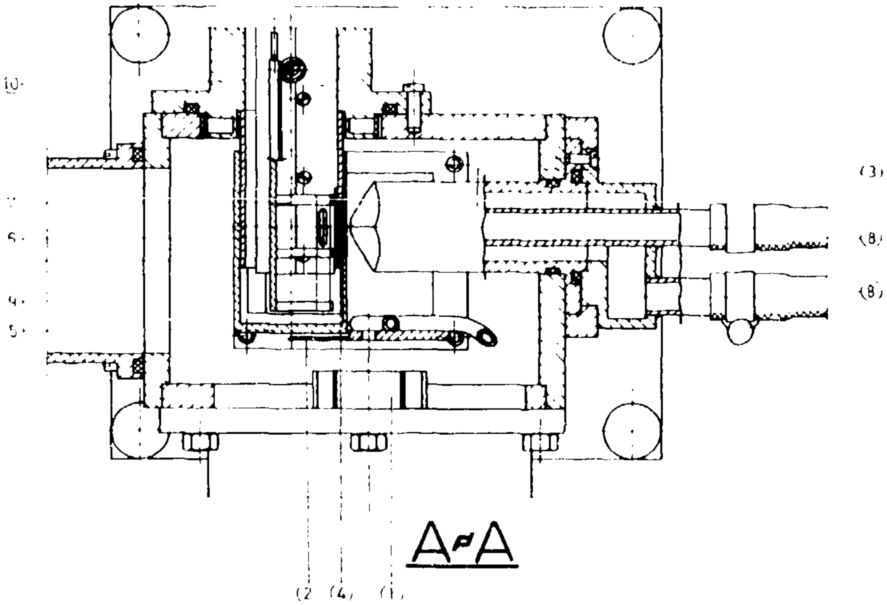

(c)

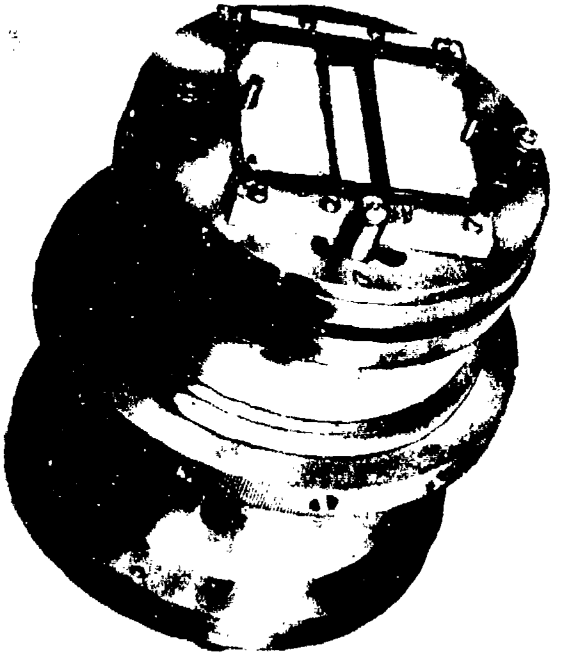

Fig. VIII:32. Photographic plate holder. The position of the plate can be adjusted without breaking vacuum. An axis through the holder is used for opening and closing the two shutter plates.

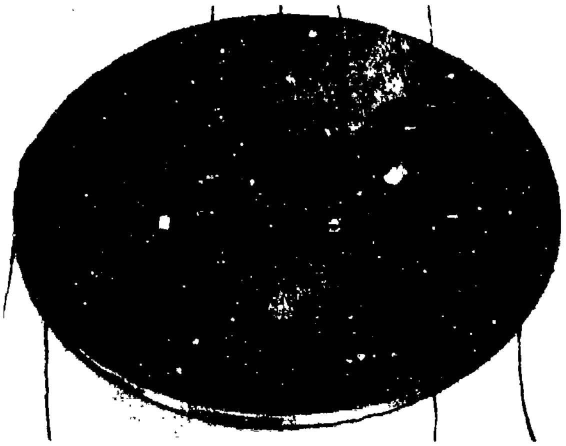

Fig. VIII:33. Array of four channel electron multipliers.

The potentiometer unit consists of a manganin resistor network with a total resistance of 25 kΩ. and a driving circuit with rotary relays by which the programmed changes of the potentiometer setting are made. A change in potentiometer setting introduces an inbalance between the voltage over the standard resistor and the potentiometer voltage. The error signal is amplified and fed back to the power supply which changes the spectrometer current so that balance is restored and the gate to the timer and scaler opens. Meanwhile, the signal from the timer that initiated the change of potentiometer setting has also initiated the printer to print out on paper tape the potentiometer setting and number of counts in the scaler. When this is done, the printer control starts the timer and scaler for the next counting cycle, provided the gate circuit is open.

The second mode of operation uses a multichannel analyser in the multiscaler mode and pulse generators for making programmed changes of the spectrometer current, see block diagram in Fig. VIII:36. A commercial power supply is employed for the spectrometer magnet in this system. It can be regulated by a program resistor and the system has a rapid response to programmed changes. A 400-channel analyser is employed which means that one counting cycle comprises up to 400 points. To avoid drifts between re-

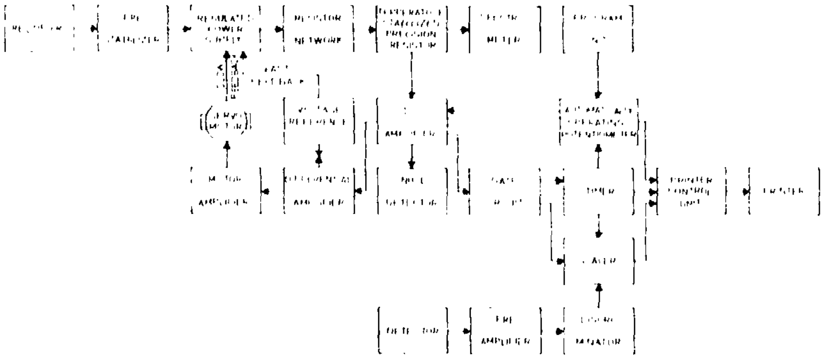

Fig. VIII:34. Block diagram showing the first method (see text) for recording spectra.

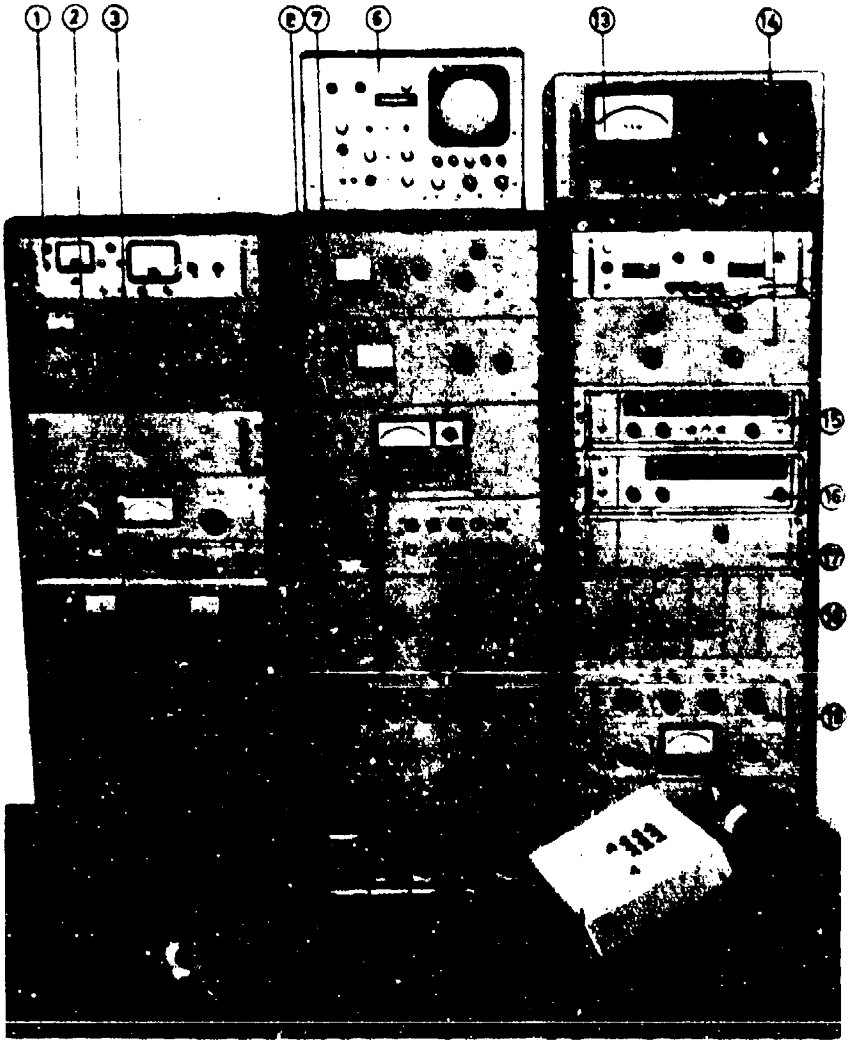

Fig. VIII:35. The electronic equipment for the new magnetic instrument. 1. Vacuumeter. 2. High voltage supply for the channel electron multipliers 3. Detector pulse discriminator. 4. High voltage supply for the ionisation pump. 5. Stepping device and current supply for the spectrometer coils in the fast stepping mode . 6. Multichannel analyser. 7. Current supply for the spectrometer coils in the slow stepping mode. 8. Null detector. 9. Automatically operating potentiometer. 10. Adjustment for current in resistor network. 11. Power supply for the potentiometer electronics. 12. Fine adjustment of start current when working in fast stepping mode. 13. Magnetometer for measurement of residual field. 14. Power supply and series resistors for Helmholtz coils. 15. Scaler. 16. Timer. 17. Printer control. 18. Control panel for pumps, cooling water, and temperature of standard cell and standard resistor. 19. High voltage supply for the focussing electrodes in electron gun. 20. Printer for potentiometer setting and number of counts.

peated cycles, the current is automatically checked and controlled at the start of each cycle. Step length and counting time at each point on the cycle are chosen according to programmed values. The accumulated counts at each point on the cycle are displayed on the screen of the multichannel analyser so that the operator can continuously follow the growth of the spectrum (see Fig. VIII:37). When he decides that a sufficient number of counts has been accumulated or when a preset number of cycles have been counted, the result is printed out.

By means of this procedure using repeated counting

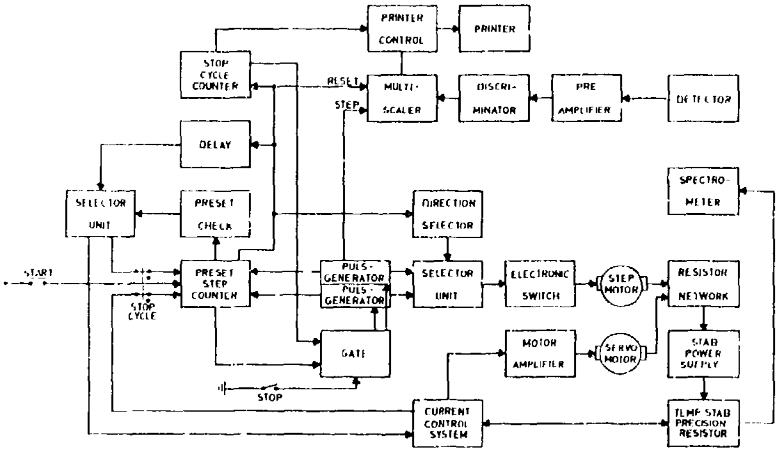

Fig. VIII:36. Block diagram showing the second mode of operation where a multichannel analyser is used for recording spectra.

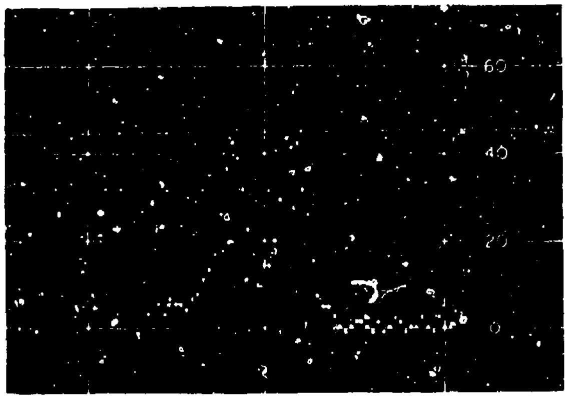

Fig. VIII:37. N_{VI} and N_{VII} electron lines from gold recorded with a multichannel analyser.

cycles, each of short duration, the variations in X-ray intensity become unimportant. This is a great virtue when one is interested not only in the chemical shifts in the ESCA spectra but also in the relative proportions of the different valence states of an element in a compound, for example as a function of time in surface reaction studies, or in elemental analysis made by ESCA.

VIII:5. The Electrostatic Spectrometer

Very few high resolution electron spectroscopic studies have previously been performed using electrostatic spectrometers. An electrostatic sector field double focussing spectrometer has, however, several advantages. There are no fields present at the source and detector positions or coils restricting the space for source and detector arrangements. Since no magnetic field is generated, the elimination of disturbing magnetic fields can be continuously controlled. There are two aberrations in electrostatic focussing devices that are not encountered in the magnetic instruments described in Sections VIII:2-4. These aberrations are due to fringing fields and relativistic effects. However, the influence from fringing fields can be reduced by grounded guard-diaphragms,[259,260] and in studying electrons with energies less than 5 keV the relativistic spread is negligible. A design study was therefore made of an electrostatic spectrometer for ESCA measurements which resulted in the construction of a new instrument.[87]

An outline of the theory for an electrostatic spectrometer and of the calculation of its focussing properties, that we have made on IBM 1620 and IBM 7090 computers, is given in Appendix 9. As the sector angle approaches 180°, the transmission-to-resolution ratio reaches a maximum. However, by using the maximum angle of 180°, the source and the detector will both be situated in the fringing field. A minor reduction of the angle will have little influence on the transmission-to-resolution ratio. A somewhat smaller sector angle could therefore be chosen and a sector angle of 157.5° was considered suitable for ESCA studies.

Electrodes and baffles

The electrostatic field is produced between sectors of two concentric spherical aluminum electrodes (Fig. VIII: 38). The radii are 32 cm and 40 cm. The sector

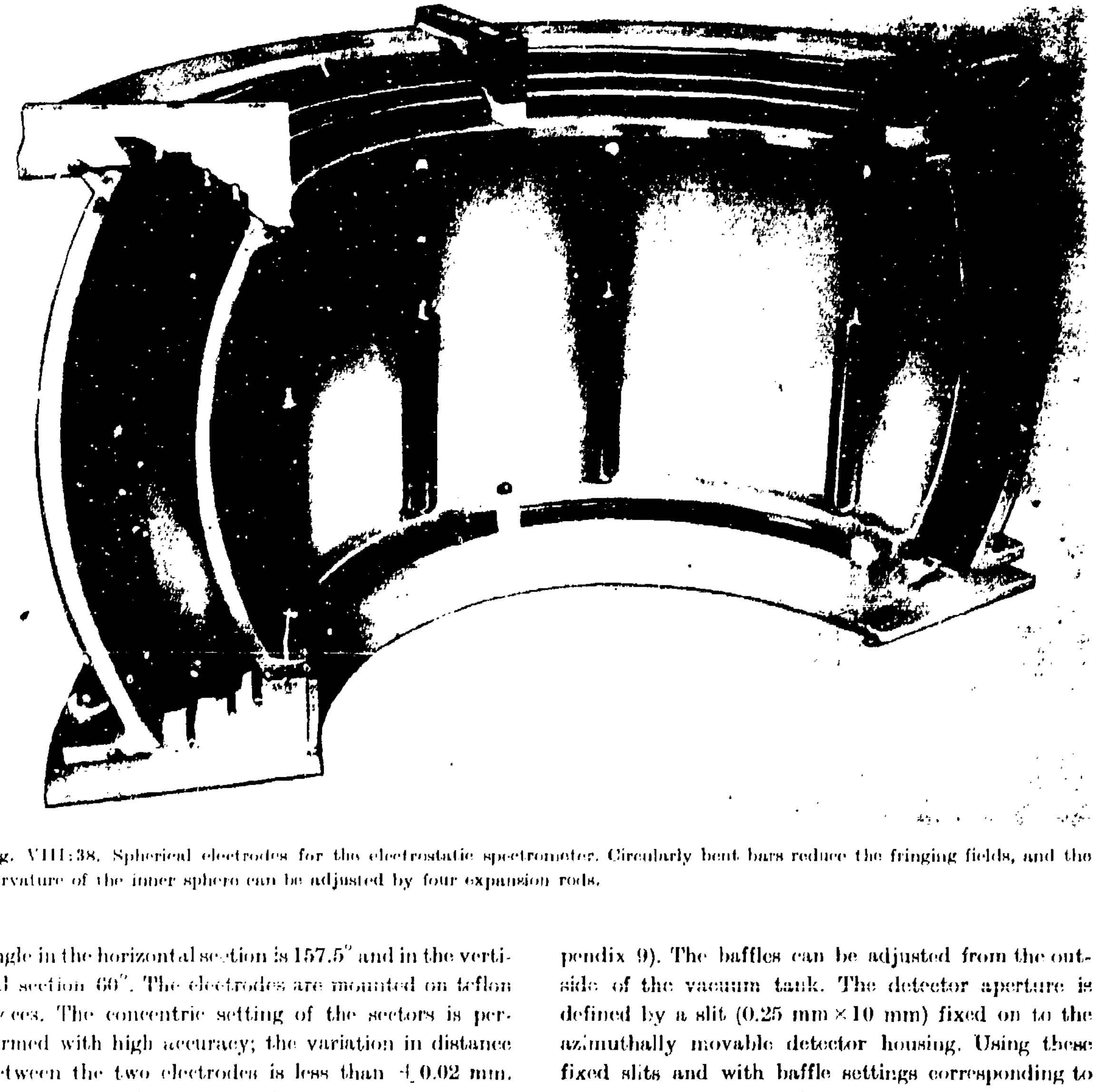

Fig. VIII:38. Spherical electrodes for the electrostatic spectrometer. Circularly bent bars reduce the fringing fields, and the curvature of the inner sphere can be adjusted by four expansion rods.

angle in the horizontal section is 157.5° and in the vertical section 60°. The electrodes are mounted on teflon pieces. The concentric setting of the sectors is performed with high accuracy; the variation in distance between the two electrodes is less than ±0.02 mm. The fringing fields at top and bottom are reduced by means of three curved bars with suitable potentials.

The end walls of the sector shaped vacuum tank in which the focussing electrodes are placed, serve as entrance and exit Herzog guard-diaphragms. A fixed slit (0.3 mm × 10 mm) placed close to the specimen, defines the electron-optical source. The accepted solid angle is defined by a system of baffles placed between the source and the electrodes (see Figs. VIII:39 and VIII:40). The vertical baffle slits are curved with radius 36 cm in order to reduce the aberrations (see Appendix 9). The baffles can be adjusted from the outside of the vacuum tank. The detector aperture is defined by a slit (0.25 mm × 10 mm) fixed on to the azimuthally movable detector housing. Using these fixed slits and with baffle settings corresponding to an accepted solid angle of 0.08 %, a resolution of 0.05 % is obtained.

Source arrangements with X-ray tube, electron gun and helium discharge lamp

The source and detector housings are mounted on the vertical end walls of the main vacuum chamber and separated from it by vacuum valves (see Figs. VIII:41 and VIII:42). Free access is therefore gained to the source and detector positions and it is easy to change source or detector without breaking vacuum

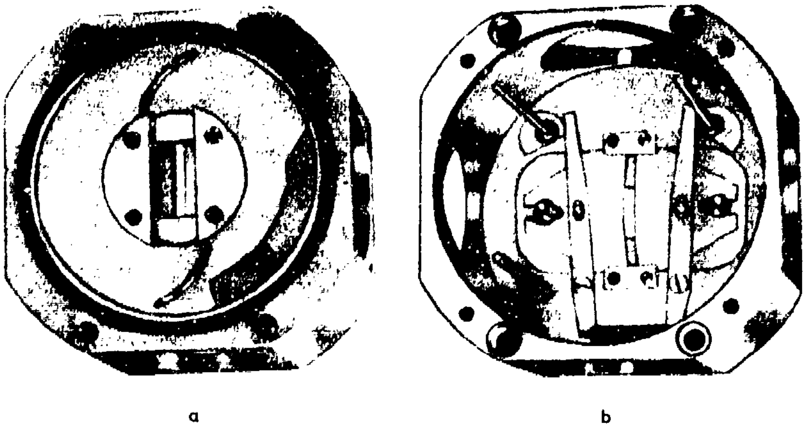

Fig. VIII:39. Adjustable electron beam defining baffles; (*a*) seen from the spectrometer side, (*b*) seen from the source side.

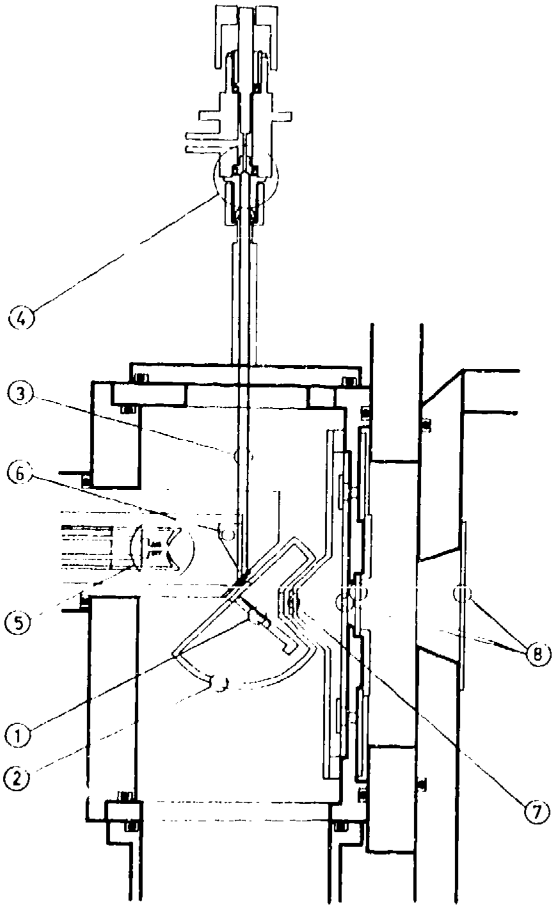

Fig. VIII:40. Horizontal section through the source housing. 1. Specimen holder. 2. Shielding cage. 3. Gas inlet tube. 4. Needle valve. 5. Cathode of X-ray tube. 6. Anode of X-ray tube. 7. Source defining slit. 8. Baffles.

in the main chamber. After letting air into the source housing, the spectrometer is in working order within two minutes. The spectrometer chamber is evacuated by a diffusion pump and a double stage roughing pump. A vacuum better than 10^{-5} torr is obtained within 20 min. The ultimate pressure is $\leq 5\cdot 10^{-7}$ torr. All components of the spectrometer are made of nonferromagnetic material. For the elimination of the earth's magnetic field, the instrument is equipped with one pair of circular coils for compensation of the vertical component and two pairs of quadratic coils for the horizontal components. For further details see Section VIII:7.

The free space around the source makes it possible to use different source arrangements. The instrument is equipped with an X-ray tube, an electron gun, and a UV light-source to expel electrons (see Section VIII:1). A drawing of the source arrangement and the X-ray tube is shown in Fig. VIII:40. The substance under investigation is deposited on a metal foil or pressed into a mesh. This foil or mesh is fixed on the grounded source holder which accomodates two different sources simultaneously. In order to eliminate scattered electrons from the anode and reduce low-energy X-radiation, the X-radiation passes through a thin aluminum foil before striking the specimen. The X-ray tube has interchangeable anodes, which are grounded and cooled by water. The cathode filament, made from tungsten wire, is placed in the center of an electrode which focusses the electrons on the anode thus giving an intense X-ray irradiation on the specimen. The power for the X-ray tube is taken from a Philips PW 1010 X-ray power supply.

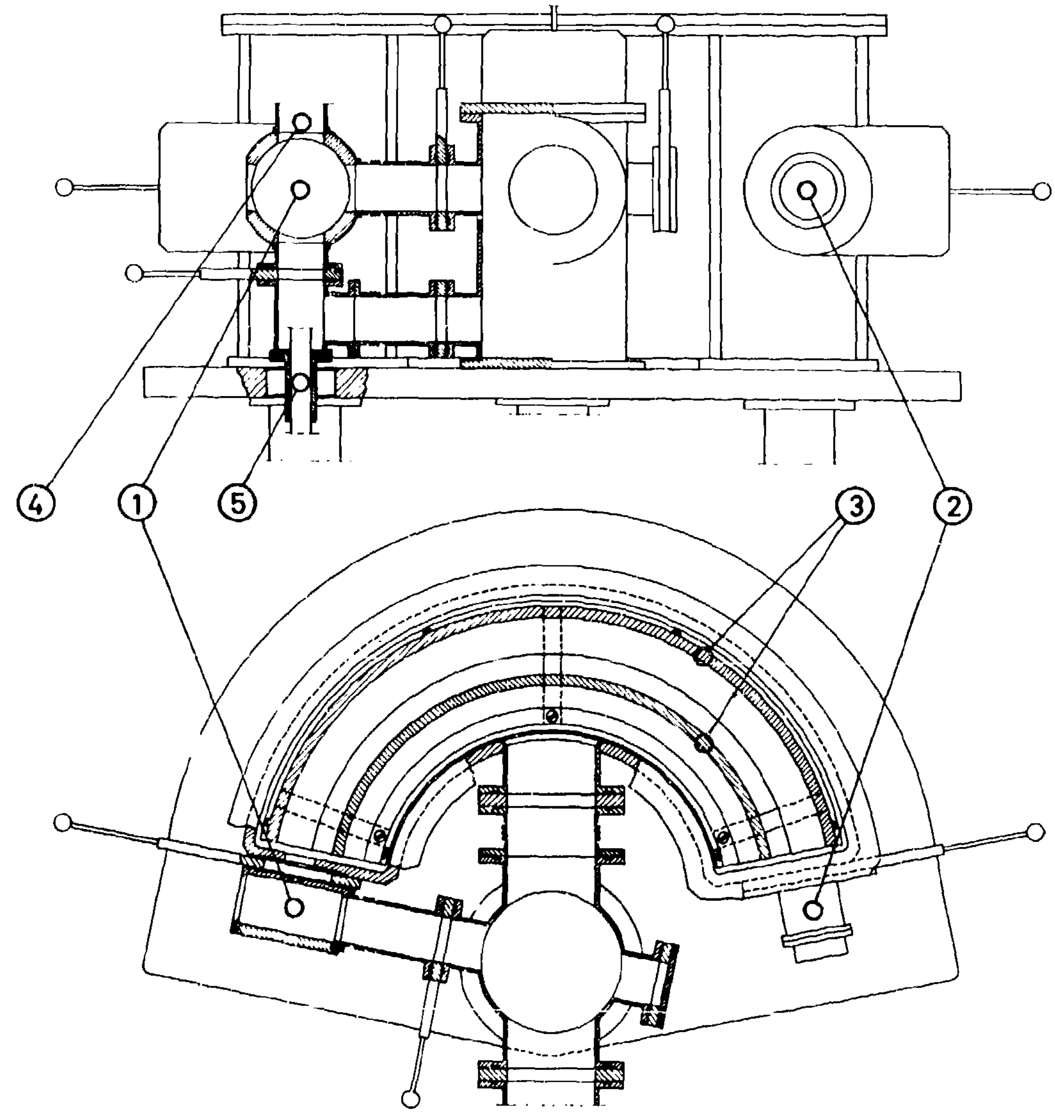

Fig. VIII:41. Drawing of the vacuum system, source and detector housings. 1. Source housing. 2. Detector housing. 3. Spherical electrodes. 4. Cryostat position. 5. Specimen inlet.

It is possible to lower or to raise the temperature of the specimen. The upper part of the specimen holder can either be connected to a cryostat containing liquid nitrogen or helium or to a heater. It is thermally insulated from the rest of the holder. To decrease the thermal radiation on the specimen and its holder, it is shielded with a cage in thermal contact with the cryostat. A cooled backing foil makes it possible to study compounds which are not solid at room temperature and low pressure. The gas or the vapour is fed through a stainless steel tube into the housing and on to the cooled foil. On the cooled foil, the compound condenses and can be studied in the normal way. The flow is regulated by a needle valve. With this freezing technique, one obtains specimen surfaces with very little adsorbed pump oil and gases. Thereby the absorption of elec-

Fig. VIII:42. Photograph of the electrostatic instrument with X-ray tube, cryostat and vapor inlet system.

trons from the specimen decreases. This can increase the intensity considerably.

The experimental arrangement for measurements with electron excitation is shown in Figs. VIII:43 and VIII:44. An electron gun with a direct heated tungsten filament, produces a vertical electron beam, which is directed into a collision chamber. A 0.2 mm slit in the chamber defines the electron-optical source. The gases or vapors under study are fed into the chamber at a rate determined by a needle valve. When the electron beam has passed the collision chamber it is collected by a Faraday cage. The current from this cage is the input signal to a servo system which monitors the beam intensity by regulating the retarding voltage of the first grid in the electron gun. The electrons can be accelerated up to 10 keV. A typical beam current is 1 μA. High absorption in the collision chamber and low absorption in the main spectrometer tank is desired. This is achieved by separate evacuation of the collision chamber region. It is possible to have a pressure of 10^{-2} torr in the collision chamber and 10^{-5} torr in the main spectrometer tank.

The gas discharge tube shown in Fig. VIII:45 is the light source for those measurements where UV-radiation is used to expel the electrons. The discharge is produced in helium which flows through the tube at a pressure of about 1 torr. In the discharge, the helium resonance line at 584 Å (21.21 eV) predominates. The radiation is collimated to a narrow beam by a capillary tube, which has an arrangement for differential

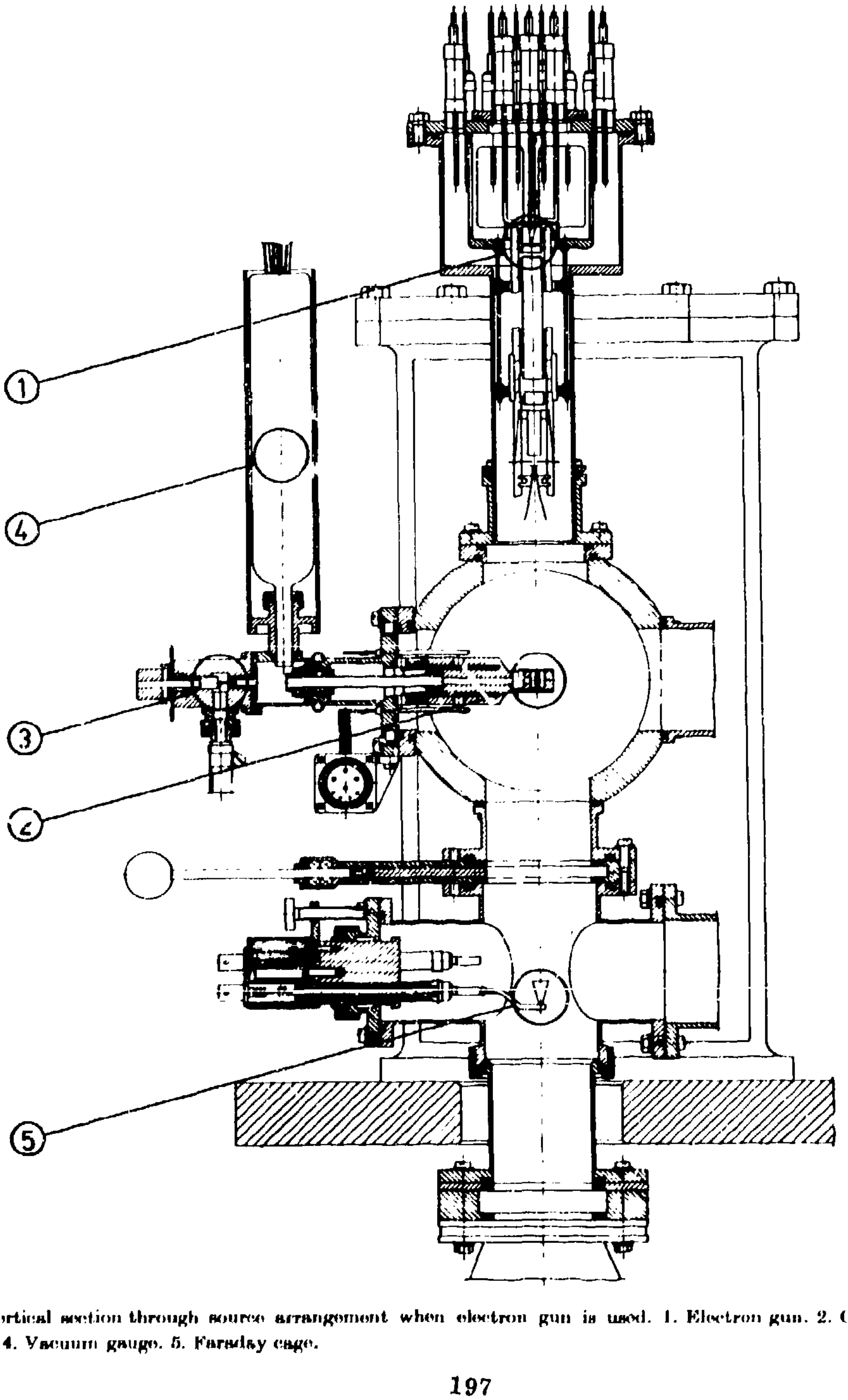

Fig. VIII:43. Vertical section through source arrangement when electron gun is used. 1. Electron gun. 2. Collision chamber. 3. Needle valve. 4. Vacuum gauge. 5. Faraday cage.

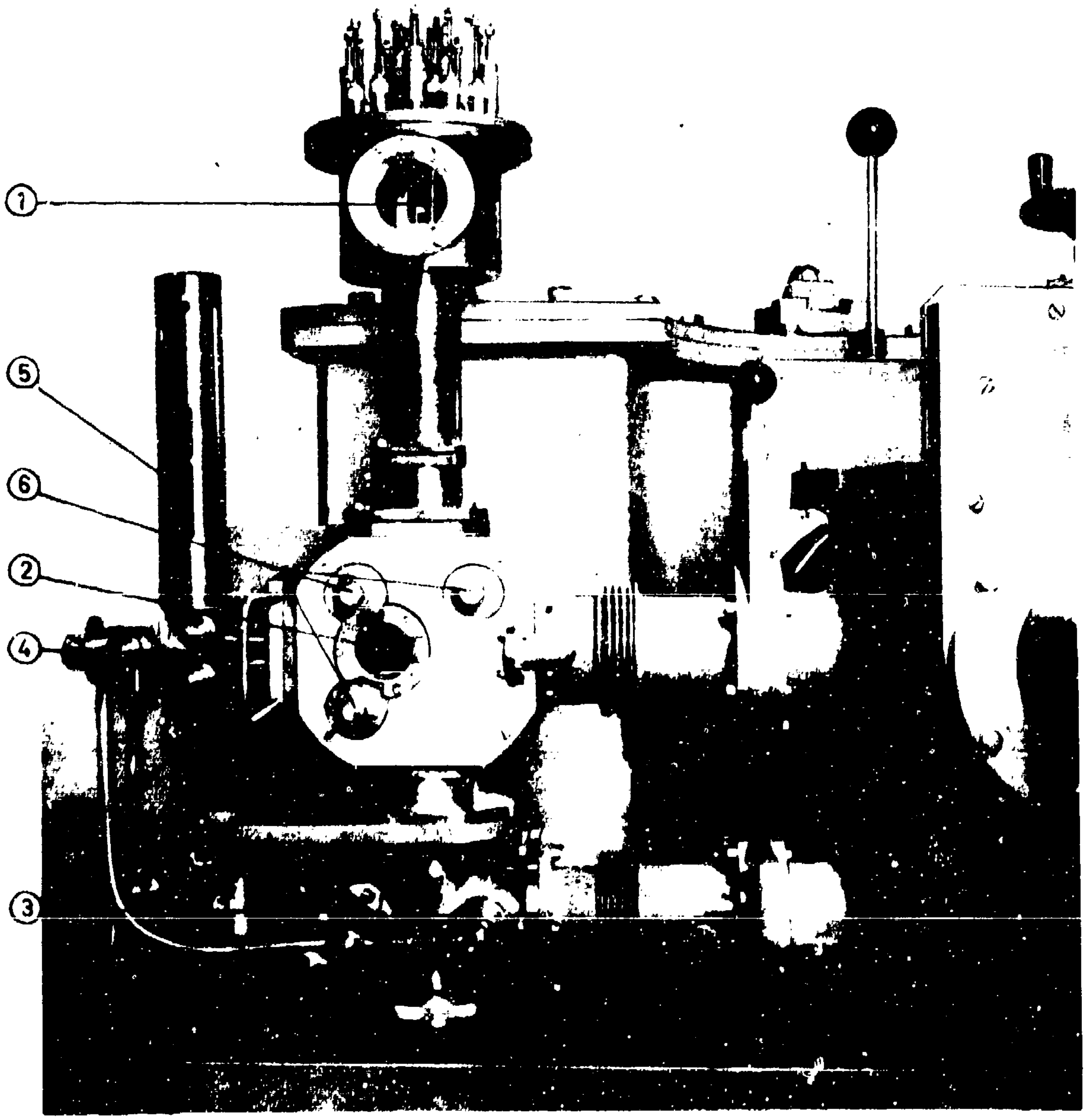

Fig. VIII:44. Photograph of the arrangement for excitation by electron impact. 1. Electron gun. 2. Collision chamber. 3. Faraday cage. 4. Needle valve for gas to the collision chamber. 5. Vacuum gauge. 6. Baffle adjustment.

pumping. The beam is directed vertically into the same collision chamber as used in the electron excitation measurements.

A channel electron multiplier is used as detector for the electrons.

Voltage regulation and data recording

Fig. VIII:46 shows a block diagram of the voltage regulation and data recording system. The focussing voltage is obtained from a high stability high accuracy voltage supply (stability $25 \cdot 10^{-6}/7$ days, accuracy 0.01 %). The voltage is measured with a digital voltmeter. Ground potential is obtained at the central orbit of the spectrometer by means of a voltage divider.

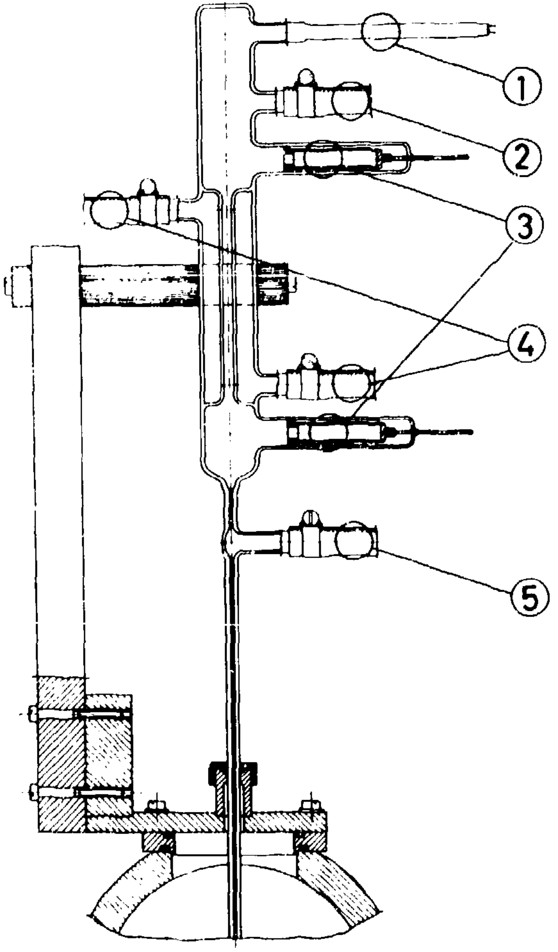

Fig. VIII:45. Vertical cut through the capillary discharge tube for UV excitation of electron spectra. 1. Vacuumeter. 2. Helium inlet. 3. Electrodes. 4. Water cooling connections. 5. Pump connection.

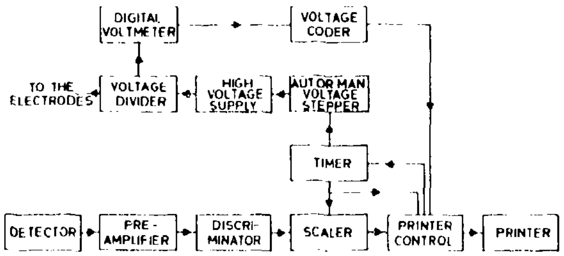

Fig. VIII:46. Block diagram of voltage regulation and data recording system when a stepping voltage supply is used.

By means of step motor driven switches, the focussing voltage is changed by pre-set steps. It is possible to step either up or down and also to program the stepping so that it proceeds a pre-set number of steps in one direction, changes step direction and steps back to the starting voltage. This procedure is repeated as many times as required. The counting time per step can be varied between 4 s and $4 \cdot 10^2$ min. After each point, the number of counts obtained and the focussing voltage are printed out. The electronic equipment is shown in Fig. VIII:47.

Spectra can also be recorded on a multichannel analyser (see Section VIII:4). Fig. VIII:48 shows a block diagram of the voltage regulation and data recording in this case. A sawtooth voltage is superimposed on a fixed voltage. The start of the sawtooth sweep is synchronized with the start of the multichannel analyser operated in multiscaler mode. This means that the channel number is changed synchronously with the focussing voltage. The sawtooth sweeptime can be varied between 0.01 s and 10 s and the amplitude between 0.1 V and 10 V. The recording is repeated until good statistics is reached. This way of recording smoothes out intensity variations during the recording.

Some spectra obtained with the different modes of excitation

Several spectra recorded with the electrostatic instrument have been shown in previous chapters (see e.g. Chapter I and VI). Some more examples will now be given of spectra obtained by the three modes of

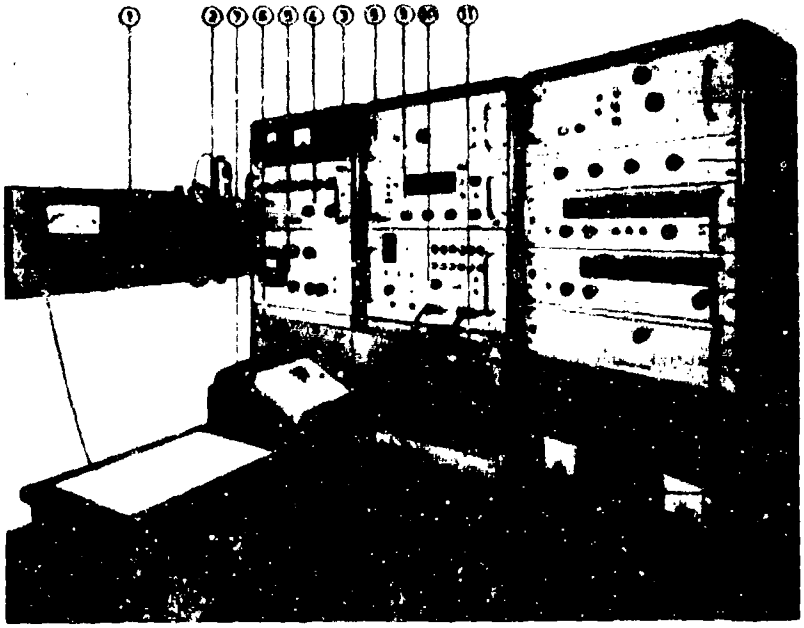

Fig. VIII:47. The electronic equipment. 1. Magnetometer for measurement of residual field. 2. Temperature controlled voltage divider. 3. Vacuumeter. 4. High voltage supply for the channel electron multiplier and for the Geiger counter with post-acceleration. 5. Potential divider for the post-acceleration system. 6. Discriminator. 7. Printer for the digital voltmeter and counter. 8. Unit for the print out of the digital voltmeter. 9. Digital voltmeter. 10. Control unit for the stepping of the focussing voltage. 11. Focussing voltage supply. 12. High voltage supply for the electron gun. 13. Servo-control of the vertical magnetic field. 14. Series resistors for the Helmholtz coils compensating the horizontal magnetic field 15. Scaler. 16. Timer. 17 Printer control. 18. Control panel for the pumps, cooling water and security circuits. 19. Power supply for the Helmholtz coils.

excitation that are used with the instrument and from samples in the solid, liquid, and gaseous phases.

Firstly, spectra of mercury and cadmium are shown in Fig. VIII:49. Liquid mercury was attached to a copper mesh. Since mercury has a low vapour pressure compared to most liquids, it does not evaporate so rapidly as to necessitate special provision for a continuous supply of the liquid. Hg N_{VI}, N_{VII}, O_{IV}, and O_V lines are shown in Fig. VIII:49a and b, the last two separated by only 1.9 eV. Cadmium was evaporated on a cadmium foil and Fig. VIII:49d shows the cadmium $N_{IV,V}$ line. Moreover, cadmium amalgam was studied and it was possible to resolve graphically Hg O_{IV} and O_V from Cd $N_{IV,V}$ as shown in Fig. VIII:49e. Al$K\alpha$ radiation was used to excite the spectra.

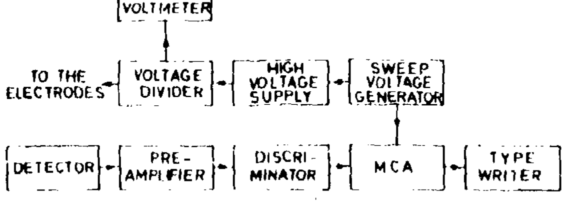

Fig. VIII:48. Block diagram of voltage regulation and data recording system when a multichannel analyser is used.

As mentioned earlier, the freezing technique gives high intensity. This makes it easy to study the low intensity spectra of molecular orbitals. The results from measurements on water are shown in Fig. VIII:50. The specimen holder was cooled by liquid nitrogen and Al$K\alpha$ radiation was used to expel the electrons. In addition to the molecular orbital levels, Fig. VIII:50 shows the oxygen 1s and 2s atomic levels. Here we can observe the broadening of the 2s levels owing to solid state and molecular effects (see Section III:2).

Fig. VIII:51 shows some Coster-Kronig and Auger electron lines from krypton. The electron gun was used for the excitation of these spectra. The Auger

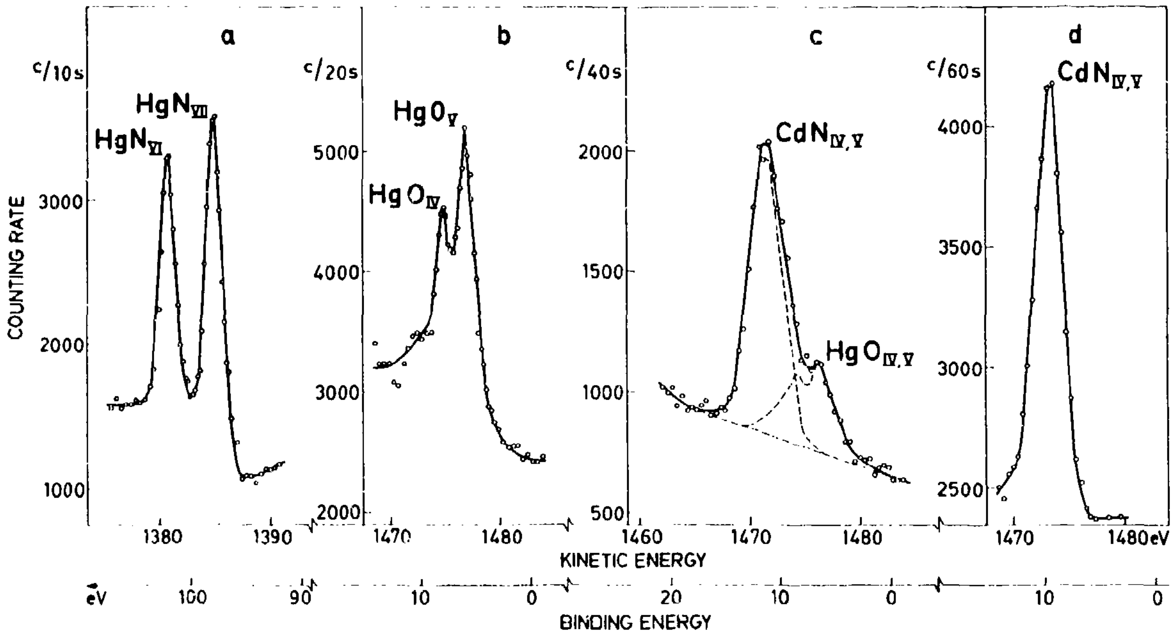

Fig. VIII:49. Electron spectra from mercury (*a*, *b*), cadmium amalgam (*c*) and cadmium (*d*), excited by Al*Kα*.

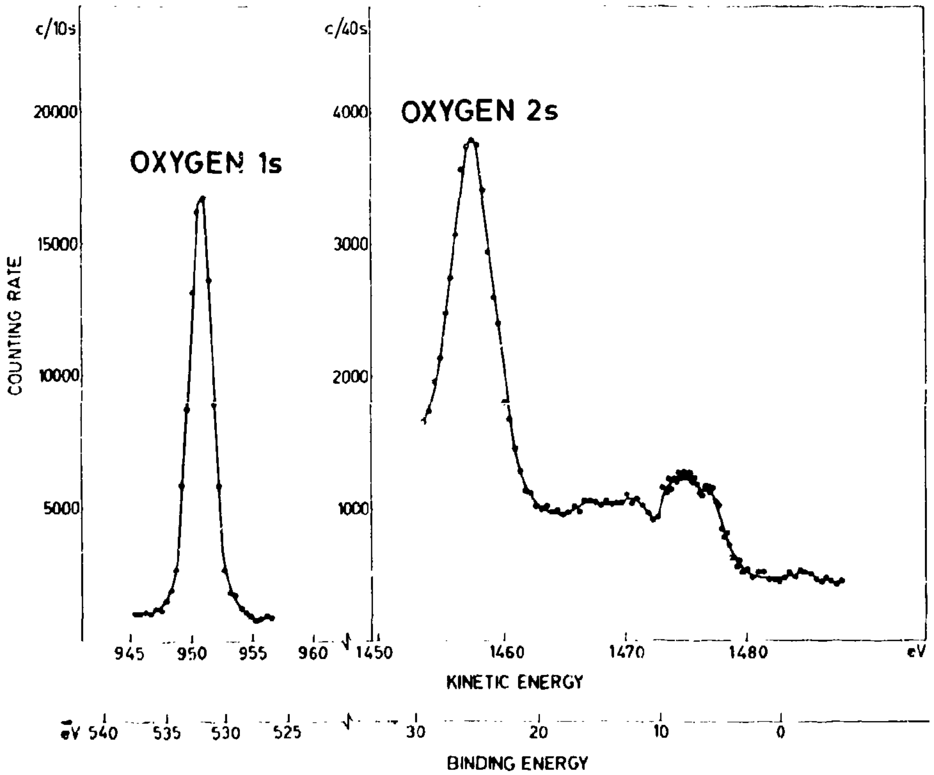

Fig. VIII:50. Electron spectrum from ice showing core electrons of oxygen and molecular orbitals excited by Al*Kα*.

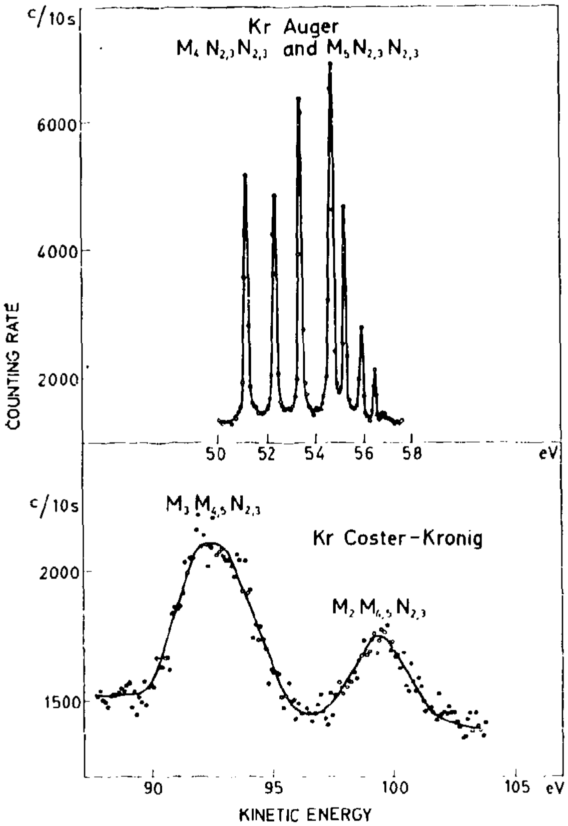

Fig. VIII:51. Coster-Kronig and Auger electron spectra from krypton excited by electron impact. The electron lines corresponding to the different transitions within the $M_3 M_{4,5} N_{2,3}$ and $M_2 M_{4,5} N_{2,3}$ groups are much broader than the Auger lines in the upper part of the figure and coalesce to two lines in the electron spectrum. This is due to the Coster-Kronig broadening of the M_2 and M_3 levels.

electron lines have a half width of 0.1 eV whereas the Coster-Kronig transitions are seen as broader distributions. The complete $M_{4,5}NN$ spectrum is shown in Fig. VI:8, and the interpretation of the spectrum is also discussed there.

The electron spectrum shown in Fig. VIII:52 is excited by helium resonance radiation and with benzene as target gas. The electrons were accelerated out of the collision chamber by about 25 V in order to increase the intensity. Several vibrational bands are seen corresponding to different ionization potentials. The energy calibration is tentative. Benzene has recently been studied by Clark and Frost[236] and by Turner[237] with similar techniques.

An electron spectrum of molecular hydrogen, excited by the helium resonance radiation is shown in Fig. VIII:53. Electrons are expelled from the hydrogen molecules in the ground state $X\,^1\Sigma_g^+$ and the molecule ions are left in the ground state $X\,^2\Sigma_g^+$. The potential curves for these two states are shown in Fig. VIII:54, which also shows some of the vibrational levels involved in the transitions seen in the spectrum.

The kinetic energy E_{kin} of an expelled electron is given by:

$$E_{\text{kin}} = E_{\text{photon}} - E_{\text{el}} - E_{\text{vibr}} - E_{\text{rot}} - E_{\text{rec}} - \varphi \qquad (6)$$

where E_{photon} is the photon energy of the UV radiation, E_{el} is the ionization energy, E_{vibr} is the difference in vibrational excitation energy of the molecule ion and the molecule, E_{rot} is the difference in rotational energy between the molecule ion and the molecule, E_{rec} is the recoil energy of the molecule ion which is usually negligible (see eq. (2) in Chapter II), and φ is due to contact and surface potentials in the spectrometer. The neutral molecule is normally not excited vibrationally. Therefore the following approximate expression holds for a diatomic molecule:

$$E_{\text{vibr}} = hc[\omega_e(v + \tfrac{1}{2}) - \omega_e x_e(v + \tfrac{1}{2})^2 - \tfrac{1}{2}\omega_e + \tfrac{1}{4}\omega_e x_e] \qquad (7)$$

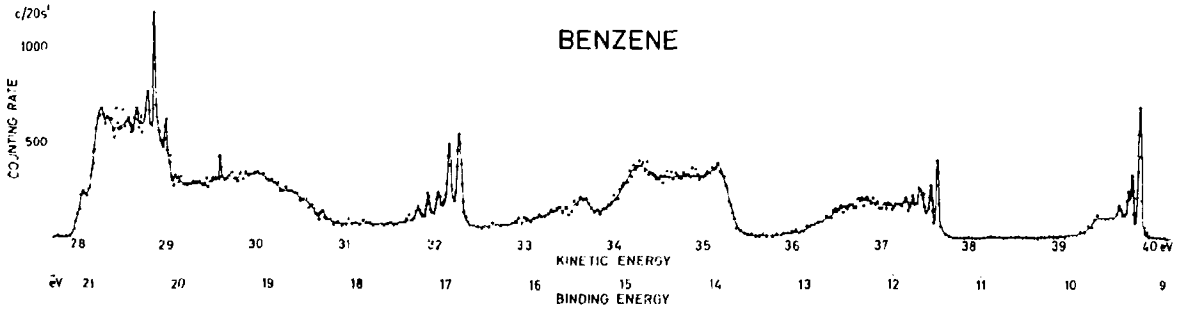

Fig. VIII:52. Electron spectrum from benzene excited by helium resonance radiation.

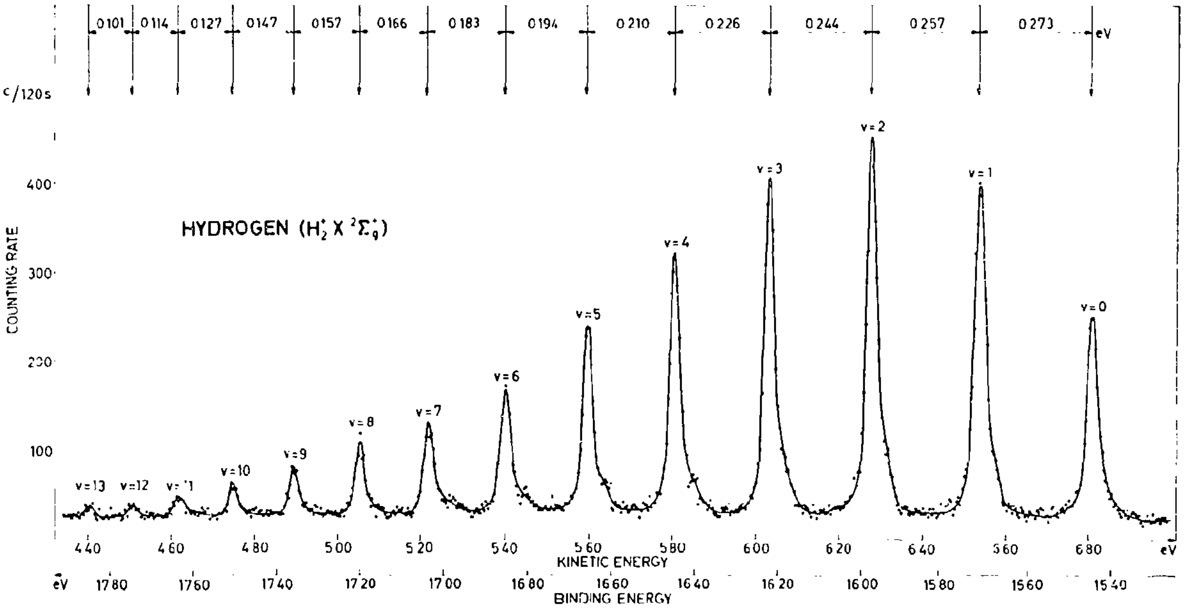

Fig. VIII:53a. Electron spectrum from molecular hydrogen, excited by helium resonance radiation. Fourteen peaks are seen, which correspond to vibrational levels of the molecule ion.

where v is the vibrational quantum number and ω_e and $\omega_e x_e$ are the first two expansion coefficients for the anharmonic oscillator; v, ω_e and $\omega_e x_e$ all refer to the molecule ion. From eqs. (6) and (7) it thus follows that the electron spectrum can show vibrational structure caused by vibrations of the molecule ion. For hydrogen this is seen in Fig. VIII:53a. The measured separations between the vibrational peaks are indicated in the figure and agree with those calculated from eq. (7), with ω_e and $\omega_e x_e$ values quoted by Herzberg.[223] The intensities of the peaks are determined by the Franck-Condon factors for the transitions.

For E_{rot} the following approximate expression holds:

$$E_{\text{rot}} = \frac{\hbar^2}{2M}\left(\frac{1}{r_0'^2} - \frac{1}{r_0^2}\right)J^2 + AJ + B \tag{8}$$

where r_0 and r_0' are the internuclear separations in the molecule and the molecule ion respectively, M is the mass of the molecule, J is the rotational quantum number and A and B are constants. Depending on whether E_{rot} is positive or negative rotational structure will be observed on the low or high energy side of the vibrational peak. For large J values E_{rot} is dominated by the first term in eq. (8) and is positive or negative depending on whether the molecule contracts or

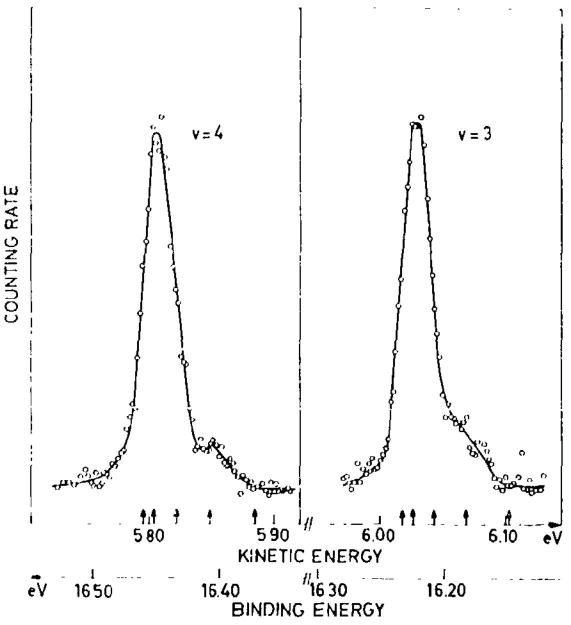

Fig. VIII:53b. More detailed recordings of the peaks corresponding to $v = 3$ and $v = 4$ for the molecule ion, showing rotational structure. The arrows indicate the positions of some of the individual rotational peaks for which $\Delta J = 0$.

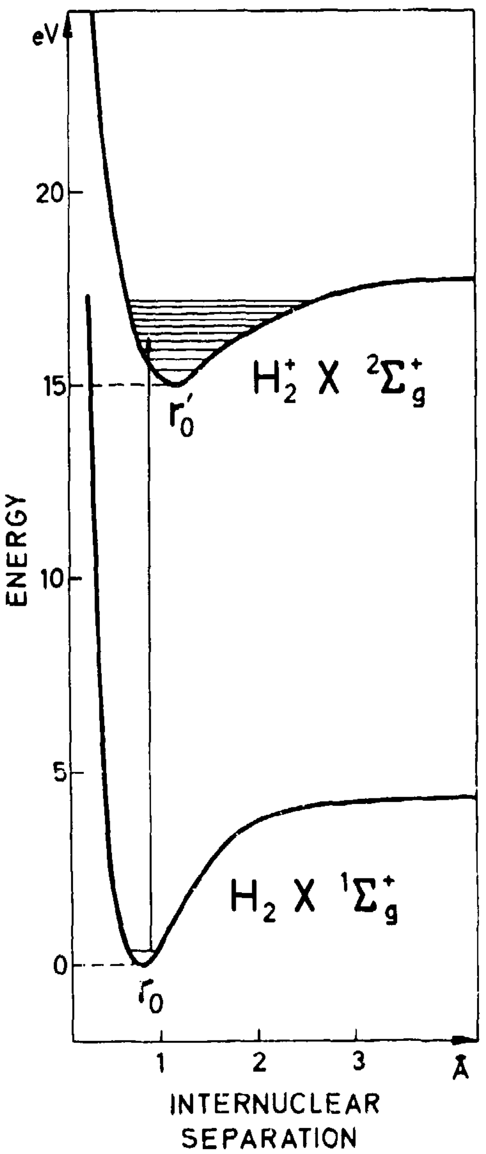

Fig. VIII:54. Potential curves for the hydrogen molecule and molecule ion in their ground states. The vibrational levels of the molecule ion are those observed in the electron spectrum shown in Fig. VIII:53. The arrow indicates a possible transition for the molecule upon ionization. The energy of the molecule then increases by $E_{el} + E_{vibr} + E_{rot}$, see eq. (7).

expands upon ionization. When the hydrogen molecule is ionized to the state $X\,^2\Sigma_g^+$ it expands, as shown in Fig. VIII: 54, and the rotational structure is observed on the high energy side as seen in Fig. VIII: 53 b.

The individual rotational lines have a width which is mainly determined by the following effects:

1. Self-reversal in the light source.
2. Doppler spread in the photoionization process:

$$\Delta E = \text{const.}\sqrt{T/M}$$

3. Time and local variations of the surface potentials in the collision chamber and on the baffles. Inside the spectrometer the local surface potentials will level out.
4. Spectrometer aberrations.

For hydrogen the Doppler spread dominates and is about 20 meV, and therefore the individual rotational peaks are not resolved. The Doppler spread can be reduced by using a molecular beam as a target for the UV radiation. We are now investigating the possibilities of using such a device.

VIII:6. The 50-cm Iron-free Instrument

Electron spectroscopy has been developed to a high degree of precision for the study of nuclear structure. High-precision spectroscopy calls for instruments of high resolution, and double focussing magnetic spectrometers have become widely used in the field of high resolution beta-ray spectroscopy, since they give the required high transmission at high resolution. Although an excellent tool for nuclear spectroscopy, the first 30-cm iron-free instrument described in Section VIII:2 soon became used exclusively for the development of ESCA. A new high precision, high resolution instrument was then built for nuclear spectroscopy work[30,46] (see Fig. VIII:55). This instrument was designed to meet a number of requirements in addition to those of the earlier instrument. Some of these requirements, such as the improved access to the source and detector regions and the higher dispersion (radius of central orbit is 50 cm), apply also if the instrument is used for ESCA. The instrument has now also been adapted for ESCA studies, and it is used both for nuclear spectroscopy, mainly high precision determinations of energies and intensities in internal conversion spectra, and for atomic spectroscopy of the extranuclear structure.

The spectrometer is situated in a laboratory which is specially built for this instrument. No ferromagnetic materials were used in the building construction and all equipment containing iron is placed far away from the spectrometer. By using two pairs of circular com-

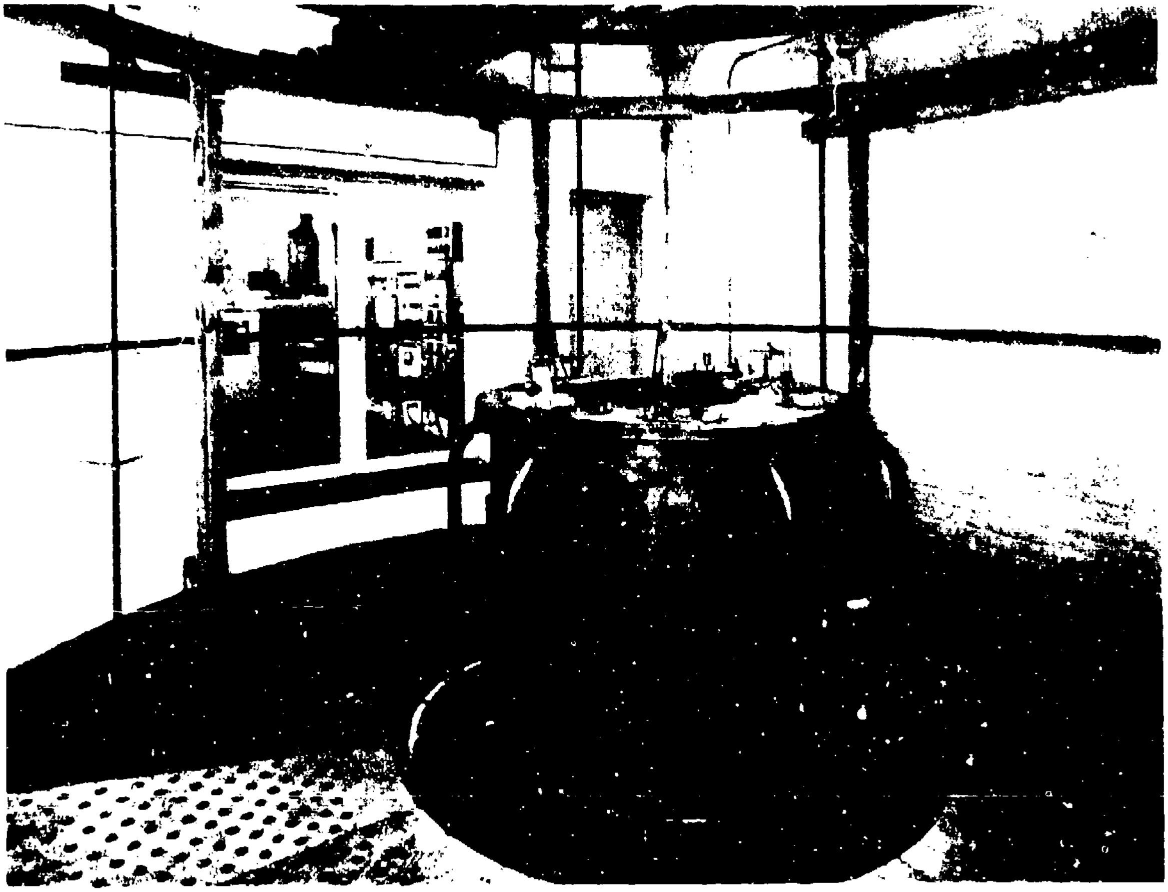

Fig. VIII:55. Photograph of the 50-cm iron-free spectrometer. The coil windings are enclosed in tanks through which transformer oil is pumped for cooling. The probe for measuring the residual magnetic field is seen to the right.

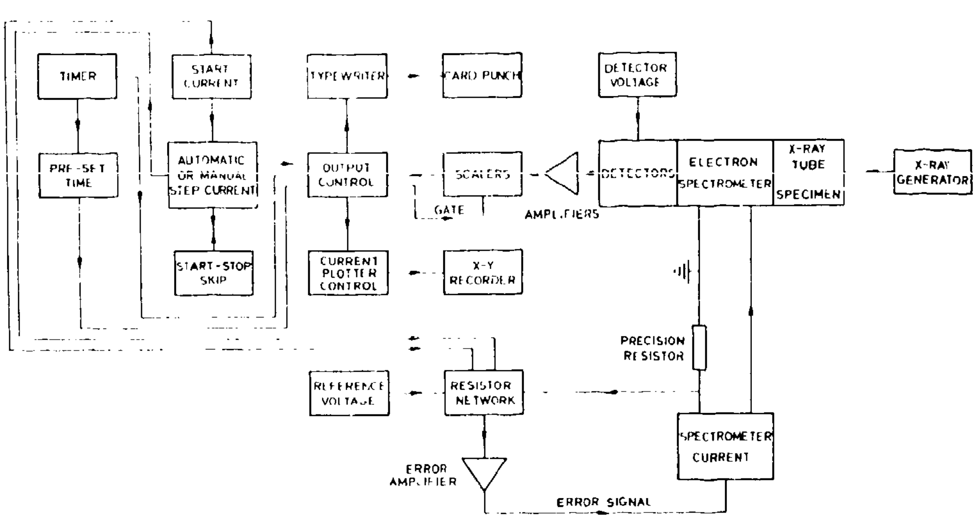

Fig. VIII:56. Block diagram of the automatic current regulation and data recording system for the 50-cm instrument.[46]

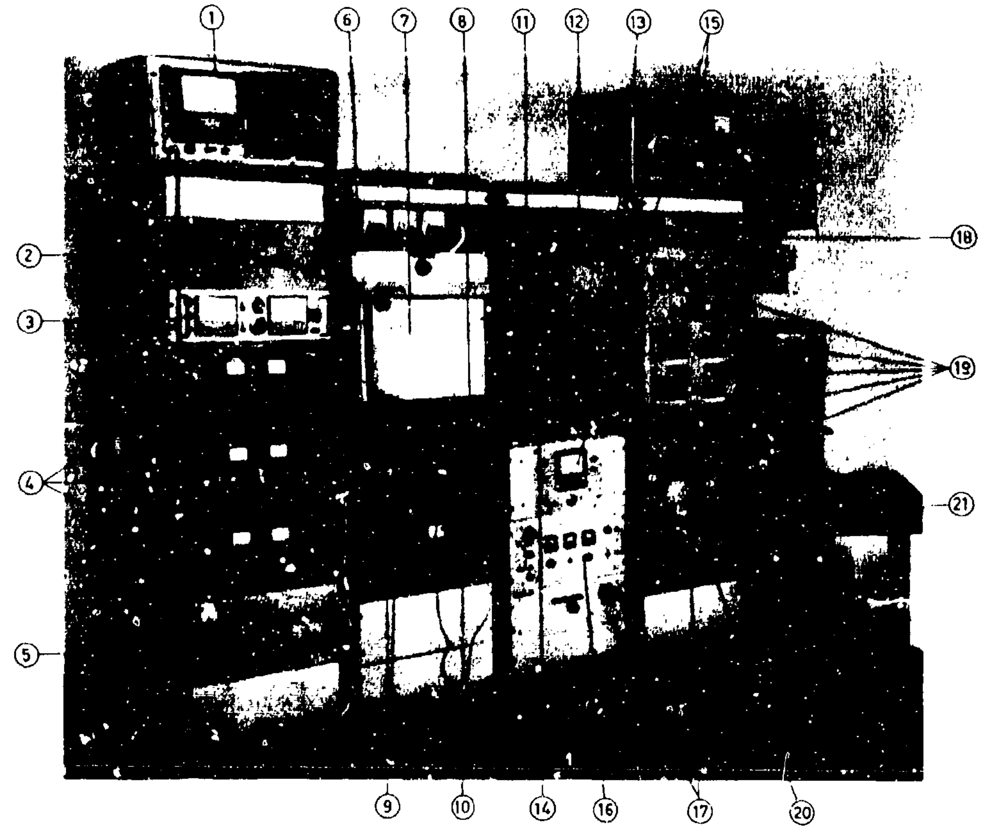

Fig. VIII:57. The electronic equipment for the 50-cm instrument:
1. Magnetometer for measurement of residual magnetic field. 2. Unit for automatic regulation of the vertical component of the magnetic field. 3. Detector voltage supply. 4. Power supplies for the Helmholtz coils. 5. Voltage supply for the multistrip source. 6. Precision resistor selector and remote on-off control of spectrometer current supply. 7. x-y-recorder. 8. Curve plotter control unit. 9. Error amplifiers. 10. Resistor network. 11. Start current selector. 12. Clock. 13. Pre-set time unit. 14. Program unit for start and stop skip, maximum current and step length. 15. Vacuum meters. 16. DC current supply for the electronics. 17. Data output control units, connected to IBM typewriter and IBM card punch (not shown on the figure). 18. High voltage supply. 19. Scalers. 20. Current and voltage supply for amplifiers. 21. High precision potentiometer. Above the potentiometer, the galvanometer amplifier and the galvanometer are seen.

pensating coils, it is possible to eliminate the vertical component of the earth's magnetic field completely. The residual vertical component of the field is within $\pm 10^{-4}$ G over the entire spectrometer area. The elimination of this component is automatically controlled using the method described in Section VIII:7 for the electrostatic instrument. The magnetic field originating from the spectrometer is eliminated at the position of the magnetometer probe by the use of a small coil connected in parallel with the spectrometer and the precision resistor. In the horizontal directions, the residual magnetic field is within $\pm 5 \cdot 10^{-4}$ G. The temperature of the spectrometer room and of the spectrometer coils are kept constant to within $\pm 0.2^\circ$ C. This temperature stability and the exceptionally good elimination of the earth magnetic field enables very accurate energy determinations with the spectrometer. The instrument also has a high resolution at a fairly good transmission. For example, the best resolution obtained is 0.012 % and the transmission at a spectrometer aberration of 0.04 % is about 0.09 %.

The current through the spectrometer coils is automatically regulated and the short time stability of the current is of the order of $3 \cdot 10^{-6}$. The long time stability and the accuracy in the definition of the current is not as good ($\approx 1.5 \cdot 10^{-5}$), so when the highest preci-

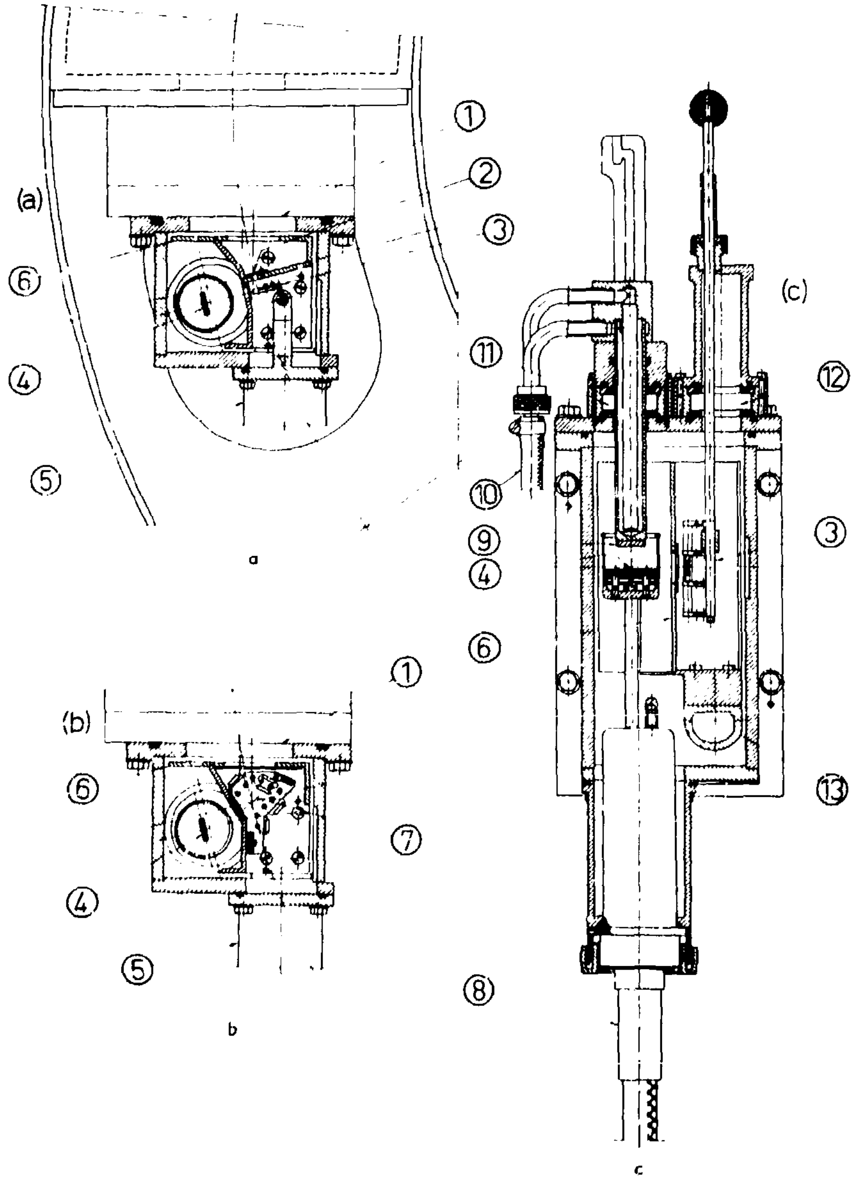

Fig. VIII:58. X-ray tube and source arrangement used in the 50-cm spectrometer. The single strip source arrangement is shown in both a horizontal (*a*) and a vertical (*c*) section. A horizontal section of the multistrip source arrangement is given in (*b*). The specially indicated parts are:

1. Opening to the spectrometer. 2. A narrow slit used to define the position of the source. 3. Single strip source holder, where three different specimens can be placed. 4. Filament of the X-ray tube, surrounded by a focussing cylinder. 5. Connection to the prevacuum system and a liquid nitrogen cryostat. 6. Inner walls insulated from the housing. 7. Multistrip source holder with potential divider. 8. Connection to the X-ray generator. 9. Anode of the X-ray tube. 10. Inlet and outlet of water used for cooling the anode. 11. Air lock for exchanging the anode without breaking vacuum. 12. Air lock for exchanging the source without breaking vacuum. 13. Connection between the inner walls of the source compartment and a cold finger cooled by the cryostat.

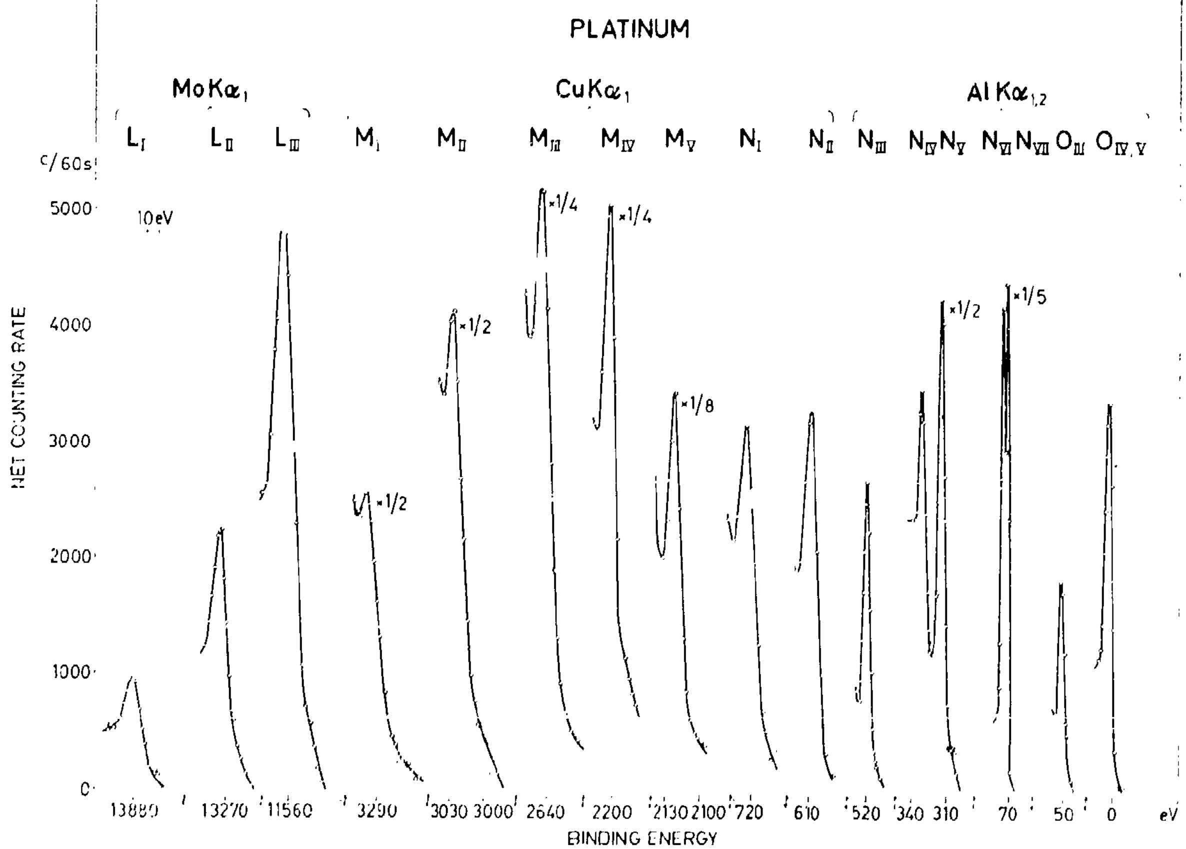

Fig. VIII:50. Electron lines of platinum recorded with the 50-cm instrument. Photoelectron lines from all *L*, *M*, *N* and some *O* shells were recorded using different X-radiations.

sion is required, the voltage drop over a precision resistor in series with the spectrometer coils is measured by means of a precision potentiometer. The data recording system is fully automatic. A block diagram of the current regulation and data recording system is given in Fig. VIII:56 and a photograph of the electronic equipment is shown in Fig. VIII:57.

The 50-cm spectrometer is very well suited for ESCA studies. To make such studies possible with the instrument, a new source housing containing an X ray tube has been built. A drawing of this housing is shown in Fig. VIII:58. The construction of the X-ray tube is very similar to that used in the 30-cm instrument (see Section VIII:2) but the dimensions are somewhat larger. It is possible to change the anode and source without breaking vacuum in the housing. One of the source assemblies used (shown in Fig. VIII:58a, c) is of the same type as that used in most of the other instruments described here. In the nuclear spectroscopy studies with the spectrometer, a multistrip source[79] of the Bergkvist[261,262] type is used. This source consists of several narrow parallel strips with very small separations. The multistrip source is connected to a high voltage supply and by *means* of a potential divider, the strips are kept at different potentials, from ground potential in equal increments up to the applied voltage. The total voltage is chosen according to the energy of the electrons studied so that all electrons with the selected energy (before acceleration) will enter the detector slit independent from which strip they originate. Investigations of the properties of a modified *multistrip* source (shown in Fig. VIII:58b) for ESCA studies have been started.

A cryostat is now being built with which it will be possible to cool the wall between the source and the X-ray tube and the wall containing the slit in front of the source. These walls are insulated from exterior walls with teflon. Pump oil and other organic materials in the vacuum chamber will condense on these cooled walls and not on the source. The amount of pump oil entering the spectrometer has previously been reduced by the installation of a water cooled baffle and a vapour trap cooled by liquid nitrogen between the diffusion pump and the spectrometer vacuum chamber. Prevacuum in the source assembly is obtained by means of a sorption pump.

The detector is a Mullard channel electron multiplier. We now use a set of such detectors placed side by side in the focal plane as in the new 30-cm instrument (see Section VIII:4). This increases the amount of information obtained per time-unit considerably.

As an example of the spectra obtained using this equipment, photoelectron lines from platinum are shown in Fig. VIII:59. The conventional source arrangement was used for this study. The spectrum shown in Fig. VIII:59 maps out a larger number of atomic core levels (seventeen) than any other spectrum that we have recorded.[93]

VIII:7. Compensating Systems for External Magnetic Fields

To be able to make accurate energy determinations with the spectrometers, the earth's magnetic field and stray fields from instruments in the neighbourhood must be compensated. The instruments are therefore surrounded by compensating coils. The classical arrangements for eliminating homogeneous magnetic fields is by the so-called Helmholtz system which consists of a pair of circular coils placed a distance equal to the coil radius apart. Such a system gives maximum homogeneity at the center of the coil system. We have used Helmholtz coils for compensating each of three perpendicular directions, one vertical and two horizontal. Four modifications of the basic Helmholtz arrangement are made at different instruments and for different magnetic field components:

(1) Maximum homogeneity of the vertical field component is required along the central electron orbit rather than at the center. The following relationship should then be fulfilled:[295]

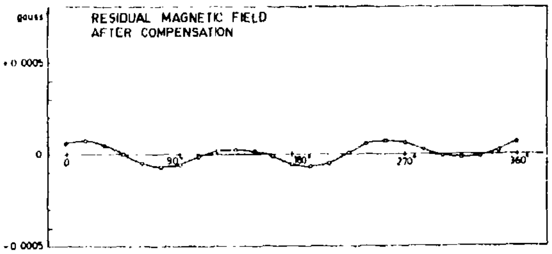

Fig. VIII:60. Residual magnetic field at the central orbit of one of the 30-cm spectrometers.

$$175a^6y^5 + 120a^8y^3 + 64a^{10}y - x^2(1200a^6y^3 + 4200a^4y^5) - x^4(640a^6y + 1800a^4y^3 - 8400a^2y^5) - x^6(2240y^5 + 1280a^4y - 480a^2y^3) - x^8(960a^2y - 960y^3) - 256x^{10}y = 0 \qquad (9)$$

where a is the coil radius, x is half the distance between the coils and y is the radius of the central electron orbit. With $a = 200$ cm and $y = 30$ cm, eq. (9) gives $x = 98$ cm which differs by 2 % from the basic Helmholtz system.

(2) For the 50-cm instrument, we have adopted a system of four coils of equal diameter (590 cm) for compensating the vertical field.[46] As many as seven terms are zero in the Taylor expansion of the magnetic field produced by this coil system, and the volume of the homogeneous field is much increased as compared to that obtained with a two-coil system.

(3) For each of the two horizontal components, one pair of quadratic coils can be used instead of circular coils. Quadratic coils are easier to construct and occupy less space than the corresponding circular coils which allows the instrument to stand on the floor at a level convenient for the operator. They give a sufficiently uniform field for the elimination of the horizontal component. The cancellation of the latter is not as critical as for the vertical component. The distance between the coils in each quadratic pair was chosen so that the vertical field component and the variation of horizontal field along the electron trajectories was kept at a minimum. Calculations of the field were made on an IBM 1620 computer and for a 30-cm instrument the calculated optimum distance between the coils (dimensions 2 m × 2 m) was 0.575 times the side of the coils.

(4) Gradients in the external magnetic field can occur if there is ferromagnetic material in the vicinity of the instrument or if there are stray fields from other magnets. For example, a gradient in the vertical component of $5 \cdot 10^{-5}$ G m^{-1} was found at the 50-cm

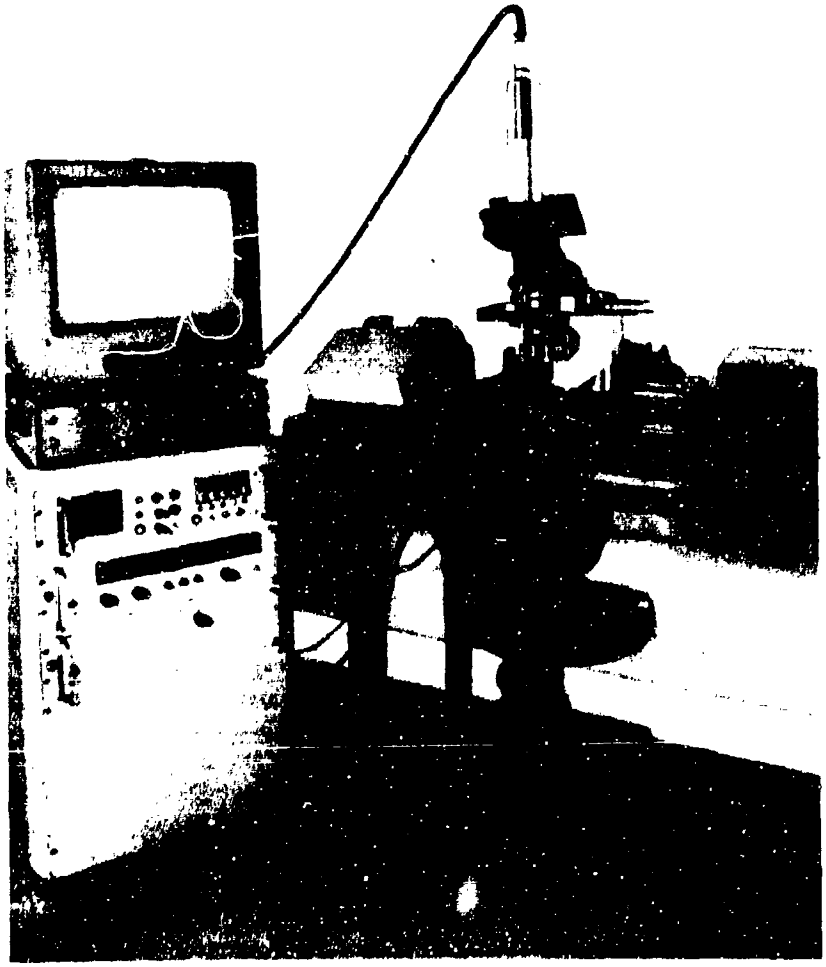

Fig. VIII:61. The TMD. The monitor is placed on top of the box containing the logic circuitry. Below are the control system for the plate movement, the scaler and the printer control. The printer, the microscope with the step motors and the television camera mounted on it and the transformers for the illumination are placed on the table.

instrument, and the stray-field of a synchro-cyclotron 100 m away was found to increase this gradient to $20 \cdot 10^{-5}$ $\mathrm{G\,m^{-1}}$. However, by making the two pairs of circular coils slightly non-coaxial[16] the vertical component of the gradient of the field was eliminated. Similar modifications of the basic symmetrical coil arrangement have also been made for the other instruments.

The compensating coil systems all eliminate the vertical external field component to within 10^{-4} G, which is about 0.02 % of the vertical component of the earth's magnetic field at Uppsala. It is less than 0.01 % of the spectrometer fields normally used in the magnetic instruments and the external fields are thus eliminated to such an extent as to justify measurements in the precision range of $1:10^5$. The residual vertical field along the electron trajectories in one of the 30-cm instruments is shown in Fig. VIII:60. The compensating coils with appropriate series resistors are connected in parallel to a highly stabilised current supply.

The absence of magnetic field originating from the spectrometer itself facilitates the control and continuous compensation of variations in the magnetic field at the electrostatic instrument. For the vertical component this is done automatically. The field meter gives an output signal proportional to the measured field. After amplification this signal, assisted by a servomotor, is used to change the setting of a potentiometer. The potentiometer determines the output current of the power supply for the compensating coils.

By this system it is possible to keep the variations of the vertical component of the magnetic field during a recording of a spectrum to within $\pm 2 \cdot 10^{-5}$ G. The other components, which are of less importance, are checked between the measurements. A continually-operating, self-correcting arrangement is also used for the 50-cm magnetic instrument (see Section VIII:6).

VIII:8. The Television Micro Densitometer

As we mentioned previously, the use of photographic detection is not straightforward in ESCA. The technique we have used is to count the tracks in a nuclear emulsion that has been exposed to electrons in the semicircular spectrograph (see Section VIII:3). (The other instruments can also be used for photographic detection, since they have a focal plane.)

At first the tracks were counted by visual observation of the tracks in a microscope;[61,65] this was of course a very tedious work. In order to speed up the scanning by several orders of magnitude, an instrument has now been constructed in which the eye has been replaced by a television camera which automatically scans the plate, counts the tracks, and prints the results on paper tape. The device is termed Televison Micro Densitometer (TMD).[71,80]

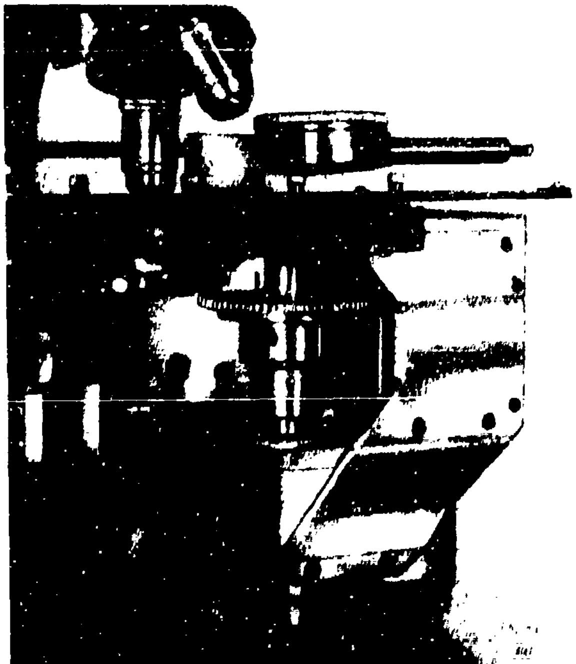

Fig. VIII:62. Photograph of the step motors and their transmission systems.

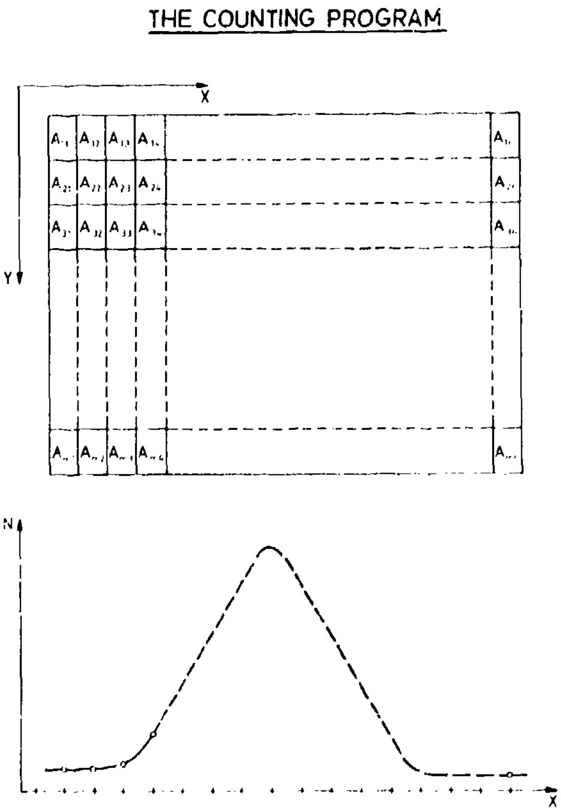

Fig. VIII:63. The principle of the counting program.

The instrument consists of several units. Some of these are commercially available and some have been specially designed for this instrument. The units are: A microscope with high magnification, light sources, a television camera, a monitor, a video amplifier, logic circuitry, a scaler, a printer control, a printer and a control system for the plate movement. The logic circuitry and the control system for the plate movement have been specially designed for this instrument and will be described below.

The microscope stage on which the plate is mounted, can be moved in two perpendicular directions by step motors. The movement is controlled electronically and the position of the plate can be determined within 1 μm. The light source used for illuminating the tracks

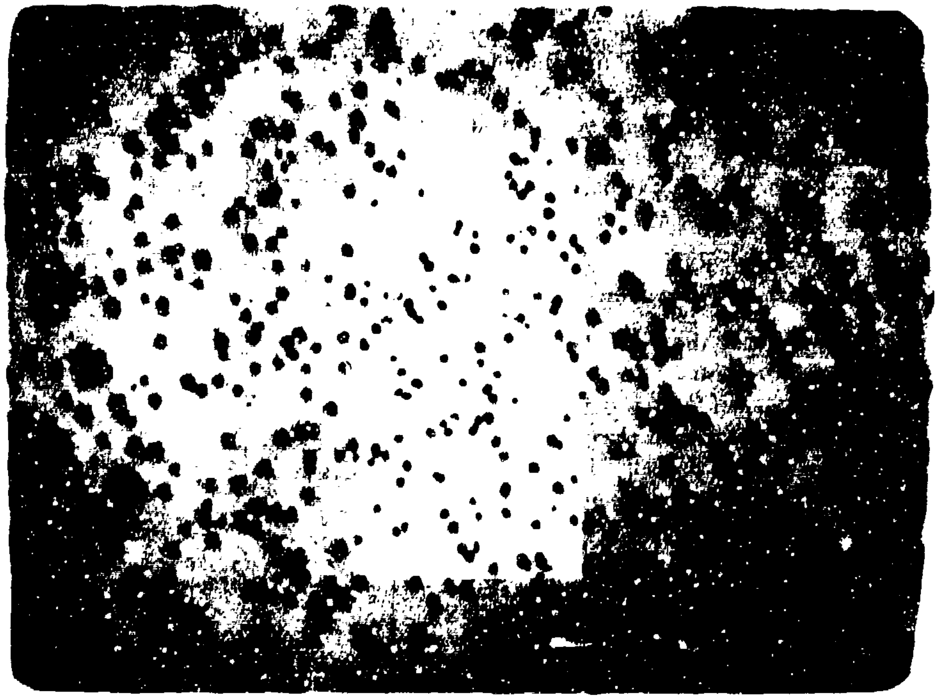

Fig. VIII:64. Photograph of the television screen with the two types of indications superimposed on the normal picture: the bright spot to the right of each detected track and the area within which the counting takes place.

is a high pressure mercury lamp equipped with necessary filters; it is also possible to use an ordinary tungsten filament lamp. Dark field illumination is used and the objective, which has a magnification of × 90, projects the image either into the binocular eyepiece for direct viewing or into the television camera that is mounted on the microscope. The scaler has a counting speed of 10 MHz and the resolution is better than 0.1 μs. The physical arrangement of the TMD is shown in Fig. VIII:61; the step motors are shown in Fig. VIII:62.

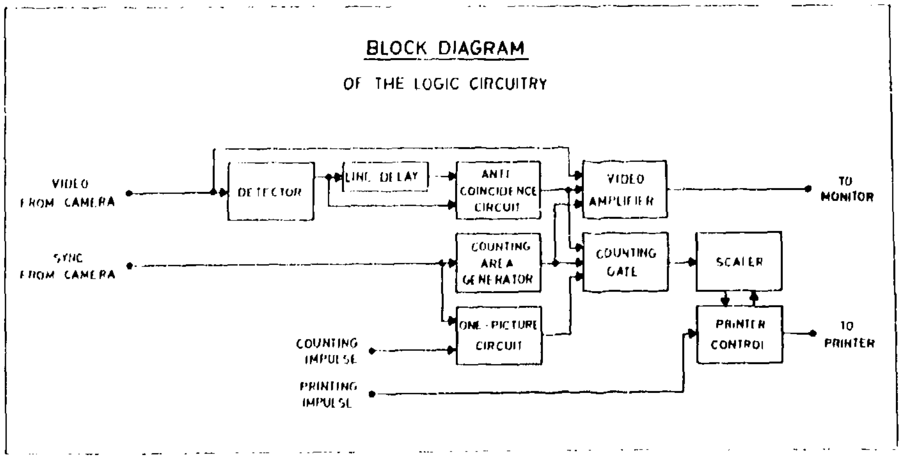

Fig. VIII:65. Block diagram of the logic circuitry.

The counting program

The field of view in the microscope is of course much smaller than the total area in which the tracks are to be counted. At any one setting of the microscope stage, the tracks are counted in a rectangular area A inside the field of view. The delineation of an electron line on the plate is thus naturally made according to the following program: (see Fig. VIII:63).

(1) Tracks are counted successively in counting areas $A_{11}, A_{21}, A_{31}, \ldots A_{m1}$; the movement of the plate between different areas is controlled by the by use of step motors attached for the microscope stage.

(2) The number of counts is stored in the scaler and when the first column has been counted the x-coordinate of the column and the total number of counts in the scaler are printed out; the scaler is reset.

(3) The microscope stage with the plate is moved by the step motor for the x direction so that the procedure can be repeated for counting areas $A_{m2}, \ldots A_{32}, A_{22}, A_{12}$ (note the reversed order).

(4) Then the third column is counted in the order $A_{13}, A_{23}, A_{33}, \ldots A_{m3}$, the fourth column in the order $A_{m4}, \ldots A_{34}, A_{24}, A_{14}$ etc.

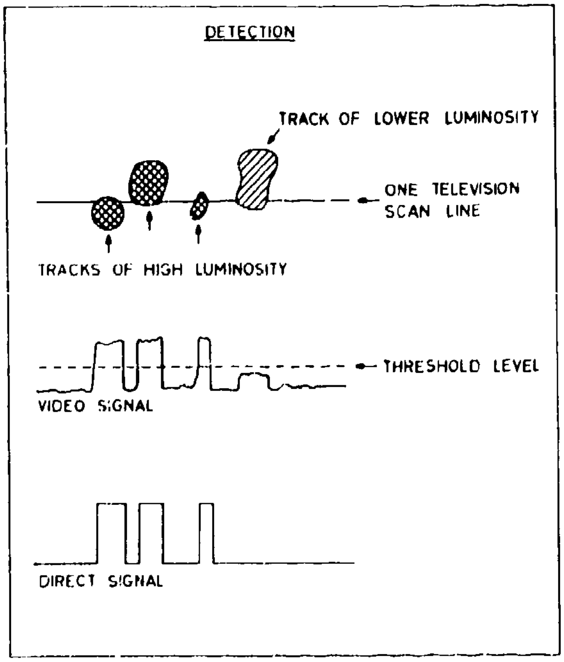

Fig. VIII:66. The principle of detection and the direct signal from the detector.

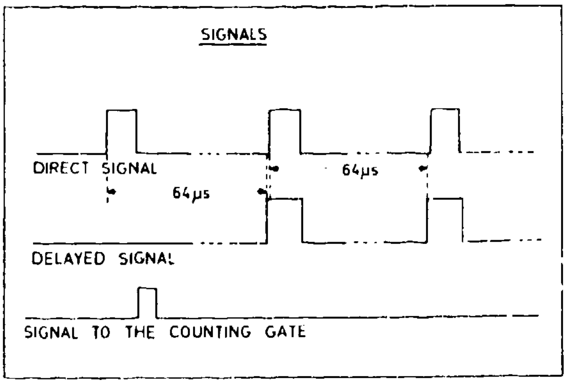

Fig. VIII:67. The direct signal from the detector, the delayed signal from the acoustic memory and the resulting signal from the anticoincidence circuit.

Logic circuitry

The logic circuitry can be used for detecting tracks of very different size and shape and each track is counted only once independent of its size and shape. The logic circuitry can discriminate tracks of different luminosity. The tracks appear dark on the television screen and each track that is detected by the logic circuitry is indicated by a bright spot (see Fig. VIII:64). The rectangular counting area is also shown on the television screen. The center of this area can be chosen anywhere inside the field of view and its height and width can be varied over a wide range. When the logic circuitry is switched off, the normal picture appears on the screen; i.e. no indication is made of the tracks or of the counting area. A block diagram of the logic circuitry is shown in Fig. VIII:65. The video signal in the detector enters a brightness threshold discriminator that determines the level above which the tracks are detected. The threshold level can be set by a control on the front panel. When leaving the detector the signals from those tracks that have been detected are converted to pulses of definite height and with duration equal to the time spent by the television scan in traversing the track (see Fig. VIII:66).

The first time the television scan intersects a track that is detected, it sends a direct signal to an anticoincidence circuit. This signal results in a pulse to the counting gate and at the same time to the bright spot of the track. The second time the television scan intersects the same track it sends a new direct signal to the anticoincidence circuit. At the same time as

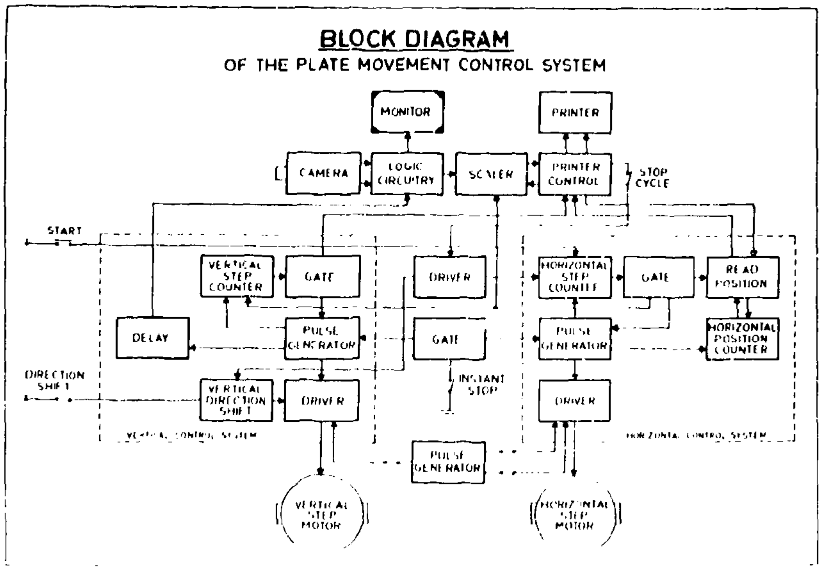

Fig. VIII:68. Block diagram of the plate movement control system.

this signal arrives, a delayed signal arrives at the anticoincidence circuit and no pulse comes out. This is repeated until the television scan has passed the lowest edge of the track when only the delayed signal arrives and nothing happens (see Fig. VIII:67). The delayed signal comes from an acoustic memory which delays the direct signal by approximately one televison line scan interval, 64 μs.

A counting area generator is used to define the rectangular area in which the tracks are counted. It consists of four multivibrators each of which can be adjusted by a control on the front panel. Two of these determine the height and width, respectively, and the others the position on the picture. It is possible to move the area without altering its dimensions. The size determining multivibrators are triggered by those which determine the position; these in turn are triggered by line and frame sync. from the camera. The video signal to the monitor consists of the video signal from the camera, the counting area indication and the indications from those tracks which are detected. The brightness of the indications can be varied by two controls on the front panel.

A one-picture circuit and a counting gate are needed as counting shall take place only for one fiftieth of a second, that is one picture, and only in the selected area. The one-picture circuit consists of three multivibrators and when counting is done automatically it is triggered by the counting impulse from the control system for the plate movement. It is also possible to count without using the control system for the plate movement. Then the counting impulse comes from a foot switch. The counting gate is controlled by the counting area generator and the one-picture circuit and allows the proper signals to pass to the scaler.

Control system for the plate movement

When the control unit for the plate movement is started (see Fig. VIII:68) the horizontal step counter is reset, the gate in the horizontal control system is opened and its pulse generator is started. The pulse generator sends pulses by means of a driver to the horizontal step motor, to the horizontal step counter and to the horizontal position counter. When the step counter has received the pre-set number of pulses, a signal is fed to the gate, which then closes, and the pulse generator is stopped. At the same time the number on the horizontal position counter is read into the printer, the scaler is opened, the vertical step counter is reset, the gate in the vertical control system is opened and its pulse generator is started. The pulse generator also sends pulses by means of a driver to the vertical step motor, to the vertical step counter and, by a delay circuit, to the logic circuity that counts the tracks. When the counter has received the preset number of pulses, it gives a signal to the gate which then closes,

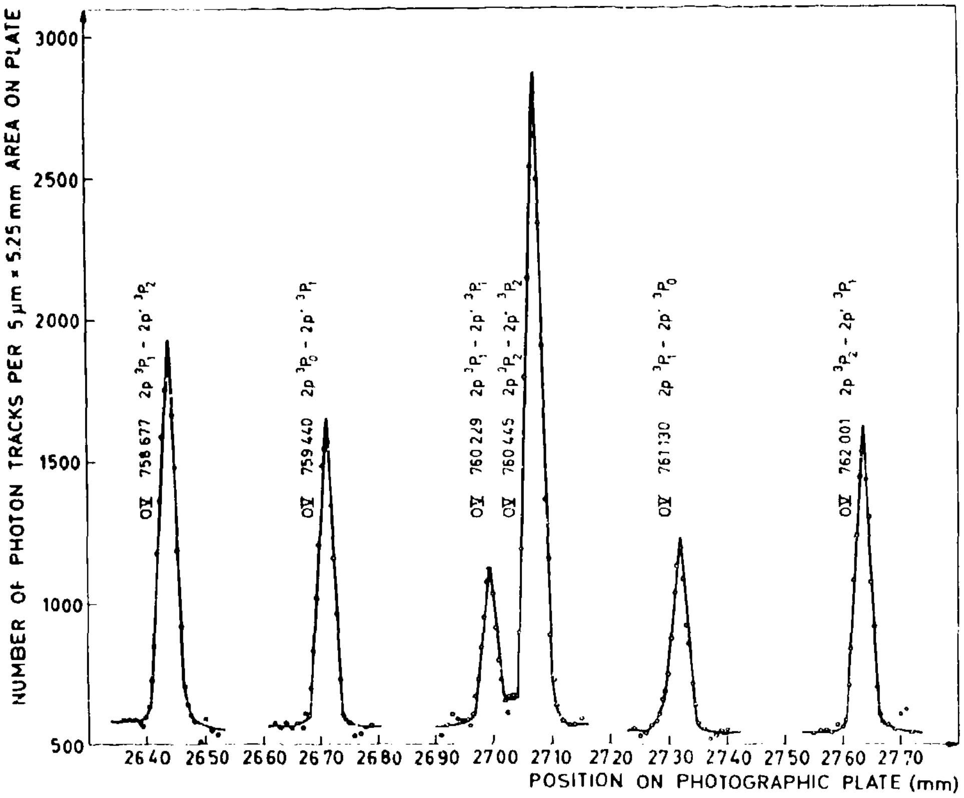

Fig. VIII:69. A photon spectrum (OV) analysed with the track counting technique. The lines were recorded with a modified E793 Hilger 3-meter normal incidence vacuum spectrograph. The photon tracks per 5 μm × 5.25 mm area on the plate are counted with the TMD.

and the pulse generator is stopped. At the same time, a signal is transmitted to the printer control unit and the number on the horizontal position counter and the number of tracks on the scaler are printed. When the printing cycle is completed the printer control unit sends a pulse to a driver that via the vertical direction shift circuit changes the stepping direction of the vertical step motor. At the same time the horizontal step counter is reset and the cycle starts again.

If the "stop cycle" switch is opened, the pulse from the printer control unit is blocked and the cycle is stopped after the vertical step motor has completed its preset number of steps and the printing is finished. When the "instant stop" switch is opened the control unit is stopped instantly by a gate that blocks the pulse generators in the vertical and the horizontal control systems.

It is possible to move the plate faster than normal and without counting. This is done with the aid of a special pulse generator, the pulses of which are fed into the driver circuits of the two step motors via push buttons. The stepping direction of the vertical step motor can be changed manually.

Before the counting starts, the operator has to decide on the size of the rectangular counting areas A and the number of counting areas in each column. The step length of the step motor for the y-direction (vertical direction) is 50 μm and therefore it is convenient to choose the height of the areas equal to this. The number of areas in the column, m, is dependent on the statistical accuracy required in the experiment. This number, m, is preset on the vertical step counter. The width of the areas must be chosen with regard to the resolution desired. The step length in the x-direction, i.e. the direction of dispersion (horizontal), is 5 μm and it is appropriate to choose the width of the areas as a multiple of this length. This can be preset on the horizontal step counter in the control system for the plate movement.

Applications

The program described above is convenient for our symmetry where the track distribution per unit area is independent of the vertical position on the plate. However, the track counting technique is not restricted to this case. It can also be used for other symmetries for example where the track density is a function of the distance from a central point (which can be difficult to localize). In this symmetry the elements of the matrix and their position must be counted and printed separately. It is still better to have the values punched on tape or cards. The information can then be handled by an electronic computer which can be used for localizing the central point and deducing the track distribution per unit area as a function of the radial distance from this point.

The instrument has in most cases been used for track counting in electron spectroscopy where it has reduced the counting time from weeks to hours. Examples of electron spectra counted by the TMD are shown in Appendix 10. An optical spectrum counted by the TMD is shown in Fig. VIII:69. It is also possible to use the instrument for other counting purposes, for examples for counting dislocations in crystals or inclusions in metal samples. If the microscope is replaced by an ordinary camera lens the instrument can be used for counting larger size objects.

ACKNOWLEDGEMENTS

We wish to thank the following persons who have contributed as co-workers during earlier phases of the ESCA project: Laborator Kay Edvarson, Fil. Dr. Evelyn Sokolowski, Docent Pär Bergvall†, Fil. Dr. Olle Hörnfeldt, and Docent Stig Hagström.

We also thank the following co-workers and visiting scientists: Fil. Lic. Robert Carlsson, Fil. Lic. Ulf Ericson, Fil. Lic. Ingemar Andersson, Fil. Lic. Örjan Nilsson, Civ.-Ing. Nils Magnusson, Fil. Kand. Ulrik Gelius, Fil. Kand. Per-Filip Hedén, Fil. Kand. Barbro Schröder, Professor Einar Stenhagen, Docent Kåre Larsson, Prosektor Sven Brolin, Dr. Lennart W. Holm, Dr. Julian Auleutner (Warsaw), Dr. Igor Nikiforov (Rostov-on-Don), Dr. Mart Elango (Tartu), Professor John K. Wood (Logan), Professor Royal G. Albridge (Nashville), and Dipl. Phys. Reimar Spohr (Freiburg).

Excellent assistance has been given by Ing. Thord Berglund, Ing. Lennart Eriksson, Ing. Rune Goldwitz, and Ing. Sven Kumlin.

The following persons have contributed by valuable discussions, by providing compounds and facilities for our studies and by other means: Professor Arne Fredga, Docent Stig Allenmark, Docent Björn Ingelman, Fil. Kand. Ernst Johnsson, Fil. Lic. Rolf Manne, Docent Olle Mårtensson, Fil. Mag. Jan Rosengren, and Docent Stig Rundqvist.

We also gratefully acknowledge the financial support which has been given by Statens Naturvetenskapliga Forskningsråd, Statens Råd för Atomforskning, Malmfonden, Magnus Bergvalls Stiftelse, Uppsala University, The Royal Academy of Sciences (K.V.A.), The Royal Society of Sciences, Uppsala, Försvarets Forskningsanstalt (FOA), Pharmacia AB, the U.S. Air Force through the European Office of Aerospace Research, the U.S. Department of Army through its European Research Office, and Fil. Dr. Anders Diös, Uppsala.

APPENDIX 1

Table of Electron Binding Energies

This table of electron binding energies is based on electron spectroscopic measurements which have been made by our research group (Chapter III). For levels which have not yet been measured by electron spectroscopy, energy differences have been taken from the table of atomic energy levels published by Bearden and Burr.[131] The *K* level has then been used as a reference level for elements with atomic number $Z \leq 34$, the L_{III} level for $35 \leq Z \leq 72$ and the M_V level for $73 \leq Z \leq 94$. Most of the binding energies in the region $Z > 94$ as well as energies for the elements below $Z < 94$ that have not yet been studied by electron spectroscopy have been taken from Bearden and Burr.[131] Their table was calculated by a least squares fit of X-ray and photoelectron energy data. For $Z \geq 97$ the binding energies were obtained from nuclear decay studies by Hollander *et al.*[276]

The precision in the binding energies of the elements measured by electron spectroscopy is better than 1 eV. However the effect of the chemical environment on the atoms being investigated must be taken into account. As discussed in previous sections, this effect can amount to several eV, and a further admonition is given in Fig. 1:1 which shows electron lines from the *K*, *L*, *M*, and *N* shells of beryllium, aluminum, antimony and bismuth, respectively. Partial oxidation of the samples results in two lines for each level or sublevel. The difference in energy between the lines from the unoxidized and the oxidized element is c. 2 eV.

No measurements have been made of the *K* level energies for the heaviest elements around $Z \approx 100$. The uncertainty in the calculated energies that are given for the *K* level in this region is of the order of 100 eV.

The tabulated binding energies are given with zero binding energy at the Fermi level. The total binding energy is therefore larger by an amount equal to the work function.

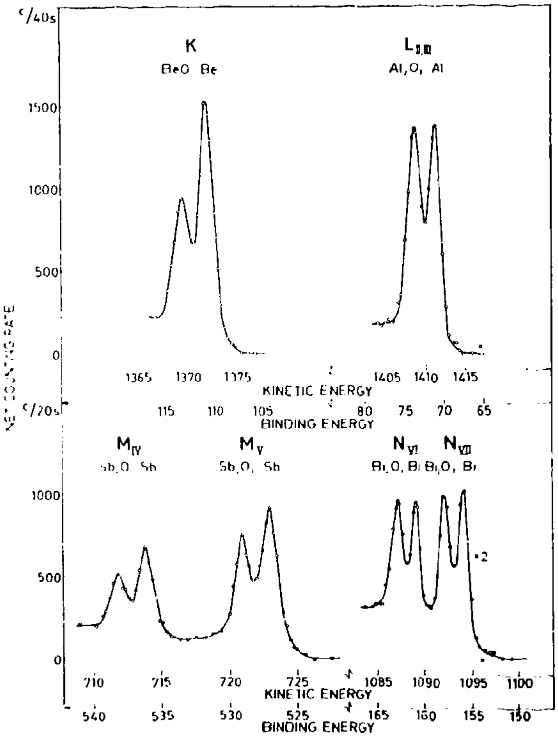

Fig. 1:1. Shifts in *K*, *L*, *M*, and *N* levels of light and heavy elements, due to oxidation.

Energy levels measured by electron spectroscopy are given with references. Information concerning the compounds which have been used for the measurements, the energy calibration etc. is found in the references given in the table. Energies obtained by interpolation are marked with an asterisk,* and extrapolated energies or energies obtained by self-consistent-field calculations are indicated by a cross †.

Electron binding energies (eV).

	$1s_{1/2}$ K	$2s_{1/2}$ L_I	$2p_{1/2}$ L_{II}	$2p_{3/2}$ L_{III}	$3s_{1/2}$ M_I	$3p_{1/2}$ M_{II}	$3p_{3/2}$ M_{III}	$3d_{3/2}$ M_{IV}	$3d_{5/2}$ M_V	$4s_{1/2}$ N_I	$4p_{1/2}$ N_{II}	$4p_{3/2}$ N_{III}	$4d_{3/2}$ N_{IV}	$4d_{5/2}$ N_V	$4f_{5/2}$ N_{VI}	$4f_{7/2}$ N_{VII}
1 H	14															
2 He	25															
3 Li	55															
4 Be	111															
5 B	188^{1}		5													
6 C	284^{1}		7													
7 N	399^{19}		9													
8 O	532^{1}	24^{2}	7													
9 F	686^{1}	31	9													
10 Ne	867	45	18													
11 Na	1 072^{1}	63^{3}	31		1											
12 Mg	1 305^{1}	89^{3}	52		2											
13 Al	1 560^{1}	118^{3}	74	73	1											
14 Si	1 839^{1}	149^{3}	100	99	8	3										
15 P	2 149^{1}	189^{3}	136	135	16	10										
16 S	2 472^{1}	229^{3}	165	164	16	8										
17 Cl	2 823^{1}	270^{3}	202	200	18	7										
18 A	3 203	320^{3}	247	245	25	12										
19 K	3 608^{1}	377^{3}	297	294	34	18										
20 Ca	4 038^{1}	438^{3}	350	347	44	26		5								
21 Sc	4 493^{1}	500^{3}	407	402	54	32		7								
22 Ti	4 965^{1}	564^{3}	461	455	59	34		3								
23 V	5 465^{1}	628^{3}	520	513	66	38		2								
24 Cr	5 989^{1}	695^{3}	584	575	74	43		2								
25 Mn	6 539^{4}	769^{3}	652	641	84	49		4								
26 Fe	7 114^{5}	846^{3}	723	710	95	56		6								
27 Co	7 709^{4}	926^{3}	794	779	101	60		3								
28 Ni	8 333^{4}	1 008^{3}	872	855	112	68		4								
29 Cu	8 979^{6}	1 096^{3}	951	931	120	74		2								
30 Zn	9 659^{6}	1 194	1 044	1 021	137	87		9								
31 Ga	10 367^{6}	1 298	1 143	1 116	158	107	103	18			1					
32 Ge	11 104^{6}	1 413^{6}	1 249	1 217	181	129	122	29			3					
33 As	11 867^{6}	1 527	1 359	1 323	204	147	141	41			3					
34 Se	12 658^{6}	1 654	1 476	1 436	232	168	162	57			6					
35 Br	13 474	1 782^{7}	1 596^{7}	1 550^{7}	257	189	182	70	69	27	5					
36 Kr	14 326	1 921	1 727	1 675	289*	223	214	89		24	11					
37 Rb	15 200	2 065^{7}	1 864^{7}	1 805^{7}	322	248	239	112	111	30	15	14				
38 Sr	16 105	2 216^{3}	2 007^{8}	1 940^{8}	358	280	269	135	133	38	20					
39 Y	17 039	2 373^{8}	2 155^{8}	2 080^{8}	395	313	301	160	158	46	26		3			
40 Zr	17 998	2 532^{8}	2 307^{8}	2 223^{8}	431	345	331	183	180	52	29		3			
41 Nb	18 986	2 698^{8}	2 465^{8}	2 371^{8}	469	379	363	208	205	58	34		4			
42 Mo	20 000	2 866^{8}	2 625^{8}	2 520^{8}	505	410	393	230	227	62	35		2			
43 Tc	21 044	3 043^{8}	2 793^{8}	2 677^{8}	544*	445	425	257	253	68*	39		2*			
44 Ru	22 117	3 224^{8}	2 967^{8}	2 838^{8}	585	483	461	284	279	75	43		2			
45 Rh	23 220	3 412^{8}	3 146^{8}	3 004^{8}	627	521	496	312	307	81	48		3			

Appendix 1 (*cont.*)

	$1s_{1/2}$ K	$2s_{1/2}$ L_{I}	$2p_{1/2}$ L_{II}	$2p_{3/2}$ L_{III}	$3s_{1/2}$ M_{I}	$3p_{1/2}$ M_{II}	$3p_{3/2}$ M_{III}	$3d_{3/2}$ M_{IV}	$3d_{5/2}$ M_{V}	$4s_{1/2}$ N_{I}	$4p_{1/2}$ N_{II}	$4p_{3/2}$ N_{III}	$4d_{3/2}$ N_{IV}	$4d_{5/2}$ N_{V}	$4f_{5/2}$ N_{VI}	$4f_{7/2}$ N_{VII}
46 Pd	24 350	3 605[8]	3 331[8]	3 173[8]	670	559	531	340	335	86	51		1			
47 Ag	25 514	3 806[9]	3 524[8,9]	3 351[8]	717	602	571	373	367	95	62	56	3			
48 Cd	26 711	4 018[9]	3 727[9]	3 538[9]	770	651	617	411	404	108	67		9			
49 In	27 940	4 238[9]	3 938[9]	3 730[8]	826	702	664	451	443	122	77		16			
50 Sn	29 200	4 465[6]	4 156[6]	3 929[6]	884	757	715	494	485	137	89		24			
51 Sb	30 491	4 699[9]	4 381[9]	4 132[8]	944	812	766	537	528	152	99		32			
52 Te	31 814	4 939[9]	4 612[9]	4 341[9]	1 006	870	819	582	572	168	110		40			
53 I	33 170	5 188[7]	4 852[7]	4 557[7]	1 072	931	875	631	620	186	123		50			
54 Xe	34 561	5 453	5 104	4 782	1 145*	999	937	685*	672	208*	147		63*			
55 Cs	35 985	5 713[7]	5 360[7]	5 012[7]	1 217	1 065	998	740	726	231	172	162	79	77		
56 Ba	37 441	5 987[7]	5 624[7]	5 247[7]	1 293	1 137	1 063	796	781	253	192	180	93	90		
57 La	38 925	6 267[10]	5 891[10]	5 483[10]	1 362	1 205	1 124	849	832	271	206	192	99			
58 Ce	40 444	6 549[10]	6 165[10]	5 724[10]	1 435	1 273	1 186	902	884	290	224	208	111		1	
59 Pr	41 991	6 835[10]	6 441[10]	5 965[10]	1 511	1 338	1 243	951	931	305	237	218	114		2	
60 Nd	43 569	7 126[10]	6 722[10]	6 208[10]	1 576	1 403	1 298	1 000	978	316	244	225	118		2	
61 Pm	45 185*	7 428*[11]	7 013*[11]	6 460*[11]	1 650*	1 472*	1 357*	1 052*	1 027*	331*	255*	237*	121*		4*	
62 Sm	46 835	7 737[10]	7 312[10]	6 717[10]	1 724	1 542	1 421	1 107	1 081	347	267	249	130		7	
63 Eu	48 519	8 052[10]	7 618[10]	6 977[10]	1 800	1 614	1 481	1 161	1 131	360	284	257	134		0	
64 Gd	50 239	8 376[10]	7 931[10]	7 243[10]	1 881	1 689	1 544	1 218	1 186	376	289	271	141		0	
65 Tb	51 996	8 708[10]	8 252[10]	7 515[10]	1 968	1 768	1 612	1 276	1 242	398	311	286	148		3	
66 Dy	53 788	9 047[10]	8 581[10]	7 790[10]	2 047	1 842	1 676	1 332	1 295	416	332	293	154		4	
67 Ho	55 618	9 395[10]	8 919[10]	8 071[10]	2 128	1 923	1 741	1 391	1 351	436	343	306	161		4	
68 Er	57 486	9 752[10]	9 265[10]	8 358[10]	2 207	2 006	1 812	1 453	1 409	449	366	320	177	168	4	
69 Tm	59 390	10 116[10]	9 618[10]	8 648[10]	2 307	2 090	1 885	1 515	1 468	472	386	337	180		5	
70 Yb	61 332	10 488[10]	9 978[10]	8 943[10]	2 397	2 172	1 949	1 576	1 527	487	396	343	197	184	6	
71 Lu	63 314	10 870[10]	10 349[10]	9 244[10]	2 491	2 264	2 024	1 640	1 589	506	410	359	205	195	7	
72 Hf	65 351	11 272[11]	10 739[11]	9 561[11]	2 601	2 365	2 108	1 716	1 662	538	437	380	224	214	19[17]	18[17]
73 Ta	67 417	11 680[12]	11 136[12]	9 881[12]	2 708	2 469[12]	2 194[12]	1 793[12]	1 735[12]	566	465	405	242	230	27[17]	25[17]
74 W	69 525	12 099[12]	11 542[12]	10 205[12]	2 820	2 575[12]	2 281[12]	1 872[12]	1 810[12]	595	492	426	259	246	37[17]	34[17]
75 Re	71 677	12 527	11 957[12]	10 535[12]	2 932	2 682[12]	2 367[12]	1 949[12]	1 883[12]	625	518	445	274	260	47[17]	45[17]
76 Os	73 871	12 968	12 385	10 871[12]	3 049	2 792[12]	2 458[12]	2 031[12]	1 960[12]	655	547	469	290	273	52[17]	50[17]
77 Ir	76 111	13 419	12 824[12]	11 215[12]	3 174	2 909[12]	2 551[12]	2 116[12]	2 041[12]	690	577	495	312	295	63[17]	60[17]
78 Pt	78 395	13 880[20]	13 273[20]	11 564[20]	3 298[20]	3 027[20]	2 646[20]	2 202[20]	2 121[20]	724[20]	608[20]	519[20]	331[20]	314[20]	74[20]	70[20]
79 Au	80 725	14 353	13 733[12]	11 918[12]	3 425[12]	3 150[12]	2 743[12]	2 291[12]	2 206[12]	759	644	546	352	334	87[17]	83[17]
80 Hg	83 103	14 839	14 209	12 284[12]	3 562	3 279	2 847[12]	2 385[12]	2 295[12]	800	677	571	379	360	103[17]	99[17]
81 Tl	85 531	15 347	14 698[12]	12 657[12]	3 704	3 416[12]	2 957[12]	2 485[12]	2 390[12]	846	722	609	407	386	122[17]	118[17]
82 Pb	88 005	15 861	15 200	13 035[12]	3 851	3 554[12]	3 067[12]	2 586[12]	2 484[12]	894	764	645	435	413	143[17]	138[17]
83 Bi	90 526	16 388	15 709[11]	13 418[17]	3 999[12]	3 697[12]	3 177[12]	2 688[12]	2 580[12]	939[12]	806[12]	679[12]	464[12]	440[12]	163[17]	153[17]
84 Po	93 105	16 939	16 244	13 814	4 149	3 854	3 302	2 798	2 683	995	851	705	500	473	184*	
85 At	95 730	17 493	16 785	14 214	4 317*	4 008	3 426	2 909	2 787	1 042*	886	740	533	507*	210*	
86 Rn	98 404	18 049	17 337	14 619	4 482*	4 159	3 538	3 022	2 892	1 097*	929	768	567	541*	238*	
87 Fr	101 137	18 639	17 906	15 031	4 652*	4 327*	3 663	3 136	3 000	1 153*	980	810	603	577	268*	
88 Ra	103 922	19 237	18 484	15 444	4 822*	4 490	3 792	3 248	3 105	1 208*	1 058	879	636	603	299	
89 Ac	106 755	19 840	19 083	15 871	5 002	4 656	3 909	3 370	3 219	1 269*	1 080	890	675	639*	319*	
90 Th	109 651	20 472	19 693	16 300[13]	5 182[13]	4 831[13]	4 046[13]	3 491[13]	3 332[13]	1 330[13]	1 168[13]	968[13]	714[13]	677[13]	344[13]	335[13]

$5s_{1/2}$ O_{I}	$5p_{1/2}$ O_{II}	$5p_{3/2}$ O_{III}	$5d_{3/2}$ O_{IV}	$5d_{5/2}$ O_{V}	$6s_{1/2}$ P_{I}	$6p_{1/2}$ P_{II}	$6p_{3/2}$ P_{III}	$6d_{3/2}$ P_{IV}	$6d_{5/2}$ P_{V}
	2								
	1								
1	1								
7	2								
12	2								
14	3								
18*	7*								
23	13	12							
40	17	15							
33	15								
38	20								
38	23								
38	22								
38*	22*								
39	22								
32	22								
36	21								
40	26								
63	26								
51	20								
60	29								
53	32								
53	23								
57	28		5						
65	38	31	7						
71	45	37	6						
77	47	37	6						
83	46	35	4						
84	58	46	0						
96	63	51	4						
102	66	51^{20}	2^{20}						
108	72	54	3						
120	81	58	7						
137	100	76	16	13					
148	105	86	22	20	3	1			
160	117	93	27	25	8*	3			
177*	132*	104*	31		12*	5*			
195*	148*	116*	40*		18*	8*			
214*	164*	127*	48*		26*	11*			
234*	182*	140*	58*		34*	15*			
254	200	153	68		44	19			
272*	215*	167*	80*						
290	229	182^{13}	95^{13}	88^{13}	60	49	43	2	

Appendix 1 (*cont.*)

	$1s_{1/2}$ K	$2s_{1/2}$ L_{I}	$2p_{1/2}$ L_{II}	$2p_{3/2}$ L_{III}	$3s_{1/2}$ M_{I}	$3p_{1/2}$ M_{II}	$3p_{3/2}$ M_{III}	$3d_{3/2}$ M_{IV}	$3d_{5/2}$ M_{V}	$4s_{1/2}$ N_{I}	$4p_{1/2}$ N_{II}	$4p_{3/2}$ N_{III}	$4d_{3/2}$ N_{IV}	$4d_{5/2}$ N_{V}	$4f_{5/2}$ N_{VI}	$4f_{7/2}$ N_{VII}
91 Pa	112 601	21 105	20 314	16 733	5 367	5 001	4 174	3 611	3 442	1 387	1 224	1 007	743	708	371	360
92 U	115 606	21 758	20 948	17 168^{14}	5 548	5 181^{14}	4 304^{14}	3 728^{14}	3 552^{14}	1 442^{14}	1 273^{14}	1 045^{14}	780^{14}	738^{14}	392	381
93 Np	118 676	22 420	21 599	17 608	5 722	5 366^{15}	4 435^{15}	3 850^{15}	3 664^{14}	1 501^{15}	1 328^{15}	1 087^{15}	817^{15}	773^{15}	415^{15}	404^{15}
94 Pu	121 818	23 102	22 266	18 057	5 933	5 546	4 562	3 973^{16}	3 778^{16}	1 558	1 377	1 120	849^{16}	801^{16}	422	
95 Am	125 027	23 773	22 944	18 504	6 120	5 710	4 667	4 092	3 887	1 617	1 412	1 136†	879	828	440†	
96 Cm	128 220*	24 460*	23 779*	18 930*	6 288*	5 895*	4 797*	4 227†	3 971†	1 643*	1 440†	1 164†				
97 Bk	131 590^{18}	25 275^{18}	24 385^{18}	19 452^{18}	6 556^{18}	6 147^{18}	4 977^{18}	4 366†	4 132†	1 755^{18}	1 554†	1 235†				
98 Cf	135 960†	26 110†	25 250†	19 930†	6 754†	6 359†	5 109†	4 497†	4 253†	1 791†	1 616†	1 279†				
99 Es	139 490†	26 900†	26 020†	20 410†	6 977†	6 574†	5 252†	4 630†	4 374†	1 868†	1 680†	1 321†				
100 Fm	143 090†	27 700†	26 810†	20 900†	7 205†	6 793†	5 397†	4 766†	4 498†	1 937†	1 747†	1 366†				
101 Md	146 780†	28 530†	27 610†	21 390†	7 441†	7 019†	5 546†	4 903†	4 622†	2 010†	1 814†	1 410†				
102 No	150 540†	29 380†	28 440†	21 880†	7 675†	7 245†	5 688†	5 037†	4 741†	2 078†	1 876†	1 448†				
103 Lr	154 380†	30 240†	29 280†	22 360†	7 900†	7 460†	5 810†	5 150†	4 860†	2 140†	1 930†	1 480†				
104 Ku	158 300†	31 120†	30 140†	22 840†	8 120†	7 660†	5 910†	5 240†	4 980†	2 200†	1 970†	1 510†				

1. S. Hagström, and S.-E. Karlsson, Arkiv Fysik *26*, 451 (1964).
2. A. Fahlman, K. Hamrin, R. Nordberg, C. Nordling, and K. Siegbahn, Phys. Rev. Letters *14*, 127 (1965).
3. R. Nordberg, K. Hamrin, A. Fahlman, C. Nordling, and K. Siegbahn, Z. Phys. *192*, 462 (1966).
4. E. Sokolowski, Arkiv Fysik *15*, 1 (1959).
5. A. Fahlman, S. Hagström, K. Hamrin, R. Nordberg, C. Nordling, and K. Siegbahn, Arkiv Fysik *31*, 479 (1966).
6. C. Nordling, Arkiv Fysik *15*, 397 (1959).
7. I. Andersson, and S. Hagström, Arkiv Fysik *27*, 161 (1964).
8. A. Fahlman, O. Hörnfeldt, and C. Nordling, Arkiv Fysik *23*, 75 (1962).
9. P. Bergvall, O. Hörnfeldt, and C. Nordling, Arkiv Fysik *17*, 113 (1960).
10. P. Bergvall, and S. Hagström, Arkiv Fysik *17*, 61 (1960).
11. S. Hagström, Z. Phys. *178*, 82 (1964).
12. A. Fahlman, and S. Hagström, Arkiv Fysik *27*, 69 (1964).

$5s_{1/2}$ O_I	$5p_{1/2}$ O_{II}	$5p_{3/2}$ O_{III}	$5d_{3/2}$ O_{IV}	$5d_{5/2}$ O_V	$6s_{1/2}$ P_I	$6p_{1/2}$ P_{II}	$6p_{3/2}$ P_{III}	$6d_{3/2}$ P_{IV}	$6d_{5/2}$ P_V
310	223		94						
324	260	195	105	96	71	43	33	4	
338*	283[15]	206[15]	109[15]	101[15]					
352	279	212	116	105					
367*	290†	220†	116	103					
382*									
398[16]									
419†									
435†									
454†									
472†									
484†									
490†									
500†									

13. C. Nordling, and S. Hagström, Z. Phys. *178*, 418 (1964).
14. C. Nordling, and S. Hagström, Arkiv Fysik *15*, 431 (1959).
15. S. Hagström, Private Communication (1966) (work performed at Berkeley).
16. A. Fahlman, K. Hamrin, R. Nordberg, C. Nordling, K. Siegbahn, and L. W. Holm, Phys. Letters *19*, 643 (1966).
17. R. Nordling, J. Hedman, C. Nordling, and K. Siegbahn. To be published.
18. J. M. Hollander, M. D. Holtz, T. Novakov, and R. L. Graham, Arkiv Fysik *28*, 375.
19. R. Nordberg, R. G. Albridge, T. Bergmark, U. Ericson, J. Hedman, C. Nordling, K. Siegbahn, and B. J. Lindberg, Arkiv Kemi *28*, 257 (1968).
20. S.-E. Karlsson, C.-H. Norberg, Ö. Nilsson, S. Högberg, A. H. El-Farrash, C. Nordling, and K. Siegbahn. To be published in Arkiv Fysik.

APPENDIX 2

Comparison between Theoretical and Experimental Binding Energies

All theoretical values in this appendix are obtained by use of relativistic Hartree–Fock–Slater functions with optimized exchange correction (see Section III:9). A and B refer to the two methods described in the text. Most experimental values are taken from Appendix 1. For outer electrons some optical data are included (marked with $^+$). Measurements made on solids are corrected for the work function. All theoretical and experimental values are referred to the weighted average of the electron configuration. This implies e.g. that the values given for the outermost electrons differ somewhat from the normally quoted ionization energy, which is referred to the ground states of each configuration. All values are given in electron volts.

Comparison between theoretical and experimental binding energies (eV).

	Z = 6 C			Z = 7 N			Z = 8 O			Z = 9 F		
Shell	A	B	Exp	A	B	Exp	A	B	Exp	A	B	Exp
1*s* 1/2	310	297	288	428	412	403	564	546	536	717	697	690
2*s* 1/2	20.0	18.0	19.5$^+$	26.9	24.3	26$^+$	34.7	31.6	28; 32$^+$	42.8	39.9	(35); 40$^+$
2*p* 1/2	10.9	9.4	11; 10.7$^+$	13.8	11.7	13; 13.2$^+$	16.9	14.1	11; 15.9	19.6	16.8	13; 18.6$^+$
2*p* 3/2				14.5	12.5		17.5	14.7		19.8	17.1	

	Z = 10 Ne			Z = 11 Na			Z = 12 Mg			Z = 13 Al		
Shell	A	B	Exp	A	B	Exp	A	B	Exp	A	B	Exp
1*s* 1/2	894	870	867	1102	1079	1074	1336	1312	1309	1595	1569	1564
2*s* 1/2	53.9	49.1	(45)	75.9	71.9	65	103	97.7	93	134	128	122
2*p* 1/2	24.3	19.7	18; 21.7$^+$	41.1	36.7	33; 38$^+$	62.5		58	88.2	81.1	78
2*p* 3/2	24.2	19.6	18; 21.6$^+$	40.9	56.5		62.2			87.6	80.4	77
3*s* 1/2				5.0	5.3	3; 5.1$^+$	7.0		6; 7.6$^+$	11.1	10.1	5; 11.3$^+$
3*p* 1/2										5.6	5.4	6.0$^+$

	Z = 14 Si		Z = 15 P			Z = 16 S			Z = 17 Cl		
Shell	A	Exp	A	B	Exp	A	B	Exp	A	B	Exp
1*s* 1/2	1877	1843	2183	2154	2153	2510	2482	2476	2864	2834	2827
2*s* 1/2	168	153	206	198	193	245	238	233	290	281	274
2*p* 1/2	117	104	148	140	140	182	173	169	221	210	206
2*p* 3/2	116	103	147	138	139	180	172	168	219	208	204
3*s* 1/2	15.2	12; 15$^+$	19.6		20; 19$^+$	24.2	22.8	20; 22$^+$	29.5		22; 25.3$^+$
3*p* 1/2	7.3	7; 7.8$^+$	9.3		14; 10.1$^+$	11.3	10.4	12; 11.5$^+$	13.8		11; 13.7$^+$
3*p* 3/2			9.8			11.6	10.7		13.8		

	Z = 18 A			Z = 19 K			Z = 20 Ca		Z = 21 Sc		
Shell	A	B	Exp	A	B	Exp	A	Exp	A	B	Exp
1*s* 1/2	3240	3209	3203	3650	3618	3610	4084	4041	4539	4505	4497
2*s* 1/2	336	327	(320)	396	386	379	460	441	522	511	501
2*p* 1/2	261	250	247	315	303	299	372	353	428	415	411
2*p* 3/2	259	248	245	312	300	296	368	350	423	410	406
3*s* 1/2	34.9	33.3	25; 29$^+$	47.9		36	60.9	47	69.9		58
3*p* 1/2	16.1	14.8	12; 15.9$^+$	26.1		20; 25$^+$	36.2	29	43.4		36
3*p* 3/2	15.9	14.6	12; 15.8$^+$	25.8			35.7		41.7		
3*d* 3/2								8	8.5		11; 8.0$^+$
4*s* 1/2				4.1		4.3$^+$	5.3	6.1$^+$	5.8		6.6$^+$

Shell	Z = 22 Ti		Z = 23 V			Z = 24 Cr		Z = 25 Mn			Z = 26 Fe	
	A	Exp	A	B	Exp	A	Exp	A	B	Exp	A	Exp
1*s* 1/2	5018	4969	5521	5483	5469	6044	5993	6600	6560	6543	7177	7119
2*s* 1/2	587	569	656	641	632	723	699	802	785	773	881	851
2*p* 1/2	488	465	550	534	524	611	588	684	666	656	756	728
2*p* 3/2	481	459	542	525	517	601	579	672	653	645	742	715
3*s* 1/2	78.6	63	87.5		70	92.3	78	106		88	116	100
3*p* 1/2	50.6	37	58.1		42	61.1	47	72.3		53	78.9	61
3*p* 3/2	47.5	37	53.2		42	55.7	47	65.8		53	72.9	61
3*d* 3/2	10.3	7; 9.3[c]	12.0		6	8.9	6	14.8	11.3	8	16.0	11
3*d* 5/2						8.3		14.0	10.4		15.2	
4*s* 1/2	6.1	7.1[c]	6.4		7.5[c]	6.1	7[c]	7.0	6.6	7.5[c]	7.2	8[c]

Shell	Z = 27 Co			Z = 28 Ni		Z = 29 Cu			Z = 35 Br	
	A	B	Exp	A	Exp	A	B	Exp	A	Exp
1*s* 1/2	7778	7734	7713	8404	8338	9050	9001	8984	13562	13478
2*s* 1/2	963	943	930	1049	1013	1131	1107	1101	1823	1786
2*p* 1/2	832	810	798	911	877	986	960	956	1635	1600
2*p* 3/2	816	794	783	892	860	965	939	936	1587	1554
3*s* 1/2	126		105	136	117	140	132	125	276	261
3*p* 1/2	85.7		64	92.8	73	92.8	85.5	79	209	193
3*p* 3/2	80.3		64	88.0	73	90.0	82.9	79	202	186
3*d* 3/2	17.2	13.1	7; 15[c]	18.4	9	12.8	7.5	7; 10.6[c]	85.2	74
3*d* 5/2	16.5	12.4		17.8		12.4	7.2		84.0	73
4*s* 1/2	7.5	7.5	8[c]	7.7	9[c]	6.9	6.6	7.7[c]	27.7	31; 25[c]
4*p* 1/2									12.5	9; 12.5[c]
4*p* 3/2									12.1	

Shell	Z = 36 Kr			Z = 49 In		Z = 52 Te		Z = 53 I			Z = 54 Xe		
	A	B	Exp	A	Exp	A	Exp	A	B	Exp	A	B	Exp
1*s* 1/2	14410	14358	14326	28103	27944	31998	31819	33361	33294	33174	34756	34689	34561
2*s* 1/2	1958	1933	1921	4296	4242	5001	4911	5250	5215	5192	5507	5472	5453
2*p* 1/2	1762	1735	1727	3994	3942	4672	4617	4912	4873	4856	5159		5104
2*p* 3/2	1708	1681	1675	3782	3734	4396	4346	4612	4574	4561	4833		4782
3*s* 1/2	304	296	(289)	853	830	1035	1011	1101	1086	1076	1168		(1145)
3*p* 1/2	233	225	223	730	706	899	875	960		936	1023		999
3*p* 3/2	225	217	214	691	668	846	824	902		879	959		937
3*d* 3/2	101	93.3	89	476	455	608	587	656		635	706		(685)
3*d* 5/2	100	92.0	89	467	447	598	577	644		624	693		672
4*s* 1/2	32.2	30.9	24; 27.5[c]	144	126	193	173	210		190	229		(208)
4*p* 1/2	14.5	13.6	11; 14.7[c]	102	81	144	115	159		127	175		147
4*p* 3/2	13.8	12.9	11; 14.0[c]	94.9	81	134	115	147		127	162		147
4*d* 3/2				27.9	20	53.6	45	63.1		54	73.1		(63)
4*d* 5/2				26.9	20	52.0	45	61.3		54	71.0		(63)
5*s* 1/2				11.0	11.7[c]	20.6	17; 19[c]	24.0	22.7	14; 21[c]	27.6	26.3	(18); 23.4[c]
5*p* 1/2				5.3	5; 5.6[c]	10.0	7; 9.8[c]	11.7	10.7	7; 11[c]	13.5	12.4	(7); 13.4[c]
5*p* 3/2						9.2		10.6	9.8		12.0	11.1	(7); 12.1[c]

Shell	Z = 74 W		Z = 78 Pt		Z = 80 Hg		
	A	Exp	A	Exp	A	B	Exp
1*s*1/2	69991	69530	78947	78400	83704	83611	83108
2*s*1/2	12213	12104	14009	13885	14980	14923	14844
2*p*1/2	11650	11547	13393	13278	14336	14273	14214
2*p*3/2	10294	10210	11660	11569	12384	12328	12289
3*s*1/2	2873	2825	3356	3303	3623	3589	3567
3*p*1/2	2624	2580	3082	3032	3336		3284
3*p*3/2	2326	2286	2696	2645	2898		2852
3*d*3/2	1914	1877	2249	2207	2433		2390
3*d*5/2	1850	1815	2166	2126	2340		2300
4*s*1/2	625	600	757	729	834	817	805
4*p*1/2	521	497	640	613	711		682
4*p*3/2	451	431	547	524	604		576
4*d*3/2	281	264	357	336	403		384
4*d*5/2	267	251	339	319	382		365
4*f*5/2	51.3	42	93.3	79	122		108
4*f*7/2	48.4	39	89.6	75	117		104
5*s*1/2	94.1	82	121	107	139	133	125
5*p*1/2	62.5	52	82.0	71	96.7	91.0	86
5*p*3/2	48.8	42	65.6	56	77.7	73.1	63
5*d*3/2	9.6	11	12.8	7; 11[a]	17.9	14.8	12; 16.7[a]
5*d*5/2	8.2		11.2		15.9	13.2	12; 14.8[a]
6*s*1/2	7.4	8[a]	8.2	8.9[a]	9.3	8.5	10.4[a]

Shell	Z = 81 Tl		Z = 83 Bi		Z = 84 Po	
	A	Exp	A	Exp	A	Exp
1*s*1/2	86153	85535	91206	90530	93814	93109
2*s*1/2	15483	15351	16534	16392	17083	16943
2*p*1/2	14825	14702	15846	15713	16280	16248
2*p*3/2	12756	12661	13522	13422	13919	13818
3*s*1/2	3764	3708	4061	4003	4220	4153
3*p*1/2	3471	3420	3754	3701	3906	3858
3*p*3/2	3005	2961	3228	3181	3346	3306
3*d*3/2	2530	2489	2734	2692	2844	2802
3*d*5/2	2431	2394	2624	2584	2727	2687
4*s*1/2	878	850	971	943	1022	999
4*p*1/2	751	726	837	810	885	855
4*p*3/2	636	613	705	683	744	709
4*d*3/2	430	411	488	468	522	504
4*d*5/2	408	390	464	444	495	477
4*f*5/2	140	126	181	167	204	(188)
4*f*7/2	135	122	175	162	198	(188)
5*s*1/2	153	141	181	164	197	(181)
5*p*1/2	108	104	133	121	147	(136)
5*p*3/2	87.0	80	107	97	119	(108)
5*d*3/2	23.9	20	37.0	31	45.0	35
5*d*5/2	21.5	17	33.6	29	41.2	35
6*s*1/2	12.3	12.5[a]	18.6	(12)	22.5	(16)
6*p*1/2	5.7	6.1[a]	8.9	7; 8.1[a]	11.2	(9); 9[a]
6*p*3/2			6.7		8.1	

Shell	Z = 86 Rn		Z = 92 U		Z = 95 Am	
	A	Exp	A	Exp	A	Exp
1*s*1/2	99169	98404	116621	115609	126157	125031
2*s*1/2	18206	18049	21961	21761	24038	23777
2*p*1/2	17471	17337	21122	20951	23140	22948
2*p*3/2	14715	14619	17288	17171	18637	18508
3*s*1/2	4536	(4482)	5624	5551	6213	6124
3*p*1/2	4208	4159	5250	5184	5814	5714
3*p*3/2	3577	3538	4357	4307	4757	4671
3*d*3/2	3056	3022	3778	3731	4148	4098
3*d*5/2	2925	2892	3598	3555	3939	3891
4*s*1/2	1120	(1097)	1477	1445	1657	1621
4*p*1/2	975	929	1308	1276	1475	1416
4*p*3/2	815	768	1072	1048	1192	(1134)
4*d*3/2	582	567	806	783	908	883
4*d*5/2	552	(541)	762	741	856	832
4*f*5/2	246	(238)	411	395	482	444
4*f*7/2	239	(238)	399	384	467	444
5*s*1/2	226	(214)	341	327	386	(371)
5*p*1/2	172	(164)	274	263	313	294
5*p*3/2	138	(127)	218	198	242	224
5*d*3/2	57.6	(48)	118	108	136	120
5*d*5/2	53.0	(48)	107	99	120	107
5*f*5/2			8.8		9.0	
5*f*7/2			7.0		6.2	
6*s*1/2	28.6	26	57.6	74	61.1	
6*p*1/2	14.3	11; 14.6[a]	36.8	46	38.5	
6*p*3/2	10.0	11; 10.7[a]	25.9	36	25.4	
6*d*3/2			5.3	7		
7*s*1/2			5.5		5.2	

APPENDIX 3

Flow Diagram for the Calculation of Wave Functions, Potentials, and Energy Levels in the Atomic Core

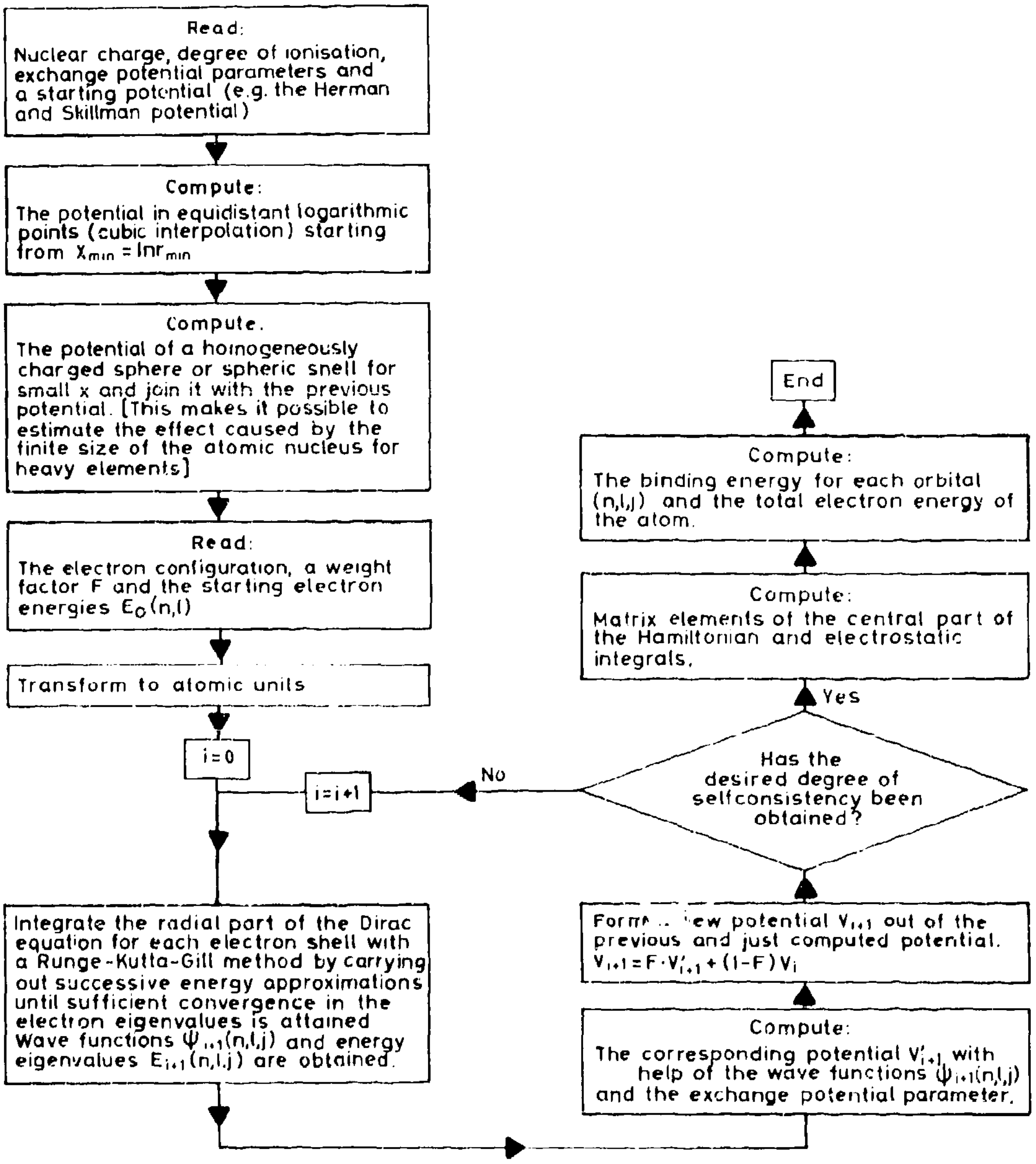

Read: Nuclear charge, degree of ionisation, exchange potential parameters and a starting potential (e.g. the Herman and Skillman potential)

Compute: The potential in equidistant logarithmic points (cubic interpolation) starting from $X_{min} = \ln r_{min}$

Compute. The potential of a homogeneously charged sphere or spheric snell for small x and join it with the previous potential. [This makes it possible to estimate the effect caused by the finite size of the atomic nucleus for heavy elements]

Read: The electron configuration, a weight factor F and the starting electron energies $E_0(n,l)$

Transform to atomic units

Integrate the radial part of the Dirac equation for each electron shell with a Runge-Kutta-Gill method by carrying out successive energy approximations until sufficient convergence in the electron eigenvalues is attained. Wave functions $\psi_{i+1}(n,l,j)$ and energy eigenvalues $E_{i+1}(n,l,j)$ are obtained.

Compute: The corresponding potential V'_{i+1} with help of the wave functions $\psi_{i+1}(n,l,j)$ and the exchange potential parameter.

Form a new potential V_{i+1} out of the previous and just computed potential. $V_{i+1} = F \cdot V'_{i+1} + (1-F) V_i$

Has the desired degree of selfconsistency been obtained?

Compute: Matrix elements of the central part of the Hamiltonian and electrostatic integrals.

Compute: The binding energy for each orbital (n,l,j) and the total electron energy of the atom.

APPENDIX 4

Table of *KLL* Auger Transition Energies

The following table of Auger energies in the *KLL* group is based on the precision measurements[33] which we have carried out in the region around $Z = 40$ (Chapter VI). The energies (in eV) have been calculated using semiempirical expressions for the energies of the *KLL* spectrum. Two sets of parameters have been used in the calculations, one[33] for elements with atomic number up to 40 and the other[35] for elements with Z higher than 40. Fig. 4 : 1 gives the relative positions of the *KLL* Auger lines as a function of atomic number Z.

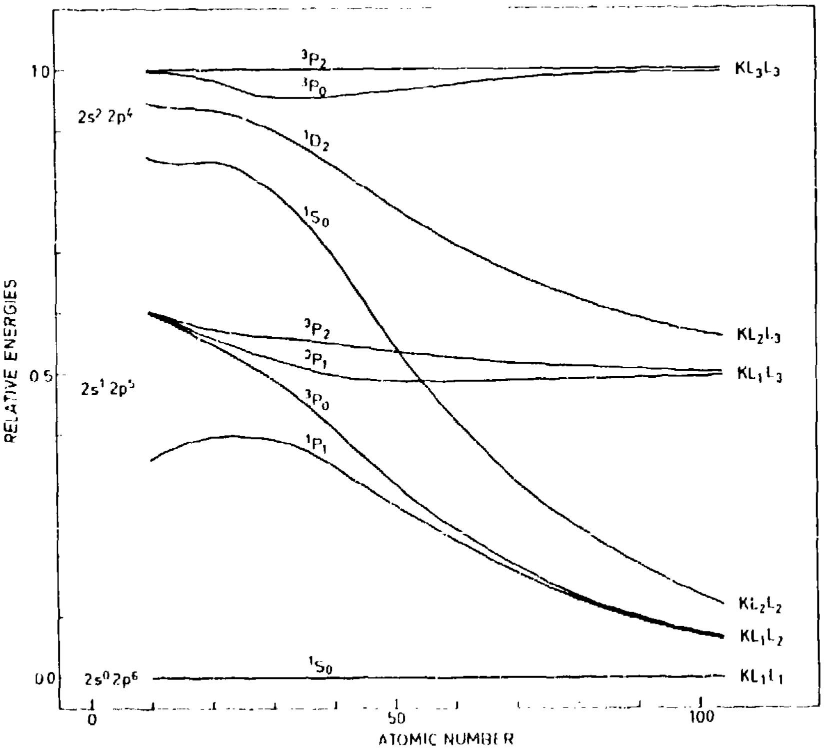

Fig. 4 : 1. Relative line positions in the *KLL* Auger group as a function of atomic number Z. The energy difference between the lines of highest and lowest energy ranges from 55 eV at $Z = 10$ to 17 keV at $Z = 104$.

KLL Auger energies (eV).

	$2s^02p^6$	$2s^12p^5$				$2s^22p^4$			
	$^1S_0$ KL_1L_1	$^1P_1$ KL_1L_2	$^3P_0$ KL_1L_2	$^3P_1$ KL_1L_3	$^3P_2$ KL_1L_3	$^1S_0$ KL_2L_2	$^1D_2$ KL_2L_3	$^3P_0$ KL_2L_3	$^3P_2$ KL_3L_3
C 6	243	252	258	258	258	265	266	267	267
N 7	356	362	369	369	369	373	375	377	377
O 8	474	486	495	495	495	504	507	509	509
F 9	610	627	638	638	638	650	654	657	657
Ne 10	761	781	794	794	794	808	813	816	816
Na 11	928	952	967	967	967	984	989	993	993
Mg 12	1 105	1 135	1 151	1 151	1 151	1 172	1 179	1 183	1 183
Al 13	1 301	1 336	1 354	1 354	1 354	1 379	1 387	1 392	1 392
Si 14	1 516	1 554	1 574	1 574	1 575	1 602	1 611	1 616	1 617
P 15	1 742	1 784	1 805	1 806	1 806	1 835	1 845	1 851	1 852
S 16	1 982	2 034	2 057	2 058	2 059	2 096	2 107	2 114	2 115
Cl 17	2 249	2 305	2 329	2 330	2 331	2 370	2 382	2 389	2 391
A 18	2 527	2 586	2 612	2 613	2 614	2 656	2 669	2 677	2 679
K 19	2 815	2 881	2 909	2 910	2 912	2 959	2 973	2 981	2 984
Ca 20	3 122	3 195	3 224	3 225	3 227	3 279	3 294	3 303	3 306
Sc 21	3 456	3 533	3 563	3 564	3 567	3 622	3 638	3 647	3 651
Ti 22	3 799	3 886	3 916	3 919	3 922	3 985	4 002	4 011	4 016
V 23	4 168	4 259	4 290	4 293	4 298	4 362	4 381	4 391	4 397
Cr 24	4 557	4 651	4 683	4 687	4 692	4 757	4 778	4 788	4 795
Mn 25	4 956	5 056	5 089	5 094	5 100	5 169	5 191	5 202	5 211
Fe 26	5 374	5 480	5 514	5 519	5 527	5 598	5 622	5 634	5 644
Co 27	5 808	5 923	5 957	5 964	5 972	6 049	6 075	6 088	6 099
Ni 28	6 264	6 384	6 419	6 426	6 436	6 514	6 542	6 556	6 568
Cu 29	6 732	6 861	6 896	6 905	6 916	7 000	7 030	7 045	7 059
Zn 30	7 214	7 348	7 384	7 394	7 407	7 493	7 526	7 543	7 558
Ga 31	7 712	7 852	7 888	7 900	7 915	8 000	8 037	8 057	8 073
Ge 32	8 216	8 365	8 401	8 416	8 433	8 523	8 563	8 586	8 603
As 33	8 749	8 903	8 939	8 957	8 975	9 063	9 107	9 133	9 152
Se 34	9 283	9 447	9 483	9 504	9 524	9 616	9 665	9 695	9 715
Br 35	9 840	10 014	10 049	10 074	10 096	10 189	10 244	10 279	10 300
Kr 36	10 412	10 594	10 630	10 658	10 682	10 777	10 837	10 877	10 899
Rb 37	10 995	11 186	11 221	11 255	11 280	11 376	11 442	11 487	11 511
Sr 38	11 595	11 795	11 830	11 870	11 897	11 992	12 066	12 118	12 143
Y 39	12 213	12 422	12 457	12 503	12 532	12 626	12 708	12 767	12 793
Zr 40	12 851	13 069	13 104	13 157	13 188	13 279	13 370	13 437	13 464
Nb 41	13 505	13 731	13 766	13 827	13 860	13 948	14 049	14 125	14 153
Mo 42	14 179	14 414	14 449	14 519	14 554	14 639	14 750	14 836	14 866
Tc 43	14 867	15 111	15 146	15 226	15 263	15 343	15 466	15 563	15 593
Ru 44	15 574	15 827	15 862	15 952	15 991	16 066	16 202	16 310	16 341
Rh 45	16 298	16 560	16 595	16 697	16 738	16 806	16 956	17 077	17 109
Pd 46	17 040	17 312	17 347	17 462	17 504	17 565	17 729	17 864	17 897
Ag 47	17 797	18 078	18 113	18 242	18 286	18 339	18 519	18 668	18 702
Cd 48	18 568	18 857	18 892	19 037	19 082	19 125	19 322	19 488	19 523
In 49	19 354	19 653	19 688	19 840	19 896	19 930	20 144	20 327	20 364
Sn 50	20 157	20 465	20 501	20 680	20 728	20 750	20 984	21 185	21 223
Sb 51	20 977	21 295	21 331	21 529	21 579	21 588	21 844	22 065	22 104
Te 52	21 814	22 142	22 179	22 398	22 449	22 444	22 722	22 965	23 005
I 53	22 668	23 006	23 043	23 284	23 338	23 316	23 618	23 884	23 925
Xe 54	23 527	22 879	23 916	24 182	24 237	24 201	24 530	24 822	24 863
Cs 55	24 426	24 783	24 820	25 111	25 167	25 106	25 463	25 781	25 823
Ba 56	25 330	25 697	25 735	26 053	26 111	26 033	26 416	26 762	26 805

	$2s^0 2p^6$	$2s^1 2p^5$				$2s^2 2p^4$			
	$^1S_0$ KL_1L_1	$^1P_1$ KL_1L_2	$^3P_0$ KL_1L_2	$^3P_1$ KL_1L_3	$^3P_2$ KL_1L_3	$^1S_0$ KL_2L_2	$^1D_2$ KL_2L_3	$^3P_0$ KL_3L_3	$^3P_2$ KL_3L_3
La 57	26 251	26 631	26 669	27 018	27 077	26 978	27 393	27 769	27 813
Ce 58	27 201	27 590	27 628	28 009	28 069	27 945	28 393	28 802	28 847
Pr 59	28 171	28 572	28 610	29 024	29 086	28 936	29 420	29 863	29 909
Nd 60	29 163	29 574	29 612	30 063	30 126	29 947	30 468	30 948	30 995
Pm 61	30 170	30 592	30 631	31 120	31 184	30 976	31 537	32 056	32 104
Sm 62	31 199	31 631	31 671	32 200	32 266	32 024	32 627	33 186	33 235
Eu 63	32 247	32 690	32 730	33 303	33 370	33 092	33 740	34 345	34 395
Gd 64	33 315	33 769	33 809	34 429	34 497	34 182	34 877	35 528	35 579
Tb 65	34 402	34 868	34 909	35 576	35 646	35 291	36 036	36 736	36 788
Dy 66	35 512	35 988	36 029	36 749	36 820	36 421	37 220	37 972	38 025
Ho 67	36 640	37 127	37 169	37 944	38 016	37 570	38 425	39 234	39 287
Er 68	37 788	38 287	38 329	39 162	39 236	38 740	39 655	40 522	40 576
Tm 69	38 958	39 469	39 512	40 406	40 481	39 934	40 91[illegible]	41 840	41 895
Yb 70	40 151	40 674	40 716	41 675	41 752	42 192	41 [illegible]49	43 186	43 242
Lu 71	41 361	41 897	41 940	42 967	43 045	42 383	43 496	44 559	44 617
Hf 72	42 589	43 137	43 181	44 280	44 359	43 635	44 821	45 957	46 015
Ta 73	43 831	44 391	44 436	45 611	45 691	44 900	46 164	47 377	47 436
W 74	45 097	45 671	45 715	46 971	47 053	46 193	47 538	48 831	48 891
Re 75	46 385	46 972	47 018	48 357	48 440	47 507	48 938	50 315	50 376
Os 76	47 690	48 291	48 337	49 767	49 851	48 839	50 361	51 830	51 892
Fr 77	49 022	49 636	49 682	51 205	51 291	50 195	51 812	53 375	53 437
Pt 78	50 375	51 003	51 050	52 672	52 759	51 575	53 292	54 954	55 017
Au 79	51 752	52 393	52 440	54 167	54 255	52 978	54 801	56 568	56 633
Hg 80	53 149	53 802	53 849	55 685	55 774	54 397	56 330	58 206	58 272
Tl 81	54 554	55 227	55 275	57 225	57 316	55 840	57 890	59 882	59 948
Pb 82	55 992	56 677	56 726	58 799	58 891	57 302	59 476	61 591	61 658
Bi 83	57 451	58 155	58 205	60 402	60 495	58 799	61 098	63 338	63 406
Po 84	58 918	59 640	59 690	62 026	62 120	60 299	62 739	65 118	65 187
At 85	60 427	61 163	61 213	63 689	63 784	61 836	64 416	66 935	67 005
Rn 86	61 986	62 720	62 771	65 392	65 489	63 397	66 124	68 789	68 860
Fr 87	63 523	64 286	64 337	67 114	67 212	64 983	67 868	70 690	70 762
Ra 88	65 103	65 887	65 939	68 879	68 978	66 604	69 654	72 640	72 712
Ac 89	66 720	67 509	67 562	70 673	70 774	68 232	71 453	74 611	74 684
Th 90	68 341	69 153	69 207	72 498	72 600	69 898	73 302	76 640	76 714
Pu 91	70 016	70 842	70 896	74 373	74 476	71 599	75 190	78 714	78 789
U 92	71 704	72 550	72 604	76 280	76 384	73 327	77 116	80 839	80 916
Np 93	73 437	74 297	74 351	78 236	78 342	75 085	79 086	83 019	83 096
Pa 94	75 204	76 080	76 135	80 237	80 344	76 884	81 103	85 254	85 332
Am 95	77 060	77 930	77 985	82 317	82 425	78 727	83 177	87 558	87 637
Cm 96	78 867	79 590	79 646	84 386	84 495	80 240	85 099	89 888	89 968
Bk 97	80 594	81 528	81 585	86 408	86 518	82 388	87 331	92 204	92 284
Cf 98	83 286	84 187	84 245	89 453	89 565	85 017	90 348	95 607	95 688
Es 99	85 219	86 146	86 204	91 701	91 814	86 997	92 617	98 165	98 248
Fm 100	87 [illegible]	88 144	88 203	93 998	94 113	89 006	94 926	100 774	100 857
Md 101	89 2[illegible]	90 192	90 251	96 356	96 471	91 085	97 315	103 472	103 556
No 102	91 267	92 260	92 320	98 763	98 880	93 173	99 744	106 240	106 325
Lr 103	93 373	94 388	94 448	101 250	101 368	95 322	102 252	109 108	109 194
Ku 104	95 518	96 565	96 615	103 796	103 915	97 510	104 820	112 056	112 142

Electron energies (keV) versus magnetic rigidity (Gcm).

Bϱ	.0	Δ	.1	Δ	.2	Δ	.3	Δ	.4	Δ	.5	Δ	.6	Δ	.7	Δ	.8	Δ	.9	Δ	Bϱ
0	0.00000	0	0.00000	0	0.00000	0	0.00001	1	0.00001	1	0.00002	1	0.00003	1	0.00004	1	0.00006	1	0.00007	2	0
1	0.00009	2	0.00011	2	0.00013	2	0.00015	2	0.00017	3	0.00020	3	0.00023	3	0.00025	3	0.00028	3	0.00032	3	1
2	0.00035	4	0.00039	4	0.00043	4	0.00047	4	0.00051	4	0.00055	4	0.00059	5	0.00064	5	0.00069	5	0.00074	5	2
3	0.00079	5	0.00085	6	0.00090	6	0.00096	6	0.00102	6	0.00108	6	0.00114	6	0.00120	7	0.00127	7	0.00134	7	3
4	0.00141	7	0.00148	7	0.00155	7	0.00163	8	0.00170	8	0.00178	8	0.00186	8	0.00194	8	0.00203	9	0.00211	9	4
5	0.00220	9	0.00229	9	0.00238	9	0.00247	9	0.00256	10	0.00266	10	0.00276	10	0.00286	10	0.00296	10	0.00306	10	5
6	0.00317	11	0.00327	11	0.00338	11	0.00349	11	0.00360	11	0.00372	12	0.00383	12	0.00395	12	0.00407	12	0.00419	12	6
7	0.00431	12	0.00443	13	0.00456	13	0.00469	13	0.00482	13	0.00495	13	0.00508	13	0.00521	14	0.00535	14	0.00549	14	7
8	0.00563	14	0.00577	14	0.00591	15	0.00606	15	0.00620	15	0.00635	15	0.00650	15	0.00666	15	0.00681	16	0.00697	16	8
9	0.00712	16	0.00728	16	0.00744	16	0.00761	16	0.00777	17	0.00794	17	0.00810	17	0.00827	17	0.00845	17	0.00862	18	9
10	0.00879	18	0.00897	18	0.00915	18	0.00933	18	0.00951	18	0.00970	19	0.00988	19	0.01007	19	0.01026	19	0.01045	19	10
11	0.01064	19	0.01083	20	0.01103	20	0.01123	20	0.01143	20	0.01163	20	0.01183	20	0.01204	21	0.01224	21	0.01245	21	11
12	0.01266	21	0.01288	21	0.01309	22	0.01330	22	0.01352	22	0.01374	22	0.01396	22	0.01418	22	0.01441	23	0.01463	23	12
13	0.01486	23	0.01509	23	0.01532	23	0.01556	23	0.01579	24	0.01603	24	0.01627	24	0.01651	24	0.01675	24	0.01699	25	13
14	0.01724	25	0.01748	25	0.01773	25	0.01798	25	0.01823	25	0.01849	26	0.01874	26	0.01900	26	0.01926	26	0.01952	26	14
15	0.01979	26	0.02005	27	0.02032	27	0.02059	27	0.02086	27	0.02113	27	0.02140	28	0.02168	28	0.02195	28	0.02223	28	15
16	0.02251	28	0.02279	28	0.02308	29	0.02336	29	0.02365	29	0.02394	29	0.02423	29	0.02452	29	0.02482	30	0.02512	30	16
17	0.02541	30	0.02571	30	0.02602	30	0.02632	31	0.02662	31	0.02693	31	0.02724	31	0.02755	31	0.02786	31	0.02818	32	17
18	0.02849	32	0.02881	32	0.02913	32	0.02945	32	0.02977	32	0.03010	33	0.03042	33	0.03075	33	0.03108	33	0.03141	33	18
19	0.03175	34	0.03208	34	0.03242	34	0.03276	34	0.03310	34	0.03344	34	0.03378	35	0.03413	35	0.03447	35	0.03482	35	19
20	0.03517	35	0.03553	35	0.03588	36	0.03624	36	0.03660	36	0.03696	36	0.03732	36	0.03768	36	0.03804	37	0.03841	37	20
21	0.03878	37	0.03915	37	0.03952	37	0.03990	38	0.04027	38	0.04065	38	0.04103	38	0.04141	38	0.04179	38	0.04218	39	21
22	0.04256	39	0.04295	39	0.04334	39	0.04373	39	0.04412	39	0.04452	40	0.04491	40	0.04531	40	0.04571	40	0.04611	40	22
23	0.04652	41	0.04692	41	0.04733	41	0.04774	41	0.04815	41	0.04856	41	0.04898	42	0.04939	42	0.04981	42	0.05023	42	23
24	0.05065	42	0.05107	42	0.05150	43	0.05192	43	0.05235	43	0.05278	43	0.05321	43	0.05365	44	0.05408	44	0.05452	44	24
25	0.05496	44	0.05540	44	0.05584	44	0.05629	45	0.05673	45	0.05718	45	0.05763	45	0.05808	45	0.05853	45	0.05899	46	25
26	0.05944	46	0.05990	46	0.06036	46	0.06082	46	0.06129	47	0.06175	47	0.06222	47	0.06269	47	0.06316	47	0.06363	47	26
27	0.06410	48	0.06458	48	0.06506	48	0.06554	48	0.06602	48	0.06650	48	0.06698	49	0.06747	49	0.06796	49	0.06845	49	27
28	0.06894	49	0.06943	50	0.06993	50	0.07043	50	0.07092	50	0.07142	50	0.07193	50	0.07243	51	0.07294	51	0.07344	51	28
29	0.07395	51	0.07446	51	0.07498	51	0.07549	52	0.07601	52	0.07652	52	0.07704	52	0.07756	52	0.07809	52	0.07861	53	29
30	0.07914	53	0.07967	53	0.08020	53	0.08073	53	0.08126	54	0.08180	54	0.08234	54	0.08288	54	0.08342	54	0.08396	54	30
31	0.08450	55	0.08505	55	0.08560	55	0.08615	55	0.08670	55	0.08725	55	0.08781	56	0.08836	56	0.08892	56	0.08948	56	31
32	0.09004	56	0.09061	57	0.09117	57	0.09174	57	0.09231	57	0.09288	57	0.09345	57	0.09402	58	0.09460	58	0.09518	58	32
33	0.09576	58	0.09634	58	0.09692	58	0.09751	59	0.09809	59	0.09868	59	0.09927	59	0.09986	59	0.10046	60	0.10105	60	33
34	0.10165	60	0.10225	60	0.10285	60	0.10345	60	0.10405	61	0.10466	61	0.10527	61	0.10588	61	0.10649	61	0.10710	61	34
35	0.10771	62	0.10833	62	0.10895	62	0.10957	62	0.11019	62	0.11081	63	0.11144	63	0.11207	63	0.11269	63	0.11333	63	35
36	0.11396	63	0.11459	64	0.11523	64	0.11586	64	0.11650	64	0.11714	64	0.11779	64	0.11843	65	0.11908	65	0.11973	65	36
37	0.12038	65	0.12103	65	0.12168	65	0.12234	66	0.12299	66	0.12365	66	0.12431	66	0.12497	66	0.12564	67	0.12630	67	37
38	0.12697	67	0.12764	67	0.12831	67	0.12898	67	0.12966	68	0.13033	68	0.13101	68	0.13169	68	0.13237	68	0.13305	68	38
39	0.13374	69	0.13443	69	0.13511	69	0.13580	69	0.13650	69	0.13719	70	0.13789	70	0.13858	70	0.13928	70	0.13998	70	39
40	0.14068	70	0.14139	71	0.14209	71	0.14280	71	0.14351	71	0.14422	71	0.14494	71	0.14565	72	0.14637	72	0.14709	72	40
41	0.14781	72	0.14853	72	0.14925	73	0.14998	73	0.15070	73	0.15143	73	0.15216	73	0.15289	73	0.15363	74	0.15436	74	41
42	0.15510	74	0.15584	74	0.15658	74	0.15733	74	0.15807	75	0.15882	75	0.15956	75	0.16031	75	0.16107	75	0.16182	76	42

APPENDIX 5

Kinetic Energy (keV) versus Magnetic Rigidity (Gcm) for Electrons with Bϱ-values below 500 Gcm (Energies below 21.5 keV)

Tabulated values are obtained from the relation

$$E = m_0c^2[\sqrt{(e/m_0c)^2(B\varrho)^2 + 1} - 1]$$

where the 1963 least-squares adjusted values of the fundamental constants[148] have been used:

$$m_0c^2 = (511.006 \pm 0.002)\ \text{keV}$$

$$e/m_0c \quad (5.86670 \pm 0.00002) \times 10^{-4}\ (\text{Gcm})^{-1}$$

To facilitate interpolation the energy differences, Δ, are also tabulated. The relation between kinetic energy and magnetic rigidity for electrons is given in graphical form in Fig. 5:1.

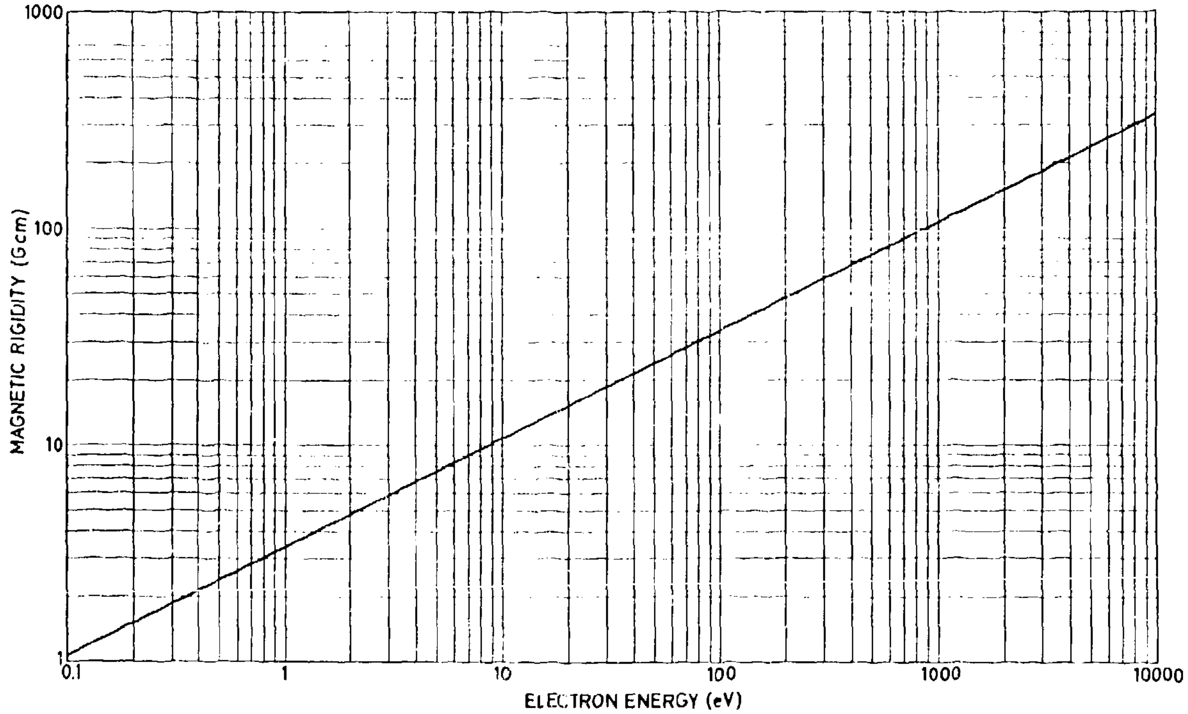

Fig. 5:1. Magnetic rigidity, $B\varrho$, versus kinetic energy for electrons.

43	0.16257	76	0.16333	76	0.16409	76	0.16485	76	0.16561	76	0.16638	77	0.16714	77	0.16791	77	0.16868	77	0.16945	77	43
44	0.17022	77	0.17100	78	0.17177	78	0.17255	78	0.17333	78	0.17411	78	0.17490	79	0.17568	79	0.17647	79	0.17726	79	44
45	0.17805	79	0.17884	79	0.17963	80	0.18043	80	0.18123	80	0.18202	80	0.18283	80	0.18363	80	0.18443	81	0.18524	81	45
46	0.18605	81	0.18686	81	0.18767	81	0.18848	81	0.18930	82	0.19011	82	0.19093	82	0.19175	82	0.19257	82	0.19340	83	46
47	0.19422	83	0.19505	83	0.19588	83	0.19671	83	0.19754	83	0.19838	84	0.19921	84	0.20005	84	0.20089	84	0.20173	84	47
48	0.20257	84	0.20342	85	0.20426	85	0.20511	85	0.20596	85	0.20681	85	0.20767	86	0.20852	86	0.20938	86	0.21024	86	48
49	0.21110	86	0.21196	86	0.21283	87	0.21369	87	0.21456	87	0.21543	87	0.21630	87	0.21717	87	0.21805	88	0.21892	88	49
50	0.21980	88	0.22068	88	0.22156	88	0.22245	89	0.22333	89	0.22422	89	0.22511	89	0.22600	89	0.22689	89	0.22778	90	50
51	0.22868	90	0.22958	90	0.23048	90	0.23138	90	0.23228	90	0.23319	91	0.23409	91	0.23500	91	0.23591	91	0.23682	91	51
52	0.23773	92	0.23865	92	0.23957	92	0.24048	92	0.24140	92	0.24233	92	0.24325	93	0.24418	93	0.24510	93	0.24603	93	52
53	0.24696	93	0.24790	93	0.24883	94	0.24977	94	0.25070	94	0.25164	94	0.25259	94	0.25353	94	0.25447	95	0.25542	95	53
54	0.25637	95	0.25732	95	0.25827	95	0.25922	96	0.26018	96	0.26114	96	0.26210	96	0.26306	96	0.26402	96	0.26498	97	54
55	0.26595	97	0.26692	97	0.26789	97	0.26886	97	0.26983	97	0.27080	98	0.27178	98	0.27276	98	0.27374	98	0.27472	98	55
56	0.27570	99	0.27669	99	0.27768	99	0.27867	99	0.27966	99	0.28065	99	0.28164	100	0.28264	100	0.28364	100	0.28464	100	56
57	0.28564	100	0.28664	100	0.28764	101	0.28865	101	0.28966	101	0.29067	101	0.29168	101	0.29269	102	0.29371	102	0.29473	102	57
58	0.29574	102	0.29676	102	0.29779	102	0.29881	103	0.29984	103	0.30086	103	0.30189	103	0.30292	103	0.30396	103	0.30499	104	58
59	0.30603	104	0.30706	104	0.30810	104	0.30915	104	0.31019	104	0.31123	105	0.31228	105	0.31333	105	0.31438	105	0.31543	105	59
60	0.31649	106	0.31754	106	0.31860	106	0.31966	106	0.32072	106	0.32178	106	0.32284	107	0.32391	107	0.32498	107	0.32605	107	60
61	0.32712	107	0.32819	107	0.32927	108	0.33034	108	0.33142	108	0.33250	108	0.33358	108	0.33467	109	0.33575	109	0.33684	109	61
62	0.33793	109	0.33902	109	0.34011	109	0.34121	110	0.34230	110	0.34340	110	0.34450	110	0.34560	110	0.34670	110	0.34781	111	62
63	0.34891	111	0.35002	111	0.35113	111	0.35224	111	0.35336	112	0.35447	112	0.35559	112	0.35671	112	0.35783	112	0.35895	112	63
64	0.36007	113	0.36120	113	0.36233	113	0.36346	113	0.36459	113	0.36572	113	0.36686	114	0.36799	114	0.36913	114	0.37027	114	64
65	0.37141	114	0.37255	115	0.37370	115	0.37485	115	0.37599	115	0.37714	115	0.37830	115	0.37945	116	0.38061	116	0.38176	116	65
66	0.38292	116	0.38408	116	0.38525	116	0.38641	117	0.38758	117	0.38874	117	0.38991	117	0.39108	117	0.39226	117	0.39343	118	66
67	0.39461	118	0.39579	118	0.39697	118	0.39815	118	0.39933	119	0.40052	119	0.40171	119	0.40289	119	0.40409	119	0.40528	119	67
68	0.40647	120	0.40767	120	0.40887	120	0.41006	120	0.41127	120	0.41247	120	0.41367	121	0.41488	121	0.41609	121	0.41730	121	68
69	0.41851	121	0.41972	122	0.42094	122	0.42216	122	0.42337	122	0.42459	122	0.42582	122	0.42704	123	0.42827	123	0.42949	123	69
70	0.43072	123	0.43195	123	0.43319	123	0.43442	124	0.43566	124	0.43690	124	0.43814	124	0.43938	124	0.44062	125	0.44187	125	70
71	0.44311	125	0.44436	125	0.44561	125	0.44686	125	0.44812	126	0.44937	126	0.45063	126	0.45189	126	0.45315	126	0.45441	126	71
72	0.45568	127	0.45694	127	0.45821	127	0.45948	127	0.46075	127	0.46202	127	0.46330	128	0.46458	128	0.46585	128	0.46713	128	72
73	0.46842	128	0.46970	129	0.47099	129	0.47227	129	0.47356	129	0.47485	129	0.47614	129	0.47744	130	0.47873	130	0.48003	130	73
74	0.48133	130	0.48263	130	0.48394	130	0.48524	131	0.48655	131	0.48785	131	0.48916	131	0.49048	131	0.49179	132	0.49311	132	74
75	0.49442	132	0.49574	132	0.49706	132	0.49838	132	0.49971	133	0.50103	133	0.50236	133	0.50369	133	0.50502	133	0.50635	133	75
76	0.50769	134	0.50902	134	0.51036	134	0.51170	134	0.51304	134	0.51439	135	0.51573	135	0.51708	135	0.51843	135	0.51978	135	76
77	0.52113	135	0.52248	136	0.52384	136	0.52520	136	0.52655	136	0.52792	136	0.52928	136	0.53064	137	0.53201	137	0.53338	137	77
78	0.53475	137	0.53612	137	0.53749	137	0.53887	138	0.54024	138	0.54162	138	0.54300	138	0.54438	138	0.54577	139	0.54715	139	78
79	0.54854	139	0.54993	139	0.55132	139	0.55271	139	0.55410	140	0.55550	140	0.55690	140	0.55830	140	0.55970	140	0.56110	140	79
80	0.56251	141	0.56391	141	0.56532	141	0.56673	141	0.56814	141	0.56955	142	0.57097	142	0.57239	142	0.57381	142	0.57523	142	80
81	0.57665	142	0.57807	143	0.57950	143	0.58092	143	0.58235	143	0.58378	143	0.58522	143	0.58665	144	0.58809	144	0.58953	144	81
82	0.59097	144	0.59241	144	0.59385	144	0.59529	145	0.59674	145	0.59819	145	0.59964	145	0.60109	145	0.60255	146	0.60400	146	82
83	0.60546	146	0.60692	146	0.60838	146	0.60984	146	0.61130	147	0.61277	147	0.61424	147	0.61571	147	0.61718	147	0.61865	147	83
84	0.62013	148	0.62160	148	0.62308	148	0.62456	148	0.62604	148	0.62753	149	0.62901	149	0.63050	149	0.63199	149	0.63348	149	84
85	0.63497	149	0.63646	150	0.63796	150	0.63946	150	0.64096	150	0.64246	150	0.64396	150	0.64547	151	0.64697	151	0.64848	151	85
86	0.64999	151	0.65150	151	0.65301	152	0.65453	152	0.65605	152	0.65756	152	0.65908	152	0.66061	152	0.66213	153	0.66366	153	86
87	0.66518	153	0.66671	153	0.66824	153	0.66978	153	0.67131	154	0.67285	154	0.67438	154	0.67592	154	0.67746	154	0.67901	154	87
88	0.68055	155	0.68210	155	0.68365	155	0.68520	155	0.68675	155	0.68830	156	0.68986	156	0.69142	156	0.69297	156	0.69453	156	88
89	0.69610	156	0.69766	157	0.69923	157	0.70079	157	0.70236	157	0.70393	157	0.70551	157	0.70708	158	0.70866	158	0.71024	158	89

Bϱ	.0	Δ	.1	Δ	.2	Δ	.3	Δ	.4	Δ	.5	Δ	.6	Δ	.7	Δ	.8	Δ	.9	Δ	Bϱ
90	0.71182	158	0.71340	158	0.71498	159	0.71657	159	0.71815	159	0.71974	159	0.72133	159	0.72292	159	0.72452	160	0.72611	160	90
91	0.72771	160	0.72931	160	0.73091	160	0.73251	160	0.73412	161	0.73572	161	0.73733	161	0.73894	161	0.74055	161	0.74217	161	91
92	0.74378	162	0.74540	162	0.74702	162	0.74864	162	0.75026	162	0.75188	163	0.75351	163	0.75513	163	0.75676	163	0.75839	163	92
93	0.76003	163	0.76166	164	0.76330	164	0.76493	164	0.76657	164	0.76821	164	0.76986	164	0.77150	165	0.77315	165	0.77480	165	93
94	0.77645	165	0.77810	165	0.77975	166	0.78141	166	0.78306	166	0.78472	166	0.78638	166	0.78804	166	0.78971	167	0.79137	167	90
95	0.79304	167	0.79471	167	0.79638	167	0.79805	167	0.79973	168	0.80140	168	0.80308	168	0.80476	168	0.80644	168	0.80813	168	95
96	0.80981	169	0.81150	169	0.81319	169	0.81488	169	0.81657	169	0.81826	170	0.81996	170	0.82165	170	0.82335	170	0.82505	170	96
97	0.82676	170	0.82846	171	0.83017	171	0.83187	171	0.83358	171	0.83529	171	0.83701	171	0.83872	172	0.84044	172	0.84216	172	97
98	0.84388	172	0.84560	172	0.84732	173	0.84905	173	0.85077	173	0.85250	173	0.85423	173	0.85597	173	0.85770	174	0.85943	174	98
99	0.86117	174	0.86291	174	0.86465	174	0.86639	174	0.86814	175	0.86989	175	0.87163	175	0.87338	175	0.87513	175	0.87689	175	99
100	0.87864	176	0.88040	176	0.88216	176	0.88392	176	0.88568	176	0.88744	177	0.88921	177	0.89098	177	0.89274	177	0.89452	177	100
101	0.89629	177	0.89806	178	0.89984	178	0.90162	178	0.90339	178	0.90518	178	0.90696	178	0.90874	179	0.91053	179	0.91232	179	101
102	0.91411	179	0.91590	179	0.91769	180	0.91949	180	0.92129	180	0.92308	180	0.92488	180	0.92669	180	0.92849	181	0.93030	181	102
103	0.93210	181	0.93391	181	0.93572	181	0.93754	181	0.93935	182	0.94117	182	0.94298	182	0.94480	182	0.94663	182	0.94845	182	103
104	0.95027	183	0.95210	183	0.95393	183	0.95576	183	0.95759	183	0.95942	184	0.96126	184	0.96310	184	0.96494	184	0.96678	184	104
105	0.96862	184	0.97046	185	0.97231	185	0.97416	185	0.97601	185	0.97786	185	0.97971	185	0.98156	186	0.98342	186	0.98528	186	105
106	0.98714	186	0.98900	186	0.99086	187	0.99273	187	0.99459	187	0.99646	187	0.99833	187	1.00021	187	1.00208	188	1.00396	188	106
107	1.00583	188	1.00771	188	1.00959	188	1.01148	188	1.01336	189	1.01525	189	1.01713	189	1.01902	189	1.02091	189	1.02281	189	107
108	1.02470	190	1.02660	190	1.02850	190	1.03040	190	1.03230	190	1.03420	191	1.03611	191	1.03801	191	1.03992	191	1.04183	191	108
109	1.04375	191	1.04566	192	1.04758	192	1.04949	192	1.05141	192	1.05333	192	1.05526	192	1.05718	193	1.05911	193	1.06104	193	109
110	1.06297	193	1.06490	193	1.06683	194	1.06877	194	1.07070	194	1.07264	194	1.07458	194	1.07652	194	1.07847	195	1.08041	195	110
111	1.08236	195	1.08431	195	1.08626	195	1.08821	195	1.09017	196	1.09212	196	1.09408	196	1.09604	196	1.09800	196	1.09996	196	111
112	1.10193	197	1.10390	197	1.10586	197	1.10783	197	1.10981	197	1.11178	198	1.11375	198	1.11573	198	1.11771	198	1.11969	198	112
113	1.12167	198	1.12366	199	1.12564	199	1.12763	199	1.12962	199	1.13161	199	1.13360	199	1.13560	200	1.13759	200	1.13959	200	113
114	1.14159	200	1.14359	200	1.14559	200	1.14760	201	1.14961	201	1.15161	201	1.15363	201	1.15564	201	1.15765	202	1.15967	202	114
115	1.16168	202	1.16370	202	1.16572	202	1.16775	202	1.16977	203	1.17180	203	1.17382	203	1.17585	203	1.17788	203	1.17992	203	115
116	1.18195	204	1.18399	204	1.18603	204	1.18807	204	1.19011	204	1.19215	205	1.19420	205	1.19624	205	1.19829	205	1.20034	205	116
117	1.20239	205	1.20445	206	1.20650	206	1.20856	206	1.21062	206	1.21268	206	1.21474	206	1.21681	207	1.21887	207	1.22094	207	117
118	1.22301	207	1.22508	207	1.22715	207	1.22923	208	1.23131	208	1.23338	208	1.23546	208	1.22755	208	1.23963	208	1.24171	209	118
119	1.24380	209	1.24589	209	1.24798	209	1.25007	209	1.25217	210	1.25426	210	1.25636	210	1.25846	210	1.26056	210	1.26266	210	119
120	1.26477	211	1.26687	211	1.26898	211	1.27109	211	1.27320	211	1.27532	211	1.27743	212	1.27955	212	1.28167	212	1.28379	212	120
121	1.28591	212	1.28803	213	1.29016	213	1.29228	213	1.29441	213	1.29654	213	1.29868	213	1.30081	214	1.30295	214	1.30508	214	121
122	1.30722	214	1.30936	214	1.31151	214	1.31265	215	1.31580	215	1.31795	215	1.32010	215	1.32225	215	1.32440	216	1.32656	215	122
123	1.32871	216	1.33087	216	1.33303	216	1.33519	216	1.33736	217	1.33952	217	1.34169	217	1.34586	217	1.34603	217	1.34820	218	123
124	1.35038	218	1.35255	218	1.35473	218	1.35691	218	1.35909	218	1.36128	218	1.36346	219	1.36565	219	1.36784	219	1.37002	219	124
125	1.37222	219	1.37441	220	1.37661	220	1.37880	220	1.38100	220	1.38320	220	1.38540	220	1.38761	221	1.38981	221	1.39202	221	125
126	1.39423	221	1.39644	221	1.39865	221	1.40087	222	1.40308	222	1.40530	222	1.40752	222	1.40974	222	1.41196	223	1.41419	223	126
127	1.41642	223	1.41865	223	1.42088	223	1.42311	223	1.42534	224	1.42758	224	1.42981	224	1.43205	224	1.43429	224	1.45654	224	127
128	1.43878	225	1.44103	225	1.44327	225	1.44552	225	1.44777	225	1.45003	225	1.45228	226	1.45454	226	1.45680	226	1.45906	226	128
129	1.46132	226	1.46358	226	1.46584	227	1.46811	227	1.47038	227	1.47265	227	1.47492	227	1.47720	228	1.47947	228	1.48175	228	129
130	1.48403	228	1.48631	228	1.48859	228	1.49087	229	1.49316	229	1.49545	229	1.49774	229	1.50003	229	1.50232	229	1.50462	230	130
131	1.50691	230	1.50921	230	1.51151	230	1.51381	230	1.51612	231	1.51842	231	1.52073	231	1.52304	231	1.52535	231	1.52766	231	131
132	1.52997	232	1.53229	232	1.53461	232	1.53692	232	1.53925	232	1.54157	232	1.54389	233	1.54622	233	1.54855	233	1.55088	233	132
133	1.55321	233	1.55554	233	1.55787	234	1.56021	234	1.56255	234	1.56489	234	1.56723	234	1.56957	235	1.57192	235	1.57427	235	133

134	1.57661	235	1.57897	235	1.58132	235	1.58367	236	1.58603	236	1.58838	236	1.59074	236	1.59310	236	1.59547	236	1.59783	237	134
135	1.60020	237	1.60256	237	1.60493	237	1.60731	237	1.60968	237	1.61205	238	1.61443	238	1.61681	238	1.61919	238	1.62157	238	135
136	1.62395	239	1.62634	239	1.62873	239	1.63111	239	1.63351	239	1.63590	239	1.63829	240	1.64069	240	1.64308	240	1.64548	240	136
137	1.64788	240	1.65029	240	1.65269	241	1.65510	241	1.65751	241	1.65992	241	1.66233	241	1.66474	241	1.66715	242	1.66957	242	137
138	1.67199	242	1.67441	242	1.67683	242	1.67926	243	1.68168	243	1.68411	243	1.68654	243	1.68897	243	1.69140	243	1.69383	244	138
139	1.69627	244	1.69871	244	1.70115	244	1.70359	244	1.70603	244	1.70847	245	1.71092	245	1.71337	245	1.71582	245	1.71827	245	139
140	1.72072	245	1.72318	246	1.72563	246	1.72809	246	1.73055	246	1.73301	246	1.73548	247	1.73794	247	1.74041	247	1.74288	247	140
141	1.74535	247	1.74782	247	1.75030	248	1.75277	248	1.75525	248	1.75773	248	1.76021	248	1.76269	248	1.76518	249	1.76766	249	141
142	1.77015	249	1.77264	249	1.77513	249	1.77763	249	1.78012	250	1.78262	250	1.78512	250	1.78762	250	1.79012	250	1.79262	251	142
143	1.79513	251	1.79763	251	1.80014	251	1.80265	251	1.80517	251	1.80768	252	1.81020	252	1.81271	252	1.81523	252	1.81775	252	143
144	1.82028	252	1.82280	253	1.82533	253	1.82786	253	1.83039	253	1.83292	253	1.83545	253	1.83799	254	1.84052	254	1.84306	254	144
145	1.84560	254	1.84814	254	1.85069	255	1.85323	255	1.85578	255	1.85833	255	1.86088	255	1.86343	255	1.86599	256	1.86854	256	145
146	1.87110	256	1.87366	256	1.87622	256	1.87878	256	1.88135	257	1.88391	257	1.88648	257	1.88905	257	1.89162	257	1.89420	257	146
147	1.89677	258	1.89935	258	1.90193	258	1.90451	258	1.90709	258	1.90967	259	1.91226	259	1.91484	259	1.91743	259	1.92002	259	147
148	1.92262	259	1.92521	260	1.92781	260	1.93040	260	1.93300	260	1.93560	260	1.93821	260	1.94081	261	1.94342	261	1.94603	261	148
149	1.94864	261	1.95125	261	1.95386	261	1.95648	262	1.95909	262	1.96171	262	1.96433	262	1.96695	262	1.96958	263	1.97220	263	149
150	1.97483	263	1.97746	263	1.98009	263	1.98272	263	1.98536	264	1.98799	264	1.99063	264	1.99327	264	1.99591	264	1.99855	264	150
151	2.00120	265	2.00384	265	2.00649	265	2.00914	265	2.01179	265	2.01445	265	2.01710	266	2.01976	266	2.02242	266	2.02508	266	151
152	2.02774	266	2.03040	267	2.03307	267	2.03573	267	2.03840	267	2.04107	267	2.04375	267	2.04642	268	2.04910	268	2.05177	268	152
153	2.05445	268	2.05713	268	2.05982	268	2.06250	269	2.06519	269	2.06788	269	2.07056	269	2.07326	269	2.07595	269	2.07864	270	153
154	2.08134	270	2.08404	270	2.08674	270	2.08944	270	2.09215	271	2.09485	271	2.09756	271	2.10027	271	2.10298	271	2.10569	271	154
155	2.10840	272	2.11112	272	2.11384	272	2.11656	272	2.11928	272	2.12200	272	2.12472	273	2.12745	273	2.13018	273	2.13291	273	155
156	2.13564	273	2.13837	273	2.14111	274	2.14384	274	2.14658	274	2.14932	274	2.15206	274	2.15481	275	2.15755	275	2.16030	275	156
157	2.16305	275	2.16580	275	2.16855	275	2.17131	276	2.17406	276	2.17682	276	2.17958	276	2.18234	276	2.18510	276	2.18787	277	157
158	2.19063	277	2.19340	277	2.19617	277	2.19894	277	2.20172	277	2.20449	278	2.20727	278	2.21005	278	2.21283	278	2.21561	278	158
159	2.21839	279	2.22118	279	2.22396	279	2.22675	279	2.22954	279	2.23233	279	2.23513	280	2.23792	280	2.24072	280	2.24352	280	159
160	2.24632	280	2.24912	280	2.25193	281	2.25473	281	2.25754	281	2.26035	281	2.26316	281	2.26598	281	2.26879	282	2.27161	282	160
161	2.27443	282	2.27725	282	2.28007	282	2.28289	283	2.28572	283	2.28854	283	2.29137	283	2.29420	283	2.29703	283	2.29987	284	161
162	2.30270	284	2.30554	284	2.30838	284	2.31122	284	2.31406	284	2.31691	285	2.31975	285	2.32260	285	2.32545	285	2.32830	285	162
163	2.33115	285	2.33401	286	2.33687	286	2.33972	286	2.34258	286	2.34545	286	2.34831	287	2.35117	287	2.35404	287	2.35691	287	163
164	2.35978	287	2.36265	287	2.36553	288	2.36840	288	2.37128	288	2.37416	288	2.37704	288	2.37992	288	2.38280	289	2.38569	289	164
165	2.38858	289	2.39147	289	2.39436	289	2.39725	289	2.40015	290	2.40304	290	2.40594	290	2.40884	290	2.41174	290	2.41465	290	165
166	2.41755	291	2.42046	291	2.42337	291	2.42628	291	2.42919	291	2.43210	292	2.43502	292	2.43793	292	2.44085	292	2.44377	292	166
167	2.44670	292	2.44962	293	2.45255	293	2.45547	293	2.45840	293	2.46133	293	2.46427	293	2.46720	294	2.47014	294	2.47307	294	167
168	2.47601	294	2.47896	294	2.48190	294	2.48484	295	2.48779	295	2.49074	295	2.49369	295	2.49664	295	2.49959	296	2.50255	296	168
169	2.50551	296	2.50846	296	2.51143	296	2.51439	296	2.51735	297	2.52032	297	2.52328	297	2.52625	297	2.52922	297	2.53220	297	169
170	2.53517	298	2.53815	298	2.54113	298	2.54410	298	2.54709	298	2.55007	298	2.55305	299	2.55604	299	2.55903	299	2.56202	299	170
171	2.56501	299	2.56800	300	2.57100	300	2.57400	300	2.57699	300	2.57999	300	2.58300	300	2.58600	301	2.58901	301	2.59201	301	171
172	2.59502	301	2.59803	301	2.60104	301	2.60406	302	2.60707	302	2.61009	302	2.61311	302	2.61613	302	2.61916	302	2.62218	303	172
173	2.62521	303	2.62823	303	2.63126	303	2.63430	303	2.63733	303	2.64036	304	2.64340	304	2.64644	304	2.64948	304	2.65252	304	173
174	2.65556	305	2.65861	305	2.66166	305	2.66471	305	2.66776	305	2.67081	305	2.67386	306	2.67692	306	2.67998	306	2.68304	306	174
175	2.68610	306	2.68916	306	2.69222	307	2.69529	307	2.69836	307	2.70143	307	2.70450	307	2.70757	307	2.71065	308	2.71372	308	175
176	2.71680	308	2.71988	308	2.72296	308	2.72605	309	2.72913	309	2.73222	309	2.73531	309	2.73840	309	2.74149	309	2.74458	310	176
177	2.74768	310	2.75078	310	2.75387	310	2.75698	310	2.76008	310	2.76318	311	2.76629	311	2.76940	311	2.77251	311	2.77562	311	177
178	2.77873	311	2.78184	312	2.78496	312	2.78808	312	2.79120	312	2.79432	312	2.79744	312	2.80057	313	2.80369	313	2.80682	313	178
179	2.80995	313	2.81308	313	2.81622	314	2.81935	314	2.82249	314	2.82563	314	2.82877	314	2.83191	314	2.83506	315	2.83820	315	179
180	2.84135	315	2.84450	315	2.84765	315	2.85080	315	2.85396	316	2.85711	316	2.86027	316	2.86343	316	2.86659	316	2.86975	316	180

Bϱ	.0	Δ	.1	Δ	.2	Δ	.3	Δ	.4	Δ	.5	Δ	.6	Δ	.7	Δ	.8	Δ	.9	Δ	Bϱ
181	2.87292	317	2.87609	317	2.87925	317	2.88242	317	2.88560	317	2.88877	318	2.89194	318	2.89512	318	2.89830	318	2.90148	318	181
182	2.90466	318	2.90785	319	2.91103	319	2.91422	319	2.91741	319	2.92060	319	2.92379	319	2.92698	320	2.93018	320	2.93338	320	182
183	2.93658	320	2.93978	320	2.94298	320	2.94619	321	2.94939	321	2.95260	321	2.95581	321	2.95902	321	2.96223	321	2.96545	322	183
184	2.96867	322	2.97188	322	2.97510	322	2.97833	322	2.98155	323	2.98478	323	2.98800	323	2.99123	323	2.99446	323	2.99769	323	184
185	3.00093	324	3.00416	324	3.00740	324	3.01064	324	3.01388	324	3.01712	324	3.02037	325	3.02361	325	3.02686	325	3.03011	325	185
186	3.03336	325	3.03661	325	3.03987	326	3.04313	326	3.04638	326	3.04964	326	3.05291	326	3.05617	327	3.05943	327	3.06270	327	186
187	3.06597	327	3.06924	327	3.07251	327	3.07578	328	3.07906	328	3.08234	328	3.08562	328	3.08890	328	3.09218	328	3.09546	329	187
188	3.09875	329	3.10204	329	3.10533	329	3.10862	329	3.11191	329	3.11520	330	3.11850	330	3.12180	330	3.12510	330	3.12840	330	188
189	3.13170	330	3.13501	331	3.13831	331	3.14162	331	3.14493	331	3.14824	331	3.15156	332	3.15487	332	3.15819	332	3.16151	332	189
190	3.16483	332	3.16815	332	3.17147	333	3.17480	333	3.17812	333	3.18145	333	3.18478	333	3.18812	333	3.19145	334	3.19479	334	190
191	3.19812	334	3.20146	334	3.20480	334	3.20815	334	3.21149	335	3.21484	335	3.21819	335	3.22153	335	3.22489	335	3.22824	335	191
192	3.23159	336	3.23495	336	3.23831	336	3.24167	336	3.24503	336	3.24839	337	3.25176	337	3.25513	337	3.25849	337	3.26186	337	192
193	3.26524	337	3.26861	338	3.27199	338	3.27536	338	3.27874	338	3.28212	338	3.28551	338	3.28889	339	3.29228	339	3.29566	339	193
194	3.29905	339	3.30244	339	3.30584	339	3.30923	340	3.31263	340	3.31602	340	3.31942	340	3.32283	340	3.32623	340	3.32963	341	194
195	3.33304	341	3.33645	341	3.33986	341	3.34327	341	3.34668	342	3.35010	342	3.35352	342	3.35693	342	3.36036	342	3.36378	342	195
196	3.36720	343	3.37063	343	3.37405	343	3.37748	343	3.38091	343	3.38435	343	3.38778	344	3.39122	344	3.39465	344	3.39809	344	196
197	3.40153	344	3.40498	344	3.40842	345	3.41187	345	3.41532	345	3.41877	345	3.42222	345	3.42567	345	3.42912	346	3.43258	346	197
198	3.43604	346	3.43950	346	3.44296	346	3.44642	347	3.44989	347	3.45336	347	3.45683	347	3.46030	347	3.46377	347	3.46724	348	198
199	3.47072	348	3.47419	348	3.47767	348	3.48115	348	3.48464	348	3.48812	349	3.49161	349	3.49509	349	3.49858	349	3.50207	349	199
200	3.50557	349	3.50906	350	3.51256	350	3.51606	350	3.51956	350	3.52306	350	3.52656	350	3.53006	351	3.53357	351	3.53708	351	200
201	3.54059	351	3.54410	351	3.54761	352	3.55113	352	3.55465	352	3.55817	352	3.56169	352	3.56521	352	3.56873	353	3.57226	353	201
202	3.57578	353	3.57931	353	3.58284	353	3.58638	353	3.58991	354	3.59345	354	3.59698	354	3.60052	354	3.60406	354	3.60761	354	202
203	3.61115	355	3.61470	355	3.61825	355	3.62179	355	3.62535	355	3.62890	355	3.63245	356	3.63601	356	3.63957	355	3.61313	356	203
204	3.64669	356	3.65025	357	3.65382	357	3.65739	357	3.66095	357	3.66452	357	3.66810	357	3.67167	358	3.67525	358	3.67882	358	204
205	3.68240	358	3.68598	358	3.68956	358	3.69315	359	3.69673	359	3.70032	359	3.70391	359	3.70750	359	3.71109	359	3.71469	360	205
206	3.71828	360	3.72188	360	3.72548	360	3.72908	360	3.73269	360	3.73629	361	3.73990	361	3.74351	361	3.74712	361	3.75073	361	206
207	3.75434	362	3.75796	362	3.76157	362	3.76519	362	3.76881	362	3.77243	362	3.77606	363	3.77968	363	3.78331	363	3.78694	363	207
208	3.79057	363	3.79420	363	3.79783	364	3.80147	364	3.80511	364	3.80875	364	3.81239	364	3.81603	364	3.81967	365	3.82332	365	208
209	3.82697	365	3.83062	365	3.83427	365	3.83792	365	3.84158	366	3.84523	366	3.84889	366	3.85255	366	3.85621	366	3.85987	366	209
210	3.86354	367	3.86721	367	3.87087	367	3.87454	367	3.87822	367	3.88189	368	3.88556	368	3.88924	368	3.89292	368	3.89660	368	210
211	3.90028	368	3.90397	369	3.90765	369	3.91134	369	3.91503	369	3.91872	369	3.92241	369	3.92611	370	3.92980	370	3.93350	370	211
212	3.93720	370	3.94090	370	3.94460	370	3.94831	371	3.95201	371	3.95572	371	3.95943	371	3.96314	371	3.96685	371	3.97057	372	212
213	3.97429	372	3.97800	372	3.98172	372	3.98545	372	3.98917	373	3.99289	373	3.99662	373	4.00035	373	4.00408	373	4.00781	373	213
214	4.01154	374	4.01528	374	4.01902	374	4.02276	374	4.02650	374	4.03024	374	4.03398	375	4.03773	375	4.04148	375	4.04522	375	214
215	4.04898	375	4.05273	375	4.05648	376	4.06024	376	4.06400	376	4.06776	376	4.07152	376	4.07528	376	4.07904	377	4.08281	377	215
216	4.08658	377	4.09035	377	4.09412	377	4.09789	377	4.10167	378	4.10544	378	4.10922	378	4.11300	378	4.11678	378	4.12057	379	216
217	4.12435	379	4.12814	379	4.13193	379	4.13572	379	4.13951	379	4.14330	380	4.14710	380	4.15090	380	4.15470	380	4.15850	380	217
218	4.16230	380	4.16610	381	4.16991	381	4.17372	381	4.17753	381	4.18134	381	4.18515	381	4.18896	382	4.19278	382	4.19660	382	218
219	4.20042	382	4.20424	382	4.20806	382	4.21189	383	4.21571	383	4.21954	383	4.22337	383	4.22720	383	4.23103	383	4.23487	384	219
220	4.23871	384	4.24254	384	4.24638	384	4.25023	384	4.25407	385	4.25792	385	4.26176	385	4.26561	385	4.26946	385	4.27331	385	220
221	4.27717	386	4.28102	386	4.28488	386	4.28874	386	4.29260	386	4.29646	386	4.30033	387	4.30419	387	4.30806	387	4.31193	387	221
222	4.31580	387	4.31967	387	4.32355	388	4.32742	388	4.33130	388	4.33518	388	4.33906	388	4.34294	388	4.34683	389	4.35072	389	222
223	4.35460	389	4.35849	389	4.36238	389	4.36628	389	4.37017	390	4.37407	390	4.37797	390	4.38187	390	4.38577	390	4.38967	391	223
224	4.39358	391	4.39749	391	4.40139	391	4.40531	391	4.40922	391	4.41313	392	4.41705	392	4.42096	392	4.42488	392	4.42880	392	224

225	4.43273	392	4.43665	393	4.44058	393	4.44450	393	4.44843	393	4.45236	393	4.45630	393	4.46023	394	4.46417	394	4.46810	394	225
226	4.47204	394	4.47599	394	4.47993	394	4.48387	395	4.48782	395	4.49177	395	4.49572	395	4.49967	395	4.50362	395	4.50758	396	226
227	4.51153	396	4.51549	396	4.51945	396	4.52341	396	4.52738	397	4.53134	397	4.53531	397	4.53928	397	4.54325	397	4.54722	397	227
228	4.55119	398	4.55517	398	4.55915	398	4.56313	398	4.56711	398	4.57109	398	4.57507	399	4.57906	399	4.58305	399	4.58704	399	228
229	4.59103	399	4.59502	399	4.59901	400	4.60301	400	4.60701	400	4.61101	400	4.61501	400	4.61901	400	4.62302	401	4.62702	401	229
230	4.63103	401	4.63504	401	4.63905	401	4.64306	401	4.64708	402	4.65110	402	4.65511	402	4.65913	402	4.66316	402	4.66718	403	230
231	4.67120	403	4.67523	403	4.67926	403	4.68329	403	4.68732	403	4.69136	404	4.69539	404	4.69943	404	4.70347	404	4.70751	404	231
232	4.71155	404	4.71559	405	4.71964	405	4.72369	405	4.72774	405	4.73179	405	4.73584	405	4.73989	406	4.74395	406	4.74801	406	232
233	4.75207	406	4.75613	406	4.76019	406	4.76426	407	4.76832	407	4.77239	407	4.77646	407	4.78053	407	4.78460	407	4.78868	408	233
234	4.79276	408	4.79683	408	4.80091	408	4.80499	408	4.80908	409	4.81316	409	4.81725	409	4.82134	409	4.82543	409	4.82952	409	234
235	4.83361	410	4.83771	410	4.84181	410	4.84591	410	4.85001	410	4.85411	410	4.85821	411	4.86232	411	4.86642	411	4.87053	411	235
236	4.87464	411	4.87876	411	4.88287	412	4.88698	412	4.89110	412	4.89522	412	4.89934	412	4.90347	412	4.90759	413	4.91172	413	236
237	4.91584	413	4.91997	413	4.92411	413	4.92824	413	4.93237	414	4.93651	414	4.94065	414	4.94479	414	4.94893	414	4.95307	414	237
238	4.95722	415	4.96136	415	4.96551	415	4.96966	415	4.97381	415	4.97797	416	4.98212	416	4.98628	416	4.99044	416	4.99460	416	238
239	4.99876	416	5.00292	417	5.00709	417	5.01126	417	5.01542	417	5.01959	417	5.02377	417	5.02794	418	5.03212	418	5.03629	418	239
240	5.04047	418	5.04465	418	5.04884	418	5.05302	419	5.05721	419	5.06139	419	5.06558	419	5.06977	419	5.07397	419	5.07816	420	240
241	5.08236	420	5.08655	420	5.09075	420	5.09496	420	5.09916	420	5.10336	421	5.10757	421	5.11178	421	5.11599	421	5.12020	421	241
242	5.12441	421	5.12863	422	5.13284	422	5.13706	422	5.14128	422	5.14550	422	5.14973	423	5.15395	423	5.15818	423	5.16241	423	242
243	5.16664	423	5.17087	423	5.17510	424	5.17934	424	5.18258	424	5.18781	424	5.19205	424	5.19630	424	5.20054	425	5.20479	425	243
244	5.20903	425	5.21328	425	5.21753	425	5.22179	425	5.22604	426	5.23030	426	5.23455	426	5.23881	426	5.24307	426	5.24734	426	244
245	5.25160	427	5.25587	427	5.26013	427	5.26440	427	5.26867	427	5.27295	427	5.27722	428	5.28150	428	5.28578	428	5.29006	428	245
246	5.29434	428	5.29862	428	5.30291	429	5.30719	429	5.31148	429	5.31577	429	5.32006	429	5.32436	430	5.32865	430	5.33295	430	246
247	5.33725	430	5.34155	430	5.24585	430	5.35015	431	5.35446	431	5.35876	431	5.36307	431	5.36738	431	5.37169	431	5.37601	432	247
248	5.38032	432	5.38464	432	5.38896	432	5.39328	432	5.39760	432	5.40193	433	5.40625	433	5.41058	433	5.41491	433	5.41924	433	248
249	5.42357	433	5.42791	434	5.43224	434	5.43658	434	5.44092	434	5.44526	434	5.44960	434	5.45395	435	5.45829	435	5.46264	435	249
250	5.46699	435	5.47134	435	5.47570	435	5.48005	436	5.48441	436	5.48877	436	5.49313	436	5.49749	436	5.50185	436	5.50622	437	250
251	5.51058	437	5.51495	437	5.51932	437	5.52369	437	5.52807	438	5.53244	438	5.53682	438	5.54120	438	5.54558	438	5.54996	438	251
252	5.55434	439	5.55873	439	5.56311	439	5.56750	439	5.57189	439	5.57629	439	5.58068	440	5.58508	440	5.58947	440	5.59387	440	252
253	5.59827	440	5.60267	440	5.60708	441	5.61148	441	5.61589	441	5.62030	441	5.62471	441	5.62912	441	5.63354	442	5.63795	442	253
254	5.64237	442	5.64679	442	5.65121	442	5.65564	442	5.66006	443	5.66449	443	5.66891	443	5.67334	443	5.67778	443	5.68221	443	254
255	5.68664	444	5.69108	444	5.69552	444	5.69996	444	5.70440	444	5.70884	444	5.71329	445	5.71773	445	5.72218	445	5.72663	445	255
256	5.73108	445	5.73554	446	5.73999	446	5.74445	446	5.74891	446	5.75337	446	5.75783	446	5.76229	447	5.76676	447	5.77123	447	256
257	5.77569	447	5.78017	447	5.78464	447	5.78911	448	5.79359	448	5.79806	448	5.80254	448	5.80702	448	5.81151	448	5.81599	449	257
258	5.82048	449	5.82496	449	5.82945	449	5.83394	449	5.83844	449	5.84293	450	5.84743	450	5.85192	450	5.85642	450	5.86092	450	258
259	5.86543	450	5.86993	451	5.87444	451	5.87894	451	5.88345	451	5.88797	451	5.89248	451	5.89699	452	5.90151	452	5.90603	452	259
260	5.91055	452	5.91507	452	5.91959	452	5.92412	453	5.92864	453	5.93317	453	5.93770	453	5.94223	453	5.94677	454	5.95130	454	260
261	5.95584	454	5.96038	454	5.96492	454	5.96946	454	5.97400	455	5.97855	455	5.98309	455	5.98764	455	5.99219	455	5.99675	455	261
262	6.00130	456	6.00585	456	6.01041	456	6.01497	456	6.01953	456	6.02409	456	6.02866	457	6.03322	457	6.03779	457	6.04236	457	262
263	6.04693	457	6.05150	457	6.05608	458	6.06065	458	6.06523	458	6.06981	458	6.07439	458	6.07897	458	6.08356	459	6.08814	459	263
264	6.09273	459	6.09732	459	6.10191	459	6.10650	459	6.11110	460	6.11569	460	6.12029	460	6.12489	460	6.12949	460	6.13409	460	264
265	6.13870	461	6.14331	461	6.14791	461	6.15252	461	6.15714	461	6.16175	461	6.16636	462	6.17098	462	6.17560	462	6.18022	462	265
266	6.18484	462	6.18946	462	6.19409	463	6.19871	463	6.20334	463	6.20797	463	6.21260	463	6.21724	464	6.22187	464	6.22651	464	266
267	6.23115	464	6.23579	464	6.24043	464	6.24507	465	6.24972	465	6.25437	465	6.25902	465	6.26367	465	6.26832	465	6.27297	466	267
268	6.27763	466	6.28228	466	6.28694	466	6.29160	466	6.29627	466	6.30093	467	6.30560	467	6.31026	467	6.31493	467	6.31960	467	268
269	6.32428	467	6.32895	468	6.33363	468	6.33830	468	6.34298	468	6.34766	468	6.35235	468	6.35703	469	6.36172	469	6.36640	469	269
270	6.37109	469	6.37578	469	6.38048	469	6.38517	470	6.38987	470	6.39457	470	6.39927	470	6.40397	470	6.40867	470	6.41337	471	270
271	6.41808	471	6.42279	471	6.42750	471	6.43221	471	6.43692	471	6.44164	472	6.44636	472	6.45107	472	6.45579	472	6.46051	472	271

Ƀϱ	.0	Δ	.1	Δ	.2	Δ	.3	Δ	.4	Δ	.5	Δ	.6	Δ	.7	Δ	.8	Δ	.9	Δ	Bϱ
272	6.46524	473	6.46996	473	6.47469	473	6.47942	473	6.48415	473	6.48888	473	6.49361	474	6.49835	474	6.50309	474	6.50782	474	272
273	6.51256	474	6.51731	474	6.52205	475	6.52680	475	6.53154	475	6.53629	475	6.54104	475	6.54579	475	6.55055	476	6.55530	476	273
274	6.56006	476	6.56482	476	6.56958	476	6.57434	476	6.57911	477	6.58387	477	6.58864	477	6.59341	477	6.59818	477	6.60293	477	274
275	6.60772	478	6.61250	478	6.61728	478	6.62206	478	6.62684	478	6.63162	478	6.63640	479	6.64119	479	6.64598	479	6.65077	479	275
276	6.65556	479	6.66035	479	6.66515	480	6.66994	480	6.67474	480	6.67954	480	6.68434	480	6.68914	480	6.69395	481	6.69875	481	276
277	6.70356	481	6.70837	481	6.71318	481	6.71800	481	6.72281	482	6.72763	482	6.73245	482	6.73726	482	6.74209	482	6.74691	482	277
278	6.75173	483	6.75656	483	6.76139	483	6.76622	483	6.77105	483	6.77588	483	6.78072	484	6.78556	484	6.79039	484	6.79523	484	278
279	6.80008	484	6.80492	485	6.80976	485	6.81461	485	6.81946	485	6.82431	485	6.82916	485	6.83402	486	6.83887	486	6.84373	486	279
280	6.84859	486	6.85345	486	6.85831	486	6.86317	487	6.86804	487	6.87290	487	6.87777	487	6.88264	487	6.88752	487	6.89239	488	280
281	6.89727	488	6.90214	488	6.90702	488	6.91190	488	6.91678	488	6.92167	489	6.92655	489	6.93144	489	6.93633	489	6.94122	489	281
282	6.94611	489	6.95101	490	6.95590	490	6.96080	490	6.96570	490	6.97060	490	6.97550	490	6.98041	491	6.98531	491	6.99022	491	282
283	6.99513	491	7.00004	491	7.00496	491	7.00987	492	7.01479	492	7.01970	492	7.02462	492	7.02954	492	7.03447	492	7.03939	493	283
284	7.04432	493	7.04925	493	7.05418	493	7.05911	493	7.06404	493	7.06897	494	7.07391	494	7.07885	494	7.08379	494	7.08873	494	284
285	7.09367	494	7.09862	495	7.10356	495	7.10851	495	7.11346	495	7.11841	495	7.12337	495	7.12832	496	7.13328	496	7.13824	496	285
286	7.14320	496	7.14816	496	7.15312	497	7.15809	497	7.16305	497	7.16802	497	7.17299	497	7.17796	497	7.18294	498	7.18791	498	286
287	7.19289	498	7.19787	498	7.20285	498	7.20783	498	7.21281	499	7.21780	499	7.22279	499	7.22777	499	7.23276	499	7.23776	499	287
288	7.24275	500	7.24775	500	7.25274	500	7.25774	500	7.26274	500	7.26774	500	7.27275	501	7.27775	501	7.28276	501	7.28777	501	288
289	7.29278	501	7.29779	501	7.30281	502	7.30782	502	7.31284	502	7.31786	502	7.32288	502	7.32790	502	7.33292	503	7.33795	503	289
290	7.34298	503	7.34801	503	7.35304	503	7.35807	503	7.36310	504	7.36814	504	7.37318	504	7.37822	504	7.38326	504	7.38830	504	290
291	7.39334	505	7.39839	505	7.40344	505	7.40849	505	7.41354	505	7.41859	505	7.42365	506	7.42870	506	7.42376	506	7.43882	506	291
292	7.44388	506	7.44894	506	7.45401	507	7.45907	507	7.46414	507	7.46921	507	7.47428	507	7.47935	507	7.48443	508	7.48951	508	292
293	7.49458	508	7.49966	508	7.50474	508	7.50983	508	7.51491	509	7.52000	509	7.52509	509	7.53018	509	7.53527	509	7.54036	509	293
294	7.54546	510	7.55055	510	7.55565	510	7.56075	510	7.56585	510	7.57095	510	7.57606	511	7.58117	511	7.58627	511	7.59138	511	294
295	7.59650	511	7.60161	511	7.60672	512	7.61184	512	7.61696	512	7.62208	512	7.62720	512	7.63232	513	7.63745	513	7.64258	513	295
296	7.64770	513	7.65283	513	7.65797	513	7.66310	514	7.66824	514	7.67337	514	7.67851	514	7.68365	514	7.68879	514	7.69394	515	296
297	7.69908	515	7.70423	515	7.70938	515	7.71453	515	7.71968	515	7.72483	516	7.72999	516	7.73515	516	7.74030	516	7.74546	516	297
298	7.75063	516	7.75579	517	7.76096	517	7.76612	517	7.77129	517	7.77646	517	7.78163	517	7.78681	518	7.79198	518	7.79716	518	298
299	7.80234	518	7.80752	518	7.81270	518	7.81789	519	7.82307	519	7.82826	519	7.83345	519	7.83864	519	7.84383	519	7.84902	520	299
300	7.85422	520	7.85942	520	7.86462	520	7.86982	520	7.87502	520	7.88022	521	7.88543	521	7.89064	521	7.89585	521	7.90106	521	300
301	7.90627	521	7.91148	522	7.91670	522	7.92192	522	7.92714	522	7.93236	522	7.93758	522	7.94280	523	7.94803	523	7.95326	523	301
302	7.95849	523	7.96372	523	7.96895	523	7.97418	524	7.97942	524	7.98466	524	7.98990	524	7.99514	524	8.00038	524	8.00563	525	302
303	8.01087	525	8.01612	525	8.02137	525	8.02662	525	8.03187	525	8.03713	526	8.04238	526	8.04764	526	8.05290	526	8.05816	526	303
304	8.06342	526	8.06869	527	8.07396	527	8.07922	527	8.08449	527	8.08976	527	8.09504	527	8.10031	528	8.10559	528	8.11087	528	304
305	8.11615	528	8.12143	528	8.12671	528	8.13199	529	8.13728	529	8.14257	529	8.14786	529	8.15315	529	8.15844	529	8.16374	530	305
306	8.16903	530	8.17433	530	8.17963	530	8.18493	530	8.19024	530	8.19554	531	8.20085	531	8.20616	531	8.21147	531	8.21678	531	306
307	8.22209	531	8.22741	532	8.23272	532	8.23804	532	8.24336	532	8.24868	532	8.25400	532	8.25933	533	8.26466	533	8.26998	533	307
308	8.27551	533	8.28065	533	8.28598	533	8.29131	534	8.29665	534	8.30199	534	8.30733	534	8.31267	534	8.31801	535	8.32336	535	308
309	8.32871	535	8.33405	535	8.33940	535	8.34476	535	8.35011	536	8.35546	536	8.36082	536	8.36618	536	8.37154	536	8.37690	536	309
310	8.38226	537	8.38763	537	8.39300	537	8.39836	537	8.40373	537	8.40911	537	8.41448	538	8.41986	538	8.42523	538	8.43061	538	310
311	8.43599	538	8.44137	538	8.44676	539	8.45214	539	8.45753	539	8.46292	539	8.46831	539	8.47370	539	8.47909	540	8.48449	540	311
312	8.48988	540	8.49528	540	8.50068	540	8.50609	540	8.51149	541	8.51689	541	8.52230	541	8.52771	541	8.53312	541	8.53853	541	312
313	8.54395	542	8.54936	542	8.55478	542	8.56020	542	8.56562	542	8.57104	542	8.57646	543	8.58189	543	8.58732	543	8.59274	543	313
314	8.59817	543	8.60361	543	8.60904	544	8.61448	544	8.61991	544	8.62535	544	8.63079	544	8.63623	544	8.64168	545	8.64712	545	314
315	8.65257	545	8.65802	545	8.66347	545	8.66892	545	8.67438	546	8.67983	546	8.68529	546	8.69075	546	8.69621	546	8.70167	546	315

316	8.70713	547	8.71260	547	8.71807	547	8.72354	547	8.72901	547	8.73448	547	8.73995	548	8.74543	548	8.75090	548	8.75638	548	316
317	8.76186	548	8.76735	548	8.77283	549	8.77832	549	8.78380	549	8.78929	549	8.79478	549	8.80028	549	8.80577	550	8.81126	550	317
318	8.81676	550	8.82226	550	8.82776	550	8.83326	550	8.83877	551	8.84427	551	8.84978	551	8.85529	551	8.86080	551	8.86631	551	318
319	8.87183	552	8.87734	552	8.88286	552	8.88838	552	8.89390	552	8.89942	552	8.90495	553	8.91047	553	8.91600	553	8.92153	553	319
320	8.92706	553	8.93259	553	8.93812	554	8.94366	554	8.94920	554	8.95474	554	8.96028	554	8.96582	554	8.97136	555	8.97691	555	320
321	8.98246	555	8.98801	555	8.99356	555	8.99911	555	9.00466	556	9.01022	556	9.01578	556	9.02134	556	9.02690	556	9.03246	556	321
322	9.03802	557	9.04359	557	9.04916	557	9.05472	557	9.06030	557	9.06587	557	9.07144	558	9.07702	558	9.08259	558	9.08817	558	322
323	9.09375	558	9.09934	558	9.10492	559	9.11051	559	9.11609	559	9.12168	559	9.12727	559	9.13287	559	9.13846	560	9.14406	560	323
324	9.14965	560	9.15525	560	9.16085	560	9.16646	560	9.17206	561	9.17767	561	9.18327	561	9.18888	561	9.19449	561	9.20011	561	324
325	9.20572	562	9.21134	562	9.21695	562	9.22257	562	9.22819	562	9.23382	562	9.23944	563	9.24507	563	9.25069	563	9.25632	563	325
326	9.26195	563	9.26759	563	9.27322	564	9.27885	564	9.28449	564	9.29013	564	9.29577	564	9.30141	564	9.30706	565	9.31270	565	326
327	9.31835	565	9.32400	565	9.32965	565	9.33530	565	9.34096	566	9.34661	566	9.35227	566	9.35793	566	9.36359	566	9.36925	566	327
328	9.37492	567	9.38058	567	9.38625	567	9.39192	567	9.39759	567	9.40526	567	9.40894	568	9.41461	568	9.42029	568	9.42597	568	328
329	9.43165	568	9.43733	568	9.44302	569	9.44870	569	9.45439	569	9.46008	569	9.46577	569	9.47146	569	9.47716	570	9.48285	570	329
330	9.48855	570	9.49425	570	9.49995	570	9.50565	570	9.51136	571	9.51706	571	9.52277	571	9.52848	571	9.53419	571	9.53990	571	330
331	9 54561	572	9.55133	572	9.55705	572	9.56277	572	9.56849	572	9.57421	572	9.57993	573	9.58566	573	9.59139	573	9.59712	573	331
332	9.60285	573	9.60858	573	9.61431	574	9.62005	574	9.62579	574	9.63152	574	9.63727	574	9.64301	574	9.64875	575	9.65450	575	332
333	9.66024	575	9.66599	575	9.67174	575	9.67750	575	9.68325	576	9.68901	576	9.69476	576	9.70052	576	9.70628	576	9.71205	576	333
334	9.71781	577	9.72357	577	9.72934	577	9.73511	577	9.74088	577	9.74665	577	9.75243	578	9.75820	578	9.76398	578	9.76976	578	334
335	9.77554	578	9.78132	578	9.78711	579	9.79289	579	9.79868	579	9.80447	579	9.81026	579	9.81605	579	9.82184	580	9.82764	580	335
336	9.83344	580	9.83924	580	9.84504	580	9.85084	580	9.85664	581	9.86245	581	9.86825	581	9.87406	581	9.87987	581	9.88569	581	336
337	9.89150	582	9.89731	582	9.90313	582	9.90895	582	9.91477	582	9.92059	582	9.92642	583	9.93224	583	9.93807	583	9.94390	583	337
338	9.94973	583	9.95556	583	9.96139	584	9.96723	584	9.97307	584	9.97890	584	9.98475	584	9.99059	584	9.99643	585	10.00228	585	338
339	10.00812	585	10.01397	585	10.01982	585	10.02567	585	10.03153	586	10.03738	586	10.04324	586	10.04910	586	10.05496	586	10.06082	586	339
340	10.06668	587	10.07255	587	10.07842	587	10.08428	587	10.09015	587	10.09603	587	10.10190	588	10.10778	588	10.11365	588	10.11953	588	340
341	10.12541	588	10.13129	588	10.13718	589	10.14306	589	10.14895	589	10.15484	589	10.16073	589	10.16662	589	10.[illegible]251	590	10.17841	590	341
342	10.18430	590	10.19020	590	10.19610	590	10.20200	590	10.20791	591	10.21381	591	10.21972	591	10.22563	591	10.23154	591	10.23745	591	342
343	10.24336	591	10.24928	592	10.25519	592	10.26111	592	10.26703	592	10.27295	592	10.27888	592	10.28480	593	10.29073	593	10.29666	593	343
344	10.30259	593	10.30852	593	10.31445	593	10.32038	594	10.32632	594	10.33226	594	10.33820	594	10.34414	594	10.35008	594	10.35603	595	344
345	10.36198	595	10.36792	595	10.37387	595	10.37982	595	10.38578	595	10.39173	596	10.39769	596	10.40365	596	10.40961	596	10.41557	596	345
346	10.42153	596	10.42750	597	10.43346	597	10.43943	597	10.44540	597	10.45137	597	10.45734	597	10.46332	598	10.46929	598	10.47527	598	346
347	10.48125	598	10.48723	598	10.49322	598	10.49920	599	10.50519	599	10.51117	599	10.51716	599	10.52315	599	10.52915	599	10.53514	600	347
348	10.54114	600	10.54714	600	10.55313	600	10.55914	600	10.56514	600	10.57114	601	10.57715	601	10.58316	601	10.58917	601	10.59518	601	348
349	10.60119	691	10.60720	602	10.61322	602	10.61924	602	10.62526	602	10.63128	602	10.63730	602	10.64332	603	10.64935	603	10.65538	603	349
350	10.66141	603	10.66744	603	10.67347	603	10.67950	604	10.68554	604	10.69158	604	10.69762	604	10.70366	604	10.70970	604	10.71574	605	350
351	10.72179	605	10.72784	605	10.73389	605	10.73994	605	10.74599	605	10.75204	606	10.75810	606	10.76415	606	10.77021	606	10.77627	606	351
352	10.78234	606	10.78840	607	10.79447	607	10.80053	607	10.80660	607	10.81267	607	10.81874	607	10.82482	608	10.83089	608	10.83697	608	352
353	10.84305	608	10.84913	608	10 85521	608	10.86130	609	10.86738	609	10.87347	609	10.87956	609	10.88565	609	10.89174	609	10.89783	610	353
354	10.90393	610	10.91002	610	10.91612	610	10.92222	610	10.92832	610	10.93443	611	10.94053	611	10.94664	611	10.95275	611	10.95886	611	354
355	10.96497	611	10.97108	612	10.97720	612	10.98332	612	10.98943	612	10.99555	612	11.00168	612	11.00780	612	11.01392	613	11.02005	613	355
356	11.02618	613	11.03231	613	11.03844	613	11.04457	613	11.05071	614	11.05684	614	11.06298	614	11.06912	614	11.07526	614	11.08141	614	356
357	11.08755	615	11.09370	615	11.09985	615	11.10606	615	11.11215	615	11.11830	615	11.12445	616	11.13061	616	11.13677	616	11.14293	616	357
358	11.14909	616	11.15525	616	11.16142	617	11.16758	617	11.17375	617	11.17992	617	11.18609	617	11.19226	617	11.19844	618	11.20461	618	358
359	11.21079	618	11.21697	618	11.22315	618	11.22934	618	11.23552	619	11.24171	619	11.24789	619	11.25408	619	11.26027	619	11.26647	619	359
360	11.27266	620	11.27886	620	11.28505	620	11.29125	620	11.29745	626	11.30366	620	11.30986	621	11.31607	621	11.32227	621	11.32848	621	360
361	11.33469	621	11.34091	621	11.34712	622	11.35333	622	11.35955	622	11.36577	622	11.37199	622	11.37821	622	11.38444	623	11.39066	623	361
362	11.39689	623	11.40312	623	11.40935	623	11.41558	623	11.42181	624	11.42805	624	11.43429	624	11.44053	624	11.44677	624	11.45301	624	362

Bϱ	.0	Δ	.1	Δ	.2	Δ	.3	Δ	.4	Δ	.5	Δ	.6	Δ	.7	Δ	.8	Δ	.9	Δ	Bϱ
363	11.45925	625	11.46550	625	11.47174	625	11.47799	625	11.48424	625	11.49049	625	11.49675	626	11.50300	626	11.50926	626	11.51552	626	363
364	11.52178	626	11.52804	626	11.53430	626	11.54057	627	11.54683	627	11.55310	627	11.55937	627	11.56564	627	11.57192	627	11.57819	628	364
365	11.58447	628	11.59075	628	11.59703	628	11.60331	628	11.60959	628	11.61588	629	11.62216	629	11.62845	629	11.63474	629	11.64103	629	365
366	11.64732	629	11.65362	630	11.65991	630	11.66621	630	11.67251	630	11.67881	630	11.68512	630	11.69142	631	11.69773	631	11.70403	631	366
367	11.71034	631	11.71665	631	11.72297	631	11.72928	632	11.73560	632	11.74191	632	11.74823	632	11.75455	632	11.76088	632	11.76720	633	367
368	11.77353	633	11.77985	633	11.78618	633	11.79251	633	11.79885	633	11.80518	634	11.81152	634	11.81785	634	11.82419	634	11.83053	634	368
369	11.83688	634	11.84322	635	11.84956	635	11.85591	635	11.86226	635	11.86861	635	11.87496	635	11.88132	636	11.88767	636	11.89403	636	369
370	11.90039	636	11.90675	636	11.91311	636	11.91947	637	11.92584	637	11.93221	637	11.93857	637	11.94494	637	11.95132	637	11.95769	638	370
371	11.96406	638	11.97044	638	11.97682	638	11.98320	638	11.98958	638	11.99596	638	12.00235	639	12.00874	639	12.01512	639	12.02151	639	371
372	12.02790	639	12.03430	639	12.04069	640	12.04709	640	12.05349	640	12.05989	640	12.06629	640	12.07269	640	12.07910	641	12.08550	641	372
373	12.09191	641	12.09832	641	12.10473	641	12.11114	641	12.11756	642	12.12397	642	12.13039	642	12.13681	642	12.14323	642	12.14965	642	373
374	12.15608	643	12.16250	643	12.16893	643	12.17536	643	12.18179	643	12.18822	643	12.19466	644	12.20109	644	12.20753	644	12.21397	644	374
375	12.22041	644	12.22685	644	12.23330	645	12.23974	645	12.24619	645	12.25264	645	12.25909	645	12.26554	645	12.27199	646	12.27845	646	375
376	12.28491	646	12.29137	646	12.29783	646	12.30429	646	12.31075	647	12.31722	647	12.32368	647	12.33015	647	12.33662	647	12.34309	647	376
377	12.34957	648	12.35604	648	12.36252	648	12.36900	648	12.37548	648	12.38196	648	12.38844	648	12.39493	649	12.40141	649	12.40790	649	377
378	12.41439	649	12.42088	649	12.42738	649	12.43387	650	12.44037	650	12.44686	650	12.45336	650	12.45986	650	12.46637	650	12.47287	651	378
379	12.47938	651	12.48589	651	12.49240	651	12.49891	651	12.50542	651	12.51193	652	12.51845	652	12.52497	652	12.53149	652	12.53801	652	379
380	12.54453	652	12.55105	653	12.55758	653	12.56411	653	12.57064	653	12.57717	653	12.58370	653	12.59023	654	12.59677	654	12.60331	654	380
381	12.60984	654	12.61638	654	12.62293	654	12.62947	655	12.63602	655	12.64256	655	12.64911	655	12.65566	655	12.66221	655	12.66877	656	381
382	12.67532	656	12.68188	656	12.68844	656	12.69500	656	12.70156	656	12.70812	656	12.71469	657	12.72125	657	12.72782	657	12.73439	657	382
383	12.74096	657	12.74754	657	12.75411	658	12.76069	658	12.76727	658	12.77385	658	12.78023	658	12.78701	658	12.79359	659	12.80018	659	383
384	12.80677	659	12.81336	659	12.81995	659	12.82654	659	12.83314	660	12.83973	660	12.84633	660	12.85293	660	12.85953	660	12.86613	660	384
385	12.87274	661	12.87934	661	12.88595	661	12.89256	661	12.89917	661	12.90578	661	12.91240	662	12.91901	662	12.92563	662	12.93225	662	385
386	12.93887	662	12.94549	662	12.95211	663	12.95874	663	12.96537	663	12.97199	663	12.97863	663	12.98526	663	12.99189	664	12.99853	664	386
387	13.00516	664	13.01180	664	13.01844	664	13.02508	664	13.03173	664	13.03837	665	13.04502	665	13.05167	665	13.05832	665	13.06497	665	387
388	13.07162	665	13.07827	666	13.08493	666	13.09159	666	13.09825	666	13.10491	666	13.11157	666	13.11824	667	13.12490	667	13.13157	667	388
389	13.13824	667	13.14491	667	13.15158	667	13.15826	668	13.16493	668	13.17161	668	13.17829	668	13.18497	668	13.19165	668	13.19834	669	389
390	13.20502	669	13.21171	669	13.21840	669	13.22509	669	13.23178	669	13.23848	670	13.24517	670	13.25187	670	13.25857	670	13.26527	670	390
391	13.27197	670	13.27867	671	13.28538	671	13.29209	671	13.29880	671	13.30551	671	13.31222	671	13.31893	672	13.32565	672	13.33236	672	391
392	13.33908	672	13.34580	672	13.35252	672	13.35925	672	13.36597	673	13.37270	673	13.37942	673	13.38615	673	13.39289	673	13.39962	673	392
393	13.40635	674	13.41309	674	13.41983	674	13.42657	674	13.43331	674	13.44005	674	13.44679	675	13.45354	675	13.46029	675	13.46704	675	393
394	13.47379	675	13.48054	675	13.48729	676	13.49405	676	13.50081	676	13.50757	676	13.51433	676	13.52109	676	13.52785	677	13.53462	677	394
395	13.54139	677	13.54815	677	13.55492	677	13.56170	677	13.56847	678	13.57525	678	13.58202	678	13.58880	678	13.59558	678	13.60236	678	395
396	13.60915	678	13.61593	679	13.62272	679	13.62951	679	13.63630	679	13.64309	679	13.64988	679	13.65667	680	13.66347	680	13.67027	680	396
397	13.67707	680	13.68387	680	13.69067	680	13.69748	681	13.70428	681	13.71109	681	13.71790	681	13.72471	681	13.73152	681	13.73834	682	397
398	13.74515	682	13.75197	682	13.75879	682	13.76561	682	13.77243	682	13.77926	683	13.78608	683	13.79291	683	13.79974	683	13.80657	683	398
399	13.81340	683	13.82024	684	13.82707	684	13.83391	684	13.84075	684	13.84759	684	13.85443	684	13.86127	685	13.86812	685	13.87496	685	399
400	13.88181	685	13.88866	685	13.89551	685	13.90237	685	13.90922	686	13.91608	686	13.92294	686	13.92980	686	13.93666	686	13.94352	686	400
401	13.95038	687	13.95725	687	13.96412	687	13.97099	687	13.97786	687	13.98473	687	13.99161	688	13.99848	688	14.00536	688	14.01224	688	401
402	14.01912	688	14.02600	688	14.03288	689	14.03977	689	14.04666	689	14.05355	689	14.06044	689	14.06733	689	14.07422	690	14.08112	690	402
403	14.08802	690	14.09491	690	14.10181	690	14.10872	690	14.11562	691	14.12252	691	14.12943	691	14.13634	691	14.14325	691	14.15016	691	403
404	14.15707	691	14.16399	692	14.17091	692	14.17782	692	14.18474	692	14.19166	692	14.19859	692	14.20551	693	14.21244	693	14.21937	693	404
405	14.22630	693	14.23323	693	14.24016	693	14.24709	694	14.25403	694	14.26097	694	14.26791	694	14.27485	694	14.28179	694	14.28873	695	405
406	14.29568	695	14.30263	695	14.30957	695	14.31652	695	14.32348	695	14.33043	696	14.33739	696	14.34434	696	14.35130	696	14.35826	696	406

407	14.36522	696	14.37219	697	14.37915	697	14.38612	697	14.39309	697	14.40006	697	14.40703	697	14.41400	697	14.42097	698	14.42795	698	407
408	14.43493	698	14.44191	698	14.44889	698	14.45587	698	14.46286	699	14.46984	699	14.47683	699	14.48382	699	14.49081	699	14.49780	699	408
409	14.50480	700	14.51179	700	14.51879	700	14.52579	700	14.53279	700	14.53979	700	14.54680	701	14.55380	701	14.56081	701	14.56782	701	409
410	14.57483	701	14.58184	701	14.58885	702	14.59587	702	14.60289	702	14.60990	702	14.61692	702	14.62394	702	14.63097	702	14.63799	703	410
411	14.64502	703	14.65205	703	14.65908	703	14.66611	703	14.67314	703	14.68018	704	14.68721	704	14.69425	704	14.70129	704	14.70833	704	411
412	14.71537	704	14.72242	705	14.72946	705	14.73651	705	14.74356	705	14.75061	705	14.75766	705	14.76472	706	14.77177	706	14.77883	706	412
413	14.78589	706	14.79295	706	14.80001	706	14.80707	707	14.81414	707	14.82121	707	14.82827	707	14.83534	707	14.84242	707	14.84949	707	413
414	14.85656	708	14.86364	708	14.87072	708	14.87780	708	14.88488	708	14.89196	708	14.89905	709	14.90613	709	14.91322	709	14.92031	709	414
415	14.92740	709	14.93449	709	14.94159	710	14.94868	710	14.95578	710	14.96288	710	14.96998	710	14.97708	710	14.98419	711	14.99129	711	415
416	14.99840	711	15.00551	711	15.01262	711	15.01973	711	15.02685	712	15.03396	712	15.04108	712	15.04820	712	15.05532	712	15.06244	712	416
417	15.06956	712	15.07669	713	15.08381	713	15.09094	713	15.09807	713	15.10520	713	15.11233	713	15.11947	714	15.12661	714	15.13374	714	417
418	15.14088	714	15.14802	714	15.15517	714	15.16231	715	15.16946	715	15.17660	715	15.18375	715	15.19090	715	15.19806	715	15.20521	716	418
419	15.21237	716	15.21952	716	15.22668	716	15.23384	716	15.24100	716	15.24817	717	15.25533	717	15.26250	717	15.26967	717	15.27684	717	419
420	15.28401	717	15.29118	717	15.29836	718	15.30553	718	15.31271	718	15.31989	718	15.32707	718	15.33426	718	15.34144	719	15.34863	719	420
421	15.35581	719	15.36300	719	15.37019	719	15.37739	719	15.38458	720	15.39178	720	15.39897	720	15.40617	720	15.41337	720	15.42058	720	421
422	15.42778	721	15.43498	721	15.44219	721	15.44940	721	15.45661	721	15.46382	721	15.47104	722	15.47825	722	15.48547	722	15.49269	722	422
423	15.49991	722	15.50713	722	15.51435	722	15.52157	723	15.52880	723	15.53603	723	15.54326	723	15.55049	723	15.55772	723	15.56496	724	423
424	15.57219	724	15.57943	724	15.58667	724	15.59391	724	15.60115	724	15.60840	725	15.61564	725	15.62289	725	15.63014	725	15.63739	725	424
425	15.64464	725	15.65189	726	15.65915	726	15.66641	726	15.67366	726	15.68692	726	15.68819	726	15.69545	726	15.70271	727	15.70998	727	425
426	15.71725	727	15.72452	727	15.73179	727	15.73906	727	15.74634	728	15.75361	728	15.76089	728	15.76817	728	15.77545	728	15.78273	728	426
427	15.79002	729	15.79730	729	15.80459	729	15.81188	729	15.81917	729	15.82646	729	15.83376	730	15.84105	730	15.84835	730	15.85565	730	427
428	15.86295	730	15.87025	730	15.87755	731	15.88486	731	15.89217	731	15.89947	731	15.90678	731	15.91409	731	15.92141	731	15.92872	732	428
429	15.93604	732	15.94336	732	15.95068	732	15.95800	732	15.96532	732	15.97264	733	15.97997	733	15.98730	733	15.99463	733	16.00196	733	429
430	16.00929	733	16.01662	734	16.02396	734	16.03130	734	16.03863	734	16.04597	734	16.05332	734	16.06066	735	16.06801	735	16.07535	735	430
431	16.08270	735	16.09005	735	16.09740	735	16.10475	735	16.11211	736	16.11947	736	16.12682	736	16.13418	736	16.14154	736	16.14891	736	431
432	16.15627	737	16.16364	737	16.17101	737	16.17837	737	16.18574	737	16.19312	737	16.20049	738	16.20787	738	16.21524	738	16.22262	738	432
433	16.23000	738	16.23738	738	16.24477	739	16.25215	739	16.25954	739	16.26693	739	16.27432	739	16.28171	739	16.28910	739	16.29650	740	433
434	16.30389	740	16.31129	740	16.31869	740	16.32609	740	16.33350	740	16.34090	741	16.34831	741	16.35571	741	16.36312	741	16.37053	741	434
435	16.37795	741	16.38536	742	16.39278	742	16.40019	742	16.40761	742	16.41503	742	16.42245	742	16.42988	743	16.43730	743	16.44473	743	435
436	16.45216	743	16.45959	743	16.46702	743	16.47445	743	16.48189	744	16.48932	744	16.49676	744	16.50420	744	16.51164	744	16.51909	744	436
437	16.52653	745	16.53398	745	16.54142	745	16.54887	745	16.55632	745	16.56378	745	16.57123	746	16.57868	746	16.58614	746	16.59360	746	437
438	16.60106	746	16.60852	746	16.61599	747	16.62345	747	16.63092	747	16.63839	747	16.64586	747	16.65333	747	16.66080	747	16.66828	748	438
439	16.67575	748	16.68323	748	16.69071	748	16.69819	748	16.70567	748	16.71316	749	16.72064	749	16.72813	749	16.73562	749	16.74311	749	439
440	16.75060	749	16.75810	750	16.76559	750	16.77309	750	16.78059	750	16.78809	750	16.79559	750	16.80309	751	16.81060	751	16.81811	751	440
441	16.82561	751	16.83312	751	16.84064	751	16.84815	751	16.85566	752	16.86318	752	16.87070	752	16.87822	752	16.88574	752	16.89326	752	441
442	16.90078	753	16.90831	753	16.91584	753	16.92337	753	16.93090	753	16.93843	753	16.94596	754	16.95350	754	16.96103	754	16.96857	754	442
443	16.97611	754	16.98366	754	16.99120	754	16.99874	755	17.00629	755	17.01384	755	17.02139	755	17.02894	755	17.03649	755	17.04405	756	443
444	17.05160	756	17.05916	756	17.06672	756	17.07428	756	17.08184	756	17.08941	757	17.09697	757	17.10454	757	17.11211	757	17.11968	757	444
445	17.12725	757	17.13483	758	17.14240	758	17.14998	758	17.15756	758	17.16514	758	17.17272	758	17.18030	758	17.18789	759	17.19547	759	445
446	17.20306	759	17.21065	759	17.21824	759	17.22583	759	17.23343	760	17.24102	760	17.24862	760	17.25622	760	17.26382	760	17.27142	760	446
447	17.27903	761	17.28663	761	17.29424	761	17.30185	761	17.30946	761	17.31707	761	17.32468	762	17.33230	762	17.33991	762	17.34753	762	447
448	17.35515	762	17.36277	762	17.37040	762	17.37802	763	17.38565	763	17.39328	763	17.40090	763	17.40854	763	17.41617	763	17.42380	764	448
449	17.43144	764	17.43908	764	17.44671	764	17.45435	764	17.46200	764	17.46964	765	17.47729	765	17.48493	765	17.49258	765	17.50023	765	449
450	17.50788	765	17.51554	765	17.52319	766	17.53085	766	17.53851	766	17.54616	766	17.55383	766	17.56149	766	17.56915	767	17.57682	767	450
451	17.58449	767	17.59216	767	17.59983	767	17.60750	767	17.61517	768	17.62285	768	17.63052	768	17.63820	768	17.64588	768	17.65357	768	451
452	17.66125	768	17.66893	769	17.67662	769	17.68431	769	17.69200	769	17.69969	769	17.70738	769	17.71508	770	17.72277	770	17.73047	770	452
453	17.73817	770	17.74587	770	17.75357	770	17.76128	771	17.76898	771	17.77669	771	17.78440	771	17.79211	771	17.79982	771	17.80753	772	453

Bo	.0	Δ	.1	Δ	.2	Δ	.3	Δ	.4	Δ	.5	Δ	.6	Δ	.7	Δ	.8	Δ	.9	Δ	Bo
454	17.81525	772	17.82297	772	17.83068	772	17.83840	772	17.84613	772	17.85385	772	17.86157	773	17.86930	773	17.87703	773	17.88476	773	454
455	17.89249	773	17.90022	773	17.90796	774	17.91569	774	17.92343	774	17.93117	774	17.93891	774	17.94665	774	17.95439	775	17.96214	775	455
456	17.96989	775	17.97763	775	17.98538	775	17.99314	775	18.00089	775	18.00864	776	18.01640	776	18.02416	776	18.03192	776	18.03968	776	456
457	18.04744	776	18.05521	777	18.06297	777	18.07074	777	18.07851	777	18.08628	777	18.09405	777	18.10182	778	18.10960	778	18.11738	778	457
458	18.12516	778	18.13294	778	18.14072	778	18.14850	778	18.15629	779	18.16407	779	18.17186	779	18.17965	779	18.18744	779	18.19523	779	458
459	18.20303	780	18.21082	780	18.21862	780	18.22642	780	18.23422	780	18.24202	780	18.24983	781	18.25763	781	18.26544	781	18.27325	781	459
460	18.28106	781	18.28887	781	18.29668	781	18.30450	782	18.31232	782	18.32013	782	18.32795	782	18.33578	782	18.34360	782	18.35142	783	460
461	18.35925	783	18.36708	783	18.37491	783	18.38274	783	18.39057	783	18.39840	784	18.40624	784	18.41408	784	18.42191	784	18.42975	784	461
462	18.43760	784	18.44544	785	18.45329	785	18.46113	785	18.46898	785	18.47683	785	18.48468	785	18.49253	785	18.50039	786	18.50824	786	462
463	18.51610	786	18.52396	786	18.53182	786	18.53968	786	18.54755	787	18.55541	787	18.56328	787	18.57115	787	18.57902	787	18.58689	787	463
464	18.59477	788	18.60264	788	18.61052	788	18.61840	788	18.62628	788	18.63416	788	18.64204	788	18.64992	789	18.65781	789	18.66570	789	464
465	18.67359	789	18.68148	789	18.68937	789	18.69727	790	18.70516	790	18.71306	790	18.72096	790	18.72886	790	18.73676	790	18.74466	791	465
466	18.75257	791	18.76047	791	18.76838	791	18.77629	791	18.78420	791	18.79212	791	18.80003	792	18.80795	792	18.81586	792	18.82378	792	466
467	18.83171	792	18.83963	792	18.84755	793	18.85548	793	18.86340	793	18.87133	793	18.87926	793	18.88720	793	18.89513	794	18.90306	794	467
468	18.91100	794	18.91894	794	18.92688	794	18.93482	794	18.94276	794	18.95071	795	18.95865	795	18.96660	795	18.97455	795	18.98250	795	468
469	18.99045	795	18.99841	796	19.00636	796	19.01432	796	19.02228	796	19.03024	796	19.03820	796	19.04616	797	19.05413	797	19.06210	797	469
470	19.07006	797	19.07803	797	19.08601	797	19.09398	797	19.10195	798	19.10993	798	19.11791	798	19.12589	798	19.13387	798	19.14185	798	470
471	19.14983	799	19.15782	799	19.16580	799	19.17379	799	19.18178	793	19.18978	799	19.19777	799	19.20576	800	19.21376	800	19.22176	800	471
472	19.22976	800	19.23776	800	19.24576	890	19.25377	801	19.26177	801	19.26978	801	19.27779	801	19.28580	801	19.29381	801	19.30183	802	472
473	19.30984	802	19.31786	802	19.32588	802	19.33390	802	19.34192	802	19.34994	802	19.35797	803	19.36599	803	19.37402	803	19.38205	803	473
474	19.39008	803	19.39811	803	19.40615	804	19.41418	804	19.42222	804	19.43026	804	19.43830	804	19.44634	804	19.45439	805	19.46243	805	474
475	19.47048	805	19.47853	805	19.48658	805	19.49463	805	19.50268	805	19.51074	806	19.51879	806	19.52685	806	19.53491	806	19.54297	806	475
476	19.55103	806	19.55910	807	19.56716	807	19.57523	807	19.58330	807	19.59137	807	19.59944	807	19.60752	808	19.61559	808	19.62367	808	476
477	19.63175	808	19.63983	808	19.64791	808	19.65599	808	19.66408	809	19.67216	809	19.68025	809	19.68834	809	19.69643	809	19.70452	809	477
478	19.71262	810	19.72071	810	19.72881	810	19.73691	810	19.74501	810	19.75311	810	19.76121	810	19.76932	811	19.77742	811	19.78553	811	478
479	19.79364	811	19.80175	811	19.80987	811	19.81798	812	19.82610	812	19.83421	812	19.84233	812	19.85045	812	19.85858	812	19.86670	813	479
480	19.87483	813	19.88295	813	19.89108	813	19.89921	813	19.90734	813	19.91548	813	19.92361	814	19.93175	814	19.93989	814	19.94802	814	480
481	19.95617	814	19.96431	814	19.97245	815	19.98060	815	19.98875	815	19.99689	815	20.00505	815	20.01320	815	20.02135	816	20.02951	816	481
482	20.03766	816	20.04582	816	20.05398	816	20.06214	816	20.07031	816	20.07847	817	20.08664	817	20.09480	817	20.10297	817	20.11114	817	482
483	20.11932	817	20.12749	818	20.13567	818	20.14384	818	20.15202	818	20.16020	818	20.16838	818	20.17657	818	20.18475	819	20.19294	819	483
484	20.20113	819	20.20932	819	20.21751	819	20.22570	819	20.23389	820	20.24209	820	20.25029	820	20.25849	820	20.26669	820	20.27489	820	484
485	20.28209	821	20.29130	821	20.29951	821	20.30771	821	20.31592	821	20.32414	821	20.33235	821	20.34056	822	20.34878	822	20.35700	822	485
486	20.36522	822	20.37344	822	20.38166	822	20.38988	823	20.39811	823	20.40634	823	20.41457	823	20.42280	823	20.43103	823	20.43926	824	486
487	20.44750	824	20.45573	824	20.46397	824	20.47221	824	20.48045	824	20.48869	824	20.49694	825	20.50518	825	20.51343	825	20.52168	825	487
488	20.52993	825	20.53818	825	20.54644	826	20.55469	826	20.56295	826	20.57121	826	20.57947	826	20.58773	826	20.59599	826	20.60426	827	488
489	20.61252	827	20.62079	827	20.62906	827	20.63733	827	20.64561	827	20.65388	828	20.66215	828	20.67043	828	20.67871	828	20.68699	828	489
490	20.69527	828	20.70356	829	20.71184	829	20.72013	829	20.72842	829	20.73671	829	20.74500	829	20.75329	829	20.76158	830	20.76988	830	490
491	20.77818	830	20.78648	830	20.79478	830	20.80308	830	20.81138	831	20.81969	831	20.82800	831	20.83630	831	20.84461	831	20.85293	831	491
492	20.86124	831	20.86955	832	20.87787	832	20.88619	832	20.89451	832	20.90283	832	20.91115	832	20.91947	833	20.92780	833	20.93613	833	492
493	20.94446	833	20.95279	833	20.96112	833	20.96945	833	20.97779	834	20.98612	834	20.99446	834	21.60280	834	21.01114	834	21.01948	834	493
494	21.02783	835	21.03617	835	21.04452	835	21.05287	835	21.06122	835	21.06957	835	21.07793	836	21.08628	836	21.09464	836	21.10300	836	494
495	21.11136	836	21.11972	836	21.12808	836	21.13644	837	21.14481	837	21.15318	837	21.16155	837	21.16992	837	21.17829	827	21.18666	838	495
496	21.19504	838	21.20342	838	21.21180	838	21.22018	838	21.22856	838	21.23694	838	21.24533	839	21.25371	839	21.26210	839	21.27049	839	496
497	21.27888	839	21.28727	839	21.29567	840	21.30406	840	21.31246	840	21.32086	840	21.32926	840	21.33766	840	21.34606	840	21.35447	841	497
498	21.36288	841	21.37128	841	21.37969	841	21.38810	841	21.39652	841	21.40493	842	21.41335	842	21.42177	842	21.43018	842	21.43860	842	498
499	21.44703	842	21.45545	843	21.46388	843	21.47230	843	21.48073	843	21.48916	843	21.49759	843	21.50602	843	21.51446	844	21.52290	844	499

APPENDIX 6

Radiations for Excitation of Electron Spectra and Conversion Factors between Energy Units

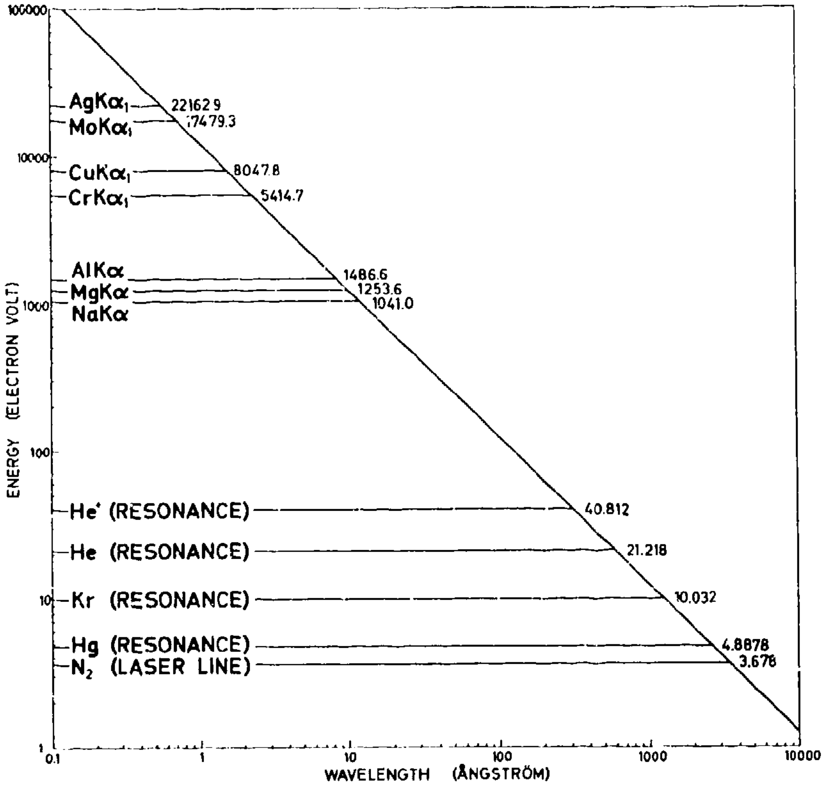

Fig. 6:1. Diagram of energy versus wavelength for photons. Some X-ray lines which are particularly useful in ESCA are indicated in the diagram (energies in eV[115]). In the UV region the He resonance line at 584 Å is indicated together with some other lines which can be useful for particular purposes. The laser line of N_2, also indicated in the diagram, is presently the one with the shortest wave-length which can be conveniently produced without using higher harmonics. The energy of this radiation is generally too low to excite electron spectra but either this radiation or those from similar light sources may become useful in more elaborate arrangements for electron spectroscopy (for example, double beam experiments). It would also be of great interest to fill the gap of exciting radiations between the sodium X-ray line and the helium UV line. The difficulties in doing this are due to the broadening of X-ray lines at lower energies on one side, and the low intensities in UV at higher energies on the other side. The situation would be improved if compensation for the inherent width of soft X-ray lines could be achieved (for example, according to the scheme discussed in Appendix 10), or if more intense sources of UV light from ionized atoms such as neon could be designed (He^+ has another line at 256 Å = 48.4 eV,[299] which could possibly be used). The ideal source of excitation, namely the X-ray laser, still seems far from becoming an accomplished fact.

Energy conversion factors between the eV unit employed in electron spectroscopy and units frequently used in other kinds of spectroscopy and chemistry. The 1963 set of fundamental constants[148] is used.

Unit	eV	Ry	cm^{-1}	s^{-1}	J	$kcal_{th} \cdot mole^{-1}$
1 eV	1	$7.35005 \cdot 10^{-2}$	8065.73	$2.41804 \cdot 10^{14}$	$1.60210 \cdot 10^{-19}$	23.061
1 Ry = ½ H	13.60535	1	$1.09737 \cdot 10^{5}$	$3.28983 \cdot 10^{15}$	$2.17971 \cdot 10^{-18}$	313.75
1 cm^{-1} ≙ 1 K	$1.23981 \cdot 10^{-4}$	$9.1127 \cdot 10^{-6}$	1	$2.997925 \cdot 10^{10}$	$1.98630 \cdot 10^{-23}$	$2.8591 \cdot 10^{-3}$
1 s^{-1} ≙ 1 Hz	$4.13558 \cdot 10^{-15}$	$3.03967 \cdot 10^{-16}$	$3.335640 \cdot 10^{-11}$	1	$6.62559 \cdot 10^{-34}$	$9.5371 \cdot 10^{-14}$
1 J	$6.24181 \cdot 10^{18}$	$4.58776 \cdot 10^{17}$	$5.03448 \cdot 10^{22}$	$1.50930 \cdot 10^{33}$	1	$1.4294 \cdot 10^{20}$
1 $kcal_{th} \cdot mole^{-1}$	$4.3363 \cdot 10^{-2}$	$3.1872 \cdot 10^{-3}$	349.76	$1.0485 \cdot 10^{13}$	$6.9472 \cdot 10^{-21}$	1

APPENDIX 7

Graphical Representation of Photoelectric Cross Sections

The absorption of photons traversing matter (Section V:7) is described by the exponential law

$$I = I_0 e^{-\mu \varrho t}$$

I_0 primary photon intensity,
I — photon intensity at a depth t,
μ — mass absorption coefficient,
ϱ — density of the absorbing material.

The mass absorption coefficient is a measure of the probability of photoelectric and scattering processes. For X-ray quanta, the scattering contribution to the mass absorption coefficient is much smaller than the photoelectric part and μ therefore reflects essentially the photoelectric cross section in an element. The main part of this cross section is due to photoelectric absorption in the K shell for radiation wavelengths smaller than the K absorption limit. For wavelengths between the K and the L absorption limits, the main contribution is due to L absorption, etc. The mass absorption coefficient thus gives information about the line intensities that can be expected in an ESCA spectrum. Furthermore, in some cases it may be necessary to use a suitable material for filtering the X-ray beam (Section VIII:1). The choice of filter material is then based on mass absorption coefficient data.

An illustration of the wavelength and Z dependence of the mass absorption coefficient is given in Fig. 7:1. The figures show the approximate variation of μ with atomic number Z for some X-ray lines which are commonly used in ESCA.

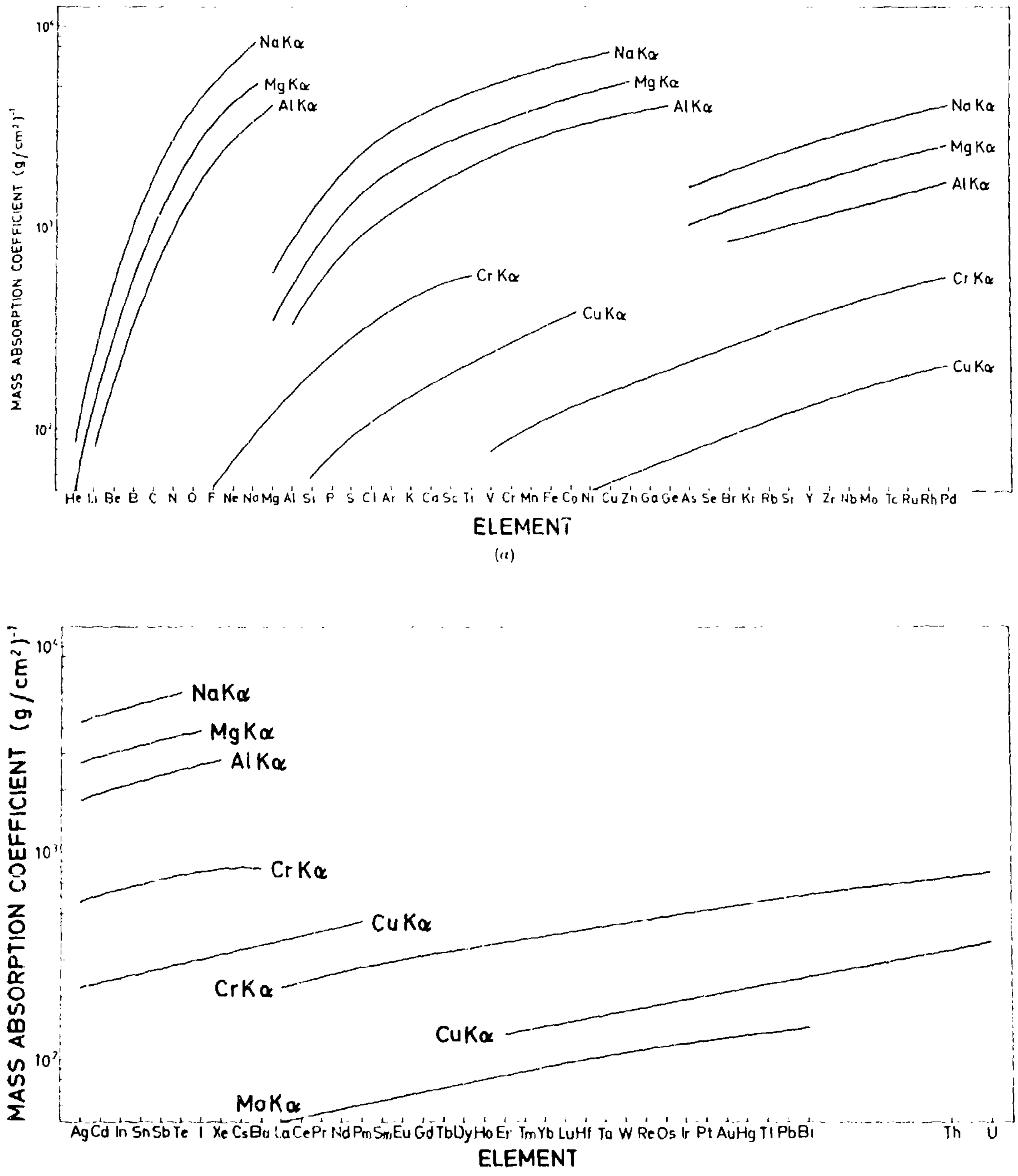

(*a*)

(*b*)

Fig. 7·1. The approximate variation of mass absorption coefficient with atomic number Z for some X-ray lines commonly used in ESCA.

APPENDIX 8

Theory of Double Focussing Magnetic Instrument and Calculation of Focussing Properties

A magnetic field having cylindrical symmetry with respect to the z direction and a symmetry plane, $x-y$, orthogonal to z, is completely defined by its analytical expression $B(\varrho,z)$ in this plane. (For notations see Fig. 8:1.) A charged particle with velocity v has a stationary motion in a circular path with radius ϱ_0 in the $x-y$ plane ($z=0$), if the equation

$$B(\varrho_0) = \frac{mv}{e\varrho_0} \tag{1}$$

is satisfied; m is the mass of the particle and e its charge. If the initial direction of the particle in the $x-y$ plane differs from the direction of the tangent to the stationary path ($\varrho=\varrho_0$) (the optic circle) by an angle φ_0, then the particle will return to the optic circle after an azimuthal angle ϕ_ϱ, the radial focussing angle, that depends on φ_0. If the angle of emission in the z-direction is ψ_0, we have a corresponding focussing angle ϕ_z. For small angles φ_0, the following relations hold between the focussing angles ϕ_ϱ and ϕ_z and the field (see e.g. Ref. 52).

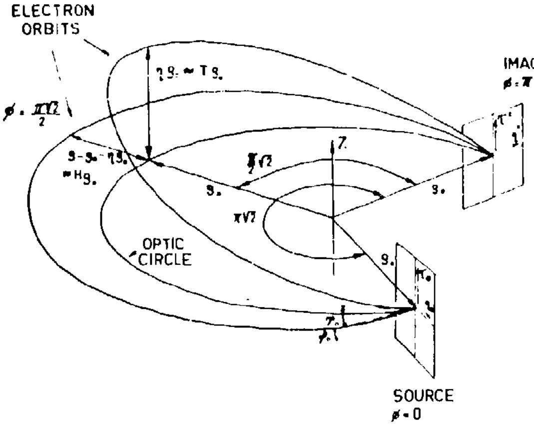

Fig. 8:1. Electron trajectories in a double focussing magnetic spectrometer.

$$\phi_\varrho = \pi\left[1+\frac{\varrho_0 B'(\varrho_0)}{B(\varrho_0)}\right]^{-\frac{1}{2}} \tag{2}$$

$$\phi_z = \pi\left[-\frac{\varrho_0 B'(\varrho_0)}{B(\varrho_0)}\right]^{-\frac{1}{2}} \tag{3}$$

From eq. (2) and (3), the following relation between the focussing angles is derived

$$\frac{1}{\phi_\varrho^2}+\frac{1}{\phi_z^2}=\frac{1}{\pi^2} \tag{4}$$

An an-astigmatic system is obtained if $\phi_\varrho=\phi_z$, which gives the following conditions for double focussing:

$$\phi_\varrho=\phi_z=\pi\sqrt{2} \tag{5}$$

$$B'(\varrho_0) = -\frac{1}{2\varrho_0}B(\varrho_0) \tag{6}$$

The solution of the latter equation imposes the condition that the magnetic field should decrease as $1/\sqrt{\varrho}$ in the vicinity of $\varrho=\varrho_0$. According to (5), double focussing takes place after an angle of $\pi\sqrt{2}\approx 255°$.

Although it is found that the field obtained using the $1/\sqrt{\varrho}$ relationship is a good choice, extensive analyses show that other slightly different fields can also be employed. The general field form may be expressed as:

$$B_z(\varrho,0) = B_0[1+\alpha\eta+\beta\eta^2+\gamma\eta^3+\delta\eta^4+\ldots] \tag{7}$$

where B_0 is the vertical component of the magnetic field on the optic circle, $\eta=(\varrho-\varrho_0)/\varrho_0$ and $\alpha,\beta,\ldots$ are the expansion coefficients which are determined to minimize aberrations.

The equations of motion are solved for a particle leaving the source at a point $\eta_0=\delta\varrho/\varrho_0$, $\tau_0=\delta z/\varrho_0$ and with angles of emission φ_0 and ψ_0. It is then found, in agreement with eq. (5) and (6), that first order an-astigmatic focussing occurs after $\phi=\pi\sqrt{2}$ when $\alpha=-\frac{1}{2}$. The particle will strike the plane $\phi=\pi\sqrt{2}$ at a point defined by the coordinates

$$\eta^* = -\eta_0+\tfrac{1}{3}(2-4\beta)\eta_0^2+\tfrac{1}{3}(4\beta-3)\tau_0^2+\tfrac{1}{3}(2-16\beta)\times$$
$$\times\varphi_0^2+\tfrac{1}{3}(16\beta-6)\psi_0^2 \tag{8}$$

$$\tau^* = -\tau_0+\tfrac{8}{3}\beta\eta_0\tau_0+\tfrac{1}{3}(32\beta-12)\varphi_0\psi_0 \tag{9}$$

Table 8:1 Expansion coefficients for some different types of magnetic field.

Coefficient	Optimal field (Ref. 277)	$1/\sqrt{\varrho}$ field	Two solenoidal coils (Section VIII:3)	Four pairs of circular coils (Ref. 279)	Two divided solenoidal coils (Section VIII:4)
α	−0.5	−0.5	−0.49993	−0.50003	−0.50005
β	+0.375	+0.375	+0.3752	+0.37517	+0.37518
γ	−0.2986	−0.3125	+0.113	−0.2983	−0.2987
δ	+0.2400	+0.2734	−0.30	+0.2392	−6.10
ε	−0.2017	−0.2461		−1.889	
ζ	+0.1768	+0.2256		+1.024	

From eq. (8) it is apparent that η^* will be independent of φ_0^2 when β equals 1/8, while for $\beta = 3/8$, η^* will be independent of ψ_0^2. Other values of β are possible, but all involve a lower resolution for a given transmission than that obtained in the two cases given above; these two are approximately of equal merit. However, the alternative $\beta = 3/8$ has a number of slight advantages over $\beta = 1/8$. Thus, for $\beta = 3/8$, the coefficient of the last term in the expression (9) for τ^* will be zero. Further, a focal plane is obtained, so that several energies can be studied simultaneously with good resolution. This is of considerable significance now that arrays of semiconductor detectors have been developed.

If, for the above reasons, the alternative $\alpha = -\frac{1}{2}$ and $\beta = 3/8$ is chosen, third order calculations give the following image coordinates as functions of γ

$$\begin{aligned}\eta^* = {} & -\eta_0 + \tfrac{1}{6}\eta_0^2 - \tfrac{1}{36}\eta_0^3 - \tfrac{1}{2}\tau_0^2 + \tfrac{7}{12}\eta_0\tau_0^2 - \tfrac{4}{3}\varphi_0^2 - \tfrac{3}{2}\pi\sqrt{2} \\ & \times(\gamma + \tfrac{43}{144})\varphi_0^3 - \tfrac{3}{4}\pi\sqrt{2}(\gamma + \tfrac{43}{144})\eta_0^2\varphi_0 + \tfrac{3}{4}\pi\sqrt{2} \\ & \times(\gamma + \tfrac{25}{48})\tau_0^2\varphi_0 + \tfrac{9}{2}\pi\sqrt{2}(\gamma + \tfrac{43}{144})\varphi_0\psi_0^2 + \tfrac{3}{2}\pi\sqrt{2} \\ & \times(\gamma + \tfrac{3}{16})\eta_0\tau_0\psi_0 - \tfrac{2}{9}\eta_0\varphi_0^2 - \tfrac{4}{3}\tau_0\varphi_0\psi_0 \end{aligned} \qquad (10)$$

$$\begin{aligned}\tau^* = {} & \tau_0 + \eta_0\tau_0 + \tfrac{1}{4}\tau_0^3 - \tfrac{7}{12}\eta_0^2\tau_0 + \tfrac{9}{2}\pi\sqrt{2}(\gamma + \tfrac{43}{144})\varphi_0^2\psi_0 \\ & - \tfrac{3}{2}\pi\sqrt{2}(\gamma + \tfrac{17}{48})\psi_0^3 + \tfrac{3}{4}\pi\sqrt{2}(\gamma + \tfrac{25}{48})\eta_0^2\psi_0 + \tfrac{3}{2}\pi\sqrt{2} \\ & \times(\gamma + \tfrac{3}{16})\eta_0\tau_0\varphi_0 - \tfrac{3}{4}\pi\sqrt{2}(\gamma + \tfrac{17}{48})\tau_0^2\psi_0 + \tfrac{2}{3}\tau_0\varphi_0^2 \end{aligned} \qquad (11)$$

From the above expressions, it is apparent that the minimum aberration error will be obtained when γ is equal to $-43/144$. Calculations of the optimal values for several expansion coefficients have been carried out by Lee-Whiting and Taylor.[277] From Table 8:1 it can be seen that these optimal values very nearly agree with the expansion coefficients for $1/\sqrt{\varrho}$ field.

A computer program has now been developed and used for the study of the electron trajectories in a magnetic field of the above described type. The program first computes the magnetic field generated by the coils and then calculates the electron trajectories in this field. Any system of coaxial cylindrical coils can be used and the B_ϱ and B_z components of the field are calculated in a two-dimensional (ϱ, z) array of points. Field values at intermediate points are obtained by cubic interpolation. When calculating the trajectories one can choose different radial and axial angles of emission and for each trajectory, one can calculate its point of intersection with the focal plane and the baffle plane, or any other azimuthal plane. Thus, by use of this program one can calculate all electron optical properties of the spectrometer which means that iso-aberration curves and optimal baffle aperture contours can be obtained.

APPENDIX 9

Theory of Double Focussing Electrostatic Instrument and Calculation of Second Order Image Distortion and of Stray Fields

The electric field in the space between the two electrodes in a spherical condenser varies as $1/r^2$. In this type of field, charged particles describe elliptical paths.[258,52] In a given field, particles with suitable energy and angle of emission move in a circular path with radius a. Particles with the same energy but with other angles of emission from a point source will move in ellipses with major axis $2a$. By analogy with the case for the homogeneous magnetic field, first-order focussing will occur after an angle π. Since the field possesses spherical symmetry, double focussing will also be obtained, which means that the transmission at a given resolution will be greater for the electrostatic condenser than for the homogeneous magnetic field.

Let us consider a sector of the spherical condenser. The symbols used are shown in Fig. 9:1, where areas I and II are free of fields. To begin with, all edge effects between the field and the field-free areas are neglected. The condition for electrons with velocity v_0 and energy E moving in circular paths within area III is

$$\frac{V_f R_1 R_2}{(R_2 - R_1)} = \frac{a m v_0^2}{e}, \tag{1}$$

where V_f is the potential difference between the spheres.

Since $E = \frac{1}{2} \cdot m v_0^2$ for non-relativistic energies we obtain, if $a = \frac{1}{2}(R_1 + R_2)$:

$$V_f = \frac{E}{e}\left(\frac{R_2}{R_1} - \frac{R_1}{R_2}\right). \tag{2}$$

The solution of the equations of motion in area III will be:

$$\frac{1}{r} = P \cos \varphi + Q \sin \varphi + k^2/A^2, \tag{3}$$

where $k^2 = a v_0^2$ and $A = r^2 \dot{\varphi}$. The inclusion of boundary conditions determines P and Q. For electrons with velocity $v = v_0(1 + \beta)$, the y-coordinate in area II is given by the expression

$$y_2 = a\left[\alpha \sin \phi + \left(\alpha \frac{x_{10}}{a} - 2\beta\right) \cos \phi + 2\beta\right] + x_2\left[\alpha \cos \phi - \left(\alpha \frac{x_{10}}{a} - 2\beta\right) \sin \phi\right]. \tag{4}$$

The condition for focussing is that for a given value of x_2, e.g. x_{20}, y_2 shall be independent of α. (4) gives:

$$a(x_{10} + x_{20}) = \tan \phi (x_{10} x_{20} - a^2). \tag{5}$$

From Fig. 9:1 it is apparent that $\tan \gamma = x_{20}/a$ and $\tan \theta = x_{10}/a$. Insertion in (5) gives:

$$\tan \phi = \frac{\tan \gamma + \tan \theta}{\tan \gamma \cdot \tan \theta - 1} = -\tan (\theta + \gamma). \tag{6}$$

From this it follows that A, O and F are colinear, which makes it possible to utilize the whole volume between the spheres and still obtain a point focus. Inserting (5) in (4) gives the distance at which an electron with velocity $v_0\,(1 + \beta)$ passes F:

$$y_2 = 2\beta a\left(1 - \cos \phi + \frac{x_{20}}{a} \sin \phi\right). \tag{7}$$

The dispersion D_v is obtained by dividing by β. The insertion of p and q instead of ϕ and x_{20} in (7) gives:

$$D_v = \frac{y_2}{\beta} = 2a(1 + q/p). \tag{8}$$

This is twice as much as for a spectrometer with a homogeneous magnetic field. In order to derive the resolution, the calculations must be extended to the second order in α. We then obtain:

$$\frac{B}{a} = \frac{y_2}{a} = \alpha^2 (\cos^2 \gamma / \cos^2 \theta + \cos \theta / \cos \gamma) \tag{9}$$

$$= \alpha^2 (p^2/q^2 + q/p),$$

which is also twice the corresponding value for the homogeneous magnetic field. The reduced velocity dispersions are therefore identical. The resolution in a

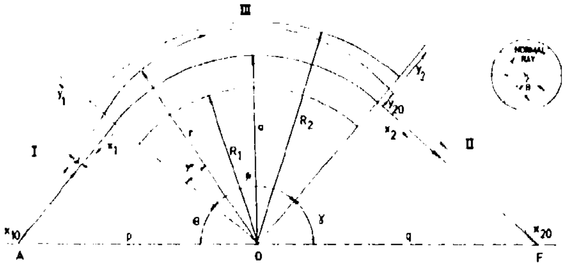

Fig. 9:1. Particle orbits in an electrostatic sector field.

spectrometer in which the field is proportional to $1/r^2$ will be:

$$R_v = \left|\frac{B}{D_v}\right| = \frac{\alpha^2}{2}\left(1 - \frac{p}{q} + \left(\frac{p}{q}\right)^2\right). \qquad (10)$$

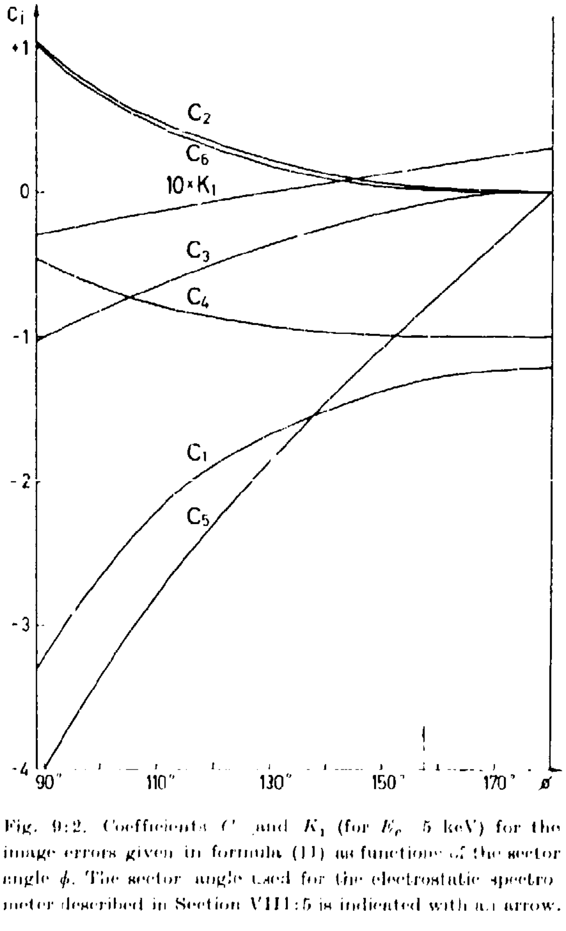

Fig. 9:2. Coefficients C and K_1 (for $E_e = 5$ keV) for the image errors given in formula (11) as functions of the sector angle ϕ. The sector angle used for the electrostatic spectrometer described in Section VIII:5 is indicated with an arrow.

Table 9:1. Calculated resolutions using eq. (12) for different transmissions and specimen areas in an electrostatic spectrometer with sector angle $\phi = 157.5°$ and orbit radius $a = 36$ cm.

(a) Rectangular baffle. Electron energy $E_e = 5$ keV.

Transmission %	Source: width × height mm × mm	Resolution (R) %
0.19	0.7 × 10	0.10
0.08	0.35 × 10	0.05
0.08	0.1 × 7	0.03
0.05	0.2 × 7	0.03
0.011	0.05 × 7	0.01

(b) Shaped baffle and detector slit. In the calculation it has been assumed that hereby the influence of the terms $C_2 a\alpha_z^2$ and $C_4 a\left(\frac{z_0}{a}\right)^2$ in (12) are negligible for $|\alpha_z| \leq 10°$ and $|z_0| \leq 7.5$ mm.

Transmission %	Source, width × height mm × mm	Resolution (R) % $E_e = 5$ keV	 $E_e = 1$ keV
0.29	0.7 × 15	0.12	0.10
0.21	0.3 × 15	0.07	0.05
0.15	0.3 × 15	0.04	0.03
0.07	0.05 × 15	0.016	0.01

The above equations apply for a point source. By extensive calculations, the dependence on the finite size of the specimen can also be obtained. Calculations of this type have been carried out by Ewald and Liebl[280] (in connection with mass spectroscopy) for the general case with a toroid condenser. If edge effects are neglected, an electron leaving the specimen at a point with coordinates (x_{10}, y_0, z_0) and with the angles of emission α_r (equal to α in Fig. 9:1) and α_z will for the correct applied voltage over the condenser reach the focal plane ($x = x_{20}$) at a point, which has the y-coordinate:

$$y = a\left(C_1\alpha_r^2 + C_2\alpha_z^2 + C_3\left(\frac{y_0}{a}\right)^2 + C_4\left(\frac{z_0}{a}\right)^2 + C_5\alpha_r\frac{y_0}{a} + C_6\alpha_z\frac{z_0}{a}\frac{y_0}{a} + K_1\alpha_r\right). \qquad (11)$$

The coefficients C_i in this formula have been calculated for a symmetrical radiation path (i.e. $p = q$) and for different values of the sector angles using the equations published by Ewald and Liebl. The term $a\,K_1\alpha_r$ is, as discussed below, due to the relativistic spread of the electrons and varies with the energy of the electrons studied. C_4 and K_1 (for $E_e = 5$ keV) are given as a function of the sector angle in Fig. 9:2. When $\phi = 180°$, all coefficients, except C_4 and K_1, have their minimum absolute values. It is thus clear that for optimum focussing properties, ϕ should be chosen as near 180° as possible. In Table 9:1, some sets of values of specimen size, transmission and resolution for a spectrometer with $\phi = 157.5°$ and $a = 36$ cm are given. As a first guide the resolution (given in Table 9:1 a) has been calculated by replacing B in eq. (10) by the sum of the absolute values of the different image errors, thus giving:

$$R_e = \left(|C_1\alpha_r^2| + |C_2\alpha_z^2| + \left|C_3\left(\frac{y_0}{a}\right)^2\right| + \left|C_4\left(\frac{z_0}{a}\right)^2\right| + \left|2C_5\alpha_r\frac{y_0}{a}\right|\right.$$
$$\left. + \left|2C_6\alpha_z\frac{y_0}{a}\right| + 2\frac{y_0}{a} + 2\frac{d}{a} + |K_1\alpha_r|\right)\cdot a/|D_v|, \quad (12)$$

where $2y_0$ and $2z_0$ are the width and the height of the specimen respectively and $2d$ is the width of the detector slit. The value R_e for the resolution gives the base width, while the full width at half maximum is the most commonly used value. The value given in Table 9:1 is accordingly $R = \frac{1}{2}R_e$. However, as shown in Fig. 9:2 the various image distortions have different signs, so that by a suitable choice of baffle shape it is possible to increase the transmission considerably while retaining the same resolution. This applies principally to the effect of $C_2a\alpha_z^2$, which can be eliminated by not having α_r equal to zero for large values for α_z. It should be possible to cancel the effect of the term $C_4a(z_0/a)^2$ to a large extent by using a curved detector slit. The detailed shape of the slits and the baffle should be determined with reference to the experimental results, since the effect of stray fields, non-uniformities in the electrical field and small errors in the adjustment of the two sectors with respect to each other can have a considerable effect on the appearance of the image. The magnitude of the increase in transmission which can be expected is shown in Table 9:1b. The values for the transmission and resolution quoted in this table have been calculated assuming that the effect of the term $C_2\alpha_z^2$ is negligible for $|\alpha_z| < 10°$, and that the curved detector slit allows the use of specimens with a height of 15 mm without the resolution being affected. By using a suitably shaped baffle it should be possible, for example, to obtain 0.15 % transmission at a resolution of 0.03 % for electrons with an energy of 1 keV.

Image distortion originating from relativistic effects is one disadvantage of the electrostatic instrument. This appears as a broadening of the electron beam which is proportional to α_r. For low electron energies, the proportionality factor is of course very small, but for high resolutions its effect cannot be neglected. If y_r is the distance from the relativistic path to the non-relativistic focus, the magnitude of the coefficient K_1 in the series expansion $y_r/a = K_1\alpha_r + K_2\alpha_r^2 + \ldots$ must

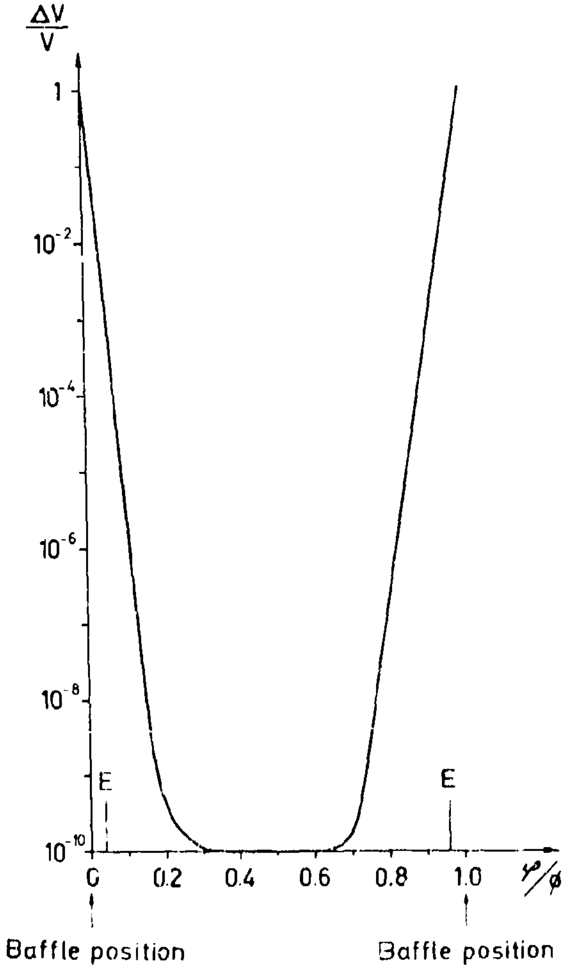

Fig. 9:3. Relative difference between the $1/r$ potential and the potential obtained when using grounded baffles as a function of φ/ϕ. The beginning and end of the spherical electrodes are indicated by E. The curve is given for $r = 33$ cm in an electrostatic field between sectors with radii $R_1 = 32$ cm and $R_2 = 40$ cm. The limit $\Delta V/V = 10^{-10}$ is set by the numerical accuracy in the calculations.

be taken into consideration. K_1 varies of course with β, where $\beta = v/c$, and the relationship is:[258]

$$K_1 = \frac{1+\beta^2}{1-\beta^2} \cdot \frac{x_{10}}{a} \cdot \cos\gamma\,\phi + \frac{\sin\gamma\,\phi}{\gamma} - \frac{2\beta^2 x_{10}}{a(1-\beta^2)} + \frac{x_{20}}{a} \times \left[\cos\gamma\,\phi - \frac{x_{10}\gamma}{a}\sin\gamma\phi\,\frac{1+\beta^2}{1-\beta^2}\right] \tag{13}$$

where $\gamma^2 = 1 - \beta^2 - 2\beta^4\alpha_r$. The variation of K_1 with sector angle has been calculated for an electron energy of 5 keV and is shown in Fig. 9:2. The difference between the resolutions expected for electrons with energies of 1 and 5 keV is shown in Table 9:1b.

In the above treatment, the edge effects in the regions between the field and field-free areas have been neglected. It is possible to eliminate these effects by the use of grounded diaphragms. Herzog[259,260] has carried out calculations for plane condensers and cylindrical condensers and his results can also be used to some extent for spherical sector condensers. The field can then be replaced by a substitution field with the same character as the ideal field, but with altered geometrical dimensions.

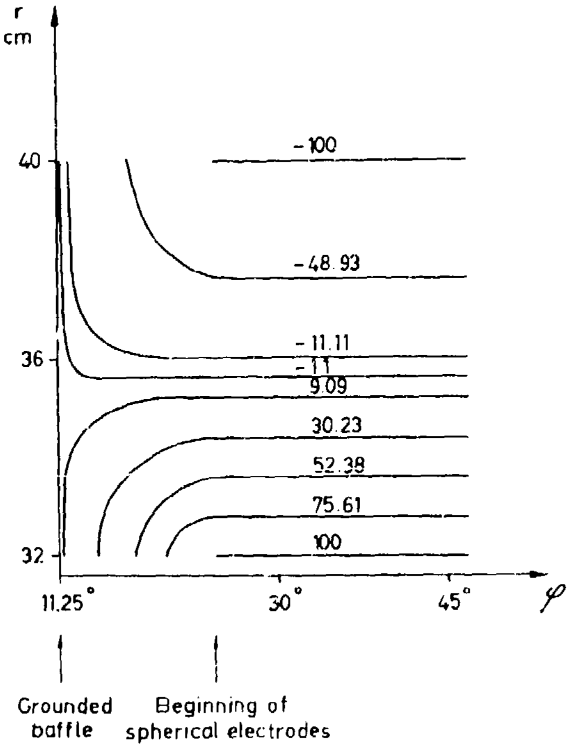

Fig. 9:4. Equipotential curves for an electrostatic spectrometer with $R_1 = 32$ cm and $R_2 = 40$ cm. The grounded baffle is placed 13.5° from the electrodes. In the calculations a symmetrical potential has been chosen whereby $V = 0$ at a radius which is somewhat smaller than the mean radius.

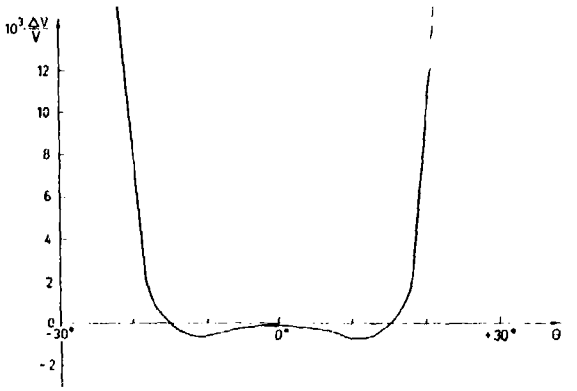

Fig. 9:5. Relative difference between the $1/r$ potential and the potential obtained using grounded limiting surfaces in the z direction. As in Fig. 9:3, the calculations are performed for a radius $r = 33$ cm with the radii of the electrodes $R_1 = 32$ cm and $R_2 = 40$ cm. The total angle between the limiting areas is 60°. Θ is the angular deviation from the symmetry plane with O chosen as origin. ΔV is positive when the $1/r$ potential is higher than the potential calculated numerically. Within the region $-15° < \Theta < 15°$, the difference has a very small influence on the shape of the image.

A more exact calculation of the peripheral field has been carried out by a numerical solution of Laplace's equation

$$\Delta V = 0. \tag{14}$$

The results of these calculations,* performed on an IBM 1620 and an IBM 7090, are shown in Figs. 9:3 and 9:4. The rapid transition of the potential to the analytical $1/r$ form is shown in Fig. 9:3. Fig. 9:4 shows the appearance of the equipotential surfaces.

When a sector condenser is used, edge effects are introduced at two additional limiting surfaces. Fig. 9:5 shows the deviation of the numerically obtained potential from the $1/r$ potential as a function of the angle Θ, where Θ is the angle taken from the symmetry plane in a plane through O at right angles to the line AOF (see Fig. 9:1). The total sector angle is 60° and the limiting surfaces are grounded. It is possible to reduce the edge effects still further by inserting into

---

* Thanks are due to Fil.lic. Göran Pettersson for performing the calculations.

the limiting surface some strips, each placed at an appropiate potential.

Attempts have also been made to calculate the electron paths. For this, it is necessary to know the electric field or grad V. However, the above calculations yield V and for each integration point in the path, $\partial V/\partial r$ and $\partial V/\partial \varphi$ must be evaluated. These derivatives are obtained as differences between numerical values which are often nearly equal, so that the numerical error in the difference, expressed as a percentage, will be very great. This makes it impossible to carry out sufficiently accurate calculations of the paths. One method of avoiding this problem is to set up analytical potential functions which are very similar to the numerically determined ones. One possible approach is to use a potential of the type:

$$V = \left(\frac{C}{r} + B\right)\left(1 - e^{\alpha\varphi^{\beta}}\right) \qquad (15)$$

which applies for $\varphi \leq \phi/2$. Preliminary results obtained in attempts to fit the variables in this potential to the numerically obtained potential show the same trends in the dependence of image distortion on ϕ as Fig. 9:2, i.e. a large sector angle gives the best focussing.

APPENDIX 10

Combined Crystal and Magnetic (Electrostatic) Focussing for Eliminating Inherent Width of X-radiation

The width of an electron line in an ESCA spectrum is determined by several factors (Section VIII:1). The main contributions to the width are, in most cases, the inherent width of the X-ray line and the width of the level studied. Under certain conditions, it is possible to compensate for the contribution of the inherent width of the X-ray line to the total width of an electron line by using an X-ray crystal monochromator in combination with an electron spectrometer (Section VIII:1). As a consequence of this compensation, the width of an electron line will be reduced considerably, which facilitates the measurements of small chemical shifts with high precision. Since, with the X-ray line width eliminated, the electron lines essentially reflect the widths of the atomic levels in the target, it may also be possible to measure the widths of these levels directly from ESCA spectra. The principle of the compensation is applicable to different types of electron spectrometers. A derivation of formulae for the compensation is given for the case of a homogeneous field magnetic spectrograph. The electron paths are semicircular in a plane orthogonal to the magnetic field.

From the triangle SPP′ of Fig. 10:1, one obtains

$$(2\varrho)^2 = \{2\cdot\varrho_0\cdot\sin\omega + x\cdot\sin(\omega+\alpha)\}^2 + \{x\cdot\cos(\omega+\alpha) + 2\cdot\varrho_0\cdot\cos\omega + y\}^2 \quad (1)$$

where ϱ_0 and ϱ are the radii of curvature of the trajectories for electrons with kinetic energy E_0 and $E_0 + \Delta E$, respectively. If the width of the source x, and the separation of the electron lines, y, are both small compared to ϱ_0, terms containing x^2, y^2 and xy can be neglected. This gives

$$\left(\frac{\varrho}{\varrho_0}\right)^2 = 1 + (x\cos\alpha + y\cos\omega)/\varrho_0 \quad (2)$$

If ΔE is small compared with the photoelectron energy E_0, one obtains for non-relativistic energies

$$E_0 + \Delta E = E_0\cdot\left(\frac{\varrho}{\varrho_0}\right)^2. \quad (3)$$

Furthermore according to Fig. 10:1

$$x = D\cdot\Delta E/\sin\beta \quad (4)$$

where the crystal dispersion $D = dx/d(h\nu)$.
Eq. (2), (3), and (4) give the distance, y, at the detector, between electrons with energies E_0 and $E_0 + \Delta E$.

$$y = \frac{\varrho_0\cdot\Delta E}{E_0\cos\omega}\cdot\left(1-\frac{DE_0\cos\alpha}{\varrho_0\sin\beta}\right) \quad (5)$$

If the contribution, ΔE, from the inherent width of the X-ray line is not allowed to contribute to the total width of the electron line y must be zero i.e.

$$E_0 = \varrho_0\sin\beta/D\cos\alpha \quad (6)$$

Experimental

The semicircular spectrograph described in Section VIII:3 has been used for an experimental verification of equations (5) and (6). The spectrograph is equipped with an X-ray tube for copper radiation and a crystal monochromator that focusses the radiation on the

THE COMPENSATION

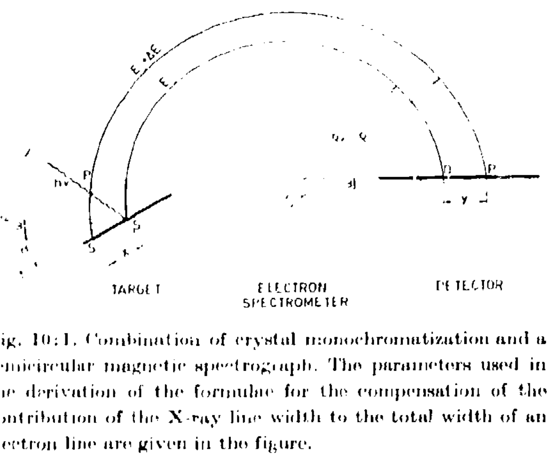

Fig. 10:1. Combination of crystal monochromatization and a semicircular magnetic spectrograph. The parameters used in the derivation of the formulae for the compensation of the contribution of the X-ray line width to the total width of an electron line are given in the figure.

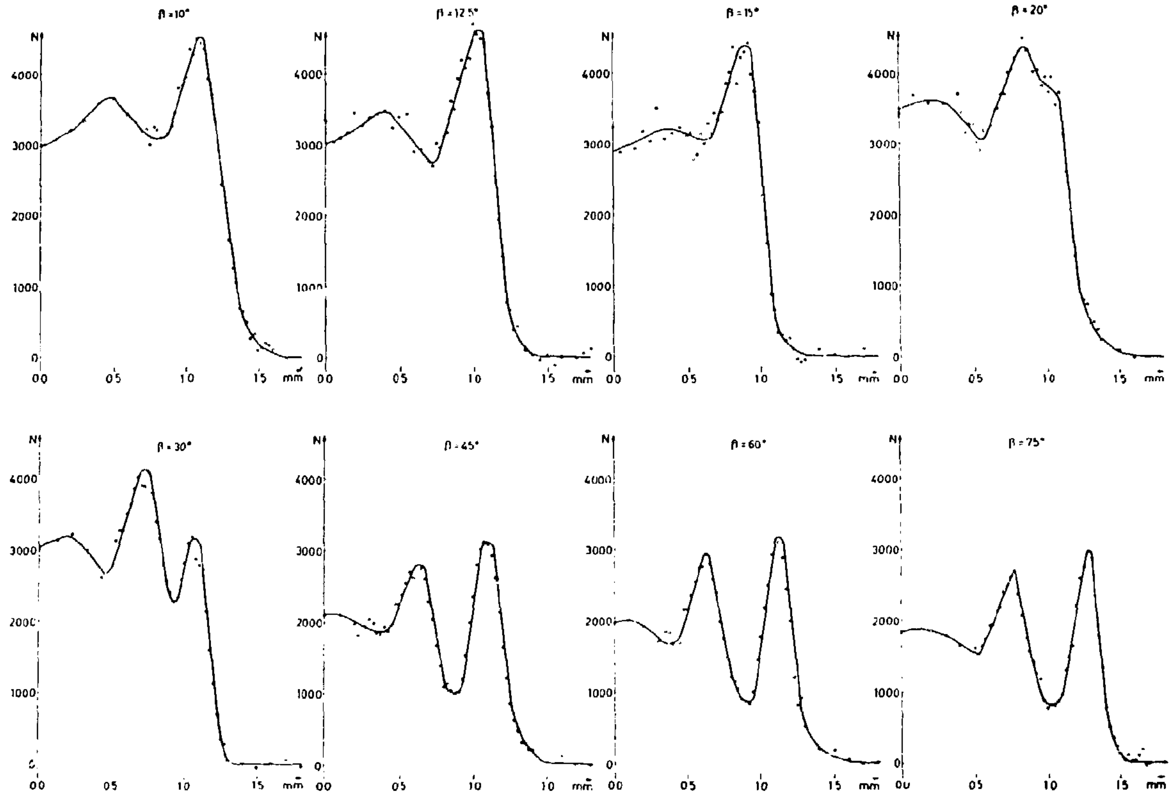

Fig. 10:2. Experimental recordings of the electron lines $ClK(CuK\alpha_1)NaCl$ and $ClK(CuK\alpha_2)NaCl$ for different angles β. The lines coalesce for $\beta = 12.5°$ in accordance with equation (7). Track counting was made by the TMD (Section VIII:8).

target. The X-ray tube and the monochromator occupy a fixed position relative to the spectrograph. The angle between the target and the X-ray beam is the only degree of freedom available. If this angle is varied, the target will not always be situated on the Rowland circle of the crystal monochromator. This experimental restriction would not allow a satisfactory study of the variation of the width of individual electron lines. We have therefore chosen to verify the compensation method described by studying the separation of two electron lines instead of the width of one electron line.

The target was a very thin film of sodium chloride evaporated on to an aluminum foil and the distance y between the electron lines ClK ($Cu\ K\alpha_1$) NaCl and ClK ($CuK\alpha_2$) NaCl was measured as a function of the angle α (see Fig. 10:1). Detection was performed photographically and the photographic plates were analysed using the track counting technique. The experimental results are shown in Fig. 10:2. As can be seen in the figure, the distance between the two lines decreases with decreasing angle α. Finally the two electron lines, $ClK(CuK\alpha_1)$ and $ClK(CuK\alpha_2)$ coalesce for $\beta = 12.5°$ which corresponds to an angle $\alpha = 16.5°$ (since in our geometry $\omega = 4.0°$ and $\alpha = \beta + \omega$).

The solid curves in Fig 10:3 show the calculated distance between the electron lines. The analytical expression which corresponds to eq. (5) for the right hand branch is

$$y = \frac{\varrho_0 \cdot \Delta E}{E_0 \cdot \cos\omega} \cdot \left(1 - \frac{DE_0}{\varrho_0 \cos\omega} \cdot \frac{1}{\tan\alpha - \tan\omega}\right) \quad (7)$$

in our geometry, where $\beta = \alpha - \omega$. For this case eq. (6) is replaced by

$$\alpha = \arctan\left(\frac{DE_0}{\varrho_0 \cos\omega} + \tan\omega\right). \quad (8)$$

A numerical calculation shows that compensation is attained when $\alpha = 16.5^\circ$ which was also found experimentally (see Fig. 10:3). The equation for the left hand branch is

$$y = \frac{\varrho_0 \cdot \Delta E}{E_0 \cos \omega}\left(1 + \frac{DE_0}{\varrho_0 \cos \omega} \cdot \frac{1}{\tan(-\alpha) + \tan \omega}\right) \quad (9)$$

since in this case $\beta = -\alpha + \omega,\ \alpha < 0,$

and $$x = -D \cdot \Delta E / \sin \beta.$$

This branch is only of theoretical interest and has therefore not been checked experimentally. The experimental values corresponding to the right hand branch are shown in Fig. 10:3 and are in good agreement with the theoretical curve. Eq. (5) and (6) have thus been verified experimentally.

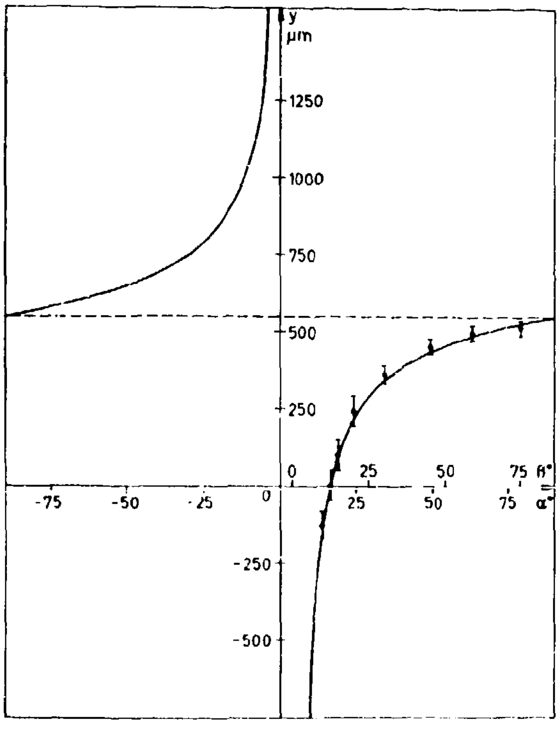

Fig. 10:3. The solid curves are calculated from equation (6) (the branch to the right) and from equation (8) (the branch to the left) and show the distance between the electron lines $ClK(CuK\alpha_1)NaCl$ and $ClK(CuK\alpha_2)NaCl$ as a function of the angle α in our experimental arrangement. Experimental points are shown for the branch to the right.

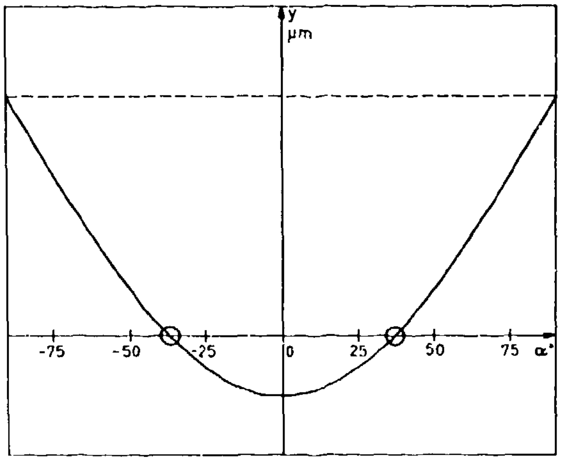

Fig. 10:4. Distance between two electron lines as a function of the angle α in the ideal case. The lines are reduced to one single line for two different angles α.

The ideal case

We have thus shown that it is possible to combine crystal monochromatized radiation with a magnetic spectrometer in such a way that focussing of photoelectrons from two different radiation wavelengths onto the same place in the spectrometer focal plane can be achieved. The inherent spread in wavelength of a single X-ray line requires that the focussing on the target must be perfect. It is thus essential that the target be placed on the Rowland circle of the crystal monochromator and that the width of the diffraction pattern (the rocking curve) of the crystal be small compared to the width of the X-ray line. Likewise, the intensity of the X-ray line must be high so that the measurements can be carried out in a reasonably short period of time. These two requirements are contradictory. The need for high intensity per crystal area means that a bent crystal has to be used and that the radius of the Rowland circle is small. The necessity for perfection means that the radius must be large since it is easier to obtain a perfect crystal in this case. The need for high intensity is less critical if a double focussing spectrometer is used for the subsequent electron analysis. Perfect focussing on the target means that $\beta = \beta_R$, where β_R is the angle between the radiation direction and the tangent to the Rowland circle. In the ideal case the X-ray tube, the crystal monochromator and the target have fixed positions in relation to each other but the whole system must be rotated around an axis through S′ (see Fig. 10:1). The spectrometer is fixed and the target is always placed on the Rowland circle of the crystal monochromator. Eq. (5) is then reduced to

$$y \approx \frac{\varrho_0 \cdot \Delta E}{E_0 \cos \omega} \cdot \left(1 - \frac{DE_0}{\varrho_0 \sin \beta_R} \cdot \cos \alpha\right) \qquad (10)$$

and eq. (6) becomes

$$\alpha = \arccos\,(\varrho_0 \sin \beta_R / DE_0). \qquad (11)$$

The solid curve shown in Fig. 10:4 is obtained from eq. (10). Eq. (11) shows that compensation is achieved for two different angles or not at all. The condition for compensation is thus

$$\varrho_0 \sin \beta_R < DE_0. \qquad (12)$$

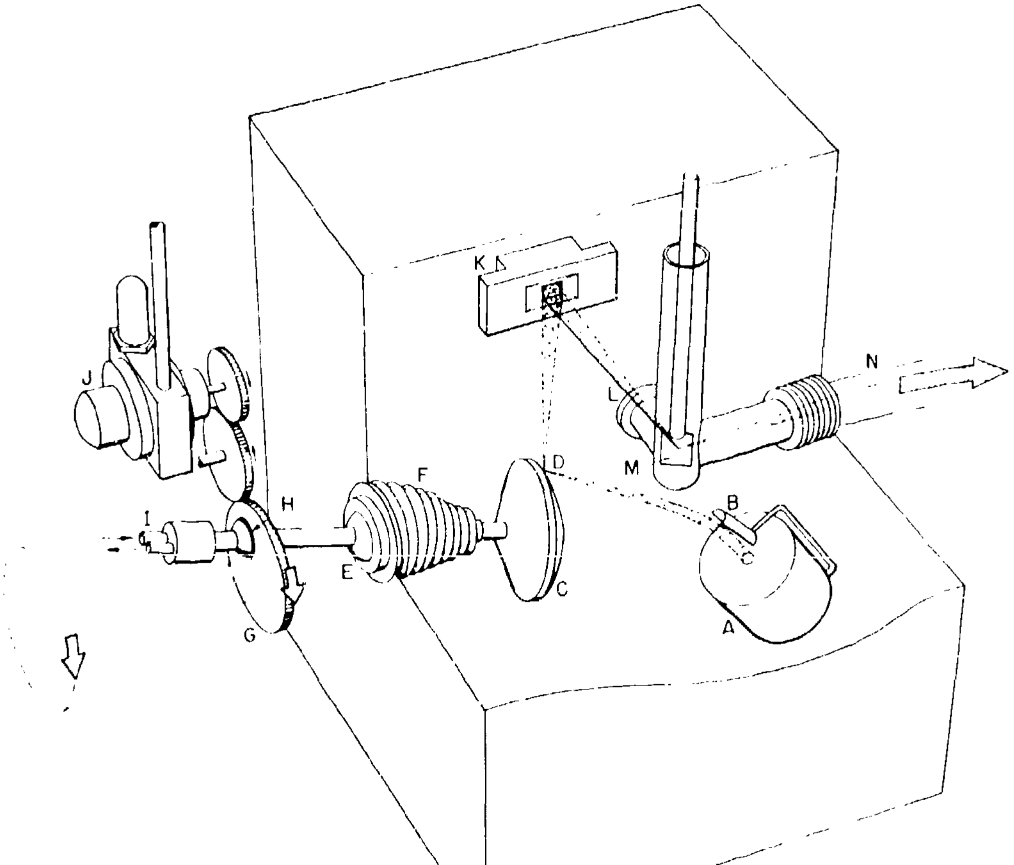

Fig. 10:5. (*Added in proof*). Schematic view of the proposed high-power X ray monochromator.

Added in proof

Fig. 10:5 shows a schematic view of a proposed high power X-ray monochromator presently under study. The arrangement consists of a precessing, water cooled aluminum anode (C) and a curved quartz crystal (K). The electron gun (A) with an electrostatic deflector (B) will give 300 mA electrons at 20 kV. The electron beam is focussed at D near the periphery of the spherically shaped anode surface. The diameter of the precession circle is 6 cm. The precession takes place around a steel ball (E), which is fixed to the anode stem and with its external spherical bearing soldered onto the X-ray housing. An ultraflexible bellow (F) is soldered onto the housing around the bearing and onto the anode stem near the anode. The anode is thus able to precess in vacuum at high speed without use of greased bearings exposed to high vacuum. Since the anode does not rotate around its axis but only makes a precession movement, water coolant can be supplied from the outside without twisting the flexible pipes for the inlet and outlet (I). The cooling water is forced to flow through an internal tube in the stem to the mushroom shaped anode and back again between this internal tube and the stem. An air jet motor (J) (no electromagnetic stray fields) with gear-wheels provides the fast rotation of the wheel G, to which the anode stem is asymmetrically connected by means of the steel bearing at H.

After diffraction at the curved quartz crystal (K) (bent to a radius of about 10 cm) the Al$K\alpha$ radiation is focussed on the sample (M) after having passed through a thin window (L). The angle between the incident beam and the source surface can be adjusted from the outside. The expelled photoelectrons (N) are analysed in a high-resolution, double focussing, electron spectrometer.

It should be emphasized that there are some quite severe problems connected with the realization of the above proposed scheme. In fact, very little is known about the details of the diffraction properties of a quartz crystal bent to such an extremely small radius as 10 cm. Dislocations and other imperfections in the crystal may have serious effects on the mechanical properties at bending and also on the attained width of the rocking curve. This latter may be broadened to the extent that the reduction of width of an ESCA line, discussed in this appendix, becomes insignificant. (If only a moderate X-ray resolution could be achieved the scheme might still be useful to improve the signal-to-background ratio in ESCA and to reduce radiation damage.) In order to overcome some of the difficulties a carefully selected crystal which is very thin ($\lesssim$0.1 mm) and properly etched has to be used. High precision is required in the machining of the crystal holder. According to recent studies at Uppsala quartz seems to be superior to other crystals like KAP for soft radiation (pers. comm. from E. Noreland; cf. E. Noreland *et al.*, UUIP-511 (Dec. 1966) and B. Nordfors, Arkiv Fysik *10*, 279 (1956)). For reflexion we intend to try the (100) plane with the lattice constant 2d = 8.51 Å. The angle between incident and reflected beams is then 23° for Al$K\alpha_{1,2}$. The inherent width of around 1 eV for the Al$K\alpha_{1,2}$ line would in the ideal case be dispersed 0.75 mm along the Rowland circle where the source is situated. With a central orbit radius of 30 cm in the double focussing electron spectrometer the source has to be tilted $\approx$ 60° relative to the X-ray beam in order to achieve compensation for the width of the Al$K\alpha_{1,2}$ line. The curvature of the X-ray line at the focus limits the useful height of the source to around 6 mm. The geometry is such that there will be only a negligible extra line broadening due to the fact that the plane of the source does not fall along the Rowland circle.

As previosly discussed in this publication (Section VIII:1) any sort of monochromatization of the X-radiation results in a great loss of intensity in the electron spectrum. The two main factors contributing to this loss are: 1. the small useful solid angle subtended by the diffracting crystal and 2. the finite reflectivity of the crystal. Unfortunately, only a very rough theoretical estimate can be made of the combined effects of these two factors. A loss factor of 50 compared to the conventional X-ray arrangement does not seem unrealistic. In any case a substantial increase in X-ray output is desirable. Most of the spectra studied in this publication have been recorded at a power dissipation of a few hundred watt at the anode. The use of a water cooled rotating anode should improve this figure considerably. The proposed arrangement shown in the figure is only one of several possible alternatives. However, if it works properly it has compared to other types of rotating anodes some special features which are important in ESCA. The X-ray output can be concentrated to a very small spot. This spot is not subject to any movement in spite of the fact that the heat is dissipated over a large area (a circular band with a diameter of 6 cm and a width of 3 mm). A heat dissipation 6 kW, evenly distributed over this area (≈ 5.7 cm²), would not cause too much of a problem whereas a concentrated beam (⌀ ≈3 mm) on the precessing anode changes the heat transport completely. Superimposed on a moderate heating of the circular band on the anode one then encounters a sudden increase in temperature of the surface element that is, at anyone moment, exposed to the electron beam. Calculations show that a very high speed of precession is required at a constant power level of 6 kW, if the instantaneous heating will not cause immediate anode evaporation. (For a discussion of the heat dissipation in X-ray anodes see e. g. W. J. Osterkamp, Philips Res. Rep. *3*, pp. 49, 161, 303 (1948)). For an electron beam forming a circular spot on an aluminum anode the temperature rise in the surface during the passage through the beam will be

$$\Delta T = 0.09 P \cdot R^{-\frac{1}{2}} r^{-\frac{3}{2}} \nu^{-\frac{1}{2}}$$

where P is the beam power in watt, R the radius of the precession movement in cm, ν the number of revolutions per second, and r the focal spot radius in cm. In the pr[illegible] e this means that the maximum power can be atta[illegible] only at a speed of precession exceeding 1000 rpm and provided that the size of the focal spot is carefully adjusted (most likely it must be increased somewhat). An infrared thermometer is therefore incorporated with our arrangement in order to make it possible to measure continuously the temperature at the spot. Provisions are also made for instantaneous shut-down in case of overheating. As mentioned above, a high power anode without subsequent crystal monochromatization would be suitable for ESCA in order to increase speed of recording in ordinary measurements.

Preliminary design studies of this proposed high power monochromator have recently been initiated by two of us (K. S. and S.-E. K.) during a stay at Lawrence Radiation Laboratory in Berkeley, Calif. These studies are performed in collaboration with D. H. Templeton, J. M. Nitschke, C. A. Corum and H. P. Robinson at Lawrence Radiation Laboratory. We want to acknowledge our gratitude to our colleagues I. Perlman, J. M. Hollander, D. A. Shirley and A. Ghiorso for their interest and support of this research project.

APPENDIX 11

Definition of Oxidation Number and Formal Charge

The *oxidation number* of an atom in a chemical compound is defined as the number which represents the electrical charge which the atom would have, if the electrons in the compound were assigned to the atoms according to the following rules.

1. The oxidation number of a monatomic ion in an ionic substance is equal to its electrical charge in units of the elementary charge.

2. The oxidation number of atoms in an elemental substance is zero.

3. In a covalent compound of a known structure, the oxidation number of each atom is the charge remaining on the atom when each shared electron pair is assigned completely to the more electronegative of the two bonding atoms. An electron pair shared by two atoms of the same element is divided between them.

Valency, which is an ambiguous and less precise concept, should not be substituted for oxidation number, and the terms valency or valence should not be used without an explicit definition. Oxidation numbers are very useful for balancing oxidation reduction equations. They also have a great instructional value in the classification of chemical compounds. They are, however, only formal quantities and a strict physical meaning can not be attached to them, as the definition arbitrarily approximates every bond between elements of different electronegativities to a fully ionized bond.

The *formal charge* is the net charge on an atom, if all electrons shared in bonds are divided equally between the atoms. (Ref. 188 and p. 8, Ref. 193).

APPENDIX 12

Some Basic Concepts in Resonance Theory

(Ch. 1, Ref. 193, and Ref. 194)

If a molecule can be represented by several different arrangements of the valence electrons corresponding to Structures I, II, III ..., the wave function for the molecule can be expressed by a linear combination of the wave functions for the individual structures:

$$\psi = a\psi_{\mathrm{I}} + b\psi_{\mathrm{II}} + c\psi_{\mathrm{III}} + \ldots$$

The coefficients a, b, c ... are determined in such a way that the energy of the system becomes a minimum. It has become customary to speak of such a system as resonating between Structures I, II, III ... or as being a resonance hybrid of the structures. The extra stability gained through the resonance is called the resonance energy.

Molecules can often be represented by a large number of different structures. The approximative relative weight of the contribution of each structure to the resonance hybrid can very often be estimated directly from the structural formula by application of simple empirical rules, and as a result most often only a few structures need to be considered. The normal state of the molecule is then represented as a system of a few chemical structures interconnected with the symbol ↔ (cf. Fig. V:23):

$$\mathrm{I} \leftrightarrow \mathrm{II} \leftrightarrow \mathrm{III} \leftrightarrow \mathrm{IV} \leftrightarrow \ldots$$

This simple application of the resonance theory has proved very fruitful in chemistry (cf. elementary textbooks. Refs. in Chapter 1 of Ref. 193). It is essentially qualitative and the theory of the chemical bond is still far from perfect (Section 6-5, Ref. 193).

APPENDIX 13

The Electronegativity Scale

The electronegativity scale mostly used by chemists has been derived by Pauling from thermochemical data (Chapter 3, Ref. 193). In terms of the resonance theory, a bond between two unlike atoms $A-B$ can be described by a linear combination of the wave functions for the bonds $A-A$ and $B-B$. In the wave function for a bond between two like atoms, e.g. $A-A$, the ratio b/a determining the relative contribution of the ionic structures is small.

$$\psi = a\psi_{AA} + b\psi_{A^+A^-} + b\psi_{A^-A^+}$$

In the wave function for a bond between two unlike atoms of different electronegativities, e.g. $A-B$, the ratios c/a and d/a differ from b/a, since they assume values that give the system extra resonance energy.

$$\psi = a\psi_{AB} + c\psi_{A^+B^-} + d\psi_{A^-B^+}$$

The additional bond energy is due to the ionic character of the bonds. The difference between the resulting bond energy $D(A-B)$ and the geometric mean of the bond energies $D(A-A)$ and $D(B-B)$ is a measure of the extra ionic energy, $\Delta' AB$:

$$\Delta'_{AB} = D(A-B) - [D(A-A)D(B-B)]^{\frac{1}{2}}$$

Using thermochemically determined bond energies, Pauling has found that $\sqrt{\Delta'_{AB}}$ satisfies an additivity relation, and the electronegativity difference between atoms A and B, $\chi_A - \chi_B$ is defined as:

$$|\chi_A - \chi_B| = 0.18\sqrt{\Delta'_{AB}}.$$

The electronegativities of elements are represented in Table 13:1. The electronegativity scale applies to atoms with formal charge zero. Charge affects the electronegativity and corrections for this may be introduced, see below. However, since calculations based on the electronegativity scale only have approximate significance, these corrections are unnecessary in most cases (p. 101, Ref. 193). Moreover, the electroneutrality principle implies, that charges on atoms tend to be neutralized.

There are several other electronegativity scales[281,298] beside that of Pauling. The most common of these is that of Mulliken,[283,284] in which the electronegativity of an atom, χ_A, is defined as:

$$\chi_A = \tfrac{1}{2}(I_A + E_A)$$

I_A is the ionization potential and E_A the electron affinity for the appropriate valence states. This definition implies that equal energy is expended in transforming the covalent molecule AB to the ionic states A^+B^- and A^-B^+, if A and B have the same electronegativity. The electronegativity values obtained

Table 13:1. Electronegativities of the elements as given by Pauling[174]

Li	Be	B					H						C	N	O	F
1.0	1.5	2.0					2.1						2.5	3.0	3.5	4.0
Na	Mg	Al											Si	P	S	Cl
0.9	1.2	1.5											1.8	2.1	2.5	3.0
K	Ca	Sc	Ti	V	Cr	Mn	Fe	Co	Ni	Cu	Zn	Ga	Ge	As	Se	Br
0.8	1.0	1.3	1.5	1.6	1.6	1.5	1.8	1.8	1.8	1.9	1.6	1.6	1.8	2.0	2.4	2.8
Rb	Sr	Y	Zr	Nb	Mo	Tc	Ru	Rh	Pd	Ag	Cd	In	Sn	Sb	Te	I
0.8	1.0	1.2	1.4	1.6	1.8	1.9	2.2	2.2	2.2	1.9	1.7	1.7	1.8	1.9	2.1	2.5
Cs	Ba	La-Lu	Hf	Ta	W	Re	Os	Ir	Pt	Au	Hg	Tl	Pb	Bi	Po	At
0.7	0.9	1.1–1.2	1.3	1.5	1.7	1.9	2.2	2.2	2.2	2.4	1.9	1.8	1.8	1.9	2.0	2.2
Fr	Ra	Ac	Th	Pa	U	Np-No										
0.7	0.9	1.1	1.3	1.5	1.7	1.3										

from Mulliken's equation are, to a good approximation, proportional to Pauling's values.

According to Pauling, a unit formal charge changes the electronegativity value of an element by approximately two-thirds of the electronegativity difference to the next atom to the right in the Periodic Table (pp. 65, 72, Ref. 193). This was deduced in the following way: The increasing electronegativity for a series of atoms in the Periodic Table can be attributed to the increase in effective nuclear charge acting on the valence electrons. The screening constant of one valence electron on another is about 0.4, and hence in going for instance from $\mathrm{N}\cdot$ to $\cdot\mathrm{O}$ the increase in effective nuclear charge is 1 0.4 0.6. In going from $-\mathrm{N}<$ to $>\overset{(+)}{\mathrm{N}}<$ the increase in effective nuclear charge is accordingly 0.4. Thus a unit positive charge can be expected to change the χ value for an atom by about two-thirds of the electronegativity difference to the next atom to the right in the Periodic Table, and a negative formal charge similarly decreases the χ value.

APPENDIX 14

Electronegativity Difference and Partial Ionic Character of Bonds

Application of the resonance theory has led to the concept of partial ionic character of bonds between unlike atoms. If ionic structures contribute to the resonance hybrid, the hybrid bonds have a partial ionic character which will be determined by the relative weights of the contributing ionic structures, i.e. $(c/a)^2$ and $(d/a)^2$ in the wave function:

$$\psi = a\psi_{AB} + c\psi_{A^+B^-} + d\psi_{A^-B^+}$$

The partial ionic character of bonds may be estimated from the electronegativity scale. Pauling has derived the following empirical equation for the calculation of amount of ionic character, I, from the dipole moments of halides:

$$I = 1 - e^{0.25(\chi_A - \chi_B)^2}$$

This function is represented in Fig. 14:1.

Our definition of modified oxidation number is so chosen, that a bond is considered as fully covalent in the application of the rule for formal charge when $(\chi_A - \chi_B) < 0.5$ (Section V:4). This corresponds to an ionic character < 6 %. The corresponding covalent bond character is thus > 94 %.

Partial ionic character has also been estimated from a consideration of nuclear quadrupole moments.[285] This approach results in greater ionic character than the dipole moment treatment. The interpretation of the significance of quadrupole coupling constant is, however, not straightforward (p. 100, Ref. 193). With dipole moments, polarization of ionic bonds is considered as covalent character.[285]

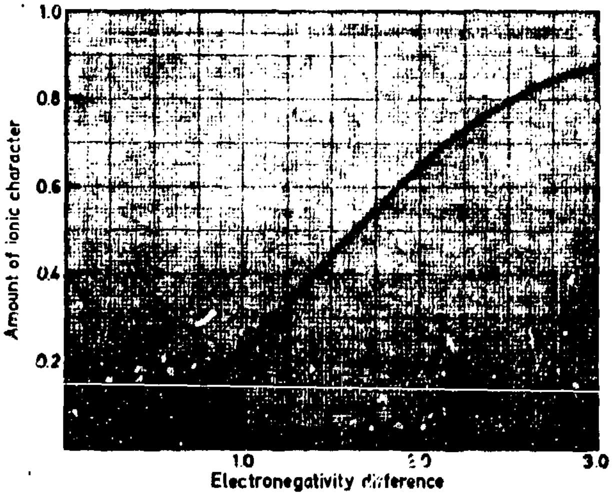

Fig. 14:1. Amount of ionic character versus electronegativity difference.[174]

APPENDIX 15

Calculation of Bond Number

(Ch. 7, Ref. 193)

The estimation of bond number from bond lengths (interatomic distances) is based on the fact that multiple bonds (double or triple) are shorter than covalent single bonds. Application of the resonance theory to this phenomenon has led to the concept of fractional bonds. The total degree of bonding is represented by the bond number, *n*.

Bond shortening is interpreted as a higher degree of bonding, or in terms of resonance or valence bond theory as a greater contribution from multiply bonded structures to the resonance hybrid. (In terms of molecular orbital theory this means a contribution of $p_\pi - p_\pi$ or $d_\pi - p_\pi$ bonding in addition to the σ bonds.) The hybrid bond corresponds to a degree of bonding intermediate between the individual resonating structures, and the resonance hybrid assumes a bond length intermediate between those of the individual resonating structures. Using resonance theory, Pauling has derived the following equation for the calculation of *n*:

$$D - D_2 = \frac{(3-n)^2(D_1 - D_2) - 4(n-1)^2(D_2 - D_3)}{(n+1)^2}$$

D is the observed bond length, D_1, D_2 and D_3 are the corresponding pure single, double and triple bond lengths. These are obtained by addition of the respective single, double and triple bond radii of the atoms and correction for differences in electronegativity with empirically derived correction terms. Accurate bond radii are only known for a limited number of elements.

If $2 > n > 1$, $100\ (n - 1)$ represents the percentage of double bond character.

If $3 > n > 2$, $100\ (n - 2)$ represents the percentage of triple bond character.

An estimation of the amount of ionic character of the bonds is obtained by multiplying *I* for the corresponding single bond by *n*.

APPENDIX 16

Equalization of Electronegativity, Orbital and Group Electronegativities

The idea of equalization of electronegativity was first introduced by Sanderson, who postulated that if atoms which are initially different in electronegativity form a bond, they will change their average electronic density in the process of combination, until they are of equal electronegativity in the molecule.[188] This concept is in principle very similar to the electroneutrality principle and leads to low absolute values for calculated charges. Sanderson's electronegativity scale represents average bond electronegativities. The application of the concept of equalization of electronegativity to orbital electronegativity theory has made it possible to calculate group electronegativities for a large number of important chemical groups.

Based on Mulliken's definition of electronegativity (Appendix 13), Hinze and Jaffé have derived orbital electronegativities for different valence states.[189] The valence state can be considered as formed from a molecule by removing from one atom all the other atoms with their electrons in an adiabatic manner, i.e. without allowing any electronic rearrangement. The valence state ionization potentials, I_v, and the valence state electron affinities, E_v, needed for the calculation of the electronegativity are obtained from the ground state ionization potentials, I_g, and the ground state electron affinities, E_g, in the following manner:

$$I_v = I_g + P^+ - P_0$$
$$E_v = E_g + P_0 - P^-$$

P_0, P^+, and P^- are the valence state promotion energies for the atom, the positive ion and the negative ion respectively. The parameters required are obtained from spectroscopic data.

Based on the concept of orbital electronegativity Hinze *et al.* defined bond electronegativity as the electronegativity of orbitals forming a bond, after charge has been exchanged between them.[190]

A new definition of orbital electronegativity permitted the determination of orbital electronegativities of groups:

$$\chi_j = \frac{\partial E}{\partial n_j}$$

E = energy of the atom in its valence state, n_j = the occupation number of the j'th orbital, the orbital electronegativity of which is χ_j.

It was assumed that n_j could have both integral and non-integral values, and that E is a continuous differentiable function of n_j. For singly occupied orbitals, this definition is identical with that of Mulliken.

This concept has been applied by Huheey for the calculation of group electronegativities.[191,192] The treatment of Jaffé and co-workers leads to an understanding of ionic character in terms of charge transferred between bond-forming orbitals.[189,190] It has been suggested that electronegativity equalization by charge transfer, gives a minimum in the ionization potential and electron affinity energy[191]. The minimum for the sum of these energies for a diatomic molecule occurs when their electronegativities are equal. The energy of an atom, E, is given by the equation:

$$E = a\delta + \frac{b}{2}\delta^2$$

where $a = \frac{1}{2}(I - A)$
$b = I + A$
δ = partial charge from electron loss or gain.
I = ionization potential.
A = electron affinity.

The orbital electronegativity χ is defined as:

$$\chi = \frac{dE}{d\delta} = a + b\delta$$

a corresponds approximately to the previously assigned electronegativities.

b is the charge coefficient.

Equalization of the orbital electronegativities for the atoms in a diatomic molecule, AB, leads to the following equation:

$$\chi_A = a_A + b_A\delta_A = \chi_B = a_B + b_B\delta_B$$

$$\delta_A = -\delta_B$$

$$\delta_A = \frac{a_B - a_A}{b_A + b_B}$$

This procedure can be generalized to apply to polyatomic groups, and Huheey has tabulated a and b for a large number of the most common groups. This method does not distinguish between isomeric groups, and can not be strictly applied to bonds of Si, P or S containing d orbitals, because of lack of data for these orbitals. Group electronegativities have been correlated with polar substituent constants.[286]

The Periodic Table of the Element

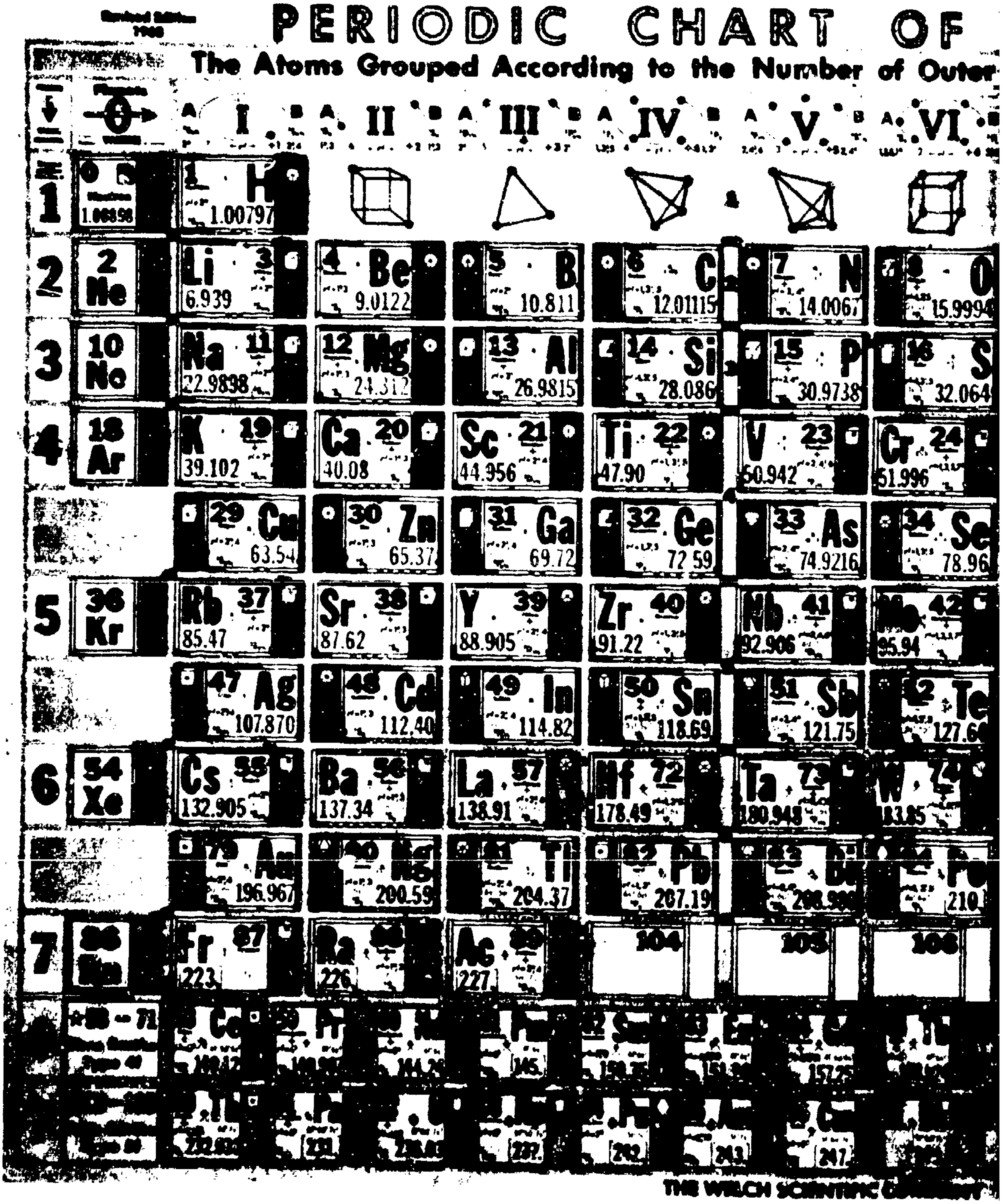

Revised Edition 1968

PERIODIC CHART OF

The Atoms Grouped According to the Number of Outer

	0	I	II	III	IV	V	VI
1	1.00898	1 H 1.00797					
2	2 He	Li 3 6.939	4 Be 9.0122	5 B 10.811	6 C 12.01115	7 N 14.0067	8 O 15.9994
3	10 Ne	Na 11 22.9898	12 Mg 24.312	13 Al 26.9815	14 Si 28.086	15 P 30.9738	16 S 32.064
4	18 Ar	K 19 39.102	Ca 20 40.08	Sc 21 44.956	Ti 22 47.90	V 23 50.942	Cr 24 51.996
		29 Cu 63.54	30 Zn 65.37	31 Ga 69.72	32 Ge 72.59	33 As 74.9216	34 Se 78.96
5	36 Kr	Rb 37 85.47	Sr 38 87.62	Y 39 88.905	Zr 40 91.22	Nb 41 92.906	Mo 42 95.94
		47 Ag 107.870	48 Cd 112.40	49 In 114.82	50 Sn 118.69	51 Sb 121.75	52 Te 127.6
6	54 Xe	Cs 55 132.905	Ba 56 137.34	La 57 138.91	Hf 72 178.49	Ta 73 180.948	W 74 183.85
		79 Au 196.967	80 Hg 200.59	81 Tl 204.37	82 Pb 207.19	83 Bi 208.980	84 Po 210
7	86 Rn	Fr 87 223	Ra 88 226	Ac 89 227	104	105	106

THE WELCH SCIENTIFIC C

Reproduced by due permission from the Welch Scientific Comp

APPENDIX 17

The Periodic Table of the Elements

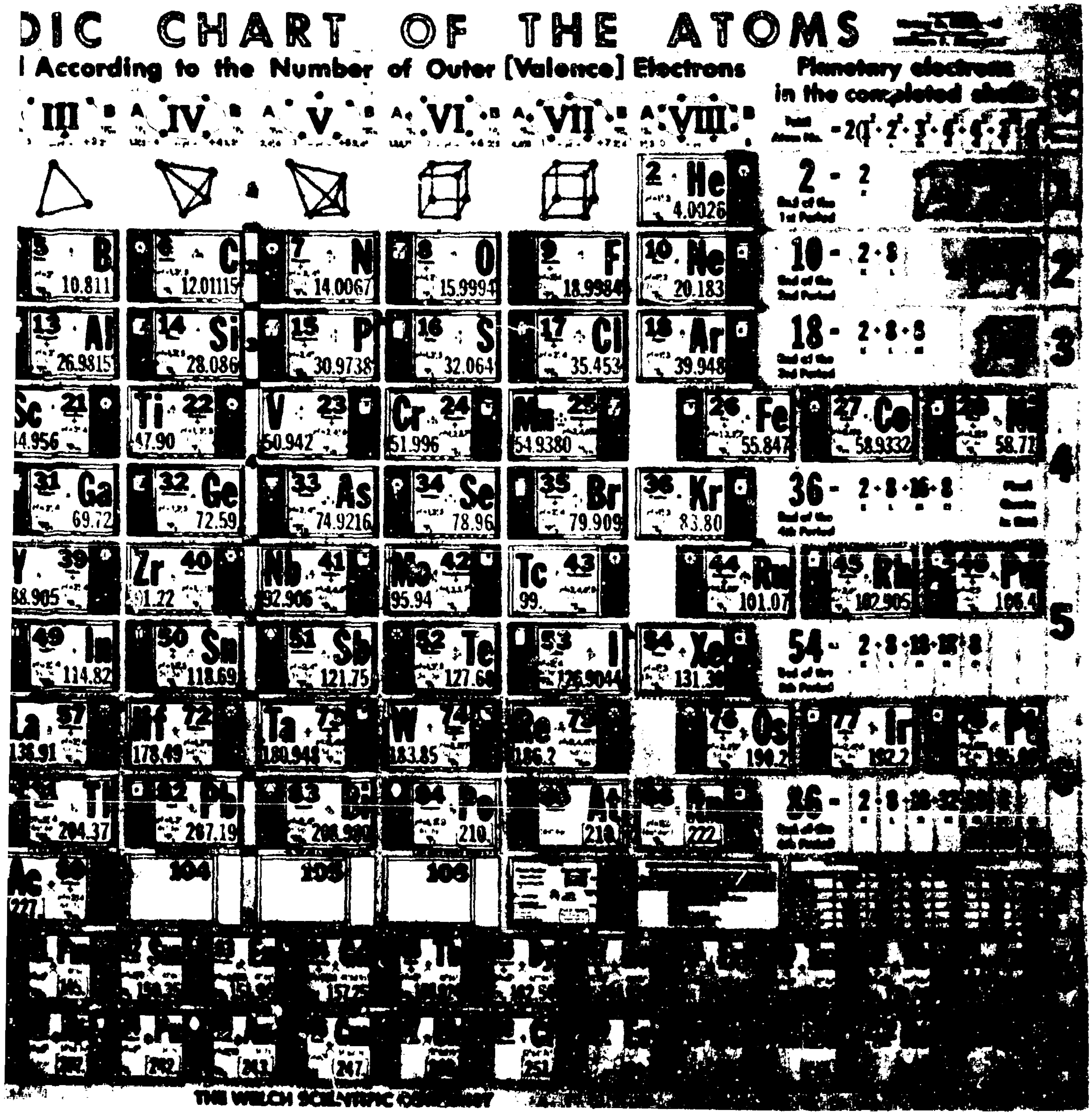

DIC CHART OF THE ATOMS

l According to the Number of Outer [Valence] Electrons

Planetary electrons in the completed shells

III	IV	V	VI	VII	VIII			
					2 He 4.0026	2 - 2 End of the 1st Period		
5 B 10.811	6 C 12.01115	7 N 14.0067	8 O 15.9994	9 F 18.9984	10 Ne 20.183	10 - 2·8 End of the 2nd Period		
13 Al 26.9815	14 Si 28.086	15 P 30.9738	16 S 32.064	17 Cl 35.453	18 Ar 39.948	18 - 2·8·8 End of the 3rd Period		
Sc 21 4.956	Ti 22 47.90	V 23 50.942	Cr 24 51.996	Mn 25 54.9380	26 Fe 55.847	27 Co 58.9332	28 Ni 58.71	
31 Ga 69.72	32 Ge 72.59	33 As 74.9216	34 Se 78.96	35 Br 79.909	36 Kr 83.80	36 - 2·8·18·8 End of the 4th Period		
Y 39 88.905	Zr 40 1.22	Nb 41 92.906	Mo 42 95.94	Tc 43 99.	44 Ru 101.07	45 Rh 102.905	46 Pd 106.4	
49 In 114.82	50 Sn 118.69	51 Sb 121.75	52 Te 127.6	53 I 126.9044	54 Xe 131.3	54 - 2·8·18·18·8 End of the 5th Period		
La 57 138.91	Hf 72 178.49	Ta 73 180.948	W 74 183.85	Re 75 186.2	76 Os 190.2	77 Ir 192.2	Pt	
81 Tl 204.37	82 Pb 207.19	83 Bi 208.980	84 Po 210	85 At 210	86 Rn 222	86 - 2·8·18·32·18·8 End of the 6th Period		
Ac 89 227	104	105	106					

THE WELCH SCIENTIFIC COMPANY

Reproduced by due permission from the Welch Scientific Company, Illinois.

1

2

23. Atomic energy levels determined by the photoelectron method.
Nordling, C., and Hagström, S., Arkiv Fysik *16*, 515 (1960). (Conference report).

24. Atomic level energies in rare earth elements.
Bergvall, P., and Hagström, S., Arkiv Fysik *17*, 61 (1960).

25. Crystal diffraction and photo electron measurements of K and L levels in the elements 47 Ag to 52 Te.
Bergvall, P., Hörnfeldt, O., and Nordling, C., Arkiv Fysik *17*, 113 (1960).

26. Investigations of atomic and nuclear energy levels by crystal diffraction and photo electron spectroscopy. (Thesis.)
Bergvall, P., Almqvist & Wiksell, Uppsala 1960.

27. Direct measurements of conversion lines in the eV scale.
Hagström, S., Nordling, C., and Siegbahn, K., Arkiv Fysik *22*, 408 (1962). (Conference report).

28. Precision measurements of Auger lines and L level energies in the elements $_{38}$Sr – $_{47}$Ag.
Hörnfeldt, O., and Fahlman, A., Arkiv Fysik *22*, 412 (1962). (Conference report).

29. Application of the photoelectron method to a study of the fundamental constant combination h/e.
Nordling, C., Hagström, S., and Siegbahn, K., Arkiv Fysik *22*, 428 (1962). (Conference report).

30. A new high-precision instrument for electron and nuclear spectroscopy.
Siegbahn, K. and Nordling, C., Arkiv Fysik *22*, 436 (1962). (Conference report).

31. Photo electron measurements of L levels in the elements strontium (Z = 38) to palladium (Z = 46).
Fahlman, A., Hörnfeldt, O., and Nordling, C., Arkiv Fysik *23*, 75 (1962).

32. The photo electron method of determining h/e.
Hagström, S., Hörnfeldt, O., Nordling, C., and Siegbahn, K., Arkiv Fysik *23*, 145 (1962).

33. Auger spectra in the intermediate coupling region.
Hörnfeldt, O., Fahlman, A., and Nordling, C., Arkiv Fysik *23*, 155 (1962).

34. Investigation of the Fermi level position in doped silicon and n-CdTe using electron spectroscopy.
Auleytner, J., and Hörnfeldt, O., Arkiv Fysik *23*, 165 (1962).

35. The Z-dependence of energies and relative intensities in the K–LL Auger spectrum.
Hörnfeldt, O., Arkiv Fysik *23*, 235 (1962).

36. Studies of atomic level energies and Auger spectra. (Thesis.)
Hörnfeldt, O., Almqvist & Wiksell, Uppsala 1962.

37. Atomic level energies in hafnium.
Hagström, S., Z. Phys. *178*, 82 (1964).

38. Some internal effects in nuclear decay, the Auger effect.
Bergström, I., and Nordling, C., "Alpha-, Beta- and Gamma-Ray Spectroscopy", Chapter XXV. Ed. K. Siegbahn. North-Holland Publ. Co., Amsterdam 1965.

39. Tables of electron binding energies and kinetic energy versus magnetic rigidity.
Hagström, S., Nordling, C., and Siegbahn, K., "Alpha-, Beta- and Gamma-Ray Spectroscopy", Appendix 2. Ed. K. Siegbahn. North-Holland Publ. Co., Amsterdam 1965.

40. Photo electron measurements of K energy levels in light elements.
Hagström, S., and Karlsson, S.-E., Arkiv Fysik *26*, 252 (1964). (Conference report).

41. X-ray produced Auger electrons from elements of low and intermediate atomic number.
Fahlman, A., and Nordling, C., Arkiv Fysik *26*, 248 (1964). (Conference report).

42. Extension of the photo electron method to elements of low atomic number.
Hagström, S., and Karlsson, S.-E., Arkiv Fysik *26*, 451 (1964).

43. Determination of atomic energy levels in the elements $_{73}$Ta to $_{83}$Bi by the photo electron method.
Fahlman, A., and Hagström, S., Arkiv Fysik *27*, 69 (1964).

44. Precision measurements of L levels in the elements $_{35}$Br, $_{37}$Rb, $_{53}$I, $_{55}$Cs, and $_{56}$Ba.
Andersson, I., and Hagström, S., Arkiv Fysik *27*, 161 (1964).

45. Electron binding energies in thorium.
Nordling, C., and Hagström, S., Z. Phys. *178*, 418 (1964).

46. A 50-cm double focusing beta spectrometer of the current sheet type.
Siegbahn, K., Nordling, C., Karlsson, S.-E., Hagström, S., Fahlman, A., and Andersson, I., Nucl. Instr. and Meth. *27*, 173 (1964).
An iron-free double-focusing β spectrometer.
Siegbahn, K., Nordling, C. L., and Hollander, J. M., UCRL-10023, 232 (1962).

47. Electron spectroscopy for chemical analysis.
Hagström, S., Nordling, C., and Siegbahn, K., Phys. Lett. *9*, 235 (1964).

48. Application of electron spectroscopy to chemical analysis.
Nordling, C., Hagström, S., and Siegbahn, K., Z. Phys. *178*, 433 (1964).

49. Electron spectroscopic determination of the chemical valence state.
Hagström, S., Nordling, C., and Siegbahn, K., Z. Phys. *178*, 439 (1964).

50. Studies of some atomic properties by electron spectroscopy. (Thesis.)
Hagström, S., Almqvist & Wiksell, Uppsala 1964.

REFERENCES

The list of references given below is divided in two sections. The first section, with reference numbers below 100, contains all ESCA publications from our research group, arranged in chronological order, and with titles given. The second section contains other papers to which reference has been made in the text. These are arranged approximately in the same order as they appear in the text, and are listed without titles.

1. Energy calibration of instruments.
   Siegbahn, K. Proceedings of the International Conference on Beta and Gamma Radioactivity, Amsterdam 1952, invited lecture, p. 1043. Physica XVIII, 1952.
2. Introductory lecture on beta- and gamma-ray transitions.
   Siegbahn, K., Proceedings of the 1954 Glasgow Conference on Nuclear and Meson Physics, invited lecture, p. 168. Pergamon Press, London and New York 1955.
3. A new method for the precise determination of h/e.
   Siegbahn, K., Appl. sci. Res. *B4*, 25 (1954).
4. Beta-ray-spectrometer theory and design. High resolution spectroscopy.
   Siegbahn, K., Beta- and gamma-ray spectroscopy", p. 52. Ed. K. Siegbahn. North-Holland Publ. Co., Amsterdam 1955.
5. Beta-ray spectroscopy in the precision range of $1:10^5$.
   Siegbahn, K., and Edvarson, K., Nucl. Phys. *1*, 137 (1956).
6. Relative conversion probabilities in the K, L_I and L_{II} shells of the 238.6 keV γ-line of Th B.
   Sokolowski, E., Edvarson, K., and Siegbahn, K., Nucl. Phys. *1*, 160 (1956).
7. Possible finite nuclear size effect on the 279 keV transition in Tl^{203}.
   Nordling, C., Siegbahn, K., and Sokolowski, E., Nucl. Phys. *1*, 326 (1956).
8. Precision method for obtaining absolute values of atomic binding energies.
   Nordling, C., Sokolowski, E., and Siegbahn, K., Phys. Rev. *105*, 1676 (1957).
9. Magnetic analysis of X-ray produced photo and Auger electrons.
   Sokolowski, E., Nordling, C., and Siegbahn, K., Arkiv Fysik *12*, 301 (1957).
10. Chemical shifts of photo- and Auger electron lines.
    Siegbahn, K., Nordling, C., and Sokolowski, E., Proc. Rehovoth Conf. Nucl. Structure 1957, p. 291. North-Holland Publ. Co., Amsterdam.
11. Chemical shift effect in inner electronic levels of Cu due to oxidation.
    Sokolowski, E., Nordling, C., and Siegbahn, K., Phys. Rev. *110*, 776 (1958).
12. Auger effect in copper.
    Nordling, C., Sokolowski, E., and Siegbahn, K., Arkiv Fysik *13*, 282 (1958). (Conference report).
13. Binding energies of internal shells in Cu, Cr and Zn studied by means of a new precision method.
    Sokolowski, E., Nordling, C., and Siegbahn, K., Arkiv Fysik *13*, 288 (1958). (Conference report).
14. Evidence of chemical shifts of the inner electronic levels in a metal relative to its oxides (Cu, Cu$_2$O, CuO).
    Nordling, C., Sokolowski, E., and Siegbahn, K., Arkiv Fysik *13*, 483 (1958).
15. Experimental studies of the KLL Auger spectra of Cu and Ge.
    Sokolowski, E., and Nordling, C., Arkiv Fysik *14*, 557 (1959).
16. Systematic study of electron binding energies of some fourth and sixth period elements by means of the photo electron method.
    Sokolowski, E., Arkiv Fysik *15*, 1 (1959).
17. Energy shifts of L-levels in some 5th period elements due to oxidation and alloying.
    Nordling, C., Arkiv Fysik *15*, 241 (1959).
18. K and L energy levels in some fourth and fifth period elements.
    Nordling, C., Arkiv Fysik *15*, 397 (1959).
19. Electron binding energies in uranium.
    Nordling, C., and Hagström, S., Arkiv Fysik *15*, 431 (1959).
20. Investigations of inner electron shells by spectroscopic studies of photo- and Auger electrons. (Thesis.)
    Sokolowski, E., Almqvist & Wiksell, Uppsala 1959.
21. Experimental studies of electron binding energies and Auger spectra. (Thesis.)
    Nordling, C., Almqvist & Wiksell, Uppsala 1959.
22. Precision measurements of K and L levels in heavier elements by means of crystal diffraction and photo electron methods.
    Bergvall, P., and Hagström, S., Arkiv Fysik *16*, 485 (1960). (Conference report).

51. Revision of electron binding energies in light elements.
Fahlman, A., Hamrin, K., Nordberg, R., Nordling, C., and Siegbahn, K., Phys. Rev. Lett. *14*, 127 (1965).

52. Beta-ray spectrometer theory and design. Magnetic alpha-ray spectroscopy. High resolution spectroscopy.
Siegbahn, K., "Alpha-, Beta- and Gamma-Ray Spectroscopy", Chapter III. Ed. K. Siegbahn. North-Holland Publ. Co., Amsterdam 1965.

53. The photoeffect in Cu using $\mathrm{Cu}K\alpha_1$ X-radiation.
Sevier, K. D., Fahlman, A., and Siegbahn, K., Arkiv Fysik *29*, 367 (1965).

54. A note on the Hartree-Fock-Slater approximation.
Lindgren, I., Phys. Lett. *19*, 382 (1965).

55. An improved Hartree-Fock-Slater method for atomic structure calculations.
Lindgren, I., Arkiv Fysik *31*, 59 (1966).

56. An electron spectroscopic determination of the L_{I} energy in the elements sodium ($Z = 11$) to copper ($Z = 29$).
Nordberg, R., Hamrin, K., Fahlman, A., Nordling, C., and Siegbahn, K., Z. Phys. *192*, 462 (1966).

57. Electron spectroscopic determination of electron binding energies in plutonium.
Fahlman, A., Hamrin, K., Nordberg, R., Nordling, C., Siegbahn, K., and Holm, L. W., Phys. Lett. *19*, 643 (1966).

58. Auger spectra for elements of low atomic number.
Fahlman, A., Nordberg, R., Nordling, C., and Siegbahn, K., Z. Phys. *192*, 476 (1966).

59. Excitation lines and multiple ionization in Auger spectra.
Fahlman, A., Hamrin, K., Axelson, G., Nordling, C., and Siegbahn, K., Z. Phys. *192*, 484 (1966).

60. Electron spectroscopy and chemical binding.
Fahlman, A., Hamrin, K., Hedman, J., Nordberg, R., Nordling, C., and Siegbahn, K., Nature *210*, 4 (1966).

61. Energy shifts in inner atomic levels of chlorine.
Fahlman, A., Carlsson, R., and Siegbahn, K., Arkiv Kemi *25*, 301 (1966).

62. Chemical shift in Auger spectra.
Fahlman, A., Hamrin, K., Nordberg, R., Nordling, C., and Siegbahn, K., Phys. Lett. *20*, 159 (1966).

63. An apparatus for the ESCA method.
Fahlman, A., Hagström, S., Hamrin, K., Nordberg, R., Nordling, C., and Siegbahn, K., Arkiv Fysik *31*, 479 (1966).

64. The ESCA method using monochromatic X-rays and a permanent magnet spectrograph.
Fahlman, A., and Siegbahn, K., Arkiv Fysik *32*, 111 (1966).

65. A track counting method for low energy electron and optical spectroscopy.
Carlsson, R., Fahlman, A., Hallin, R., and Siegbahn, K., Arkiv Fysik *32*, 99 (1966).

66. *L* subshell photoelectron emission in germanium.
Carlsson, R., Fahlman, A., and Siegbahn, K., Arkiv Fysik *32*, 103 (1966).

67. Electron spectroscopy of atoms and molecules. (Thesis.)
Fahlman, A., Acta Universitatis Upsaliensis 73 (1966).

68. Calculation of electron binding energies and chemical shifts.
Lindgren, I., "Röntgenspektren und chemische Bindung", p. 182. Physikalisch-Chemisches Institut der Karl-Marx-Universität Leipzig (1966).

69. Chemical shifts by electron spectroscopy.
Nordling, C., and Siegbahn, K., "Röntgenspektren und chemische Bindung", p. 248. Physikalisch-Chemisches Institut der Karl-Marx-Universität Leipzig (1966).

70. A new precision spectroscopy of atoms and molecules.
Nordling, C., and Siegbahn, K., Rev. Roum. Phys. *11*, 797 (1966).

71. A method using a television microscope for counting electron and photon tracks in photographic plates.
Carlsson, R., Fahlman, A., and Siegbahn, K., UUIP-485 (July 1966).

72. Relativistic self-consistent-field calculations for heavy elements.
Lindgren, I., and Rosén, A., UUIP-491 (July 1966).

73. Bindningsenergier och Augerenergier beräknade med en modifierad Hartree-Fock-Slater-metod. (In Swedish).
Gelius, U., och Nordqvist, L.-A., UUIP-495 (August 1966).

74. Photoelectron spectroscopy of fatty acid multilayers.
Larsson, K., Nordling, C., Siegbahn, K., and Stenhagen, E., Acta Chem. Scand. *20*, 2880 (1966).

75. New approach to structure studies in organic chemistry.
Axelson, G., Ericsson, U., Fahlman, A., Hamrin, K., Hedman, J., Nordberg, R., Nordling, C., and Siegbahn, K., Nature *213*, 70 (1967).

76. Shifts in electron spectra of nitrogen in organic molecules.
Nordberg, R., Albridge, R. G., Bergmark, T., Ericson, U., Fahlman, A., Hamrin, K., Hedman, J., Johansson, G., Nordling, C., Siegbahn, K., and Lindberg, B., Nature *214*, 481 (1967).

77. Electron spectroscopic evidence of the thiolsulfonate structure of cystine S-dioxide.
    Axelson, G., Hamrin, K., Fahlman, A., Nordling, C., and Lindberg, B. J., Spectrochim. Acta. *23A*, 2015 (1967).

78. Relativistic calculations of electron binding energies by a modified Hartree-Fock-Slater method.
    Rosén, A., and Lindgren, I., To be published in Phys. Rev.

79. Array detectors and extended source used in a double focusing beta spectrometer.
    Nilsson, Ö., Karlsson, S.-E., Andersson, I., Nordling, C., and Siegbahn, K., Nucl. Instr. and Meth. *47*, 13 (1967).

80. A control system for the plate movement of a television microscope used as a photometer.
    Berglund, T., Carlsson, R., Fahlman, A., and Siegbahn, K., UUIP-544 (May 1967).

81. Molecular spectroscopy by means of ESCA. Charge distribution in nitrogen compounds.
    Nordberg, R., Albridge, R. G., Bergmark, T., Ericson, U., Hedman, J., Nordling, C., Siegbahn, K., and Lindberg, B. J., Arkiv Kemi *28*, 257 (1968).

82. The *KLL* Auger spectrum of fluorine.
    Albridge, R. G., Hamrin, K., Johansson, G., and Fahlman, A., Z. Phys. *209*, 419 (1968).

83. Structure studies of sulphur compounds by ESCA.
    Hamrin, K., Johansson, G., Fahlman, A., Nordling, C., Siegbahn, K., and Lindberg, B., To be published in Chem. Phys. Lett.

84. The *K* level energy of beryllium in metal, oxide and fluoride.
    Hamrin, K., Johansson, G., Fahlman, A., Nordling, C., and Siegbahn, K., UUIP-548 (May 1967).

85. Electron binding energies in some ionic single-crystals.
    Nordberg, R., Elango, M., Nordling, C., and Siegbahn, K., To be published.

86. A new magnetic instrument for ESCA.
    Nordberg, R., Hedman, J., Nordling, C., and Siegbahn, K., To be published.

87. An electrostatic double focussing instrument for ESCA.
    Siegbahn, K., Bergmark, T., and Karlsson, S.-E., To be published.

88. Conduction band of some gold-silver alloys studied by means of ESCA.
    Hamrin, K., Johansson, G., Fahlman, A., Nordling, C., and Siegbahn, K., To be published.

89. Electron spectroscopic studies of sulfur in organic molecules.
    Johansson, G., Fahlman, A., Hamrin, K., Nordling, C., Siegbahn, K., and Lindberg, B., To be published in Arkiv Fysik. (Conference report).

90. Energy shifts in the ls-level of nitrogen.
    Nordberg, R., Albridge, R. G., Bergmark, T., Ericson, U., Hedman, J., Nordling, C., Siegbahn, K., and Lindberg, B., To be published in Arkiv Fysik (Conference report).

91. Electron spectroscopic studies of insulin.
    Lindberg, B. J., Brolin, S., Fahlman, A., Hamrin, K., Johansson, G., Nordling, C., and Siegbahn, K., To be published in Proceedings of the 6th congress of the international diabetes federation 1967, Exerpta Medica Foundation.

92. Auger electron studies of atomic and molecular levels by electron impact.
    Bergmark, T., Spohr, R., Magnusson, N., and Siegbahn, K., To be published.

93. Electron binding energies in platinum.
    Karlsson, S.-E., Norberg, C.-H., Nilsson, Ö., Hogberg, S., El-Farrash, A. H., Nordling, C., and Siegbahn, K., To be published in Arkiv Fysik.

94. Electron excitation of electron spectra.
    Spohr, R., Bergmark, T., and Siegbahn, K., To be published in Arkiv Fysik. (Conference report).

95. Photometry by means of a television microscope.
    Carlsson, R., Fahlman, A., and Siegbahn K., To be published in Arkiv Fysik. (Conference report).

96. ESCA studies of liquids and gases.
    Bergmark, T., Magnusson, N., and Siegbahn, K., To be published in Arkiv Fysik. (Conference report).

97. Precision electron spectroscopy for studies of nuclear and atomic energy levels. (Thesis.)
    Karlsson, S.-E., Acta Universitatis Upsaliensis 99 (1967).

98. Electron spectroscopic investigation of ultraviolet photoionization processes.
    Spohr, R., Bergmark, T., Magnusson, N., and Siegbahn, K., To be published.

101. Robinson, H., and Rawlinson, W. F., Phil. Mag. *28*, 277 (1914).
102. Robinson, H., Proc. Roy. Soc. *A 104*, 455 (1923).
103. Robinson, H., Phil. Mag. *50*, 241 (1925).
104. de Broglie, M., C. R. *172*, 274 (1921).
105. Siegbahn, M., "Spektroskopie der Röntgenstrahlen", 2 Aufl. Berlin 1931.
106. Lindh, A. E., in Handbuch der Experimentalphysik, Bd 24, Teil 2, Ed. W. Wien and F. Harms, Leipzig 1930.
107. Van den Akker, J. A., and Watson, E. C., Phys. Rev. *37*, 1631 (1931).
108. Ference, M., Jr., Phys. Rev. *51*, 720 (1937).
109. Bazin, A., Zhurnal Ėksperimental'noĭ i Teoreticheskoĭ Fiziki *14*, 23 (1944).
110. Steinhardt, R. G., Jr., Granados, F. A. D., and Post, G. L., Anal. Chem. *27*, 1046 (1955).
111. Henke, B. L., Technical Report No. 6, Contract No. AF 49 (638)-394 (1962), Air Force Office of Scientific Research.
112. Svartholm, N., and Siegbahn, K., Arkiv f. Mat. Astr. Fys. *33A*, 21 (1946).
113. Rudberg, E., Proc. Roy. Soc. *A127*, 111 (1930).
114. Sandström, A. E., in Encyclopedia of Physics, Vol. XXX, p. 78. Ed. S. Flügge, Springer-Verlag, Berlin 1957.
115. Bearden, J. A., Rev. Mod. Phys. *39*, 78 (1967).
116. Skinner, H. W. B., and Johnston, J. E., Proc. Roy. Soc. Lond. Ser A *161*, 420 (1937).
117. Tomboulian, D. H., in Encyclopedia of Physics, Vol. XXX, p. 246. Ed. S. Flügge, Springer-Verlag, Berlin 1957.
118. Hodgkin, D. C., Kamper, J., Mackay, M., Pickworth, J., Trueblood, K. N., and White, J. G., Nature *178*, 64 (1956).
119. Stelling, O., Z. Physik *50*, 506 (1928).
120. Faessler, A., and Goehring, M., Die Naturwissenschaften *39*, 169 (1952).
121. Robinson, H. R., and Young, C. L., Phil. Mag. *10*, 71 (1930).
122. Turner, D. W., and Al-Joboury, M. J., J. Chem. Phys. *37*. 3007 (1962).
123. Turner, D. W., and May, D. P., J. Chem. Phys. *45*, 471 (1966).
Turner, D. W., Nature *213*, 795 (1967).
124. Kurbatov, B. L., Vilessov, F. I., and Terenin, A. N., Sov. Phys. Dokl., *6*, 490 (1961), *6*, 883 (1962).
125. Berkowitz, J., and Ehrhardt, H., Phys. Lett. *21*, 531 (1966).
126. Spohr, R., and von Puttkamer, E., Z. Naturforschg. *22a*, 705 (1967).
127. Hagedoorn, H. L., and Wapstra, A. H. Nucl. Phys *15*, 146 (1960).
128. Bardeen, J., Phys. Rev. *71*, 717 (1947).
129. Listengarten, M. A., Izv. Akad. Nauk SSSR, Ser. Fiz. *24*, 1041 (1960). (Engl. transl. Bull. Acad. Sci. USSR, phys. Ser. (USA) *24*, 1050 (1960)).
130. Parratt, L. G., Rev. Mod. Phys. *31*, 616 (1959).
131. Bearden, J. A., and Burr, A. F., Rev. Mod. Phys. *39*, 125 (1967).
132. Edlén, B., in Encyclopedia of Physics, Vol. XXVII, p. 80. Ed. S. Flügge, Springer-Verlag, Berlin 1964.
133. Hertz, G., Z. Physik *3*, 19 (1920).
134. Wapstra, A. H., Nijgh, G, J., and Van Lieshout, R., "Nuclear spectroscopy tables", North-Holland Publ. Co., Amsterdam 1959.
135. Sommerfeld, A., "Atombau und Spektrallinien", 6th ed., Vol. I, Braunschweig 1944.
136. Dirac, P. A. M. "Principles of Quantum Mechanics", 3rd ed., Oxford 1947.
137. Hagström, S. B. M., and Fadley, C. S., Bull. Am. Phys. Soc. *11*, 389 (1966).
138. Hagström, S., Private communication.
139. Bergvall, P., Arkiv Fysik *16*, 57 (1959).
140. Bethe, H. A., and Salpeter, E. E., in Encyclopedia of Physics, Vol. XXXV, p. 88. Ed. S. Flügge, Springer-Verlag, Berlin 1957.
141. Moseley, H. G. J., Phil. Mag. *27*, 703 (1914).
142. Idei, S., Sci. Rep. Tohoku Univ., Ser. I *19*, 559 (1930).
143. Sakellaridis, P., C. R. *236*, 1244 (1953); *236*, 1014 (1953); *236*, 1547 (1953); *238*, 2296 (1954).
144. Christy, R. F., and Keller, J. M., Phys. Rev. *61*, 147 (1942).
145. Bethe. H. A., and Longmire, C., Phys. Rev. *75*, 306 (1949).
146. Bergström, I., Brown, F., Davies, J. A., Geiger, J. S., Graham, R. L., and Kelly, R., Nucl. Instr. and Meth. *21*, 249 (1963).
147. Pines, D., "Elementary Excitations in Solids", W. A. Benjamin, Inc., New York 1963.
148. Cohen, E. R., and DuMond, J. W. M., Rev. Mod. Phys. *37*, 537 (1965).
149. Slater, J. C., "Quantum Theory of Atomic Structure", McGraw-Hill, New York 1960.
150. Hartree, D. R., "The Calculation of Atomic Structures", John Wiley & Sons, New York 1957.
151. Slater, J. C., Phys. Rev. *81*, 385 (1951).
152 Herman, F., and Skillman, S., "Atomic Structure Calculations", Prentice-Hall Inc., Englewood Cliffs, New Jersey 1963.
153. Kohn, W., and Sham, L. J., Phys. Rev. *140*, A 1133 (1965).
154. Tong, B. Y., and Sham, L. J., Phys. Rev. *144*, 1 (1966).
155. Cowan, R. D., Larson, A. C., Liberman, D., Mann, J. B., and Waber, J., Phys. Rev. *144*, 5 (1966).
156. Liberman, D., Waber, J. T., and Cromer, D. T., Phys. Rev. *137*, A 27 (1965).
157. Snow, E. C., Canfield, J. M., and Waber, J. T., Phys. Rev. *135*, A 969 (1964).

158. Nestor, C. W., Tucker, T. C., Carlson, T. A., Roberts, L. D., Malik, F. B., and Froese, C., Oak Ridge National Laboratory Report ORNL-4027 (Dec. 1966).

159. Koopmans, T., Physica *1*, 104 (1933).

160. Conolly, J. W. D., University of Florida Quantum Theory Project Preprint No. 94 (1966).

161. Froese, C., J. Chem. Phys. *45*, 1417 (1966), and unpublished results.

162. Coulthard, M. A., Proc. Phys. Soc. *91*, 44 (1967).

163. Berglund, C. N., and Spicer, W. E., Phys. Rev. *136*, A 1044 (1964).

164. Roberts, S., Phys. Rev. *118*, 1509 (1960).

165. Burdick, G. A., Phys. Rev. *129*, 139 (1963).

166. Slater, J. C., "Quantum theory of molecules and solids", Vol. 2, Mc Graw-Hill Inc., New York 1965.

167. Blodgett, A. J. Jr., and Spicer, W. E., Phys. Rev. *146*, 390 (1966).

168. Shoenberg, D., "The Fermi Surface", p. 74. Ed. W. A. Harrison and M. B. Webb, John Wiley & Sons, Inc., New York 1960.

169. Morse, R. W., "The Fermi Surface", p. 214. Ed. W. A. Harrison and M. B. Webb, John Wiley & Sons, Inc., New York 1960.

170. Kip, A. F., "The Fermi Surface", p. 146. Ed. W. A. Harrison and M. B. Webb, John Wiley & Sons, Inc., New York 1960.

171. Cauchois, Y., and Bonelle, C., Proceedings of the International Colloquium on Optical Properties and Electronic Structure of Metals and Alloys, Paris 1965, p. 83. Ed. F. Abelès, North-Holland Publishing Co., Amsterdam 1966.

172. Phillips, J. C., Phys. Rev. *136*, A 1705 (1964).

173. Kraushaar, J. J., Wilson, E. D., and Bainbridge, K. T., Phys. Rev. *90*, 610 (1953).

174. Pauling, L., "The Nature of the Chemical Bond", 2nd ed., New York 1945.

175. Madelung, E., Phys. Z. *19*, 524 (1918).

176. Frauenfelder, H., "The Mössbauer Effect", W. A. Benjamin, Inc. Publishers, New York 1962.

177. Craig, D. P., and Zauli, C., J. Chem. Phys. *37*, 601, 609 (1962).

178. Craig, D. P., and Thirunamachandran, T., J. Chem. Phys. *45*, 3355 (1966).

179. Moffitt, W., Proc. Roy. Soc. A *200*, 409 (1950).

180. Bishop, D. M., Randič, M., and Morton, J. R., J. Chem. Phys. *45*, 1880 (1966).

181. Wood, R. H., J. Chem. Phys. *32*, 1690 (1959).

182. Wyckoff, R. W. G., "Crystal Structures", Interscience Publishers, 2nd ed., New York 1948.

183. Meisel, A., Phys. Stat. Sol. *10*, 365 (1965).

184. Coulson, C. A., and Zauli, C., Mol. Phys. *6*, 525 (1963).

185. Palmieri, P., and Zauli, C., Theoret. Chim. Acta *7*, 89 (1967).

186. Nefedow, W., Phys. Stat. Sol. *2*, 904 (1962).

187. Gould, E. S., "Mechanism and Structure in Organic Chemistry", New York 1959.

188. Hägg, G., "Allmän och Oorganisk Kemi" (in Swedish), p. 146, Uppsala 1963.

189. Hinze, J., and Jaffé, H. H., J. Am. Chem. Soc. *84*, 540 (1962).

190. Hinze, J., Whitehead, M. A., and Jaffé, H. H., J. Am. Chem. Soc. *85*, 148 (1963).

191. Huheey, J. E., J. Phys. Chem. *69*, 3284 (1965).

192. Huheey, J. E., J. Phys. Chem. *70*, 2086 (1966).

193. Pauling, L., "The Nature of the Chemical Bond", 3rd ed., New York 1960.

194. Wheland, G. W., "The Theory of Resonance", Sections 1, 4, New York, London 1947.

195. Lewis, G. N., J. Am. Chem. Soc. *38*, 762 (1916).

196. Sanderson, R. T., J. Chem. Ed. *31*, 2 (1954).

197. Bishop, D. M., Theoret. Chim. Acta (Berl.) *8*, 285 (1967).

198. Ionov, S. P., and Porai-Koshits, M. A., Russ. J. Inorg. Chem. *10*, 1069 (1965). (Engl. transl.).

199. Price, C. S., and Oae, S., "Sulfur Bonding", pp. 62, 167, New York 1962.

200. Pauling, L., J. Phys. Chem. *56*, 361 (1952).

201. Siebert, H., Z. anorg. u. allg. Chem. *275*, 225 (1954).

202. Gillespie, R. J., and Robinson, E. A., Can. J. Chem. *41*, 2074 (1963).

203. Staab, H. A., "Einführung in die theoretische organische Chemie", 2nd ed., Ch. 3.3, Weinheim 1960.

204. Fadley, C. S., Hagström, S. B. M., Hollander, J. M., Klein, M. P., and Shirley, D. A., Science *157*, 1571 (1967).

205. Del Re, G., J. Chem. Soc. 4031 (1958).

206. Del Re, G., Pullman, B., and Yonezawa, T., Biochim. Biophys. Acta *75*, 153 (1963).

207. Momose, T., Ueda, Y., Shoji, T., and Yano, H., Chem. Pharm. Bull. (Tokyo) *6*, 669 (1955).

208. Baxter, J. N., Cymerman-Craig, J., and Willis, J. B., J. Chem. Soc. 669 (1955).

209. Hamilton, W. C., and La Placa, S. J., J. Am. Chem. Soc. *86*, 2289 (1964).

210. Lindquist, I., and Mörtsell, M., Acta Cryst. *10*, 406 (1957).

211. Abrahams, S. C., Quart. Rev. (London) *10*, 407 (1956).

212. Lindberg, B. J., Acta Chem. Scand. *21*, 2215 (1967).

213. Pauly, C., and Otto, R., Ber. *9*, 1639 (1876).

214. Pauly, C., and Otto, R., Ber. *10*, 2181 (1877).

215. Crenshaw, R. R., and Owen, T. C., Proc. Chem. Soc. 250 (1961).

216. Cymerman, J., and Willis, J. B., J. Chem. Soc. 1332 (1951).

217. Allen, P. Jr., Berner, P. J., and Malinowski, E. R., Chem. & Ind. 1164 (1961).

218. Allen, P. Jr., Berner, P. J., and Malinowski, E. R., Chem. & Ind. 208 (1963).

219. Sweetman, B. J., Nature *183*, 744 (1959).

220. Utzinger, G. E., Experimentia *17*, 374 (1961).
221. Savige, W. E., Eager, J., Maclaren, J. A., and Roxburgh, C. M., Tetrahedron Letters, *44*, 3289 (1964).
222. Block, S. S., and Weidner, I. P., Applied Spectroscopy *20*, 73 (1966).
223. Herzberg, G., "Molecular spectra and molecular structure", Vol. I, 2nd ed., D. Van Nostrand Company Inc., New York 1950.
224. Gorin, G., and Godwin, W. E., Biochem. Biophys. Res. Comm., *25*, 227 (1966).
225. Fadley, C. S., Hagström, S. B. M., Klein, M. P., and Shirley, D. A., UCRL-17005 (1967).
226. Kanter, H., and Sternglass, E. J., Phys. Rev. *126*, 620 (1962).
227. Blodgett, K. B., J. Am. Chem. Soc. *57*, 1007 (1935).
228. Clark, G. L., and Leppla, P. W. J. Am. Chem. Soc. *58*, 2199 (1936).
229. Stenhagen, E., Trans. Faraday Soc. *34*, 1328 (1938).
230. Steinhardt, R. G., Jr., and Serfass, E. J., Anal. Chem. *25*, 697 (1953).
231. Henke, B. A., "X-ray Optics and X-ray Microanalysis" pp. 157 172, Academic Press, New York and London 1963.
232. Palmieri, P., and Zauli, C., J. Chem. Soc. (A) 813 (1967).
233. Manne, R., J. Chem. Phys. *46*, 4645 (1967).
234. Asaad, W. N., and Burhop, E. H. S., Proc. Phys. Soc. (London) *71*, 369 (1958).
235. Asaad, W. N., Proc. Roy. Soc. (London) A *249*, 555 (1959).
236. Listengarten, M. A., Izv. Akad. Nauk. SSSR, Ser. Fiz. *26*, 182 (1962). (Engl. transl. Bull. Acad. Sci. USSR, phys. Ser. (USA) *26*, 182 (1962)).
237. Asaad, W. N., Nucl. Phys. *66*, 494 (1965).
238. Graham, R. L., Bergström, I., and Brown, F., Nucl. Phys. *39*, 107 (1962).
239. Mehlhorn, W., and Asaad, W. N., Z. Physik *191*, 231 (1966).
240. Körber, H., and Mehlhorn, W., Z. Physik *191*, 217 (1966).
241. Callan, E. J., Phys. Rev. *124*, 793 (1961).
242. Krause, M. O., Vestal, M. L., Johnston, W. H., and Carlson, T. A., Phys. Rev. *133*, A 385 (1964).
243. Codling, K. and Madden, R. P., Phys. Rev. Lett. *12*, 106 (1964).
244. Condon, E. U., and Shortley, C., "The theory of atomic spectra", Cambridge 1959.
245. Carlson, T. A., and Krause, M. O., Phys. Rev. Lett. *17*, 1079 (1966).
246. Mehlhorn, W., Z. Physik *187*, 21 (1965).
247. Moore, C. E., "Atomic Energy Levels", Vol. II, Washington; Nat. Bureau of Standards 1952.
248. Hultberg, S., Arkiv Fysik *15*, 307 (1959).
249. Pratt, R. H., Levee, R. D., Pexton, R. L., and Aron, W., Phys. Rev. *134*, A898 (1964).
250. Rakavy, G., and Ron, A., Phys. Lett. *19*, 207 (1965).
251. Bethe, H. A., and Salpeter, E. E. in Encyclopedia of Physics Vol. XXXV, p. 381. Ed. S. Flügge, Springer-Verlag, Berlin 1957.
252. Sommerfeld, A., and Schur, G., Ann. d. Phys. *4*, 409 (1930).
253. Schur, G., Ann. d. Phys. *4*, 433 (1930).
254. Hall, H., Rev. Mod. Phys. *8*, 358 (1936).
255. Slater, J. C., Phys. Rev. *36*, 57 (1930).
256. Futrell, J. H., and Miller, C. D., Rev. Sci. Instr. *37*, 1521 (1966).
257. Spangenberg, K. R., "Vacuum Tubes", McGraw-Hill Book Co., Inc., New York 1948.
258. Purcell, E. M., Phys. Rev. *54*, 818 (1938).
259. Herzog, R., Z. Physik *97*, 596 (1935).
260. Herzog, R., Phys. Zeitschr. *41*, 18 (1940).
261. Bergkvist, K.-E., Arkiv Fysik *27*, 383 (1965).
262. Bergkvist, K.-E., Arkiv Fysik *27*, 439 (1965).
263. Bruninx, E., and Rudstam, G., Nucl. Instr. and Meth. *13*, 131 (1961).
264. Evans, D. S., Rev. Sci. Instr. *36*, 375 (1965).
265. Al-Joboury, M. I., and Turner, D. W., J. Chem. Soc. 5141 (1963).
266. Schoen, R. I., J. Chem. Phys. *40*, 1830 (1964).
267. Frost, D. C., McDowell, C. A., and Vroom, D. A., Phys. Rev. Lett. *15*, 612 (1965).
268. Kindig, N. B., and Spicer, W. E., Rev. Sci. Instr. *36*, 759 (1965).
269. Blodgett, A. J., Jr., and Spicer, W. E., Phys. Rev. *158*, 514 (1967).
270. Bäckström, G., Bäcklin, A., Holmberg, N. E., and Bergkvist, K. E., Nucl. Instr. and Meth. *16*, 199 (1962).
271. Graham, R. L., Hollander, J. M., and Kleinheinz, P., UCRL Report, November 1962.
272. Danysz, J., Le Radium *9*, 1 (1912).
273. Danysz, J., Le Radium *10*, 4 (1913).
274. Hofmann, E. G., and Jagodzinski, H., Z. Metallk. *46*, 601 (1955).
275. Scott, R. E., Rev. Sci. Instr. *35*, 118 (1964).
276. Hollander, J. M., Holtz, M. D., Novakov, T., and Graham, R. L., Arkiv Fysik *28*, 375 (1965).
277. Lee-Whiting, G. E., and Taylor, E. A., Can. J. Phys. *35*, 1 (1957).
278. Compton, A. H., and Allison, S. K., "X-rays in Theory and Experiment", 2nd ed., p. 533, MacMillan and Co., Ltd, London 1935.
279. Graham, R. L., Ewan, G. T., and Geiger, J. S., Nucl. Instr. and Meth. *9*, 245 (1960).
280. Ewald, H., and Liebl, H., Z. Naturforschg. *12a*, 28 (1957).
281. Pritchard, H. O., and Skinner, H. A., Chem. Revs. *55*, 745 (1955).
282. Barinski, R. L., and Nefedow, V. I., "Rentgenospektralnoe Opredelenie Zarjada Atomov v Molekulach", Izdatelstvo "Nauka", Moskva 1966.
283. Mulliken, R. S., J. Chem. Phys. *2*, 782 (1934).

284. Mulliken, R. S., J. Chem. Phys. *3*, 573 (1935).

285. Nachod, F. C., and Philips, W. D. (Ed.), "Determination of Organic Structures by Physical Methods", Vol. 2, p. 699, New York, London 1962.

286. Huheey, J. E., J. Org. Chem. *31*, 2365 (1966).

287. Wetterblad, T., Z. Physik *42*, 611 (1927).

288. Klostermeyer, H., and Humbel, R. E., Angewandte Chemie *78*, 871 (1966).

289. Timusk, T., and Martienssen, W., Phys. Rev. *128*, 1656 (1962).

290. Klemperer, O., and Shepherd, J. P. G., Advances in Physics Vol. XII, p. 335 (1963).

291. Boersch, H., IVth International Conference on the Physics of Electronic and Atomic Collisions, p. 351, Science Bookcrafters, Inc., New York 1965.

292. Geiger, J., and Topschowsky, M., Z. Naturforschg. *21a*, 626 (1966).

293. Hagström, S., Private communication.

294. Seyewetz, A., and Mournier, D., Bull. Chim. France *43*, 648 (1928).

295. Ference, M., Shaw, A. E., and Stephenson, R. J., Rev. Sci. Instr. *11*, 57 (1940).

296. Clark, J. D., and Frost, D. C., J. Am. Chem. Soc. *89*, 244 (1967).

297. Turner, D. W., Tetrahedron Letters *35*, 3419 (1967).

298. Iczkowski, R. P., and Margrave, J. L., J. Am. Chem. Soc. *83*, 3547 (1961).

299. Kelly, R. L., "Vacuum ultraviolet emission lines", UCRL-5612 (1959).

DOCUMENT CONTROL DATA - R & D

(… of abstract and indexing annotation must be entered when the overall report is classified)

Department of Physics
University of Uppsala
Uppsala, Sweden

2a. REPORT SECURITY CLASSIFICATION
Unclassified

2b. GROUP

ESCA. Atomic, molecular and solid state structure studied by means of electron spectroscopy.

(Type of report and inclusive dates)
Scientific Final

(… middle initial, last name)
Kai Siegbahn, Carl Nordling, Anders Fahlman, Ragnar Nordberg, Kjell Hamrin, Jan Hedman, Gunilla Johansson, Torsten Bergmark, Sven-Erik Karlsson, Ingvar Lindgren, and Bernt Lindberg.

August 1968

7a. TOTAL NO. OF PAGES
282

7b. NO. OF REFS
299

AF 61(052)-795

7360 and 7367

Task nos 736005 and 736702

9a. ORIGINATOR'S REPORT NUMBER(S)
Nova Acta Regiae Soc. Sci. Upsaliensis Ser. IV Vol. 20 (1967)

9b. OTHER REPORT NO(S) *(Any other numbers that may be assigned this report)*
AFML-TR-68-189

This document is subject to special export controls and each transmittal to foreign governments or foreign nationals may be made only with prior approval of the Air Force Materials Laboratory (MAYA), Wright-Patterson AFB, Ohio 45433

12. SPONSORING MILITARY ACTIVITY
Air Force Materials Laboratory (AFML)
Wright-Patterson AFB
Ohio 45433

In this monograph, a report is given of our work leading to the development of a high resolution electron spectroscopy. The work started in the early part of the fifties and has now been brought to a stage where we believe that this kind of spectroscopy is ready for a more general use. The energies that can be measured by our present equipment range from 1MeV down to 0.01 eV, i.e. 26 octaves. It will be shown that new information about atoms and molecules can be obtained by electron spectroscopy. Samples may be prepared in the solid, liquid or gaseous phase. The material to be presented is comparatively extensive and we therefore start in Chapter I with a general survey in order to acquaint the reader with the main features of this type of spectroscopy before presenting a more detailed account in the chapter that follow. Some results of theoretical work and design studies are collected in appendices together with some tables required for ESCA.

DD FORM 1473

UNCLASSIFIED

Security Classification

14. KEY WORDS	LINK A		LINK B		LINK C	
	ROLE	WT	ROLE	WT	ROLE	WT
Application of electron spectroscopy (ESCA). Atomic, molecular and solid state structure. Electron spectrum of solids, liquids and gases. High resolution electron spectrometers. Binding energies of atomic electrons. Band structures of solids. Electron spectroscopy for chemical analysis. Electron emission from excited atoms. Photoelectric cross sections. Atomic and molecular charges.						

Security Classification